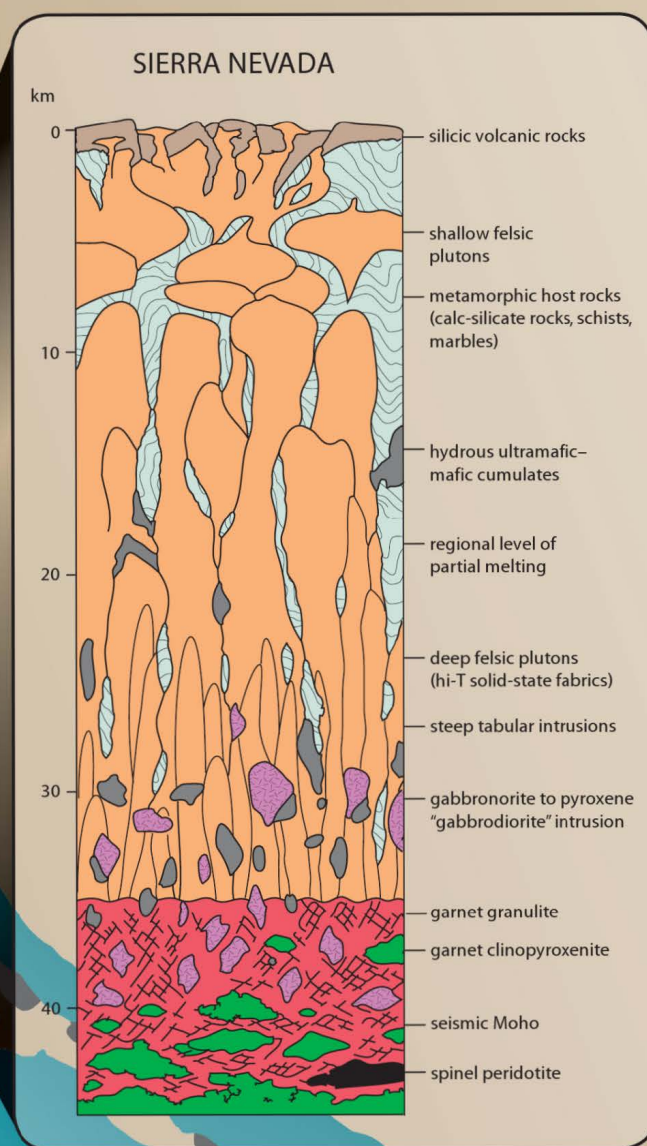


CRUSTAL CROSS SECTIONS

from the Western North American Cordillera
and Elsewhere: Implications for Tectonic
and Petrologic Processes

edited by Robert B. Miller and Arthur W. Snoke



THE
GEOLOGICAL
SOCIETY
OF AMERICA®

Special Paper 456

*Crustal Cross Sections from the Western North American Cordillera
and Elsewhere: Implications for Tectonic and Petrologic Processes*

Edited by

Robert B. Miller
Department of Geology
San José State University
San José, California 95192-0102
USA

Arthur W. Snoke
Department of Geology and Geophysics
Department 3006
1000 East University Avenue
University of Wyoming
Laramie, Wyoming 82071-2000
USA



THE
GEOLOGICAL
SOCIETY
OF AMERICA®

Special Paper 456

3300 Penrose Place, P.O. Box 9140 ■ Boulder, Colorado 80301-9140, USA

2009

Copyright © 2009, The Geological Society of America (GSA). All rights reserved. GSA grants permission to individual scientists to make unlimited photocopies of one or more items from this volume for noncommercial purposes advancing science or education, including classroom use. For permission to make photocopies of any item in this volume for other noncommercial, nonprofit purposes, contact The Geological Society of America. Written permission is required from GSA for all other forms of capture or reproduction of any item in the volume including, but not limited to, all types of electronic or digital scanning or other digital or manual transformation of articles or any portion thereof, such as abstracts, into computer-readable and/or transmittable form for personal or corporate use, either noncommercial or commercial, for-profit or otherwise. Send permission requests to GSA Copyright Permissions, 3300 Penrose Place, P.O. Box 9140, Boulder, Colorado 80301-9140, USA. GSA provides this and other forums for the presentation of diverse opinions and positions by scientists worldwide, regardless of their race, citizenship, gender, religion, or political viewpoint. Opinions presented in this publication do not reflect official positions of the Society.

Copyright is not claimed on any material prepared wholly by government employees within the scope of their employment.

Published by The Geological Society of America, Inc.
3300 Penrose Place, P.O. Box 9140, Boulder, Colorado 80301-9140, USA
www.geosociety.org

Printed in U.S.A.

GSA Books Science Editors: Marion E. Bickford and Donald I. Siegel

Library of Congress Cataloging-in-Publication Data

Crustal cross sections from the western North American cordillera and elsewhere : implications for tectonic and petrologic processes / edited by Robert B. Miller, Arthur W. Snoke.

p. cm. — (Special paper ; 456)

Includes bibliographical references and index.

ISBN 978-0-8137-2456-0 (pbk.)

1. Continental crust. 2. Geology, Stratigraphic. 3. Orogeny. 4. Geology, Structural. 5. Plate tectonics. I. Miller, Robert B. (Robert Bruce), 1951–. II. Snoke, Arthur W.

QE511.C7176 2009

551.1'3—dc22

2009021398

Cover, background image: Sketch map of the western North American Cordillera showing distribution of Mesozoic and Cenozoic plutonic rocks. **Inset, front:** Restored crustal section of the southern Sierra Nevada, California. (Modified from Saleeby, J.B., Ducea, M., and Clemens-Knott, D., 2003, Production and loss of high-density batholithic root—Southern Sierra Nevada, California: *Tectonics*, v. 22. Used with permission from the American Geophysical Union.) **Inset, back:** Diagrammatic crustal section of the accreted Jurassic Talkeetna arc of south-central Alaska. (Derived from Greene, A.R., DeBari, S.M., Kelemen, P.B., Blusztajn, J., and Clift, P.D., 2006, A detailed geochemical study of island arc crust: The Talkeetna arc section, south-central Alaska: *Journal of Petrology*, v. 47, p. 1051–1093, Fig. 2 and Table 1.) See Chapter 1 by R.B. Miller and A.W. Snoke for additional details about these crustal cross sections.

Contents

<i>CD-ROM Contents</i>	v
<i>Acknowledgments</i>	vi
1. The utility of crustal cross sections in the analysis of orogenic processes in contrasting tectonic settings	1
<i>R.B. Miller and A.W. Snoke</i>	
2. Petrology and geochronology of crustal xenoliths from the Bering Strait region: Linking deep and shallow processes in extending continental crust	39
<i>V.V. Akinin, E.L. Miller, and J.L. Wooden</i>	
3. Construction and evolution of the Kodiak Talkeetna arc crustal section, southern Alaska	69
<i>D.W. Farris</i>	
4. Mid-Cretaceous–Recent crustal evolution in the central Coast orogen, British Columbia and southeastern Alaska	97
<i>M.L. Crawford, K.A. Klepeis, G.E. Gehrels, and J. Lindline</i>	
5. Plutonism at different crustal levels: Insights from the ~5–40 km (paleodepth) North Cascades crustal section, Washington	125
<i>R.B. Miller, S.R. Paterson, and J.P. Matzel</i>	
6. Granulite- to amphibolite-facies metamorphism and penetrative deformation in a disrupted ophiolite, Klamath Mountains, California: A deep view into the basement of an accreted oceanic arc	151
<i>S.R. Garlick, L.G. Medaris Jr., A.W. Snoke, J.J. Schwartz, and S.M. Swapp</i>	
7. Mesozoic magmatism in an upper- to middle-crustal section through the Cordilleran continental margin arc, eastern Transverse Ranges, California	187
<i>S.K. Needy, J.L. Anderson, J.L. Wooden, R.J. Fleck, A.P. Barth, S.R. Paterson, V. Memeti, and G.S. Pignotta</i>	
8. Perspectives on the architecture of continental crust from integrated field studies of exposed isobaric sections	219
<i>M.L. Williams, K.E. Karlstrom, G. Dumond, and K.H. Mahan</i>	
9. Evolution of the middle and lower continental crust during the transition from contraction to extension in Fiordland, New Zealand	243
<i>K.A. Klepeis and D.S. King</i>	

<i>10. A granulite-facies normal shear zone exposed in the Arunta inlier of central Australia: Implications for deep-crustal deformation during oblique divergence</i>	267
<i>C. Waters-Tormey, L.B. Goodwin, B. Tikoff, K. Staffier, and P. Kelso</i>	
<i>Index</i>	287

CD-ROM Contents

Associated Chapter	Item
Miller and Snoke (Chapter 1)	Figures 4–10.
Akinin et al. (Chapter 2)	Tables 1–4.
Crawford et al. (Chapter 4)	Figures 6A–6C, 7A–7B, 8, 11, and 12. Appendix. Methods. Tables 2–5. (Also GSA Data Repository item 2009156.)
Garlick et al. (Chapter 6)	Appendix 1. Geologic map of the Seiad complex, Kangaroo Mountain area, Klamath Mountains, California, by Sarah R. Garlick and L. Gordon Medaris Jr. Appendix 2. Field-trip guide to the Seiad complex, Kangaroo Mountain area, Klamath Mountains, California, by Sarah R. Garlick and Arthur W. Snoke. (Also GSA Data Repository item 2009157.)

Acknowledgments

This book is a byproduct of a symposium on crustal cross sections that was convened by the editors at the 2005 Geological Society of America (GSA) Cordilleran Section Meeting held in San Jose, California. We thank the authors of the individual chapters for their contributions to this volume. We also gratefully acknowledge the reviewers listed below and an anonymous reviewer for their thorough evaluations of the manuscripts considered for this volume. Their contributions significantly improved the overall quality of this Special Paper. We also appreciate the efforts of GSA Books Science Editor M.E. "Pat" Bickford and the staff at GSA Headquarters for their assistance in the production of this volume.

Chuck Bailey	College of William and Mary
Calvin Barnes	Texas Tech University
Steven Bergman	Shell Oil Company
M.E. "Pat" Bickford	Syracuse University
Ned Brown	Western Washington University
Bill Collins	James Cook University, Australia
Susan DeBari	Western Washington University
W. Gary Ernst	Stanford University
Robert Holdsworth	Durham University, UK
Keith Howard	U.S. Geological Survey
Carl Jacobson	Iowa State University
Scott Johnson	University of Maine
Calvin Miller	Vanderbilt University
Richard Norris	University of Otago, New Zealand
John Platt	University of Southern California
Michael Roden	University of Georgia
David Schneider	University of Ottawa, Canada
David Scholl	Stanford University
Virginia Sisson	American Natural History Museum
Harold Stowell	University of Alabama

The utility of crustal cross sections in the analysis of orogenic processes in contrasting tectonic settings

Robert B. Miller*

Department of Geology, San José State University, San José, California 95192-0102, USA

Arthur W. Snoke

Department of Geology and Geophysics, Department 3006, 1000 East University Avenue, University of Wyoming, Laramie, Wyoming 82071-2000, USA

ABSTRACT

The nature of petrologic and structural properties and processes that characterize the middle and lower continental crust is a long-standing problem in the earth sciences. During the past several decades significant progress has been made on this fundamental problem by synthesizing deep-crustal seismic-reflection imaging, laboratory-based seismic-velocity determinations, xenolith studies, and detailed geological studies of exposed crustal cross sections. Geological, geochemical, and geophysical studies of crustal sections provide a crustal-scale context for a variety of important problems in the earth sciences. Crustal sections are widely used to evaluate crustal composition and petrogenesis, including lateral and vertical variations in rock types. Evidence from deep levels of crustal sections suggests seismic shear-wave anisotropy and seismic lamination result from widespread subhorizontal contacts, shear zones, and transposition fabrics, and in some sections from metamorphosed m- to km-thick, intraplated and/or underplated mafic magmatic sheets and plutons. Crustal sections also facilitate the evaluation of crustal rheology in natural settings from regional to outcrop scale. Magmatism, metamorphism, partial melting, and relatively small lithological differences control rheology, localize strain, and lead to markedly heterogeneous deformation over a wide range of crustal levels. Finally, crustal sections provide unique views of the architecture and deformation patterns of fault zones in the deep crust.

As a guide to the growth and evolution of continental crust in the past 0.5 Ga, we summarize the salient features of some examples of crustal cross sections from Phanerozoic orogens. These crustal sections represent different tectonic settings, although the variation in magmatic arcs from intra-oceanic to continental-margin settings is a major theme in our synthesis. Another theme is the importance of attenuated crustal sections in reconstructing the hinterland of orogens that have experienced large-magnitude crustal extension after an earlier history of crustal contraction. The

*rmiller@geosun.sjsu.edu

Miller, R.B., and Snoke, A.W., 2009, The utility of crustal cross sections in the analysis of orogenic processes in contrasting tectonic settings, *in* Miller, R.B., and Snoke, A.W., eds., *Crustal Cross Sections from the Western North American Cordillera and Elsewhere: Implications for Tectonic and Petrologic Processes*: Geological Society of America Special Paper 456, p. 1–38, doi: 10.1130/2009.2456(01). For permission to copy, contact editing@geosociety.org. ©2009 The Geological Society of America. All rights reserved.

Phanerozoic crustal cross sections summarized in this chapter developed during a polyphase deformational and magmatic history that spanned 10–100s of Ma and resulted in overprinting of different events. Consequently, we conclude that there is no “typical” Phanerozoic continental crustal section, and the overall crustal composition varies markedly between sections. The thickness of lower crust that existed below an exposed crustal section is difficult to quantify. Only a few sections are in contact (typically faulted) with mantle rocks, and although xenoliths can provide important information about the unexposed parts of the deep crust and upper mantle, they are absent for most sections. The exhumation of relatively intact crustal cross sections and lower-crustal rocks probably requires an unusual sequence of tectonic events, and almost all of the sections evaluated in this chapter were exhumed by multiple mechanisms. Major exhumation is most commonly attributed to normal faults and extensional shear zones.

INTRODUCTION

The purpose of this volume is to provide a synthesis of crustal cross sections with a special emphasis on the western North American Cordillera. From the North American geographic perspective, this volume includes articles that discuss examples of crustal cross sections from the Bering Shelf area, where the Russian Federation and Alaska share a common international border, followed by other studies of areas along the western North American Cordillera and the southwest of the United States (Fig. 1). These Cordilleran crustal sections, developed chiefly during Phanerozoic orogenic processes, are supplemented by articles on lower- and mid-crustal sections through Proterozoic crust in North America and Australia, and the Cretaceous section of Fiordland, New Zealand.

We begin this introductory chapter by outlining some early geologic ideas and concepts concerning the relationship of crustal depth (structural level) to structural style, plutonism, regional metamorphism, and migmatization. Further, we emphasize the importance of the study of crustal cross sections for petrologic, geochemical, structural, rheological, and geophysical context in regard to fundamental processes that occur in the crust and upper mantle. To provide some “comparative anatomy” with other crustal sections exposed worldwide, the key elements of seven classic crustal cross sections, only one of which (Fiordland) is discussed in detail in the volume, are outlined in this introductory chapter, and numerous important references on these examples are provided to the reader. We also discuss common issues for the interpretation of inferred crustal cross sections, including how crustal sections that expose deep-crustal and upper-mantle rocks are eventually exhumed.

This is not the first book (e.g., see *Exposed Cross-Sections of the Continental Crust*, edited by Matthew H. Salisbury and David M. Fountain [1990]) or synthesis article (e.g., Fountain and Salisbury, 1981; Percival et al., 1992) that attempted to integrate a variety of data concerning inferred crustal cross sections exposed throughout the world. We take a somewhat different tack in this review article by emphasizing Phanerozoic crustal sections in our analysis. This approach is compatible with the theme of

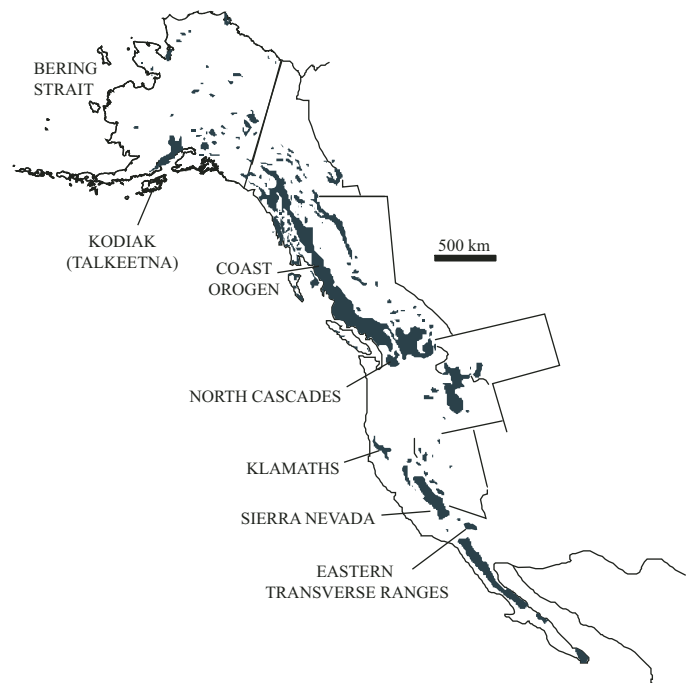


Figure 1. A sketch map of the western North American Cordillera that approximately shows the distribution of the crustal cross sections discussed in this volume. Areas shaded black are Mesozoic and Cenozoic plutons.

the volume as a whole, which emphasizes the Cordilleran orogen of western North America.

EARLY CONCEPTS ABOUT CRUSTAL COMPOSITION, DEPTH ZONES, AND RELATIONSHIP TO METAMORPHISM AND PLUTONISM

Composition of the Lower Crust

For many years, geophysicists and petrologists have taken the lead in developing whole-crustal models for various areas of Earth. In particular, the nature of the lower crust has been a major

problem in the earth sciences for more than a hundred years. In the classic, quintessential physical geology textbook by Holmes (1965) the lower crust is referred to as “crustal sima,” whereas the upper mantle is “mantle sima” with the Mohorovicic discontinuity separating these fundamental divisions of Earth. “Sima” is used for rocks that contain abundant silica but with iron oxides and magnesia as the second most abundant constituents, whereas sialic rocks consist chiefly of silica and alumina. Holmes (1965) considered rocks of basaltic composition with an average density of $\sim 2.9 \text{ g/cm}^3$ as representative of crustal sima and ultrabasic rocks with an average density of $\sim 3.3 \text{ g/cm}^3$ as representative of mantle sima (see Holmes, 1965, his figure 18). During the more than four decades since Holmes’ synthesis, significant progress has been made on this fundamental problem by synthesizing deep-crustal seismic-reflection imaging, laboratory-based seismic-velocity studies, geobarometric determinations, xenolith studies, and detailed geologic mapping of exposed deep-crustal sections (e.g., Fountain et al., 1990, 1992; Rudnick and Fountain, 1995).

Crustal Depth and Metamorphic Grade

The concept that a relationship exists between crustal depth and metamorphic grade is an idea that was prominent in geologic thinking as far back as the beginning of the twentieth century (e.g., Grubenmann, 1904). As the sub-discipline of metamorphic geology developed in the middle of the twentieth century (e.g., Turner, 1948) the importance of the metamorphic facies and phase equilibria began to dominate thinking about variations in metamorphic grade and zonation. Somewhat earlier, in the classic “Zur Deutung der Migmatite” published in *Geologische Rundschau*, C.E. Wegmann (1935), a Swiss structural geologist, developed a tectonic model that related regional metamorphism, migmatite development, and orogenic zones. Wegmann (1935) described a three-tier, in situ orogenic model based on structural level: *Unterbau*, *Oberbau*, and an intermediate transitional zone that he called “*Übergangszone*.” Haller (1956, 1971) further developed the “stockwerk”-folding hypothesis through his regional studies of the East Greenland Caledonides. He also employed a three-tier structural-metamorphic model, which involved limited lateral displacement (i.e., regional thrust faulting): (1) *infrastructure*, a deep-seated migmatitic core; (2) *a zone of disharmonic detachment* (or *Abscherungszone*) separating the lower tier (1) from the upper tier (3) *superstructure*, low-grade or non-metamorphic rocks (Fig. 2). Subsequent geologic mapping and radiometric dating (e.g., Higgins, 1976; Steiger et al., 1979; Soper and Higgins, 1993; Henriksen and Higgins, 2008) have demonstrated that the various structural levels in the East Greenland Caledonides are a product of polyphase deformation (e.g., basement-cover relationships overprinted by Caledonian reworking of Precambrian basement rocks). Furthermore, some aspects of the deformational history manifested in the East Greenland Caledonides are indicative of large-magnitude crustal extension (Hartz et al., 2001; White and Hodges, 2002; Gilotti and McClelland, 2008). Despite these problems, Culshaw

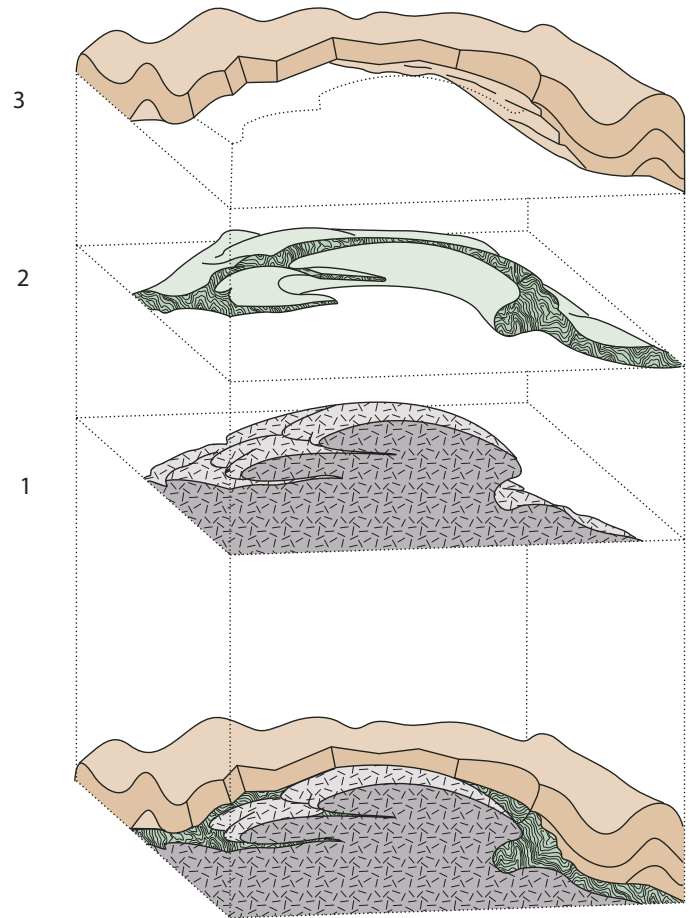


Figure 2. The “stockwerk”-folding tectonic model for the East Greenland Caledonides as summarized in Haller (1971, his figure 52). Used with permission from John Wiley & Sons. The upper tier (3), superstructure, consists of non-metamorphosed to low-grade sedimentary rocks, whereas the lower tier (1), infrastructure, consists of plastically deformed, migmatitic rocks that have welled up into large-scale recumbent folds and domes. These two contrasting structural levels are separated by a middle tier (2) of variable thickness referred to as a zone of disharmonic detachment (i.e., “*Abscherungszone*”), indicating structural decoupling between the upper tier and lower tier of the orogenic crust.

et al. (2006) argued for the validity of this tectonic model and provided two-dimensional thermal-mechanical models to account for the relationships originally hypothesized by Wegmann (1935).

Crustal Depth and Pluton Emplacement

The role of depth during pluton emplacement was strongly emphasized in Buddington’s (1959) presidential address published in the *Bulletin of the Geological Society of America*. In this classic synthesis on pluton emplacement, which utilized dominantly North America examples, Buddington (1959) outlined a classification based on depth: epizonal, mesozonal, and catazonal (Fig. 3A). Based on Buddington’s assignment of inferred range in depth of emplacement (Fig. 3B), these subdivisions were

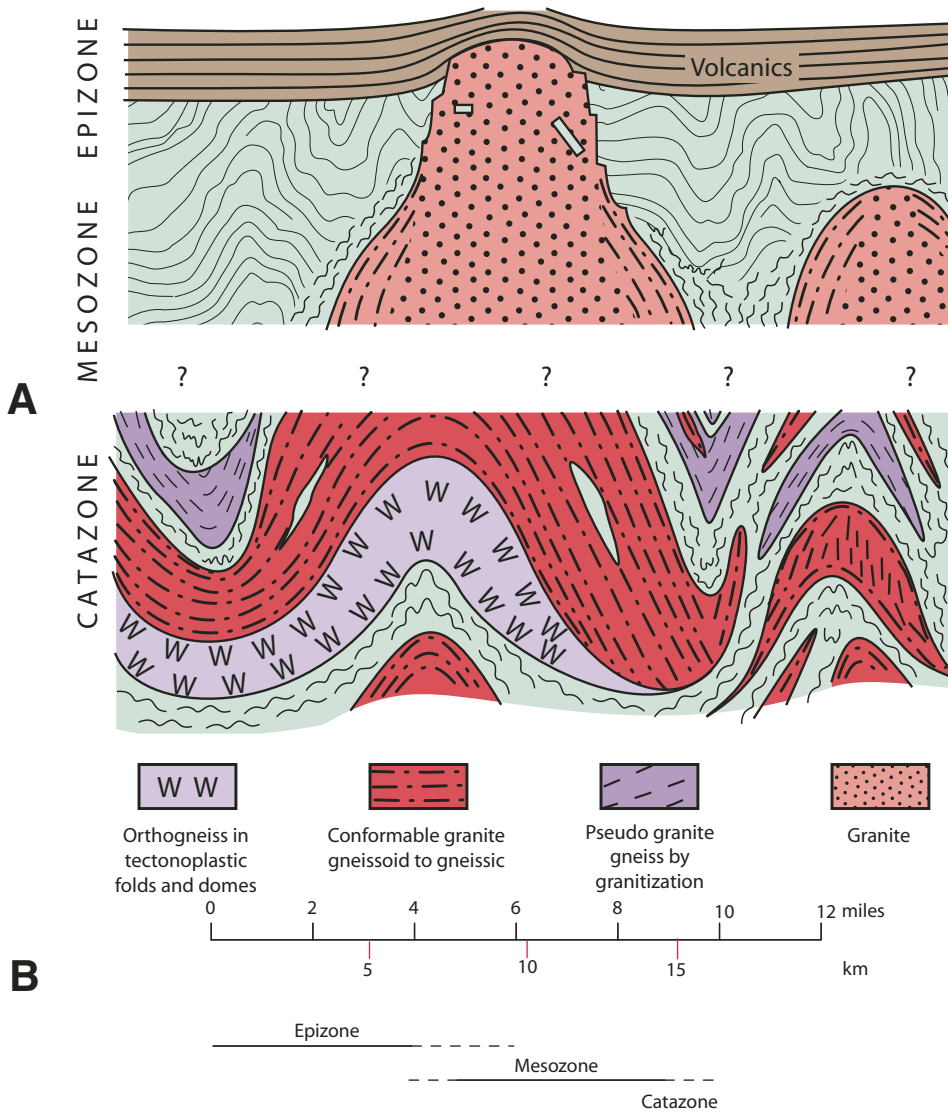


Figure 3. (A) Buddington's (1959) schematic sketch showing structural relationships of plutons in the epizone, mesozone, and catazone (his figure 19); (B) Buddington's (1959) schematic diagram illustrating the approximate depth of his three emplacement zones (his figure 1).

interpreted by many geologists as indicating upper, middle, and lower crustal levels. At the time that Buddington (1959) compiled his synthesis on pluton emplacement, there was little reliable geobarometric data available on the depth at which an exposed pluton was initially intruded into the Earth's crust. Thus, his depth assignments were chiefly based on field relationships; e.g., direct association with coeval volcanic rocks, structural discordance or concordance with the surrounding host rocks, evidence of brittle or plastic deformation during emplacement, intensity of fabric development in the pluton and adjacent host rocks, intensity and grade of metamorphism and migmatization in the host rocks, and other qualitative, field-based criteria. The distinctive characteristics of mesozonal plutons, which were somewhat vague in Buddington's (1959) model, include: no direct relationship with volcanic rocks; less intense metamorphism of the host rocks and little migmatization as compared to catazonal plutons; evidence of contact metamorphism that can be locally dynamothermal

in character; complex emplacement relationships with the surrounding host rocks that are both discordant and concordant; and widespread planar and linear fabrics in both the intrusive rocks and directly surrounding host rocks.

The depth-zone concept for pluton emplacement has survived in a general sense for the past 50 years (cf. Pitcher, 1979; Paterson et al., 1991, 1996; Cruden, 2006), although the boundaries between the different zones are blurred and relations between emplacement style and depth are complex. Buddington (1959) recognized the importance of multiple material transfer processes operating during emplacement, and that bulk composition, temperature, and volatiles characteristic of the intruded magma had a significant control on the rheology of both the pluton and host rocks. Thus, many important features associated with the intrusion of a pluton were not completely controlled by depth. Numerous subsequent workers have also demonstrated that multiple variables are important in determining emplacement style.

Several other emplacement processes have been widely proposed since Buddington's (1959) work. He did not view horizontal crustal extension as important at any level, whereas many subsequent workers have emphasized passive emplacement of magma into dilational sites in fault zones (e.g., Hutton, 1982, 1988). Floor sinking (Cruden, 1998; Wiebe and Collins, 1998) and return (downward) flow of host rock (Saleeby, 1990; Tobisch et al., 2000; Paterson and Farris, 2008) have also been emphasized in the recent literature.

Many regional case studies of plutons have further suggested that a variety of features commonly attributed to different depth zones occur at the same crustal level. Perhaps most notable is the research by Pitcher and Berger (1972) and subsequent work (e.g., Hutton, 1982; Paterson and Vernon, 1995; Stevenson et al., 2008) on the Caledonian granites of Donegal, Ireland. There, plutons intruded in close proximity to each other include: a ring-dike complex with inferred caldera collapse; a steeply sheeted granite, which has numerous host rock rafts and is marked by lateral wedging within a major shear zone; and an elliptical pluton, which has a ductilely strained aureole (Pitcher and Berger, 1972). Miller et al. (this volume) also concluded that the same material transfer processes operated at a wide range of crustal levels in the Cretaceous North Cascades (Washington) crustal section, but their relative importance varied in broad accord with Buddington's (1959) scheme.

Syntheses on the nature of batholiths and the variation in magmatic rock types and associated metamorphism in exposed crustal cross sections, which developed through significant arc magmatism, were provided by Hamilton and Myers (1967) and Hamilton (1981). They argued that batholiths are large, sheet-like bodies that had laterally spread out in the upper crust above gneissic host rocks that had flowed downward beneath rising plutons, and at a shallow level batholiths had crystallized beneath a cover of their own volcanic ejecta. According to Hamilton (1981), the lower crust is characterized by differentiated layered complexes consisting of abundant ultramafic and mafic cumulates, and locally anorthosite, and other magmatic rocks. Supracrustal rocks are metamorphosed to the granulite facies and much granitic melt has been extracted from these high-grade and now depleted rocks. The middle crust, according to Hamilton (1981, 1989) is chiefly migmatitic and varies from granulite facies in the deep part to amphibolite facies in the upper part. Granitic rocks in the middle crust crystallized from hydrated, peraluminous magmas that commonly form sheet-like, two-mica granitic plutons and abundant pegmatitic dikes and small bodies, which pervasively intrude the host rocks. In the upper crust, drier magmas rise and crystallize as batholiths above the mid-crustal migmatitic complexes and commonly erupt pyroclastically, forming voluminous ash-flow sheets and resulting in calderas at the Earth's surface.

Many of the issues raised by Hamilton remain contentious, such as the distribution of plutons in the crust (e.g., compare Collins and Sawyer, 1996, and Karlstrom and Williams, 2006, with Saleeby et al., 2008, and Miller et al., this volume), shapes of

plutons (e.g., compare Paterson et al., 1996, with Cruden, 2006), and relationships of plutons to large-volume ash flows (e.g., compare Lipman, 2007, with Glazner et al., 2004). Various aspects of these issues are also addressed in almost all of the articles in this volume.

WHY ARE CRUSTAL SECTIONS IMPORTANT?

Composition of Continental Crust and Its Petrogenesis

Continental crust is commonly subdivided into three layers consisting of upper, middle and lower crust in which P-wave velocities increase progressively with depth (Rudnick and Fountain, 1995). On the basis of seismic-reflection and refraction studies, Smithson (1978) argued that the continental crust is both laterally and vertically heterogeneous. He presented a generalized model (Smithson, 1978, his figure 3) consisting of three zones showing lateral and vertical heterogeneity: (1) an upper zone of supracrustal rocks and granitic intrusions, (2) a middle migmatite zone, and (3) a lower, more mafic (intermediate in bulk chemical composition) zone. Although a wide range of P-wave velocities are found in the middle crust (6.0–7.1 km s⁻¹), most middle-crustal P-wave velocities are in the range 6.5–6.8 km s⁻¹ (Holbrook et al., 1992). Lower-crustal P-wave velocities also exhibit a broad range (6.4–7.5 km s⁻¹), indicating much heterogeneity in composition, and consequently rock types, from place to place (Holbrook et al., 1992). However, P-wave velocities in the lower crust also exhibit a bimodal distribution beneath shields, platforms, passive margins, rifts, and volcanic plateaus in the ranges 6.7–6.8 km s⁻¹ and 7.2–7.5 km s⁻¹, suggesting that either mafic magmatic under- and/or intraplateauing or high-grade metamorphism and densification are responsible for the increase in P-wave velocity in the lower crust (Holbrook et al., 1992; Rudnick and Fountain, 1995).

Crustal sections provide samples of rocks at different crustal levels and constraints on likely *P-T* conditions, which enable the correlation of determined seismic-reflection velocities with laboratory measurements of seismic velocities of natural rocks (e.g., Fountain, 1976, 1986, 1989; Fountain and Salisbury, 1981; Christensen and Mooney, 1995; Rudnick and Fountain, 1995). Despite ever-increasing sophistication in data acquisition and processing, seismic-reflection studies continue to have significant problems in imaging complex compositional heterogeneities, particularly over small length scales, and in revealing steep structures. Crustal sections provide windows that enable evaluation of lateral and vertical variations in rock types and orientations of structures. For example, several classic crustal sections (e.g., Fiordland, New Zealand; Ivrea-Verbano zone, northern Italy and adjacent Switzerland; Kapuskasing, Canada) expose large regions of the lower crust. An alternative approach to evaluating middle- to deep-crustal heterogeneity, as emphasized by Williams et al. (this volume), is to study large tracts of isobarically equilibrated terranes (e.g., >20,000 km² for eastern Athabasca, Canada, high-pressure granulites), which consist of rocks

that were laterally contiguous at the same approximate depth and were commonly metamorphosed at the same pressure.

Arc magmatism is considered to be a fundamental process in the post-Archean (<2.5 Ga) growth of continental crust (Hamilton, 1981, 1989; Taylor and McLennan, 1985; Davidson, 1992; Rudnick and Gao, 2004), and many crustal cross sections represent ancient magmatic arcs. Magmatic arcs are either developed on oceanic lithosphere and subsequently sutured to a continent by an arc-continental margin collision (e.g., ongoing and future collision between Taiwan and continental margin of China) or constructed on continental crust (e.g., Andean arc). Other processes that can account for the growth of continental crust since 2.5 Ga are the accretion of oceanic plateaus along active continental margins (e.g., Kerr et al., 2000) and magmatic under- and/or intraplating in the lower crust (Bergantz, 1989; Fountain, 1989).

The bulk chemical composition of continental crust is overall that of an intermediate igneous rock with relatively high Mg# (Taylor and McLennan, 1985; Rudnick, 1995; Rudnick and Gao, 2004). Continental crust is enriched in incompatible elements, is depleted in niobium relative to lanthanum, and has a subchondritic Nb/Ta ratio (Rudnick and Gao, 2004). A conundrum is the intermediate bulk chemical composition, as compared to the abundance of mafic rocks in the deep crust as indicated by direct field observations (e.g., Ivrea-Verbano zone), seismic-reflection and refraction studies, and xenolith suites. Furthermore, if the chemically evolved continental crust forms a complementary geochemical reservoir to the Earth's depleted mantle, how is the intermediate bulk chemical composition explained when partial melting experiments of mantle peridotite produce mafic magmas such as basalts and picrites (Rudnick, 1995)? Delamination of dense continental lithosphere is a hypothesis that has been proposed to modify the bulk composition of continental crust in a variety of tectonic settings—*intra-oceanic island arc* (DeBari and Sleep, 1991; Greene et al., 2006), *continental magmatic arc* (Ducea and Saleeby, 1998b), and *collisional zone* (Platt and Visser, 1989; Molnar et al., 1993). Although the process of delamination may be important in modifying the bulk composition of continental crust, there are unquestionably other processes that must play a role in the development of the intermediate bulk composition of continental crust; e.g., mixing of primitive arc basalts with lower crustal melts (Kelemen et al., 2004, their figure 26).

The rocks of the lower crust (>25 km in depth) are commonly believed to consist chiefly of granulite-facies metamorphic rocks. An important characteristic of very high-grade granulite-facies terrains is the extreme depletion in large-ion lithophile elements relative to typical crustal rock types. This depletion is interpreted to represent upward removal during deep-crustal anatexis. High-pressure (10–15 kb), granulite-facies xenoliths are commonly cited as samples of the lower continental crust (Rudnick, 1992; Rudnick and Gao, 2004). Harley's (1989) survey of the *P–T* conditions of granulite-facies rocks indicated a broad range of conditions with over 50% of granulite-facies occurrences

characterized by *P–T* conditions outside of the commonly cited average granulite-facies regime of $\sim 8 \pm 1$ kb and 800 ± 50 °C (e.g., Bohlen, 1987; Bohlen and Mezger, 1989). Some granulite-facies terrains are characterized by very high-temperature conditions (900–1000 °C) and pressure conditions >10 kb. O'Brien and Rötzler (2003) argued that high-pressure granulites of non-xenolithic origin commonly represent rocks formed as a result of short-lived tectonic events that led to significant crustal thickening (e.g., collisional zones) or even subduction of crust into the mantle. High-pressure granulite-facies terrains also occur in the deep levels of magmatic arcs that have experienced crustal shortening and thickening synchronous with magmatism (e.g., Fiordland, New Zealand).

Another important aspect of granulite-facies rocks with regard to the composition of the lower crust is that there are significant compositional differences between granulite-facies xenoliths and exposed terrains (Rudnick, 1992). Granulite-facies xenoliths are dominated by mafic rock types, whereas granulite-facies terrains are dominated by evolved compositions and commonly include supracrustal rocks that, after deposition on the surface, were buried to reach granulite-facies metamorphic conditions. One explanation for these apparent contradictions is that the high-pressure xenoliths are derived from magmatically under- and/or intraplated material that underlies more felsic granulite-facies terrains (Wedepohl, 1995, see his figure 9). High seismic velocities (7.1–7.5 km/s) near the base of continental crust support this interpretation (Holbrook et al., 1992; Rudnick and Fountain, 1995); however, the lower crust clearly exhibits much heterogeneity from place to place and the presence of abundant garnet can dramatically increase the seismic velocity of rocks of more felsic bulk composition (e.g., "stronalites" of the Ivrea-Verbano crustal section—see Schmid and Wood, 1976; Schmid, 1978–1979). Regional-scale granulite-facies terrains, such as exposed in South India, are typically underlain by ≥ 30 km of crustal material, suggesting crustal thicknesses of >50 km before exhumation (e.g., Kaila et al., 1979). One model to explain such granulite-facies terrains is tectonic thickening by thrusting during continental collision (Newton, 1990). In contrast, Sandiford and Powell (1986) argued that granulite-facies metamorphism could occur in the deep crust during continental extension accommodated by a transient thermal perturbation. These authors cited the Basin and Range province of the western North American Cordillera as an actualistic example. In regions of large-magnitude crustal extension, where unusually high heat flow is expected because of asthenospheric upwelling and associated under- or intraplating mafic magmatism, temperatures required for granulite-facies metamorphism are reached at deep-crustal levels. If such a region is exhumed by younger, unrelated tectonic events, these high-grade metamorphic terrains could include broad tracts of isobaric, granulite-facies metamorphic rocks.

Magmatic under- and/or intraplating of continental crust by the intrusion of mantle-derived, mafic magmas has been commonly invoked to provide the heat for deep-crustal metamorphism and anatexis (Huppert and Sparks, 1988; Bergantz, 1989).

Under- and/or intraplate has been hypothesized as an important lower-crust process in various tectonic settings, ranging from continental magmatic arcs to rift zones (Bergantz, 1989). Fountain (1989) developed a detailed argument for the growth and modification of the lower continental crust during crustal extension with the extreme case characterized by high extension rates, large β values (stretching factor >2), and high asthenospheric temperatures. Fountain (1989) cited the Ivrea-Verbano zone as an exhumed example of deep continental crust that grew by under- and/or intraplate of mafic magmas and was extensively modified by granulite-facies metamorphism and anatexis during late Paleozoic intra-continental rifting (i.e., transtension—see Handy et al., 1999).

Interpretation of Seismic Anisotropy and Seismic Lamination

Subhorizontal seismic anisotropy and seismic lamination (densely packed, multiple sets of reflections) are recognized as important features of some seismic studies of the lower crust (e.g., Rabbel et al., 1998; Meissner et al., 2006). They are observed together in a number of locations where both seismic wide-angle measurements and teleseismic receiver functions have been utilized. Lower-crustal seismic lamination may result from intrusion of subhorizontal mafic sills that are commonly attributed to under-/intraplate of mantle-derived magmas (e.g., McCarthy and Thompson, 1988; Fountain, 1989; McCarthy and Parsons, 1994). Meissner et al. (2006) also propose that more irregularly shaped mafic intrusions are stretched into extensive, subhorizontal layers by strong ductile flow, thus contributing to the reflectivity. Major proposed causes of seismic anisotropy include: lattice-preferred orientation and shape-preferred orientation of minerals (micas, amphiboles) that define a penetrative subhorizontal foliation; alternating thin compositional layers; and aligned fluid- or gas-filled fractures (crack anisotropy; e.g., Peacock and Hudson, 1990). The latter is probably not important in the deepest crust.

In several studies, synthetic seismograms of exposed lower-crustal sections have been utilized to evaluate shear-wave anisotropy and seismic lamination. For example, Rabbel et al. (1998) compared the petrology and structure of lower-crustal xenoliths from a region of Variscan orogenesis in southwest Germany that is marked by anisotropic, laminated lower crust with synthetic seismograms constructed from profiles through the Ivrea-Verbano and Calabria (southern Italy) crustal sections. The xenolith suite is dominated by amphibolite- and granulite-facies metapelites metamorphosed at 500–730 °C and 4–7.3 kb that display anisotropy defined by lattice- and shape-preferred orientation of biotite and sillimanite. Rabbel et al. (1998) concluded that the shear-wave anisotropy and pattern of reflectivity are compatible with different compositional layers rich in metapelites analogous to Calabria and parts of the Ivrea-Verbano section (cf. Pohl et al., 1999; Weiss et al., 1999).

In their review, Meissner et al. (2006) noted that reflectivity patterns from ~15%–20% (globally) of seismic lines reveal

laminated lower crust, but fewer places have discernible crustal anisotropy. The relative scarcity of documented anisotropy may be an artifact of fewer wide-angle and receiver function experiments. In view of this difficulty in imaging the deep crust, crustal sections are a particularly fertile source for evaluating the importance of seismic anisotropy and mechanisms that form it.

Evidence of potential mechanisms for both seismic lamination and anisotropy is preserved in crustal sections and other exposures of deep crust. Gently dipping mafic magmatic sheets and plutons form the tabular, ~5–8-km-thick composite Mafic Complex in the lower crust of the Ivrea-Verbano section (e.g., Rivalenti et al., 1975, 1981, 1984; Quick et al., 1992, 1994; Peressini et al., 2007). Large regions of exhumed Precambrian lower crust in the eastern Athabasca region (Saskatchewan) contain m- to km-thick mafic granulite sills (Baldwin et al., 2006; Williams et al., this volume) that are interlayered with felsic granulites. The mafic rocks in both the Ivrea-Verbano zone and eastern Athabasca probably represent crystallized intraplate and/or underplate mafic magma, and thus are examples of deep crust that would probably record seismic lamination. Hydration of the Athabaskan granulites during exhumation, which formed micas, is a likely mechanism for the generation of mid-crustal seismic anisotropy according to Mahan (2006).

Subhorizontal transposition fabrics are common in exposures of deep continental crust (cf. Williams and Jiang, 2005). Examples include several sections described in this volume: Arunta inlier (Waters-Torney et al.), eastern Athabasca (Williams et al.), Fiordland (Klepeis and King), and North Cascades (Miller et al.). Underthrust beneath several Mesozoic Cordilleran arcs are biotite paragneisses and graphitic, white-mica schists that were metamorphosed to pressures of up to 12 kb and possess strong, flat-lying foliation and lineation, which are commonly associated with pervasive non-coaxial shear. These arc sections include the North Cascades (Paterson et al., 2004; Miller et al., 2006), southern Sierra Nevada batholith (e.g., Saleeby, 2003) and its offset equivalents of the Salinian block (Kidder et al., 2003) and eastern Transverse Ranges (Needy et al., this volume), and the Klamath Mountains (Helper, 1986; Garlick et al., this volume).

Another implication of middle- to deep-crustal exposures for seismic-reflection studies is emphasized by Williams et al. (this volume). They document extensive early subhorizontal fabrics that are overprinted by domains of steep structures. Gently dipping structures would be preferentially observed in seismic-reflection profiles, whereas steep domains may only be recorded by zones of weak reflections, if at all. Williams et al. (this volume) also suggest that the steep zones may represent the velocity transitions in teleseismic images between seismically fast and slow domains (e.g., Levander et al., 1994).

Seismic anisotropy in the upper mantle is more difficult to evaluate in crustal sections, as most sections terminate in the lower crust. One Cordilleran section where upper-mantle seismic anisotropy has been inferred is in the Jurassic Talkeetna island-arc assemblage (Burns, 1985; DeBari and Coleman, 1989; Greene et al., 2006; Farris, this volume). Mehl et al. (2003) documented

ultramafic mantle tectonites and overlying cumulates flow on horizontal foliation planes induced by slip in olivine on (001)[100]. This slip resulted in alignment of olivine [100] axes parallel to the arc, and may provide perhaps the first direct field evidence for arc-parallel flow, which could produce the arc-parallel anisotropy observed in the mantle of several modern arcs (e.g., Wiens and Smith, 2003).

One speculative implication from crustal sections is that seismic anisotropy, and potentially lamination, are common in a wide variety of tectonic settings. To date, seismic lamination is mainly recognized in extensional orogens, such as the Basin and Range province, but is also displayed in the thick, hot crust of a few collisional orogens (Alps, Tibet; Meissner et al., 2006). We predict that such lamination is common in young orogens with elevated geothermal gradients.

Lithospheric Rheological Modeling

For many years, the dominant view of lithospheric rheology has been the “jelly-sandwich model,” which postulates that a strong upper crust overlies a weak lower crust and strong uppermost mantle (e.g., Ranalli, 1995; Watts and Burov, 2003). In this model, a considerable component of the total strength is in the lithospheric mantle except when a very high geothermal gradient results in both weak lower crust and uppermost mantle. This model has been challenged by several workers (e.g., Maggi et al., 2000; Jackson, 2002) who suggest that much of the lithospheric strength is in the upper seismogenic crust, and that lower-crustal strength may exceed that of the upper mantle. These models are largely based on geophysical observations, such as earthquake distributions (seismogenic thicknesses), elastic thicknesses, and numerical modeling.

These models address the large features of the lithosphere, but are far too simplistic for orogenic belts. They commonly assume relatively lithologically homogeneous crustal layers (e.g., mafic lower crust versus felsic middle crust) and uniform flow laws for different layers. Lithospheric mantle strength is strongly controlled by geothermal gradient, and many numerical models assume that advective heat transfer is minimal and a steady-state gradient dominates. For example, the sophisticated models of Afonso and Ranalli (2004) assume that the latest tectonothermal event occurred ≥ 100 Ma before the modeled strength profile. Such models, which assume a steady-state geotherm, may not be particularly relevant to active orogens, such as the Cordillera and elsewhere where the rise of mantle-derived magmas is an important process.

Numerous field-based studies have focused on the degree of coupling between different layers of continental crust (e.g., Oldow et al., 1990; Grocott et al., 2004). Many of these studies have considered that regional-scale, subhorizontal shear zones act as detachments, separating rocks that record very different strain histories (e.g., classic concept of thin-skinned tectonics). An extreme case of decoupling is advanced in the channel-flow hypothesis (e.g., Hodges, 2000; Beaumont et al.,

2001; Grujic et al., 2002; Godin et al., 2006; Law et al., 2006) in which gently dipping shear zones separate a layer of weak, low-viscosity crust from relatively rigid, higher-viscosity rocks above and below the channel. Other researchers argue for kinematic compatibility between structures at different crustal levels that responded differently to the regional stress field (e.g., Teysier and Tikoff, 1998). Still other workers conclude that continental crust in active orogens is likely characterized at all scales by heterogeneous vertical partitioning of deformation and complex rheological stratification (e.g., Axen et al., 1998).

Studies of crustal sections reported in this volume and elsewhere have focused on crustal rheology. One theme of such studies is the importance of lithological heterogeneities in controlling rheology at different crustal levels. For example, our summary below of crustal cross sections indicates that all crustal levels of some sections contain quartz-rich rock types, including metasedimentary rocks, and simple consideration of mafic lower crust and felsic middle and upper crust is questionable and leads to overly simplistic rheological models. Similarly, Miller and Paterson (2001) documented the importance of relatively small lithological differences and related mechanical anisotropy for markedly heterogeneous deformation and rheology at paleodepths ranging from <10 km to ~ 40 km in the Cretaceous North Cascades magmatic arc. They concluded that in the ductilely deformed part of this crustal section there was an overall decrease in strength with depth, but that in detail there was marked variation in relative strengths of rocks (also see Karlstrom and Williams, 1998).

Field (e.g., Hollister and Crawford, 1986; Davidson et al., 1992; Brown and Rushmer, 1997) and laboratory studies (e.g., Dell’Angelo and Tullis, 1988; Rutter and Neumann, 1995; Rutter, 1997; Grujic and Mancktelow, 1998) indicate that one of the most important variables for crustal rheology and architecture is magmatism. It has long been recognized that magmatism weakens crust and thus may localize strain (e.g., Hollister and Crawford, 1986; cf. Crawford et al., this volume). Moreover, upon cooling below the solidus, plutons are typically stronger than their host rocks, and strain is commonly concentrated in the latter rocks (e.g., Miller and Paterson, 2001). Complex relationships between magmatism and crustal rheology are well illustrated by crustal sections, including sections discussed in this volume (e.g., Coast Mountains, Cordilleran metamorphic core complexes, Fiordland, North Cascades).

In eastern Athabasca, intrusion, heating, and migmatization of deep-crustal rocks led to major weakening and crustal flow (Williams et al., this volume). In contrast, dehydration from melt removal and cooling may lead to strengthening of the lower crust (e.g., Klepeis et al., 2003). This is well illustrated in Fiordland where the mafic to intermediate composition of lower arc crust and mineral reactions controlling melt production strongly influenced melt transfer and mechanical behavior of the lithosphere (Klepeis et al., 2003, 2004, 2007; Klepeis and King, this volume). In this arc, evolving lithospheric strength profiles during magmatism and convergence led to transient periods of vertical coupling and decoupling of crustal layers (e.g., Klepeis et al.,

2003). During periods of advection of heat by magmatism, the lower crust was weakened and decoupled from the middle and upper crust, whereas cooling following melt loss led to strengthening of the lower crust and coupling with higher levels of the crust. During coupling, a ~25-km-thick zone of interconnected deep-crustal shear zones and a mid-crustal fold-and-thrust belt developed (Klepeis et al., 2004).

The role of partial melting in leading to dramatic weakening of rocks during deformation has received much emphasis in the last decade. The mid- to deep crust (~20–40 km) of active orogens may contain significant amounts of partially melted crust (e.g., Nelson et al., 1996; Schilling and Partzsch, 2001), and the presence of regional-scale migmatite and orthogneiss complexes in ancient orogens suggests that this is a characteristic of thickened crust. This crust may flow laterally in response to lateral pressure gradients (e.g., Bird, 1991; Hodges and Walker, 1992; Royden, 1996; Clark and Royden, 2000), including those created by erosion at the orogenic front (Beaumont et al., 2001). Depending on the balance between buoyancy and lateral forces, partially molten crust may also flow vertically, creating domal structures that may be coupled with the driving forces for exhumation of the deep crust (Teyssier and Whitney, 2002).

The type example of regional-scale crustal flow of a melt-rich zone in a contractional setting is the hypothesized mid-crustal channel resulting from continental collision in the Himalayan-Tibetan orogen (e.g., Beaumont et al., 2001; Grujic et al., 2002; Godin et al., 2006). In this model, Himalayan crystalline rocks are ductilely extruded upward to the surface in a channel bounded above by the extensional South Tibetan detachment and below by the Main Central thrust (e.g., Burchfiel and Royden, 1985; Hodges et al., 1992a), and hot, thick middle crust beneath southern Tibet flows laterally, leading to the growth of the Tibetan Plateau (e.g., Clark and Royden, 2000). The channel flow model has been applied to the metamorphic hinterlands of other orogens (e.g., Appalachians—Hatcher and Merschat, 2006; Grenville—Jamieson et al., 2004; Canadian Cordillera—Brown and Gibson, 2006). Mid-crustal flow of migmatitic infrastructure in response to large-magnitude upper-crustal extension is also well-displayed by attenuated crustal sections in the hinterland to the Cordilleran fold-and-thrust belt. An example is the Ruby-East Humboldt metamorphic core complex in northeastern Nevada, where MacCready et al. (1997, see their figure 13) hypothesized inward flow and north-south channelization of the migmatitic infrastructure below a west-northwest-rooted, km-scale-thick, normal-sense, mylonitic shear zone. In the Shuswap metamorphic core complex of the southern Canadian Cordillera, Teyssier et al. (2005) proposed that following crustal thickening, partially molten crust flowed in a mid-crustal channel toward the foreland, and during a second stage of “free boundary collapse,” a rolling-hinge detachment developed that was accompanied by both lateral and vertical flow. The upward vertical flow of the partially molten crust is envisioned to have led to formation of migmatite domes (see Teyssier et al., 2005, their figure 12). The applicability of the channel-flow model remains contentious, in

part because it is probably rare that both the roof and floor of any channel are preserved in an orogen. Crustal cross sections clearly are amongst the best sites for direct field evaluation of this model.

Fault- and Shear-Zone Models

Many conceptual crustal-scale fault- and shear-zone models employ a narrow, discrete fault zone in the upper 10–15 km of the crust, which formed in the frictional regime; with increasing depth this chiefly brittle fault zone widens downward into a broader zone of non-coaxial shear-strain in the crystal-plastic regime (e.g., Sibson, 1977; Scholz, 1990). This widening is largely attributed to the decrease in the strength contrast between shear-zone rocks and adjacent rocks. Fault-zone structure is relatively well known in the shallow crust on the basis of numerous field studies, patterns of seismicity, experiments on rock mechanics, etc. (cf. Scholz, 1990, for review). There is also extensive literature on ductile shear zones. The architecture and deformation patterns of faults and shear zones traversing the brittle-to-plastic transition into the deep crust, however, are less certain and are the focus of some studies of crustal sections (e.g., Klepeis and King, this volume; Waters-Tormey et al., this volume).

The style of extensional fault systems at deep-crustal levels has been controversial, as illustrated by widely varying models for the origin of detachment faults and the deep-crustal features of metamorphic core complexes. In particular, some models of mid- to lower-crustal extension predict crustal thinning by pure shear, either by homogeneous strain or by many anastomosing shear zones (e.g., Miller et al., 1983; Hamilton, 1987; Jackson and White, 1989), or by simple shear marked by crustal- to lithospheric-scale shear zones (e.g., Wernicke, 1981). These models are difficult to evaluate because extensional fault systems in the deep crust are rarely exhumed without major disruption. Some crustal sections, however, provide excellent views of lower-crustal extension, as illustrated in the paper by Waters-Tormey et al. (this volume) on the Proterozoic Arunta inlier of central Australia. These authors documented localization of penetrative strain under granulite-facies conditions into km-scale shear zones, which are wider than typical shear zones at shallower levels. This focusing of extensional strain into discrete, high-temperature (granulite facies), moderately dipping shear zones is compatible with simple-shear models of extension (Waters-Tormey et al., this volume).

The Fiordland crustal section provides another view of deep-crustal extensional processes (see below). There, the deep (~25 km), gently dipping Doubtful Sound shear zone in the southern part of the section separates lower-crustal orthogneisses, recording penetrative extensional flow from mid-crustal orthogneisses and meta-supracrustal rocks (Oliver, 1980; Gibson, 1990). The detailed vorticity studies of Klepeis and King (this volume) demonstrate that extension was marked by vertical thinning, subhorizontal stretching, and 40%–50% pure shear. At shallower levels (15–20 km) in the northern part of the Fiordland

section, detachment faults separate weakly metamorphosed rocks from higher-grade, ductilely deformed rocks and thus display relationships more typical of Cordilleran metamorphic core complexes (Tulloch and Kimbrough, 1989). In the North Cascades crustal section, a subhorizontal extensional shear zone somewhat analogous to the Doubtful Sound shear zone separates rocks metamorphosed at 11–12 kb from only slightly lower-pressure rocks in the hanging wall (Paterson et al., 2004).

Changes in the properties of thrust faults and processes operating during contraction between the external and internal zones of orogenic belts have been an important focus of research in structural geology and tectonics for more than 100 years. We do not attempt to summarize the voluminous research on this topic, but note that as expected, the deeper levels of thrust systems are less well understood. The mid- to lower-crustal parts of crustal sections are ideal settings in which to evaluate these systems. For example, deeply exhumed attenuated sections in the hinterland of the Cordilleran fold-and-thrust system variably preserve the record of contraction at syn-orogenic depths reaching ~30 km. Perhaps the most noteworthy example in the Cordillera is the exposure of the internal zone in the Omineca belt of southern British Columbia. In the deepest levels (20–30 km) of core-complex gneiss domes (Monashee complex, Valhalla complex), many researchers have proposed that ductile decoupling zones (Monashee décollement, Gwillim Creek shear zone) transport upper-amphibolite-facies migmatitic schists and gneisses northeastward over cooler and less deformed Precambrian basement rocks (e.g., Read and Brown, 1981; Brown et al., 1986, 1992; Carr et al., 1987; Parrish, 1995; Carr and Simony, 2006). Displacement was synchronous with high-grade metamorphism and partial melting, intense folding, transposition, and pervasive top-to-the-east non-coaxial shear in the hanging wall (cf. Brown and Gibson, 2006). The basal ductile shear zone(s) are inferred to continue to the east in the transport direction into the basal décollement of the fold-and-thrust belt (Brown et al., 1986, 1992; Cook et al., 1992; Parrish, 1995; Carr and Simony, 2006). Brown and Gibson (2006) suggested that the high-grade rocks above the Monashee décollement formed a 10–20-km-thick layer of hot, weak rocks that represent an orogenic channel. In a somewhat different view, Carr and Simony (2006) conclude that the Valhalla complex forms a ~30-km thick, coherent thrust sheet above the basal décollement. Some aspects of these interpretations have been challenged by Williams and Jiang (2005), as they argued that there are no major discontinuities within the Omineca core complexes and that these rocks are involved in a crustal-scale, northeast-vergent shear zone marked by gently dipping transposition foliation, pervasive non-coaxial deformation, and regional-scale recumbent folds. These insights from the attenuated crustal sections of the Omineca belt may be applicable to the deep crust of the Cordilleran fold-and-thrust belt farther south in the hinterland of the Sevier orogenic belt. For example, in the Ruby-East Humboldt core complex large-scale fold-nappes exposed at the deepest levels (Howard, 1966, 1980, 1987, 2000; Lush et al., 1988) fold earlier low-angle

faults (contractional?) and in one case involved remobilized Precambrian basement rocks (Lush et al., 1988). One interpretation is that these hinterland structures expose the roots of the Sevier fold-and-thrust belt (Miller and Gans, 1989; McGrew, 1992; Snoke, 2005).

The majority of studies of thrust belts focus on the geometries and kinematics of contractional structures involving miogeoclinal and peri-cratonic strata, and thinned continental basement such as described in the hinterland of the Cordilleran fold-and-thrust belt. In contrast, crustal sections in the western Cordillera are illustrative of structures developed in the mid- to deep levels of accretionary belts involving arc rocks, ophiolites, and basinal sedimentary rocks. These relationships are illustrated in the Klamath Mountains (cf. Garlick et al., this volume) where various components of oceanic suprasubduction complexes are imbricated into a large-scale thrust stack that progressively evolved from east-to-west (i.e., oceanward) (Snoke and Barnes, 2006). Thick-skinned thrusting involving crustal depths reaching >30 km is well documented in the southwest-directed Coast belt thrust system of the northwest Cordillera where thrusts juxtapose rocks from markedly different crustal levels and map-scale recumbent folds formed in individual thrust sheets (cf. Rubin et al., 1990; Crawford et al., this volume). Crustal loading is recorded by increases in metamorphic pressures ranging from ~2.5 kb in the central Coast belt (Stowell and Crawford, 2000; Himmelberg et al., 2004; Crawford et al., this volume) to as much as 6 kb in the southern part of the belt (e.g., Evans and Berti, 1986; Brown and Walker, 1993; Whitney et al., 1999). Thick-skinned tectonic wedging in the hinterland is also demonstrated in the south (Journey and Friedman, 1993; Varsek et al., 1993).

Complex vertical variations in fault-zone architecture in contractional and transpressional systems are illustrated by other deep-crustal exposures described in this volume. In Fiordland, a network of linked steep and subhorizontal structures dominates the middle- to lower crust (Klepeis et al., 2003; Klepeis and King, this volume). Mid- and lower-crustal isobaric sections in Saskatchewan and the southwest United States also possess an architecture defined by domains of flat and steep shear zones (Karlstrom and Williams, 2006; Williams et al., this volume).

There is considerable discussion on the depths to which major strike-slip faults extend in the lithosphere. Some of these structures, such as the San Andreas fault, penetrate the entire lithosphere, whereas it is envisioned that other strike-slip faults terminate at mid-crustal detachments (cf. Lemiszki and Brown, 1988; Sylvester, 1988; Vauchez and Tommasi, 2003; Legg et al., 2004). Uncertainties about the deep-crustal fault-zone structure in part reflect the difficulties in seismically imaging steep structures. Most well-studied examples of deep-crustal strike-slip shear zones are from exposures of Precambrian cratons where the transition to shallower crustal levels is generally not preserved. Excellent examples include the Paleoproterozoic Great Slave Lake shear zone of the northwestern Canadian shield, which is an intra-continental transform shear zone marked by

early granulite-facies mylonites (Hoffman, 1987; Hanmer, 1988; Hanmer et al., 1992), and the Neoproterozoic Mozambique belt of Madagascar, which records deformation at 5–11 kb and temperatures of >750 °C (Pili et al., 1997; Martelat et al., 2000).

Crustal cross sections are obvious targets to evaluate the architecture of transcurrent fault zones, but few classic crustal sections are transected by strike-slip faults. Furthermore, the intersection of major strike-slip zones and detachments has not been well documented in these sections. Some sections are cut by mid-crustal strike-slip shear zones, such as in the Sierra Nevada (e.g., Sierra Crest shear system and proto-Kern Canyon fault zone; Tikoff and Greene, 1997; Nadin and Saleeby, 2008), North Cascades (Ross Lake fault zone; Miller, 1994), and perhaps the central Coast Mountains (Coast shear zone; Hollister and Andronicos, 1997; although see Crawford et al., this volume, for a different interpretation), but documented fault-zone paleodepths do not exceed 20 km. These observations may reflect the statistical likelihood that relatively few major strike-slip faults should be observed given the vertical orientations of both strike-slip faults and crustal sections. Alternatively, perhaps the lack of major crustal thickening associated with strike-slip systems does not lead to sufficient exhumation by vertical motion and erosion, and/or subsequent extensional collapse.

OROGENIC PROCESSES AS MANIFESTED IN PHANEROZOIC CRUSTAL CROSS SECTIONS

Introduction

Previous summaries (e.g., Fountain and Salisbury, 1981; Percival et al., 1992) have reviewed the features of a large number of variably preserved crustal sections and exposures of lower crust, many of which are part of Precambrian cratons. In this article, we emphasize a restricted number of classic crustal sections for which there has been much new work since the synthesis of Percival et al. (1992). These sections are arguably broadly representative of the diversity of the middle to lower crust. Our examples are from Phanerozoic orogens and represent different tectonic settings, including continental arcs, island arcs, and metamorphic core complexes and other attenuated terranes. These examples are complemented by the accompanying papers in this volume.

The set of crustal cross sections that we summarize in this article illustrate some of the important processes related to continental crustal growth and development in post-Precambrian time. These processes include: magmatic intra/underplating, accretion of an oceanic-arc to a continental margin, the transition from oceanic-arc crust to continental crust, the fate of accretionary complexes in orogenic collages, and the exhumation of deep-crustal rocks via upper-crustal extension and synchronous subduction underplating (Platt, 1986). A geodynamic process that plays a significant role in the development of some continental crustal sections is delamination of dense continental lithosphere (Houseman et al., 1981).

Ivrea-Verbano Zone, Southern Alps, Northern Italy and Southern Switzerland

The Ivrea-Verbano zone is part of a basement high within the Southern Alps of the Cretaceous–Tertiary Alpine orogenic belt. The ~100-km-long and 5- to 15-km-wide Ivrea-Verbano zone and adjacent lithotectonic units to the east and southeast (Strona-Ceneri [Serie dei Laghi—see Boriani et al., 1990b] and Val Colla zones) are commonly interpreted as a steeply upturned section through continental crust of the Southern Alps—part of the Adriatic micro-plate or indenter or Greater Apulian plate (Mehnert, 1975; Fountain, 1976; Fountain and Salisbury, 1981; Zingg et al., 1990; Rutter et al., 1993, 2007; Schmid, 1993; Schmid et al., 2004) (Fig. 4). Metamorphic grade increases across the Ivrea-Verbano zone from upper amphibolite facies in the southeast to granulite facies in the northwest (Zingg, 1980, 1983, 1990; Demarchi et al., 1998). The Ivrea-Verbano zone is juxtaposed against rock units of the Austroalpine domain along the Insubric line, a fundamental tectonic boundary in the Alps (Gansser, 1968) (Fig. 4A). The eastern boundary of the Ivrea-Verbano zone is the late Paleozoic Cossato-Mergozzo-Brissago line (Boriani et al., 1990a), which is locally overprinted by the early Mesozoic Pogallo line or shear zone (Handy, 1987; Handy et al., 1999). One interpretation is that these eastern tectonic boundaries were originally low-angle shear zones that accommodated crustal extension in the late Paleozoic (Hodges and Fountain, 1984) and early Mesozoic (Handy, 1987; Handy et al., 1999), respectively. Consequently, these inferred extensional shear zones may have excised thick slices (10–20 km in scale) of middle and lower crust prior to the upending of the Southern Alps section during the Alpine orogeny (Fig. 4).

Various geophysical studies indicate that high velocity and dense rocks (upper mantle rocks?) occur at a very shallow level in this part of the Southern Alps (see Zingg, 1990, and Percival et al., 1992, for key references that discuss these studies). A discontinuous chain of tectonic peridotite massifs (Shervais, 1979; Boudier et al., 1984; Shervais and Mukasa, 1991) forms the basal zone of the Ivrea-Verbano zone subparallel to its western and northern tectonic boundary (i.e., Insubric line, Fig. 4A). The Insubric line and other tectonic lineaments define the regionally extensive Periadriatic line, traditionally considered to mark the northern boundary of the Southern Alps (Schmid et al., 1989).

An important phase of the geologic history of the Ivrea-Verbano zone is late Paleozoic magmatism that post-dated an earlier history of contraction related to the Variscan orogeny. Handy and Zingg (1991) argued that the magmatism was synchronous with transtension (see their figure 11a) and the formation of elongated basins in the upper crust of the Southern Alps. These authors also suggested that the sinistral transtensional faults and basins of the Southern Alps may have been the conjugate to large-scale dextral strike-slip faults associated with a broad zone of shear between the American-European plate and African plate during Carboniferous to Permian time (e.g., Arthaud and Matte, 1977). In the southern Ivrea-Verbano zone, this magmatism is manifested by emplacement of the composite,

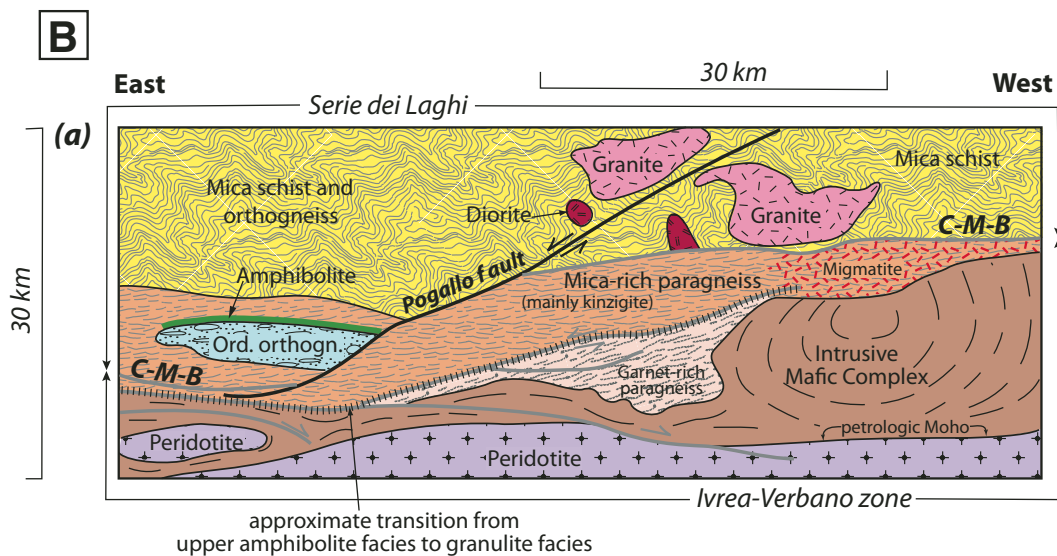
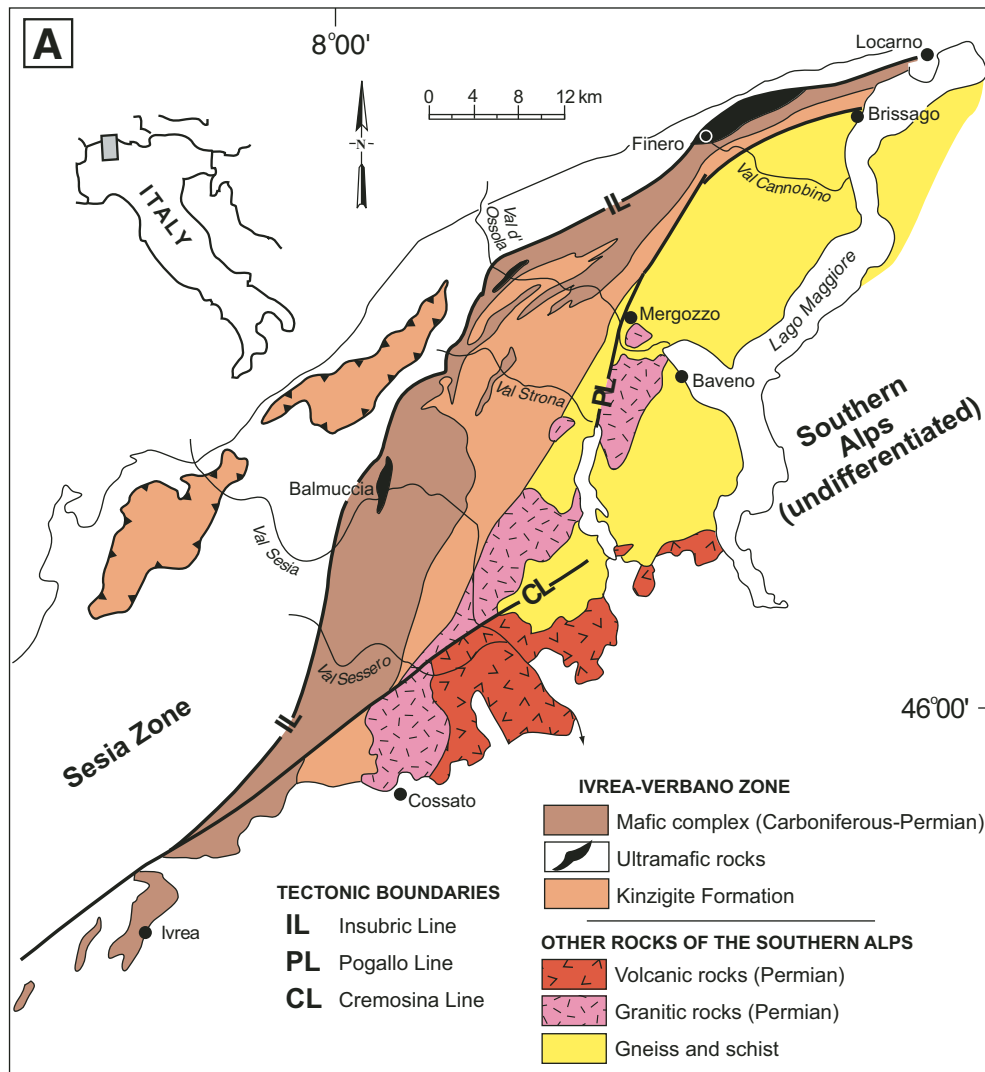


Figure 4. (A) Generalized geologic map of the Ivrea-Verbano zone and environs, northern Italy. Modified from Zingg et al. (1990) and Snoke et al. (1999). (B) Restored (Triassic time) partial crustal section through the Massiccio dei Laghi, Southern Alps, northwest Italy (after Khazanehdari et al., 2000, their figure 8a). The upper part of the section (i.e., the Serie dei Laghi) consists of middle-crustal rocks and is separated from the lower-crustal part of the section (i.e., the Ivrea-Verbano zone) by the Cossato-Mergozzo-Brissago (C-M-B) line. The C-M-B line was subsequently overprinted by the Pogallo fault.

~8-km-thick, under/intruded Late Carboniferous to Early Permian (Pin, 1986; Quick et al., 2003; Peressini et al., 2007) Mafic Complex (Fig. 4) that was subsequently tilted to subvertical (Rivalenti et al., 1981, 1984; Quick et al., 1992, 1994). An igneous contact between spinel lherzolite tectonite and overlying cumulus rocks, representing the petrologic Moho, is exposed along the eastern margin of the Balmuccia peridotite (Shervais, 1979; Rivalenti et al., 1981; Shervais and Mukasa, 1991; Quick et al., 1995, 2003). Although primary magmatic layering is commonly preserved in the Mafic Complex, many of these igneous rocks have also experienced synmagmatic deformation (Rivalenti et al., 1981; Quick et al., 1992, 1994) characterized by penetrative foliation and lineation, isoclinal folds, boudinage, and solid-state shear zones.

The Ivrea-Verbano zone is considered an important template with which to compare deep-crustal, seismic-reflection data (Hollinger and Levander, 1994; Rutter et al., 1999; Khazanehdari et al., 2000), and in understanding lower-crustal magmatic processes (Fountain, 1989; Quick et al., 1994; Henk et al., 1997) and rheological properties (Handy and Zingg, 1991; Rutter and Brodie, 1992). However, there are several controversial or poorly understood aspects of the tectonic setting and petrologic history of the Ivrea-Verbano zone. For example, all that can be said with certainty about the protolith age of the metasedimentary and meta-igneous rocks of the zone is that this age must be younger than the Proterozoic detrital components (<2500–600 Ma) contained in these rocks (Köppel, 1974; Gebauer, 1993). Many workers infer a Neoproterozoic or Early Paleozoic age for the sedimentary and igneous protoliths (e.g., Hunziker and Zingg, 1980). However, Vavra et al. (1996) demonstrated the presence of a magmatic zircon population that yielded an age of 355 ± 6 Ma through ion microprobe (SHRIMP) analyses. These zircon grains occur in an orthopyroxene-bearing quartzo-feldspathic granulite interpreted as a possible volcanic or volcanoclastic rock on the basis of morphology and chemistry of the grains. Thus, at least parts of the Ivrea-Verbano zone were in a supracrustal setting near a volcanic center during the Devonian–Lower Carboniferous time. One commonly cited tectonic setting for the metasedimentary and meta-igneous rocks of the zone is an accretionary complex (Sills and Tarney, 1984). The presence of ultramafic rocks within the Kinzigite Formation, a lithotectonic unit commonly employed to refer to the interlayered metasedimentary and meta-igneous rocks of the Ivrea-Verbano zone (i.e., host rocks for the Mafic Complex), and lack of any known basement for this formation supports such an original setting (Quick et al., 1995). Geochemical data from amphibolites of the zone likewise support such a model in that they are characterized by MORB isotopic and trace-element abundances (Sills and Tarney, 1984; Mazzucchelli and Siena, 1986).

Barboza et al. (1999) and Barboza and Bergantz (2000) have questioned the relationship between emplacement of the upper Mafic Complex and development of regional, prograde metamorphism and anatexis in the Ivrea-Verbano zone. These authors argued that the upper parts of the Mafic Complex were emplaced

during late Paleozoic crustal extension; and consequently, metamorphism and anatexis associated with this magmatism was a spatially restricted, decompression-melting event that overprinted the regional prograde metamorphic zonation. Thus, the Ivrea-Verbano zone may not reflect a causal relationship between emplacement of mantle-derived magma (magmatic underplating) and regional granulite-facies metamorphism and anatexis as previously considered by many workers (e.g., Schmid and Wood, 1976; Sills, 1984; Rutter et al., 1993; Schnetger, 1994; Henk et al., 1997).

Boriani and coworkers (e.g., Boriani et al., 1990a, 1990b; Boriani et al., 1992) have questioned the concept that the Serie dei Laghi experienced significant rotation since the emplacement of Early Permian granitic plutons (e.g., Mottarone–Baveno pluton) that intrude much of the zone—thus precluding a continuous continental cross section from the Ivrea-Verbano zone into the Serie dei Laghi. Handy and Zingg (1991), Schmid (1993), and Handy et al. (1999) have underscored the significance of the polyphase, long-lived history of the Ivrea-Verbano zone involving multiple pre-Alpine deformational phases and metamorphic events (also see Boriani and Villa, 1997). Certainly, the structural and low-grade metamorphic overprint of the mid-Tertiary Alpine orogeny is an additional important complication in deciphering the geologic history of the Ivrea-Verbano zone (Schmid et al., 1987; Zingg et al., 1990; Rutter et al., 1993; Schmid, 1993; Colombo and Tunesi, 1999).

Vavra and coworkers (Vavra et al., 1996, 1999; Vavra and Schaltegger, 1999) have reported an extensive set of U-Pb, zircon ion microprobe (SHRIMP) analyses from the Ivrea-Verbano zone. Vavra et al. (1996) concluded that the oldest zircon overgrowths formed during anatectic melt formation in a metapelitic rock at 296 ± 12 Ma. Vavra et al. (1999) and Vavra and Schaltegger (1999) also demonstrated a complex series of fluid-driven events that disturbed the U-Th-Pb systematics of both zircon and monazite in Ivrea-Verbano zone samples. These events are postulated to be related to post-Variscan regional tectonic events including: (1) late Paleozoic transtension, mafic magmatism, and exhumation, and (2) Late Triassic to Early Jurassic rifting and associated hydrothermal activity and alkaline magmatism.

The timing and mechanisms of uplift of the Ivrea-Verbano zone are also controversial (e.g., compare Zingg et al., 1990 with Boriani et al., 1990a), although an Alpine age is commonly assumed (Schmid et al., 1987; Rutter et al., 1993; Schmid, 1993). The Insubric line is a complex network of Alpine-age faults and associated fault rocks of variable affinity and protolith (Schmid et al., 1987; Zingg and Hunziker, 1990). The final uplift and rotation to subvertical of the Ivrea-Verbano zone occurred during transpressional deformation and lithospheric wedging related to the Alpine orogeny (Schmid et al., 1987, 1989; Schmid, 1993; Handy et al., 1999).

One conclusion that clearly emerges from the many studies of the Ivrea-Verbano zone is that this lithotectonic zone is composed of elements of variable age and that their structural evolution is polyphase and variable across the zone (Handy et al.,

1999). Thus, to view the Ivrea-Verbano zone as a “typical example of deep crust” disregards its obvious complex, polygenetic evolution (Rutter et al., 2007).

Kohistan Arc (Complex), Northwest Pakistan

In northwest Pakistan, the Indian and Asian plates, which to the east are juxtaposed across the Indus-Tsangpo suture zone,

are separated by a heterogeneous assemblage of arc-related rocks broadly referred to as the Kohistan complex (Fig. 5) of the Kohistan-Ladakh terrane. In the mid-Cretaceous, the Kohistan complex was in an intra-oceanic arc setting; however, the polarity of the related subduction system is still controversial (Searle et al., 1999). One model suggests a northward-facing arc with a southward-dipping subduction zone that collided with the Asian plate (= Karakoram terrane) along the Northern or Shyok

Kohistan complex, northwest Pakistan

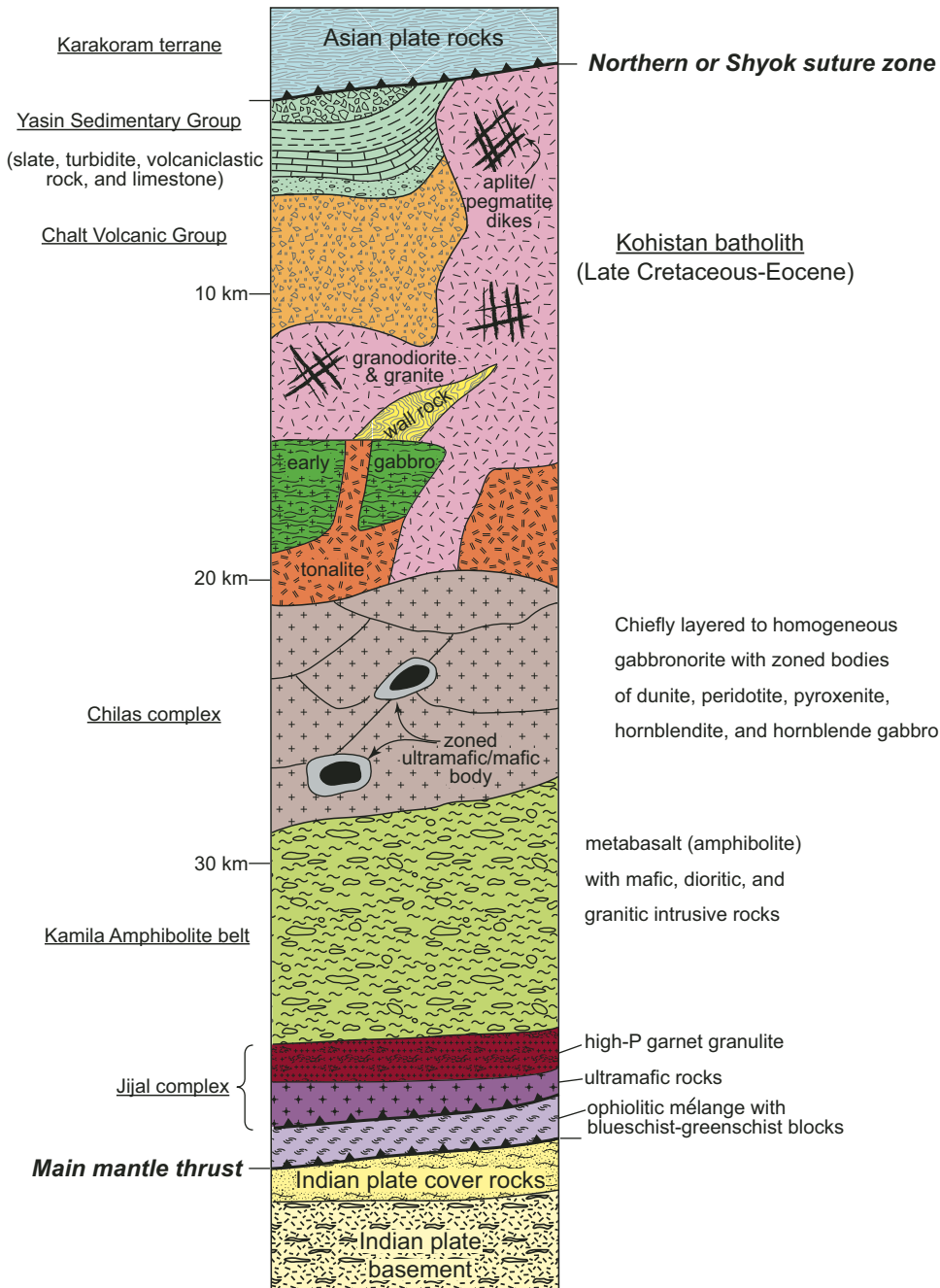


Figure 5. Diagrammatic crustal section of the Kohistan arc, northwest Pakistan (derived from Coward et al., 1986, their figure 2; Treloar et al., 1990, their figure 3; Percival et al., 1992, their figure 8-8; Searle et al., 1999, their figure 4; Burg et al., 2006, their figures 1 and 2).

suture. (Note: Burg et al. [2006] refer to this tectonic boundary as the “Karakoram-Kohistan suture zone.”) An alternative model employs a southward-facing arc with a northward-dipping subduction zone, and consequently, the Northern or Shyok suture represents the closure of a back-arc basin (Khan et al., 1997; Searle et al., 1999; their figure 5).

The Kohistan-Ladakh terrane was accreted to Asia in the latest Cretaceous before the Kohistan complex subsequently collided with India in the early to mid-Eocene (Searle et al., 1999). The closure of the ocean basin between the Asian plate and Kohistan island arc can only be bracketed between 95 and 75 Ma (Searle et al., 1999). Thus, in northwest Pakistan the subsequent Himalayan collision, during which the Kohistan complex was thrust southward over the Indian plate along the north-dipping, crustal-scale Main Mantle thrust (Gansser, 1964), was between the Kohistan complex and Indian plate.

The Kohistan complex (Fig. 5) contains rocks formed in at least two main stages of magmatic growth separated by a multiphase deformational history (Coward et al., 1982, 1986, 1987; Searle et al., 1999). The island-arc building stage occurred during Early–Late Cretaceous time, whereas the younger Andean-arc stage occurred during Late Cretaceous–Eocene time (Pettersen and Windley, 1991; Searle et al., 1999). Rocks of the island-arc stage include those of an upper level consisting of submarine and subaerial mafic to intermediate arc volcanic rocks and associated volcanoclastic rocks called the Chalt Volcanic Group; these in turn are overlain by slate, turbidites, volcanoclastic rock, and limestone of the Aptian-Albian Yasin Sedimentary Group (Pudsey, 1986).

The Andean-arc stage is manifested by the Kohistan batholith, a part of the Trans-Himalaya batholith, which extends ~2700 km in length and is 30–60 km in width (Pettersen and Windley, 1985, 1991). The plutons that comprise the Kohistan batholith range in composition from early gabbros, subsequently intruded by tonalites, granodiorites, granites, and finally a dense network of aplitite-pegmatite dikes (Pettersen and Windley, 1991). Thus, the plutons become more silicic with time.

South of the Kohistan batholith, island-arc-related metavolcanic and metasedimentary rocks are intruded by mafic to ultramafic rocks of the large (~300 × 20–40 km in area) Chilas complex (Khan et al., 1989; Percival et al., 1992; Searle et al., 1999; Jagoutz et al., 2007). This complex consists chiefly of massive to locally layered gabbro-norite that has locally undergone re-equilibration at 6–8 kb and ~750–850 °C (Jan and Howie, 1980; Bard, 1983; Khan et al., 1993; Yamamoto, 1993). The size of the Chilas complex, and various crosscutting field relationships, suggest that this large complex grew in a piecemeal fashion, consisting of numerous individual intrusive bodies (Burg et al., 2006; Jagoutz et al., 2006). Ultramafic bodies are also common throughout the Chilas complex, and are complexly zoned from dunite to peridotite to pyroxenite (Jagoutz et al., 2006). According to Jagoutz et al. (2006), the ultramafic bodies are ancient melt channels for high Mg# magmas that were parental for the widespread crystallization of gabbro-norite of the Chilas sequence. The Chilas complex is considered to be either the crystalline remains of a multi-stage

magma chamber developed at the base of the Kohistan arc, or a magmatic suite that developed during intra-arc spreading related to back-arc basin development (Khan et al., 1989, 1993). The most reliable radiometric age (U-Pb, zircon) indicates that at least part of the Chilas mafic to ultramafic suite formed in the Late Cretaceous (85.73 ± 0.5 Ma; Schaltegger et al., 2002).

Structurally, below the Chilas complex is an enigmatic zone of variably deformed amphibolite-facies rocks called the “Kamila amphibolite belt” (Treloar et al., 1990, 1996), which may include some amphibolitized gabbroic rocks of the Chilas complex. However, other components of the Chilas complex intrude the rock units of the Kamila amphibolite belt (Treloar et al., 1996; Burg et al., 2006). The amphibolite belt was interpreted by Treloar et al. (1990) as a deep-crustal shear zone that separates the Chilas complex from the deeper thrust stack of high-pressure cumulates of the Jijal ultramafic-mafic lower crustal-mantle complex. In this interpretation, southwest-directed thrusting in the Kamila shear zone is related to the southward propagation of shortening across the Kohistan complex following the initial suturing with Asia, but prior to collision with the Indian subcontinent.

The Jijal complex is bounded on the south by the Main Mantle thrust, marked in places by serpentinite or ophiolitic mélanges, which contain high-pressure assemblages typical of blueschist–greenschist-facies transition rocks (Searle et al., 1999). Directly south of the Main Mantle thrust is a greenschist-facies metasedimentary sequence of phyllites, psammites, and marbles, which have been interpreted as evidence of the drowning of the Indian shelf prior to and/or during emplacement of the Kohistan complex onto the Indian plate (DiPietro et al., 1993).

The Jijal complex consists of a lower ultramafic section chiefly composed of dunites, harzburgites, websterites, and clinopyroxenites, and an upper mafic section of mainly massive to gneissic garnetiferous granulites (Jan and Howie, 1981; Garrido et al., 2007). Some geobarometers indicate pressures as high as 12–14 kb for the igneous crystallization of the rocks (Jan and Howie, 1981). The high-pressure Jijal complex may represent an early part of the Kohistan arc that was subducted and then extruded upward in the subduction channel during Late Cretaceous, south-directed thrusting (Searle et al., 1999, see their figure 6).

Although perhaps imperfect as a true section through an island arc, the Kohistan complex does provide an excellent example of a fragment of an oceanic arc accreted to a continental margin that subsequently became an Andean-type continental margin (Pettersen and Windley, 1985; Searle et al., 1999). Thus, the deformational history related to collision and the second stage of calc-alkaline magmatic growth related to continued subduction provides a superb example of the conversion from oceanic to continental crust (Pettersen and Windley, 1991; Treloar et al., 1996).

A North American analogue to the Kohistan arc (complex) is the Early to Middle Jurassic Talkeetna arc that forms part of the composite Wrangellia-Peninsular terrane of south-central Alaska (Plafker et al., 1989; Clift et al., 2005b). This arc-section is discontinuously exposed for ~800 km (Burns, 1985; DeBari and Coleman, 1989; Farris, this volume), and the most complete

cross section is provided in the Chugach and Talkeetna Mountains, where the arc-section is built upon residual mantle peridotite and dunite (Fig. 6). The lower-crustal sequence is dominated by layered gabbronorite, although a thin zone (~0.2 km) of garnet granulite forms a transition from mantle rocks to lower-crustal cumulates (DeBari, 1997). Mid-crustal rocks consist of a heterogeneous assemblage of dioritic to tonalitic rocks mixed with gabbroic rocks and areas of abundant mafic dikes and inclusions (Greene et al., 2006). The upper-crustal part of the section consists of a thick (~7 km) sequence of lavas, tuffs, and volcanoclastic rocks of the Talkeetna Formation that compositionally ranges from basalt to rhyolite (DeBari and Coleman, 1989; Clift et al., 2005a; Greene et al., 2006).

Fiordland, New Zealand

The South Island of New Zealand exposes a nearly complete Early Cretaceous crustal section with paleodepths ranging from ≤ 8 km to >45 km (Fig. 7) (e.g., Gibson, 1990; Oliver, 1990; Klepeis et al., 2003, 2007; Klepeis and King, this volume). Fiordland

is particularly noteworthy for the large area of relatively young, deep, arc crust, as the region contains >5000 km² of high-pressure (~10–15 kb) migmatites, granulite-facies rocks, and middle- to lower-crustal plutons. The middle- to shallow-crustal parts of the section are exposed in Westland, which has been offset to the north from the deeper rocks by dextral strike-slip along the Alpine fault (Fig. 7A).

The South Island is generally considered in terms of Eastern and Western provinces (Landis and Coombs, 1967), which are separated by the Median batholith (also called Median tectonic zone). The Eastern province consists of Permian to Cretaceous arc volcanic and associated sedimentary rocks and accretionary complexes formed outboard of the Pacific margin of Gondwana (J.D. Bradshaw, 1989), which is represented by the Western province. The latter province is composed of early Paleozoic metapsammitic and pelitic schist, paragneiss, calc-silicate rock, marble, and local mafic gneiss, which are intruded by Devonian and Carboniferous granitoid plutons that are now orthogneisses (e.g., Oliver, 1990). These rocks experienced contractional deformation and low- to high-grade metamorphism during middle Paleozoic time (Oliver, 1980; Ireland and Gibson, 1998). The Median batholith contains Triassic to Early Jurassic and Late Jurassic to Early Cretaceous mafic to intermediate plutons (Kimbrough et al., 1993; Mortimer et al., 1999). Late Triassic plutons of the Median batholith intrude the Eastern province, and Early Cretaceous “stitching plutons” (Western Fiordland Orthogneiss and Separation Point Suite) intruded both the older parts of the batholith and Western province, thus providing the younger age limit on amalgamation of the provinces (J.Y. Bradshaw, 1990; Kimbrough et al., 1993; Mortimer et al., 1999).

The lower part of the Fiordland section is dominated by granulite-facies orthogneisses (Fig. 7B) (e.g., Oliver, 1980; J.D. Bradshaw, 1989; J.Y. Bradshaw, 1989; Clarke et al., 2000; Klepeis et al., 2003); the most voluminous lower-crustal unit, the mafic to intermediate Western Fiordland Orthogneiss, is a >3000 -km² tabular batholith that was emplaced between 126 and 116 Ma. Metamorphosed supracrustal rocks are scarce in the deepest crust. Intrusion of the Western Fiordland Orthogneiss resulted in a narrow (200–500-m-thick) zone of partial melting and migmatite formation above the batholith, but up to a 10-km-thick region of lower crust was partially melted below the body (Klepeis et al., 2003, 2004). This melting and granulite-facies metamorphism occurred between 850 and 750 °C and was followed by rapid, nearly isobaric, cooling to ~650 °C by ~111 Ma (J.Y. Bradshaw, 1989; Daczko et al., 2001; Hollis et al., 2004; Flowers et al., 2005). The Western Fiordland Orthogneiss is structurally overlain by Paleozoic and Mesozoic paragneiss, biotite schist, marble, and dioritic to granitic orthogneiss (Fig. 7B), largely of the Western province. Upper-amphibolite to greenschist-facies assemblages in these rocks record pressures ranging from 5 to 9 kb (Oliver, 1977; Gibson and Ireland, 1995). In Westland, lower-greenschist-facies, Ordovician turbidites constitute the shallowest levels of the section. Shallow parts of the Western Fiordland Orthogneiss and broadly similar deformed plutons

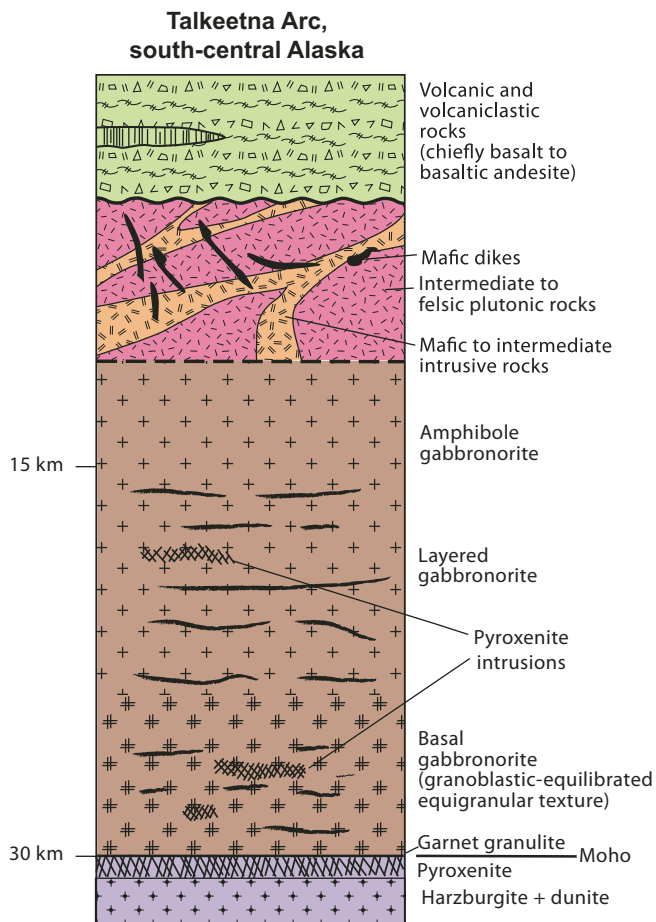


Figure 6. Diagrammatic crustal section of the accreted Jurassic Talkeetna arc of south-central Alaska (derived from Greene et al., 2006, their figure 2 and Table 1, and Kelemen et al., 2004, their figure 17).

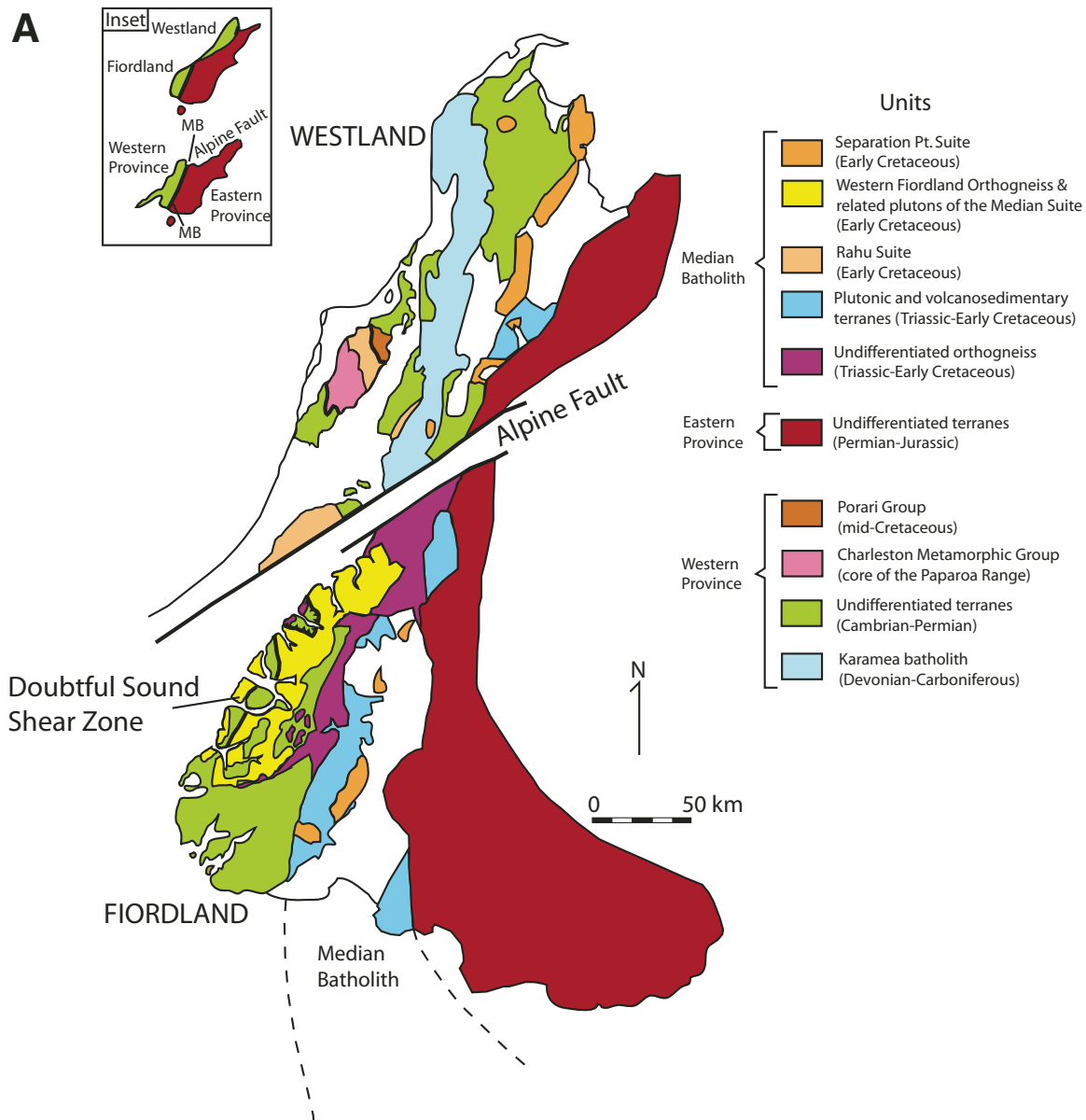


Figure 7. (Continued on following page.) (A) Simplified geologic map of the western part of the South Island of New Zealand; largely modified from Tulloch and Challis (2000) and Klepeis et al. (2004). Inset shows present configuration (top) and Cretaceous reconstruction (bottom) after removing slip on Alpine fault. (B) Restored “cartoon crustal cross section” of the Cretaceous Fiordland arc of New Zealand, compiled from Klepeis et al. (2003). This section is largely constructed for a time slice reflecting crustal shortening and thickening, and shortly before extension. The dark green layer within the Paleozoic metasedimentary rocks is a representative marker unit to show the structural style of the thrust belt. The position of the extensional Doubtful Sound shear zone and normal faults at higher levels are shown as gray faults. eK—Early Cretaceous; MB—Median batholith; WFO—Western Fiordland Orthogneiss.

form parts of the mid-crust in northern Fiordland (e.g., Tulloch and Kimbrough, 1989; Klepeis et al., 2007). These parts of the orthogneiss contain only sparse granulite-facies rocks.

The shallow to middle crust (8–27 km) of Westland contains significant volumes of ca. 126–105-Ma tonalite, granodiorite, and granite of the Separation Point suite (Fig. 7) (Tulloch and

Rabone, 1993; Tulloch and Challis, 2000). These rocks are characterized by high Na, Al, and Sr, and low K values. The high ratio of Sr/Y led Tulloch and Kimbrough (2003) to infer that the granitoids formed by partial melting of underplated mafic arc crust under high pressures, which resulted in a garnet-bearing residue. Tulloch and Kimbrough (2003) also noted that the

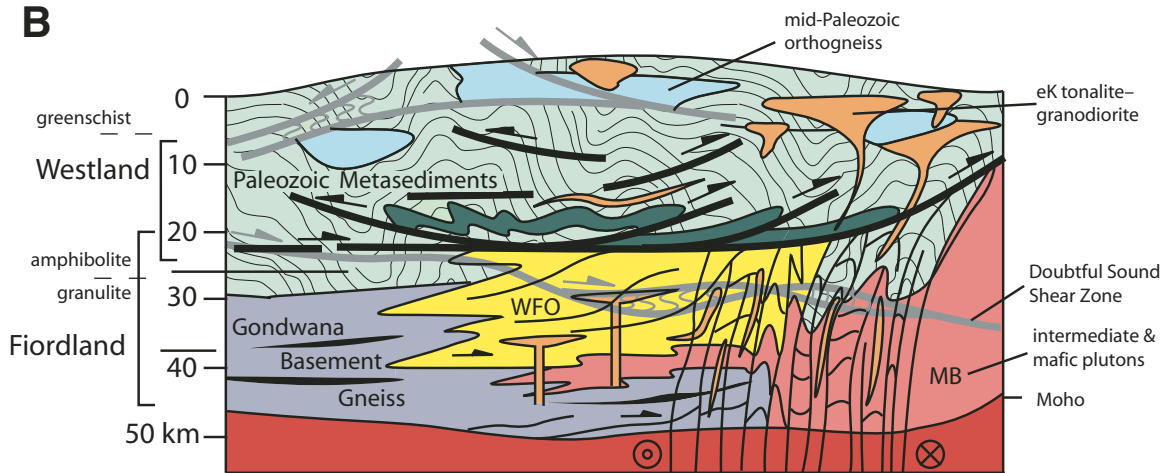


Figure 7. (Continued.)

geochemistry of these rocks resembles that of adakite and the Archean trondhjemite-tonalite-granodiorite suite.

The mid-Cretaceous tectonic regime of Fiordland is marked by shortening and crustal thickening from ca. 126–111 Ma during arc magmatism followed by plate reorganization and extension from ca. 111–90 Ma that led to opening of the Tasman Sea (Tulloch and Kimbrough, 1989). The thick Cretaceous crust in Fiordland is inferred to result largely from the crustal shortening (e.g., J.D. Bradshaw, 1989; Clarke et al., 2000; Daczko et al., 2002; Klepeis et al., 2007), although magmatic thickening may have played a role (Gibson, 1990; Brown, 1996). Prior to extension, the gross structural architecture was marked by subhorizontal, tabular, intermediate to mafic orthogneisses (Western Fiordland Orthogneiss) and associated granulite-facies host rocks, which were deformed by synchronously linked subhorizontal and steep contractional shear zones (Klepeis et al., 2007). Subsequent steep shear zones transect the lower-crustal rocks and bend upward into a décollement that forms the base of a deep mid-crustal fold-and-thrust belt above the Western Fiordland Orthogneiss (Fig. 7) (Daczko et al., 2002; Klepeis et al., 2004). Structures resulting from subsequent (ca. 111–90 Ma) extension were marked by much lateral and vertical variability. In central Fiordland, the deep crust records penetrative extensional deformation and is separated from mid-crustal orthogneisses and meta-supracrustal rocks by a major subhorizontal extensional shear zone, the Doubtful Sound décollement (Oliver, 1980; Gibson, 1990). In contrast, major extensional structures are absent in northern Fiordland. Klepeis and King (this volume) attribute these different responses to different thermal and rheological properties of the lower crust at length scales of ~100 km. The lower crust of central Fiordland was hot and weak, whereas northern Fiordland underwent rapid cooling prior to the formation of extensional structures to the south (e.g., Klepeis and King, this volume). Extension in northern Fiordland was focused above the strong lower crust, resulting in the collapse of the upper crust and exhumation of the weak mid-crust (Klepeis et al., 2007).

Major detachment faults formed at 15–20-km depth and metamorphic core complexes resulted (Fig. 7A; Paparoa core complex) (Tulloch and Kimbrough, 1989; Spell et al., 2000).

Late Mesozoic extension is inferred to have caused much of the exhumation of the section (e.g., Gibson, 1990). Final exhumation resulted from Neogene transpression across the adjacent Alpine fault, which led to rapid uplift and erosion (e.g., House et al., 2005). This late exhumation of the relatively intact section has enabled geophysical studies to trace the exhumed rocks into the present lower crust and mantle (e.g., Eberhart-Phillips and Reyners, 2001).

Southern Sierra Nevada Batholith

The Sierra Nevada batholith is the classic North American Cordillera continental magmatic arc, and the southern Sierra Nevada crustal section is one of the classic crustal sections of the Cordillera. This dominantly granodioritic and tonalitic batholith was constructed across the boundary between Proterozoic North American continental crust and accreted oceanic and island-arc terranes (e.g., Kistler, 1990; Saleeby, 1990). The batholith was largely constructed during voluminous magmatism in the Cretaceous (Bateman, 1992; Coleman and Glazner, 1997) and magmatism migrated eastward across the arc from ca. 130–85 Ma (e.g., Stern et al., 1981; Chen and Moore, 1982), presumably due to flattening of the subducting Farallon slab. Magmatism also grades from more mafic (significant gabbro to tonalite) in the west to dominantly granodiorite in the east (Bateman, 1992).

Saleeby (1990) and Saleeby et al. (2003) used ca. 100-Ma plutonic and volcanic rocks, dominantly high *T/P* assemblages in associated metamorphic rocks, and lower-crustal and mantle xenoliths in Neogene volcanic rocks to construct a synthetic crustal section through the southern part of the arc. Geophysical data helped to further refine this oblique section, which extends from surficial volcanic rocks and associated shallow plutons in the north to orthogneisses in the south derived from

ca. 100-Ma plutons that crystallized at depths reaching ≥ 35 km (Fig. 8) (Saleeby et al., 2003, 2007, 2008). In the axial part of the batholith, silicic ignimbrites, including some in well-preserved caldera complexes, dominate over andesites (Fiske and Tobisch, 1978, 1994; Busby-Spera, 1984). To the west, Early Cretaceous ring dike complexes represent the shallowest rocks constructed through accreted Paleozoic and Mesozoic oceanic and island-arc rocks (Clemens-Knott and Saleeby, 1999). In the upper ~ 15 km of the batholith, narrow screens and pendants of metamorphosed volcanic rocks, siliciclastic rocks and carbonates separate the voluminous felsic plutons. Widespread partial to nearly complete melting of pelitic and psammitic host rocks took place at ~ 15 – 20 km depth (5–6 kb) (Saleeby, 1990). Foliation and

lineation in the shallow to medium-depth part of the section are dominantly magmatic, but at paleodepths of >20 km the plutonic rocks are strongly foliated, showing increased solid-state deformation, and the deepest rocks of the section are orthogneisses (Sams and Saleeby, 1988; Saleeby, 1990; Pickett and Saleeby, 1993). Some of these orthogneisses display granulite-facies assemblages, which mostly formed during the cooling of tonalites and gabbros. Metamorphic host rocks to the orthogneisses record evidence of extreme partial melting, and rocks with refractory compositions (quartzite, marble, calc-silicate rock) are the dominant hosts. These orthogneisses are currently underlain by a regional thrust system associated with underthrusting of metasedimentary rocks of a subduction assemblage (Saleeby et al., 2003). Saleeby et al. (2007) estimate that the base of the crust at ca. 100 Ma was ~ 6 – 7 km (2 kb) below the base of the exposed section.

Rapid cooling and exhumation of the deep-crustal gneisses is thought to result from flattening of the Cretaceous subduction zone beneath the southern Sierra Nevada, the removal of much of the underlying mantle lithosphere, rock uplift and erosion, and extensional collapse (Saleeby, 2003; Saleeby et al., 2007, 2008). According to Saleeby et al. (2003), segmentation of the down-going slab and steeper dips of the slab beneath the central Sierra Nevada led to less exhumation there, and the result is the present oblique section. Similar exhumation models have been inferred for other Cretaceous arc sections that have been dispersed from the southern Sierra Nevada by the San Andreas and other strike-slip faults and earlier extensional faults. These broadly equivalent, less intact arc crustal sections are preserved in the eastern Transverse Ranges (Needy et al., this volume) and Salinian block (Ducea et al., 2003; Kidder et al., 2003). Needy et al. (this volume) also appeal to underplating of subducted metasedimentary rocks (cf. Jacobson et al., 1996) during Laramide low-angle subduction to explain the tilting and exhumation of the eastern Transverse Ranges crustal section.

Studies of xenolith suites in Miocene and Pliocene–Quaternary volcanic rocks have led to major insights into the evolution of the deep crust and mantle of the Sierra Nevada arc. The Miocene (12–8 Ma) xenolith suite, which is brought up in volcanic rocks sitting on the shallow part of the crustal section to the north, includes abundant garnet pyroxenites (15–25 kb), garnet- and spinel-bearing peridotites (13–42 kb), and mafic garnet granulites (8–13 kb) (e.g., Beard and Glazner, 1995; Ducea and Saleeby, 1996, 1998a, 1998b; Lee et al., 2000, 2001). These geobarometric data are used to construct a stratified lithospheric column below the exposed crustal section (Saleeby et al., 2003). This column has garnet peridotites with inclusions of garnet pyroxenite at the base, overlain by garnet pyroxenite with inclusions of garnet peridotite and spinel peridotite at shallower levels, and higher garnet granulites with inclusions of garnet pyroxenite. The garnet granulites, in turn, are inferred to lie beneath the felsic granitoids of the exposed Cretaceous crustal section (Fig. 8). The seismic Moho is interpreted as the transitional boundary between plagioclase-bearing and plagioclase-absent rocks, and was at ~ 45 km paleodepth. Saleeby et al. (2003) emphasize that

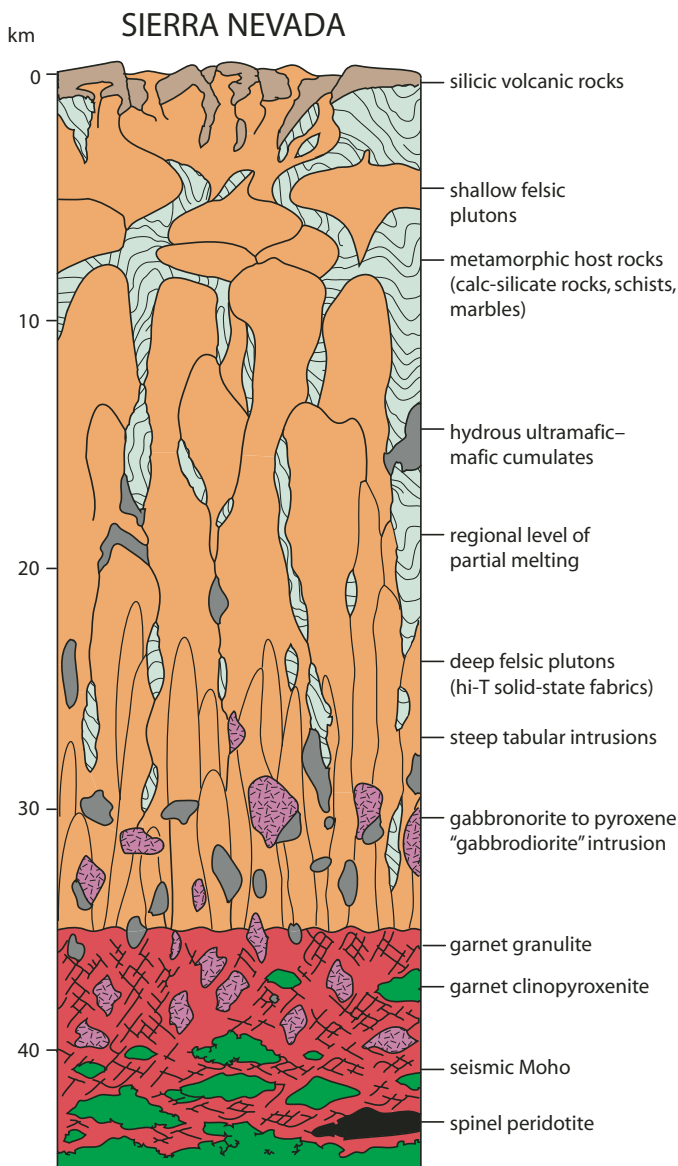


Figure 8. Restored crustal section of the southern Sierra Nevada, California, modified from Saleeby (1990) and Saleeby et al. (2003). Used with permission from the American Geophysical Union.

the garnet clinopyroxenites are the eclogitic residue of partial melting of hydrous mafic to intermediate rocks at >10 kb, which formed the Sierran arc granitoids (Wolf and Wyllie, 1993; Rapp and Watson, 1995). These garnet-bearing rocks, which extended downward to 90 km paleodepth, are thus crustal in their petrogenesis, but mantle in their seismic velocity (Ducea and Saleeby, 1998a, 1998b; Ducea, 2001; Saleeby et al., 2003).

In contrast to the Miocene xenolith suite, the Pliocene–Quaternary suite contains no garnet-bearing rocks and much spinel- and plagioclase peridotite. These data are interpreted to indicate that the garnet-bearing rocks formed a high-density root, which was subsequently delaminated. The mechanism(s) of delamination are problematic. Delamination was inferred by Saleeby et al. (2003) to have occurred during two different events that were localized along the contact between the felsic batholith and garnet-rich residue. They suggested that lithospheric mantle in the southern Sierra Nevada was removed during latest-Cretaceous-to-Paleocene Laramide low-angle subduction (see above) and more widespread convective removal occurred during Neogene Basin and Range extension directly to the east of the arc. This convectively removed garnet-pyroxenite-rich mantle lithosphere has apparently been imaged by seismic studies, which indicate that a high-velocity body of upper mantle extends from near the Moho to ~225 km depth in a roughly circular area beneath the southwestern edge of the Sierra Nevada and part of the adjacent Great Valley, forming a “mantle drip” (Zandt and Carrigan, 1993; Jones et al., 1994; Ruppert et al., 1998; Zandt et al., 2004).

The Sierra Nevada illustrates the utility of crustal cross sections to evaluate a number of important features of arcs. For example, a major feature of this crustal section is the reconstitution of much of the pre-Cretaceous crust by voluminous magmatism and the transfer of host rock (Fig. 8). The magnitude of plutonism creates a tremendous “room problem.” Saleeby (1990) accounts in part for this problem by proposing that the upward ascent of silicic magmas was accompanied by the downward (“return”) flow of metamorphic host rocks. He also showed that nearly coeval silicic volcanic rocks were rapidly transported downward adjacent to plutons to depths of 10 km. Further evidence that downward transport of host rock was a widespread process in the Sierra Nevada batholith has been provided by subsequent workers (e.g., Cruden et al., 1999; Tobisch et al., 2000; Paterson and Farris, 2008).

Another distinctive feature of the crustal section is the strong planar vertical anisotropy displayed by field relations and seismic studies (Ruppert et al., 1998). This anisotropy is particularly strong at paleodepths of >10 km, and is caused by steeply dipping tabular intrusions and intervening screens of metamorphic rocks, internal contacts of thinly sheeted plutons, and foliation in the plutons and medium- to high-grade metamorphic rocks (Saleeby et al., 2008). This vertical anisotropy and the distribution of rock units negate the view of Sierran plutons as ascending into the mid-crust (~15–20 km paleodepth) and spreading laterally over deeper, high-grade metamorphic rocks (Saleeby et al., 2008).

Attenuated Crustal Cross Sections Developed during Large-Magnitude Extension

In contrast to the crustal sections previously discussed, important “windows” into the middle and deep crust, and locally even the upper mantle are provided in numerous attenuated crustal sections that occur within the orogens of the world. These attenuated crustal sections typically occur in areas that have undergone large-magnitude extension, commonly preceded by large-magnitude contraction, in continental settings. In the past decade, oceanic core complexes have also been documented (e.g., Tucholke et al., 1998; Ranero and Reston, 1999; Karson et al., 2006; Canales et al., 2008).

Perhaps the type examples of attenuated crustal sections are the “Cordilleran metamorphic core complexes,” which extend along much of the length of the North American Cordillera (Crittenden et al., 1980; Armstrong, 1982). A representative, and one of the largest and most deeply exhumed of these core complexes is exposed in the Ruby Mountains and adjoining East Humboldt Range, northeastern Nevada. In the most general sense the Ruby-East Humboldt core complex consists of two structural tiers that are delineated by the Tertiary extensional architecture of the core complex (Fig. 9; Snoke et al., 1990; Sullivan and Snoke, 2007). The upper tier consists of non-metamorphosed to weakly metamorphosed, brittlely attenuated stratified rocks that range in age from the late Paleozoic to mid-Miocene and lie above a frictional/brittle, west-rooted, normal-sense detachment fault system (Ruby-East Humboldt detachment fault system). Throughout most of the Ruby-East Humboldt core complex, the detachment system is directly underlain by a km-thick, west-rooted, Tertiary mylonitic shear zone, which is the uppermost part of the lower structural tier, and yields a top-to-the-west-northwest sense-of-shear (Snoke and Lush, 1984; Snoke et al., 1997; McGrew and Casey, 1998). In the northern Ruby Mountains and East Humboldt Range, the lower structural tier consists of Archean through mid-Paleozoic, high-grade, migmatitic metasedimentary rocks (i.e., “metamorphic infrastructure” of Armstrong and Hansen, 1966) that have been extensively intruded by Mesozoic and Tertiary dikes, sills, and small plutons. This migmatitic infrastructure reached upper-amphibolite-facies metamorphic conditions in Late Cretaceous time as indicated by cross-cutting intrusive relationships of radiometrically dated pegmatitic leucogranitic gneiss (Hodges et al., 1992b; McGrew et al., 2000; Lee et al., 2003). $^{40}\text{Ar}/^{39}\text{Ar}$ cooling ages suggest either that this thermal event lasted until late Eocene time or that the crust was reheated to upper-amphibolite-facies conditions during the late Eocene (Dallmeyer et al., 1986; McGrew and Snee, 1994).

Late Cretaceous and mid-Tertiary granitic rocks form 50%–90% of the deepest levels of the complex (Howard, 1966, 1980, 2000; Wright and Snoke, 1993; MacCready et al., 1997). The dominant volume of Late Cretaceous plutonic rocks is two-mica, pegmatitic leucogranite gneiss that is interlayered and folded with metasedimentary rocks (Howard, 1966, 1987, 2000; Lee et al., 2003). The parental magmas were low-temperature crustal melts

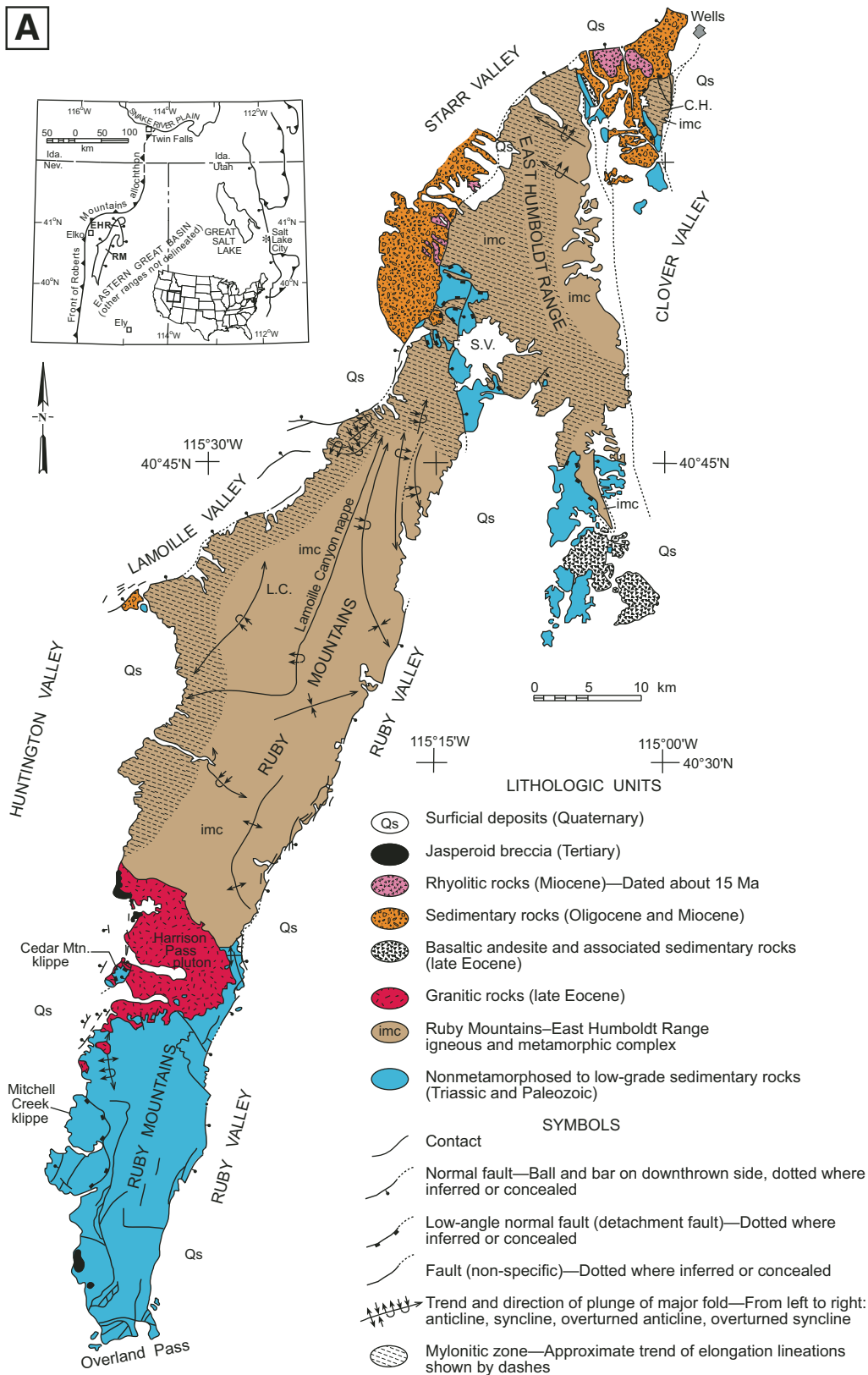


Figure 9. (Continued on following page.) (A) Generalized geologic map of the Ruby Mountains–East Humboldt Range, Nevada. C.H.—Clover Hill; S.V.—Secret Valley; L.C.—Lamoille Canyon. Modified from Snoke et al. (1997). (B) Schematic crustal sections of the Ruby–East Humboldt metamorphic core complex, northeastern Nevada through time: (1) Late Cretaceous (modified from Snoke, 2005, his figure 3), RMa = Roberts Mountains allochthon; (2) Mid-Tertiary (modified from Mueller and Snoke, 1993b, their figure 4), Tr-P = Triassic and Paleozoic rocks; and (3) Present (modified from Mueller and Snoke, 1993b, their figure 4, and Howard, 2003, his figure 3). Note that there is a change in scale from panels 1–3.

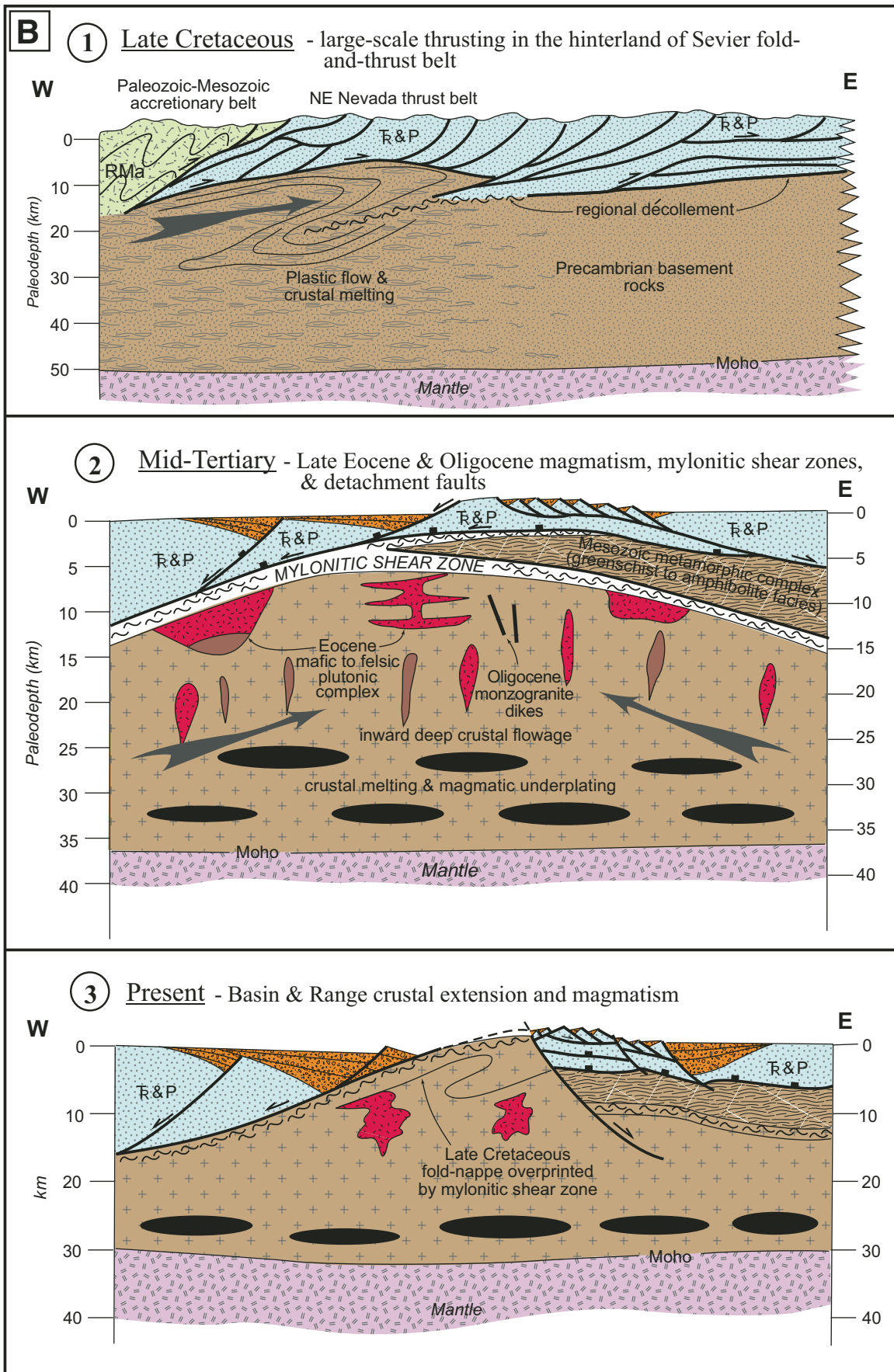


Figure 9. (Continued.)

from metasedimentary rocks of the Cordilleran miogeocline and of the underlying basement units (Lee et al., 2003). Crustal anatexis was either in direct response to crustal thickening by large-scale thrust faulting in the hinterland of the mid-Cretaceous to early Eocene Sevier fold-and-thrust belt (Miller and Gans, 1989; McGrew, 1992; Lee et al., 2003) or a result of subsequent crustal collapse and decompression (Hodges and Walker, 1992; Camilleri and Chamberlain, 1997; Wells and Hoisch, 2008). Isotopic evidence for a mantle component in the Late Cretaceous granitic rocks is absent (Kistler et al., 1981; Lee et al., 2003). The Cretaceous granitic rocks form an intimate intrusive network in the lower Paleozoic to Neoproterozoic calcareous, quartzitic, and pelitic host rocks. Even where granitic rocks greatly predominate, metasedimentary rafts form a ghost stratigraphy that traces large-scale, coherent folds (Howard, 1966, 1980, 1987, 2000).

Tertiary plutonic rocks in the Ruby–East Humboldt core complex can be subdivided into two age groups: ca. 40–36 Ma (late Eocene) and ca. 29 Ma (late Oligocene). The largest of the late Eocene intrusions is the ~140-km², ca. 36-Ma Harrison Pass composite pluton (Burton, 1997; Barnes et al., 2001; Fig. 9A). This pluton and widespread smaller late Eocene intrusive bodies encompass a wide range of bulk compositions (e.g., Howard, 1966; McGrew, 1992; Wright and Snoke, 1993; MacCready et al., 1997), and include gabbro, quartz diorite, tonalite-granodiorite, and hornblende-biotite to garnet two-mica monzogranite, some of which contains accessory sillimanite. Coeval volcanic rocks are part of the allochthonous, hanging-wall Tertiary volcanic-sedimentary sequences that occur along the margins of the core complex (Brooks et al., 1995; Snoke et al., 1997). The late Oligocene intrusive suite is characterized by steeply dipping biotite ± hornblende monzogranite dikes which, on the basis of U-Pb (zircon) ages, intruded the core complex in a narrow time interval at ca. 29 Ma (Wright and Snoke, 1993; MacCready et al., 1997). No late Oligocene volcanic rocks are known from the Tertiary volcanic sequence, either locally or regionally (Mueller and Snoke, 1993a; Brooks et al., 1995).

The evolution of the Ruby–East Humboldt detachment fault system and its relationship with the mid-Tertiary mylonitic shear zone of the lower structural tier has not been completely deciphered despite many detailed studies on various aspects of this plastic-to-brittle fault/shear-zone system (Hacker et al., 1990; Hurlow et al., 1991; Mueller and Snoke, 1993b; MacCready, 1996; McGrew and Casey, 1998). Virtually all of the brittle deformation associated with the currently exposed fault system is younger than the mid-Tertiary mylonitic shear zone, as mylonites are commonly overprinted by brittle deformation associated with the detachment fault system. Geothermobarometric data from mylonitic pelitic schists indicate a *P–T* estimate of 3.1–3.7 kb and 580–620 °C (Hurlow et al., 1991)—physical conditions well beyond the onset of quartz and feldspar plasticity (Scholz, 1990, his figure 3.19). Regional cross sections indicate that the mid-Tertiary mylonitic shear zone was captured by the younger Ruby–East Humboldt detachment fault system and offset by younger high-angle normal faults inferred to be related to the detachment

system (Mueller and Snoke, 1993b, see their Plate 2; Fig. 9). Thermochronological data indicate that mylonites were significantly below 300 °C by the late Oligocene (Dallmeyer et al., 1986; Dokka et al., 1986; McGrew and Snee, 1994), although mid-Miocene rocks locally occur in the hanging wall of the detachment system (Snoke and Lush, 1984; Mueller and Snoke, 1993b). Finally, although the bulk of the thermochronologic and radiometric data suggest that mylonitization occurred in the time interval of ca. 29–23 Ma (Wright and Snoke, 1993), some thermochronological data and field relationships suggest that late Eocene mylonitization may be related to an earlier movement history along the shear zone that was strongly overprinted by late Oligocene mylonitization (Mueller and Snoke, 1993b; Wright and Snoke, 1993; McGrew and Snee, 1994; Snoke et al., 1997; Howard, 2003). In summary, the mylonitic shear zone is part of a long-lived, west-rooted, normal-sense fault system that apparently was active from Eocene to Holocene time (Mueller and Snoke, 1993b) and indicates a protracted exhumation history for the core complex. The role of Late Cretaceous extension (Wells and Hoisch, 2008) in the exhumation of the core complex is an unresolved question that has proved difficult to evaluate given the long and complex Tertiary history of crustal extension.

The role of synchronous deep-crustal flow during large-magnitude crustal extension (Axen et al., 1998) is an important problem in the structural development of metamorphic core complexes and attenuated crustal cross sections in general. However, only a few of the Cordilleran core complexes expose crustal levels that are sufficiently deep to permit evaluation through direct analysis of rocks below the extensional, mylonitic shear zone. The Ruby–East Humboldt core complex is one of these complexes. MacCready et al. (1997) argued that there was fundamental decoupling between structural levels in this core complex in part on the basis of a near-orthogonal lineation pattern between the mylonite zone, with a pervasive west-northwest sense of slip, and the underlying migmatitic infrastructure containing approximately north–south-trending lineations with a weak indication of southward flow. MacCready et al. (1997) further argued for inflow of the middle crust and development of a convex-upward north–south channel during large-magnitude upper-crustal extension. This middle-crustal flow was considered to be synchronous with widespread magmatic under- or intraplating of the lower crust by mafic magmas, which in turn stimulated production of the late Eocene to early Oligocene granitic magmas discussed above. Similar patterns have not yet been recognized in other Cordilleran metamorphic core complexes, although Amato et al. (2002) (also see Akinin et al., this volume) described analogous structural relationships in the Kigluaik gneiss dome, Seward Peninsula, Alaska.

Another excellent example of an attenuated crustal cross section is preserved in the orogenic belts that surround the Alboran Sea of the western Mediterranean region, including the Betic Cordillera of southern Spain and Moroccan Rif (Fig. 10). These orogens form the Gibraltar arc, which defines the western margin of the Alboran Sea. Several features suggest that the

BETIC CORDILLERA, SOUTHERN SPAIN

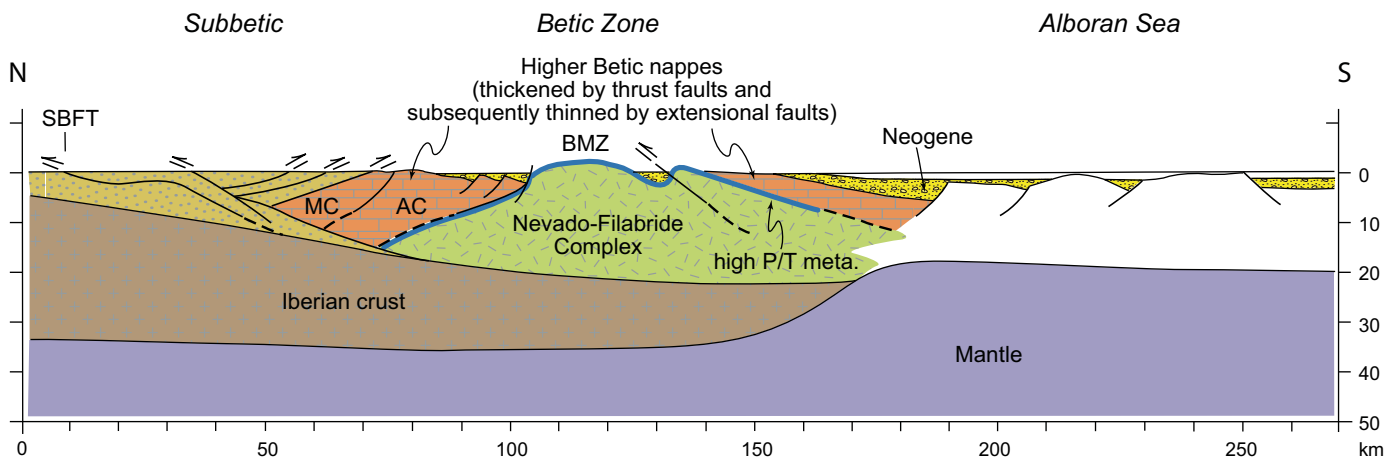


Figure 10. Schematic crustal section across the central Betic Cordillera (southern Spain) and adjacent Alboran Sea (modified from Vissers et al., 1995, their figure 2). SBFT—Subbetic frontal thrust; BMZ—Betic movement zone; AC—Alpujarride Complex; MC—Malaguide Complex.

Alboran Sea was a high collisional ridge during Paleogene time that subsequently experienced large-magnitude extensional collapse in early Miocene time (Platt et al., 2005): (1) the basin is underlain by thin (13–20 km) continental crust and anomalously low-velocity upper mantle ($V_p = 7.6\text{--}7.9$ km/s) (Banda et al., 1983); (2) has an east–west-striking horst-and-graben structure (Dillon et al., 1980); (3) was the locus of Neogene volcanism; and (4) has subsided 2–4 km since middle Miocene time (Platt and Vissers, 1989). Furthermore, the African and European plates were slowly converging during much of Tertiary time, so this is an example of large-magnitude crustal extension that occurred in a convergent geodynamic framework (Burchfiel and Royden, 1985, 1987; Dewey, 1988).

The Betic Cordillera includes a northern belt (pre-Betic and Subbetic zones) that exhibits Neogene, thin-skinned, fold-and-thrust-belt foreland deformation and a southern internal belt (Betic zone) comprised of metamorphic rocks (Vissers et al., 1995). The Betic zone is composed of a lower tectonic complex, the Nevado-Filábride, which includes high P/T metamorphic rocks, and an upper complex, the Higher Betic nappes, characterized by variable metamorphic grade from virtually non-metamorphosed rocks to high-pressure assemblages (Platt et al., 1983, 2003; Azañón et al., 1998). Stratigraphic duplication in the Higher Betic nappes indicates the development of a structural pile thickened by thrusting, and this interpretation is supported by metamorphic assemblages, which require a total structural thickness of >35 km (Tubía et al., 1997; Azañón et al., 1998; Platt et al., 2003).

The contact between the two tectonic complexes is the Betic movement zone of Vissers et al. (1995) characterized by a 100s-of-meters-thick zone of cataclasite and mylonite (Platt et al., 1984; Platt and Behrmann, 1986). Many of the tectonic contacts in the Betic zone are post-metamorphic, and they commonly place relatively low-grade rocks onto higher-grade metamorphic rocks

(Argles et al., 1999; Platt et al., 2003, 2005). The most dramatic example is the main tectonic boundary between the Higher Betic nappes (i.e., Alpujarride Complex) and the Nevado-Filábride Complex, which commonly places lower-greenschist-facies phyllites above tectonic slices of glaucophane schist, eclogite, or amphibolite-facies rocks (Platt, 1986, his figure 3; Platt and Behrmann, 1986; Vissers et al., 1995). The Betic Cordillera provides an example of a collisional orogen that has undergone an important episode of intraorogenic extensional collapse while convergent motion of the bounding plates continued (Vissers et al., 1995; Platt et al., 2006). This collapse has been interpreted as related to delamination of a gravitationally unstable, thick root of lithospheric mantle beneath the collisional zone (Platt and Vissers, 1989; Seber et al., 1996; Platt et al., 2006). By late Oligocene time, much of the lithospheric root beneath the Alboran collisional ridge had been removed by convection and replaced by asthenospheric mantle. This caused an increase in surface elevation and the region started to extend, exhuming metamorphic rocks and high-temperature peridotite from the base of the crust and upper part of the mantle along low-angle normal faults. Recent Lu-Hf radiometric dating of garnets from the structurally lowest tectonic unit, the Nevado-Filábride Complex, has yielded metamorphic ages of 18–14 Ma, which indicate that this tectonic unit was subducted *after* the extensional collapse of the overlying units (i.e., the Alpujarride Complex; see Fig. 10).

The presence of a younger structural and metamorphic history in rock units structurally *below* overlying tectonic units is widely recognized in metasedimentary rocks in various ancient accretionary complexes exposed in the U.S. Cordillera from the North Cascades (Matzel et al., 2004) to the Klamath Mountains and California Coast Ranges (Helper, 1986; Helper et al., 1989; Barth et al., 2003; Kidder et al., 2003; Kidder and Ducea, 2006) to the southern Sierra Nevada (Saleeby et al., 2003), and Transverse

Ranges/Mojave region of southern California (Jacobson et al., 2000, 2007; Grove et al., 2003). These important structural and metamorphic relationships within these ancient accretionary complexes support the tectonic model that orogenic wedges thicken by progressive subduction accretion (Scholl and von Huene, 2007), and previously accreted rocks are uplifted and subsequently exhumed by extensional faults and shear zones at higher structural levels in the wedge (Platt, 1986). The main differences between the Betic Cordillera and U.S. Cordillera systems is that the former is collisional and hanging-wall units are largely metasedimentary, whereas the other situation largely involves magmatic arcs where hanging-wall rocks are mostly plutons.

WHAT ARE SOME IMPORTANT DISTINCTIONS, QUESTIONS, AND PROBLEMS WITH REGARD TO THE INTERPRETATION OF CRUSTAL CROSS SECTIONS?

A series of issues are encountered in trying to interpret and synthesize relationships in and between crustal cross sections. We summarize a few of the most important issues below as illustrated by the crustal sections reviewed in this article and the volume.

Perhaps the most apparent issue is that there is no “typical” crustal cross section of continental crust. Arguably most striking, the overall composition of the crust differs markedly between sections (compare Figs. 4–10). This conclusion holds for sections constructed in broadly similar tectonic settings, such as magmatic arcs, which are probably the dominant tectonic element preserved in crustal cross sections. For example, much of the deep crust of the Kohistan and Talkeetna island-arc sequences is composed of mafic and lesser ultramafic rocks (Figs. 5 and 6). In contrast, the Sierra Nevada continental arc is dominated by granodiorite to tonalite downward to depths of >35 km, and mafic rocks are mainly eclogitic in composition and seismically part of the mantle (Fig. 8). The Fiordland arc probably lies compositionally between the other arcs, consisting mostly of dioritic to gabbroic orthogneisses at depths of >20 km, but containing considerable amounts of tonalite and granodiorite in the middle to upper crust (Fig. 7). These compositional differences in part reflect the contrasts between island arcs and continental magmatic arcs, and the lithosphere through and on which they were constructed. They may also reflect how much, if any, of the lower crust has been delaminated. Delamination has been increasingly proposed to have taken place in a range of orogens and future studies of crustal sections will undoubtedly evaluate the importance of this tectonic process for the composition and other features of the lower crust.

The relative amounts of metamorphosed supracrustal rocks at deep-crustal levels vary significantly between crustal sections. Such rocks are almost absent in the lower crust of the Kohistan, Talkeetna, and Fiordland sections. They are scarce in the Sierran and associated sections through the Salinian block and eastern Transverse Ranges; however, most of the deep crust there consists of plutons constructed over relatively short (<20 Ma) time

intervals, and metamorphosed supracrustal rocks do make up a significant percentage of the preserved host rocks. In contrast, the lower crust of the Ivrea-Verbano zone consists of granulite-facies metasedimentary and meta-igneous rocks intruded by mafic rocks, and supracrustal-derived rocks are important constituents of the deep levels of the Ruby–East Humboldt Range, Betic Cordillera, Klamath Mountains (Seiad complex), and Coast Mountains/North Cascades. These differences in part reflect the contrasting tectonic histories of these sections, but also the volume of arc-plutonic rocks emplaced during the development of these sections of continental crust. The Kohistan and Talkeetna island-arc sections were constructed on oceanic crust, and as expected, contain minimal quantities of metamorphosed supracrustal rocks in the deep crust. Moreover, although both of these island arcs were deformed in convergent plate settings, collisional for Kohistan and a Cordilleran-type accretionary margin for Talkeetna, neither section was intimately interleaved with other rocks by faulting during convergence. In contrast, magmatic rocks in the Ivrea-Verbano zone intruded an accretionary complex containing deeply buried supracrustal rocks, and the Klamath Mountains and Coast Mountains/North Cascades represent Cordilleran-type accretionary margins consisting in part of thrust sheets rich in metamorphosed supracrustal rocks.

Another variable feature of the sections is the geothermal gradient inferred from metamorphic assemblages. Granulite-facies rocks are widespread at depths of >25 km in many sections (e.g., Arunta, East Athabasca, Fiordland, Ivrea-Verbano, Klamath Mountains [Seiad complex], Kohistan, and Talkeetna), although not in the Sierra Nevada and North Cascades. Similarly, granulite-facies assemblages are not commonly reported from attenuated terranes; e.g., the Ruby–East Humboldt core complex, which reached >30 km in paleodepth during Late Cretaceous time based on P – T estimates from mineral assemblages in exposed rocks (McGrew et al., 2000). High-pressure assemblages are exposed in the deep levels of parts of the attenuated Betic Cordillera crustal section; this section apparently records a low geothermal gradient on the basis of the presence of blueschist- and eclogite-facies metabasic rocks and high-pressure metapelitic rocks.

The Phanerozoic sections highlighted in this volume display a range of crustal thicknesses, which reflects the different tectonic settings in which the sections evolved. It is difficult to evaluate the syn-orogenic crustal thicknesses of these sections, as this crust inherently is not static. This is particularly the case for sections that undergo major changes in thickness, such as the large crustal loading of Fiordland and Coast Mountains/North Cascades and substantial thinning of the Ruby–East Humboldt metamorphic core complex and other attenuated terranes. Nevertheless, reconstructions (Figs. 4–10) suggest that syn-orogenic paleodepths to the Moho for the sections analyzed in this article range from ≥ 45 km for Fiordland, Sierra Nevada, North Cascades, Ruby–East Humboldt core complex, and Betic Cordillera to ~ 30 km for the Talkeetna arc and Ivrea-Verbano zone. The inferred crustal thicknesses of several of these sections are significantly greater

than commonly cited average values of ~35 km for continental crust. This is not surprising given that the Fiordland and Coast Mountains/North Cascades arcs were constructed largely during regional shortening and crustal loading. Conversely, the thinner sections are compatible with their tectonic settings: island arc for the Talkeetna arc, and a transtensional regime during intrusion of mafic rocks in the Ivrea-Verbano zone.

There is considerable variability in the geometries of structures in crustal sections. The deep crust of most of the sections covered in this volume is characterized by gently dipping contacts between rock units, subhorizontal transposition foliation, recumbent folds, gently dipping shear zones, and in some sections subhorizontal sills. These subhorizontal structures formed during both regional contraction (e.g., Coast Mountains/North Cascades) and extension (e.g., Cordilleran metamorphic core complexes, Betic Cordillera). In marked contrast, the Sierra Nevada section has strong vertical anisotropy throughout its vertical extent defined by steep-sided intrusions, foliations, and shear zones. In Fiordland, a network of linked steep and subhorizontal structures dominates the middle to lower crust, and mid- and lower-crustal isobaric sections in Saskatchewan and the southwest United States also display domains of flat and steep shear zones. These differences in orientations of structures are intriguing. Gently dipping structures typify the mid- and deep crust (e.g., Williams and Jiang, 2005), and rheological differences and vertical partitioning may explain the Fiordland structures. The Sierra Nevada is more problematic; steep pluton contacts may impose a controlling anisotropy, and/or the orogen experienced a significant component of pure shear.

What were the tectonic settings of the crustal cross sections through geologic time? Many, if not most, crustal cross sections developed during a polyphase deformational history that spans 10 to 100s of million years, or even a billion years or more for Archean sections. The result is typically complex overprinting of different events. The variety of tectonic regimes and complex tectonic evolution are illustrated by the following examples from the case studies. (1) Magma in the Ivrea-Verbano zone was intruded during regional transtension in the Late Carboniferous–Permian, which followed crustal shortening during the Variscan orogeny and preceded deformation related to the Alpine orogeny. The early history of the zone is controversial, but a likely setting is an accretionary complex. (2) In the Fiordland section, a substantial component of the magmatic rocks intruded and much of the metamorphism occurred in an Early Cretaceous arc, but features formed at this time built on an earlier history of Mesozoic arc magmatism and accretion of oceanic and arc terranes. Early Cretaceous contraction was shortly followed by extension and then the opening of the Tasman Sea. The latest deformation is related to the Alpine fault. (3) Kohistan evolved from a Late Cretaceous island arc to a Late Cretaceous to Eocene Andean-type magmatic arc, and was strongly affected by both accretion to Asia and subsequent Indo-Asia collision. (4) Most of the Cenozoic Cordilleran metamorphic core complexes are in areas that were thickened by Mesozoic shortening in the hinterland to the Sevier orogenic

belt and then thinned by subsequent extension. (5) In the Betic Cordillera, continental lithosphere thickened during collision and underwent large-scale extensional collapse, probably in response to delamination of lithospheric mantle. This collapse was synchronous with continued convergent plate motion. (6) The Sierra Nevada batholith is a long-lived arc constructed across the boundary between continental crust and accreted oceanic and island-arc terranes. Magmatism ended in the Late Cretaceous when there was a major flattening of the dip of the subduction zone, perhaps due to subduction of an oceanic plateau. In the Neogene, much of the mantle lithospheric root of the batholith was removed, a process that is probably ongoing beneath other parts of the arc.

The polygenetic tectonic evolution of the crustal cross sections described in the volume makes it clear that no single crustal section (e.g., Ivrea-Verbano zone) typifies the deep crust. Schmid (1993, p. 580) made this point well when he claimed that the search for a “type section” of deep crust is a fruitless enterprise, because “it would reflect a highly immobilistic view of crustal evolution.”

How complete are crustal cross sections? Almost all crustal sections are cut by faults, reflecting the active tectonic settings in which they formed and in many cases subsequent deformation during exhumation. The amount of section excised or duplicated by faults and ductile shear zones is typically difficult to quantify. This is particularly well illustrated by attenuated crustal sections.

An important question is: how much lower crust exists below an exposed crustal section? Only a few crustal sections are in contact with mantle rocks, and in most of these cases the contacts are faults. Thus, lowermost crust is generally absent. Deep-crustal and mantle xenoliths provide important information, as illustrated for the Bering Strait region (Akinin et al., this volume) and the Sierra Nevada, but unfortunately, such xenoliths are absent for most crustal sections. A few sections can be tied by geophysical data to the present deep crust and mantle (e.g., Fiordland, Ivrea-Verbano zone), but the geophysical data do not provide the same level of detail as the exposed sections.

What were the mechanisms and processes that led to exhumation of crustal cross sections? The exhumation of relatively intact crustal sections and lower-crustal rocks probably requires an unusual sequence of tectonic events (Handy, 1990). Exhumation in general results from erosion, normal faulting, and ductile (vertical) thinning, and commonly involves more than one of these processes (see reviews by Platt, 1993, and Ring et al., 1999). The contribution of each of these processes is very difficult to quantify. For example, erosion is presumably always a factor, but the numerous variables which control erosion rates (e.g., climate, tectonics, rock types) hinder determination of these rates, particularly for Mesozoic and older orogens. Different combinations of processes have been proposed for exhumation of crustal sections discussed in this paper and in the subsequent articles, and these sections illustrate the types of tectonic events that may lead to exhumation of deep crust.

Major exhumation is probably most commonly attributed to normal faults and extensional shear zones. Numerous studies have

demonstrated that these structures exhume metamorphic core complexes (e.g., Ruby Mountains–East Humboldt Range) and other attenuated sections as described above. Large-magnitude extension, such as in the eastern Great Basin, typically does not bring to the Earth's surface high-pressure (>10 kb) metamorphic rocks, but exhumation of deeper levels may result from more than one extensional event (Ring et al., 1999; Forster and Lister, 1999). In this context, it is noteworthy that some Cordilleran core complexes may have experienced both Late Cretaceous and Cenozoic extension (e.g., Hodges and Walker, 1992; Wells and Hoisch, 2008).

Gently dipping mid- to deep-crustal shear zones in Fiordland (Doubtful Sound shear zone; see Klepeis et al., this volume) and Coast Mountains/North Cascades (e.g., Andronicos et al., 2003; Paterson et al., 2004; Crawford et al., this volume), which formed during extensional and transtensional regimes, respectively, were also at least in part responsible for the exhumation of these magmatic arc sections. These shear zones were marked by significant vertical ductile thinning. Transtension also drove early exhumation of the Ivrea-Verbano zone (see above).

Delamination of lithospheric mantle, and in some cases lowermost continental crust, as a result of major crustal thickening resulting from collision or from depression of deep arc crust into the eclogite facies (e.g., southern Sierra Nevada) is an important driving mechanism for exhumation by extension and erosion. Removal of the lithospheric root in the Betic Cordillera collisional orogen is probably responsible for extension and exhumation of this attenuated section. Cenozoic extension in the western North American Cordillera and at least part of the Basin and Range province has also been attributed to collapse of thickened crust (Coney and Harms, 1984), possibly due to delamination (Sonder et al., 1987), and Late Cretaceous extension and exhumation arguably were driven by delamination (Wells and Hoisch, 2008). Removal of lithospheric mantle and the rise of asthenospheric mantle also result in heating of the crust and uplift, which should enhance erosion, as has been proposed for the Sierra Nevada. Similarly, slab breakoff during continent-continent collision (e.g., Davies and von Blanckenburg, 1995) may lead to crustal heating and uplift, but is not the dominant mechanism proposed for many crustal sections.

Lithospheric mantle and in some cases lowermost crust may also be removed by structural underplating of clastic trench deposits and minor oceanic crust during low-angle subduction, processes that can lead to exhumation (e.g., Jacobson et al., 2007). The relatively buoyant underplated metasedimentary rocks may drive surface uplift and erosional exhumation, and/or lead to ductile thinning of lower crust and initiation of normal faulting. Variations of this scenario have been applied to exhumation of the southern Sierra Nevada, eastern Transverse Ranges, Seiad complex (Klamath Mountains), and North Cascades sections.

Intra-continental thrusting has been viewed as an important, albeit indirect component of the exhumation history of some Precambrian deep-crustal terranes (see early review by Handy, 1990). For example, exhumation of an exposed area of >20,000 km² of

lower crust in the Athabasca granulite terrane was ultimately driven by continent-continent collision (Trans-Hudson orogeny), in which thrust displacements with ≥ 20 km of throw resulted in rock uplift that was accompanied by erosion and/or tectonic denudation of surface material (Mahan et al., 2003). A later stage of normal faulting is envisioned to have brought granulites from the middle crust to near the surface. Also in the Canadian Shield, the Kapuskasing section is bounded below by a crustal-scale thrust (Ivanhoe Lake fault zone), and rock uplift associated with this fault zone probably happened at rates similar to erosional denudation (Percival, 1990). Finally, the Arunta block is in the hanging wall to the Redbank thrust, which offsets the fossil Moho (Goleby et al., 1989; see Waters-Tormey et al., this volume). This block records Proterozoic exhumation during extension or transtension and Paleozoic exhumation (rapid erosion?) associated with the Redbank thrust (Biermeier et al., 2003; Claoue-Long and Hoatson, 2005; Waters-Tormey et al., this volume).

Transpression across major fault zones may lead to extensive surface uplift and exhumation largely by erosion. For example, Alpine transpressional deformation and lithospheric wedging along and near the Insubric line resulted in rock uplift of the Ivrea-Verbano zone. In Fiordland, oblique convergence between the Pacific and Indo-Australian plates led to Neogene transpression across the Alpine fault and rapid erosion.

In summary, almost all of the crustal cross sections evaluated in this volume were exhumed by multiple mechanisms, which is probably generally a prerequisite for exhumation of deep crust. Although the exhumation of several of these sections is not well documented, they do illustrate the wide-ranging combinations of tectonic events that exhume deep crust. Examples of these combinations include: (1) underplating of metasedimentary rocks and extension and erosion, followed by delamination of an eclogitic root, uplift and erosion, and late uplift and erosion due to ridge subduction and formation of an asthenospheric window (Sierra Nevada); (2) transtension followed by much later collision, transpression, and erosion (Ivrea-Verbano zone); (3) extension/transtension and subsequent intra-continental thrusting and erosion (Arunta); (4) extension and vertical ductile thinning of an arc followed by much later transpression, uplift, and erosion (Fiordland); and (5) multiple periods of extension during and after crustal thickening (Cordilleran metamorphic core complexes).

ACKNOWLEDGMENTS

We thank Jonathan Miller and Scott Paterson for helpful discussions. We gratefully acknowledge Paterson, Sarah Garlick, and Dan Jones for helpful informal reviews, and Pat Bickford and John Platt for their formal reviews, all of which led to improvements in the manuscript. Miller's research on crustal sections was supported in part by the National Science Foundation (EAR-9980623, EAR-0074099, and EAR-0511062). Snoke's studies on deep-crustal rocks were also supported by National Science Foundation EAR-9017894 (Ivrea-Verbano zone) and EAR-9627958 (Ruby–East Humboldt core complex).

REFERENCES CITED

- Afonso, J.C., and Ranalli, G., 2004, Crustal and mantle strengths in continental lithosphere: Is the jelly sandwich model obsolete?: *Tectonophysics*, v. 394, p. 221–232, doi: 10.1016/j.tecto.2004.08.006.
- Akinin, V.V., Miller, E.L., and Wooden, J.L., 2009, this volume, Petrology and geochronology of crustal xenoliths from the Bering Strait region: Linking deep and shallow processes in extending continental crust, in Miller, R.B., and Snoko, A.W., eds., *Crustal cross sections from the western North American Cordillera and elsewhere: Implications for tectonic and petrologic processes: Geological Society of America Special Paper 456*, doi: 10.1130/2009.2456(02).
- Amato, J., Miller, E.L., and Hannula, K.A., 2002, Orthogonal flow direction in extending continental crust: An example from the Kigluak gneiss dome, Seward Peninsula, Alaska, in Miller, E.L., Grantz, A., and Klempner, S., eds., *Tectonic evolution of the Bering Shelf-Chukchi Sea-Arctic margin and adjacent landmasses: Geological Society of America Special Paper 360*, p. 133–146.
- Andronicos, C.L., Chardon, D., Hollister, L.S., Gehrels, G.E., and Woodsworth, G.J., 2003, Strain partitioning in an obliquely convergent orogen, plutonism, and synorogenic collapse: Coast Mountains batholith, British Columbia, Canada: *Tectonics*, v. 22, no. 2, doi: 10.1029/2001TC001312.
- Argles, T.W., Platt, J.P., and Waters, D.J., 1999, Attenuation and excision of a crustal section during extensional exhumation: The Carratraca Massif, Betic Cordillera, southern Spain: *Journal of the Geological Society of London*, v. 156, p. 149–162, doi: 10.1144/gsjgs.156.1.0149.
- Armstrong, R.L., 1982, Cordilleran metamorphic core complexes—From Arizona to southern Canada: *Annual Review of Earth and Planetary Sciences*, v. 10, p. 129–154, doi: 10.1146/annurev.earth.10.050182.001021.
- Armstrong, R.L., and Hansen, E., 1966, Cordilleran infrastructure in the eastern Great Basin: *American Journal of Science*, v. 264, p. 112–127.
- Arthaud, F., and Matte, P., 1977, Late Paleozoic strike-slip faulting in southern Europe and northern Africa: Result of a right-lateral shear zone between the Appalachians and the Urals: *Geological Society of America Bulletin*, v. 88, p. 1305–1320, doi: 10.1130/0016-7606(1977)88<1305:LPSFIS>2.0.CO;2.
- Axen, G.J., Selverstone, J., Byrne, T., and Fletcher, J.M., 1998, If the strong crust leads, will the weak crust follow?: *GSA Today*, v. 8, no. 12, p. 1–8.
- Azañón, J.M., García-Dueñas, V., and Goffé, B., 1998, Exhumation of high-pressure metapelites and coeval crustal extension in the Alpujarride complex (Betic Cordillera): *Tectonophysics*, v. 285, p. 231–252, doi: 10.1016/S0040-1951(97)00273-4.
- Baldwin, J.A., Bowring, S.A., Williams, M.L., and Mahan, K.H., 2006, Geochronological constraints on the crustal evolution of felsic high-pressure granulites, Snowbird tectonic zone, Canada: *Lithos*, v. 88, p. 173–200, doi: 10.1016/j.lithos.2005.08.009.
- Banda, E., Udias, A., Mueller, S., Mezcuca, J., Boloix, M., Qallart, J., and Aparicio, A., 1983, Crustal structure beneath Spain from deep seismic sounding experiments: *Physics of the Earth and Planetary Interiors*, v. 31, p. 277–280, doi: 10.1016/0031-9201(83)90087-0.
- Barboza, S.A., and Bergantz, G.W., 2000, Metamorphism and anatexis in the Mafic Complex contact aureole, Ivrea zone, northern Italy: *Journal of Petrology*, v. 41, p. 1307–1327, doi: 10.1093/petrology/41.8.1307.
- Barboza, S.A., Bergantz, G.W., and Brown, M., 1999, Regional granulite facies metamorphism in the Ivrea zone: Is the Mafic Complex the smoking gun or a red herring?: *Geology*, v. 27, p. 447–450, doi: 10.1130/0091-7613(1999)027<0447:RGFMIT>2.3.CO;2.
- Bard, J.P., 1983, Metamorphism of an obducted island arc: Example of the Kohistan sequence (Pakistan) in the Himalayan collided range: *Earth and Planetary Science Letters*, v. 65, p. 133–144, doi: 10.1016/0012-821X(83)90195-4.
- Barnes, C.G., Burton, B.R., Burling, T.C., Wright, J.E., and Karlsson, H.R., 2001, Petrology and geochemistry of the late Eocene Harrison Pass pluton, Ruby Mountains core complex, northeastern Nevada: *Journal of Petrology*, v. 42, p. 901–929, doi: 10.1093/petrology/42.5.901.
- Barth, A.P., Wooden, J.L., Grove, M., Jacobson, C.E., and Pedrick, J.N., 2003, U-Pb zircon geochronology of rocks in the Salinas Valley region of California: A reevaluation of the crustal structure and origin of the Salinian block: *Geology*, v. 31, p. 517–520, doi: 10.1130/0091-7613(2003)031<0517:UZGORI>2.0.CO;2.
- Bateman, P.C., 1992, Plutonism in the central part of the Sierra Nevada batholith, California: U.S. Geological Survey Professional Paper 1483, 186 p.
- Beard, B.L., and Glazner, A.F., 1995, Trace element and Sr and Nd isotopic composition of mantle xenoliths from the Big Pine volcanic field, California: *Journal of Geophysical Research*, v. 100, p. 4169–4179, doi: 10.1029/94JB02883.
- Beaumont, C., Jamieson, R.A., Nguyen, M.H., and Lee, B., 2001, Himalayan tectonics explained by extrusion of a low-viscosity crustal channel coupled to focused surface denudation: *Nature*, v. 414, p. 738–742, doi: 10.1038/414738a.
- Bergantz, G.W., 1989, Underplating and partial melting: Implications for melt generation and extraction: *Science*, v. 245, p. 1093–1095, doi: 10.1126/science.245.4922.1093.
- Biermeier, C., Stuwe, K., Foster, D.A., and Finger, F., 2003, Thermal evolution of the Redbank thrust system, central Australia: Geochronological and phase-equilibrium constraints: *Tectonics*, v. 22, 1002, doi: 10.1029/2001TC901033.
- Bird, P., 1991, Lateral extrusion of lower crust from under high topography, in the isostatic limit: *Journal of Geophysical Research*, v. 96, p. 10,275–10,286.
- Bohlen, S.R., 1987, Pressure-temperature-time paths and a tectonic model for the evolution of granulites: *The Journal of Geology*, v. 95, p. 617–632.
- Bohlen, S.R., and Mezger, K., 1989, Origin of granulite terranes and the formation of the lowermost continental crust: *Science*, v. 244, p. 326–329, doi: 10.1126/science.244.4902.326.
- Boriani, A.C., and Villa, I.M., 1997, Geochronology of regional metamorphism in the Ivrea-Verbano zone and Serie dei Laghi, Italian Alps: *Schweizerische Mineralogische und Petrographische Mitteilungen*, v. 77, p. 381–401.
- Boriani, A., Burlini, L., and Sacchi, R., 1990a, The Cossato-Mergozzo-Brissago line and the Pogallo line (Southern Alps, northern Italy) and their relationships with the late-Hercynian magmatic and metamorphic events: *Tectonophysics*, v. 182, p. 91–102, doi: 10.1016/0040-1951(90)90344-8.
- Boriani, A., Giobbi Origoni, E., Borghi, A., and Caironi, V., 1990b, The evolution of the “Serie dei Laghi” (Strona-Ceneri and Scisti dei Laghi): The upper components of the Ivrea-Verbano crustal section; Southern Alps, North Italy and Ticino, Switzerland: *Tectonophysics*, v. 182, p. 103–118, doi: 10.1016/0040-1951(90)90345-9.
- Boriani, A., Caironi, V., Giobbi Origoni, E., and Vannucci, R., 1992, The Permian intrusive rocks of Serie dei Laghi (Western Southern Alps): *Acta Vulcanologica*, v. 2, p. 73–86.
- Boudier, F., Jackson, M., and Nicolas, A., 1984, Structural study of the Balmuccia massif (western Alps): A transition from mantle to lower crust, in Zwart, H.J., Hartman, P., and Tobi, A.C., eds., *Ophiolites and ultramafic rocks—A tribute to Emile den Tex: Geologie en Mijnbouw*, v. 63, p. 179–188.
- Bradshaw, J.D., 1989, Cretaceous geotectonic patterns in the New Zealand region: *Tectonics*, v. 8, p. 803–820, doi: 10.1029/TC008i004p00803.
- Bradshaw, J.Y., 1989, Origin and metamorphic history of an Early Cretaceous polybaric granulite terrain, Fiordland, southwest New Zealand: *Contributions to Mineralogy and Petrology*, v. 103, p. 346–360, doi: 10.1007/BF00402921.
- Bradshaw, J.Y., 1990, Geology of the crystalline rocks of northern Fiordland: Details of the granulite facies Western Fiordland Orthogneiss and associated rock units: *New Zealand Journal of Geology and Geophysics*, v. 33, p. 465–484.
- Brooks, W.E., Thorman, C.H., and Snee, L.W., 1995, The ⁴⁰Ar/³⁹Ar ages and tectonic setting of the middle Eocene northeast Nevada volcanic field: *Journal of Geophysical Research*, v. 100, p. 10,403–10,416, doi: 10.1029/94JB03389.
- Brown, E.H., 1996, High-pressure metamorphism caused by magma loading in Fiordland, New Zealand: *Journal of Metamorphic Geology*, v. 14, p. 441–452, doi: 10.1046/j.1525-1314.1996.06024.x.
- Brown, E.H., and Walker, N.W., 1993, A magma loading model for Barrovian metamorphism in the SE Coast Plutonic Complex, British Columbia and Washington: *Geological Society of America Bulletin*, v. 105, p. 479–500, doi: 10.1130/0016-7606(1993)105<0479:AMLMFB>2.3.CO;2.
- Brown, M., and Rushmer, T., 1997, The role of deformation in the movement of granitic melt: Views from the laboratory and the field, in Holness, M.B., ed., *Deformation-enhanced fluid transport in the Earth’s crust and mantle: London, UK, Chapman & Hall*, p. 111–144.

- Brown, R.L., and Gibson, H.D., 2006, An argument for channel flow in the southern Canadian Cordillera and comparison with Himalayan tectonics, *in* Law, R.D., Searle, M.P., and Godin, L., eds., Channel flow, ductile extrusion and exhumation in continental collision zones: Geological Society of London Special Publication 268, p. 543–559.
- Brown, R.L., Journeay, J.M., Lane, L.S., Murphy, D.C., and Rees, C.J., 1986, Obduction, backfolding and piggyback thrusting in the metamorphic hinterland of the southeastern Canadian Cordillera: *Journal of Structural Geology*, v. 8, p. 255–268, doi: 10.1016/0191-8141(86)90047-7.
- Brown, R.L., Carr, S.D., Johnson, B.L., Coleman, V.J., Cook, F.A., and Varsek, J.L., 1992, The Monashee decollement of the southern Canadian Cordillera: A crustal-scale shear zone linking the Rocky Mountain foreland belt to lower crust beneath accreted terranes, *in* McClay, K.R., ed., Thrust tectonics: London, UK, Chapman & Hall, p. 357–364.
- Buddington, A.F., 1959, Granitic emplacement with special reference to North America: *Geological Society of America Bulletin*, v. 70, p. 671–747, doi: 10.1130/0016-7606(1959)70[671:GEWSRT]2.0.CO;2.
- Burchfiel, B.C., and Royden, L.H., 1985, North-south extension within the convergent Himalayan region: *Geology*, v. 13, p. 679–682, doi: 10.1130/0091-7613(1985)13<679:NEWTCH>2.0.CO;2.
- Burchfiel, B.C., and Royden, L.H., 1987, Thin-skinned N–S extension within the convergent Himalayan region: Gravitational collapse of a Miocene topographic front, *in* Coward, M.P., Dewey, J.F., and Hancock, P.L., eds., Continental extensional tectonics: Geological Society of London Special Publication 28, p. 611–619.
- Burg, J.-P., Jagoutz, O., Dawood, H., and Shahid Hussain, S., 2006, Precollision tilt of crustal blocks in rifted island arcs: Structural evidence from the Kohistan Arc: *Tectonics*, v. 25, p. TC5005, doi: 10.1029/2005TC001835.
- Burns, L.E., 1985, The Border Ranges ultramafic and mafic complex, south-central Alaska: Cumulate fractionates of island-arc volcanics: *Canadian Journal of Earth Sciences*, v. 22, p. 1020–1038.
- Burton, B.R., 1997, Structural geology and emplacement history of the Harrison Pass pluton, central Ruby Mountains, Elko County, Nevada [Ph.D. thesis]: Laramie, University of Wyoming, 295 p.
- Busby-Spera, C.J., 1984, Large-volume rhyolitic ash flow eruptions and submarine caldera collapse in lower Mesozoic Sierra Nevada, California: *Journal of Geophysical Research*, v. 89, p. 8417–8427, doi: 10.1029/JB089iB10p08417.
- Camilleri, P.A., and Chamberlain, K.R., 1997, Mesozoic tectonics and metamorphism in the Pequoop Mountains and Wood Hills region, northeast Nevada: Implications for the architecture and evolution of the Sevier orogen: *Geological Society of America Bulletin*, v. 109, p. 74–94, doi: 10.1130/0016-7606(1997)109<0074:MTAMIT>2.3.CO;2.
- Canales, J.P., Tuelholke, B.E., Xu, M., Collins, J.A., and DuBois, D.L., 2008, Seismic evidence for large-scale compositional heterogeneity of oceanic core complexes: *Geochemistry Geophysics Geosystems*, v. 9, doi: 10.1029/2008GC002009.
- Carr, S.D., and Simony, P.S., 2006, Ductile thrusting versus channel flow in the southeastern Canadian Cordillera: Evolution of a coherent crystalline thrust sheet, *in* Law, R.D., Searle, M.P., and Godin, L., eds., Channel flow, ductile extrusion and exhumation in continental collision zones: Geological Society of London Special Publication 268, p. 561–587.
- Carr, S.D., Parrish, R.R., and Brown, R.L., 1987, Eocene structural development of the Valhalla Complex, southeastern British Columbia: *Tectonics*, v. 6, p. 175–196, doi: 10.1029/TC006i002p0175.
- Chen, J.H., and Moore, J.G., 1982, Uranium-lead isotopic ages from the Sierra Nevada batholith, California: *Journal of Geophysical Research*, v. 87, p. 4761–4784, doi: 10.1029/JB087iB06p04761.
- Christensen, N.I., and Mooney, W.D., 1995, Seismic velocity structure and composition of the continental crust: A global view: *Journal of Geophysical Research*, v. 100, p. 9761–9788, doi: 10.1029/95JB00259.
- Clark, M.C., and Royden, L.H., 2000, Topographic ooze: Building the eastern margin of Tibet by lower crustal flow: *Geology*, v. 28, p. 703–706, doi: 10.1130/0091-7613(2000)28<703:TOBTEM>2.0.CO;2.
- Clarke, G.L., Klepeis, K.A., and Daczko, N.R., 2000, Cretaceous high-P granulites at Milford Sound, New Zealand: Metamorphic history and emplacement in a convergent margin setting: *Journal of Metamorphic Geology*, v. 18, p. 359–374, doi: 10.1046/j.1525-1314.2000.00259.x.
- Claoue-Long, J.C., and Hoatson, D.M., 2005, Proterozoic mafic-ultramafic intrusions in the Arunta region, central Australia, Part 2: Event chronology and regional correlations: *Precambrian Research*, v. 142, p. 134–158, doi: 10.1016/j.precamres.2005.08.006.
- Clemens-Knott, D., and Saleeby, J.B., 1999, Impinging ring-dike complexes in the Sierra Nevada batholith, California: Roots of the Early Cretaceous volcanic arc: *Geological Society of America Bulletin*, v. 111, p. 484–496, doi: 10.1130/0016-7606(1999)111<0484:IRDCIT>2.3.CO;2.
- Clift, P.D., Pavlis, T., DeBari, S.M., Draut, A.E., Rioux, M., and Kelemen, P.B., 2005a, Subduction erosion of the Jurassic Talkeetna-Bonanza arc and the Mesozoic accretionary tectonics of western North America: *Geology*, v. 33, p. 881–884, doi: 10.1130/G21822.1.
- Clift, P.D., Draut, A.E., Kelemen, P.B., Blusztajn, J., and Greene, A., 2005b, Stratigraphic and geochemical evolution of an oceanic arc upper crustal section: The Jurassic Talkeetna Volcanic Formation, south-central Alaska: *Geological Society of America Bulletin*, v. 117, p. 902–925, doi: 10.1130/B25638.1.
- Coleman, D.S., and Glazner, A.F., 1997, The Sierra Crest magmatic event: Rapid formation of juvenile crust during the Late Cretaceous in California, *in* Ernst, W.G., and Nelson, C.A., eds., Integrated earth and environmental evolution of the southwestern United States: Columbia, Maryland, Bellwether Publishing, p. 253–272.
- Collins, W.J., and Sawyer, E.W., 1996, Pervasive magma transfer through the lower-middle crust during non-coaxial compressional deformation: An alternative to dyking: *Journal of Metamorphic Geology*, v. 14, p. 565–579, doi: 10.1046/j.1525-1314.1996.00442.x.
- Colombo, A., and Tunesi, A., 1999, Alpine metamorphism of the Southern Alps west of the Giudicarie line: *Schweizerische Mineralogische und Petrographische Mitteilungen*, v. 79, p. 183–189.
- Coney, P.J., and Harms, T.A., 1984, Cordilleran metamorphic core complexes: Cenozoic extensional relics of Mesozoic compression: *Geology*, v. 12, p. 550–554, doi: 10.1130/0091-7613(1984)12<550:CMCCCE>2.0.CO;2.
- Cook, F.A., Varsek, J.L., Clowes, R.M., Kanasevich, E.R., Spencer, C.S., Parrish, R.R., Brown, R.L., Carr, S.D., Johnson, B.J., and Price, R.A., 1992, Lithoprobe crustal reflection cross section of the southern Canadian Cordillera, 1. Foreland thrust and fold belt to Fraser fault: *Tectonics*, v. 11, p. 12–35, doi: 10.1029/91TC02332.
- Coward, M.P., Jan, M.Q., Rex, D., Tarney, J., Thirlwall, M., and Windley, B.F., 1982, Geo-tectonic framework of the Himalaya of N Pakistan: *Journal of the Geological Society of London*, v. 139, p. 299–308, doi: 10.1144/gsjgs.139.3.0299.
- Coward, M.P., Windley, B.F., Broughton, R.D., Luff, I.W., Petterson, M.G., Pudsey, C.J., Rex, D.C., and Khan, A., 1986, Collision tectonics in the NW Himalayas, *in* Coward, M.P., and Ries, A.C., eds., Collision tectonics: Geological Society of London Special Publication 19, p. 203–219.
- Coward, M.P., Butler, R.W.H., Asif Khan, M., and Knipe, R.J., 1987, The tectonic history of the Kohistan and its implications for Himalayan structure: *Journal of the Geological Society of London*, v. 144, p. 377–391, doi: 10.1144/gsjgs.144.3.0377.
- Crawford, M.L., Lindline, J., Gehrels, G.E., and Klepeis, K.A., 2009, this volume, Mid-Cretaceous–Recent crustal evolution in the central Coast orogen, British Columbia and southeastern Alaska, *in* Miller, R.B., and Snoke, A.W., eds., Crustal cross sections from the western North American Cordillera and elsewhere: Implications for tectonic and petrologic processes: Geological Society of America Special Paper 456, doi: 10.1130/2009.2456(04).
- Crittenden, M.D., Jr., Coney, P.J., and Davis, G.H., eds., 1980, Cordilleran metamorphic core complexes: Geological Society of America Memoir 153, 490 p.
- Cruden, A.R., 1998, On the emplacement of tabular granites: *Journal of the Geological Society of London*, v. 155, p. 853–862, doi: 10.1144/gsjgs.155.5.0853.
- Cruden, A.R., 2006, Emplacement and growth of plutons: Implications for rates of melting and mass transfer in continental crust, *in* Brown, M., and Rushmer, T., eds., Evolution and differentiation of continental crust: Cambridge, UK, Cambridge University Press, p. 455–519.
- Cruden, A.R., Tobisch, O.T., and Launeau, P., 1999, Magnetic fabric evidence for conduit-fed emplacement of a tabular intrusion: Dinkey Creek pluton, central Sierra Nevada batholith, California: *Journal of Geophysical Research*, v. 104, p. 10,511–10,530, doi: 10.1029/1998JB009093.
- Culshaw, N.G., Beaumont, C., and Jamieson, R.A., 2006, The orogenic superstructure-infrastructure concept: Revisited, quantified, and revived: *Geology*, v. 34, p. 733–736, doi: 10.1130/G22793.1.

- Daczko, N.R., Clarke, G.L., and Klepeis, K.A., 2001, Transformation of two-pyroxene hornblende granulite to garnet granulite involving simultaneous melting and fracturing of the lower crust, Fiordland, New Zealand: *Journal of Metamorphic Geology*, v. 19, p. 549–560, doi: 10.1046/j.0263-4929.2001.00328.x.
- Daczko, N.R., Klepeis, K.A., and Clarke, G.L., 2002, Thermomechanical evolution of the crust during convergence and deep crustal pluton emplacement in the Western Province of Fiordland, New Zealand: *Tectonics*, v. 21, 1022, doi: 10.1029/2001TC001282.
- Dallmeyer, R.D., Snoko, A.W., and McKee, E.H., 1986, The Mesozoic-Cenozoic tectonothermal evolution of the Ruby Mountains, East Humboldt Range, Nevada: A Cordilleran metamorphic core complex: *Tectonics*, v. 5, p. 931–954, doi: 10.1029/TC005i006p00931.
- Davidson, C., Hollister, L.S., and Schmid, S.M., 1992, Role of melt in the formation of a deep-crustal convergence shear zone: The Maclaren Glacier metamorphic belt, south central Alaska: *Tectonics*, v. 11, p. 348–359, doi: 10.1029/91TC02907.
- Davidson, J.P., 1992, Continental and island arcs, in Nierenberg, W.A., ed., *Encyclopedia of Earth system science*, v. 1 (A–Co): San Diego, California, Academic Press, p. 615–626.
- Davies, J.H., and von Blanckenburg, F., 1995, Slab breakoff: A model of lithosphere detachment and its test in the magmatism and deformation of collisional orogens: *Earth and Planetary Science Letters*, v. 129, p. 85–102, doi: 10.1016/0012-821X(94)00237-S.
- DeBari, S.M., 1997, Evolution of magmas in continental and oceanic arcs: The role of the lower crust: *Canadian Mineralogist*, v. 35, p. 501–519.
- DeBari, S.M., and Coleman, R.G., 1989, Examination of the deep levels of an island arc: Evidence from the Tonsina ultramafic-mafic assemblage, Tonsina, Alaska: *Journal of Geophysical Research*, v. 94, p. 4373–4391, doi: 10.1029/JB094iB04p04373.
- DeBari, S.M., and Sleep, N.H., 1991, High-Mg, low-Al bulk composition of the Talkeetna island arc, Alaska: Implications for primary magmas and the nature of arc crust: *Geological Society of America Bulletin*, v. 103, p. 37–47, doi: 10.1130/0016-7606(1991)103<0037:HMLABC>2.3.CO;2.
- Dell'Angelo, L.N., and Tullis, J., 1988, Experimental deformation of partially melted granitic aggregates: *Journal of Metamorphic Geology*, v. 6, p. 495–515, doi: 10.1111/j.1525-1314.1988.tb00436.x.
- Demarchi, G., Quick, J.E., Sinigoi, S., and Meyer, A., 1998, Pressure gradient and original orientation of a lower-crustal intrusion in the Ivrea-Verbano zone, northern Italy: *The Journal of Geology*, v. 106, p. 609–622.
- Dewey, J.F., 1988, Extensional collapse of orogens: *Tectonics*, v. 7, p. 1123–1139, doi: 10.1029/TC007i006p01123.
- Dillon, W.P., Robb, J.M., Greene, M.G., and Lucena, J.C., 1980, Evolution of the continental margin of southern Spain and the Alboran Sea: *Marine Geology*, v. 36, p. 205–226, doi: 10.1016/0025-3227(80)90087-0.
- DiPietro, J.A., Pogue, K.R., Lawrence, R.D., Baig, M.S., Hussain, A., and Amad, I., 1993, Stratigraphy south of the Main Mantle thrust, lower Swat, Pakistan, in Treloar, P.J., and Searle, M.P., eds., *Himalayan tectonics*: Geological Society of London Special Publication 74, p. 207–220.
- Dokka, R.K., Mahaffie, M.J., and Snoko, A.W., 1986, Thermochronologic evidence of major tectonic denudation associated with detachment faulting, northern Ruby Mountains–East Humboldt Range, Nevada: *Tectonics*, v. 5, p. 995–1006, doi: 10.1029/TC005i007p00995.
- Ducea, M.N., 2001, The California arc: Thick granitic batholiths, eclogitic residues, lithospheric-scale thrusting, and magmatic flare-ups: *GSA Today*, v. 11, p. 4–10, doi: 10.1130/1052-5173(2001)011<0004:TCATGB>2.0.CO;2.
- Ducea, M.N., and Saleeby, J.B., 1996, Buoyancy sources for a large, unrooted mountain range, the Sierra Nevada, California: Evidence from xenolith thermobarometry: *Journal of Geophysical Research*, v. 101, p. 8229–8244, doi: 10.1029/95JB03452.
- Ducea, M.N., and Saleeby, J.B., 1998a, The age and origin of a thick mafic-ultramafic keel from beneath the Sierra Nevada batholith: Evidence from xenolith thermobarometry: *Journal of Geophysical Research*, v. 101, p. 8229–8244, doi: 10.1029/95JB03452.
- Ducea, M.N., and Saleeby, J.B., 1998b, A case for delamination of deep batholithic crust beneath the Sierra Nevada, California: *International Geology Review*, v. 133, p. 78–93.
- Ducea, M.N., Kidder, S., and Zandt, G., 2003, Arc composition at mid-crustal depths: Insights from the Coast Ridge Belt, Santa Lucia Mountains, California: *Geophysical Research Letters*, v. 30, p. 1703, doi: 10.1029/2002GL016297.
- Eberhart-Phillips, D., and Reyners, M., 2001, A complex, young subduction zone imaged by three-dimensional seismic velocity, Fiordland, New Zealand: *Geophysical Journal International*, v. 146, p. 731–746, doi: 10.1046/j.0956-540x.2001.01485.x.
- Evans, B.W., and Berti, J.W., 1986, Revised metamorphic history for the Chawaukum Schist, North Cascades, Washington: *Geology*, v. 14, p. 695–698, doi: 10.1130/0091-7613(1986)14<695:RMHFTC>2.0.CO;2.
- Farris, D.W., 2009, this volume, Construction and evolution of the Kodiak Talkeetna arc crustal section, southern Alaska, in Miller, R.B., and Snoko, A.W., eds., *Crustal cross sections from the western North American Cordillera and elsewhere: Implications for tectonic and petrologic processes*: Geological Society of America Special Paper 456, doi: 10.1130/2009.2456(03).
- Fiske, R.S., and Tobisch, O.T., 1978, Paleogeographic significance of volcanic rocks of the Ritter Range pendant, central Sierra Nevada, California, in Howell, D.G., and McDougal, K.A., eds., *Mesozoic paleogeography of the western United States*: Sacramento, California, Society of Economic Paleontologists and Mineralogists, Pacific Section, Pacific Coast Paleogeography Symposium 2, p. 209–219.
- Fiske, R.S., and Tobisch, O.T., 1994, Middle Cretaceous ash-flow tuff and caldera collapse deposit in the Minarets caldera, east-central Sierra Nevada, California: *Geological Society of America Bulletin*, v. 106, p. 582–593, doi: 10.1130/0016-7606(1994)106<0582:MCAFTA>2.3.CO;2.
- Flowers, R.M., Bowring, S.A., Tulloch, A.J., and Klepeis, K.A., 2005, Tempo of burial and exhumation within the deep roots of a magmatic arc, Fiordland, New Zealand: *Geology*, v. 33, p. 17–20, doi: 10.1130/G21010.1.
- Forster, M., and Lister, G.S., 1999, Detachment faults in the Aegean core complex of Ios, Cyclades, Greece, in Ring, U., Brandon, M.T., Willett, S.D., and Lister, G.S., eds., *Exhumation processes: Normal faulting, ductile flow and erosion*: Geological Society of London Special Publication 154, p. 305–323.
- Fountain, D.M., 1976, The Ivrea-Verbano and Strona-Ceneri zones, northern Italy: A cross-section of the continental crust—New evidence from seismic velocities: *Tectonophysics*, v. 33, p. 145–165, doi: 10.1016/0040-1951(76)90054-8.
- Fountain, D.M., 1986, Implications of deep crustal evolution seismic reflection seismology, in Barazangi, M., and Brown, L., eds., *Reflection seismology: The continental crust*: Washington, D.C., American Geophysical Union, Geodynamic Series 14, p. 1–7.
- Fountain, D.M., 1989, Growth and modification of lower continental crust in extended terrains: The role of extension and magmatic underplating, in Mereu, R.F., Mueller, S., and Fountain, D.M., eds., *Lower crust: Properties and processes*: Washington, D.C., American Geophysical Union Monograph, v. 51, p. 287–299.
- Fountain, D.M., and Salisbury, M.H., 1981, Exposed cross-sections through the continental crust: Implications for crustal structure, petrology and evolution: *Earth and Planetary Science Letters*, v. 56, p. 263–277, doi: 10.1016/0012-821X(81)90133-3.
- Fountain, D.M., Percival, J., and Salisbury, M.H., 1990, Exposed cross sections of the continental crust—Synopsis, in Salisbury, M.H., and Fountain, D.M., eds., *Exposed cross-sections of the continental crust*: Dordrecht, the Netherlands, Kluwer Academic Publishers, p. 653–662.
- Fountain, D.M., Arculus, R., and Kay, R.W., eds., 1992, *Continental lower crust*: Amsterdam, the Netherlands, Elsevier, 485 p.
- Gansser, A., 1964, *Geology of the Himalayas*: New York, Interscience Publishers, John Wiley & Sons, 289 p.
- Gansser, A., 1968, The Insubric line, a major tectonic problem: *Schweizerische Mineralogische und Petrographische Mitteilungen*, v. 48, p. 123–143.
- Garlick, S.R., Medaris, L.G., Jr., Snoko, A.W., Schwartz, J.J., and Swapp, S.M., 2009, this volume, Granulite- to amphibolite-facies metamorphism and penetrative deformation in a disrupted ophiolite, Klamath Mountains, California: A deep view into the basement of an accreted oceanic island arc, in Miller, R.B., and Snoko, A.W., eds., *Crustal cross sections from the western North American Cordillera and elsewhere: Implications for tectonic and petrologic processes*: Geological Society of America Special Paper 456, doi: 10.1130/2009.2456(06).
- Garrido, C.J., Bodinier, J.-L., Dhuime, B., Bosch, D., Chanefo, I., Bruguier, O., Hussain, S.S., Dawood, H., and Burg, J.-P., 2007, Origin of the island arc Moho transition zone via melt-rock reaction and its implications for intracrustal differentiation of island arcs: Evidence from the Jijal complex (Kohistan complex, northern Pakistan): *Geology*, v. 35, p. 683–686, doi: 10.1130/G23675A.1.

- Gebauer, D., 1993, The pre-Alpine evolution of the continental crust of the central Alps—An overview, *in* von Raumer, J.F., and Neubauer, F., eds., Pre-Mesozoic geology in the Alps: Berlin, Springer-Verlag, p. 93–117.
- Gibson, G.M., 1990, Uplift and exhumation of middle and lower crustal rocks in an extensional tectonic setting, Fiordland, New Zealand, *in* Salisbury, M.H., and Fountain, D.M., eds., Exposed cross-sections of the continental crust: Dordrecht, the Netherlands, Kluwer Academic Publishers, p. 71–101.
- Gibson, G.M., and Ireland, T.R., 1995, Granulite formation during continental extension in Fiordland, New Zealand: *Nature*, v. 375, p. 479–482, doi: 10.1038/375479a0.
- Gilotti, J.A., and McClelland, W.C., 2008, Geometry, kinematics, and timing of extensional faulting in the Greenland Caledonides—A synthesis, *in* Higgins, A.K., Gilotti, J.A., and Smith, M.P., eds., The Greenland Caledonides: Evolution of the northeast margin of Laurentia: Geological Society of America Memoir 202, p. 251–271, doi: 10.1130/2008.1202(10).
- Glazner, A.F., Bartley, J.M., Coleman, D.S., Gray, W., and Taylor, R.Z., 2004, Are plutons assembled over millions of years by amalgamation of small magma chambers?: *GSA Today*, v. 14, no. 4/5, p. 4–11, doi: 10.1130/1052-5173(2004)014<0004:APAOMO>2.0.CO;2.
- Godin, L., Grujic, D., Law, R.D., and Searle, M.P., 2006, Channel flow, ductile extrusion and exhumation in continental collision zones: An introduction, *in* Law, R.D., Searle, M.P., and Godin, L., 2006, eds., Channel flow, ductile extrusion and exhumation in continental collision zones: Geological Society of London Special Publication 268, p. 1–23.
- Goleby, B.R., Shaw, R.D., Wright, C., Kennett, B.L.N., and Lambeck, K., 1989, Geophysical evidence for “thick-skinned” crustal deformation in central Australia: *Nature*, v. 337, p. 325–330, doi: 10.1038/337325a0.
- Greene, A.R., DeBari, S.M., Kelemen, P.B., Blusztajn, J., and Clift, P.D., 2006, A detailed geochemical study of island arc crust: The Talkeetna arc section, south-central Alaska: *Journal of Petrology*, v. 47, p. 1051–1093, doi: 10.1093/petrology/egl002.
- Grocott, J., McCaffrey, K.J.W., Taylor, G., and Tikoff, B., 2004, eds., Vertical coupling and decoupling in the lithosphere: Geological Society of London Special Publication 227, 344 p.
- Grove, M., Jacobson, C.E., Barth, A.P., and Vučić, A., 2003, Temporal and spatial trends of Late Cretaceous–early Tertiary underplating of Pelona and related schist beneath southern California and southwestern Arizona, *in* Johnson, S.E., Paterson, S.R., Fletcher, J.M., Girty, G.H., Kimbrough, D.L., and Martin-Barajas, A., eds., Tectonic evolution of northwestern México and the southwestern USA: Geological Society of America Special Paper 374, p. 381–406.
- Grubenmann, U., 1904, Die kristallinen schiefer: Berlin, Borntraeger.
- Grujic, D., and Mancktelow, N.S., 1998, Melt-bearing shear zones: Analogue experiments and comparison with examples from southern Madagascar: *Journal of Structural Geology*, v. 20, p. 673–680, doi: 10.1016/S0191-8141(98)00006-6.
- Grujic, D., Hollister, L., and Parrish, R., 2002, Himalayan metamorphic sequence as an orogenic channel: Insight from Bhutan: *Earth and Planetary Science Letters*, v. 198, p. 177–191, doi: 10.1016/S0012-821X(02)00482-X.
- Hacker, B.R., Yin, A., Christie, J.M., and Snoke, A.W., 1990, Differential stress, strain rate, and temperatures of mylonitization in the Ruby Mountains, Nevada: Implications for the rate and duration of uplift: *Journal of Geophysical Research*, v. 95, p. 8569–8580, doi: 10.1029/JB095iB06p08569.
- Haller, J., 1956, Probleme der tiefentektonik: Bauformen im migmatit-stockwerk der Ostgrönländischen Kaledoniden: *Geologische Rundschau*, v. 45, p. 159–167, doi: 10.1007/BF01802002.
- Haller, J., 1971, *Geology of the East Greenland Caledonides*: New York, Interscience Publishers, John Wiley & Sons, 413 p.
- Hamilton, W., 1981, Crustal evolution by arc magmatism: *Royal Society of London Philosophical Transactions*, ser. A, v. 301, p. 279–291.
- Hamilton, W., 1987, Crustal extension in the Basin and Range province, southwestern United States, *in* Coward, M.P., Dewey, J.F., and Hancock, P.L., eds., Continental extensional tectonics: Geological Society of London Special Publication 28, p. 155–176.
- Hamilton, W.B., 1989, Crustal geologic processes of the United States, *in* Pakiser, L.C., and Mooney, W.D., eds., Geophysical framework of the continental United States: Geological Society of America Memoir 172, p. 743–781.
- Hamilton, W., and Myers, W.B., 1967, The nature of batholiths: U.S. Geological Survey Professional Paper 554-C, p. C1–C30.
- Handy, M.R., 1987, The structure, age and kinematics of the Pogallo fault zone: Southern Alps, northwestern Italy: *Eclogae Geologicae Helveticae*, v. 80, p. 593–632.
- Handy, M.R., 1990, The exhumation of cross sections of the continental crust: Structure, kinematics and rheology, *in* Salisbury, M.H., and Fountain, D.M., eds., Exposed cross-sections of the continental crust: Dordrecht, the Netherlands, Kluwer Academic Publishers, p. 485–507.
- Handy, M.R., and Zingg, A., 1991, The tectonic and rheological evolution of an attenuated cross-section of the continental crust: Ivrea crustal section, southern Alps, northwestern Italy and southern Switzerland: *Geological Society of America Bulletin*, v. 103, p. 236–253, doi: 10.1130/0016-7606(1991)103<0236:TTAREO>2.3.CO;2.
- Handy, M.R., Franz, L., Heller, F., Janott, B., and Zurbriggen, R., 1999, Multistage accretion, orogenic stacking, and exhumation of continental crust (Ivrea crustal section, Italy and Switzerland): *Tectonics*, v. 18, p. 1154–1177, doi: 10.1029/1999TC900034.
- Hanmer, S., 1988, Great Slave Lake shear zone, Canadian Shield: Reconstructed vertical profile of a crustal-scale fault zone: *Tectonophysics*, v. 149, p. 245–264, doi: 10.1016/0040-1951(88)90176-X.
- Hanmer, S., Bowring, S., Van Breeman, O., and Parrish, R., 1992, Great Slave Lake shear zone, NW Canada: Mylonitic record of Early Proterozoic continental convergence, collision and indentation: *Journal of Structural Geology*, v. 14, p. 757–773, doi: 10.1016/0191-8141(92)90039-Y.
- Harley, S.L., 1989, The origins of granulites: A metamorphic perspective: *Geological Magazine*, v. 126, p. 215–247.
- Hartz, E.H., Andresen, A., Hodges, K.V., and Martin, M.W., 2001, Syncontractional extension and exhumation of deep crustal rocks in the east Greenland Caledonides: *Tectonics*, v. 20, p. 58–77, doi: 10.1029/2000TC900020.
- Hatcher, R.D., Jr., and Merschat, A.J., 2006, The Appalachian inner Piedmont: An exhumed strike-parallel, tectonically forced orogenic channel, *in* Law, R.D., Searle, M.P., and Godin, L., eds., Channel flow, ductile extrusion and exhumation in continental collision zones: Geological Society of London Special Publication 268, p. 517–541.
- Helper, M.A., 1986, Deformation and high P/T metamorphism in the central part of the Condrey Mountain window, north-central Klamath Mountains, California and Oregon, *in* Evans, B.W., and Brown, E.H., eds., Blueschists and eclogites: Geological Society of America Memoir 164, p. 125–141.
- Helper, M.A., Walker, N.W., and McDowell, F.W., 1989, Early Cretaceous metamorphic ages and Middle Jurassic U-Pb zircon protolith ages for the Condrey Mountain Schist, Klamath Mtns., NW Calif. and SW Oregon: *Geological Society of America Abstracts with Programs*, v. 21, no. 5, p. 92.
- Henk, A., Franz, L., Teufel, S., and Oncken, O., 1997, Magmatic underplating, extension, and crustal reequilibration: Insights from a cross-section through the Ivrea Zone and Strona-Ceneri Zone, northern Italy: *The Journal of Geology*, v. 105, p. 367–377.
- Henriksen, N., and Higgins, A.K., 2008, Geological research and mapping in the Caledonian orogen of East Greenland, 70°N–82°N, *in* Higgins, A.K., Gilotti, J.A., and Smith, M.P., eds., The Greenland Caledonides: Evolution of the northeast margin of Laurentia: Geological Society of America Memoir 202, p. 1–27, doi: 10.1130/2008.1202(01).
- Higgins, A.K., 1976, Pre-Caledonian metamorphic complexes within the southern part of the East Greenland Caledonides: *Journal of the Geological Society of London*, v. 132, p. 289–305, doi: 10.1144/gsjgs.132.3.0289.
- Himmelberg, G.R., Haeussler, P.J., and Brew, D.A., 2004, Emplacement, rapid burial, and exhumation of 90-Ma plutons in southeastern Alaska: *Canadian Journal of Earth Sciences*, v. 41, p. 87–102, doi: 10.1139/e03-087.
- Hodges, K.V., 2000, Tectonics of the Himalaya and Tibet from two perspectives: *Geological Society of America Bulletin*, v. 112, p. 324–350, doi: 10.1130/0016-7606(2000)112<0324:TOTHAS>2.3.CO;2.
- Hodges, K.V., and Fountain, D.M., 1984, Pogallo line, South Alps, northern Italy: An intermediate crustal level, low-angle normal fault?: *Geology*, v. 12, p. 151–155, doi: 10.1130/0091-7613(1984)12<151:PLSANI>2.0.CO;2.
- Hodges, K.V., and Walker, J.D., 1992, Extension in the Cretaceous Sevier orogen, North American Cordillera: *Geological Society of America Bulletin*, v. 104, p. 560–569, doi: 10.1130/0016-7606(1992)104<0560:EITCSO>2.3.CO;2.
- Hodges, K.V., Parrish, R.R., Housh, T.B., Lux, D.R., Burchfiel, B.C., Royden, L.H., and Chen, Z., 1992a, Simultaneous Miocene extension and shortening in the Himalayan orogen: *Science*, v. 258, p. 1466–1470, doi: 10.1126/science.258.5087.1466.

- Hodges, K.V., Snoke, A.W., and Hurlow, H.A., 1992b, Thermal evolution of a portion of the Sevier hinterland: The northern Ruby Mountains–East Humboldt Range and Wood Hills, northern Nevada: *Tectonics*, v. 11, p. 154–164, doi: 10.1029/91TC01879.
- Hoffman, P.F., 1987, Continental transform tectonics: Great Slave Lake shear zone (ca. 1.9 Ga), northwest Canada: *Geology*, v. 15, p. 785–788, doi: 10.1130/0091-7613(1987)15<785:CTTGSL>2.0.CO;2.
- Holbrook, W.S., Mooney, W.D., and Christensen, N.I., 1992, The seismic velocity structure of the deep continental crust, in Fountain, D.M., Arculus, R., and Kay, R.W., eds., *Continental lower crust: Amsterdam, Elsevier, Developments in Geotectonics* 23, p. 1–43.
- Holliger, K., and Levander, A., 1994, Structure and seismic response of extended continental crust: Stochastic analysis of the Strona–Ceneri and Ivrea zones: *Geology*, v. 22, p. 79–82, doi: 10.1130/0091-7613(1994)022<79:SASROE>2.3.CO;2.
- Hollis, J.A., Clarke, G.L., Klepeis, K.A., Daczko, N.R., and Ireland, T.R., 2004, The regional significance of Cretaceous magmatism and metamorphism in Fiordland, New Zealand, from U–Pb zircon geochronology: *Journal of Metamorphic Geology*, v. 22, p. 607–627, doi: 10.1111/j.1525-1314.2004.00537.x.
- Hollister, L.S., and Andronicos, C., 1997, A candidate for the Baja British Columbia fault system: *GSA Today*, v. 7, no. 11, p. 1–7.
- Hollister, L.S., and Crawford, M.L., 1986, Melt-enhanced deformation; a major tectonic process: *Geology*, v. 14, p. 558–561, doi: 10.1130/0091-7613(1986)14<558:MDAMTP>2.0.CO;2.
- Holmes, A., 1965, *Principles of physical geology* (2nd edition): New York, Ronald Press Company, 1288 p.
- House, M.A., Gurnis, M., Sutherland, R., and Kamp, P.J.J., 2005, Patterns of Late Cenozoic exhumation deduced from apatite and zircon U–He ages from Fiordland, New Zealand: *Geochemistry Geophysics Geosystems*, v. 6, doi: 10.1029/2005GC000968.
- Houseman, G.A., McKenzie, D.P., and Molnar, P., 1981, Convective instability of a thickened boundary layer and its relevance for the thermal evolution of continental convergence belts: *Journal of Geophysical Research*, v. 86, p. 6115–6132, doi: 10.1029/JB086iB07p06115.
- Howard, K.A., 1966, Structure of the metamorphic rocks of the northern Ruby Mountains, Nevada [Ph.D. thesis]: New Haven, Yale University, 170 p.
- Howard, K.A., 1980, Metamorphic infrastructure in the northern Ruby Mountains, Nevada, in Crittenden, M.D., Jr., Coney, P.J., and Davis, G.H., eds., *Cordilleran metamorphic core complexes: Geological Society of America Memoir* 153, p. 335–347.
- Howard, K.A., 1987, Lamoille Canyon nappe in the Ruby Mountains metamorphic core complex, Nevada, in Hill, M.L., ed., *Cordilleran Section of the Geological Society of America: Geological Society of America Centennial Field Guide*, v. 1, p. 95–100.
- Howard, K.A., 2000, Geologic map of the Lamoille quadrangle, Elko County, Nevada: Nevada Bureau of Mines and Geology Map 125, scale 1:24,000, 1 sheet.
- Howard, K.A., 2003, Crustal structure in the Elko–Carlin region, Nevada, during Eocene gold mineralization: Ruby–East Humboldt metamorphic core complex as a guide to the deep crust: *Economic Geology and the Bulletin of the Society of Economic Geologists*, v. 98, p. 249–268.
- Hunziker, J.C., and Zingg, A., 1980, Lower Paleozoic amphibolite to granulite facies metamorphism in the Ivrea Zone (Southern Alps, northern Italy): *Schweizerische Mineralogische und Petrographische Mitteilungen*, v. 60, p. 181–213.
- Huppert, H.E., and Sparks, R.S.J., 1988, The generation of granitic magmas by intrusion of basalt into continental crust: *Journal of Petrology*, v. 29, p. 599–624.
- Hurlow, H.A., Snoke, A.W., and Hodges, K.V., 1991, Temperature and pressure of mylonitization in a Tertiary extensional shear zone, Ruby Mountains–East Humboldt Range, Nevada: *Tectonic implications: Geology*, v. 19, p. 82–86, doi: 10.1130/0091-7613(1991)019<0082:TAPOMI>2.3.CO;2.
- Hutton, D.H.W., 1982, A tectonic model for the emplacement of the Main Donegal Granite, NW Ireland: *Journal of the Geological Society of London*, v. 139, p. 615–631, doi: 10.1144/gsjgs.139.5.0615.
- Hutton, D.H.W., 1988, Granite emplacement mechanisms and tectonic controls: Inferences from deformation studies: *Transactions of the Royal Society of Edinburgh: Earth Sciences*, v. 79, p. 245–255.
- Ireland, T.R., and Gibson, G.M., 1998, SHRIMP monazite and zircon geochronology of high-grade metamorphism in New Zealand: *Journal of Metamorphic Geology*, v. 16, p. 149–167, doi: 10.1111/j.1525-1314.1998.00112.x.
- Jackson, J.A., 2002, Strength of the continental lithosphere: Time to abandon the jelly sandwich?: *GSA Today*, v. 12, no. 9, p. 4–10, doi: 10.1130/1052-5173(2002)012<0004:SOTCLT>2.0.CO;2.
- Jackson, J.A., and White, N.J., 1989, Normal faulting in the upper continental crust: Observations from regions of active extension: *Journal of Structural Geology*, v. 11, p. 15–36, doi: 10.1016/0191-8141(89)90033-3.
- Jacobson, C.E., Oyarzabal, F.R., and Haxel, G.B., 1996, Subduction and exhumation of the Pelona–Orocopia–Rand Schists, southern California: *Geology*, v. 24, p. 547–550, doi: 10.1130/0091-7613(1996)024<0547:SAEOTP>2.3.CO;2.
- Jacobson, C.E., Barth, A.P., and Grove, M., 2000, Late Cretaceous protolith age and provenance of the Pelona and Orocopia Schists, southern California: Implications for evolution of the Cordilleran margin: *Geology*, v. 28, p. 219–222, doi: 10.1130/0091-7613(2000)28<219:LCPAAP>2.0.CO;2.
- Jacobson, C.E., Grove, M., Vučić, A., Pedrick, J.N., and Ebert, K.A., 2007, Exhumation of the Orocopia Schist and associated rocks of southeastern California: Relative roles of erosion, synsubduction tectonic denudation, and middle Cenozoic extension, in Cloos, M., Carlson, W.D., Gilbert, M.C., Liou, J.G., and Sorenson, S.S., eds., *Convergent margin terranes and associated regions: A tribute to W.G. Ernst: Geological Society of America Special Paper* 419, p. 1–37, doi: 10.1130/2007.2419(01).
- Jagoutz, O., Müntener, O., Burg, J.-P., Ulmer, P., and Jagoutz, E., 2006, Lower continental crust formation through focused flow in km-scale melt conduits: The zoned ultramafic bodies of the Chilas Complex in the Kohistan island arc (NW Pakistan): *Earth and Planetary Science Letters*, v. 242, p. 320–342, doi: 10.1016/j.epsl.2005.12.005.
- Jagoutz, O., Müntener, O., Ulmer, P., Pettke, T., Burg, J.-P., Dawood, H., and Hussain, S., 2007, Petrology and mineral chemistry of lower crustal intrusions: The Chilas Complex, Kohistan (NW Pakistan): *Journal of Petrology*, v. 48, p. 1895–1953, doi: 10.1093/petrology/egm044.
- Jamieson, R.A., Culshaw, N., Beaumont, C., Nguyen, M.H., and Lee, B., 2004, Hot nappes and lumpy channels: Mid-crustal flow modes in the western Grenville orogen, in Searle, M.P., Law, R.D., and Godin, L., convenors, *Channel flow, ductile extrusion and exhumation of lower-mid crust in continental collision zones, Abstracts Volume: Geological Society of London*.
- Jan, M.Q., and Howie, R.A., 1980, Ortho- and clinopyroxenes from the pyroxene granulites of Swat Kohistan, northern Pakistan: *Mineralogical Magazine*, v. 43, p. 715–726, doi: 10.1180/minmag.1980.043.330.04.
- Jan, M.Q., and Howie, R.A., 1981, The mineralogy and geochemistry of the metamorphosed basic and ultrabasic rocks of the Jijal complex, Kohistan, NW Pakistan: *Journal of Petrology*, v. 22, p. 85–126.
- Jones, C.H., Kanimori, H., and Roecker, S.W., 1994, Missing roots and mantle “drips”: Regional P_n and teleseismic arrival times in the southern Sierra Nevada and vicinity, California: *Journal of Geophysical Research*, v. 99, p. 4567–4601, doi: 10.1029/93JB01232.
- Journey, J.M., and Friedman, R.M., 1993, The Coast Belt thrust system: Evidence of Late Cretaceous shortening in southwest British Columbia: *Tectonics*, v. 12, p. 756–775, doi: 10.1029/92TC02773.
- Kaila, K.L., Roy Chowdury, K., Reddy, P.R., Krishna, V.G., Narain, H., Subbotin, S.I., Sollogub, V.B., Chekunov, A.V., Kharetchko, G.E., Lazarenko, M.A., and Ilchenko, T.V., 1979, Crustal structure along Kavali–Udipi profile in the Indian Peninsular Shield from deep seismic sounding: *Journal of the Geological Society of India*, v. 20, p. 307–333.
- Karlstrom, K.E., and Williams, M.L., 1998, Heterogeneity of the middle crust: Implications for strength of continental lithosphere: *Geology*, v. 26, p. 815–818, doi: 10.1130/0091-7613(1998)026<0815:HOTMCI>2.3.CO;2.
- Karlstrom, K.E., and Williams, M.L., 2006, Nature and evolution of the middle crust: Heterogeneity of structure and process due to pluton-enhanced tectonism, in Brown, M., and Rushmer, T., eds., *Evolution and differentiation of continental crust: Cambridge, UK, Cambridge University Press*, p. 268–295.
- Karson, J.A., Fruh-Green, G.L., Kelley, D.S., Williams, E.A., Yoerger, D.R., and Jakuba, M., 2006, Detachment shear zone of the Atlantis Massif core complex, Mid-Atlantic Ridge, 30°N: *Geochemistry Geophysics Geosystems*, v. 7, doi: 10.1029/2005GC001109.
- Kelemen, P.B., Hanghøj, K., and Greene, A.R., 2004, One view of the geochemistry of subduction-related magmatic arcs, with an emphasis on primitive andesite and lower crust, in Rudnick, R.L., volume ed., *The crust*, v. 3:

- Treatise on geochemistry (Holland, H.D., and Turekian, K.K., exec. eds.): Oxford, Elsevier Pergamon, p. 593–659.
- Kerr, A.C., White, R.V., and Saunders, A.D., 2000, LIP reading: Recognizing oceanic plateaux in the geological record: *Journal of Petrology*, v. 41, p. 1041–1056, doi: 10.1093/ptrology/41.7.1041.
- Khan, M.A., Jan, M.Q., Windley, B.F., Tarney, J., and Thirlwall, M.F., 1989, The Chilas mafic-ultramafic igneous complex: The root of the Kohistan island arc in the Himalaya of northern Pakistan, *in* Malinconico, L.L., Jr., and Lillie, R.J., eds., *Tectonics of the western Himalayas*: Geological Society of America Memoir 232, p. 75–94.
- Khan, M.A., Jan, M.Q., and Weaver, B.L., 1993, Evolution of the lower arc crust in Kohistan, N. Pakistan: Temporal arc magmatism through early, mature, and intra-arc rift stages, *in* Treloar, P.J., and Searle, M.P., eds., *Himalayan tectonics*: Geological Society of London Special Publication 74, p. 123–138.
- Khan, M.A., Stern, R.J., Gribble, R.F., and Windley, B.F., 1997, Geochemical and isotopic constraints on subduction polarity, magma sources, and palaeogeography of the Kohistan intra-oceanic arc, northern Pakistan Himalaya: *Journal of the Geological Society of London*, v. 154, p. 935–946, doi: 10.1144/gsjgs.154.6.935.
- Khazanehdari, J., Rutter, E.H., and Brodie, K.H., 2000, High-pressure–high-temperature seismic velocity structure of the midcrustal and lower crustal rocks of the Ivrea-Verbano zone and Serie dei Laghi, NW Italy: *Journal of Geophysical Research*, v. 105, p. 13,843–13,858, doi: 10.1029/2000JB900025.
- Kidder, S., and Ducea, M.N., 2006, High temperatures and inverted metamorphism in the schist of Sierra de Salinas, California: *Earth and Planetary Science Letters*, v. 241, p. 422–437, doi: 10.1016/j.epsl.2005.11.037.
- Kidder, S., Ducea, M., Gehrels, G., Patchett, P.J., and Vervoort, J., 2003, Tectonic and magmatic development of the Salinian Coast Ridge belt, California: *Tectonics*, v. 22, p. 1058, doi: 10.1029/2002TC001409.
- Kimbrough, D.L., Tulloch, A.J., Geary, E., Coombs, D.S., and Landis, C.A., 1993, Isotopic ages from the Nelson region of South Island, New Zealand: Crustal structure and the definition of the Median tectonic zone: *Tectonophysics*, v. 225, p. 433–448, doi: 10.1016/0040-1951(93)90308-7.
- Kistler, R.W., 1990, Two different types of lithosphere in the Sierra Nevada, California, *in* Anderson, J.L., ed., *The nature and origin of Cordilleran magmatism*: Geological Society of America Memoir 174, p. 271–282.
- Kistler, R.W., Ghent, E.D., and O’Neil, J.R., 1981, Petrogenesis of garnet-w mica granites in the Ruby Mountains, Nevada: *Journal of Geophysical Research*, v. 86, p. 10,591–10,606, doi: 10.1029/JB086iB11p10591.
- Klepeis, K.A., and King, D.S., 2009, this volume, Evolution of the middle and lower crust during the transition from contraction to extension in Fiordland, New Zealand, *in* Miller, R.B., and Snoke, A.W., eds., *Crustal cross sections from the western North American Cordillera and elsewhere: Implications for tectonic and petrologic processes*: Geological Society of America Special Paper 456, doi: 10.1130/2009.2456(09).
- Klepeis, K.A., Clarke, G.L., and Rushmer, T.R., 2003, Magma transport and coupling between deformation and magmatism in the continental lithosphere: *GSA Today*, v. 13, no. 1, p. 4–11, doi: 10.1130/1052-5173(2003)013<0004:MTACBD>2.0.CO;2.
- Klepeis, K.A., Clarke, G.L., Gehrels, G., and Vervoort, J., 2004, Processes controlling vertical coupling and decoupling between the upper and lower crust of orogens: Results from Fiordland, New Zealand: *Journal of Structural Geology*, v. 26, p. 765–791, doi: 10.1016/j.jsg.2003.08.012.
- Klepeis, K.A., King, D.S., De Paoli, M., Clarke, G.L., and Gehrels, G., 2007, Interaction of strong lower and weak middle crust during lithospheric extension in western New Zealand: *Tectonics*, v. 26, p. TC4017, doi: 10.1029/2006TC002003.
- Köppel, V., 1974, Isotopic U–Pb ages of monazites and zircons from the crust–mantle transition and adjacent units of the Ivrea–Ceneri Zones (S. Alps, Italy): *Contributions to Mineralogy and Petrology*, v. 43, p. 55–70.
- Landis, C.A., and Coombs, D.S., 1967, Metamorphic belts and orogenesis in southern New Zealand: *Tectonophysics*, v. 4, p. 501–518, doi: 10.1016/0040-1951(67)90014-5.
- Law, R.D., Searle, M.P., and Godin, L., 2006, eds., *Channel flow, ductile extrusion and exhumation in continental collision zones*: Geological Society of London Special Publication 268, 620 p.
- Lee, C.-T., Yin, Q., Rudnick, R.L., Chesley, J.T., and Jacobsen, S.B., 2000, Re-Os isotopic evidence for pre-Miocene delamination of lithospheric mantle beneath the Sierra Nevada, California: *Science*, v. 289, p. 1912–1916, doi: 10.1126/science.289.5486.1912.
- Lee, C.-T., Rudnick, R.L., and Brimhall, G.H., 2001, Deep lithospheric dynamics beneath the Sierra Nevada during Mesozoic and Cenozoic as inferred from xenolith petrology: *Geochemistry Geophysics Geosystems*, v. 2, 2001GC000152.
- Lee, S.-y., Barnes, C.G., Snoke, A.W., Howard, K.A., and Frost, C.D., 2003, Petrogenesis of Mesozoic peraluminous granites in the Lamoille Canyon area, Ruby Mountains, Nevada, USA: *Journal of Petrology* v. 44, p. 713–732.
- Legg, M.R., Kamerling, M.J., and Francis, R.D., 2004, Termination of strike-slip faults at convergence zones within continental transform boundaries: Examples from the California Continental Borderland, *in* Grocott, J., et al., eds., *Vertical and decoupling in the lithosphere*: Geological Society of London Special Publication 227, p. 65–82.
- Lemiszi, P.J., and Brown, L.D., 1988, Variable crustal structure of strike-slip fault zones as observed on deep seismic reflection profiles: *Geological Society of America Bulletin*, v. 100, p. 665–676, doi: 10.1130/0016-7606(1988)100<0665:VCSOSS>2.3.CO;2.
- Levander, A., Hobbs, R.W., Smith, S.K., England, R.W., Snyder, D.B., and Holliger, K., 1994, The crust as a heterogeneous ‘optical’ medium, or ‘crocodiles in the mist’: *Tectonophysics*, v. 232, p. 281–297, doi: 10.1016/0040-1951(94)90090-6.
- Lipman, P.W., 2007, Incremental assembly and prolonged consolidation of Cordilleran magma chambers: Evidence from the southern Rocky Mountain volcanic field: *Geosphere*, v. 3, p. 42–70, doi: 10.1130/GES00061.1.
- Lush, A.P., McGrew, A.J., Snoke, A.W., and Wright, J.E., 1988, Allochthonous Archean basement in the northern East Humboldt Range, Nevada: *Geology*, v. 16, p. 349–353, doi: 10.1130/0091-7613(1988)016<0349:AABITN>2.3.CO;2.
- MacCready, T., 1996, Misalignment of quartz c-axis fabrics and lineations due to oblique final strain increments in the Ruby Mountains core complex, Nevada: *Journal of Structural Geology*, v. 18, p. 765–776, doi: 10.1016/S0191-8141(96)80010-1.
- MacCready, T., Snoke, A.W., Wright, J.E., and Howard, K.A., 1997, Mid-crustal flow during Tertiary extension in the Ruby Mountains core complex, Nevada: *Geological Society of America Bulletin*, v. 109, p. 1576–1594, doi: 10.1130/0016-7606(1997)109<1576:MCFDTE>2.3.CO;2.
- Maggi, A., Jackson, J.A., McKenzie, D., and Priestley, K., 2000, Earthquake focal depths, effective elastic thickness, and the strength of the continental lithosphere: *Geology*, v. 28, p. 495–498, doi: 10.1130/0091-7613(2000)28<495:EFDEET>2.0.CO;2.
- Mahan, K., 2006, Retrograde mica in deep crustal granulites: Implications for crustal seismic anisotropy: *Geophysical Research Letters*, v. 33, p. L24301, doi: 10.1029/2006GL028130.
- Mahan, K.H., Williams, M.L., and Baldwin, J.A., 2003, Contractional uplift of deep crustal rocks along the Legs Lake shear zone, western Churchill province, Canadian Shield: *Canadian Journal of Earth Sciences*, v. 40, p. 1085–1110, doi: 10.1139/e03-039.
- Martelat, J.-E., Lardeaux, J.M., Nicollet, C., and Rakotondrazafy, R., 2000, Strain pattern and late Precambrian deformation history in southern Madagascar: *Precambrian Research*, v. 102, p. 1–20, doi: 10.1016/S0301-9268(99)00083-2.
- Matzel, J.P., Bowring, S.A., and Miller, R.B., 2004, Protolith age of the Swakane Gneiss, North Cascades, Washington: Evidence of rapid underthrusting of sediments beneath an arc: *Tectonics*, v. 23, doi: 10.1029/2003TC001577.
- Mazzucchelli, M., and Siena, F., 1986, Geotectonic significance of the metabasites of the Kinzigite Series, Ivrea-Verbano zone (Western Italian Alps): *Tschermak’s Mineralogische und Petrographische Mitteilungen*, v. 35, p. 99–116, doi: 10.1007/BF01140842.
- McCarthy, J., and Parsons, T., 1994, Insights into the kinematic Cenozoic evolution of the Basin and Range–Colorado Plateau transition from coincident seismic refraction and reflection data: *Geological Society of America Bulletin*, v. 106, p. 747–759, doi: 10.1130/0016-7606(1994)106<0747:IITKCE>2.3.CO;2.
- McCarthy, J., and Thompson, G.A., 1988, Seismic imaging of extended crust with emphasis on the western United States: *Geological Society of America Bulletin*, v. 100, p. 1361–1374, doi: 10.1130/0016-7606(1988)100<1361:SIOECW>2.3.CO;2.
- McGrew, A.J., 1992, *Tectonic evolution of the northern East Humboldt Range, Elko County, Nevada* [Ph.D. thesis]: Laramie, University of Wyoming, 191 p.
- McGrew, A.J., and Casey, M., 1998, Quartzite fabric transition in a Cordilleran metamorphic core complex, *in* Snoke, A.W., Tullis, J., and Todd, V.R.,

- eds., *Fault-related rocks: A photographic atlas*: Princeton, New Jersey, Princeton University Press, p. 484–489.
- McGrew, A.J., and Snee, L.W., 1994, $^{40}\text{Ar}/^{39}\text{Ar}$ thermochronologic constraints on the tectonothermal evolution of the northern East Humboldt Range metamorphic core complex, Nevada: *Tectonophysics*, v. 238, p. 425–450, doi: 10.1016/0040-1951(94)90067-1.
- McGrew, A.J., Peters, M.T., and Wright, J.E., 2000, Thermobarometric constraints on the tectonothermal evolution of the East Humboldt Range metamorphic core complex, Nevada: *Geological Society of America Bulletin*, v. 112, p. 45–60, doi: 10.1130/0016-7606(2000)112<0045:TCOTTE>2.3.CO;2.
- Mehl, L., Hacker, B.R., Hirth, G., and Kelemen, P.B., 2003, Arc-parallel flow within the mantle wedge: Evidence from the accreted Talkeetna arc, south central Alaska: *Journal of Geophysical Research*, v. 108, p. 2375, doi: 10.1029/2002JB002233.
- Mehnert, K., 1975, The Ivrea zone: A model of the deep crust: *Neues Jahrbuch für Mineralogie-Abhandlungen*, v. 125, p. 156–199.
- Meissner, R., Rabbel, W., and Kern, H., 2006, Seismic lamination and anisotropy of lower continental crust: *Tectonophysics*, v. 416, p. 81–99, doi: 10.1016/j.tecto.2005.11.013.
- Miller, E.L., and Gans, P.B., 1989, Cretaceous crustal structure and metamorphism in the hinterland of the Sevier thrust belt, western U.S. Cordillera: *Geology*, v. 17, p. 59–62, doi: 10.1130/0091-7613(1989)017<0059:CCSAMI>2.3.CO;2.
- Miller, E.L., Gans, P.B., and Garing, J., 1983, The Snake Range decollement: An exhumed mid-Tertiary ductile-brittle transition: *Tectonics*, v. 2, p. 239–263, doi: 10.1029/TC002i003p00239.
- Miller, R.B., 1994, A mid-crustal contractional stepover zone in a major strike-slip system, North Cascades, Washington: *Journal of Structural Geology*, v. 16, p. 47–60, doi: 10.1016/0191-8141(94)90017-5.
- Miller, R.B., and Paterson, S.R., 2001, Influence of lithological heterogeneity, mechanical anisotropy, and magmatism on the rheology of an arc, North Cascades, Washington: *Tectonophysics*, v. 342, p. 351–370, doi: 10.1016/S0040-1951(01)00170-6.
- Miller, R.B., Paterson, S.R., Lebit, H., Alsleben, H., and Luneburg, C., 2006, Significance of composite lineations in the mid- to deep crust: A case study from the North Cascades, Washington: *Journal of Structural Geology*, v. 28, p. 302–322, doi: 10.1016/j.jsg.2005.11.003.
- Miller, R.B., Paterson, S.R., and Matzel, J.P., 2009, this volume, Plutonism at different crustal levels: Insights from the ~5–40 km (paleodepth) North Cascades crustal section, Washington, in Miller, R.B., and Snoke, A.W., eds., *Crustal cross sections from the western North American Cordillera and elsewhere: Implications for tectonic and petrologic processes*: Geological Society of America Special Paper 456, doi: 10.1130/2009.2456(05).
- Molnar, P., England, P., and Martinod, J., 1993, Mantle dynamics, uplift of the Tibetan Plateau, and the Indian monsoon: *Reviews of Geophysics*, v. 31, p. 357–396, doi: 10.1029/93RG02030.
- Mortimer, N., Tulloch, A.J., Spark, R.N., Walker, N.W., Ladley, E., Allibone, A.H., and Kimbrough, D.L., 1999, Overview of the Median batholith, New Zealand: A new interpretation of the geology of the Median tectonic zone and adjacent rocks: *Journal of African Earth Sciences*, v. 29, p. 257–268, doi: 10.1016/S0899-5362(99)00095-0.
- Mueller, K.J., and Snoke, A.W., 1993a, Cenozoic basin development and normal fault systems associated with the exhumation of metamorphic complexes in northeast Nevada, in Lahren, M.M., Trexler, J.H., Jr., and Spinoso, C., eds., *Crustal evolution of the Great Basin and Sierra Nevada: Cordilleran/Rocky Mountain Section*, Geological Society of America Guidebook, Department of Geological Sciences, University of Nevada, Reno, p. 1–34.
- Mueller, K.J., and Snoke, A.W., 1993b, Progressive overprinting of normal fault systems and their role in Tertiary exhumation of the East Humboldt-Wood Hills metamorphic complex, northeast Nevada: *Tectonics*, v. 12, p. 361–371, doi: 10.1029/92TC01967.
- Nadin, E.S., and Saleeby, J.B., 2008, Disruption of regional primary structure of the Sierra Nevada batholith by the Kern Canyon fault system, California, in Wright, J.E., and Shervais, J.W., eds., *Ophiolites, arcs, and batholiths: A tribute to Cliff Hopson*: Geological Society of America Special Paper 438, p. 429–454, doi: 10.1130/2008.2438(15).
- Needy, S.K., Anderson, J.L., Wooden, J.L., Fleck, R.J., Barth, A.P., Paterson, S.R., Memeti, V., and Pignotta, G.S., 2009, this volume, Mesozoic magmatism in an upper- to middle-crustal section through the Cordilleran continental margin arc, eastern Transverse Ranges, California, in Miller, R.B., and Snoke, A.W., eds., *Crustal cross sections from the western North American Cordillera and elsewhere: Implications for tectonic and petrologic processes*: Geological Society of America Special Paper 456, doi: 10.1130/2009.2456(07).
- Nelson, K.D., Zhao, W., Brown, L.D., Kuo, J., Jinkai Che, Xianwen Liu, Klemperer, S.L., Makovsky, Y., Meissner, R., Mechie, J., Kind, R., Wenzel, F., Ni, J., Nabelek, J., Chen Leshou, Handong Tan, Wenbo Wei, Jones, A.G., Booker, J., Unsworth, M., Kidd, W.S.F., Hauck, M., Alsdorf, D., Ross, A., Cogan, R., Changde Wu, Sandvol, E., and Edwards, M., 1996, Partially molten middle crust beneath southern Tibet; synthesis of Project INDEPTH results: *Science*, v. 274, p. 1684–1688, doi: 10.1126/science.274.5293.1684.
- Newton, R.C., 1990, The late Archean high-grade terrain of South India and the deep structure of the Dharwar craton, in Salisbury, M.H., and Fountain, D.M., eds., *Exposed cross-sections of the continental crust*: Dordrecht, the Netherlands, Kluwer Academic Publishers, p. 305–326.
- O'Brien, P.J., and Rötzler, J., 2003, High-pressure granulites: Formation, recovery of peak conditions and implications for tectonics: *Journal of Metamorphic Geology*, v. 21, p. 3–20, doi: 10.1046/j.1525-1314.2003.00420.x.
- Oldow, J.S., Bally, A.W., Avé Lallemant, H.G., and Leeman, W.P., 1990, Transpression, orogenic float, and lithospheric balance: *Geology*, v. 18, p. 991–994, doi: 10.1130/0091-7613(1990)018<0991:TOFALB>2.3.CO;2.
- Oliver, G.J.H., 1977, Feldspathic hornblende and garnet granulites and associated anorthosite pegmatites from Doubtful Sound, Fiordland, New Zealand: *Contributions to Mineralogy and Petrology*, v. 65, p. 111–121, doi: 10.1007/BF00371051.
- Oliver, G.J.H., 1980, Geology of the granulite and amphibolite facies gneisses of Doubtful Sound, Fiordland, New Zealand: *New Zealand Journal of Geology and Geophysics*, v. 23, p. 27–41.
- Oliver, G.J.H., 1990, An exposed cross-section of continental crust, Doubtful Sound, Fiordland, New Zealand: Geophysical & geological setting, in Salisbury, M.H., and Fountain, D.M., eds., *Exposed cross-sections of the continental crust*: Dordrecht, the Netherlands, Kluwer Academic Publishers, p. 43–69.
- Parrish, R.R., 1995, Thermal evolution of the southeastern Canadian Cordillera: *Canadian Journal of Earth Sciences*, v. 32, p. 1618–1642.
- Paterson, S.R., and Farris, D.W., 2008, Downward host rock transport and the formation of rim monoclines during the emplacement of Cordilleran batholiths: *Transactions of the Royal Society of Edinburgh: Earth Sciences; Special Issue: Plutons and batholiths (The Wallace Pitcher Memorial Volume)*, v. 97, p. 397–413.
- Paterson, S.R., and Vernon, R.H., 1995, Bursting the bubble of ballooning plutons—A return to nested diapirs emplaced by multiple processes: *Geological Society of America Bulletin*, v. 107, p. 1356–1380, doi: 10.1130/0016-7606(1995)107<1356:BTBOBP>2.3.CO;2.
- Paterson, S.R., Fowler, T.K., Jr., and Miller, R.B., 1996, Pluton emplacement in arcs: A crustal-scale exchange process: *Transactions of the Royal Society of Edinburgh: Earth Sciences*, v. 87, p. 115–124.
- Paterson, S.R., Vernon, R.H., and Fowler, T.K., Jr., 1991, Aureole tectonics, in Kerrick, D.M., ed., *Contact metamorphism*: Chelsea, Michigan, Mineralogical Society of America, *Reviews in Mineralogy*, v. 26, p. 673–722.
- Paterson, S.R., Miller, R.B., Alsleben, H., Whitney, D.L., Valley, P.M., and Hurlow, H., 2004, Driving mechanisms for 40 km of exhumation during contraction and extension in a continental arc, Cascades core, Washington: *Tectonics*, v. 23, doi: 10.1029/2002TC001440.
- Peacock, S., and Hudson, J.A., 1990, Seismic properties of rocks with distributions of small cracks: *Geophysical Journal International*, v. 102, p. 471–484, doi: 10.1111/j.1365-246X.1990.tb04479.x.
- Percival, J.A., 1990, A field guide to the Kapuskasing uplift, a cross section through the Archean Superior province, in Salisbury, M.H., and Fountain, D.M., eds., *Exposed cross-sections of the continental crust*: Dordrecht, the Netherlands, Kluwer Academic Publishers, p. 227–283.
- Percival, J.A., Fountain, D.M., and Salisbury, M.H., 1992, Exposed crustal cross sections as windows on the lower crust, in Fountain, D.M., Arculus, R., and Kay, R.W., eds., *Continental lower crust*: Amsterdam, the Netherlands, Elsevier, p. 317–362.
- Peressini, G., Quick, J.E., Singoi, S., Hofmann, A.W., and Fanning, M., 2007, Duration of a large mafic intrusion and heat transfer in the lower crust: A SHRIMP U-Pb zircon study in the Ivrea-Verbano zone (Western Alps, Italy): *Journal of Petrology*, v. 48, p. 1185–1218, doi: 10.1093/petrology/egm014.

- Petterson, M.G., and Windley, B.F., 1985, Rb-Sr dating of the Kohistan arc batholith in the Trans-Himalaya of north Pakistan, and tectonic implications: *Earth and Planetary Science Letters*, v. 74, p. 45–57, doi: 10.1016/0012-821X(85)90165-7.
- Petterson, M.G., and Windley, B.F., 1991, Changing source regions of magmas and crustal growth in the Trans-Himalayas: Evidence from the Chalt volcanics and Kohistan batholith, Kohistan, northern Pakistan: *Earth and Planetary Science Letters*, v. 102, p. 326–341, doi: 10.1016/0012-821X(91)0027-F.
- Pickett, D.A., and Saleeby, J.B., 1993, Thermobarometric constraints on the depth of exposure and conditions of plutonism and metamorphism at deep levels of the Sierra Nevada batholith, Tehachapi Mountains, California: *Journal of Geophysical Research*, v. 98, p. 609–629, doi: 10.1029/92JB01889.
- Pili, E., Ricard, Y., Lardeaux, J.-M., and Sheppard, S.M.F., 1997, Lithospheric shear zones and mantle-crust connections: *Tectonophysics*, v. 280, p. 15–29, doi: 10.1016/S0040-1951(97)00142-X.
- Pin, C., 1986, Datation U-Pb sur zircons à 285 Ma du complexe du gabbro-dioritique du Val Sesia-Val Mastellone et age tardi-Hercynien du métamorphisme granulitique de la zone Ivrea-Verbano (Italie): *Comptes Rendus de l'Académie des Sciences, Série 2, Mécanique, Physique, Chimie, Sciences de l'Univers: Sciences de la Terre*, v. 303, p. 827–830.
- Pitcher, W.S., 1979, The nature, ascent and emplacement of granitic magmas: *Journal of the Geological Society of London*, v. 136, p. 627–662, doi: 10.1144/gsjgs.136.6.627.
- Pitcher, W.S., and Berger, A.R., 1972, *The geology of Donegal: A study of granite emplacement and unroofing: Regional Geology Series*: New York, Wiley Interscience, 435 p.
- Plafker, G., Nokleberg, W.J., and Lull, J.S., 1989, Bedrock geology and tectonic evolution of the Wrangellia, Peninsular, and Chugach terranes along the trans-Alaska crustal transect in the Chugach Mountains and southern Copper River basin, Alaska: *Journal of Geophysical Research*, v. 94, p. 4255–4295, doi: 10.1029/JB094iB04p04255.
- Platt, J.P., 1986, Dynamics of orogenic wedges and the uplift of high-pressure metamorphic rocks: *Geological Society of America Bulletin*, v. 97, p. 1037–1053, doi: 10.1130/0016-7606(1986)97<1037:DOOWAT>2.0.CO;2.
- Platt, J.P., 1993, Exhumation of high-pressure rocks: A review of concepts and processes: *Terra Nova*, v. 5, p. 119–133, doi: 10.1111/j.1365-3121.1993.tb00237.x.
- Platt, J.P., and Behrmann, J.H., 1986, Structure and fabrics in a crustal-scale shear zone, Betic Cordillera, SE Spain: *Journal of Structural Geology*, v. 8, p. 15–33, doi: 10.1016/0191-8141(86)90014-3.
- Platt, J.P., and Vissers, R.L.M., 1989, Extensional collapse of thickened continental lithosphere: A working hypothesis for the Alboran Sea and the Gibraltar arc: *Geology*, v. 17, p. 540–543, doi: 10.1130/0091-7613(1989)017<0540:ECOTCL>2.3.CO;2.
- Platt, J.P., van den Eeckhout, B., Janzen, E., Konert, G., Simon, O.J., and Weijermars, R., 1983, The structure and tectonic evolution of the Aguilón fold-nappe, Sierra Alhamilla, Betic Cordilleras, SE Spain: *Journal of Structural Geology*, v. 5, p. 519–538, doi: 10.1016/0191-8141(83)90057-3.
- Platt, J.P., Behrmann, J.H., Martínez, J.-M.M., and Vissers, R.L.M., 1984, A zone of mylonite and related ductile deformation beneath the Alpujarride nappe complex, Betic Cordilleras, S. Spain: *Geologische Rundschau*, v. 73, p. 773–785, doi: 10.1007/BF01824981.
- Platt, J.P., Argles, T.W., Carter, A., Kelley, S.P., Whitehouse, M.J., and Loneragan, L., 2003, Exhumation of the Ronda peridotite and its crustal envelope: Constraints from thermal modeling of a *P–T–time* array: *Journal of the Geological Society of London*, v. 160, p. 655–676, doi: 10.1144/0016-764902-108.
- Platt, J.P., Kelley, S.P., Carter, A., and Orozco, M., 2005, Timing of tectonic events in the Alpujarride Complex, Betic Cordillera, southern Spain: *Journal of the Geological Society of London*, v. 162, p. 451–462, doi: 10.1144/0016-764903-039.
- Platt, J.P., Anczkiewicz, R., Soto, J.-I., Kelley, S.P., and Thirlwall, M., 2006, Early Miocene continental subduction and rapid exhumation in the western Mediterranean: *Geology*, v. 34, p. 981–984, doi: 10.1130/G22801A.1.
- Pohl, M., Wenzel, F., Weiss, T., Siegesmund, S., Bohlen, T., and Rabbel, W., 1999, Realistic models of anisotropic laminated lower crust: Pure and Applied Geophysics, v. 156, p. 139–156, doi: 10.1007/s000240050293.
- Pudsey, C.J., 1986, The Northern Suture, Pakistan: Margin of a Cretaceous island arc: *Geological Magazine*, v. 123, p. 405–423.
- Quick, J.E., Sinigoi, S., and Mayer, A., 1992, Synmagmatic deformation in the underplated igneous complex of the Ivrea-Verbano zone: *Geology*, v. 20, p. 613–616, doi: 10.1130/0091-7613(1992)020<0613:SDITUI>2.3.CO;2.
- Quick, J.E., Sinigoi, S., and Mayer, A., 1994, Emplacement dynamics of a large mafic intrusion in the lower crust, Ivrea-Verbano zone, northern Italy: *Journal of Geophysical Research*, v. 99, p. 21,559–21,573, doi: 10.1029/94JB00113.
- Quick, J.E., Sinigoi, S., and Mayer, A., 1995, Emplacement of mantle peridotite in the lower continental crust, Ivrea-Verbano zone, northwest Italy: *Geology*, v. 23, p. 739–742, doi: 10.1130/0091-7613(1995)023<0739:EOMPIT>2.3.CO;2.
- Quick, J.E., Sinigoi, S., Snoke, A.W., Kalakay, T.J., and Mayer, A., 2003, Geological map of Ivrea zone with explanatory notes: U.S. Geological Survey Miscellaneous Field Investigations Map I-2776, scale 1:50,000, 1 sheet and 22 p. pamphlet.
- Rabbel, W., Siegesmund, S., Weiss, T., Pohl, M., and Bohlen, T., 1998, Shear wave anisotropy of laminated lower crust beneath Urach (SW Germany): A comparison with xenoliths and with exposed lower crustal sections: *Tectonophysics*, v. 298, p. 337–356, doi: 10.1016/S0040-1951(98)00174-7.
- Ranalli, G., 1995, *Rheology of the Earth*: London, Chapman and Hall, 413 p.
- Ranero, C.R., and Reston, T.J., 1999, Detachment faulting at oceanic core complexes: *Geology*, v. 27, p. 983–986, doi: 10.1130/0091-7613(1999)027<0983:DFAOCC>2.3.CO;2.
- Rapp, R.P., and Watson, E.B., 1995, Dehydration melting of metabasalts at 8–32 kbar: Implications of continental growth and crust-mantle recycling: *Journal of Petrology*, v. 35, p. 891–931.
- Read, P.B., and Brown, R.L., 1981, Columbia River fault zone: Southeastern margin of the Shuswap and Monashee complexes, southern British Columbia: *Canadian Journal of Earth Sciences*, v. 18, p. 1127–1145.
- Ring, U., Brandon, M.T., Willett, S.D., and Lister, G.S., 1999, Exhumation processes, in Ring, U., Brandon, M.T., Willett, S.D., and Lister, G.S., eds., *Exhumation processes: Normal faulting, ductile flow and erosion*: Geological Society of London Special Publication 154, p. 1–27.
- Rivalenti, G., Garuti, G., and Rossi, A., 1975, The origin of the Ivrea-Verbano Basic Formation (western Italian Alps)—Whole rock geochemistry: *Bollettino della Società Geologica Italiana*, v. 94, p. 1149–1186.
- Rivalenti, G., Garuti, G., Rossi, A., Siena, F., and Sinigoi, S., 1981, Existence of different peridotite types and of a layered igneous complex in the Ivrea zone of the Western Alps: *Journal of Petrology*, v. 22, p. 127–153.
- Rivalenti, G., Rossi, A., and Sinigoi, S., 1984, The layered series of the Ivrea igneous complex: *Tschermak's Mineralogische und Petrographische Mitteilungen*, v. 33, p. 77–99, doi: 10.1007/BF01083065.
- Royden, L.H., 1996, Coupling and decoupling of crust and mantle in convergent orogens: Implications for strain partitioning in the crust: *Journal of Geophysical Research*, v. 101, p. 17,679–17,705, doi: 10.1029/96JB00951.
- Rubin, C.M., Saleeby, J.B., Cowan, D.S., Brandon, M.T., and McGroder, M.F., 1990, Regionally extensive mid-Cretaceous west-vergent thrust system in the Northwestern Cordillera: *Geology*, v. 18, p. 276–280, doi: 10.1130/0091-7613(1990)018<0276:REMCWV>2.3.CO;2.
- Rudnick, R.L., 1992, Xenoliths—Samples of the lower continental crust, in Fountain, D.M., Arculus, R., and Kay, R.W., eds., *Continental lower crust*: Amsterdam, Elsevier, *Developments in Geotectonics* 23, p. 269–316.
- Rudnick, R.L., 1995, Making continental crust: *Nature*, v. 378, p. 571–578, doi: 10.1038/378571a0.
- Rudnick, R.L., and Fountain, D.M., 1995, Nature and composition of the continental crust: A lower crustal perspective: *Reviews of Geophysics*, v. 33, p. 267–309, doi: 10.1029/95RG01302.
- Rudnick, R.L., and Gao, S., 2004, Composition of the continental crust, in Rudnick, R.L., ed., *The crust*, in Rudnick, R.L., volume ed., *The crust*, v. 3: *Treatise on geochemistry* (Holland, H.D., and Turekian, K.K., exec. eds.): Oxford, Elsevier Pergamon, p. 593–659.
- Ruppert, S., Fliedner, M.M., and Zandt, G., 1998, Thin crust and active upper mantle beneath the southern Sierra Nevada in the western United States: *Tectonophysics*, v. 286, p. 237–252, doi: 10.1016/S0040-1951(97)00268-0.
- Rutter, E.H., 1997, The influence of deformation on the extraction of crustal melts: A consideration of the role of melt-assisted granular flow, in Holness, M.B., ed., *Deformation-enhanced fluid transport in the Earth's crust and mantle*: London, UK, Chapman & Hall, p. 82–110.

- Rutter, E.H., and Brodie, K.H., 1992, Rheology of the lower crust, *in* Fountain, D.M., Arculus, R., and Kay, R.W., eds., *Continental lower crust: Amsterdam, Elsevier, Developments in Geotectonics* 23, p. 201–267.
- Rutter, E.H., and Neumann, D.H.K., 1995, Experimental deformation of partially molten Westerly granite, with implications for the extraction of granitic magmas: *Journal of Geophysical Research*, v. 100, p. 15,697–15,715, doi: 10.1029/94JB03388.
- Rutter, E.H., Brodie, K.H., and Evans, P.E., 1993, Structural geometry, lower crustal magmatic underplating and lithospheric stretching in the Ivrea-Verbano zone, northern Italy: *Journal of Structural Geology*, v. 15, p. 647–662, doi: 10.1016/0191-8141(93)90153-2.
- Rutter, E.H., Khazanehdari, J., Brodie, K.H., Blundell, D.J., and Waltham, D.A., 1999, Synthetic seismic reflection profile through the Ivrea zone—Serie dei Laghi continental crustal section, northwestern Italy: *Geology*, v. 27, p. 79–82, doi: 10.1130/0091-7613(1999)027<0079:SSRPTT>2.3.CO;2.
- Rutter, E., Brodie, K., James, T., and Burlini, L., 2007, Large-scale folding in the upper part of the Ivrea-Verbano zone, NW Italy: *Journal of Structural Geology*, v. 29, p. 1–17, doi: 10.1016/j.jsg.2006.08.013.
- Saleeby, J.B., 1990, Progress in tectonic and petrogenetic studies in an exposed cross-section of young (~100 Ma) continental crust, southern Sierra Nevada, California, *in* Salisbury, M.H., and Fountain, D.M., eds., *Exposed cross-sections of the continental crust: Dordrecht, the Netherlands, Kluwer Academic Publishers*, p. 137–158.
- Saleeby, J.B., 2003, Segmentation of the Laramide—Evidence from the southern Sierra Nevada region: *Geological Society of America Bulletin*, v. 115, p. 655–668, doi: 10.1130/0016-7606(2003)115<0655:SOTLSF>2.0.CO;2.
- Saleeby, J.B., Ducea, M., and Clemens-Knott, D., 2003, Production and loss of high-density batholithic root—Southern Sierra Nevada, California: *Tectonics*, v. 22, doi: 10.1029/2002TC001374.
- Saleeby, J.B., Farley, K.A., Kistler, R.W., and Fleck, R., 2007, Thermal evolution and exhumation of deep-level batholithic exposures, southernmost Sierra Nevada, California, *in* Cloos, M., Carlson, W.D., Gilbert, M.C., Liou, J.G., and Sorenson, S.S., eds., *Convergent margin terranes and associated regions: A tribute to W.G. Ernst: Geological Society of America Special Paper* 419, p. 39–66, doi: 10.1130/2007.2419(02).
- Saleeby, J.B., Ducea, M.N., Busby, C.J., Nadin, E.S., and Wetmore, P.H., 2008, Chronology of pluton emplacement in the southern Sierra Nevada batholith, California, *in* Wright, J.E., and Shervais, J.W., eds., *Ophiolites, arcs, and batholiths: A tribute to Cliff Hopson: Geological Society of America Special Paper* 438, p. 397–427, doi: 10.1130/2008.2438(14).
- Salisbury, M., and Fountain, D., 1990, eds., *Exposed cross-sections of the continental crust: Dordrecht, the Netherlands, Kluwer Academic Publishers*, 662 p.
- Sams, D.B., and Saleeby, J.B., 1988, Geology and petrotectonic significance of crystalline rocks of the southernmost Sierra Nevada, California, *in* Ernst, W.G., ed., *Rubey Volume VII, Metamorphism and crustal evolution in the western United States: Englewood Cliffs, New Jersey, Prentice-Hall*, p. 866–893.
- Sandiford, M., and Powell, R., 1986, Deep crustal metamorphism during continental extension: Modern and ancient examples: *Earth and Planetary Science Letters*, v. 79, p. 151–158, doi: 10.1016/0012-821X(86)90048-8.
- Schaltegger, U., Zeilinger, G., Frank, M., and Burg, J.-P., 2002, Multiple mantle sources during island arc magmatism: U-Pb and Hf isotopic evidence from the Kohistan arc complex, Pakistan: *Terra Nova*, v. 14, p. 461–468, doi: 10.1046/j.1365-3121.2002.00432.x.
- Schilling, F.R., and Partzsch, G.M., 2001, Quantifying partial melt fraction in the crust beneath the central Andes and the Tibetan Plateau: *Physics and Chemistry of the Earth*, v. 26, p. 239–246, doi: 10.1016/S1464-1895(01)00051-5.
- Schmid, R., 1978–1979, Are the metapelites in the Ivrea zone restites?: *Memorie degli Istituti di Geologia e Mineralogia dell'Università di Padova*, v. 33, p. 67–69.
- Schmid, R., and Wood, B.J., 1976, Phase relationships in granulitic metapelites from the Ivrea-Verbano zone (Northern Italy): *Contributions to Mineralogy and Petrology*, v. 54, p. 255–279, doi: 10.1007/BF00389407.
- Schmid, S.M., 1993, Ivrea zone and adjacent Southern Alpine basement, *in* von Raumer, J.F., and Neubauer, F., eds., *Pre-Mesozoic geology in the Alps: Berlin, Springer-Verlag*, p. 567–583.
- Schmid, S.M., Zingg, A., and Handy, M., 1987, The kinematics of movement along the Insubric line and the emplacement of the Ivrea zone: *Tectonophysics*, v. 135, p. 47–66, doi: 10.1016/0040-1951(87)90151-X.
- Schmid, S.M., Aebli, H.R., Heller, F., and Zingg, A., 1989, The role of the Periadriatic line in the tectonic evolution of the Alps, *in* Coward, M.P., Dietrich, D., and Park, R.G., eds., *Alpine tectonics: Geological Society of London Special Publication* 45, p. 153–171.
- Schmid, S.M., Fügenschuh, B., Kissling, E., and Schuster, E., 2004, Tectonic map and overall architecture of the Alpine orogen: *Eclogae Geologicae Helvetiae*, v. 97, p. 93–117, doi: 10.1007/s00015-004-1113-x.
- Schnetger, B., 1994, Partial melting during the evolution of the amphibolite- to granulite-facies gneisses of the Ivrea zone, northern Italy: *Chemical Geology*, v. 113, p. 71–101, doi: 10.1016/0009-2541(94)90006-X.
- Scholl, D.W., and von Huene, R., 2007, Crustal recycling at modern subduction zones applied to the past—Issues of growth and preservation of continental basement crust, mantle geochemistry, and supercontinent reconstruction, *in* Hatcher, R.D., Jr., Carlson, M.P., McBride, J.H., and Martínez Catalán, J.R., eds., *4-D framework of continental crust: Geological Society of America Memoir* 200, p. 9–32, doi: 10.1130/2007.1200(02).
- Scholz, C.H., 1990, *The mechanics of earthquakes and faulting: Cambridge, UK, Cambridge University Press*, 439 p.
- Searle, M.P., Asif Khan, M., Fraser, J.E., and Gough, S.J., 1999, The tectonic evolution of the Kohistan-Karakoram collision belt along the Karakoram Highway transect, north Pakistan: *Tectonics*, v. 18, p. 929–949, doi: 10.1029/1999TC900042.
- Seber, D., Barazangi, M., Ibenbrahim, A., and Demnati, A., 1996, Geophysical evidence for lithospheric delamination beneath the Alboran Sea and Rif-Betic Mountains: *Nature*, v. 379, p. 785–790, doi: 10.1038/379785a0.
- Shervais, J.W., 1979, Thermal emplacement model for the alpine lherzolite massif at Balmuccia, Italy: *Journal of Petrology*, v. 20, p. 795–820.
- Shervais, J.W., and Mukasa, S.B., 1991, The Balmuccia orogenic lherzolite massif, Italy: *Journal of Petrology, Special Lherzolites Issue*, p. 155–174.
- Sibson, R.H., 1977, Fault rocks and fault mechanics: *Journal of the Geological Society of London*, v. 133, p. 191–213, doi: 10.1144/gsjgs.133.3.0191.
- Sills, J.D., 1984, Granulite facies metamorphism in the Ivrea zone, N.W. Italy: *Schweizerische Mineralogische und Petrographische Mitteilungen*, v. 64, p. 169–191.
- Sills, J.D., and Tarney, J., 1984, Petrogenesis and tectonic significance of amphibolites interlayered with metasedimentary gneisses in the Ivrea zone, Southern Alps, NW Italy: *Tectonophysics*, v. 107, p. 187–206, doi: 10.1016/0040-1951(84)90251-8.
- Smithson, S.B., 1978, Modeling continental crust: Structural and chemical constraints: *Geophysical Research Letters*, v. 5, p. 749–752, doi: 10.1029/GL005i009p00749.
- Snoke, A.W., 2005, Southern Cordillera, *in* Selley, R.C., Cocks, L.R.M., and Plimer, I.R., eds., *Encyclopedia of geology*, v. 4: Amsterdam, Academic Press, p. 48–61.
- Snoke, A.W., and Barnes, C.G., 2006, The development of tectonic concepts for the Klamath Mountains province, California and Oregon, *in* Snoke, A.W., and Barnes, C.G., eds., *Geological studies in the Klamath Mountains Province, California and Oregon—A volume in honor of William P. Irwin: Geological Society of America Special Paper* 410, p. 1–29.
- Snoke, A.W., and Lush, A.P., 1984, Polyphase Mesozoic-Cenozoic deformational history of the northern Ruby Mountains—East Humboldt Range, Nevada, *in* Lintz, J., Jr., ed., *Western geological excursions*, v. 4, Geological Society of America 1984 Annual Meeting, Reno, Nevada, p. 232–260.
- Snoke, A.W., McGrew, A.J., Valasek, P.A., and Smithson, S.B., 1990, A crustal cross-section for a terrain of superimposed shortening and extension: Ruby Mountains—East Humboldt Range metamorphic core complex, Nevada, *in* Salisbury, M.H., and Fountain, D.M., eds., *Exposed cross-sections of the continental crust: Dordrecht, the Netherlands, Kluwer Academic Publishers*, p. 103–135.
- Snoke, A.W., Howard, K.A., McGrew, A.J., Burton, B.R., Barnes, C.G., Peters, M.T., and Wright, J.E., 1997, The grand tour of the Ruby—East Humboldt metamorphic core complex, northeastern Nevada: Part 1—Introduction & road log, *in* Link, P.K., and Kowallis, B.J., eds., *Proterozoic to Recent stratigraphy, tectonics, and volcanology, Utah, Nevada, southern Idaho and central Mexico: Provo, Utah, Brigham Young University Geology Studies*, v. 42, Part 1, p. 225–269.
- Snoke, A.W., Kalakay, T.J., Quick, J.E., and Sinigoi, S., 1999, Development of a deep-crustal shear zone in response to syntectonic intrusion of mafic magma into the lower crust, Ivrea-Verbano zone, Italy: *Earth and Planetary Science Letters*, v. 166, p. 31–45, doi: 10.1016/S0012-821X(98)00280-5.
- Sonder, L.J., England, P.C., Wernicke, B.P., and Christiansen, R.L., 1987, A physical model for Cenozoic extension of western North America, *in*

- Coward, M.P., Dewey, J.F., and Hancock, P.L., eds., Continental extensional tectonics: Geological Society of London Special Publication 28, p. 187–201.
- Soper, N.J., and Higgins, A.K., 1993, Basement–cover relationships in the East Greenland Caledonides: Evidence from the Eleonore Bay Supergroup at Ardencape Fjord: *Transactions of the Royal Society of Edinburgh: Earth Sciences*, v. 84, p. 103–115.
- Spell, T.L., McDougall, I., and Tulloch, A.J., 2000, Thermochronological constraints on the breakup of the Pacific Gondwana margin: The Paparoa metamorphic core complex, South Island, New Zealand: *Tectonics*, v. 19, p. 433–451, doi: 10.1029/1999TC900046.
- Steiger, R.H., Hansen, B.T., Schuler, Ch., Bär, M.T., and Henriksen, N., 1979, Polyorogenic nature of the southern Caledonian fold belt in East Greenland: An isotopic age study: *Journal of Geology*, v. 87, p. 475–495.
- Stern, T.W., Bateman, P.C., Morgan, B.A., Newell, M.F., and Peck, D.L., 1981, Isotopic U–Pb ages of zircon from the granitoids of the central Sierra Nevada, California: U.S. Geological Society of America Professional Paper 1185, 17 p.
- Stevenson, C.T.E., Hutton, D.H.W., and Price, A.R., 2008, The Trawenagh Bay Granite and a new model for the emplacement of the Donegal batholith: *Transactions of the Royal Society of Edinburgh: Earth Sciences*, v. 97, p. 455–477, doi: 10.1017/S0263593300001565.
- Stowell, H.H., and Crawford, M.L., 2000, Metamorphic history of the Coast Mountains orogen, western British Columbia and southeastern Alaska, *in* Stowell, H.H., and McClelland, W.C., eds., *Tectonics of the Coast Mountains, southeastern Alaska and British Columbia*: Geological Society of America Special Paper 343, p. 257–283.
- Sullivan, W.A., and Snoke, A.W., 2007, Comparative anatomy of core–complex development in the northeastern Great Basin, U.S.A.: *Rocky Mountain Geology*, v. 42, p. 1–29, doi: 10.2113/gsrocky42.1.1.
- Sylvester, A.G., 1988, Strike-slip faults: Geological Society of America Bulletin, v. 100, p. 1666–1703, doi: 10.1130/0016-7606(1988)100<1666:SSF>2.3.CO;2.
- Taylor, S.R., and McClennan, S.M., 1985, *The continental crust: Its composition and evolution*: Oxford, UK, Blackwell Scientific Publications, 312 p.
- Teyssier, C., and Tikoff, B., 1998, Strike-slip partitioned transpression of the San Andreas fault system: A lithospheric scale approach, *in* Holdsworth, R., Strachan, R.A., and Dewey, J.F., eds., *Continental transpression and transtension tectonics*: Geological Society of London Special Publication 135, p. 143–158.
- Teyssier, C., and Whitney, D.L., 2002, Gneiss domes and orogeny: *Geology*, v. 30, p. 1139–1142, doi: 10.1130/0091-7613(2002)030<1139:GDAO>2.0.CO;2.
- Teyssier, C., Ferre, E.C., Whitney, D.L., Norlander, B., Vanderhaeghe, O., and Parkinson, D., 2005, Flow of partially molten crust and origin of detachments during collapse of the Cordilleran orogen, *in* Bruhn, D., and Burlini, L., eds., *High-strain zones: Structure and physical properties*: Geological Society of London Special Publication 245, p. 39–64.
- Tikoff, B., and Greene, D., 1997, Stretching lineations in transpressional shear zones: An example from the Sierra Nevada batholith, California: *Journal of Structural Geology*, v. 19, p. 29–39, doi: 10.1016/S0191-8141(96)00056-9.
- Tobisch, O.T., Fiske, R.S., Saleeby, J.B., Holt, E., and Sorenson, S.S., 2000, Steep tilting of metavolcanic rocks by multiple mechanisms, central Sierra Nevada, California: Geological Society of America Bulletin, v. 112, p. 1043–1058, doi: 10.1130/0016-7606(2000)112<1043:STOMRB>2.3.CO;2.
- Treloar, P.J., Brodie, K.H., Coward, M.P., Jan, M.Q., Khan, M.A., Knipe, R.J., Rex, D.C., and Williams, M.P., 1990, The evolution of the Kamila shear zone, Kohistan, Pakistan, *in* Salisbury, M.H., and Fountain, D.M., eds., *Exposed cross-sections of the continental crust*: Dordrecht, the Netherlands, Kluwer Academic Publishers, p. 175–214.
- Treloar, P.J., Petterson, M.G., Jan, M.Q., and Sullivan, M.A., 1996, A re-evaluation of the stratigraphy and evolution of the Kohistan arc sequence, Pakistan Himalaya: Implications for magmatic and tectonic arc-building processes: *Journal of the Geological Society of London*, v. 153, p. 681–693, doi: 10.1144/gsjgs.153.5.0681.
- Tubía, J.M., Cuevas, J., and Gil Ibarguchi, J.I., 1997, Sequential development of the metamorphic aureole beneath the Ronda peridotites and its bearing on the tectonic evolution of the Betic Cordillera: *Tectonophysics*, v. 279, p. 227–252, doi: 10.1016/S0040-1951(97)00124-8.
- Tucholke, B.E., Lin, J., and Kleinrock, M.C., 1998, Megamullions and multilion structure defining oceanic core complexes on the Mid-Atlantic Ridge: *Journal of Geophysical Research*, v. 103, p. 9857–9866, doi: 10.1029/98JB00167.
- Tulloch, A.J., and Challis, G.A., 2000, Emplacement depths of Paleozoic–Mesozoic plutons from western New Zealand estimated by hornblende–Al geobarometry: *New Zealand Journal of Geology and Geophysics*, v. 43, p. 555–567.
- Tulloch, A.J., and Kimbrough, D.L., 1989, The Paparoa metamorphic core complex, Westland–Nelson, New Zealand: Cretaceous extension associated with fragmentation of the Pacific margin of Gondwana: *Tectonics*, v. 8, p. 1217–1234, doi: 10.1029/TC008i006p01217.
- Tulloch, A.J., and Kimbrough, D.L., 2003, Paired plutonic belts in convergent margins and the development of high Sr/Y magmatism: The Peninsular Ranges batholith of California and the Median batholith of New Zealand, *in* Johnson, S.E., et al., eds., *Tectonic evolution of northwestern México and the southwestern USA*: Geological Society of America Special Paper 374, p. 275–295.
- Tulloch, A.J., and Rabone, S.D.C., 1993, Mo-bearing granodiorite porphyry plutons in the Early Cretaceous Separation Point Suite, west Nelson, New Zealand: *New Zealand Journal of Geology and Geophysics*, v. 36, p. 401–408.
- Turner, F.J., 1948, Mineralogical and structural evolution of metamorphic rocks: Geological Society of America Memoir 30, 342 p.
- Varsek, J.L., Cook, F.A., Clowes, R.M., Journey, J.M., Monger, J.W.H., Parrish, R.R., and Kanasevich, E.R., 1993, LITHOPROBE crustal reflection structure of southwestern Canada, 2: Coast Mountains transect: *Tectonics*, v. 12, p. 334–360, doi: 10.1029/92TC00598.
- Vauchez, A., and Tommasi, A., 2003, Wrench faults down to the asthenosphere: Geological and geophysical evidence and thermo-mechanical effects, *in* Storti, F., Holdsworth, R.E., and Salvini, F., eds., *Intraplate strike-slip deformation belts*: Geological Society of London Special Publication 210, p. 15–34.
- Vavra, G., and Schaltegger, U., 1999, Post-granulite facies monazite growth and rejuvenation during Permian to Lower Jurassic thermal and fluid events in the Ivrea zone (Southern Alps): *Contributions to Mineralogy and Petrology*, v. 134, p. 405–414, doi: 10.1007/s004100050493.
- Vavra, G., Gebauer, D., Schmid, R., and Compston, W., 1996, Multiple zircon growth and recrystallization during polyphase Late Cambrian to Triassic metamorphism in granulites of the Ivrea zone (Southern Alps): An ion microprobe (SHRIMP) study: *Contributions to Mineralogy and Petrology*, v. 122, p. 337–358, doi: 10.1007/s004100050132.
- Vavra, G., Schmid, R., and Gebauer, D., 1999, Internal morphology, habit and U–Th–Pb microanalysis of amphibolite-to-granulite facies zircons: Geochronology of the Ivrea zone (Southern Alps): *Contributions to Mineralogy and Petrology*, v. 134, p. 380–404, doi: 10.1007/s004100050492.
- Vissers, R.L.M., Platt, J.P., and van der Wal, D., 1995, Late orogenic extension of the Betic Cordillera and the Alboran Domain: A lithospheric view: *Tectonics*, v. 14, p. 786–803, doi: 10.1029/95TC00086.
- Waters-Torney, C., Goodwin, L.B., Tikoff, B., Staffier, K., and Kelso, P., 2009, This volume, A granulite-facies normal shear zone exposed in the Arunta inlier of central Australia: Implications for deep-crustal deformation during oblique divergence, *in* Miller, R.B., and Snoke, A.W., eds., *Crustal cross sections from the western North American Cordillera and elsewhere: Implications for tectonic and petrologic processes*: Geological Society of America Special Paper 456, doi: 10.1130/2009.2456(10).
- Watts, A.B., and Burov, E.B., 2003, Lithospheric strength and its relationship to the elastic and seismogenic layer thickness: *Earth and Planetary Science Letters*, v. 213, p. 113–131, doi: 10.1016/S0012-821X(03)00289-9.
- Wedepohl, K.H., 1995, The composition of the continental crust: *Geochimica et Cosmochimica Acta*, v. 59, p. 1217–1232, doi: 10.1016/0016-7037(95)00038-2.
- Wegmann, C.E., 1935, Zur deutung der migmatite: *Geologische Rundschau*, v. 26, no. 5, p. 305–350, doi: 10.1007/BF01802849.
- Weiss, T., Siegesmund, S., Rabbel, W., Bohlen, T., and Pohl, M., 1999, Seismic velocities and anisotropy in the lower continental crust: *Pure and Applied Geophysics*, v. 156, p. 97–122, doi: 10.1007/s000240050291.
- Wells, M.L., and Hoisch, T.D., 2008, The role of mantle delamination in widespread Late Cretaceous extension and magmatism in the Cordilleran orogen, western United States: *Geological Society of America Bulletin*, v. 120, p. 515–530, doi: 10.1130/B26006.1.

- Wernicke, B., 1981, Low-angle normal faults in the Basin and Range Province: Nappe tectonics in an extending orogen: *Nature*, v. 291, p. 645–648, doi: 10.1038/291645a0.
- White, A.P., and Hodges, K.V., 2002, Multistage extensional evolution of the central East Greenland Caledonides: *Tectonics*, v. 21, p. 1048, doi: 10.1029/2001TC001308.
- Whitney, D.L., Miller, R.B., and Paterson, S.R., 1999, *P-T-t* evidence for mechanisms of vertical tectonic motion in a contractional orogen: North-western US and Canadian Cordillera: *Journal of Metamorphic Geology*, v. 17, p. 75–90, doi: 10.1046/j.1525-1314.1999.00181.x.
- Wiebe, R.A., and Collins, W.J., 1998, Depositional features and stratigraphic sections in granitic plutons: Implications for the emplacement and crystallization of granitic magma: *Journal of Structural Geology*, v. 20, p. 1273–1289, doi: 10.1016/S0191-8141(98)00059-5.
- Wiens, D.A., and Smith, G.P., 2003, Seismological constraints on structure and flow patterns within the mantle wedge, *in* Eiler, J.M., ed., *Inside the subduction factory*: Washington, D.C., Geophysical Monograph 138, p. 59–81.
- Williams, M.L., Karlstrom, K.E., Dumond, G., and Mahan, K.H., 2009, this volume, Perspectives on the architecture of continental crust from integrated field studies of exposed isobaric sections, *in* Miller, R.B., and Snoke, A.W., eds., *Crustal cross sections from the western North American Cordillera and elsewhere: Implications for tectonic and petrologic processes*: Geological Society of America Special Paper 456, doi: 10.1130/2009.2456(08).
- Williams, P.F., and Jiang, D., 2005, An investigation of lower crustal deformation: Evidence for channel flow and its implications for tectonics and structural studies: *Journal of Structural Geology*, v. 27, p. 1486–1504, doi: 10.1016/j.jsg.2005.04.002.
- Wolf, M.B., and Wyllie, P.J., 1993, Garnet growth during amphibolite anatexis: Implications of a garnetiferous restite: *The Journal of Geology*, v. 101, p. 357–373.
- Wright, J.E., and Snoke, A.W., 1993, Tertiary magmatism and mylonitization in the Ruby–East Humboldt metamorphic core complex, northeastern Nevada: U–Pb geochronology and Sr, Nd, Pb isotope geochemistry: *Geological Society of America Bulletin*, v. 105, p. 935–952, doi: 10.1130/0016-7606(1993)105<0935:TMAMIT>2.3.CO;2.
- Yamamoto, H., 1993, Contrasting metamorphic P–T–time paths of the Kohistan granulites and tectonics of the western Himalayas: *Journal of the Geological Society of London*, v. 150, p. 843–856, doi: 10.1144/gsjgs.150.5.0843.
- Zandt, G., and Carrigan, R., 1993, Small-scale convective instability and upper mantle viscosity under California: *Science*, v. 261, p. 460–463, doi: 10.1126/science.261.5120.460.
- Zandt, G., Gilbert, H., Owens, T.J., Ducea, M., Saleeby, J., and Jones, C.H., 2004, Active foundering of a continental arc root beneath the southern Sierra Nevada in California: *Nature*, v. 431, p. 41–46, doi: 10.1038/nature02847.
- Zingg, A., 1980, Regional metamorphism in the Ivrea zone (southern Alps, N-Italy): Field and microscopic investigations: *Schweizerische Mineralogische und Petrographische Mitteilungen*, v. 60, p. 153–179.
- Zingg, A., 1983, The Ivrea and Strona-Ceneri zones (Southern Alps, Ticino and N-Italy)—A review: *Schweizerische Mineralogische und Petrographische Mitteilungen*, v. 63, p. 361–392.
- Zingg, A., 1990, The Ivrea crustal cross-section (northern Italy and southern Switzerland), *in* Salisbury, M.H., and Fountain, D.M., eds., *Exposed cross-sections of the continental crust*: Dordrecht, the Netherlands, Kluwer Academic Publishers, p. 1–19.
- Zingg, A., and Hunziker, J., 1990, The age of movements along the Insubric line west of Locarno (northern Italy and southern Switzerland): *Eclogae Geologicae Helveticae*, v. 83, p. 629–644.
- Zingg, A., Handy, M.R., Hunziker, J.C., and Schmid, S.M., 1990, Tectono-metamorphic history of the Ivrea zone and its relationship to the crustal evolution of the Southern Alps: *Tectonophysics*, v. 182, p. 169–192, doi: 10.1016/0040-1951(90)90349-D.

MANUSCRIPT ACCEPTED BY THE SOCIETY 24 FEBRUARY 2009

Petrology and geochronology of crustal xenoliths from the Bering Strait region: Linking deep and shallow processes in extending continental crust

Vyacheslav V. Akinin*

North East Interdisciplinary Science Research Institute, Russian Academy of Sciences, Portovaya 16, Magadan 685000, Russian Federation

Elizabeth L. Miller

Department of Geological and Environmental Sciences, Stanford University, Bld. 320, Stanford, California 94305, USA

Joseph L. Wooden

U.S. Geological Survey, Menlo Park, California 94305, USA

ABSTRACT

Petrologic, geochemical, and metamorphic data on gneissic xenoliths derived from the middle and lower crust in the Neogene Bering Sea basalt province, coupled with U-Pb geochronology of their zircons using sensitive high-resolution ion microprobe–reverse geometry (SHRIMP-RG), yield a detailed comparison between the P-T-t and magmatic history of the lower crust and magmatic, metamorphic, and deformational history of the upper crust. Our results provide unique insights into the nature of lithospheric processes that accompany the extension of continental crust. The gneissic, mostly mafic xenoliths (constituting less than two percent of the total xenolith population) from lavas in the Enmelen, RU, St. Lawrence, Nunivak, and Seward Peninsula fields most likely originated through magmatic fractionation processes with continued residence at granulite-facies conditions. Zircon single-grain ages ($n = 125$) are interpreted as both magmatic and metamorphic and are entirely Cretaceous to Paleocene in age (ca. 138–60 Ma). Their age distributions correspond to the main ages of magmatism in two belts of supracrustal volcanic and plutonic rocks in the Bering Sea region. Oscillatory-zoned igneous zircons, Late Cretaceous to Paleocene metamorphic zircons and overgrowths, and lack of any older inheritance in zircons from the xenoliths provide strong evidence for juvenile addition of material to the crust at this time. Surface exposures of Precambrian and Paleozoic rocks locally reached upper amphibolite-facies (sillimanite grade) to granulite-facies conditions within a series of extension-related metamorphic culminations or gneiss domes, which developed within the Cretaceous magmatic belt. Metamorphic gradients and inferred geotherms (~30–50 °C/km) from both the gneiss domes and xenoliths are

*akinin@neisri.ru

Akinin, V.V., Miller, E.L., and Wooden, J.L., 2009, Petrology and geochronology of crustal xenoliths from the Bering Strait region: Linking deep and shallow processes in extending continental crust, *in* Miller, R.B., and Snoke, A.W., eds., *Crustal Cross Sections from the Western North American Cordillera and Elsewhere: Implications for Tectonic and Petrologic Processes*: Geological Society of America Special Paper 456, p. 39–68, doi: 10.1130/2009.2456(02). For permission to copy, contact editing@geosociety.org. ©2009 The Geological Society of America. All rights reserved.

too high to be explained by crustal thickening alone. Magmatic heat input from the mantle is necessary to explain both the petrology of the magmas and elevated metamorphic temperatures.

Deep-crustal seismic-reflection and refraction data reveal a 30–35-km-thick crust, a sharp Moho and reflective lower and middle crust. Velocities do not support a largely mafic (underplated) lower crust, but together with xenolith data suggest that Late Cretaceous to early Paleocene mafic intrusions are likely increasingly important with depth in the crust and that the elevated temperatures during granulite-facies metamorphism led to large-scale flow of crustal rocks to produce gneiss domes and the observed subhorizontal reflectivity of the crust. This unique combined data set for the Bering Shelf region provides compelling evidence for the complete reconstitution/re-equilibration of continental crust from the bottom up during mantle-driven magmatic events associated with crustal extension. Thus, despite Precambrian and Paleozoic rocks at the surface and Alaska's accretionary tectonic history, it is likely that a significant portion of the Bering Sea region lower crust is much younger and related to post-accretionary tectonic and magmatic events.

INTRODUCTION

The tectonic and petrologic processes involved in the growth and modification of continental crust are topics of broad interest across many disciplines in the solid earth sciences (e.g., Rudnick and Gao, 2003; Brown and Rushmer, 2006; Levander et al., 2006). One of the fundamental contributions to our understanding of these processes has been the acquisition of deep-crustal seismic-reflection and refraction profiles. These rough snapshots of the structure of the deep crust and upper mantle have provided new data and insights that have revolutionized our thinking about what processes occur at depth beneath both ancient and modern orogens (e.g., Klempner et al., 1986; Allmendinger et al., 1987; Mooney and Meissner, 1992; Nelson, 1992; Fuis et al., 1995; Cook et al., 1999; Levander et al., 2006). These data in turn provide new challenges: How do we integrate the complex structural and petrologic histories revealed by geologic studies to what commonly appears to be a simpler (and contemporary) structure of the deep crust? How can surface geologic studies be used to predict the nature, history, and structure of the deep crust? Xenolith suites from the crust and upper mantle provide one of the most direct and highly valued means of addressing aspects of these questions, but are scarce worldwide. As noted by Rudnick and Gao (2003), where lower-crustal xenoliths have been dated, they are commonly younger than supracrustal rock sequences, re-enforcing the nature of this general challenge.

The Bering Shelf region of Arctic Alaska and Russia (Fig. 1) provides a unique opportunity to directly address these challenges: Neogene basalt fields entrain xenoliths of the lower crust and mantle, which have also been seismically imaged (Klempner et al., 2002). The evolving geologic and petrologic database for this region provides evidence for a much younger history of the lower crust than is apparent from Alaska's geologic history: The northern Cordillera is commonly cited as a classic example of an accretionary Phanerozoic orogenic belt which included

orogenic thickening of Neoproterozoic crust and its Paleozoic to early Mesozoic cover during arc collision and terrane accretion in the Mesozoic (e.g., Coney et al., 1980; Monger et al., 1991; Nokleberg et al., 1998). Widespread Cretaceous to early Tertiary magmatism post-dates this accretionary history. The role of this magmatism in the crustal evolution of the orogen at this latitude was generally believed to be minor (e.g., Nokleberg et al., 1998) until geologic studies in Alaska and Russia, focused on gneiss domes, alternatively suggested that the Cordilleran orogenic "collage" may have been significantly extended during the time-span of Cretaceous magmatism (e.g., Miller and Hudson, 1991; Miller et al., 1992; Hannula et al., 1995; BSGFP [Bering Strait Geologic Field Party], 1997; Calvert, 1999; Amato et al., 2002; Akinin and Calvert, 2002; Amato and Miller, 2004). The collection of deep-crustal seismic-reflection and refraction data indicates that the crust beneath western Alaska and the Bering Strait is now only ~30–35 km thick and the middle and lower crust characterized by subhorizontal reflectivity and little Moho relief (Klempner et al., 2002). Preliminary geochronologic studies of crustal xenoliths from St. Lawrence Island indicate young Late Cretaceous and Tertiary ages, suggesting that additional studies of xenolith suites would be useful to elucidate the history of the lower crust beneath this region and help to better link it to surface geologic studies (Miller et al., 2002).

Here we present new data and compile existing data on the petrologic, geochemical, metamorphic, and geochronologic histories of crustal xenoliths from five basalt fields in the Bering Strait region, with a focus on their geochronology. High-precision U-Pb dating of individual zircon grains from extremely small, mostly mafic xenoliths is now routinely possible utilizing the spatial and mass resolution of ion microprobes such as the SHRIMP-RG. One hundred and seventeen new U-Pb ages on single zircon grains from crustal xenoliths in the Bering Strait region provide a geochronologic data set with which to better address and understand the temporal links

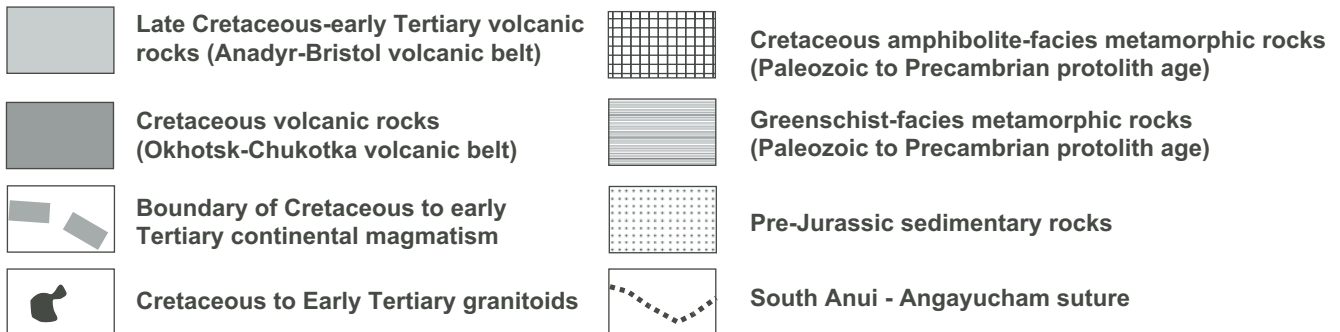
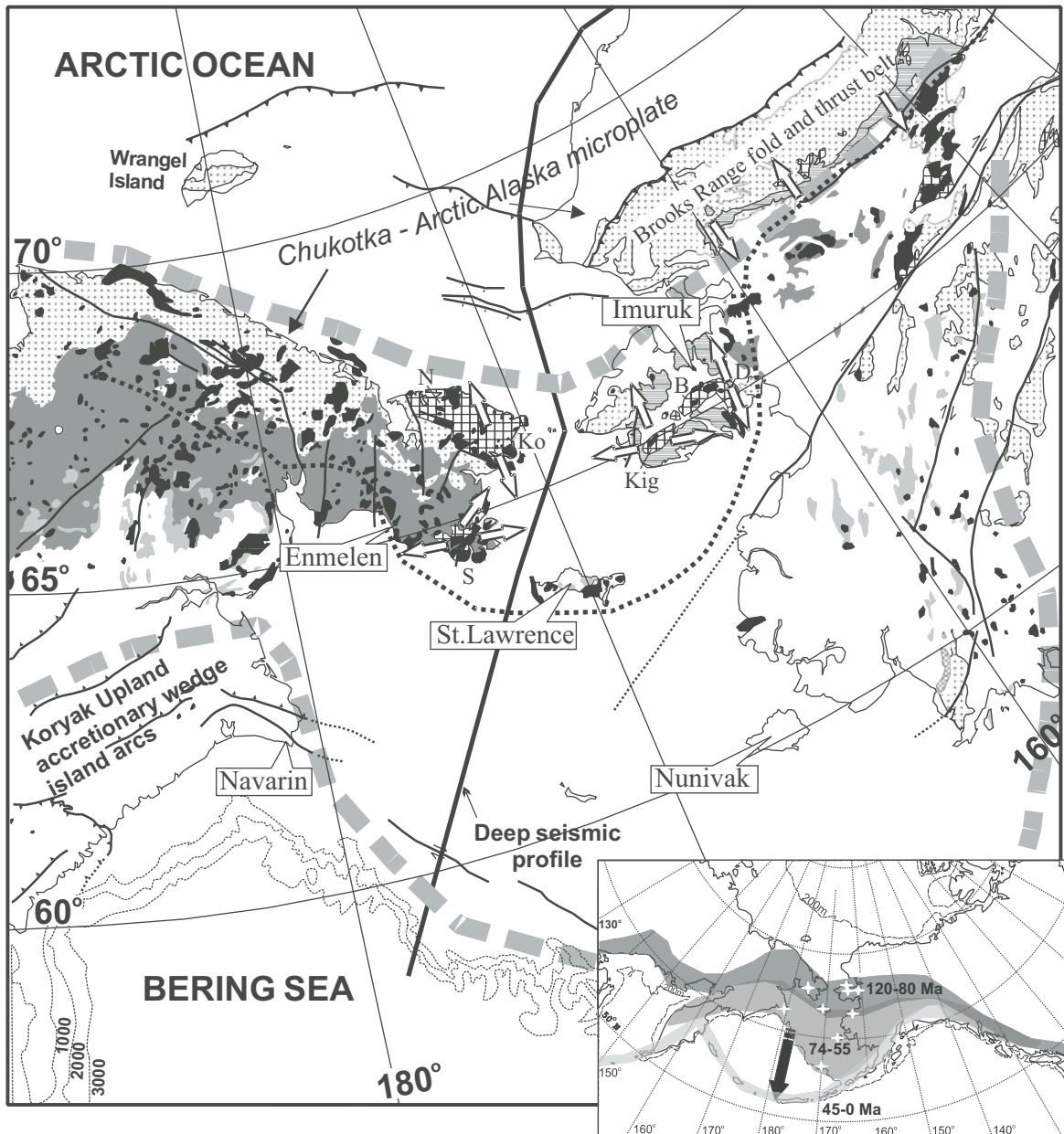


Figure 1. Index map of Alaska and eastern Chukotka showing main geologic features discussed in text. The localities of crustal xenoliths studied are labeled with square boxes: Enmelen, Imuruk, Saint Lawrence Island, Nunivak, and Navarin volcanic fields. The deep-crustal seismic-reflection profile is delineated with a black line (from Klemperer et al. [2002]). The approximate northern and southern limits of Cretaceous to early Tertiary continental calc-alkaline magmatism are shown by light-gray dashed lines. Inset shows southward-migrating, synextensional arc magmatism following crustal thickening and accretion in the Bering Strait region (white stars—Bering Sea basalt province volcanoes). Metamorphic culminations are labeled: Kig—Kigluai Mountains; B—Bendeleben Mountains; D—Darby Mountains; Ko—Koolen dome, N—Neshkan dome; S—Senyavin uplift. Stretching directions in metamorphic rocks shown by white arrows (Till and Dumoulin, 1994; BSGFP, 1997; Miller et al., 2002). White regions on continents correspond to Cretaceous, Tertiary, and Cenozoic sedimentary rocks.

between the history of magmatism, metamorphism, and deformation documented by geologic studies and those in the deeper crust. Together, these three data sets (surface geology, seismic, and xenolith) provide a more detailed characterization of magmatic and orogenic processes during continental extension at the scale of the lithosphere. In the case of the Bering Strait, and perhaps continental extensional provinces worldwide, the new data provide strong evidence for heating of the lower crust to granulite-facies metamorphic conditions by mantle-derived magmas. This heating in turn provides the explanation for the extreme metamorphic gradients and large-scale flow of crustal rocks documented in gneiss domes and for the pervasive sub-horizontal seismic reflectivity observed in the middle and lower crust (e.g., Klemperer et al., 1986; Klemperer, 1987; Klemperer and Hobbs, 1991; Costa and Rey, 1995). More provocatively, the U-Pb isotopic data on zircons from crustal xenoliths provide insight into the extent and degree to which continental crust is modified or reconstituted from the bottom up during magmatism in an extensional tectonic setting.

REGIONAL TECTONIC, MAGMATIC, AND METAMORPHIC CONSTRAINTS ON CRUSTAL EVOLUTION

Tectonic History

All of northern Alaska and adjacent Russia, together with their continental shelves, constitute part of the Arctic Alaska-Chukotka microplate (e.g., Lawver et al., 2002), bound to the south by a belt of ophiolitic rocks that includes the Angayucham terrane of the southern Brooks Range (e.g., Moore et al., 1994) and the South Anyui zone of western Chukotka (e.g., Seslavinskiy, 1979; Sokolov et al., 2002) (Fig. 1). The northern boundary of the Arctic Alaska microplate is the edge of the Arctic continental shelf. The xenolith-bearing basalt fields on the Seward Peninsula, Enmelen and St. Lawrence Island were erupted across the middle and southernmost extent of this continental microplate in the Bering Strait region (Fig. 1). The Nunivak fields were erupted through accreted terranes that lay to the south of the microplate and which have unknown basement ages.

The Arctic Alaska-Chukotka microplate is characterized by Neoproterozoic volcanic and plutonic basement rocks with U-Pb zircon ages ranging from 750 to 550 Ma (Kos'ko et al., 1993; Moore et al., 1994; Amato et al., 2003; Amato, 2004). Broad similarities in the overlying Paleozoic to early Mesozoic cover sequences (e.g., Kos'ko et al., 1993; Natal'in et al., 1999; Dumoulin et al., 2002) allow one to infer the extent of Precambrian basement despite its limited actual exposure (Fig. 1). Devonian plutons with U-Pb ages ranging from 390 to 340 Ma transect basement and some of the cover units of the Arctic Alaska microplate (e.g., Kos'ko et al., 1993; Till and Dumoulin, 1994; Moore et al., 1994; BSGFP, 1997; Toro et al., 2002). Emplacement of oceanic and ophiolitic rocks along the southern boundary of the microplate occurred in the Middle Jurassic as

a consequence of arc collision with a south-facing continental margin, followed by north-vergent thrust faulting of shelf-facies strata into the Early Cretaceous, forming the Brooks Range orogen (e.g., Moore et al., 1994; Miller and Hudson, 1991). Precambrian and Paleozoic rocks in the southernmost Brooks Range (Schist belt) and on the Seward Peninsula (Nome Group) (Fig. 1) have relict blueschist-facies assemblages formed under estimated conditions of 12 MPa and 450 °C (Forbes et al., 1984; Evans and Patrick, 1987; Patrick and Evans, 1989; Patrick and Lieberman, 1988). Because these conditions were obtained in subducted continental crust and its sedimentary cover, they imply that crustal thicknesses may have at least locally doubled during Jurassic-Cretaceous collisional orogenesis. Extensional unroofing of the blueschist terrane occurred soon after its inferred development. ⁴⁰Ar/³⁹Ar data, summarized for the Seward Peninsula, suggest peak metamorphic conditions were reached prior to ca. 125 Ma (Hannula et al., 1995).

Magmatic History

Cretaceous granitoid plutons, dikes and volcanic rocks form a broad and diffuse belt of magmatism that crosses the Bering Strait into Arctic Russia (Fig. 1). Volcanic rocks are more prevalent on the Russian side of the Bering Strait and form the extensive Okhotsk-Chukotka volcanic belt (OCVB) (Fig. 1). The intrusive rocks range in age of 120–80 Ma, and the volcanic rocks range in age 107–59 Ma (Fig. 2) but the existing data set is by no means complete. Although it is widely accepted that Cretaceous plutonic and volcanic rocks post-date and transect the accretionary/collisional deformation and the terranes described above (e.g., Nokleberg et al., 1998), geologic studies have demonstrated that Cretaceous magmatism was accompanied by significant regional metamorphism and crustal thinning (see discussion in Miller et al., 2002). This deformation is quite extreme in the Bering Strait region where it is responsible for the genesis of a series of gneissic culminations that expose upper amphibolite-facies (sillimanite zone) to granulite-facies mid-crustal rocks that underwent high-temperature flow during this magmatic event (e.g., Miller et al., 1992; BSGFP, 1997; Amato et al., 1994, 2002; Amato and Miller, 2004) (Fig. 1).

The limited geochemical and isotopic data for Cretaceous plutonic and volcanic rocks of the Bering Strait region have been summarized for Alaska by Amato and Wright (1997) and for Chukotka by Rowe (1998), Polin and Moll-Stalcup (1999), and Akinin and Kotlyar (2002) (Figs. 3A, 3B). Isotopic data from the best-dated plutons and dikes indicate that Cretaceous magmas contain a significant mantle component and variable crustal input (Fig. 3B). Although isotopic systematics vary between the areas studied, magmatism reflects assimilation-fractional crystallization processes associated with the contamination of mafic magmas by sialic crust (Fig. 3A). Amato and Wright (1997) suggest that magmatism was associated with northward subduction beneath the Bering Strait region and that the source region for more mafic magmas was enriched lithospheric mantle.

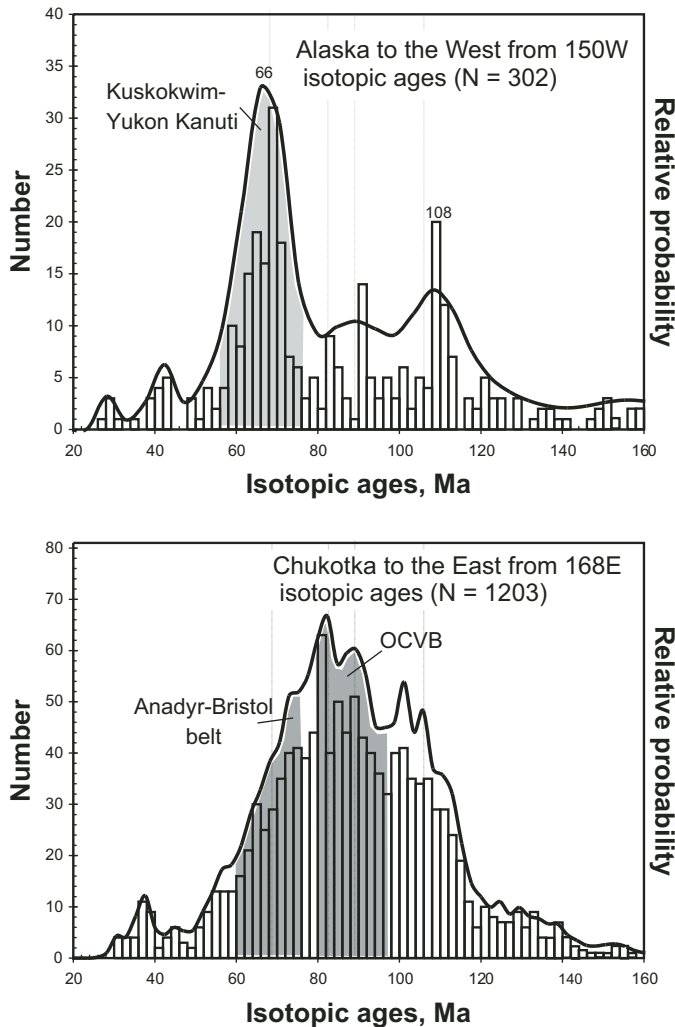


Figure 2. Age distributions of Cretaceous magmatic rocks in Alaska (K-Ar, Rb-Sr and U-Pb data from Wilson et al., 1994) and Chukotka (K-Ar, Rb-Sr, and U-Pb data from GEOCHRON database, Akinin and Kotlyar, 1997). Shaded areas are main age ranges for the Kuskokwim and Yukon-Kanuti magmatic belts (Alaska), and OCVB—Okhotsk-Chukotka volcanic belt (Chukotka).

Magmatism in the Bering Strait region largely migrates southward with time (Fig. 1, inset). The Cretaceous plutons described above cover a wide region of the Arctic Alaska-Chukotka plate (Fig. 1) and are inferred to have been intruded during an extensional tectonic regime (Amato and Wright, 1997). The younger Okhotsk-Chukotka volcanic belt is organized in a more linear fashion parallel to the Pacific margin of northeastern Russia (Fig. 1, inset) and its volcanic units are mostly flat lying to gently dipping (Belyi, 1994). The Okhotsk-Chukotka volcanic belt does not exist in Alaska, but coeval plutons have been dated on the Seward Peninsula and St. Lawrence Island. (Amato and Wright, 1997; Amato et al., 2003). Based on its length and linearity, the Okhotsk-Chukotka volcanic belt has been traditionally attributed to subduction beneath the northeastern margin of Russia. A slight gap in age separates volcanic rocks of the Okhotsk-Chukotka

volcanic belt from younger Latest Cretaceous to early Eocene volcanic rocks (74–55 Ma) mapped in Alaska and offshore along the Bering shelf margin (Moll-Stalcup, 1994; Worrall, 1991) (Fig. 1, inset). The northernmost outcrops of rocks of this age occur on St. Lawrence Island (Patton and Csejtey, 1980). The belt as a whole occurs along the southern margin of the slightly older Cretaceous magmatic belt (Fig. 1, inset).

Metamorphism

Vast regions of subhorizontally foliated to gently south-dipping metamorphic rocks are exposed across the Seward Peninsula and along the southern flanks of the Brooks Range, Alaska (Patrick and Lieberman, 1988; Miller and Hudson, 1991; Little et al., 1994; Hannula et al., 1995). These widespread fabrics (white arrows in Fig. 1) are interpreted as post-collisional, extensional flow fabrics related to vertical thinning and horizontal stretching of the crust (e.g., Little et al., 1994; Hannula et al., 1995; Miller et al., 2002). On the Seward Peninsula, the Precambrian to Paleozoic Nome Group is noted for its relict blueschist-facies metamorphism (Fig. 4) (e.g., Patrick and Lieberman, 1988) which predates metamorphism associated with its pronounced, superimposed, high-strain, subhorizontal foliation and north-south-trending stretching lineations formed during Cretaceous extension (e.g., Hannula et al., 1995). The lower grade Nome Group flanks high-grade gneiss domes in the Kigluaik and nearby Bendeleben and Darby Mountains (Fig. 1) (Till et al., 1986; Miller et al., 1992; Amato et al., 1994). High-grade rocks also occur across the Bering Strait in the Koolen dome (BSGFP, 1997) and adjacent Neshkan dome (Figs. 1, 4). Metamorphic rocks in the Senyavin uplift (Fig. 1) reached peak conditions at a slightly earlier time under a different metamorphic gradient (Fig. 4) (Calvert, 1999). The well-documented ages of peak metamorphism in the synextensional gneiss domes are ca. 91 Ma (Kigluaik) and 108–94 Ma (Koolen). All P-T determinations from the gneiss domes are summarized in Figure 4.

The Kigluaik Mountains are the best studied of these gneiss domes and provides glaciated exposures of amphibolite- to granulite-facies metamorphic rocks that exhibit pronounced strains related to vertical thinning of cover during the rise of the gneiss dome into the shallow crust (Miller et al., 1992; Amato et al., 2002). The Kigluaik gneiss dome is intruded at depth by the gabbroic 91-Ma Kigluaik pluton, invoked as part of the heat source for high-grade metamorphism and crustal melting (Amato et al., 1994; Amato and Wright, 1997). Barrovian isograds along the margins of the dome are spaced closely together and include biotite, garnet, staurolite, sillimanite, and sillimanite + K-feldspar (Lieberman, 1988; Patrick and Evans, 1989; Miller et al., 1992) (Fig. 4). The field metamorphic gradient in the Kigluaik gneiss dome is “collapsed” in the sense that a total of 0.6–0.7 GPa is traversed in less than 6 km of rock section, yielding a field pressure gradient of ~0.1 GPa (1 kb) and a temperature gradient of about 50–100 °C per km. Similarly, the metamorphic field gradient is ~50–100 °C/km (Lieberman, 1988; Hannula et al., 1995;

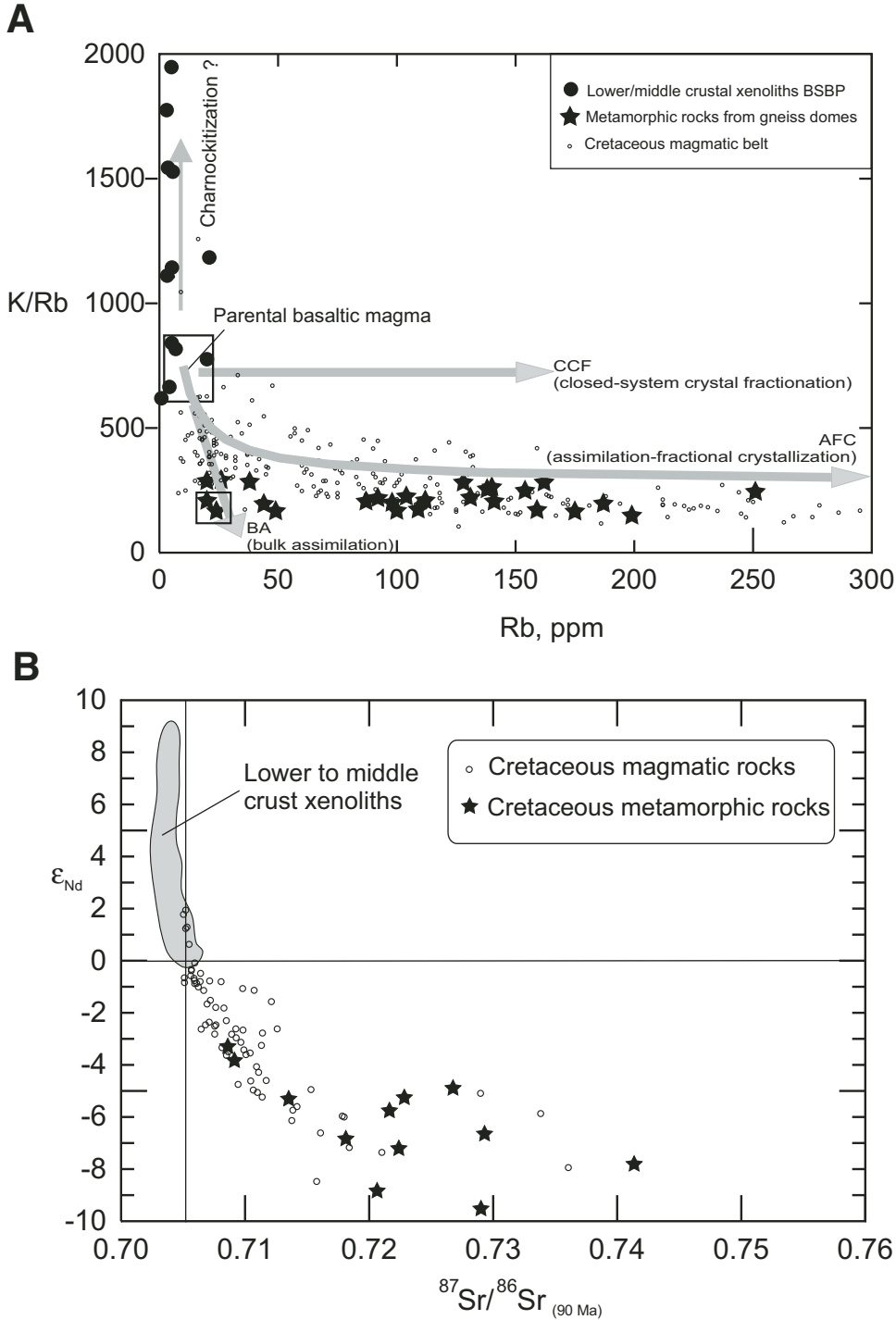


Figure 3. Compositional data for Cretaceous magmatic and metamorphic rocks. (A) K/Rb versus Rb and comparison to general trends for bulk assimilation (BA), concurrent assimilation-fractional crystallization (AFC) and closed-system crystal fractionation (CCF) of a basaltic parent magma. AFC trend calculated according to DePaolo (1981), for parental high alumina basalts from the Okhotsk-Chukotka volcanic belt (OCVB) (Akinin and Kotlyar, 2002) and for amphibolites from Koolen metamorphic dome (Akinin and Calvert, 2002). Ratio of the rate of assimilation to the rate of crystallization used is 0.5. (B) ϵ_{Nd} versus initial $^{87}Sr/^{86}Sr$ (assuming 90 Ma age) plot of magmatic and metamorphic rocks from the Bering Sea region. Rocks represent Cretaceous plutons and dikes from the Kigluaik gneiss dome, Alaska, Koolen gneiss dome and Senyavin uplift, Russia. Sources of data for Cretaceous magmatic and metamorphic rocks include Rowe (1998), Amato and Wright (1997), Polin and Moll-Stalcup (1999), Amato et al. (2003), and Akinin and Kotlyar (2002). Crustal-xenolith isotopic data are from Akinin et al. (2005). BSBP—Bering Sea basalt province; C—Cretaceous.

Miller et al., 1992; Amato and Miller, 2004). This relationship has been attributed to the synmetamorphic flow of rocks in the dome during their ascent into the shallow crust at ca. 91 Ma as the Kigluaik pluton was intruded (Miller et al., 1992; Amato et al., 1994; Amato and Miller, 2004; Fig. 4).

Crustal Geophysics

Seismic-reflection data image the deep crust and mantle across the Bering Shelf near the xenolith localities (Fig. 1) and provide the structural framework for relating rocks at depth

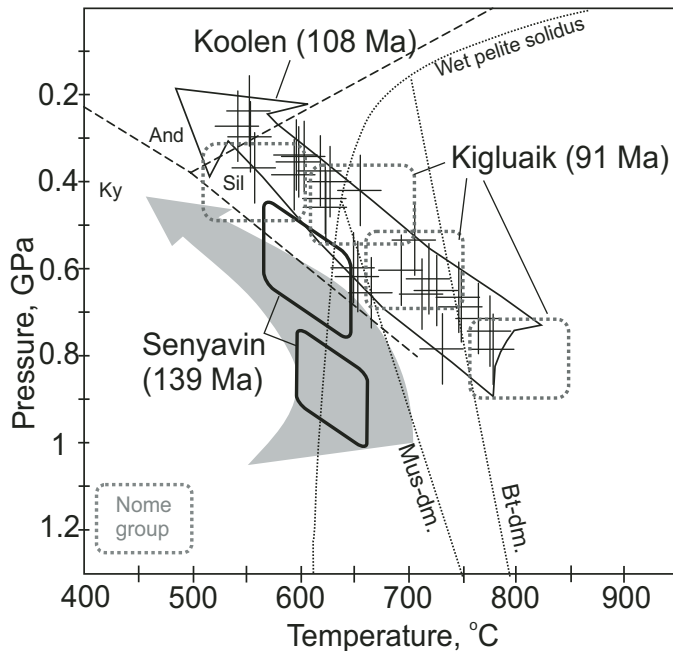


Figure 4. Summary of pressure-temperature conditions obtained from rocks in Cretaceous metamorphic culminations (gneiss domes) in the Bering Strait region, the Koolen dome, Kigluaik dome, and Senyavin uplift, with U-Pb ages for peak metamorphism shown in parentheses. Gray dashed boxes outline P-T conditions for progressively deeper levels of the Kigluaik gneiss dome. The box labeled “Nome group” represents conditions of earlier blueschist-facies metamorphism on the Seward Peninsula. The white arrow encompasses all calculated P-T conditions for rocks in the Koolen dome with their uncertainties. Black boxes are P-T conditions experienced by rocks in the Senyavin uplift. Gray arrow represents typical Barrovian P-T path (Jamieson et al., 1998) shown for comparison. Protolith ages for samples studied are all Paleozoic and older (Till and Dumoulin, 1994; Natal’in et al., 1999; Amato et al., 2003). Mineral thermobarometry calculations have been made using garnet-biotite equilibria, garnet-plagioclase- Al_2SiO_5 -quartz and garnet-plagioclase-muscovite-biotite equilibria, clinopyroxene-garnet equilibria, and multi-equilibria intersections from THERMOCALC (Holland and Powell, 1998). Details of thermobarometric calculations are described in Akinin and Calvert (2002). Mineral compositions data sources: Kigluaik dome—Lieberman (1988); Patrick and Evans (1989); Koolen dome—Akinin and Calvert (2002); Senyavin uplift—Calvert (1999). “Mus-dm.” and “Bt-dm.” are muscovite- and biotite-melting curves (Thompson and Connolly, 1995). And—andalusite; Ky—kyanite; Sil—sillimanite.

(xenoliths) to the geology of the upper crust (Fig. 5) (Klemperer et al., 2002).

A gradual but significant change in the character of lower-crustal reflections and the Moho reflection occur just south of the westward projection of the Brooks Range and Hope Basin (Fig. 5); the lower crust becomes reflective and the Moho becomes shallower (Fig. 5). Subhorizontal reflectivity occurs in the lower 1/3–2/3 of the crust and is most prominent from north of the Bering Strait to south of St. Lawrence Island, an across-strike distance of ~500 km. Across this same distance the crust is also fairly

uniform in thickness at ~32 km depth (Fig. 5) (Klemperer et al., 2002). Near the Seward Peninsula (Fig. 5), the shallowest reflectivity occurs at ~5–10 km depth. The region of uniform crustal thickness and onset of subhorizontal reflectivity corresponds to the locus of Cretaceous magmatism at the surface (Fig. 1).

Lower-crustal reflectivity was first observed and interpreted to be characteristic of thin crust beneath young extensional provinces such as the North Sea and Basin and Range province of the western United States (e.g., Matthews and Cheadle, 1986; Klemperer et al., 1986; Klemperer, 1987; Allmendinger et al., 1987). In general, reflectivity is thought to represent tectonically imposed layering (produced by crustal flow) and/or primary igneous layering produced by mafic intrusions into the lower crust (e.g., Green et al., 1990; Warner, 1990; summary by Levander et al., 2006). The lower part of the crust beneath the Bering Strait has velocities that range from 6.1–6.7 km/sec (Fig. 5). These velocities are not consistent with large volumes of underplated mafic magmas, which should have higher velocities on the order of ~7 km/sec. The velocities are, however, consistent with some intraplating of mafic sills and lenses into the lower crust, leading to a bimodal velocity structure at a small scale that could be generated by ~6.5 km/sec felsic to intermediate igneous and metamorphic rock types and ~7 km/sec gabbroic intrusions (Klemperer et al., 2002). These postulated gabbroic bodies are a likely source for mafic xenoliths entrained in Neogene basalts and discussed in detail below. The crust between 16 and 24 km depth, however, is characterized by fairly low velocities of 6.1–6.4 km/sec (Wolf et al., 2002), precluding a large component of mafic intrusions at these depths, and providing independent evidence that the xenoliths studied originate from the lower crust beneath this region. The low mid-crustal velocities suggest that the reflectivity observed higher in the crust must represent subhorizontally transposed compositional layering in older metamorphic and felsic igneous rocks (paragneisses and orthogneisses), probably similar to gneisses exposed in the metamorphic culminations described above. The xenoliths and their ages, discussed next, provide a robust test for the inferences and conclusions above and a strong basis for understanding the crustal-scale tectonic and magmatic processes involved in the formation of seismically imaged, reflective continental crust.

LOWER- TO MIDDLE-CRUSTAL XENOLITHS OF THE BERING STRAIT REGION

Introduction

The Neogene Bering Sea basalt province (Moll-Stalcup, 1994; Akinin and Apt, 1994) includes over 17 volcanic fields of tholeiitic and alkalic olivine basalt flows with subordinate basanite and nephelinite cones, flows, and maars (white stars on inset of Fig. 1). Most of the volcanic fields are dominated by relatively light rare earth elements (LREE)-enriched basalts with intra-plate geochemical characteristics and thus compositionally resemble

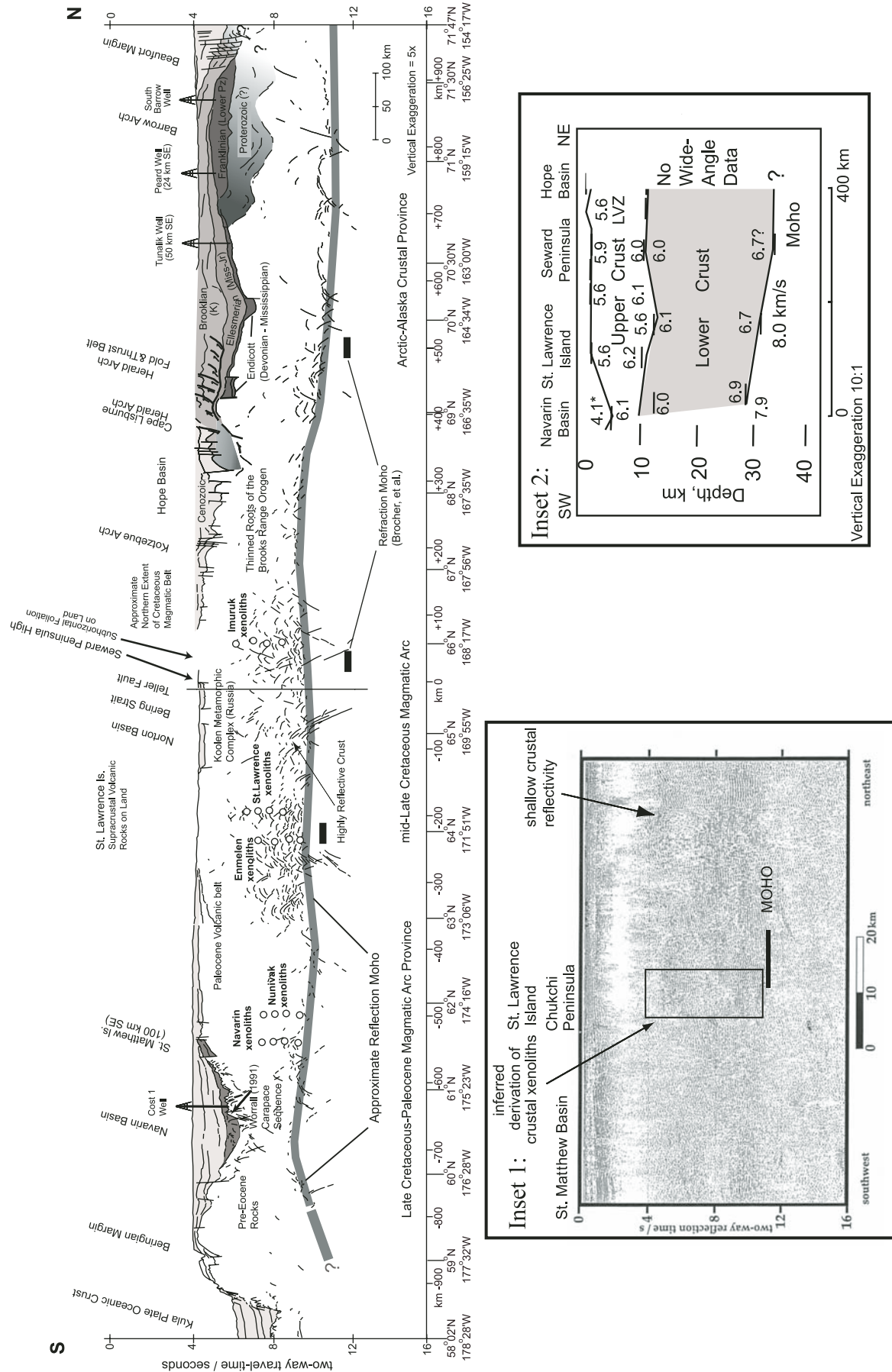


Figure 5. Line drawing and interpretation of reflectors in a deep-crustal seismic-reflection profile (location shown in Fig. 1) with the projected location and range of depths of the xenoliths discussed in this study (modified from Klempner et al., 2002). Inset 1 illustrates the nature of lower-crustal reflectivity observed along the profile from the Bering Strait to St. Matthew Basin. Inset 2 shows results of refraction studies and crustal velocity model from Miller et al. (2002). LVZ—low velocity zone.

those erupted on oceanic islands or in some continental settings (e.g., Clague and Frey, 1982).

Many of the alkali basalts contain upper-mantle and lower-crustal xenoliths. The most abundant and well-studied xenolith suites are those from Nunivak Island (Francis, 1976, 1978; Menzies and Murthy, 1980; Roden et al., 1984, 1995), St. Lawrence Island (Wirth et al., 2002), and the Enmelen volcanoes, Chukchi Peninsula (Akinin and Apt, 1994; Akinin et al., 1997; Akinin et al., 2005) (Fig. 1). Spinel lherzolites are the dominant rock type represented by the xenoliths, which is a common aspect of xenolith suites worldwide. For example, ~80%–90% of all Enmelen xenoliths are spinel lherzolites. Clinopyroxene megacrysts (7%), Fe-Ti oxide megacrysts (3%), gabbro and granulites (1.6%), and orthopyroxene megacrysts (1.1%) form the remainder of the population, whereas websterite, dunite, harzburgite, clinopyroxenite, pyroxene pegmatite, glimmerite, and olivine or biotite megacrysts constitute less than 1% of inclusions in the Enmelen basalts (Akinin, 1995). The plagioclase-bearing granulite and gabbroic xenolith suite which is the main focus of this study, constitutes <2% of the xenolith population. On Nunivak Island, corona-bearing pyroxene granulite xenoliths comprise 9% of the xenolith population. These xenoliths are interpreted as original troctolite cumulates whose olivine and plagioclase subsequently reacted to form coronas of aluminous clinopyroxene-spinel symplectite and aluminous orthopyroxene at ~950°C and at $P > 9$ kb (Francis, 1976; Roden et al., 1995).

Petrography

Fifty samples of plagioclase-bearing xenoliths (30 samples from Enmelen, 18 samples from Imuruk, and 2 samples from St. Lawrence) were petrographically and geochemically studied (Figs. 6–11). These xenoliths are 3–5 cm in diameter and are commonly gneissic in texture with pyroxene-rich and plagioclase-rich layers (Fig. 6). Medium-grained, polygonal-granoblastic textures are common in thin section and represent static equilibration at high temperatures for an extended period of time. All plagioclase-bearing xenoliths lack hydrous phases, suggesting granulite-facies conditions. In addition to plagioclase, the xenoliths contain orthopyroxene, clinopyroxene, quartz, K-feldspar, and Fe-Ti oxides (Table 1). Accessory minerals include apatite, zircon, and rutile. Apatite occurs as inclusions within plagioclase and pyroxene. Disequilibrium-melting textures are observed in some samples and are attributed to decompression-related incongruent melting of orthopyroxene during the ascent of host lavas. Based on their textures and geochemistry, the plagioclase-bearing xenoliths can be divided into three groups (Figs. 7, 10, and 11): Group 1 (Figs. 7A–7C) consists of mafic to intermediate charnockites and includes norites, jotunites, and two-pyroxene granulites. Group 2 (Figs. 7D–7F) consists of pyroxene-plagioclase cumulates and includes norites, gabbro-norites, and pegmatitic olivine gabbro. Group 3 (Figs. 7G–7I) consists of kelyphitic, initially garnet-bearing gabbro. Differences between these three groups can be seen in their light rare earth elements (LREE)

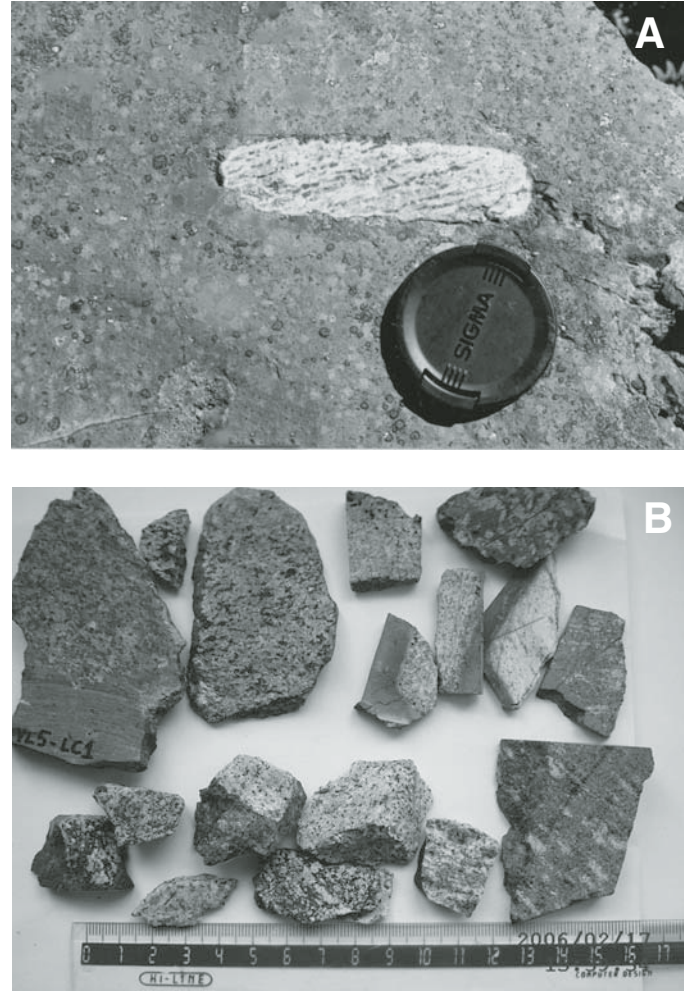


Figure 6. (A) Photograph of plagioclase-bearing gneissic xenolith in basaltic lava flow from Imuruk volcanic field, Seward Peninsula. Camera lens cap is ~50 mm in diameter. (B) Collection from Enmelen volcanic field, Chukotka Peninsula. Centimeter scale at base of photograph.

enrichments and Eu anomalies (Figs. 7C, 7F, 7I). Plagioclase in all xenoliths is typically more abundant than other minerals and ranges in composition from An_{41} to An_{51} . Group 1 xenoliths contain an equilibrium assemblage of orthopyroxene and K-feldspar (usually mesoperthite), an assemblage characteristic of charnockite series rocks. Two xenoliths from St. Lawrence Island have mesoperthitic feldspar with plagioclase lamella that are low in anorthite (An_{17}) and rich in orthoclase (Or_{15}). Group 2 xenoliths have allotriomorphic-granular textures and in a few cases, clinopyroxenes occur as small subidiomorphic inclusions within large mesoperthitic feldspars producing poikilitic textures (Fig. 7D). Group 3 gabbros contain up to 30% of dark kelyphite or extremely fine-grained plagioclase+pyroxene+spinel symplectite (kel on Figs. 7G, 7H), which is interpreted as a product of garnet breakdown during decompression melting (Padovani and Carter, 1977).

TABLE 1. MODAL COMPOSITIONS OF LOWER TO MIDDLE CRUST XENOLITHS FROM BERING SEA REGION

Sample	Longitude (°W)	Latitude (°N)	Group	Rock	Location	Mode mineral composition (%)						Texture
						Pl+Kfs	Opx	Cpx	Qtz	Fe-Ti oxide	Kelephylite	
En136-2	175.1924	65.0351	1	Granulite, intermediate	Enmelen	86.4	8	0.8	4.4	0.4		Granoblastic
En131-8	175.19431	65.04100	1	Norite, charnockite series	Enmelen	80.5	14.4	2.4		2.7		Equigranular
G3s	175.33560	65.06420	1	Norite, charnockite series	Enmelen	78.7	19.5	0		1.8		Equigranular
GYT28s	175.36360	65.10520	1	Norite, charnockite series	Enmelen	75.1	23.1	1.2		0.7		Equigranular
En131-26	175.19431	65.04100	1	Granulite, intermediate	Enmelen	72.6	0.5	14	12.7	0.3		Granoblastic
EN131-5	175.19431	65.04100	1	Norite, charnockite series	Enmelen	72	24.1	3.6		0.2		Equigranular
EN132	175.28439	65.06230	2	Pyroxene-plagioclase cumulate, norite	Enmelen	79.3	19.6	0.68		0.4		Cumulate equigranular
EN126-16	175.1842	65.0715	2	Norite	Enmelen	65	33.3	1.4		0.3		Equigranular
En131-20	175.19431	65.04100	2	Gabbronorite	Enmelen	40.4	8.2	51.2		0.2		Equigranular
En131-2	175.19431	65.04100	3	Kelyphytic (garnet) gabbro	Enmelen	56.6		13.9		0.2	29.3	Equigranular
En131-15	175.19431	65.04100	3	Kelyphytic (garnet) gabbro	Enmelen	53.2	2.4	25.8		1.6	17	Equigranular
En131-16	175.19431	65.04100	3	Kelyphytic (garnet) gabbro	Enmelen	33.1	6.9	32.1		0.9	27	Equigranular
SV21F	170.5	63.5	1	Cumulate anorthosite	St. Lawrence	94.3	2.1	3.5		0.2		Poikilitic, coarse grained
SV21B	170.5	63.5	1	Granulite, intermediate	St. Lawrence	82.8	6	1	9.9	0.3		Granoblastic
16-11k	163.20390	65.45480	1	Granulite, intermediate	Imuruk	75.3	24.4			0.3		Granoblastic
16-12k	163.20390	65.45480	1	Granulite, felsic	Imuruk	60.1	13.5		26.1	0.3		Granoblastic
16-9k	163.20390	65.45480	2	Gabbronorite	Imuruk	23.1	15	61.5		0.4		Gabbroic, foliated
8-1k	162.57170	65.33160	2	Pegmatite olivine gabbro	Imuruk	50	15(ol)	25				Coarse grained, contain 10% of olivine

Note: Modal composition was estimated by area calculated in thin sections using ArcView software. Error for estimation is less than 5 relative percent.

The composition of clinopyroxene in the xenoliths ranges from $Wo_{36}En_{31}Fs_{12}$ to $Wo_{49}En_{48}Fs_{24}$ with Mg-numbers range 0.57–0.77 (Table 2). There are notable differences between the clinopyroxenes from the three xenolith groups. Clinopyroxenes from Group 1 charnockites have $Al_2O_3 < 5$ wt%, $TiO_2 < 0.5$ wt%, and $Na_2O < 0.7$ wt%, which are lower than Group 2 and 3 where Al_2O_3 ranges from 4.8 to 10.4 wt%, and TiO_2 , and Na_2O both exceed 0.7 wt% (Table 1). Orthopyroxenes from Group 1 xenoliths also have lower Al_2O_3 than those from other groups. Zoning in pyroxene is not pronounced except in a few cases where it is characterized by slightly decreasing Mg-numbers toward crystal rims which we attribute to slow cooling and possible magmatic differentiation.

Major-Element Geochemistry

Whole-rock geochemistry of xenoliths from Enmelen and Imuruk volcanic fields (Table 3), compiled with published data on plagioclase-bearing xenoliths from Nunivak Island (Francis, 1976), Cape Navarin (Fedorov et al., 1993), and St. Lawrence Island (Wirth et al., 2002) (Figs. 8 and 9) indicate that most xenoliths are mafic, with 44.7–53.1 wt% SiO_2 and 3.1–11.5 wt% MgO (Table 3, Fig. 8). Xenoliths from Imuruk are somewhat more silica-rich than those from Enmelen and St. Lawrence Island (Fig. 9). Two intermediate-composition xenoliths from Imuruk are close to granodiorite and quartz monzonite in terms of their modal mineralogy and whole rock geochemistry (Figs. 8, 9).

Na_2O (1.7–4.6 wt%) is greater than K_2O (0.2–2.5 wt%) in all xenoliths, as is typical for most igneous rock suites. Charnockites have the highest $Na_2O + K_2O$ (3.4 – 7.1 wt%) as compared to Group 2 xenoliths where alkalis range from 1.9 to 2.7 wt% and in Group 3 from 2.1 to 4.3 wt% (Table 3). Broad negative correlations are observed between MgO and SiO_2 and more pronounced negative correlations exist between MgO and $Na_2O + K_2O$, compatible with observed variations in the modal percent feldspar and clinopyroxene (Fig. 8). CaO increases with MgO (Fig. 8). These variations are typical of fractional crystallization trends, supporting a magmatic origin for the protoliths of the granulite-facies xenoliths. The observed behavior of compatible and incompatible elements (Fig. 8), where decreasing MgO and Sc and increasing La/Sm ratios with increasing feldspar also support a magmatic cumulate origin.

All of the xenoliths overlap in composition with the world-wide suite of lower crust xenoliths as compiled by Kempton and Harmon (1992), but there are also distinct differences between the various xenolith groups studied (Fig. 9). Enmelen Group 2 and the St. Lawrence xenoliths plot between the Mafic-1 and Mafic-2 xenolith fields of Kempton and Harmon (1992) and display decreasing Mg-numbers with increasing SiO_2/Al_2O_3 (Fig. 9). This trend is compatible with the inferred cumulate origin of Enmelen Group 2 xenoliths whose protoliths may have been parental magmas that followed a calc-alkaline igneous fractionation trend (Fig. 9). Groups-1 and 3 xenoliths from Enmelen scatter within the Mafic-3 field. Nunivak and Cape Navarin xenoliths

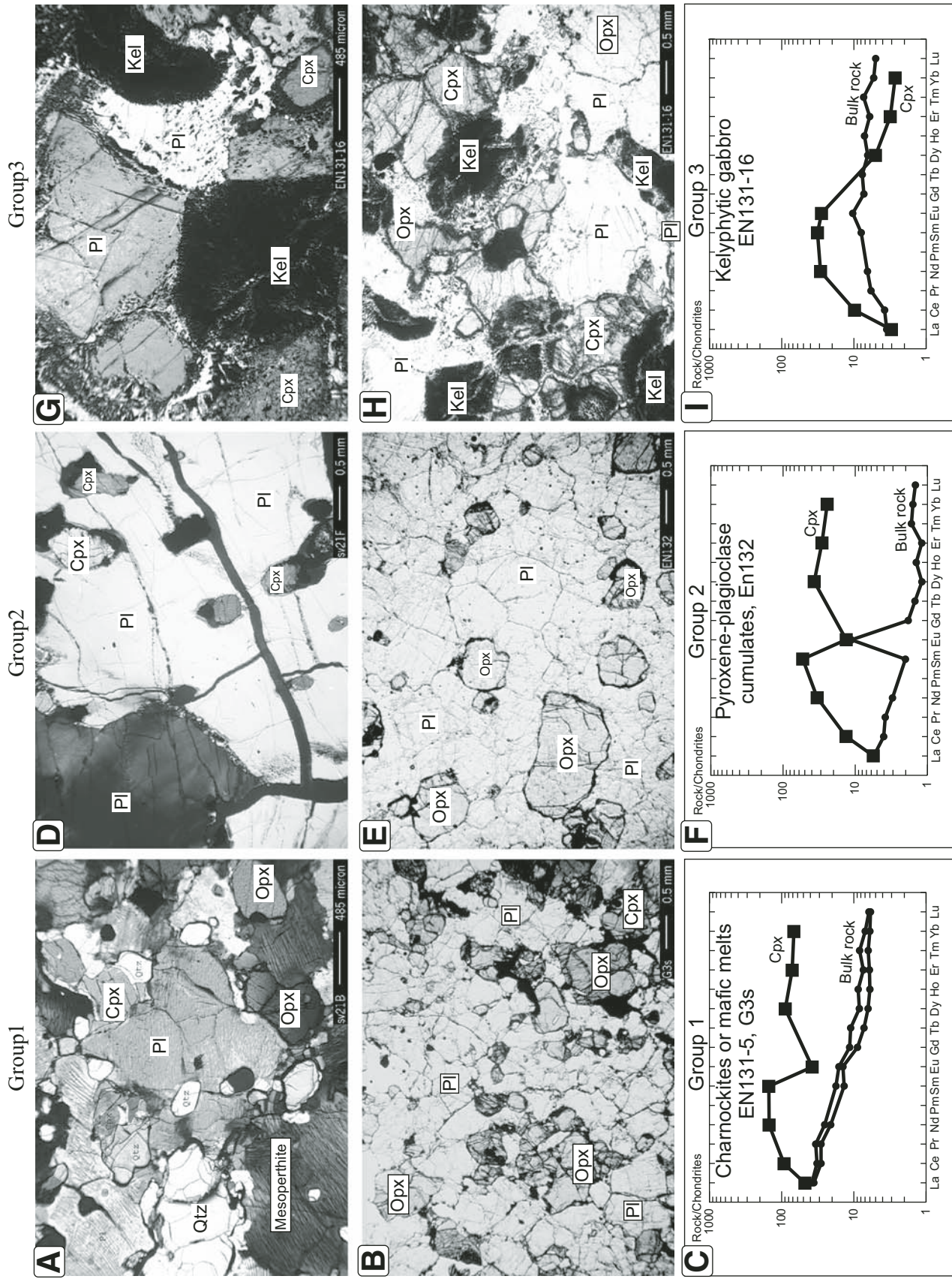


Figure 7. Three groups of plagioclase-bearing xenoliths from St. Lawrence (A, D), and Emmelen, Chukotka Peninsula (B, C, E, F, G, H, I). Upper images of thin sections taken with cross-polarized light, lower images with plane-polarized light. Chondrite-normalized REE patterns for bulk-rock and clinopyroxene separates from representative samples of those three groups are shown at the bottom. Cpx—clinopyroxene; Opx—orthopyroxene; Pl—plagioclase; Qtz—quartz; Kel—kelyphite.

TABLE 2. MINERAL COMPOSITIONS AND THERMOBAROMETRY FOR BERING SEA LOWER/MIDDLE CRUST XENOLITHS

Xenolith group	Sample	Location	Grain zone	Temperature (°C), Pressure (GPa)	Ab(pl)	An(pl)	Or(pl)	Mg#(cpx)	Wo_cpx	En_cpx	Fs_cpx	Mg#(opx)	Wo_opx	En_opx	Fs_opx	Al ₂ O ₃ (wt%)
1	130-1	Enmelen	Core		0.521	0.457	0.022	0.777	0.382	0.480	0.138					0.25
1	130-1	Enmelen	Rim		0.547	0.429	0.025	0.625	0.440	0.350	0.210					2.35
1	131-5G	Enmelen	Core		0.486	0.466	0.048	0.768	0.384	0.473	0.143	58.74	0.014	0.579	0.407	0.3
1	131-5G	Enmelen	Rim									63.22	0.013	0.624	0.363	3.2
1	EN131-14	Enmelen	Core	820 ¹ , 0.65 ¹	0.514	0.456	0.030	0.583	0.452	0.319	0.228					2.9
1	EN131-19	Enmelen	Core	836 ¹ , 0.52 ⁴	0.507	0.461	0.032	0.589	0.445	0.327	0.228	48.89	0.025	0.477	0.499	2.6
1	EN131-5	Enmelen	Core	838 ¹ , 0.89 ⁵	0.492	0.475	0.034	0.586	0.445	0.325	0.230	50.49	0.018	0.496	0.486	4.5
1	EN131-8	Enmelen	Core	890 ² , 0.99 ⁴	0.523	0.435	0.042	0.578	0.452	0.317	0.231					4
1	G3s	Enmelen	Core	960 ³	0.551	0.415	0.034					48.37	0.015	0.476	0.508	
1	GYT28s	Enmelen	Core	760 ¹ , 0.62 ⁵	0.542–0.447	0.429–0.515	0.028–0.038	0.579	0.455	0.315	0.229					2.1
1	125-1	Enmelen	Rim		0.489	0.472	0.039									
1	125-1	Enmelen	Core	775 ¹ , 0.6 ⁵	0.493	0.464	0.043	0.682	0.459	0.369	0.172	55.97	0.014	0.552	0.434	2.8
1	EN131-26	Enmelen	Core	841 ¹ , 0.56 ⁴	0.564	0.385	0.050	0.616–0.647	0.449–0.472	0.339–0.342	0.211–0.186	50.5–48.1	0.041–0.026	0.485–0.486	0.474–0.506	2.3
2	EN131-20	Enmelen	Core	744 ¹ , 0.96 ⁵	0.310	0.676	0.014	0.701	0.488	0.359	0.153	67.0–67.9	0.009–0.016	0.664–0.665	0.326–0.319	8.1
2	EN132	Enmelen	Core	837 ¹ , 1.04 ⁴	0.400	0.576	0.025	0.761	0.473	0.401	0.126	67.9–67.6	0.027–0.011	0.660–0.669	0.312–0.321	4.8
3	EN131-16	Enmelen	Core	1090 ² , 1.2 ⁵	0.582	0.399	0.018	0.651	0.491	0.332	0.178					10.4
4	EN136-2	Enmelen	Core	740 ¹ , 0.6 ⁴	0.572	0.381	0.047	0.665–0.667	0.462–0.371	0.357–0.420	0.180–0.210	46.1–46.5	0.016–0.046	0.453–0.444	0.530–0.511	0.1
1	16-11k	Imuruk	Core	880 ¹ , 0.6 ⁵	0.464	0.505	0.031	0.748	0.453	0.409	0.138	57.38	0.016	0.564	0.419	0.3
4	16-12k	Imuruk	Core		0.574	0.385	0.041					54.08	0.015	0.533	0.452	
1	SV-21B	St. Lawrence	Core	912 ¹ , 0.86 ⁴	0.646	0.197	0.158	0.676–0.649	0.432–0.440	0.383–0.363	0.184–0.197	54.73	0.017	0.538	0.445	2.3
1	SV-21F	St. Lawrence	Core	914 ¹ , 0.74 ⁶				0.606	0.411	0.357	0.232	51.37	0.019	0.504	0.477	2.3
1	SV-21F	St. Lawrence	Rim	990 ² , 0.7 ⁴				0.601	0.405	0.357	0.237	51.37	0.018	0.504	0.477	2.5

Note: Thermobarometers used: ¹Wells (1977); ²Lindsley (1983); ³Brey and Kohler (1990); ⁴McCarthy and Patino Douce (1998); ⁵Nimis (1999); ⁶THERMOCALC software. Microprobe mineral analyses were carried out on a Cameca SX100 electron microprobe equipped with four wavelength-dispersive spectrometers at the University of Vienna, Institute of Petrology, and the JEOL-7031 microprobe at Stanford University. The acceleration voltage and beam current were 15kV and 20nA, and standard correction procedures were applied. The error for all elements is below 5% and only for Na is in the range of 10%. Minerals were analyzed at 3 to 10 points and proved to be quite homogeneous for most of samples. Whole microprobe data can be obtained upon request from the authors.

TABLE 3. MAJOR AND TRACE ELEMENT COMPOSITION OF LOWER TO MIDDLE CRUSTAL XENOLITHS FROM THE BERING SEA REGION

Sample #	GY128s	EN131-5	G3s	EN132	EN131-24	EN131-2	EN131-16	EN131-15	16-11k	16-12k	16-9k	8-1k	LC_XEN
Group	Enmelen	Enmelen	Enmelen	Enmelen	Enmelen	Enmelen	Enmelen	Enmelen	Imuruk	Imuruk	Imuruk	Imuruk	
location	175.34	175.19	175.36	175.28	175.19	175.19	175.19	175.19	163.2	163.2	163.2	162.57	
Longitude	175.34	175.19	175.36	175.28	175.19	175.19	175.19	175.19	163.2	163.2	163.2	162.57	
(°W)													
Latitude	65.06	65.04	65.11	65.06	65.04	65.04	65.04	65.04	65.45	65.45	65.45	65.33	
(°N)													
SiO ₂	49.33	51.52	53.07	52.39	45.36	44.92	47.83	47.86	58.23	64.43	50.99	46.48	50.4
TiO ₂	0.93	0.81	1.24	0.19	0.45	0.48	1.2	1.18	0.49	0.23	0.5	1.79	1
Al ₂ O ₃	19.29	19.82	16.7	22.28	20.52	23.15	17.41	17.63	13.42	14.74	8.71	17.21	16.8
FeO	7.99	7.85	11.3	5.06	8.81	6.79	10.2	10.16	7.79	5.99	12.39	9.98	9
MnO	0.1	0.11	0.22	0.09	0.1	0.09	0.17	0.16	0.24	0.12	0.27	0.13	0.15
MgO	3.13	4.49	5.53	5.65	10.43	7.26	6.71	6.84	6	3.94	11.54	6.26	7.7
CaO	7.11	8.88	6.22	9.71	10.59	14.43	10.7	10.68	5.84	3.82	11.61	10.08	10.3
Na ₂ O	4.57	4.32	3.45	3.41	2.26	1.73	3.46	3.19	3.95	4.11	1.91	2.84	1.27
K ₂ O	2.53	1.13	0.63	0.6	0.45	0.33	0.86	0.8	3.01	1.89	0.67	0.37	0.81
P ₂ O ₅	0.35	0.18	0.31	0.02	0.03	0.07	0.34	0.35	0.07	0.01	0.03	0.08	0.22
LOI ¹	3.77	0.07	0.07	0.05					0.08	0.05		3.65	
Total	99.99	99.98	99.99	100.01	99.98	100	100.01	99.98	99.98	99.99	100	99.98	97.65
Mg-number	0.451	0.545	0.507	0.701	0.713	0.692	0.58	0.585	0.618	0.58	0.661	0.568	0.642
Cr	45	73	90	108	194	258	54	203	230.2	128.3	351.9	108.5	302
Ni	166	55	43	92	126	69	28	65	83.6	32.2	78.8	81.2	147
Sc	16.2	26.6	20.4	18.9	10.6	22.2	38.7	31.7	24.7	18.2	61.7	21.2	34
Pb	4.7	3.9	6.5		1.8			1.5	2.6	5.9	2.1		5.9
Cs	0.29	0.03	0.21	0.02	0.04	0.04	0.02	0.02	0.10	0.08	0.03	0.04	1
Rb	75	4.8	2.9	3.2	3.3	3.3	1.5	4.3	21	20.1	4.9	1.6	21
Ba	826	293	346	119	160	53	87	358	229	458	96	49	502
Sr	559.4	595.9	423.5	725	885.8	610.2	545.8	934.1	345.6	300.3	209.5	767.4	405
Ta	0.4	0.4	0.6	0	0.1	1.5	0.1	0.3	0.8	0.2	0.2	0.5	
Nb	5.9	7.2	6.6	0.5	1.9	11	0.9	4.4	12.4	2.9	3	6	12
Hf	1.5	1.9	0.4	0.2	0.6	1.6	0.4	0.8	1.4	0.6	2.1	1.6	2.9
Zr	60.3	67.3	9.3	7.5	20.8	62.9	9.8	27.1	58.2	20.2	62.5	52.8	99
Y	15.4	16.7	13.5	2.4	3.7	4.8	14.2	17.5	30.3	18.9	34.2	16.9	19
Th	0.3	0.4	0.1	0.1	0.5	1.3	0.1	0.3	0.7	0.2	0.6	0.3	2.8
U	1.2	0.2	0.2	0	0.1	0.6	0.1	0.2	0.3	0.9	0.2	0.2	0.4
La	17.5	12.6	11.8	1.8	5.4	4.4	1.2	7.9	6.1	5.4	7.4	9	14.6
Ce	35.7	28	24.6	3.5	10.1	8.6	3.3	19.5	13.9	9.1	22.5	15.8	29.9
Pr	4.6	3.8	3.2	0.4	1.1	1.1	0.7	2.9	1.8	1	3.8	2.6	
Nd	19.3	16	13.2	1.9	4.6	4.7	4.1	14.3	7.8	3.7	20.5	12	15.6
Sm	4.3	3.6	2.8	0.4	1	1.2	1.6	3.6	2.2	0.9	6.3	3.1	3.8
Eu	1.5	1.2	1.1	0.9	0.5	0.6	0.8	1.4	1.4	1.3	1.5	1.4	1.2
Gd	3.3	3.2	2.5	0.5	0.8	1.1	2	3.8	3.4	1.4	6.7	3.1	4.1
Tb	0.5	0.5	0.3	0.1	0.1	0.2	0.4	0.5	0.7	0.3	1.2	0.5	0.7
Dy	2.6	2.9	2.2	0.4	0.8	1	2.2	3.1	5	2.3	7.1	3.2	
Ho	0.5	0.6	0.4	0.1	0.2	0.2	0.5	0.6	1.2	0.6	1.4	0.6	0.7
Er	1.4	1.7	1.4	0.3	0.4	0.5	1.4	1.7	3.6	2.1	3.5	1.6	2.2
Tm	0.2	0.3	0.2	0.1	0.1	0.1	0.2	0.2	0.6	0.4	0.5	0.2	
Yb	1.2	1.5	1.3	0.4	0.4	0.5	1.2	1.5	3.6	2.4	3	1.4	2.2
Eu/Eu*	1.18	1.11	1.26	5.84	1.62	1.44	1.37	1.17	1.59	3.64	0.68	1.32	0.95

Note: Care was taken that the analyzed samples do not have macroscopic or microscopic evidence for invasion of the host lava. Major element oxides (wt%) of xenoliths by XRF (North East Interdisciplinary Research Institute, Magadan, T. Manuilova and T. Borkhodoeva, analysts). Trace element analyses (ppm) by ICP-MS (Institute of Earth Crust, Irkutsk). Sample "LC_XEN"—average composition of lower crust xenoliths from (Rudnick, 1992). LOI—loss on ignition.

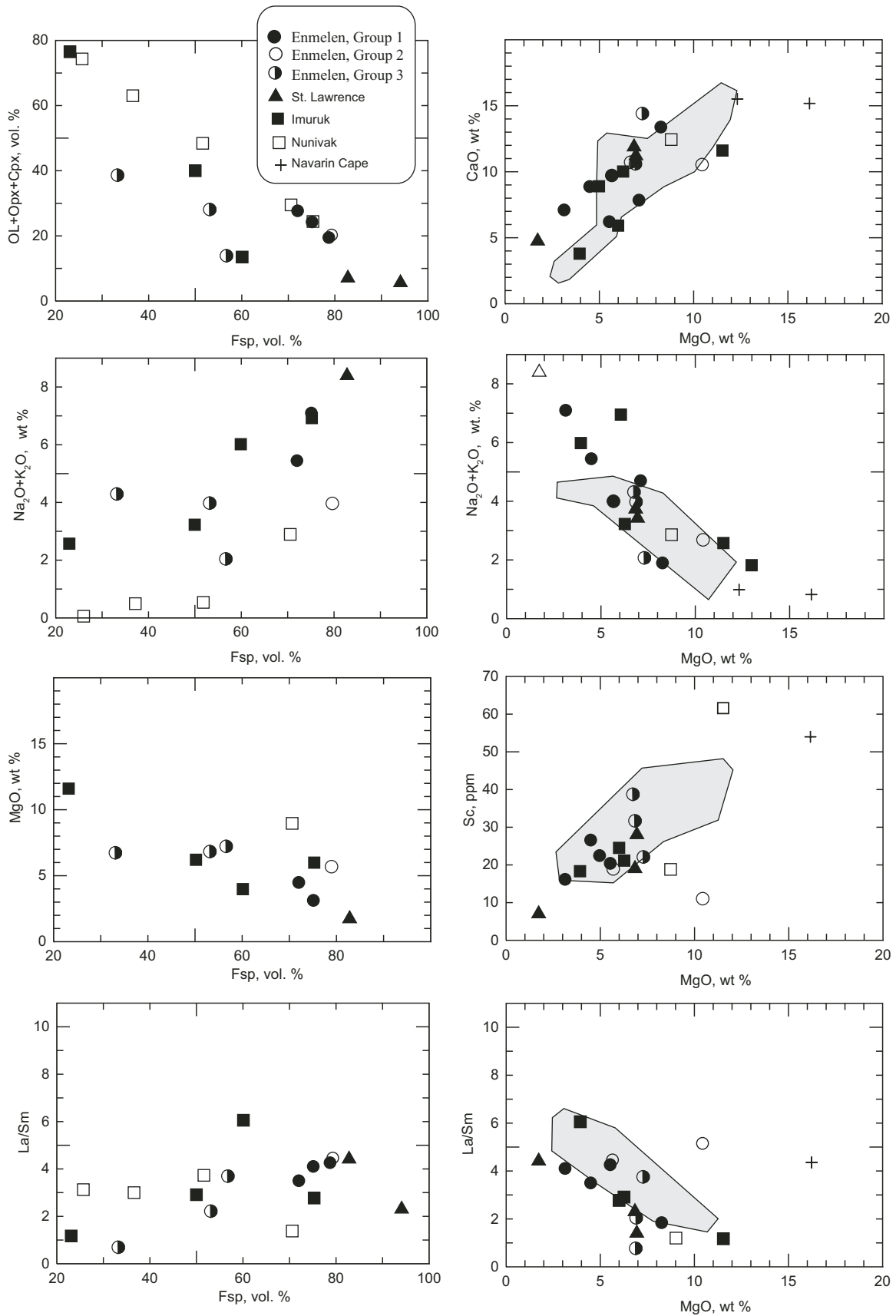


Figure 8. Major and trace elements versus mode (expressed as volume %) of plagioclase+K-feldspar (Fsp) and olivine+pyroxenes (ol+opx+cpx) for Bering Sea province lower-crustal xenoliths. Trace-element data for Nunivak xenoliths are from Roden (1982), and inferred primary dome are from Francis (1976). Gray field on diagrams shows the compositional range of lower-crustal xenoliths worldwide (Rudnick, 1992).

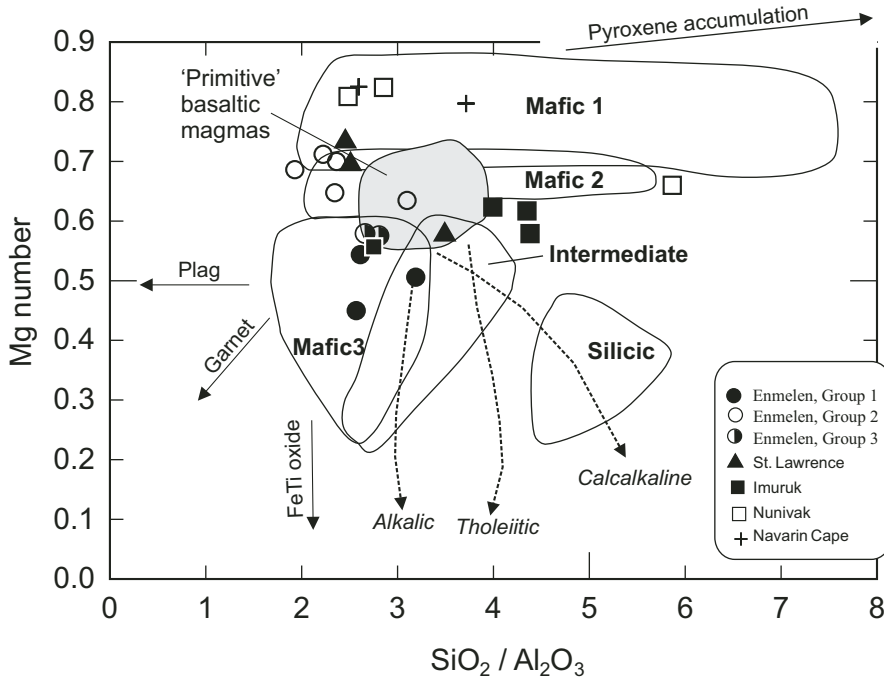


Figure 9. Mg# versus $\text{SiO}_2/\text{Al}_2\text{O}_3$ diagram for lower-crustal xenoliths from the Bering Sea basalt province compared to fields represented by other granulite-xenolith suites. Dashed arrows denote average differentiation trends for alkalic, tholeiitic, and calc-alkaline melts. Continuous arrows show general direction of compositional changes with accumulation of different minerals. Definition of fields and trends are from Kempton and Harmon (1992). Symbols used for individual samples are the same as in Figure 8. Plag—plagioclase.

fall into the relatively high-magnesium, Mafic-1 field whose protolith compositions roughly follow a pyroxene or olivine (troctolite) accumulation trend, whereas Imuruk xenoliths have lower Mg-number and the highest $\text{SiO}_2/\text{Al}_2\text{O}_3$ ratios (Fig. 9).

Trace-Element Geochemistry

Ni contents of the Bering Sea basalt province xenoliths (Table 3) do not exceed 100 ppm and are lower than expected for primary mafic melts (e.g., Sato, 1977), suggesting that their protoliths may represent fractionated magmas or layered igneous rocks in which olivine was not a main cumulate phase except for Nunivak samples. Cr contents range from 21 to 1460 ppm (highest values are for Nunivak xenoliths, Roden, 1982) and increase with Mg-number, whereas La/Sm ratios are negatively correlated with MgO (Fig. 8). These variations could be interpreted as the result of crystal accumulation.

Bering Sea basalt province xenoliths have low values of the most incompatible trace elements, resembling those of the average worldwide lower-crustal xenolith suite (Rudnick, 1992) (Table 3, Fig. 11). One exception is sample GYT28s, which has high Rb (75 ppm), Ba (710 ppm) and K_2O (2.53 wt%) perhaps reflecting contamination by host melanephelinitic lava. Most of the incompatible trace elements (Rb, U, Th, Sr, Nb, Ta, Hf) show scattered distributions relative to Mg-number, whereas Ba, Pb, and REE show a negative correlation. These relations are also compatible with magmatic fractionation. Rb/Sr ratios of xenoliths range from 0.0005 to 0.0669 (averaging 0.011), which encompass average values for the lower crust (0.032, Rudnick and Fountain, 1995).

Rare earth elements (REE) are believed to be relatively immobile during high-grade metamorphism and low $a_{\text{H}_2\text{O}}$. Thus REE distributions can provide a useful additional petrogenetic tool to help determine the protoliths for the xenoliths. Bering Sea basalt province xenoliths from different localities are distinctive in their whole-rock REE contents (total REE range from 0.6 to 150 ppm, and average 52 ppm, Table 3). The most depleted and flat REE patterns are those of Nunivak and Navarin samples (total REE = 0.6–12.4 ppm, $\text{La}/\text{Yb}_N = 1$ –3) which also have unusual major element compositions (Fig. 10D). Imuruk xenoliths have relatively flat REE distributions (total REE = 31–85 ppm, $\text{La}/\text{Yb}_N = 1.1$ –1.7) and have more or less pronounced Eu anomalies ($\text{Eu}/\text{Eu}^* = 0.6$ –3.6, Fig. 10C). Enmelen and St. Lawrence xenoliths range from LREE depleted to LREE enriched with variable enrichments in Eu. Three types of REE patterns can be distinguished from Enmelen and St. Lawrence (Table 3, Figs. 10A and 10B). Group 1 xenoliths (charnockites) have smooth, slightly LREE enriched patterns (total REE = 65–93 ppm, $\text{La}/\text{Yb}_N = 5.6$ –9.6) without pronounced Eu anomalies (Fig. 10A). Group 2 xenoliths are characterized by lower total contents of REE and positive Eu anomalies (total REE = 10–25 ppm, $\text{Eu}/\text{Eu}^* = 1.6$ –5.8, Fig. 10A). Sample EN132 has a notable pattern with the lowest total REE and a strong positive Eu anomaly, common to plagioclase cumulates. Kelyphitic gabbro, sample EN131-16 (Group 3 xenoliths, Fig. 10A) is the only sample where slight LREE depletion ($\text{La}/\text{Yb}_N = 0.6$) is observed, compatible with the fact that it was originally garnet bearing.

Extended incompatible element diagrams (Fig. 11) highlight additional aspects of Bering Sea basalt province xenoliths. The most obvious are positive anomalies for Sr and Ba, particularly in Group 2 cumulate xenoliths (Fig. 11B). Combining this

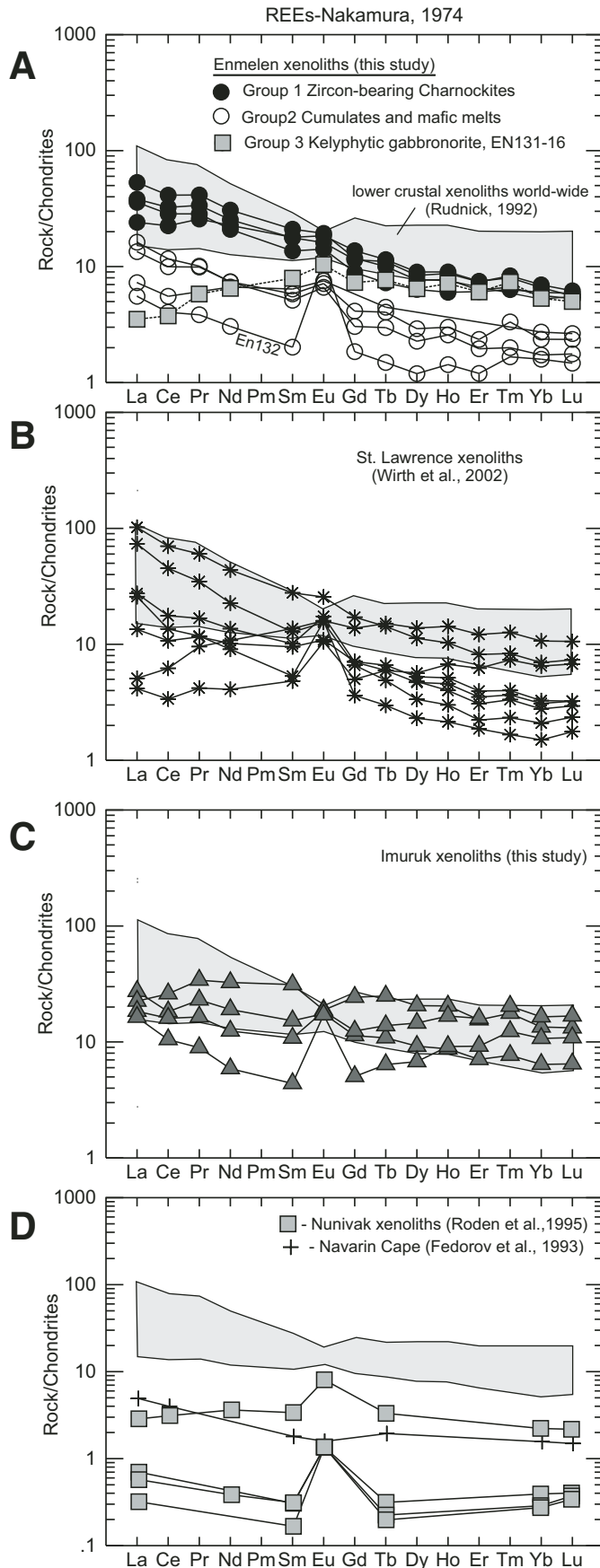


Figure 10. Chondrite-normalized REE (rare earth element) patterns for Bering Strait region plagioclase-bearing xenoliths. (A) Enmelen xenoliths (this study), (B) xenoliths from St. Lawrence Island (Wirth et al., 2002), (C) xenoliths from Imuruk volcanic field, Seward Peninsula (this study), (D) Nunivak Island (Rodén et al., 1995) and Navarin Cape (Fedorov et al., 1993). Shaded fields are average compositions of lower-crustal xenoliths worldwide (Rudnick, 1992). Normalizing values from Nakamura (1974).

characteristic with the similar behavior of Pb and Eu, which are strongly partitioned into feldspar, we can conclude that the magmatic protoliths of Group 2 xenoliths were rich in plagioclase.

Pressure and Temperature Estimates

Pressure and temperature estimates for the equilibration of the xenoliths provide a means of comparing these xenoliths to upper crustal rocks and help determine where they originated in the crust. Garnet is not present in any of the xenoliths studied, thus pressure estimates have relatively large uncertainties (assigned as 0.2–0.3 GPa). Equilibrium pressures were calculated using silica-Ca-tschermak's-anorthite (SCAn) geobarometer (McCarthy and Patino Douce, 1998), which is empirically calibrated for garnet-free granulites. The clinopyroxene geobarometer of Nimis (1999) was used for xenoliths of presumably magmatic origin with Cpx Mg-numbers > 0.7. THERMOCALC software (Holland and Powell, 1998) was used to determine equilibrium pressures for xenoliths with appropriate mineral assemblages (cpx+opx+pl+kfs+qtz+ilm+mag). The results of these calculations indicate that most xenoliths equilibrated in the deep crust, at depths between 15 and 30 km (Table 2, Fig. 12). The temperatures based on two-pyroxene geothermometry (Wells, 1977) are close to graphically estimated ones plotted on the clinopyroxene quadrilateral (Lindsley, 1983) and are 740–1090 °C. The ilmenite-magnetite thermobarometer of Andersen and Lindsley (1988), used on assemblages in xenolith SV21F, yields temperatures from 830 to 850 °C, and log f_{O_2} (QFM) = +1 to +1.3. The mineral cores were used in most cases for those calculations in order to exclude increasing temperature during late decompression melting effects which occur on grain edges. Estimated uncertainty in the thermometers used is ~50–70 °C. The xenoliths clearly record elevated temperatures that are common to granulite-facies rocks worldwide (Fig. 12).

Geochronologic Data

Ion microprobe dating of single zircons is a powerful tool that can constrain the multistage histories of zircons (e.g., Black et al., 1986; Rudnick and Williams, 1987). Cathodoluminescence (CL) imaging is used to characterize the internal structure of the zircons prior to analysis. These structures can commonly be attributed to distinct periods of igneous or metamorphic growth (e.g., Hanchar and Rudnick, 1995). In general, zircons

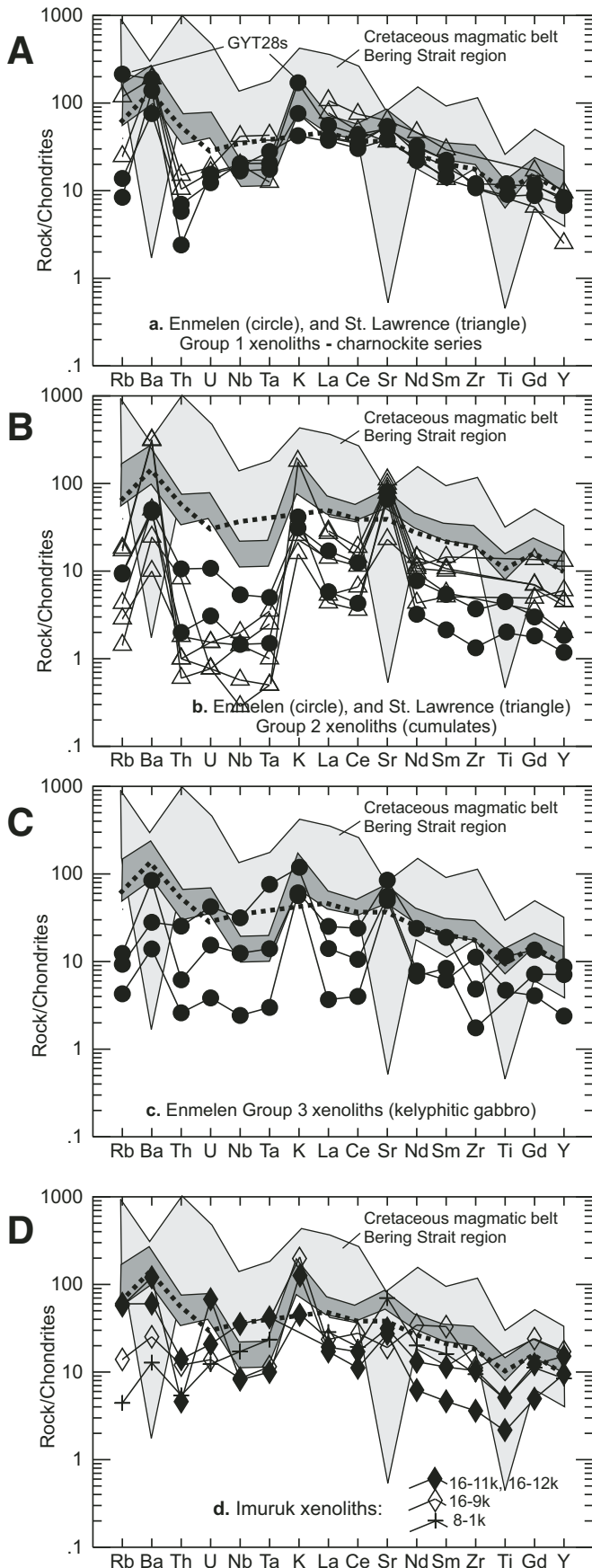


Figure 11. Chondrite-normalized incompatible trace element diagrams (spidergrams) for Bering Sea basalt province crustal xenoliths compared to existing data from Cretaceous calc-alkaline magmatic rocks (mafic volcanic rocks denoted by dark shaded field and felsic rocks are light shaded field) across the Bering Strait region. (A) Group 1 xenoliths from Enmelen and St. Lawrence, (B) Group 2 xenoliths from Enmelen and St. Lawrence, (C) Group 3 xenoliths from Enmelen, and (D) Imuruk xenoliths. Note that Group 2 xenoliths and Cretaceous calc-alkaline magmatic rocks have complementary data for most elements, particularly Rb, Ba, Th, U, and Sr. Sources for Cretaceous magmatic belt data include: Rowe (1998), Amato and Wright (1997), Polin and Moll-Stalcup (1999), Amato et al. (2003), and Akinin and Kotlyar (2002). Dotted line represents the average composition of lower-crust xenoliths (Rudnick, 1992). Chondrite composition is from Sun (1980).

from deep-crustal xenoliths have commonly resided at high temperatures for prolonged time intervals, and thus may not have behaved as entirely closed systems (e.g., Schmitz and Bowring, 2000). An important goal in this case can be to find preserved and not wholly reset domains of crystals, in order to analyze as many zircons as possible.

Zircons were separated from 3 to 5 cm diameter xenoliths using standard techniques including grinding, heavy liquids, and Frantz magnetic separation. A hand mortar was used for crushing because of the small sample size and the desire to exclude any contamination. Approximately 10–30 zircons from each sample were hand-picked and mounted in epoxy together with the R33 zircon standard (Black et al., 2004). The grains were polished to their mid-section to expose the internal structure of the zircons. Transmitted and reflected light images at 20×–500× magnification were used to identify crack and inclusion free zones for subsequent ion microprobe analysis. A custom-built cathodoluminescence detector mounted on a JEOL JSM 5600 scanning electron microscope was used to illuminate fine-scale trace-element zonation and the internal structure of the polished zircons. In situ U-Pb isotopic measurements were performed on a SHRIMP-RG (sensitive high-resolution ion microprobe–reverse geometry) at the USGS-Stanford Micro-Analytical Center using standard operating procedures described by Williams (1998). A 5–6 nA mass-filtered O₂ primary beam was focused to produce a 25–30 μm diameter analysis area with positive secondary ions extracted. The mass resolution at 10% of peak height was 6000 with a ²⁰⁶Pb sensitivity measured by CZ3 of ~14 cps/nA/ppm. Each analysis consisted of five cycles through the run table. An analysis of the R33 standard zircon (419 Ma) was run after every fourth unknown for robust Pb/U calibration throughout the analytical session. Uranium and thorium concentrations were calibrated to CZ3 (550 ppm U). The ages reported have been subjected to ²⁰⁷Pb-correction (Williams, 1998) which assumes that slightly discordant zircons are simple mixtures of trace common Pb and radiogenic Pb. Using the measured ²⁰⁷Pb/²⁰⁶Pb ratio to monitor common lead, ages are calculated by extrapolating the measured data point onto concordia along a line extending from

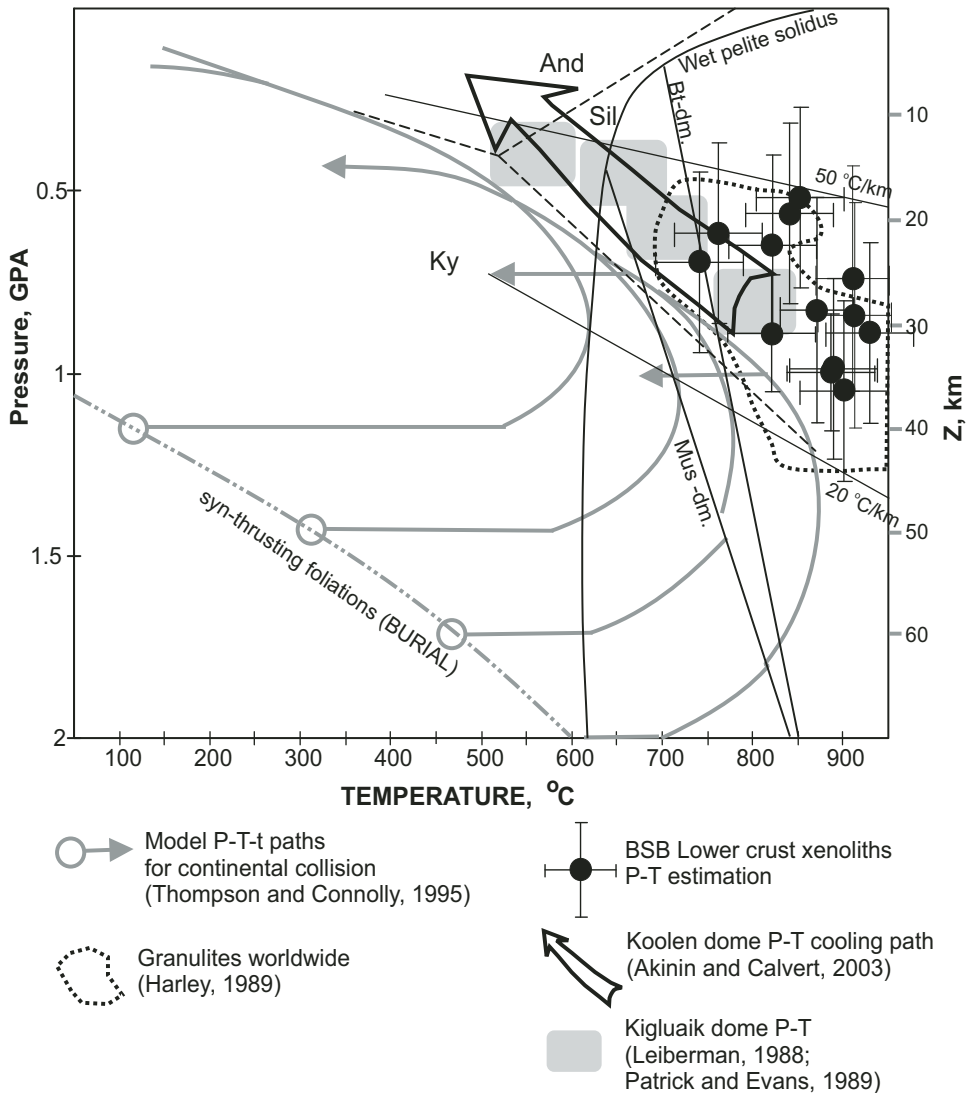


Figure 12. Pressure-temperature estimates compiled for plagioclase-bearing crustal xenoliths of Bering Strait region and their comparison with data from Bering Strait region gneiss domes. Pressure-temperature paths modeled for continental collision (gray lines and arrows) (Thompson and Connolly, 1995) show that such conditions are not sufficient to attain the temperature conditions recorded in high-grade metamorphic rocks and studied lower- to middle-crustal xenoliths. “Mus-dm.” and “Bt-dm.” are muscovite- and biotite-melting curves (Thompson and Connolly, 1995). And—andalusite; Ky—kyanite; Sil—sillimanite; BSB—Bering Sea basalt.

the model common Pb composition at an approximation for the individual grain-age. There is no obvious evidence in the cathodoluminescence images for the presence of xenocrystic cores as a source of inheritance-related discordance. The uncorrected data (Table 4) are plotted on histogram and Tera-Wasserburg concordia diagram (Fig. 13).

Forty-eight xenoliths from Enmelen, Chukchi Peninsula, and Imuruk, Seward Peninsula (Fig. 1) were processed for zircons. Eight samples of Group 1 (charnokites and two-pyroxene granulites) from Enmelen and one sample from Imuruk yielded zircons. Zircon inclusions in plagioclase were identified in two Enmelen thin-sections. In addition, 17 zircons were dated from plagioclase-bearing crustal xenoliths on St. Lawrence Island (Miller et al., 2002). Our most complete geochronological data set is that for the Enmelen xenoliths from the Chukotka Peninsula, ~250 km to the west of St. Lawrence Island (Fig. 1). Here, a total of 90 individual zircons were dated of which rim and core ages were obtained on thirteen (Figs. 13, 14, and 15; Table 4).

The majority of zircons separated from the xenoliths are 100 ± 50 microns in diameter, rounded and equidimensional to stubby in shape, and more rarely elongated with a length to width ratio of ~1:5–1:2. Crystals are transparent, colorless or light pink under transmitted light and have poorly defined faces; some grains have rounded overgrowths. CL imaging shows that the zircons are not zoned in any systematic fashion and that their zoning varies from grain to grain, even in individual xenoliths, although featureless gray domains commonly cut or rim darker oscillatory zoned zircon (Fig. 15). Concentric and sector zoning, which is presumably magmatic in origin, is present in some cores of grains and is rather irregular (Figs. 14 and 15).

When all of the Enmelen and St. Lawrence concordant ages are viewed together they show a large scatter in ages spanning 60–107 Ma; one Imuruk xenolith has zircon with the oldest age of 134.1 ± 4.4 Ma (Fig. 13A). Zircons from individual xenoliths show the same variability (Table 4). This inconsistency might be explained by differential growth and/or equilibration of zircon

TABLE 4. U-Pb SHRIMP ISOTOPIC DATA FOR ZIRCONS FROM THE ENMELLEN AND IMURUK LOWER/MIDDLE CRUST XENOLITHS

Sample grain number	Population according CL zonation	$^{206}\text{Pb}_c$ (%)	U (ppm)	Th (ppm)	$^{232}\text{Th}/^{238}\text{U}$	$^{206}\text{Pb}_R$ (ppm)	$^{238}\text{U}/^{206}\text{Pb}$	1 sd. (%)	$^{207}\text{Pb}/^{206}\text{Pb}$	1 sd. (%)	$^{206}\text{Pb}/^{238}\text{U}$ (Ma)	1 sd. (Ma)
GYT28s-1	2	0.57	449	219	0.50	4.5	85.10	5.2	.0520	6.7	74.9	3.9
GYT28s-2	1	0.00	54	24	0.45	0.6	78.20	10.3	.0313	20.7	83.6	8.6
GYT28s-3	1	0.18	333	143	0.44	3.8	75.61	3.3	.0491	7.5	84.5	2.8
GYT28s-4	3	0.14	720	302	0.43	9.0	68.40	3.0	.0490	5.3	93.4	2.8
GYT28s-5	3	0.83	464	151	0.34	5.0	79.89	3.3	.0542	6.3	79.5	2.6
GYT28s-6	3	0.00	618	366	0.61	7.7	68.94	3.1	.0447	5.7	93.2	2.9
GYT28s-7	2	0.00	706	260	0.38	8.3	72.95	3.9	.0433	5.5	88.3	3.4
GYT28s-8	1	0.00	311	189	0.63	3.5	76.75	4.2	.0471	11.3	83.5	3.6
GYT28s-9	2	0.07	801	96	0.12	8.5	80.97	3.1	.0481	5.3	79.1	2.5
GYT28s-10c	2	0.00	304	213	0.72	3.4	77.71	3.9	.0443	8.8	82.8	3.3
GYT28s-11r	2	0.00	97	33	0.36	1.1	78.06	5.2	.0422	20.6	82.6	4.4
GYT28s-12c	1	0.52	73	66	0.93	0.8	74.20	5.5	.0519	16.3	85.9	4.8
GYT28s-13r	1	0.00	61	29	0.49	0.6	80.67	5.6	.0432	21.2	79.9	4.5
g3s-1	3	0.42	289	120	0.43	3.8	65.44	4.2	.0513	8.0	97.4	4.1
g3s-2c	2	0.00	1132	374	0.34	16.1	60.46	3.3	.0459	3.5	106.0	3.5
g3s-3	2	0.17	425	118	0.29	5.5	66.40	8.1	.0493	10.3	96.2	7.8
g3s-4r	2	0.00	859	305	0.37	11.9	61.89	2.9	.0451	4.0	103.7	3.0
g3s-5	1	0.00	913	351	0.40	8.4	93.67	2.9	.0447	4.8	68.7	2.0
g3s-6	1	0.00	273	71	0.27	2.6	90.87	4.1	.0436	22.1	70.9	3.0
g3s-7	2	0.02	280	75	0.28	2.8	84.94	4.0	.0477	8.9	75.4	3.0
g3s-8	1	0.05	593	196	0.34	6.4	79.79	4.3	.0480	9.1	80.3	3.5
g3s-9c	2	0.00	804	226	0.29	10.3	67.34	2.9	.0434	5.0	95.6	2.8
g3s-10r	2	0.01	801	287	0.37	8.6	80.00	3.1	.0477	5.1	80.1	2.5
g3s-11	1	0.00	314	118	0.39	2.5	106.24	4.5	.0410	10.0	60.9	2.7
g3s-12	1	1.51	163	74	0.47	1.8	75.90	3.9	.0597	10.3	83.1	3.3
g3s-13	1	0.00	204	84	0.43	1.9	94.13	3.9	.0454	12.1	68.3	2.7
g3s-14	3	0.56	397	150	0.39	5.1	67.38	5.3	.0524	6.9	94.4	5.0
g3s-14d	3	0.22	534	182	0.35	7.2	64.14	3.3	.0498	4.3	99.5	3.3
EN136-2-1	1	9.26	67	30	0.47	0.6	88.09	4.6	.1207	14.5	66.1	3.4
EN136-2-2	3	0.14	218	56	0.27	2.6	71.40	2.6	.0489	9.7	89.5	2.4
EN136-2-3	2	0.99	343	90	0.27	4.0	72.90	2.2	.0556	8.1	87.0	2.0
EN136-2-4	3	0.59	249	58	0.24	2.5	84.72	2.6	.0522	9.4	75.2	2.0
EN136-2-5	2	0.42	581	421	0.75	6.5	76.76	3.1	.0510	6.2	83.1	2.6
EN136-2-6	2	0.00	236	70	0.31	2.6	78.60	5.2	.0454	9.4	81.7	4.3
EN136-2-7	1	0.33	406	171	0.43	3.7	94.68	8.7	.0500	7.7	67.5	5.9
EN136-2-8	3	0.00	435	201	0.48	5.4	68.94	3.9	.0440	7.1	93.3	3.6

(Continued)

TABLE 4. U-Pb SHRIMP ISOTOPIIC DATA FOR ZIRCONS FROM THE ENMELEN AND IMURUK LOWERMIDDLE CRUST XENOLITHS (Continued)

Sample grain number	Population according CL zonation	$^{206}\text{Pb}/^{238}\text{U}$ (%)	U (ppm)	Th (ppm)	$^{232}\text{Th}/^{238}\text{U}$	$^{206}\text{Pb}_A$ (ppm)	$^{238}\text{U}/^{206}\text{Pb}$	1 sd. (%)	$^{207}\text{Pb}/^{206}\text{Pb}$	1 sd. (%)	$^{206}\text{Pb}/^{238}\text{U}$ (Ma)	1 sd. (Ma)
EN136-2-9	2	0.00	403	305	0.78	4.8	72.78	1.9	.0478	9.9	88.0	1.8
EN136-2-10	2	0.00	307	150	0.51	3.5	75.17	4.3	.0453	7.0	85.5	3.7
EN136-2-11	3	0.00	481	401	0.86	5.6	74.27	2.1	.0453	6.7	86.5	1.8
EN136-2-12	3	0.00	445	194	0.45	6.4	59.41	3.4	.0465	6.5	107.8	3.6
EN136-2-13	2	0.19	297	115	0.40	3.3	77.32	3.5	.0492	8.7	82.7	2.9
EN131-5-1	1	0.42	152	50	0.34	1.6	82.24	6.6	.0509	13.8	77.6	5.2
EN131-5-2	1	0.56	431	307	0.74	4.5	81.60	3.1	.0520	6.2	78.1	2.5
EN131-5-3	1	0.00	24	4	0.18	0.2	94.75	7.7	.0403	19.1	68.3	5.3
EN131-5-4	2	0.43	201	71	0.37	2.2	79.79	3.7	.0511	10.3	79.9	3.0
EN131-5-5c	2	0.39	153	55	0.37	1.7	75.65	3.7	.0508	9.6	84.3	3.1
EN131-5-6r	1	-3.00	10	1	0.13	0.1	91.80	10.2	.0236	41.8	71.9	7.4
EN131-5-7	2	0.00	462	263	0.59	5.5	72.57	3.7	.0420	5.9	88.9	3.3
EN131-5-8	1	0.31	389	214	0.57	4.0	83.85	3.1	.0500	7.5	76.2	2.4
EN131-5-9	2	0.31	164	53	0.33	1.9	74.49	3.7	.0502	10.3	85.7	3.2
EN131-5-10	3	0.00	371	223	0.62	4.5	70.23	5.2	.0471	6.5	91.2	4.7
EN131-5-11	3	0.30	426	160	0.39	5.7	64.10	4.0	.0504	6.2	99.5	4.0
EN131-5-12	3	0.42	658	396	0.62	6.4	87.82	3.0	.0508	5.3	72.7	2.2
EN131-5-13	1	0.27	87	44	0.53	0.9	85.45	4.4	.0497	14.0	74.8	3.3
EN131-5-14	2	0.00	623	335	0.56	7.9	67.59	5.6	.0442	8.4	95.1	5.3
EN131-5-15c	2	0.09	316	148	0.48	2.5	106.74	5.1	.0479	8.8	60.1	3.1
EN131-5-16r	1	3.12	20	6	0.29	0.2	93.26	9.4	.0721	30.8	66.6	6.5
EN131-8-1	2	0.00	273	110	0.42	2.5	92.61	3.8	.0420	15.2	69.7	2.7
EN131-8-2	1	3.52	15	2	0.13	0.1	87.87	4.3	.0753	13.4	70.4	3.2
EN131-8-4	1	1.53	17	2	0.14	0.2	79.58	3.8	.0597	11.5	79.3	3.1
EN131-8-5	1	0.00	30	4	0.15	0.3	90.24	3.2	.0455	10.3	71.2	2.3
EN131-8-7	1	4.33	20	3	0.13	0.2	93.84	10.5	.0816	23.4	65.4	7.0
EN131-8-8	3	-0.47	257	137	0.55	3.2	69.96	3.2	.0441	6.3	91.9	2.9
EN131-8-9	3	-0.12	442	164	0.38	5.6	67.35	3.3	.0470	4.6	95.1	3.1
EN131-19-1	3	0.00	552	253	0.47	7.1	66.96	3.1	.0474	6.2	95.6	3.0
EN131-19-2	1	0.83	65	24	0.39	0.7	81.26	3.9	.0542	7.0	78.2	3.1
EN131-19-3	3	0.24	423	168	0.41	5.0	72.34	2.1	.0497	2.7	88.3	1.8
EN131-19-4	2	0.00	433	216	0.52	5.4	69.31	8.4	.0467	2.7	92.5	7.8
EN131-19-5	1	0.59	50	13	0.27	0.5	81.00	2.9	.0523	9.1	78.6	2.3

(Continued)

TABLE 4. U-Pb SHRIMP ISOTOPIC DATA FOR ZIRCONS FROM THE ENMELEN AND IMURUK LOWER/MIDDLE CRUST XENOLITHS (Continued)

Sample grain number	Population according CL zonation	$^{206}\text{Pb}_c$ (%)	U (ppm)	Th (ppm)	$^{232}\text{Th}/^{238}\text{U}$	$^{206}\text{Pb}_R$ (ppm)	$^{238}\text{U}/^{206}\text{Pb}$	1 sd. (%)	$^{207}\text{Pb}/^{206}\text{Pb}$	1 sd. (%)	$^{206}\text{Pb}/^{238}\text{U}$ (Ma)	1 sd. (Ma)
EN131-19-6	3	0.02	334	157	0.49	4.3	67.23	2.1	.0481	3.0	95.2	2.0
EN131-19-7	3	0.27	801	445	0.57	10.3	66.65	2.0	.0500	1.9	95.7	1.9
EN131-19-8	1	0.38	194	83	0.44	2.3	71.13	2.3	.0508	4.0	89.7	2.0
EN131-19-9	2	0.14	943	365	0.40	10.0	81.46	2.0	.0487	2.0	78.5	1.6
EN131-19-10	1	0.00	321	174	0.56	3.3	83.17	2.2	.0463	3.4	77.2	1.7
EN131-19-11	2	0.00	194	60	0.32	2.3	71.36	2.7	.0471	4.1	89.8	2.4
EN131-19-12	1	1.10	38	14	0.39	0.4	77.85	3.1	.0564	8.4	81.4	2.5
EN131-19-13	3	0.00	726	236	0.34	8.7	71.76	2.1	.0460	2.2	89.4	1.8
EN131-19-14	2	0.45	161	45	0.29	1.8	77.52	2.3	.0513	4.3	82.3	1.9
EN131-19-15	1	1.31	50	11	0.22	0.5	92.71	3.0	.0577	10.1	68.3	2.1
EN131-19-16r	3	0.22	409	127	0.32	5.2	68.17	2.3	.0497	2.6	93.7	2.2
EN131-19-17c	3	0.02	376	161	0.44	5.0	64.30	4.1	.0482	2.7	99.5	4.1
EN131-14-1c	3	0.00	665	519	0.81	7.9	72.42	3.0	.0453	5.8	88.7	2.7
EN131-14-2c	3	0.00	176	67	0.39	2.1	71.97	2.2	.0468	4.2	89.1	2.0
EN131-14-3r	1	8.64	11	3	0.32	0.1	85.72	5.3	.1159	12.8	68.3	3.9
EN131-14-4	3	0.05	225	110	0.51	2.4	80.77	10.3	.0480	3.7	79.3	8.1
EN131-14-5	3	0.39	169	63	0.39	2.1	69.57	2.5	.0509	4.1	91.6	2.3
EN131-14-6	3	0.08	442	226	0.53	5.3	72.03	2.1	.0484	2.6	88.8	1.9
EN131-14-7	2	0.00	341	139	0.42	3.8	77.28	2.1	.0473	3.2	82.9	1.7
EN131-14-8	2	0.12	471	312	0.68	5.2	77.42	2.1	.0486	2.7	82.6	1.7
EN131-14-9	3	0.00	373	128	0.35	4.5	71.70	2.1	.0474	3.7	89.3	1.9
EN131-14-10	1	2.05	25	8	0.31	0.2	86.94	3.6	.0637	10.4	72.2	2.7
EN131-14-11r	3	0.00	481	264	0.57	5.1	80.23	2.5	.0436	2.9	80.3	2.0
EN131-14-12	2	0.68	173	56	0.33	2.0	75.60	2.3	.0531	4.1	84.1	1.9
EN131-14-13	3	0.08	592	457	0.80	7.1	71.58	2.5	.0484	2.3	89.4	2.3
EN126-15-1	1	0.43	176	125	0.74	2.0	74.52	2.3	.0511	4.3	85.6	1.9
15-7k-3*		0.00	147	98	0.69	2.1	60.20	6.0	.0414	10.6	107.1	6.5
15-7k-2*		0.00	187	166	0.92	3.4	47.62	3.3	.0481	8.0	134.1	4.4
15-7k-1r*		0.78	186	146	0.81	2.9	55.02	8.1	.0545	16.6	115.2	9.4

Note: Errors as 1 sd. are 1-σ; Pb_c and Pb_R indicate the common and radiogenic portions, respectively. Error in standard calibration of R33 analyses ranges from 0.57% to 0.65% (not included in above errors). $^{206}\text{Pb}/^{238}\text{U}$ ages are as common Pb corrected by assuming $^{206}\text{Pb}/^{238}\text{U}$ age concordance. "c" and "r" for "Sample" denote cores and rims, respectively. CL—cathodoluminescence; SHRIMP—sensitive high resolution ion microprobe. One zircon grain from Imuruk xenolith, Seward Peninsula, at the bottom (15-7 k) marked with an asterisk (*).

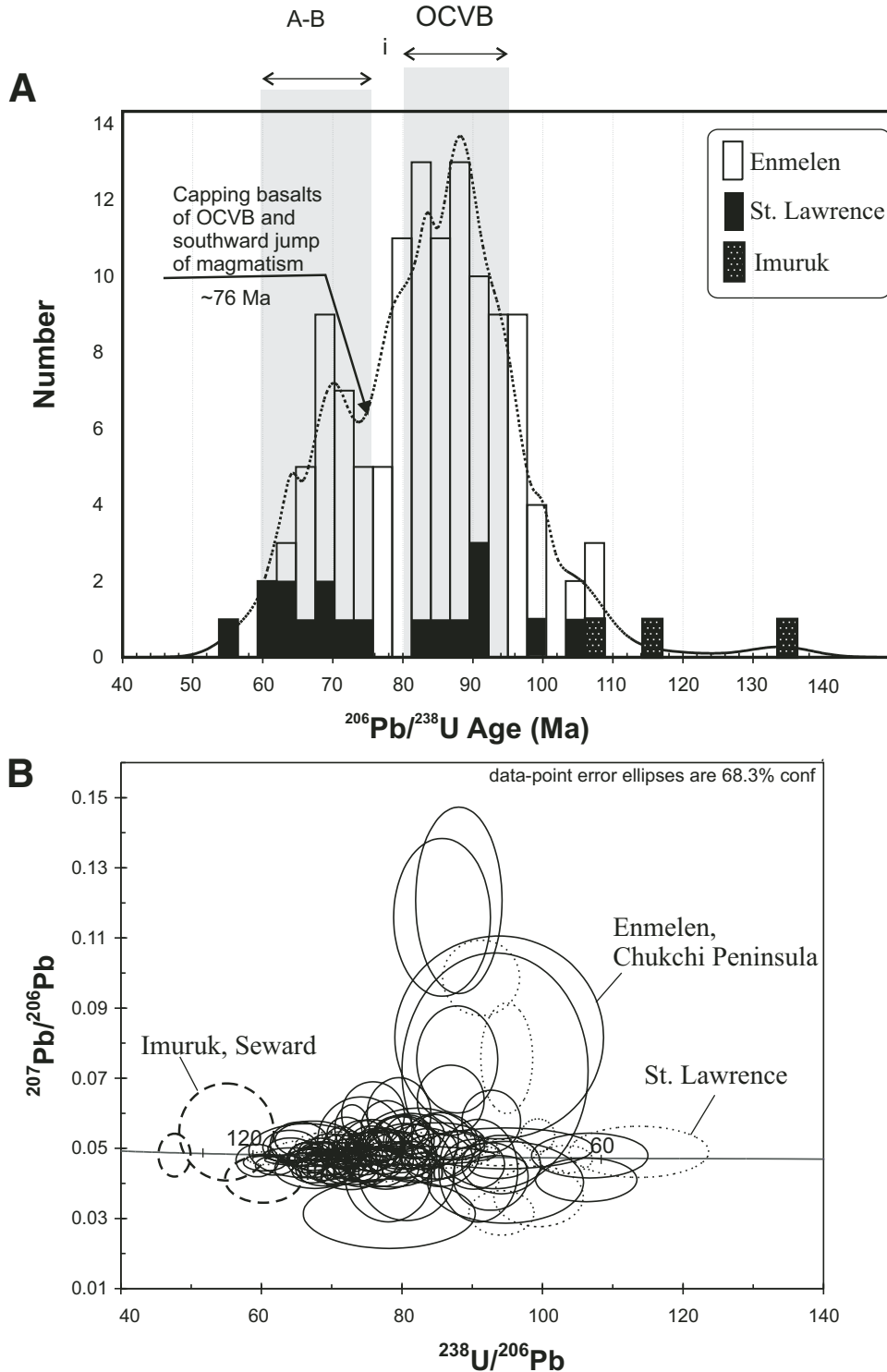


Figure 13. Histogram of SHRIMP U-Pb ages for zircons from Bering Strait region crustal xenoliths (A) and Tera-Wasserburg concordia diagram (B). Gray bars on 13A show the inferred peak of magmatic activity in the Anadyr-Bristol & Kuskokwim-Kanuti and Okhotsk-Chukotka volcanic belt (A-B and OCVB) from Figure 2.

during superimposed high grade metamorphic events, even at the scale of the samples themselves. Zircon cores are sometimes older than rims but this is not a systematic relationship (Fig. 14).

Zircons from Enmelen xenoliths can be divided into three populations according to their zonation as seen in the CL images

(Fig. 16). The first population exhibits oscillatory-zoned cores and very thin or no obvious rims. They yield an age peak on an age probability density plot at or near 90 Ma but represent two age ranges: 88–90 Ma and 92–96 Ma) (Fig. 13). The second population exhibits both cores and slightly younger rims, yielding a peak

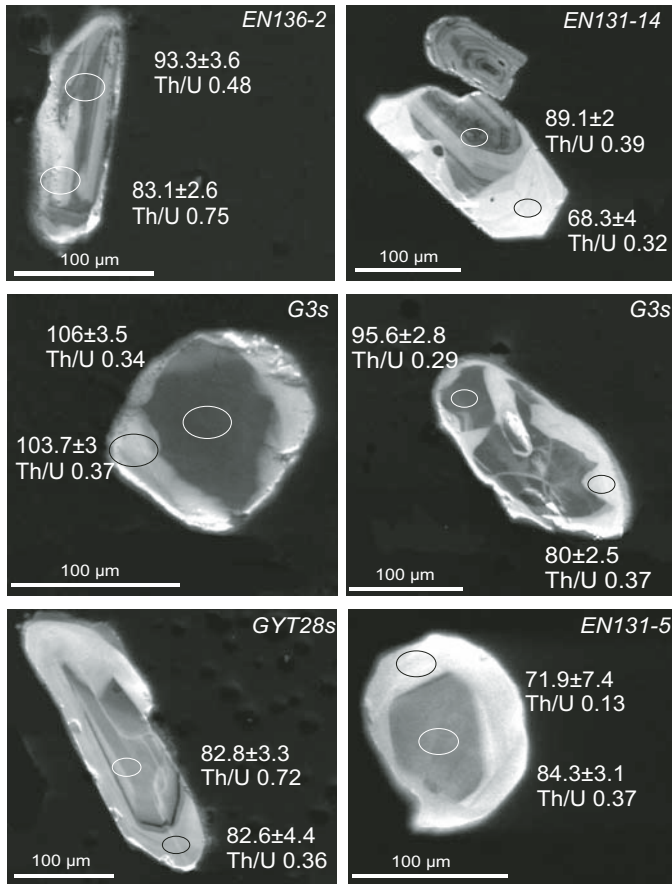


Figure 14. Cathodoluminescence images of zircon from lower-crust xenoliths from the Enmelen field. Oscillatory zoning seen in the cores of some zircons is presumed to be magmatic, and unzoned U-depleted rims are likely younger metamorphic overgrowths. White circles are individually analyzed spots by SHRIMP RG (~30 μ diameter). Numbers refer to U-Pb ages (± 1 sigma errors) and Th/U ratios presented in Table 4.

on the probability density plot at or near 83.5 Ma represented by two major age ranges: 82–86 Ma and 88–90 Ma (Fig. 13). The third population exhibits no zoning, is U-poor and homogeneous in appearance. These zircons yield two peaks on the probability density plot with ages at or near 70 Ma and 78 Ma, corresponding to three groupings of single grain age ranges on the histograms: 66–72 Ma, 76–80 Ma, and 82–86 Ma. All three types of zircon are found in individual xenoliths (Figs. 14, 15). Most of the zircons belong to the second group and exhibit oscillatory- or sector-zoned cores overgrown by younger homogeneous and U-poor rims. The best example of such a relationship is found in sample EN131-14 where homogeneous, extremely low uranium rims ($U = 11$ ppm) cut discordantly across oscillatory zoned cores (Fig. 14).

Based on the CL images, we interpret the zircons as mostly magmatic in origin as supported by the relatively high Th/U ratio of the cores (Rubatto et al., 2001; Hoskin and Schaltegger, 2003) with variable amounts of metamorphic recrystallization

by overgrowth. Decreasing Th/U ratios toward the U-poor rims were observed only in a few rare cases where different domains of the same crystals were dated (e.g., EN131-5 on Fig. 14). More often, relatively low Th/U ratios, typical of metamorphic zircons, characterize the overgrowths (e.g., Rubatto et al., 2001) as illustrated by the third type of zircon population (Fig. 17). Most of the first and second populations of zircons contain mineral-melt inclusions whereas the third population is clear and inclusion-free. Preliminary microprobe study allowed the identification of orthopyroxene as an inclusion phase in zircons from samples EN131-5 and G3s. This pyroxene is similar in composition to host rock orthopyroxenes. Combined mineral-melt inclusions in zircon are more common and are composed of Si-rich glass and orthopyroxene. Rare clinopyroxene and olivine were also found. The bulk composition of mineral-melt inclusions are mafic to intermediate. Thus most of the first and second population zircons appear to preserve evidence for their crystallization from liquid magmas.

We interpret the ages of the three populations of zircons from the Enmelen xenoliths to record both the time of magmatic events as well as accompanying high-grade metamorphism in the deep crust. The age of these events appear to coincide well with the major pulses of calc-alkaline and basaltic magmatism represented by plutons and volcanic rocks (Fig. 13). The calc-alkaline part of the Okhotsk-Chukotka continental margin volcanic belt was mostly erupted in the age range 107–80 Ma (Hourigan and Akinin, 2004; Akinin and Khanchuk, 2005) (Fig. 2). Basalts that have within-plate extension-related geochemical signatures form the youngest capping units in this belt and were erupted 78–76 Ma. This event marked the termination of volcanism in Okhotsk-Chukotka belt. The Anadyr-Bristol volcanic belt is located south of the Okhotsk-Chukotka belt (Ivanov, 1985) (Fig. 1). This belt is inferred to underlie the outer part of the Bering Sea and is also forms the basement of the Anadyr Basin of Chukotka. Its continuation on the Alaska mainland is represented by the Kuskokwim and Yukon-Kanuti magmatic belts (Agapitov et al., 1973; Marlow et al., 1976; Worrall, 1991; Moll-Stalcup, 1994). The age range of volcanic rocks within these belts is 76–55 Ma (Figs. 1 and 2).

DISCUSSION AND CONCLUSIONS

Petrologic, geochemical, and geochronologic investigations of lower- to middle-crustal xenoliths entrained in Late Neogene alkali basalts of the Bering Sea constrain the composition, conditions of equilibration, and age of the deep crust beneath the Bering Shelf allowing comparison with the geologically documented history of supracrustal magmatism, metamorphism, and deformation. This comparison is intended to help understand the processes leading to crustal growth, evolution, and modification during crustal extension. The two data sets from the deep crust (xenoliths) and shallow crust (geologic relationships) are tied together in 3-D by seismic-reflection profiles and in 4-D by geochronologic studies and P–T histories (Fig. 18).

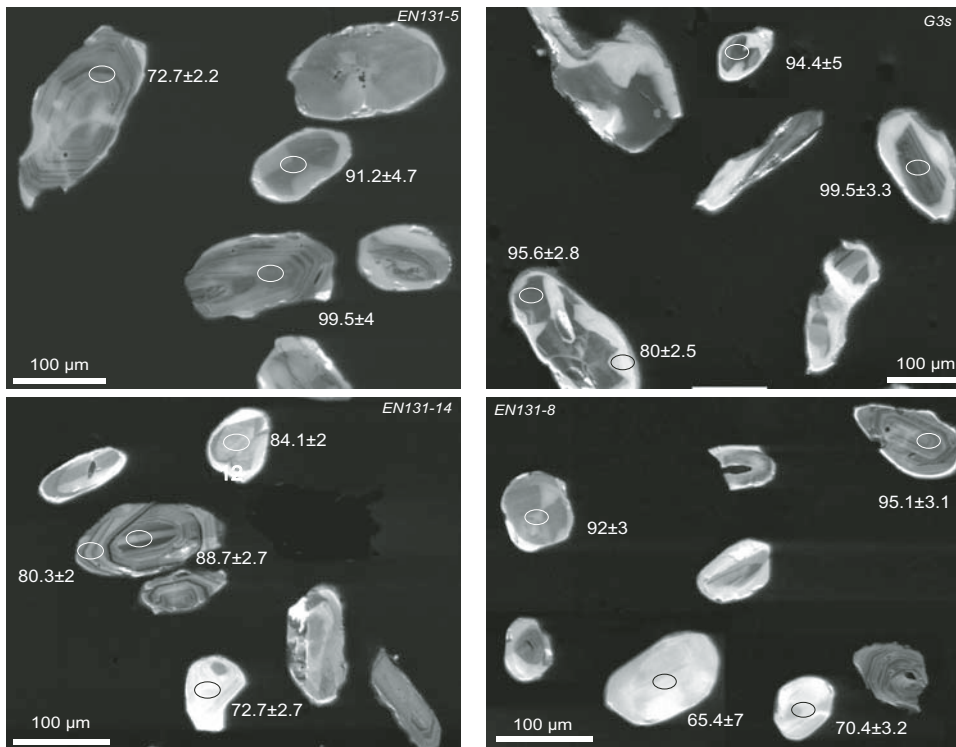


Figure 15. Cathodoluminescence images of zircon from Enmelen lower-crust xenoliths. Most of zircons are rounded and not zoned in any systematic fashion. Featureless gray domains commonly cut or rim darker oscillatory zoned zircon.

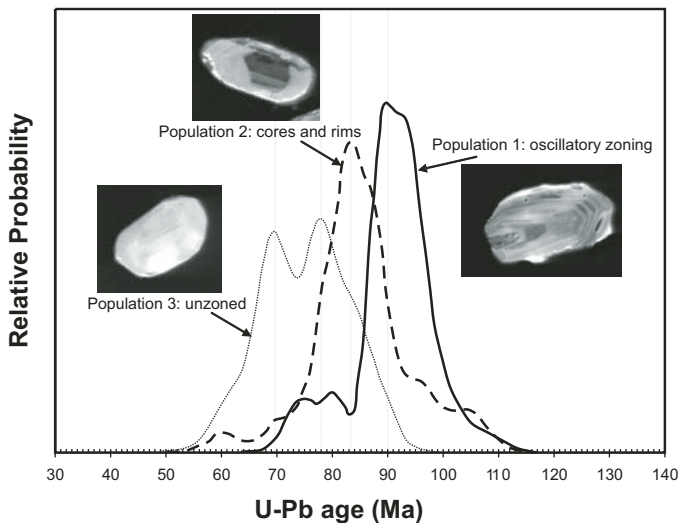


Figure 16. Zonation-based differences between zircon populations from Enmelen field xenoliths, based on their cathodoluminescence images.

Bering Sea basalt province plagioclase-bearing xenoliths represent a diverse suite of lithologic assemblages that are distinct from region to region: Chukchi Peninsula-St. Lawrence Island (Enmelen and St. Lawrence xenoliths), Seward Peninsula (Imuruk xenoliths), and the southern edge of the Bering shelf (Nunivak and Navarin xenoliths). There are no apparent genetic links between these three sets of xenoliths, but there are commonalities in those from each area. Most xenoliths are

mafic, and their geochemistry suggests they originated by magmatic fractionation processes and accumulated and resided at high temperatures to explain their subsequent granulite facies metamorphism (Fig. 12). We suggest that mafic to intermediate charnockitic rocks may reflect compositional modification of the crust induced by mantle fluids and magmatism. One of the main reactions involved in the formation of charnockites is: $\text{biotite} + \text{quartz} = \text{orthopyroxene} + \text{K-feldspar} + \text{H}_2\text{O}$ (Korzhin-ski, 1962). A metamorphic-metasomatic origin for charnockites may be related to fluids either enriched in CO_2 and depleted in H_2O as suggested by Newton (1992) or to fluids with relatively high potassium activity (Perchuk and Gerya, 1992). A magmatic origin for charnockites has also been suggested (Newton, 1992; Wilson et al., 1996). Although it is clear that both igneous and metamorphic charnockites exist, all develop under granulite-facies conditions and low H_2O activity where dehydration reactions are responsible for their anhydrous parageneses.

We interpret the notable positive anomalies for Sr and Ba in Group 2 cumulate xenoliths as reflections of feldspar-rich magmatic protolith(s). High Ba and Sr are found in granulite xenoliths from eastern Australia and from the Southwest U.S. and have been interpreted to represent Ba- and Sr-enriched lower crust produced in an island-arc environment (Arculus and Johnson, 1981). Rudnick and Taylor (1987) reported that Ba and Sr enrichment in lower-crustal xenoliths may reflect contamination of xenoliths by host lava (kimberlites or alkali basalts) and thus may not be indicative of the geochemical composition of deep crust. Here there is clear evidence that the Bering Sea basalt province xenoliths are enriched in Sr and Ba because of their high

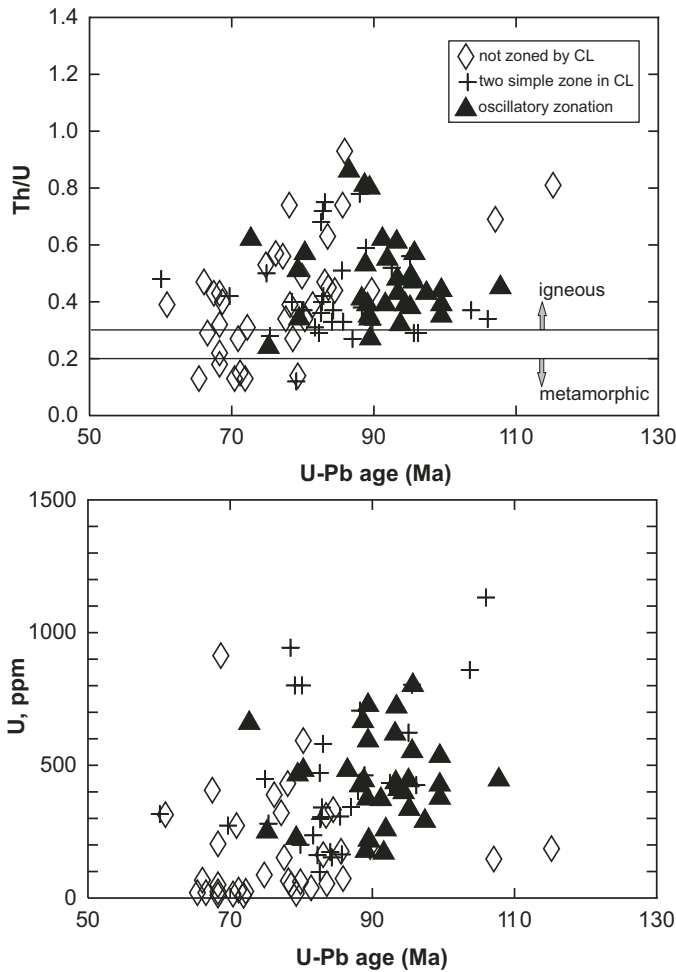


Figure 17. Th/U and U versus U-Pb age of zircons from this study indicating possible magmatic origin for most of the lower- to middle-crustal xenolith samples. Relatively low Th/U ratios and U contents are more commonly typical for metamorphic zircons (Rubatto et al., 2001; Hoskin and Schaltegger, 2003).

modal feldspar (Table 1, Fig. 8). Group 1 charnockite xenoliths have similar REE patterns to basaltic andesites and basalts of the Okhotsk-Chukotka volcanic belt, except for their negative Th and U anomalies (Fig. 11A). It is notable that Group 2 xenoliths have pronounced positive Sr and Ba anomalies compared to the observed negative anomalies of the Cretaceous magmatic belt (Fig. 11B). These differences and similarities suggest that some Group 2 xenoliths might represent feldspar-rich cumulates crystallized from calc-alkaline parent magma.

Radiogenic isotopes measured in pyroxene and plagioclase separates have mantle array type ratios attributed to an OIB-like mantle source ($^{87}\text{Sr}/^{86}\text{Sr} = 0.7040\text{--}0.70463$; $^{143}\text{Nd}/^{144}\text{Nd} = 0.51252\text{--}0.51289$; $^{206}\text{Pb}/^{204}\text{Pb} = 18.32\text{--}18.69$) (Akinin et al., 2004). The isotopic data indicate a genetic relationship between some of the xenoliths and Cretaceous calc-alkaline magmatic rocks exposed at the surface (Akinin et al., 2004). Nunivak and Navarin xenoliths located along the southern edge of the Bering

Shelf are MORB-like (Roden et al., 1995; Fedorov et al., 1993) and different in their geochemistry and isotopic ratios from the OIB-like northern xenoliths, suggesting a different composition of the lower crust beneath the area south of the Arctic-Alaska-Chukotka plate (Fig. 1).

Mineral thermobarometry indicates that the xenoliths were derived from the middle and lower crust (pressures of 0.3–1 GPa or ~10–35 km depths). Their elevated temperatures (740–1090 °C) are compatible with the range of temperatures documented in the gneiss domes, suggesting the xenoliths represent a deeper expression of the extreme temperature gradients documented in surface exposures (Fig. 4). Temperatures are also compatible with magmatic conditions as suggested by the compositions and inferred protoliths of the xenoliths. The implied geotherms are too high to be explained by terrane accretion and continental collision (Thompson and Connolly, 1995) (Fig. 12) and suggest that mantle-derived magmas or asthenospheric upwelling/lithosphere thinning supplied heat to the crust. Despite their equigranular textures, the xenoliths all possess a gneissic foliation at the hand-specimen scale, suggesting flow at high temperatures during this metamorphism; this flow was undoubtedly one of the main factors involved in producing the subhorizontal reflectivity observed in the lower crust across this region (Klemperer et al., 2002) (Figs. 5 and 18). Similarly, the reflection Moho observed across this region developed in Cretaceous to Paleogene time. In the upper crust, the earlier stages of this flow are represented by the Cretaceous gneiss domes of the Bering Strait region (Fig. 18). Their petrology and P–T paths indicate rapid rise and decompression of hot middle crustal material to the shallow crust during magmatic activity and thus in a very general sense represent gravitationally driven instabilities (Fig. 18). Multiple geochronologic studies of zircons from metasedimentary and metaigneous rocks of the gneiss domes have shown that they preserve their earlier Precambrian and Paleozoic histories and isotopic systematics, despite Cretaceous upper amphibolite- to granulite-facies metamorphic overprints (e.g., Amato, 2004).

Single grain U-Pb ages on zircons in charnockite and granulite xenoliths obtained with the SHRIMP-RG, on the other hand, are exclusively much younger and range from 60 to 107 Ma. Zircon-zonation patterns, whole-rock geochemical characteristics, and U-Pb ages as well as how these features vary with rock type and mineral content were used to reconstruct the evolution of the deep crust and tie that history to the geologic history of the upper crust. We interpret the variation in $^{206}\text{Pb}/^{238}\text{U}$ ages of zircons from xenoliths to reflect fine-scale Pb loss and the fact that mid- to Late Cretaceous magmatic ages may have been partially reset during latest Cretaceous–early Paleocene high-grade metamorphism induced by a second major pulse of mantle-derived magmas into the crust at a slightly younger time and in a slightly more southerly position (Fig. 1, inset). Elevated equilibrium temperatures calculated for xenoliths (740–890°C in most samples) are close to critical closure temperature for zircon of 900°C (Lee et al., 1997) and thus slow cooling and/or heating by younger magmatism/metamorphism may have helped to reset

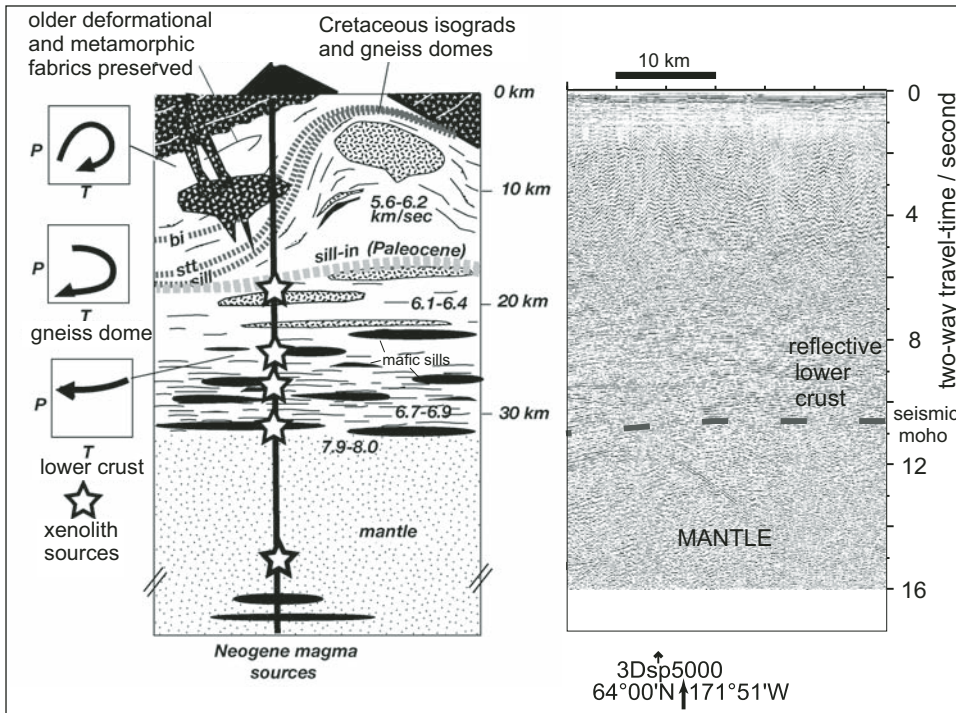


Figure 18. Schematic cross section summarizing and interpreting data presented in this study in the context of the history of extended continental crust beneath the Bering Shelf region. Portion of seismic-reflection profile is from Klemperer et al. (2002). bi—biotite, sill— sillimanite, stt—staurolite isograds.

isotopic systems. However, we do not conclude that the whole U-Pb isotopic system in the zircons has been completely reset; e.g., magmatic oscillatory zoning cores in zircons preclude complete resetting.

The Imuruk xenolith field lies far north of any exposures of Paleogene magmatic rocks and close to the northern boundary of mid- to Late Cretaceous plutons. Only one zircon grain was found in the Imuruk xenoliths; the data from this sample is considered very preliminary. One part of that zircon revealed the oldest U-Pb age obtained so far from Bering Sea xenoliths, 134.1 ± 4.4 Ma (Table 4). Although this datum is not statistically representative, it is located on the Tera-Wasserburg concordia (Fig. 13B) and thus may reflect a real geological event. This age may be related to: regional metamorphism dated in the Senyavin uplift of Russia at 139 Ma (Calvert, 1999), high-P/low-T metamorphism across the southern Brooks Range and Seward Peninsula (>125 Ma, Hannula et al., 1995), or earliest magmatic activity represented by the Yukon-Koyukuk volcanic rocks (137–120 Ma; Box and Patton, 1989; Miller and Hudson, 1991).

Perhaps the most surprising aspect of the geochronologic data is that all of the zircons, whether igneous or metamorphic, are Late Cretaceous to early Paleocene in age. A total of 125 U-Pb SHRIMP zircon ages from a wide sampling area including the Enmelen, St. Lawrence, and Imuruk fields are not only young, but have no evidence for inheritance despite the fact that the geology of this region indicates the crust beneath this region is in large part Precambrian to Paleozoic. Worldwide, lower-crustal xenoliths are commonly younger than the main rock units at the surface (e.g., Costa and Rey, 1995; Chen et al., 1994; Davis et al., 2003; Rudnick and Gao, 2003); and this is certainly the

case here. The zircon geochronology suggests that beneath the Bering Shelf, mafic to intermediate magmatism of Cretaceous to Paleogene age was the most important event to have formed and reconstituted the present-day middle and lower crust despite its Precambrian age and its older accretionary history. This conclusion was tentatively based on the nature of Cretaceous metamorphism in gneiss domes where regional strain patterns, extreme temperatures, magma compositions, and their isotopic systematics could not be explained solely as the products of crustal thickening (Fig. 12) (e.g., discussions in Amato et al., 1994, 2002; Amato and Wright, 1997; BSGFP, 1997; Akinin and Calvert, 2002; Amato and Miller, 2004).

One of the main conclusions of this geochronologic data set is that the lower crust beneath the Bering Shelf has been significantly modified during Cretaceous (107–80 Ma) magmatic intrusion, resided at elevated temperatures and was subjected to a younger thermal/metamorphic event at 75–60 Ma. These two events coincide with the age of two major pulses of calc-alkaline magmatism, represented by plutons and volcanic rocks at the surface. These two events occurred together with, and partially post-dated, stretching of previously thickened crust. Despite the fact that the xenolith localities are few, the geochronologic data show remarkable consistency across a broad geographic region, attesting to the regional nature of these conclusions about the magmatic and tectonic evolution of the deep crust. Mantle-derived magmatism is thus inferred to be the main petrologic process modifying the deep crust beneath the Bering Shelf during the Cretaceous to Paleogene. We suggest that the lower crust contains a large amount of juvenile Cretaceous (to the north) and Paleogene (to the south) magmatic rocks of both mafic and

intermediate composition. As evident from geophysical studies, there is no clear-cut zone of >7.0 km/sec velocities observed in the lower crust which could represent entirely mafic material (Figs. 5 and 18). As in many other regions, such as the Sierra Nevada and geophysically studied parts of the Basin and Range, mafic magmatic additions to the crust, predicted petrologically, are either missing or may have become part of the mantle during delamination (Ducea and Saleeby, 1996; Lee et al., 2001).

Because the locus of magmatism becomes younger southward toward the Bering Shelf edge, and actually undergoes a geographic and possibly an age jump between 80 and 76 Ma, our data provide further support for the view that the magmas originated in mantle source regions above a subducting slab that retreated southward during extension (Amato et al., 1994; Amato and Wright, 1997). Heating (and weakening) of the crust during 76–55 Ma magmatism may have controlled the locus of crustal thinning and rapid subsidence history of pull-apart transtensional basins developed along the Bering Shelf edge, which represent the youngest tectonic events that modified the deep crust beneath the outer edge of the Bering Shelf (Worrall, 1991; Klemperer et al., 2002).

Granulite-facies metamorphism has been studied in many regions on Earth and mantle-derived magmatism has commonly been implicated as the driver for the documented high temperatures, thus our conclusions are not unexpected (e.g., discussions in Sandiford and Powell, 1986; Mezger, 1992). Studies of high-grade metamorphic culminations or gneiss domes in extensional provinces have also commonly been used to argue for elevated temperatures and large-scale flow of continental crust at depth (e.g., MacCready et al., 1997; Snoke et al., 1999; Amato and Miller, 2004). Heat flow in the actively extending Basin and Range is sufficiently high to suggest granulite-facies metamorphic conditions in the deep crust and the strong subhorizontal reflectivity observed beneath the Basin and Range is believed to have developed as a consequence of this extension, thus the Basin and Range might represent a reasonable modern analog to the Bering Shelf. What is most surprising is the fact that we found no evidence for older or inherited zircons from lower-crustal xenoliths, suggesting more juvenile magma than indicated geophysically and/or total re-equilibration of the zircon isotopic systems regardless of rock types or that any older zircons completely dissolved in the high-temperature mafic melts. Whatever the age of the original Precambrian basement and the accreted terrane rocks which formed the lower crust of most of the Bering Shelf and surrounding landmasses prior to magmatism and extension, they now are replaced or remobilized and reconstituted, and form a much younger granulite-facies terrane of Cretaceous to Paleogene age. Relicts of the region's older history are preserved only in supracrustal rocks, despite Cretaceous deformational and metamorphic overprints (Fig. 18). This conclusion stands in strong contrast to the general perception, based on surface geology, that crustal growth in the Alaska and adjacent Russia Cordillera is the result of the successive addition of arc and oceanic terranes to the continental margin. Across the Bering Shelf, this collage of

terrane now forms only the uppermost part of the crustal section (Fig. 18). Looking more closely, the history and volumes of Cretaceous to Paleogene magmas, the development of sillimanite-grade gneiss domes in the Cretaceous, and the detailed geologic studies that argued for regional extension during the formation of magmatic belts in both Alaska and Russia were the main clues to understanding the broader lithospheric context of these events and their importance to interpreting the deeper crustal evolution of this region (e.g., Klemperer et al., 2002).

ACKNOWLEDGMENTS

This work was supported by RFBR grants 09-05-91005-ANF and 06-05-64824a, FEB RAS 09-1-III16-11, FMF 1201-N10, and Blaustein Visiting Scholar endowment (Stanford) to V.V. Akinin and Continental Dynamics Program (NSF) award EAR-93-17087 to S. Klemperer and E.L. Miller. We thank Jeremy Hourigan for his assistance in the fieldwork and Theo Ntaflou and Bob Jones (Stanford) for their help with microprobe analytical work. We thank Chris Mattinson for review of an earlier copy of the manuscript. Detailed reviews by Michael Roden, Steven Bergman, and editorial suggestions by Arthur Snoke improved the focus and content of the manuscript.

REFERENCES CITED

- Agapitov, D.I., Ivanov, V.V., and Krainov, V.G., 1973, New data on geology and perspective of oil and gas resources in Anadyr basin (in Russian), *in* The problems of oil and gas potential in the North-East of USSR (Novye dannye po geologii i perspektivam neftegazonosnosti Anadyrskogo basseina. V kn: Problemy neftegazonosnosti Severo-Vostoka SSSR): Magadan, Russia, Northeast Interdisciplinary Science Research Institute, v. 49, p. 23–39.
- Akinin, V.V., 1995, Petrology of alkali lavas and deep-seated inclusions of Enmelen volcanoes, Chukchi Peninsula, *in* Simakov, K.V., and Thurston, D.K., eds., Proceedings of the International Conference on Arctic Margins: Magadan, Russia, Northeast Science Center, Far East Branch of the Russian Academy of Science, p. 138–146.
- Akinin, V.V., and Apt, J.E., 1994, Enmelen volcanoes, Chukchi Peninsula: Petrology of alkaline lavas and deep-seated inclusions (in Russian): Magadan, Russia, Northeast Interdisciplinary Science Research Institute, 97 p.
- Akinin, V.V., and Calvert, A.T., 2002, Mid-crustal metamorphism and three-stage exhumation of the Koolen gneiss dome, Chukotka Peninsula, NE Russia—Constraints from thermobarometry and ⁴⁰Ar/³⁹Ar thermochronology, *in* Miller, E.L., Grantz, A., and Klemperer, S., eds., Tectonic evolution of the Bering Shelf–Chukchi Sea–Arctic Margin and adjacent landmasses: Geological Society of America Special Paper 360, p. 147–165.
- Akinin, V.V., and Khanchuk, A.I., 2005, The Okhotsk–Chukotka volcanogenic belt: Age revision based on new ⁴⁰Ar/³⁹Ar and U–Pb isotope data: Doklady Earth Sciences, v. 405, no. 8, p. 1131–1135.
- Akinin, V.V., and Kotlyar, I.N., 1997, GEOCHRON: The computer database of isotopic dating of minerals, rocks, and ores in Northeastern Siberia, *in* Byalobzeski, S.G., ed., Magmatism and mineralization in northeastern Siberia: Magadan, Russia, Northeast Interdisciplinary Science Research Institute, p. 314–318 (in Russian).
- Akinin, V.V., and Kotlyar, I.N., 2002, Origin of andesitic formation from Okhotsk–Chukotsk volcanic belt, *in* Structure, geodynamics and metallogeny of the Okhotsk region and adjacent parts of the north-western Pacific Plate: Yuzhno-Sakhalinsk, Institute of Marine Geology and Geophysics, v. 1, p. 152–153.
- Akinin, V.V., Roden, M.F., Francis, D.M., Apt, J.E., and Moll-Stallcup, E., 1997, Compositional and thermal state of the upper mantle beneath the

- Bering Sea basalt province: Evidence from the Chukchi Peninsula of Russia: *Canadian Journal of Earth Sciences*, v. 34, p. 789–800.
- Akinin, V.V., Miller, E.L., Mukasa, S., and Andronikov, A., 2004, Mesozoic-Cenozoic reworking of the deep crust beneath the Bering Sea plate: Data from lower to middle crust xenoliths: *Eos (Transactions, American Geophysical Union)*, v. 85, no. 47, abstract GP44A-07.
- Akinin, V.V., Sobolev, A.V., Ntafos, Th., and Richter, W., 2005, Clinopyroxene megacrysts from Enmelen melanephelinitic volcanoes (Chukchi Peninsula, Russia): Application to composition and evolution of mantle melts: *Contributions to Mineralogy and Petrology*, v. 150, p. 85–101, doi: 10.1007/s00410-005-0007-x.
- Allmendinger, R.W., Hauge, T.A., Hauser, E.C., Potter, C.J., Klemperer, S.L., Nelson, K.D., Knuepfer, P., and Oliver, J., 1987, Overview of the COCORP 40 N transect, western United States: The fabric of an orogenic belt: *Geological Society of America Bulletin*, v. 98, p. 308–319, doi: 10.1130/0016-7606(1987)98<308:OOTCNT>2.0.CO;2.
- Amato, J.M., 2004, Crystalline basement ages, detrital zircon ages and metamorphic ages from Seward Peninsula: Implications for Proterozoic and Cambrian–Ordovician paleogeographic reconstructions of the Arctic Alaska terrane: *Geological Society of America Abstracts with Programs*, v. 36, no. 5, p. 22.
- Amato, J.M., and Miller, E.L., 2004, Geologic map and summary of the evolution of the Kigluai Mountains gneiss dome, Seward Peninsula, Alaska, *in* Whitney, D.L., Teyssier, C., and Siddoway, C.S., eds., *Gneiss domes in orogeny: Geological Society of America Special Paper 380*, p. 295–306.
- Amato, J.M., and Wright, J.E., 1997, Potassic mafic magmatism in the Kigluai gneiss dome, Northern Alaska: A geochemical study of arc magmatism in an extensional tectonic setting: *Journal of Geophysical Research*, v. 102, p. 8065–8084, doi: 10.1029/96JB03224.
- Amato, J.M., Wright, J.E., Gans, P.B., and Miller, E.L., 1994, Magmatically induced metamorphism and deformation in the Kigluai gneiss dome, Seward Peninsula, Alaska: *Tectonics*, v. 13, p. 515–527, doi: 10.1029/93TC03320.
- Amato, J., Miller, E.L., and Hannula, K.A., 2002, Orthogonal flow direction in extending continental crust: An example from the Kigluai gneiss dome, Seward Peninsula, Alaska, *in* Miller, E.L., Grantz, A., and Klemperer, S., eds., *Tectonic evolution of the Bering Shelf–Chukchi Sea–Arctic Margin and adjacent landmasses: Geological Society of America Special Paper 360*, p. 133–146.
- Amato, J.M., Miller, E.L., and Gehrels, G.E., 2003, Lower Paleozoic through Archean detrital zircon ages from metasedimentary rocks of the Nome Group, Seward Peninsula, Alaska: *Eos (Transactions, American Geophysical Union)*, v. 84, no. 46, abstract T31F-0891.
- Andersen, D.J., and Lindsley, D.H., 1988, Internally consistent solution models for Fe–Mg–Mn–Ti oxides: Fe–Ti oxides: *The American Mineralogist*, v. 79, no. 7/8, p. 714–726.
- Arculus, R.J., and Johnson, R.W., 1981, Island-arc magma sources: A geochemical assessment of the roles of slab-derived components and crustal contamination: *Geochemical Journal*, v. 15, p. 109–133.
- Belyi, V.F., 1994, *Geologiya Okhotsko-Chukotskogo volcanogennogo poyasa (Geology of the Okhotsk-Chukotka volcanic belt): Magadan, Russia, Northeast Interdisciplinary Science Research Institute*, 76 p. (in Russian).
- Bering Strait Geologic Field Party (BSGFP), 1997, Koolen metamorphic complex, NE Russia: Implications for the tectonic evolution of the Bering Strait region: *Tectonics*, v. 16, p. 713–729, doi: 10.1029/97TC01170.
- Black, L.P., Williams, I.S., and Compston, W., 1986, Four zircon ages from one rock: The history of a 3930 Ma-old granulite from Mount Somes, Enderby Land, Antarctica: *Contributions to Mineralogy and Petrology*, v. 94, p. 427–437, doi: 10.1007/BF00376336.
- Black, L.P., Kamo, S.L., Allen, C.M., Davis, D.W., Aleinikoff, J.N., Valley, J.W., Mundil, R., Campbell, I.H., Korsch, R.J., Williams, I.S., and Foudoulis, C., 2004, Improved ²⁰⁶Pb/²³⁸U microprobe geochronology by the monitoring of a trace-element-related matrix effect; SHRIMP, ID–TIMS, ELA–ICP–MS and oxygen isotope documentation for a series of zircon standards: *Chemical Geology*, v. 205, p. 115–140, doi: 10.1016/j.chemgeo.2004.01.003.
- Box, S.E., and Patton, W.W., Jr., 1989, Igneous history of the Koyukuk terrane, western Alaska: Constraints of the origin, evolution and ultimate collision of an accreted island arc terrane: *Journal of Geophysical Research*, v. 94, p. 15,843–15,868, doi: 10.1029/JB094iB11p15843.
- Brey, G.P., and Kohler, T., 1990, Geothermobarometry in four-phase lherzolites II. New thermobarometers, and practical assessment of existing thermobarometers: *Journal of Petrology*, v. 31, p. 1353–1378.
- Brown, M., and Rushmer, T., 2006, Introduction, *in* Brown, M., and Rushmer, T., eds., *Evolution and differentiation of the continental crust: Cambridge, UK, Cambridge University Press*, p. 1–20.
- Calvert, A.T., 1999, *Metamorphism and exhumation of mid-crustal gneiss domes in the Arctic Alaska terrane [Ph.D. thesis]: Santa Barbara, University of California*, 198 p.
- Chen, Y.D., O'Reilly, S.Y., Kinny, P.D., and Griffin, W.L., 1994, Dating lower crustal and upper mantle events: An ion microprobe study of xenoliths from kimberlitic pipes: *Lithos*, v. 32, p. 77–94, doi: 10.1016/0024-4937(94)90022-1.
- Clague, D.A., and Frey, F.A., 1982, Petrology and trace element geochemistry of the Honolulu Volcanics, Oahu: Implications for the oceanic mantle below Hawaii: *Journal of Petrology*, v. 23, p. 447–504.
- Coney, P.J., Jones, D.L., and Monger, J.W.H., 1980, Cordilleran suspect terranes: *Nature*, v. 288, p. 329–333, doi: 10.1038/288329a0.
- Cook, F., van der Velden, A., Hall, K., and Roberts, B., 1999, Frozen subduction in Canada's Northwest Territories: Lithoprobe deep lithospheric profiling of the western Canadian shield: *Tectonics*, v. 18, p. 1–24, doi: 10.1029/1998TC900016.
- Costa, S., and Rey, P., 1995, Lower crustal rejuvenation and growth during post-thickening collapse: Insights from a crustal cross section through a Variscan metamorphic core complex: *Geology*, v. 23, p. 905–908, doi: 10.1130/0091-7613(1995)023<0905:LCRAGD>2.3.CO;2.
- Davis, W.J., Canil, D., MacKenzie, J.M., and Carbone, G.B., 2003, Petrology and U–Pb geochronology of lower crustal xenoliths and the development of a craton, Slave province, Canada: *Lithos*, v. 71, p. 541–573, doi: 10.1016/S0024-4937(03)00130-0.
- DePaolo, D.J., 1981, Trace element and isotopic effects of combined wallrock assimilation and fractional crystallization: *Earth and Planetary Science Letters*, v. 53, p. 189–202, doi: 10.1016/0012-821X(81)90153-9.
- Ducea, M.N., and Saleeby, J.B., 1996, Buoyancy sources for a large, unrooted mountain range, the Sierra Nevada, California: Evidence from xenolith thermobarometry: *Journal of Geophysical Research*, v. 101, p. 8229–8244, doi: 10.1029/95JB03452.
- Dumoulin, J.A., Harris, A.G., Gagiev, M., Bradley, D.C., and Repetski, J.E., 2002, Lithostratigraphic, conodont, and other faunal links between lower Paleozoic strata in northern and central Alaska and northeastern Russia, *in* Miller, E.L., Grantz, A., and Klemperer, S.L., eds., *Tectonic evolution of the Bering Shelf–Chukchi Sea–Arctic Margin and adjacent landmasses: Geological Society of America Special Paper 360*, p. 291–312.
- Evans, B.W., and Patrick, B.E., 1987, Phengite-3T in high-pressure metamorphosed granitic orthogneisses, Seward Peninsula, Alaska: *Canadian Mineralogist*, v. 25, p. 141–158.
- Fedorov, P.I., Koloskov, A.V., and Lyapunov, S.M., 1993, Deep-seated xenoliths from alkali basalts of Navarin Cape (East of Koryak Upland): *Doklady Earth Science*, v. 336, no. 2, p. 246–249.
- Forbes, R.B., Evans, B.W., and Thurston, S.P., 1984, Regional progressive high-pressure metamorphism, Seward Peninsula, Alaska: *Journal of Metamorphic Geology*, v. 2, p. 43–54, doi: 10.1111/j.1525-1314.1984.tb00284.x.
- Francis, D.M., 1976, Corona-bearing pyroxene granulite xenoliths and the lower crust beneath Nunivak Island, Alaska: *Canadian Mineralogist*, v. 14, p. 291–298.
- Francis, D.M., 1978, The implications of the compositional dependence of texture in spinel lherzolite xenoliths: *The Journal of Geology*, v. 86, p. 473–485.
- Fuis, G.S., Levander, A.R., Lutter, W.J., Wissinger, E.S., Moore, T.E., and Christensen, N.I., 1995, Seismic images of the Brooks Range, Arctic Alaska, reveal crustal-scale duplexing: *Geology*, v. 23, p. 65–68, doi: 10.1130/0091-7613(1995)023<0065:SIOTBR>2.3.CO;2.
- Green, A.G., Milkereit, B., Percival, J.A., Davidson, A., Parrish, R.R., Cook, F.A., Geis, W.T., Cannon, W.F., Hutchinson, D.R., West, G.E., and Clowes, R.M., 1990, Origin of deep crustal reflections: Seismic profiling across high-grade metamorphic terranes in Canada: *Tectonophysics*, v. 173, p. 627–638, doi: 10.1016/0040-1951(90)90250-C.
- Hanchar, J.M., and Rudnick, R.L., 1995, Revealing hidden structures: The application of cathodoluminescence and back-scattered electron imaging to dating zircons from lower crustal xenoliths: *Lithos*, v. 36, p. 289–303, doi: 10.1016/0024-4937(95)00022-4.

- Hannula, K.A., Miller, E.L., Dumitru, T.A., Lee, J., and Rubin, C.M., 1995, Structural and metamorphic relations in the southwest Seward Peninsula, Alaska: Crustal extension and the unroofing of blueschists: *Geological Society of America Bulletin*, v. 107, p. 536–553, doi: 10.1130/0016-7606(1995)107<0536:SAMRIT>2.3.CO;2.
- Holland, T.J.B., and Powell, R., 1998, An internally-consistent thermodynamic data set for phases of petrological interest: *Journal of Metamorphic Geology*, v. 16, p. 309–343, doi: 10.1111/j.1525-1314.1998.00140.x.
- Hoskin, P.W.O., and Schaltegger, U., 2003, The composition of zircon and igneous and metamorphic petrogenesis, in Hanchar, J.M., and Hoskin, P.W.O., eds., *Zircon*: Washington, D.C., Mineralogical Society of America, *Reviews in Mineralogy and Geochemistry*, v. 53, p. 27–62.
- Hourigan, J.K., and Akinin, V.V., 2004, Tectonic and chronostratigraphic implications of new ⁴⁰Ar/³⁹Ar geochronology and geochemistry of the Arman and Maltan-Ola volcanic fields, Okhotsk-Chukotka volcanic belt, north-eastern Russia: *Geological Society of America Bulletin*, v. 116, p. 637–654, doi: 10.1130/B25340.1.
- Ivanov, V.V., 1985, Sedimentary basins of north-eastern Asia (comparative oil and geological analysis): Moscow, Nauka, 208 p. (in Russian).
- Jamieson, R.A., Beaumont, C., Fullsack, P., and Lee, B., 1998, Barrovian regional metamorphism: Where's the heat, in Treloar, P.J., and O'Brien, P.J., eds., *What drives metamorphism and metamorphic reactions*: Geological Society of London Special Publication 138, p. 23–51.
- Kempton, P.D., and Harmon, R.S., 1992, Oxygen isotope evidence for large-scale hybridization of the lower crust during magmatic underplating: *Geochimica et Cosmochimica Acta*, v. 56, p. 971–986, doi: 10.1016/0016-7037(92)90041-G.
- Klemperer, S.L., 1987, A relation between continental heat flow and the seismic reflectivity of the lower crust: *Journal of Geophysics*, v. 61, p. 1–11.
- Klemperer, S.L., and Hobbs, R., 1991, The BIRPS atlas: Deep seismic reflection profiles around the British Isles: Cambridge, UK, Cambridge University Press, 124 p. + 99 sections.
- Klemperer, S.L., Hauge, T.A., Hauser, E.C., Oliver, J.E., and Potter, C.J., 1986, The Moho in the northern Basin and Range province, Nevada, along the COCORP 40 N seismic-reflection transect: *Geological Society of America Bulletin*, v. 97, p. 603–618, doi: 10.1130/0016-7606(1986)97<603:TMITNB>2.0.CO;2.
- Klemperer, S.L., Miller, E.L., Grantz, A., and Scholl, D.W., and Bering-Chukchi Working Group, 2002, Crustal structure of the Bering and Chukchi shelves: Deep seismic reflection profiles across the North American continent between Alaska and Russia, in Miller, E.L., Grantz, A., and Klemperer, S.L., eds., *Tectonic evolution of the Bering Shelf–Chukchi Sea–Arctic Margin and adjacent landmasses*: Geological Society of America Special Paper 360, p. 1–24.
- Korzhinski, D.S., 1962, Role of alkalis in origin of charnockitic gneisses, in *Geology and petrology of Pre Cambrian. Main and regional problems*: Moscow, Academy of Science USSR, v. 5, p. 50–61 (in Russian).
- Kos'ko, M.K., Cecile, M.P., Harrison, J.C., Ganelin, V.G., and Khandoshko, N.V., and Lopatin, B.G., 1993, Geology of Wrangel Island, between Chukchi and East Siberian seas, northeastern Russia: *Ottawa, Geological Survey of Canada Bulletin* 461, 101 p.
- Lawver, L.A., Grantz, A., and Gahagan, L.M., 2002, Plate kinematic evolution of the present Arctic region since the Ordovician, in Miller, E.L., Grantz, A., and Klemperer, S.L., eds., *Tectonic evolution of the Bering Shelf–Chukchi Sea–Arctic Margin and adjacent landmasses*: Geological Society of America Special Paper 360, p. 333–358.
- Lee, C.T., Yin, Q., Rudnick, R.L., and Jacobsen, S.B., 2001, Preservation of ancient and fertile lithospheric mantle beneath the southwestern United States: *Nature*, v. 411, p. 69–73, doi: 10.1038/35075048.
- Lee, J.K., Williams, I.S., and Ellis, D.J., 1997, Pb, U and Th diffusion in natural zircon: *Nature*, v. 390, p. 159–162, doi: 10.1038/36554.
- Levander, A., Lenardic, A., and Karlstrom, K., 2006, Structure of the continental lithosphere, in Brown, M., and Rushmer, T., eds., *Evolution and differentiation of the continental crust*: Cambridge, UK, Cambridge University Press, p. 21–66.
- Lieberman, J.E., 1988, Metamorphic and structural studies of the Kigluak Mountains, western Alaska [Ph.D. thesis]: Seattle, University of Washington, 192 p.
- Lindsley, D.H., 1983, Pyroxene thermometry: *The American Mineralogist*, v. 68, p. 477–493.
- Little, T.A., Miller, E.L., Lee, J., and Law, R.D., 1994, Extensional origin of ductile fabrics in the Schist Belt, Central Brooks Range, Alaska I. Geologic and structural studies: *Journal of Structural Geology*, v. 16, p. 899–918, doi: 10.1016/0191-8141(94)90075-2.
- MacCready, T., Snoko, A.W., Wright, J.E., and Howard, K.A., 1997, Mid-crustal flow during Tertiary extension in the Ruby Mountains core complex, Nevada: *Geological Society of America Bulletin*, v. 109, p. 1576–1594, doi: 10.1130/0016-7606(1997)109<1576:MCFDTE>2.3.CO;2.
- Marlow, M.S., Scholl, D.W., Cooper, A.K., and Buffington, E.C., 1976, Structure and evolution of Bering Sea shelf south of St. Lawrence Island: *American Association of Petroleum Geologists Bulletin*, v. 60, p. 161–183.
- Mathews, D.H., and Cheadle, M.J., 1986, Deep reflections from the Caledonides and Variscides west of Britain and comparison with the Himalayas, in Barazangi, M., and Brown, L.D., eds., *Reflection seismology: A global perspective*: Washington, D.C., American Geophysical Union Geodynamics Series, v. 13, p. 5–19.
- McCarthy, T.C., and Patino Douce, A.E., 1998, Empirical calibration of the silica-Ca-tschermak's-anorthite (SCAN) geobarometer: *Journal of Metamorphic Petrology*, v. 16, p. 675–686.
- Menzies, M., and Murthy, V.R., 1980, Nd and Sr isotope geochemistry of hydrous mantle nodule and their host alkali basalts: Implications for local heterogeneities in metasomatically veined mantle: *Earth and Planetary Science Letters*, v. 46, p. 323–334, doi: 10.1016/0012-821X(80)90048-5.
- Mezger, K., 1992, Temporal evolution of regional granulite terranes: Implications for the formation of lowermost continental crust, in Fountain, D.M., Arculus, R., and Kay, R.W., eds., *Continental lower crust*: Amsterdam, the Netherlands, Elsevier, *Development in Geotectonics* 23, p. 447–478.
- Miller, E.L., and Hudson, T.L., 1991, Mid-Cretaceous extensional fragmentation of a Jurassic-Early Cretaceous compressional orogen, Alaska: *Tectonics*, v. 10, p. 781–796, doi: 10.1029/91TC00044.
- Miller, E.L., Calvert, A.T., and Little, T.A., 1992, Strain-collapsed metamorphic isograds in a sillimanite gneiss dome, Seward Peninsula, Alaska: *Geology*, v. 20, p. 487–490, doi: 10.1130/0091-7613(1992)020<0487:SCMIIA>2.3.CO;2.
- Miller, E.L., Ireland, T., Klemperer, S.L., Wirth, K.A., Akinin, V.V., and Brocher, T., 2002, SHRIMP zircon dating of reflective crust and Moho beneath the Bering Shelf, Alaska and Russia, in Miller, E.L., Grantz, A., and Klemperer, S., eds., *Tectonic evolution of the Bering Shelf–Chukchi Sea–Arctic Margin and adjacent landmasses*: Geological Society of America Special Paper 360, p. 195–208.
- Moll-Stalcup, E.J., 1994, Latest Cretaceous and Cenozoic magmatism in mainland Alaska, in Plafker, G., and Berg, H.C., eds., *The Geology of Alaska: Boulder, Colorado, Geological Society of America, Geology of North America*, v. G-1, p. 589–619.
- Monger, J.W.H., Wheeler, J.O., Tipper, H.W., Gabrielse, H., Harms, T., Struik, L.C., Campbell, R.B., Dodds, C.J., Gehrels, G.E., and O'Brien, J., 1991, Cordilleran terranes, in Gabrielse, H., and Yorath, C.J., eds., *Geology of the Cordilleran orogen, Geology of Canada*: Ottawa, Geological Survey of Canada, no. 4, p. 281–327.
- Mooney, W.D., and Meissner, R., 1992, Multi-genetic origin of crustal reflectivity: A review of seismic reflection profiling of the continental lower crust and Moho, in Fountain, D.M., Arculus, R., and Kay, R.W., eds., *Continental lower crust*: Amsterdam, the Netherlands, Elsevier, *Development in Geotectonics* 23, p. 45–79.
- Moore, T.E., Wallace, W.K., Bird, K.J., Karl, S.M., Mull, C.G., and Dillon, J.T., 1994, Geology of northern Alaska, in Plafker, G., and Berg, H.C., eds., *The Geology of Alaska: Boulder, Colorado, Geological Society of America, Geology of North America*, v. G-1, p. 49–140.
- Nakamura, N., 1974, Determination of REE, Ba, Fe, Mg, Na and K in carbonaceous and ordinary chondrites: *Geochimica et Cosmochimica Acta*, v. 38, p. 757–775.
- Natal'in, B.A., Amato, J.M., Toro, J., and Wright, J.E., 1999, Paleozoic rocks of northern Chukotka Peninsula, Russian Far East: Implications for the tectonics of the Arctic region: *Tectonics*, v. 18, p. 977–1003, doi: 10.1029/1999TC900044.
- Nelson, K.D., 1992, Are crustal thickness variations in old mountain belts like the Appalachians a consequence of lithospheric delamination?: *Geology*, v. 20, p. 498–502, doi: 10.1130/0091-7613(1992)020<0498:ACTVIO>2.3.CO;2.
- Newton, R.C., 1992, An overview of charnockite: *Precambrian Research*, v. 55, p. 399–405, doi: 10.1016/0301-9268(92)90036-N.

- Nimis, P., 1999, Clinopyroxene geobarometry of magmatic rocks, Part 2: Structural geobarometers for basic to acid, tholeiitic and mildly alkaline magmatic systems: Contributions to Mineralogy and Petrology, v. 135, p. 62–74, doi: 10.1007/s004100050498.
- Nokleberg, W.J., Parfenov, L.M., Monger, J.W.H., Norton, I.O., Khanchuk, A.I., Stone, D.B., Scholl, D.W., and Fujita, K., 1998, Phanerozoic tectonic evolution of the circum-north Pacific: U.S. Geological Survey Open-File Report 98-754, 125 p.
- Padovani, E.R., and Carter, J.L., 1977, Non-equilibrium partial fusion due to decompression and thermal effects in crustal xenoliths, in Dick, H.B.J., ed., Magma genesis: Portland, Oregon, Department of Geology and Mineral Industries Bulletin 96, p. 43–57.
- Patrick, B.E., and Evans, B.W., 1989, Metamorphic evolution of the Seward Peninsula blueshist Terrane: Journal of Petrology, v. 30, p. 531–555.
- Patrick, B.E., and Lieberman, J.E., 1988, Thermal overprint on blueschists of the Seward Peninsula: The Lepontine in Alaska: Geology, v. 16, p. 1100–1103, doi: 10.1130/0091-7613(1988)016<1100:TOOBOT>2.3.CO;2.
- Patton, W.W., and Csejtey, B., 1980, Geologic map of Saint Lawrence Island: U.S. Geological Survey Miscellaneous Investigation Series Map 1-203, scale 1:250,000, 1 sheet.
- Perchuk, L.L., and Gerya, T.V., 1992, The fluid regime of metamorphism and the charnockite reaction in granulites: A review: International Geology Review, v. 34, p. 1–58.
- Polin, V.F., and Moll-Stalcup, E.J., 1999, Petrologo-geokhimicheskie kriterii tektonicheskikh uslovii formirovaniye Chukotskovo zvena Okhotsko-Chukotskogo volcanicheskogo poyasa (Petrologic-geochemical criteria of the tectonic conditions of formation of the Chukotka section of the Okhotsk Chukotka volcanic belt): Tikhokeanskaya geologia: Geology of the Pacific Ocean, v. 18, no. 4, p. 29–47 (in Russian).
- Roden, M.F., 1982, Geochemistry of the Earth's mantle, Nunivak Island, Alaska, and other areas: Evidence from xenolith studies [Ph.D. thesis]: Cambridge, Massachusetts, Massachusetts Institute of Technology, 413 p.
- Roden, M.F., Francis, D.M., and Frey, F.A., 1984, An example of consequent mantle metasomatism in peridotite inclusions from Nunivak Island, Alaska: Journal of Petrology, v. 25, p. 546–577.
- Roden, M.F., Francis, D.M., and Frey, F.A., 1995, Upper mantle composition beneath the eastern Bering Sea, in Simakov, K.V., and Thurston, D.K., eds., Proceedings of the International Conference on Arctic Margins: Magadan, Russia, North East Science Center Russian Academy of Science, p. 147–152.
- Rowe, H., 1998, Petrogenesis of plutons and hypabyssal rocks of the Bering Strait Region, Chukotka, Russia [M.S. thesis]: Houston, Texas, Rice University, 90 p.
- Rubatto, D., Williams, I.S., and Buck, I.S., 2001, Zircon and monazite response to prograde metamorphism in the Reynolds Range, central Australia: Contributions to Mineralogy and Petrology, v. 140, p. 458–468, doi: 10.1007/PL00007673.
- Rudnick, R.L., 1992, Xenoliths—Samples of the lower continental crust, in Fountain, D.M., Arculus, R., and Kay, R.W., eds., Continental lower crust: Amsterdam, the Netherlands, Elsevier, Development in Geotectonics 23, p. 269–316.
- Rudnick, R.L., and Fountain, D.M., 1995, Nature and composition of the continental crust: A lower crustal perspective: Reviews of Geophysics, v. 33, p. 267–309, doi: 10.1029/95RG01302.
- Rudnick, R.L., and Gao, S., 2003, Composition of the continental crust, in Holland, H.D., and Turekian, K.K., eds., Treatise on Geochemistry, Crust, v. 3: Oxford, UK, Elsevier, p. 1–64.
- Rudnick, R.L., and Taylor, S.R., 1987, The composition and petrogenesis of the lower crust: A xenolith study: Journal of Geophysical Research, v. 92, p. 13,981–14,005, doi: 10.1029/JB092iB13p13981.
- Rudnick, R.L., and Williams, I.S., 1987, Dating the lower crust by ion microprobe: Earth and Planetary Science Letters, v. 85, p. 145–161, doi: 10.1016/0012-821X(87)90028-8.
- Sandiford, M., and Powell, R., 1986, Deep crustal metamorphism during continental extension: Modern and ancient examples: Earth and Planetary Science Letters, v. 79, p. 151–158, doi: 10.1016/0012-821X(86)90048-8.
- Sato, M., 1977, Nickel content of basaltic magmas: identification of primary magmas and measure of the degree of olivine fractionation: Lithos, v. 10, p. 113–120, doi: 10.1016/0024-4937(77)90037-8.
- Schmitz, M.D., and Bowring, S.A., 2000, The significance of U–Pb zircon dates in lower crustal xenoliths from the southwestern margin of the Kaapvaal craton, southern Africa: Chemical Geology, v. 172, p. 59–76, doi: 10.1016/S0009-2541(00)00236-9.
- Seslavinskiy, K.B., 1979, The South Anyui suture (western Chukotka): Doklady Akademii Nauk SSSR, v. 249, p. 1181–1185.
- Sokolov, S.D., Bondarenko, G.Y., Morozov, O.L., Shekhovtsov, V.A., Glovtov, S.P., Ganelin, A.V., and Kravchenko-Berezhnoy, I.R., 2002, South Anyui suture, Northeast Arctic Russia, facts and problems, in Miller, E.L., Grantz, A., and Klemperer, S.L., eds., Tectonic Evolution of the Bering Shelf–Chukchi Sea–Arctic Margin and adjacent landmasses: Geological Society of America Special Paper 360, p. 209–224.
- Snoke, A.W., Kalakay, T.J., Quick, J.E., and Sinigoi, S., 1999, Development of a deep-crustal shear zone in response to syntectonic intrusion of mafic magma into the lower crust, Ivrea-Verbano zone, Italy: Earth and Planetary Science Letters, v. 166, p. 31–45, doi: 10.1016/S0012-821X(98)00280-5.
- Sun, S.S., 1980, Lead isotopic study of young volcanic rocks from mid-ocean ridges, ocean islands, and island arcs: Royal Society of London Philosophical Transactions, ser. A, v. 297, p. 409–445.
- Till, A.B., and Dumoulin, J.A., 1994, Geology of Seward Peninsula and Saint Lawrence Island, in Plafker, G., and Berg, H.C., eds., The Geology of Alaska: Boulder, Colorado Geological Society of America, Geology of North America, v. G-1, p. 141–152.
- Till, A.B., Dumoulin, J.A., Gamble, B., Kaufman, D., and Carroll, P.I., 1986, Preliminary geologic map and fossil data, Solomon, Bendeleben and southern Kotzebue quadrangles, Seward Peninsula, Alaska: U.S. Geological Survey Open-File Report 86-276, scale 1:250,000, 71 p. + 3 plates.
- Thompson, A.B., and Connolly, J., 1995, Melting of the continental crust: some thermal and petrological constraints on anatexis in continental collisional zones and other tectonic settings: Journal of Geophysical Research, v. 100, p. 15,565–15,579, doi: 10.1029/95JB00191.
- Toro, J., Gans, P.B., McClelland, W.B., and Dumitru, T., 2002, Deformation and exhumation of nappes in the Mt. Igipak region, central Brooks Range, Alaska, in Miller, E.L., Grantz, A., and Klemperer, S.L., eds., Tectonic evolution of the Bering Shelf–Chukchi Sea–Arctic Margin and adjacent landmasses: Geological Society of America Special Paper 360, p. 111–132.
- Warner, M.R., 1990, Basalts, water, or shear zones in the lower continental crust?: Tectonophysics, v. 173, p. 163–174, doi: 10.1016/0040-1951(90)90214-S.
- Wells, P.R.A., 1977, Pyroxene thermometry in simple and complex systems: Contributions to Mineralogy and Petrology, v. 62, p. 129–139, doi: 10.1007/BF00372872.
- Williams, I.S., 1998, U–Th–Pb geochronology by ion microprobe: Applications of microanalytical techniques to understanding mineralizing processes: Reviews in Economic Geology, v. 7, p. 1–35.
- Wilson, F.W., Shew, N., and DuBois, G.D., 1994, Map and table showing isotopic age data in Alaska, in Plafker, G., and Berg, H.C., eds., The Geology of Alaska: Boulder, Colorado Geological Society of America, Geology of North America, v. G-1, Plate 8, scale 1:2,500,000, 1 sheet with tables.
- Wilson, J.R., Robins, B., Nielsen, F.M., Duchesne, J.C., and Vander Auwera, J., 1996, The Bjerkreim-Sokndal layered intrusion, southwest Norway, in Cawthorn, R.G., ed., Layered intrusions: Amsterdam, Elsevier, p. 231–255.
- Wirth, K.R., Grandy, J., Kelley, K., and Sadofsky, S., 2002, Evolution of crust and mantle beneath the Bering Sea region: evidence from xenoliths and late Cenozoic basalts, in Miller, E.L., Grantz, A., and Klemperer, S.L., eds., Tectonic Evolution of the Bering Shelf–Chukchi Sea–Arctic Margin and adjacent landmasses: Geological Society of America Special Paper 360, p. 167–193.
- Wolf, L.W., McCaleb, R.C., Stone, D.B., Brocher, Th.M., Fujita, K., and Klemperer, S.L., 2002, Crustal structure across the Bering Strait, Alaska: onshore recordings of a marine seismic survey, in Miller, E.L., Grantz, A., and Klemperer, S.L., eds., Tectonic evolution of the Bering Shelf–Chukchi Sea–Arctic Margin and adjacent landmasses: Geological Society of America Special Paper 360, p. 25–37.
- Worrall, D.M., 1991, Tectonic history of the Bering Sea and the evolution of Tertiary strike-slip basins of the Bering Shelf: Geological Society of America Special Paper 257, 120 p.

Construction and evolution of the Kodiak Talkeetna arc crustal section, southern Alaska

David W. Farris*

Department of Geological Sciences, Florida State University, Tallahassee, Florida 32306, USA

ABSTRACT

The Kodiak Border Ranges ultramafic complex, Afognak batholith, and Shuyak Formation on Kodiak and Afognak Islands together form the lower, middle, and upper portions, respectively, of a Jurassic–Triassic island-arc crustal section. The Kodiak section exhibits structural and geochemical trends similar, but not identical to, the Tonsina-Nelchina segment of the Talkeetna arc, located >500 km to the northeast. Exposed at the base of the Kodiak section is cumulate clinopyroxenite with associated dunite, wehrlite, and layered gabbro. In the inferred middle to upper crust, tonalite and quartz diorite of the Afognak batholith intrude Shuyak Formation basaltic flows, basaltic pillow lavas, and volcanoclastic sedimentary rocks.

Despite the fault-bounded nature of the lower crustal and mantle rocks, continuous chemical trends in elements such as MgO, Ni, Cr, Nb, Sr, Y, and rare-earth elements exist across all three units. Modeling of these data suggest that Kodiak arc evolution occurred in two main stages: (1) a gabbroic initial melt underwent fractional crystallization that produced a pyroxenitic root and a gabbroic lower crust, and (2) melt in equilibrium with the gabbroic lower crust underwent assimilation-fractional crystallization to produce mid-crustal plutonic and upper-crustal volcanic rocks.

Kodiak Island exposes the oldest and thinnest portion of the Talkeetna arc, with ages from the Afognak batholith ranging from ca. 215–185 Ma. In the eastern and western Talkeetna arc, magmatism migrated northward after ca. 180 Ma in response to inferred forearc erosion. Forearc erosion coupled with differential subduction-channel movement juxtaposed blueschist-facies rocks with middle and lower crustal arc rocks. These processes occurred earlier and to a greater degree in the western Talkeetna arc, causing the arc to split in half, separating the Kodiak and Alaskan Peninsula parts of the Talkeetna arc.

INTRODUCTION

The Talkeetna arc is a Late Triassic to Early Jurassic island arc that extends for over 800 km along the southern margin of the Peninsular terrane portion of the Wrangellia composite terrane

in southern Alaska (Plafker et al., 1989, 1994). The Wrangellia composite terrane was accreted to North America prior to the mid-Cretaceous (Plafker et al., 1989; Nokleberg et al., 1994). The southern edge of the Talkeetna arc is juxtaposed against the Chugach accretionary terrane by the Border Ranges fault system.

*farris@gly.fsu.edu

Farris, D.W., 2009, Construction and evolution of the Kodiak Talkeetna arc crustal section, southern Alaska, in Miller, R.B., and Snoke, A.W., eds., *Crustal Cross Sections from the Western North American Cordillera and Elsewhere: Implications for Tectonic and Petrologic Processes*: Geological Society of America Special Paper 456, p. 69–96, doi: 10.1130/2009.2456(03). For permission to copy, contact editing@geosociety.org. ©2009 The Geological Society of America. All rights reserved.

Associated with the volcanic and plutonic units of the Talkeetna arc are a discontinuous series of ultramafic and mafic bodies that crop out along the Border Ranges fault (Fig. 1). These bodies are known as the Border Ranges ultramafic and mafic complexes, and Burns (1985) proposed that these bodies formed at the base of an island arc. Previous interpretations include: obducted ophiolite fragments (Beyer, 1980; Toth, 1981), zoned ultramafic-mafic complexes (Clark and Greenwood, 1972), garnet-bearing mantle residue (Forbes and Swainbank, 1974), and alpine-type ultramafic complexes (Hoffman, 1974). Of particular significance for this study is the Ph.D. dissertation by Beyer (1980) in which the most detailed geologic mapping of the Kodiak Border Ranges ultramafic-mafic complex is presented. Most subsequent studies of the Talkeetna arc were centered in the Tonsina-Nelchina region north of Valdez (e.g., DeBarì and Coleman, 1989). Pearcy et al. (1990) and DeBarì and Sleep (1991) were the first papers to examine the entire Talkeetna arc as a crustal section, and focused on mass balance exchange between the upper and lower parts of the arc. More recent studies include Mehl et al. (2003), who studied mantle flow recorded in the associated ultramafic

rocks; Rioux et al. (2001, 2004, 2005, 2007), who reported new geochronologic data from the upper part of the arc; Clift et al. (2005a), who made a detailed study of the volcanic rocks of the Talkeetna Formation; Clift et al. (2005b), who suggested that significant subduction erosion occurred while the arc was still active; and Greene et al. (2006), who conducted a detailed geochemical study and documented a continuous chemical linkage between the upper and lower parts of the arc.

The Talkeetna arc is important because mantle rocks through upper-crustal volcanic rocks are preserved, albeit discontinuously. This allows for high-resolution determination of the arc structure and composition (Fountain et al., 1990), which in turn is of value because magmatic arcs are a key feature in the growth and modification of continental crust. Detailed knowledge of arc structure and composition will allow a better understanding of arc processes including: how material is transported from the mantle into the crust (Paterson and Vernon, 1995), mantle-root formation and delamination (Kay and Kay, 1993), variations in the crustal rheological structure (Kohlstedt et al., 1995; Jackson, 2002), generation and redistribution of magma (Brown et al., 1995), and the interplay between magmatic activity and tectonics (Paterson and Schmidt, 1999). Due to exhumation from the mantle to the upper crust, the Talkeetna arc provides an opportunity to address and provide important insights in regard to these fundamental problems of arc evolution.

The focus of this paper is on the along-strike equivalent of the Talkeetna arc on the northwest side of Kodiak Island, southern Alaska. These rocks are located more than 500 km southwest of the Tonsina-Nelchina section. The goal of this study is: (1) to verify that the Kodiak equivalent units constitute an island-arc crustal section; (2) if the Kodiak rocks do form a crustal section, to compare them to the eastern Talkeetna arc and determine what they can tell us about arcs processes in general; (3) to produce a geochemical model of the Kodiak arc evolution; and (4) to use structural, tectonic, and petrologic relationships to postulate a model for how this crustal section was exhumed.

KODIAK LITHIC UNITS

Introduction

The Kodiak Talkeetna arc is composed of a number of independently defined lithic units (Fig. 2). The Kodiak Border Ranges ultramafic-mafic complexes, Afognak batholith, and Shuyak Formation form the lower, middle, and upper sections of the arc, respectively, whereas the Uyak Complex and Raspberry Schist are accretionary units involved in the exhumation of the arc. Each unit is described, and how these units fit into a potential arc-crustal section is examined.

Kodiak Border Ranges Ultramafic-Mafic Complexes

The Kodiak Border Ranges ultramafic-mafic complexes are a series of km-scale, fault-bounded blocks of layered gabbro,

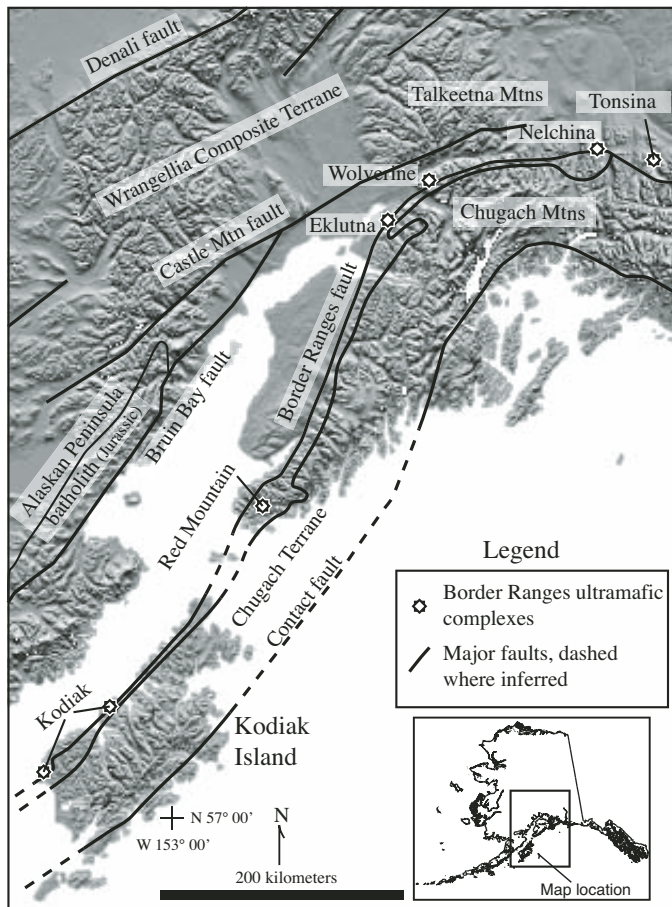


Figure 1. Map of south-central Alaska showing physiographic features; some major faults and terranes; and localities of the Border Ranges ultramafic-mafic complexes, which form the base of the accreted Jurassic–Triassic Talkeetna island arc.

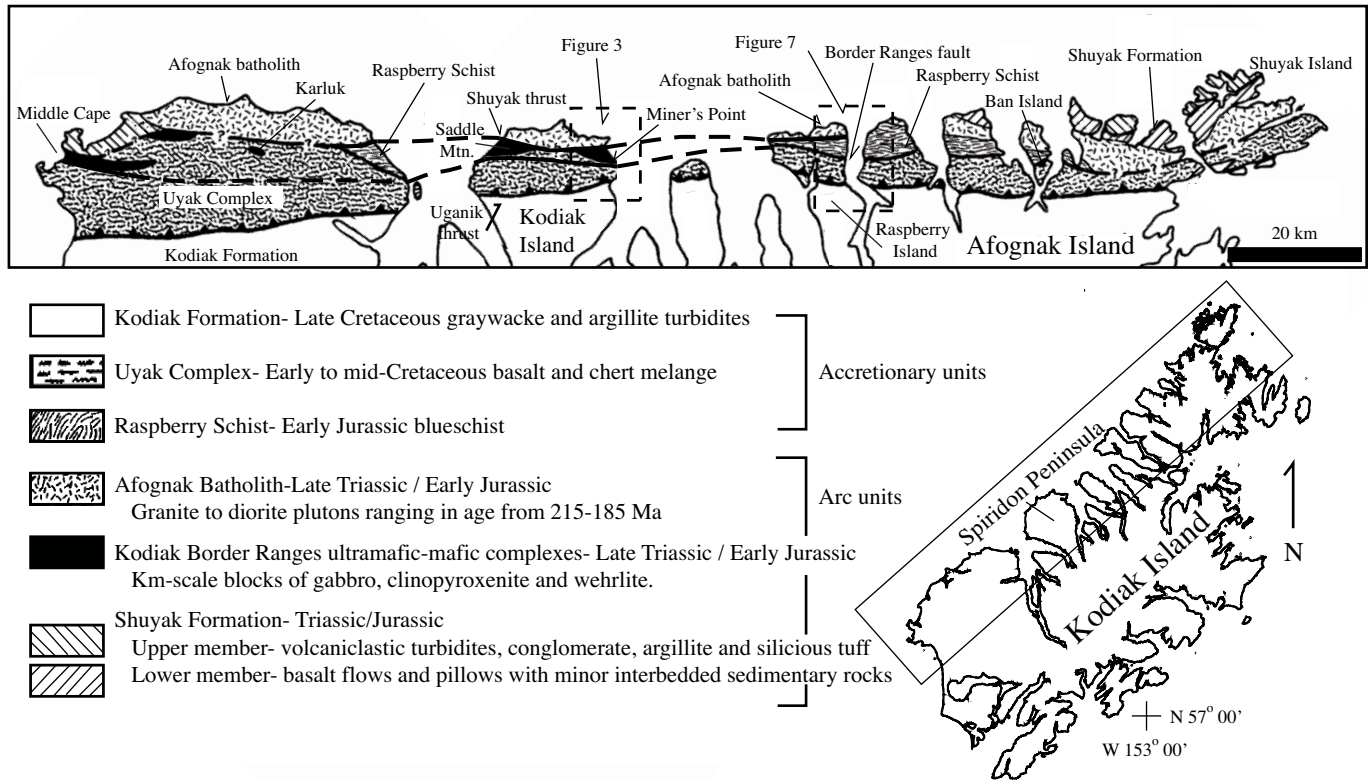


Figure 2. Geologic map of the northwest side of the Kodiak Islands. The distribution of the main units of the arc section are shown, as well as major faults and the accretionary units to the south (after Connelly, 1978).

clinopyroxenite, and dunite that occur along the northern boundary of the accretionary Uyak Complex (Beyer, 1980; Burns, 1985). The largest of the ultramafic complexes with the thickest pyroxenite section occurs on the Spiridon Peninsula of Kodiak Island (Fig. 2), where excellent coastal exposures of this body occur along its northeast and southwest margins. The northeastern exposure is known as the Miner's Point body (Fig. 3), and the southeast exposure occurs at Saddle Mountain (Fig. 2). Exposure between these two localities is poor, and it is not known if the two bodies are continuous. However, their internal stratigraphy is sufficiently similar to suggest that these separate bodies are likely related (Beyer, 1980).

The other major exposure of rocks from the Kodiak Border Ranges ultramafic-mafic complex occurs on the southwestern end of Kodiak Island and is known as the Middle Cape body. The Middle Cape body lacks ultramafic rocks and shares some affinity with the Afognak batholith. From south to north the Middle Cape body becomes less mafic. Its southern boundary is a serpentinite shear zone. Immediately north of this shear zone lies ferrogabbro cut by basaltic dikes. The ferrogabbro grades into a quartz gabbro and the mafic dikes die out. North of that locality is tonalite and a thick section of volcanic rocks (i.e., Middle Cape volcanic rocks) that are considered correlative with the Shuyak Formation. Beyer (1980) states that the nature of the contact between the quartz gabbro and tonalite-volcanic rocks is uncertain.

The two other exposures considered related to the Kodiak Border Ranges ultramafic-mafic complex are small (1.0 × 0.2 km), poorly exposed slivers surrounded by accretionary rocks (Beyer, 1980). These are the Karluk body, located inland of Uyak Bay, and the Ban Island body, located on Ban Island off the northwestern coast of Afognak Island. The Karluk body is a small lens of layered clinopyroxenite, dunite, and gabbro-norite bounded by small serpentinite shear zones and surrounded on all sides by mélangé of the Uyak Complex. The Ban Island body is exposed between Raspberry Schist and rocks of the Uyak Complex. The two smaller bodies are in different stratigraphic positions than the two larger bodies, and therefore suggest somewhat different structural histories.

Afognak Batholith

The Afognak batholith is composed of a suite of quartz dioritic to granitic plutons that range in age from ca. 215–184 Ma (Carden et al., 1977; Roeske et al., 1989). The batholith is elongated parallel to regional strike and extends throughout the Kodiak Islands region. Older ages from the batholith are from Afognak and Raspberry Islands, whereas the younger ages are from west of Uyak Bay on Kodiak Island. The rocks of the batholith are chiefly composed of plagioclase, quartz, hornblende, and biotite, with trace amounts Fe-Ti oxides and apatite (Hill, 1979). Typically,

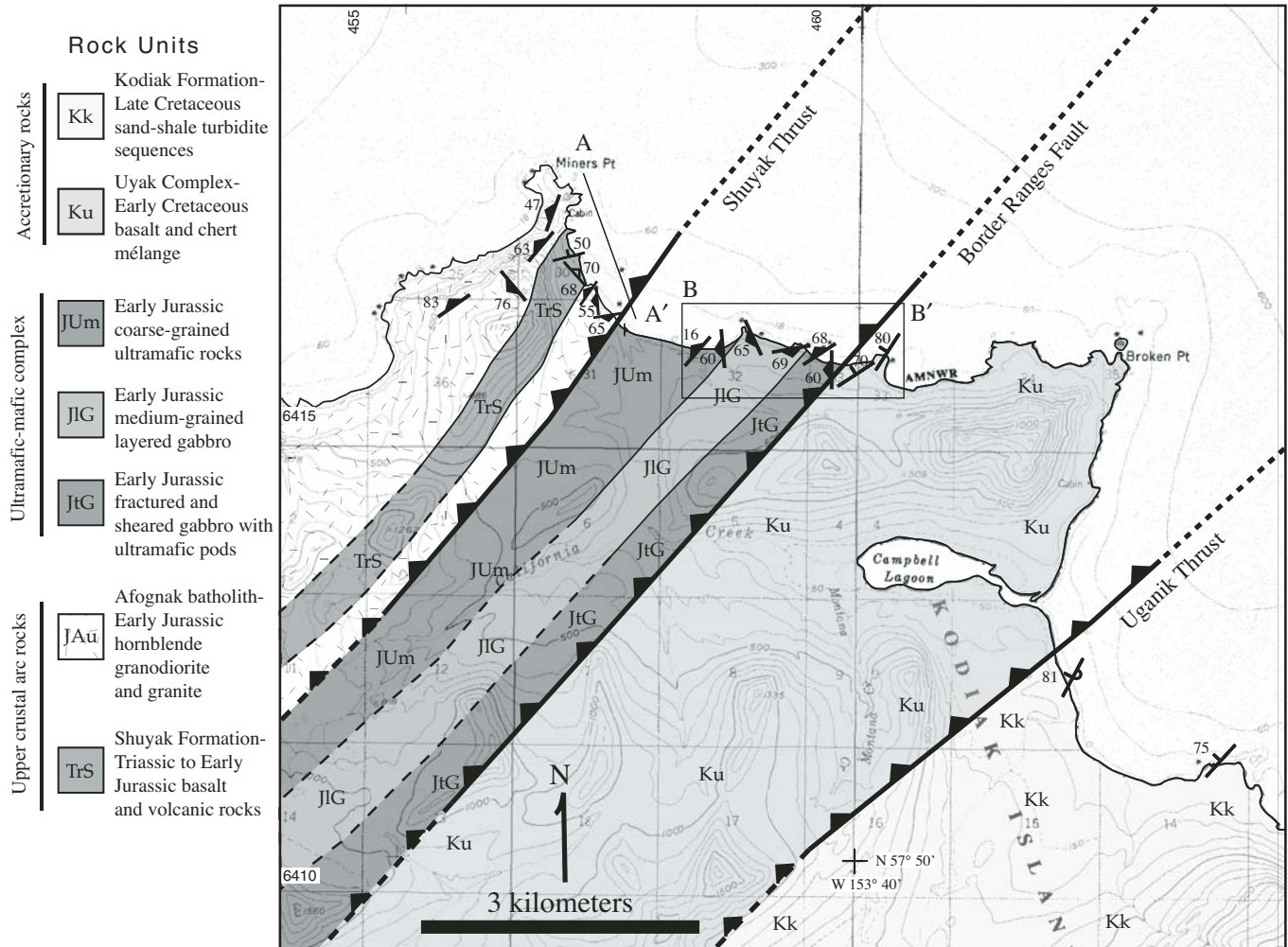


Figure 3. Geologic map of Miner's Point on the Spiridon Peninsula (see Fig. 2 for general location). Upper-crustal exposures of the Afognak batholith and the thickest example of the Kodiak Border Ranges ultramafic-mafic complex occur at this locality (after Moore, 1967; Beyer, 1980; new mapping by author conducted during summer 2003).

hornblende is euhedral and exhibits green to brown pleochroism. Texturally some of the rocks are plagioclase + hornblende cumulates, but most have hypidomorphic-granular to porphyritic textures (Hill, 1979). No pyroxene has been reported from these rocks. On the Spiridon Peninsula, the rocks are granitic in composition with subhedral to anhedral hornblende. Hill (1979) suggested an island-arc setting, similar to the modern Tonga-Kermadec arc, for the development of the Afognak batholith.

Shuyak Formation

The Upper Triassic Shuyak Formation is a sequence of basaltic flows, basaltic pillow lavas, and volcanoclastic sedimentary rocks, which are exposed on the northwestern side of Kodiak, Afognak, and Shuyak Islands (Connelly, 1978). Based on trace-element data, Hill and Gill (1976) suggest that most of the basaltic rocks are island-arc tholeiites. The thickest portion of the unit occurs on Shuyak and Afognak Islands. Connelly

(1978) has subdivided the unit into upper and lower members. The upper member is predominantly composed of sedimentary rocks including: volcanoclastic turbidites, conglomerate, argillite, and siliceous tuff. The lower and southernmost member is composed of basaltic flows and pillow lavas with minor tuff. The upper and lower members are presently fault-bounded, but the volcanic-rich member has more extensive sedimentary interbeds near its upper boundary suggesting an original gradational contact. The upper sedimentary unit contains the pelecypod *Halobia* cf. *H. halorcica*, which is of Norian age (Connelly, 1978). The southern boundary of the Shuyak Formation is an intrusive contact with the Afognak batholith.

Uyak Complex

The Uyak Complex forms the southern boundary of the Kodiak crustal section and is dominantly an oceanic mélange composed of radiolarian chert and pillow basalt (Connelly,

1978). Fossil ages from this unit range from Paleozoic (cryptozoic Nassellariina) to Early Cretaceous (*Thanarla conica* and *Archaeodictyomitra* with late Valanginian to late Aptian ages [Connelly, 1978]). The younger mid-Cretaceous fossils are likely close to a depositional age, whereas the older Paleozoic fossils are interpreted as blocks caught up in the mélangé. Connelly (1978) included the Kodiak ultramafic-mafic complexes as blocks of oceanic crust within Uyak Complex, however, subsequent workers have suggested that they are older and part of the Talkeetna arc (Burns, 1985). The mélangé of the Uyak Complex is bound by major faults. Its southern boundary is the Uganik thrust, where the Uyak Complex is thrust above the Upper Cretaceous Kodiak Formation, and its northern boundary is the Border Ranges fault, which separates arc-related rocks from the accretionary units to the south.

Raspberry Schist

The Raspberry Schist is an Early Jurassic high-pressure/low-temperature blueschist-facies unit composed of metabasitic and tuffaceous metasedimentary rocks. Roeske et al. (1989) report pumpellyite-actinolite and lawsonite-albite-chlorite blueschist-facies mineral assemblages. Roeske (1986, 1989) split the schist into two units: Js1 and Js2, based on different metamorphic histories. According to Roeske (1986), Js1 has a lower-metamorphic grade and experienced minimum pressures of ~3.4 kb and maximum temperatures of ~350 °C. Js2 is more strongly deformed and has a greater maximum temperature estimate of ~475 °C at pressures of 6–8 kb. Unit Js1 contains abundant lawsonite, whereas glaucophane is common and lawsonite scarce in unit Js2. The Raspberry Schist is a fault-bounded lithic unit. To the south it is juxtaposed against the Uyak Complex by the Border Ranges fault, whereas to the north the Shuyak fault separates the Raspberry Schist from rocks of the Afognak batholith.

MAP AREAS

Introduction

Detailed geologic and structural mapping were conducted in two parts of the Kodiak arc section that exhibit contrasting field relations. The two areas are Miner's Point on the Spiridon Peninsula and Raspberry Strait between Raspberry and Afognak Islands. The structural and petrologic differences between these two localities provide important controls on the exhumation history of the arc.

Miner's Point Kodiak Border Ranges Ultramafic-Mafic Complex

The crustal section near Miner's Point contains the best and largest exposure of the Kodiak Border Ranges ultramafic-mafic complex (Figs. 3 and 4B). Bounding the ultramafic-mafic complex are 50–100-m-wide serpentinite gouge zones (Fig. 5). To

the north of the Kodiak Border Ranges ultramafic-mafic complexes, rocks of the Afognak batholith intrude basaltic rocks of the Shuyak Formation, and to the south, the accretionary Uyak Complex is exposed.

The Kodiak Border Ranges ultramafic-mafic complex is highly sheared and faulted, however, it can be divided into three semi-coherent units. The northwestern side of the complex contains the best preserved ultramafic rocks. These include sheared dunite, coarse-grained (up to 1–3 cm) layered clinopyroxenite, and large phacoids of black pyroxenite surrounded by serpentinite mélangé. Every few tens of meters, large, 1–2-m-wide shear zones occur.

The middle unit in the Miner's Point Kodiak Border Ranges ultramafic-mafic complex is the most structurally coherent, and is composed of medium-grained layered gabbro-norite (Figs. 3, 4B, 5B). Individual compositional layers range from 5 to 30 cm in width and are composed of alternating light and dark bands rich in plagioclase and pyroxene, respectively. Also, compositional bands and a layer-parallel magmatic foliation strike ~150° and dip 50–80° to the west–southwest in the western part of the middle unit, and on its eastern edge, the foliation strikes ~80° and dips 65° S. Together, the changes in the orientation of layering define a southwest-plunging antiform. However, displacement on numerous minor shear zones in this zone is not known. Consequently, it is uncertain if the antiform is due to folding or due to fault rotation of individual blocks within the unit as a whole.

The easternmost ultramafic unit is compositionally similar to the westernmost unit; however, it has experienced greater internal shearing. Alternating zones of gabbro-norite and clinopyroxenite merge eastward into cataclastic clinopyroxenite and dunite. These cataclastic rocks grade into phacoids of black pyroxenite surrounded by serpentinite mélangé and in turn strike into a 50–100-m-wide section of serpentinite gouge that separates the ultramafic-mafic complex from the mélangé of the Uyak Complex (Fig. 5A). A 3-m-wide rhyodacite dike intrudes the gouge zone near the contact.

Afognak Batholith at Miner's Point

The Afognak batholith at this location is composed of moderately coarse-grained granite and granodiorite that exhibit a mutually intrusive relationship with basalt and greenstone of the Shuyak Formation (Figs. 3 and 4A). The southeast boundary of the granitic rocks is a northwest-dipping shear zone with steeply plunging lineations and fault grooves. The granite grades westward through a zone of cataclasis into rocks with a sugary texture before grading into coherent, moderately coarse-grained hornblende ± biotite granite. Continuing westward, small, near-vertical basaltic dikes intrude the granite, some of which have incorporated angular granitic xenoliths (Fig. 6B). Locally there appears to be some hybridization between the granitic and basaltic magmas. The spatial density of basaltic dikes increases to the northwest until a thick section of massive basalt is encountered. A small valley with no outcrop, possibly containing a fault,

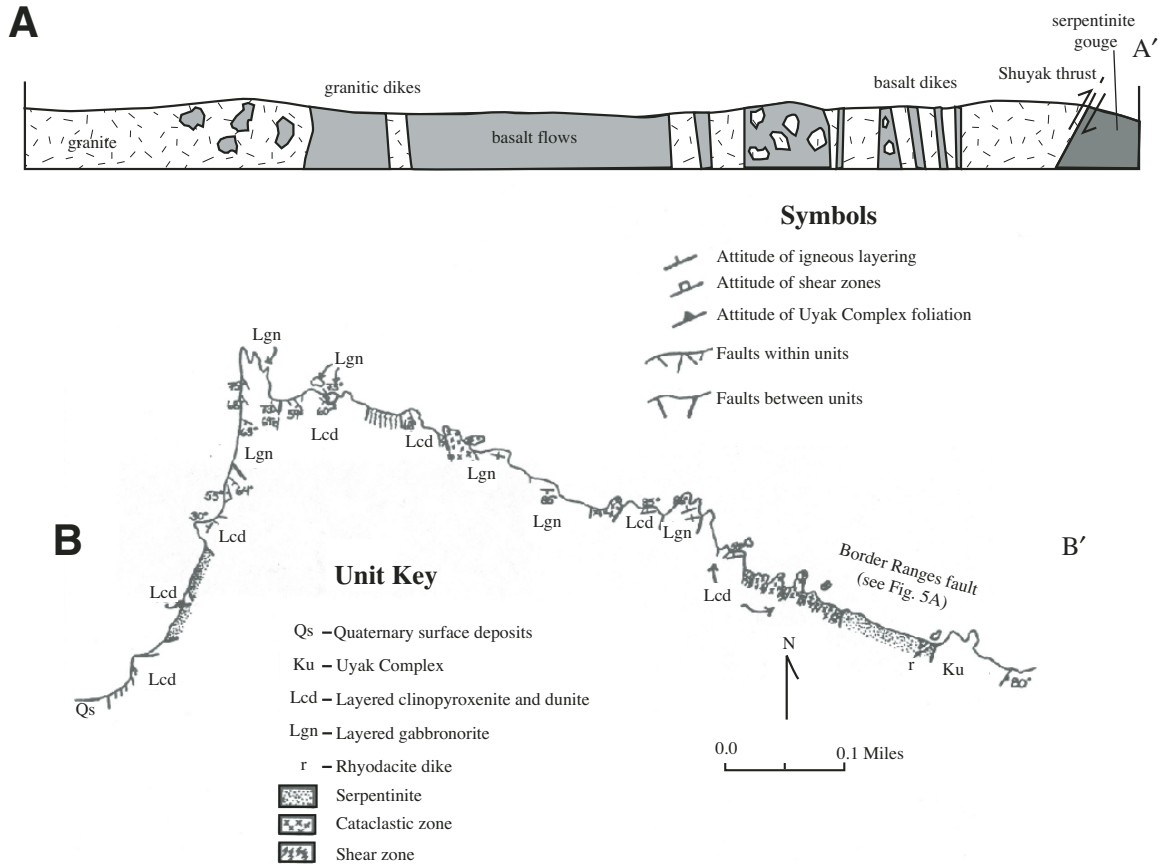


Figure 4. Geologic cross sections and shoreline map of Miner's Point area. (A) Schematic cross section across the Afognak batholith (topography is also schematic; most data are from sea cliff exposures). The granite and basaltic rocks exhibit mutually intrusive relationships suggesting a shallow level of emplacement for the coarse-grained plutonic rocks. (B) Detailed shoreline map of the ultramafic-mafic complex (after Beyer, 1980).

separates the granite with basaltic dikes from the massive basalt flows. The massive basalts have experienced more alteration to greenschist-facies mineral assemblages (i.e., now greenstones) than the intrusive basaltic dikes. Boundaries between flows are difficult to observe, but one potential chilled margin had a strike and dip of 256° , 50° NW, respectively. Northwest of the massive basalt flows, granite and granodiorite with conspicuous sulfide mineralization intrude the basalt, and large basaltic blocks occur within the granite (Fig. 6A). Farther to the northwest, basalt is not present and the granite becomes coarse-grained and continues westward out of the map area.

Raspberry Strait

The second area of detailed mapping is along Raspberry Strait, near Afognak Island (Fig. 7). This region is along strike with the Miner's Point area, and contains the same major fault geometry with the Uganik thrust, Border Ranges fault, and Shuyak thrust. However, the ultramafic-mafic complex is not present. Instead a thick section of blueschist-facies Raspberry

Schist occurs in a similar structural position (e.g., Roeske, 1986; Roeske et al., 1989).

Afognak Batholith, Raspberry Strait

Along Raspberry Strait, the Afognak batholith is composed primarily of hornblende-rich tonalite and diorite, which intrude volcanic rocks of the Shuyak Formation. Parts of two plutons are exposed in this area, and are separated by a wall-rock screen and an extensive zone of blocks of the Shuyak Formation (Fig. 7). The southwestern pluton is dioritic, whereas the northeastern one is tonalitic. Also, the southeastern plutonic contact is marked by strongly migmatitic volcanic rocks of the Shuyak Formation with extensive lit-par-lit injections of tonalite and partial anatexis of the wall rocks as suggested by geochemical modeling (Fig. 8). Farther from the contact, and close to the Shuyak thrust, the volcanic rocks exhibit iron staining and hydrothermal alteration. Within the pluton, the intrusive rocks of the margin are cut by numerous small-scale shear zones. The hornblende at this location is euhedral, moderate to coarse

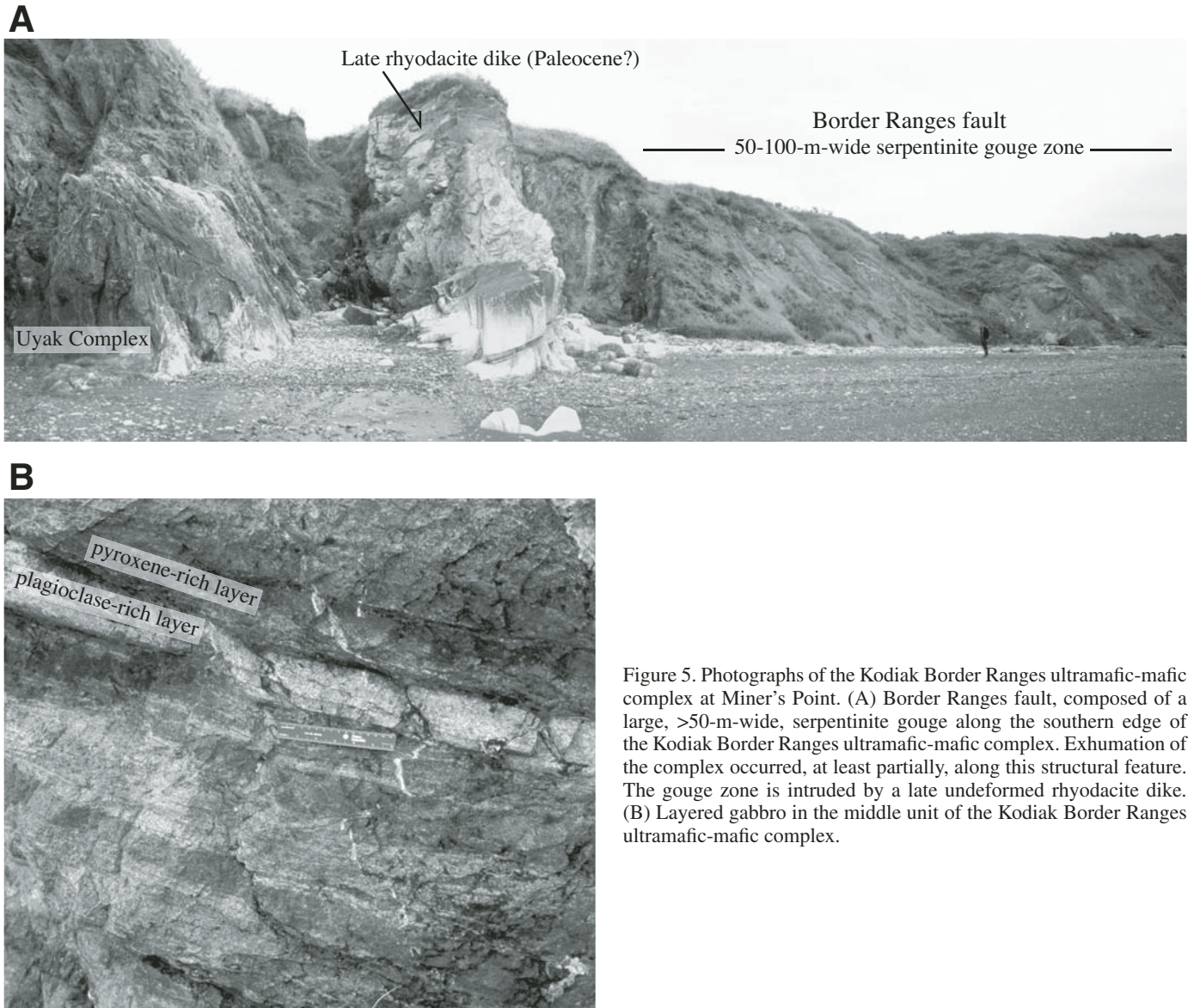


Figure 5. Photographs of the Kodiak Border Ranges ultramafic-mafic complex at Miner's Point. (A) Border Ranges fault, composed of a large, >50-m-wide, serpentinite gouge along the southern edge of the Kodiak Border Ranges ultramafic-mafic complex. Exhumation of the complex occurred, at least partially, along this structural feature. The gouge zone is intruded by a late undeformed rhyodacite dike. (B) Layered gabbro in the middle unit of the Kodiak Border Ranges ultramafic-mafic complex.

grained, and constitutes >20% of the rocks by volume (Fig. 8). Overall, the rocks of the Afognak batholith along Raspberry Strait are more mafic than those that occur near Miner's Point on the Spiridon Peninsula.

GEOCHEMICAL DATA

Introduction

In this section the geochemical character of the Kodiak-arc rocks are summarized and evaluated. The chemical data are from Beyer (1980) and Hill (1979) and are previously unpublished. Major- and selected trace-element data were collected using X-ray fluorescence (XRF) techniques, whereas the REE data and

other trace elements were obtained through Instrumental Neutron Activation Analysis (INAA). Elements such as FeO^* , Na_2O , and Ni among others were analyzed by both XRF and INAA, and yield similar results, indicating the data are robust. Major-element mineral data are from an electron microprobe, and REE pyroxene and plagioclase data was obtained through INAA. Samples from the Kodiak Border Ranges ultramafic-mafic complexes are primarily located in the Miner's Point and Middle Cape complexes. Afognak batholith data are from Raspberry and Afognak Island, and Shuyak Formation data are from Afognak and Shuyak Islands. These data do not cover all of the lithologic variations of the inferred Kodiak arc section (e.g., the Afognak batholith at Miner's Point is not represented in the data set), however, each of the three major crustal units is represented.

Major-Element Data

Variations between the three crustal units are visible on a variety of Harker diagrams (e.g., MgO, Al_2O_3 , CaO, etc.; Fig. 9), and in general overlap with the Tonsina-Nelchina data from Greene et al. (2006) and DeBari and Sleep (1991). (See Table DR1.1.) Differences between the ultramafic cumulate and the gabbroic through volcanic rocks are most clearly defined in terms of MgO and Al_2O_3 . The ultramafic rocks exhibit >20% MgO and <7% Al_2O_3 , whereas the rest of the units form a negative slope trend with increasing silica starting at ~10% MgO. However, Al_2O_3 evolution is flat. Most of the ultramafic samples are clinopyroxenites that form a flattened cluster around 20% MgO. Dunite samples plot closer to 30% MgO. The abundance of clinopyroxenitic rocks in the sample set reflects its abundance among the ultramafic rock types. Large bodies of dunite, such as found in parts of the eastern Talkeetna arc (e.g., Mehl et al., 2003), are not present in the Kodiak section. However, the eastern Talkeetna arc dunite bodies are likely of asthenospheric mantle origin and are not related to the geochemical evolution of the arc (Mehl et al., 2003; Greene et al., 2006). Between the ultramafic rocks and the rest of the units there is a significant MgO gap. However, between gabbro of the Kodiak Border Ranges ultramafic-mafic complex and the rest of the Kodiak arc units there is a continuous downward MgO trend (Fig. 9A). In terms of decreasing MgO and increasing SiO_2 , the gabbroic rocks are followed by the basaltic rocks of the Shuyak Formation, then by basaltic dikes that cut the ultramafic-mafic complex, and finally by the Afognak batholith. One exception is a 58% SiO_2 quartz gabbro, which came from the Middle Cape body (Fig. 9). This sample has a composition similar to the Afognak batholith.

Overall, eastern Talkeetna arc data from Greene et al. (2006) exhibit broad trends similar to the Kodiak data. However, when compared to the average compositions of DeBari and Sleep (1991) there are some differences. The Afognak batholith has a composition similar to the Talkeetna Formation (Clift et al., 2005a), despite the fact that the Talkeetna Formation is composed of upper-crustal volcanic rocks, and the Afognak batholith is composed of intrusive rocks. The stratigraphically similar mid-crustal intrusive rocks in the Tonsina-Nelchina region have a composition between the basaltic dikes and Shuyak Formation volcanic rocks. Although the bulk geochemical trends between Kodiak and Tonsina-Nelchina are similar, variations between the individual units exist.

Other geochemical trends include: both FeO^*/MgO and K_2O indicate that the Kodiak arc rocks are transitional between

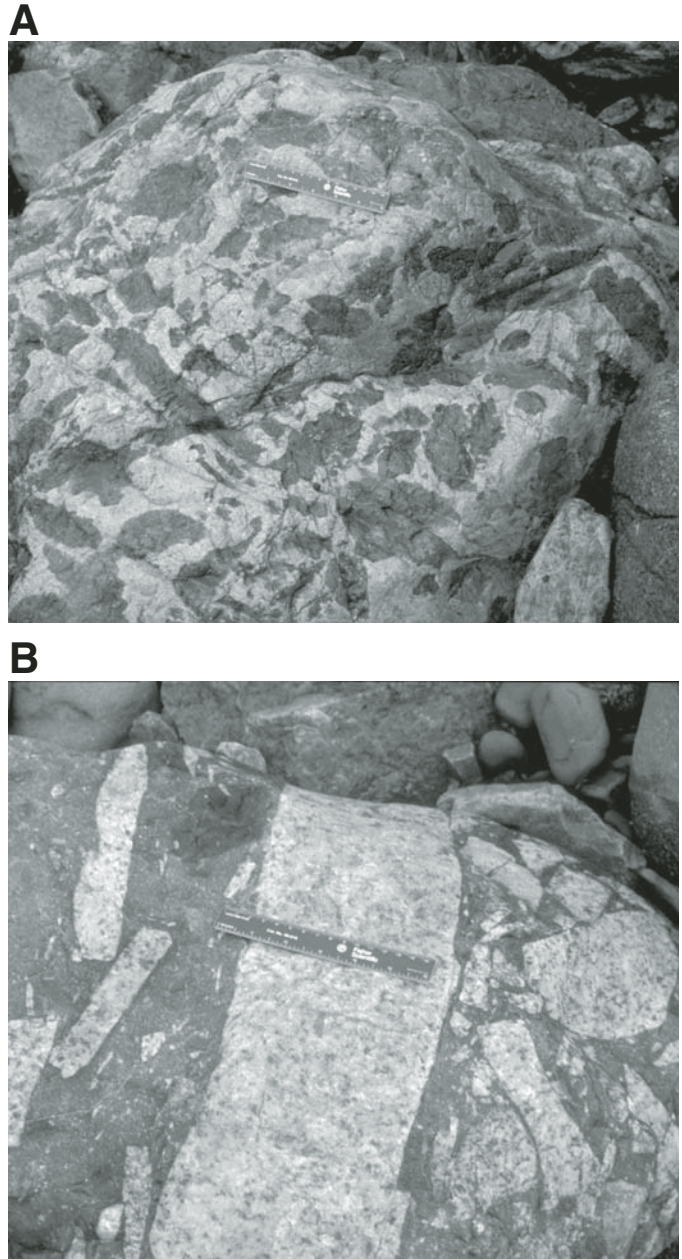


Figure 6. Photographs of the Afognak batholith at Miner's Point. (A) Enclaves of chilled basalt entrained in granite. (B) Sharp-edged blocks of granite entrained in a basaltic dike.

tholeiitic and calc-alkalic as are those from the eastern Talkeetna arc (Greene et al., 2006). TiO_2 data overlap with that of Greene et al. (2006), but trend lower at higher SiO_2 values (e.g., Afognak batholith) and higher for some rocks of the Shuyak Formation. A subset of rocks from the Shuyak Formation has TiO_2 values up to 3%, and P_2O_5 values up to 0.6%; such values, coupled with high K_2O , are more characteristic of oceanic alkali basalts (Mullen, 1983). However overall, the rocks from the Kodiak units are quite similar to those of the eastern Talkeetna crustal section

¹GSA Data Repository Item 2009188—Tables DR1 (geochemical data from the Kodiak Talkeetna arc crustal section), DR2–DR3 (Kodiak Border ranges mafic-ultramafic complex data from Beyer, 1980), DR4 (data used in geochemical models for the Kodiak Talkeetna arc crustal section), and DR5 (geochronologic data from the Kodiak Island area)—is available at www.geosociety.org/pubs/ft2009.htm, or on request from editing@geosociety.org, Documents Secretary, GSA, P.O. Box 9140, Boulder, CO 80301-9140, USA.

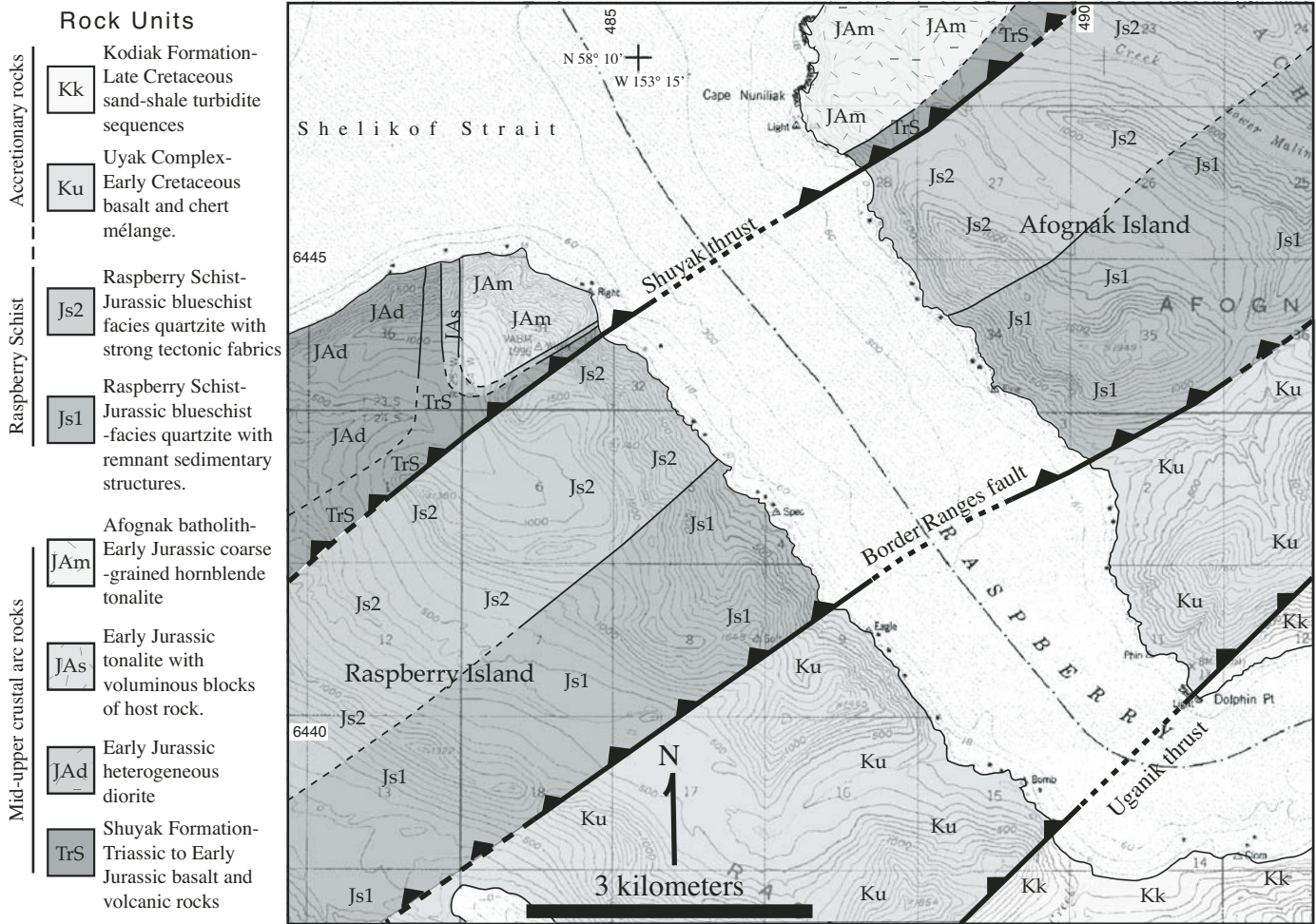


Figure 7. Geologic map of Raspberry Strait. Note that the ultramafic-mafic complex is not present at this locality, whereas the blueschist-facies Raspberry Schist occupies the same structural position (geologic mapping by Farris conducted during summer 2003; some geologic data from Roeske, 1986).

(e.g., Greene et al., 2006), and exhibit major-element characteristics diagnostic of an island-arc setting.

Rare-Earth-Element Data

Rare-earth-element (REE) data from the different Kodiak units exhibit a continuous trend of increasing concentration from the ultramafic-mafic complexes upwards to the Afognak batholith and upper-crustal volcanic rocks of the Shuyak Formation (Fig. 10A). The Kodiak Border Ranges ultramafic-mafic complexes exhibit strongly depleted LREE with HREE that approach chondritic values. The gabbroic rocks of the Kodiak Border Ranges ultramafic-mafic complexes are still LREE depleted, but the HREEs have values just greater than chondrite (Taylor and McLennan, 1985). Basaltic dikes that cut the Border Ranges ultramafic-mafic complexes have a nearly flat REE trend, except for a moderate positive Eu anomaly. Ultramafic, gabbroic, and basaltic rocks of the Kodiak Border Ranges

ultramafic-mafic complex exhibit a slight to moderate positive Eu anomaly that becomes more pronounced at higher REE concentrations. Such an Eu anomaly is indicative of plagioclase accumulation. Averaged values for the Afognak batholith and Shuyak Formation are almost identical with values above 10 times chondrite, flat to slightly LREE enriched trends, and small negative Eu anomalies (Fig. 10B). However, individual samples from the Shuyak Formation have much more variation with some having LREE depletion and some having LREE enrichment. Overall, REE values increase from less than 1× chondrite in the Kodiak Border Ranges ultramafic-mafic complexes to 10–20× chondrite in the upper crustal volcanic and intrusive rocks.

The Tonsina-Nelchina data cover a similar compositional range as the Kodiak data, however, there are some differences. The Greene et al. (2006) data set does not contain significant pyroxenites. Therefore, the lowest REE compositions are somewhat higher than in the Kodiak rocks. Even the lowest REE

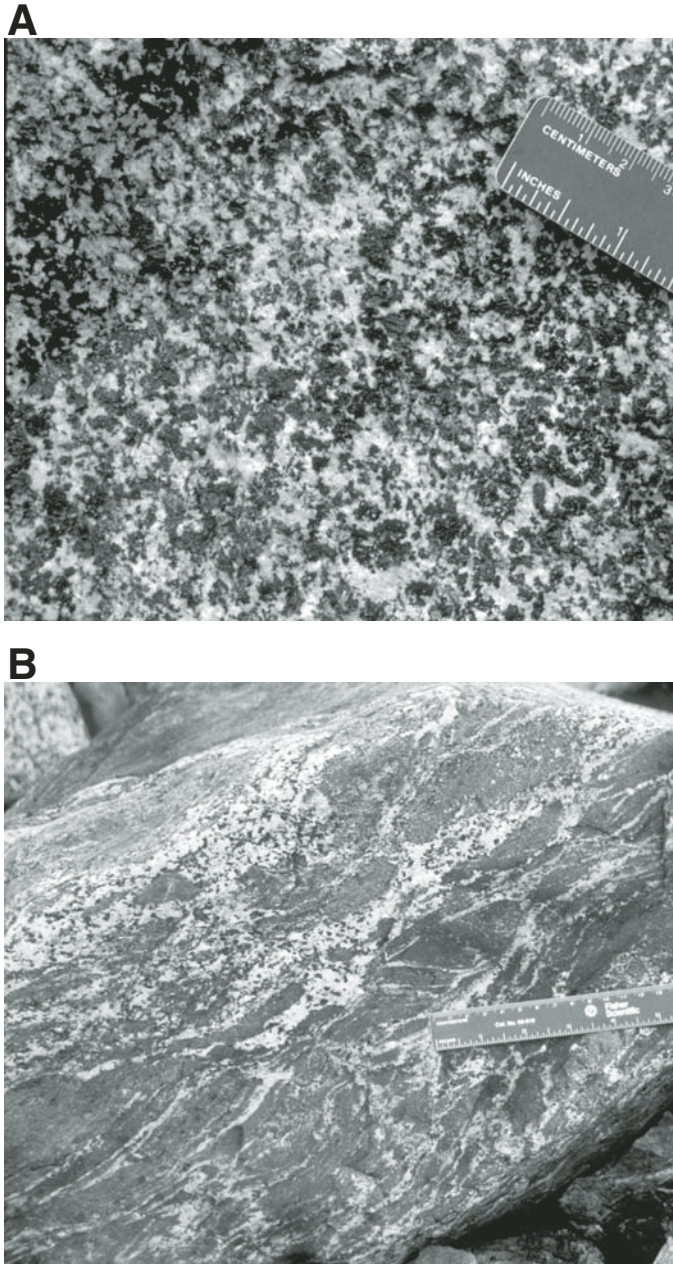


Figure 8. Photographs of the Afognak batholith along Raspberry Strait. (A) Hornblende-rich tonalite containing 30–40 percent modal hornblende. This is much more than the 5–10 modal percent hornblende found in the Miner's Point granitic rocks. (B) Gneissic wall rock surrounding the Afognak batholith. Field observations coupled with geochemical modeling and geochronology suggest the wall rock underwent partial melting and slow cooling coupled with multiple injections of tonalitic and dioritic magma.

gabbro from Greene et al. (2006) and DeBari and Sleep (1991) has greater concentrations than the average gabbro from the Kodiak Border Ranges ultramafic-mafic complex (Fig. 10A). However, at the more evolved end of each data set, REE concentrations are similar at 10–20× chondrite.

Trace-Element Data

Outside of REE data, the trace-element data set for the Kodiak arc rocks is somewhat incomplete. However, sufficient data exist for a general comparison to other parts of the Talkeetna arc system. Figure 11 contains four different trace-element plots, which elucidate aspects of the each unit. Figure 11A is a plot of La versus Sm: note that the Kodiak data overlaps with the Tonsina-Nelchina data for concentrations greater than 0.5 ppm. However, the Tonsina-Nelchina data contains a gabbro tail not present in the Kodiak data, and as noted above, the Kodiak clinopyroxenite and gabbro data have substantially lower La than reported in Greene et al. (2006). The three solid lines are trace-element models for different portions of the arc. Details of the models will be discussed in a following section.

A plot of Cr versus Ni indicates that the Kodiak Border Ranges ultramafic-mafic complex is substantially enriched in Cr (3000–5000 ppm) relative to the eastern Talkeetna arc, whereas the Afognak batholith is depleted (5–10 ppm). However, the Shuyak Formation basaltic rocks have high Cr relative to the Talkeetna Formation (DeBari and Sleep, 1991).

In plots of Sr/Y versus Y and Nb versus Y, both the Kodiak and Tonsina-Nelchina data fall within island-arc classification fields (Pearce et al., 1984; Figs. 11D, 11E). One exception is that some of the Tonsina-Nelchina data exhibit high adakite-like Sr/Y ratios. However, Greene et al. (2006) explain this by stating that those samples are gabbroites that contain substantial plagioclase accumulation. The Kodiak rock contains more Nb than the Tonsina-Nelchina rocks, and produce a parallel, but elevated Nb/Y trend. Nb/Y data exist for only two of the Kodiak units, near the lower level of precision for the analytical technique, however the trend does appear to be real. Overall, trace-element data corroborate a linked island-arc origin for the different Kodiak units and are once again similar to the eastern Talkeetna arc with some variation.

Mineral-Chemistry Data

In Beyer (1980) there is a large, previously unpublished data set of clinopyroxene compositions (Fig. 12) and other mineral data (Fig. 13) from the Kodiak Border Ranges ultramafic-mafic complex (see Tables DR2 and DR3, see footnote 1). Clinopyroxene data are plotted with respect to magnesium-number ($Mg \# = 100Mg/(Mg + Fe)$) according to the different rock types of the Kodiak Border Ranges ultramafic-mafic complex. Mineral-chemistry data from rocks from the Afognak batholith and Shuyak Formation are not represented in the Beyer (1980) data. Clinopyroxenes from gabbroite and ferrogabbro are essentially identical to those reported in Greene et al. (2006). The few eastern Talkeetna clinopyroxenes from pyroxenite also plot at the low Mg # end of the Kodiak trend and so are also compositionally similar, but more evolved.

The one large compositional difference is in terms of Cr composition. Some of the Kodiak clinopyroxene, particularly

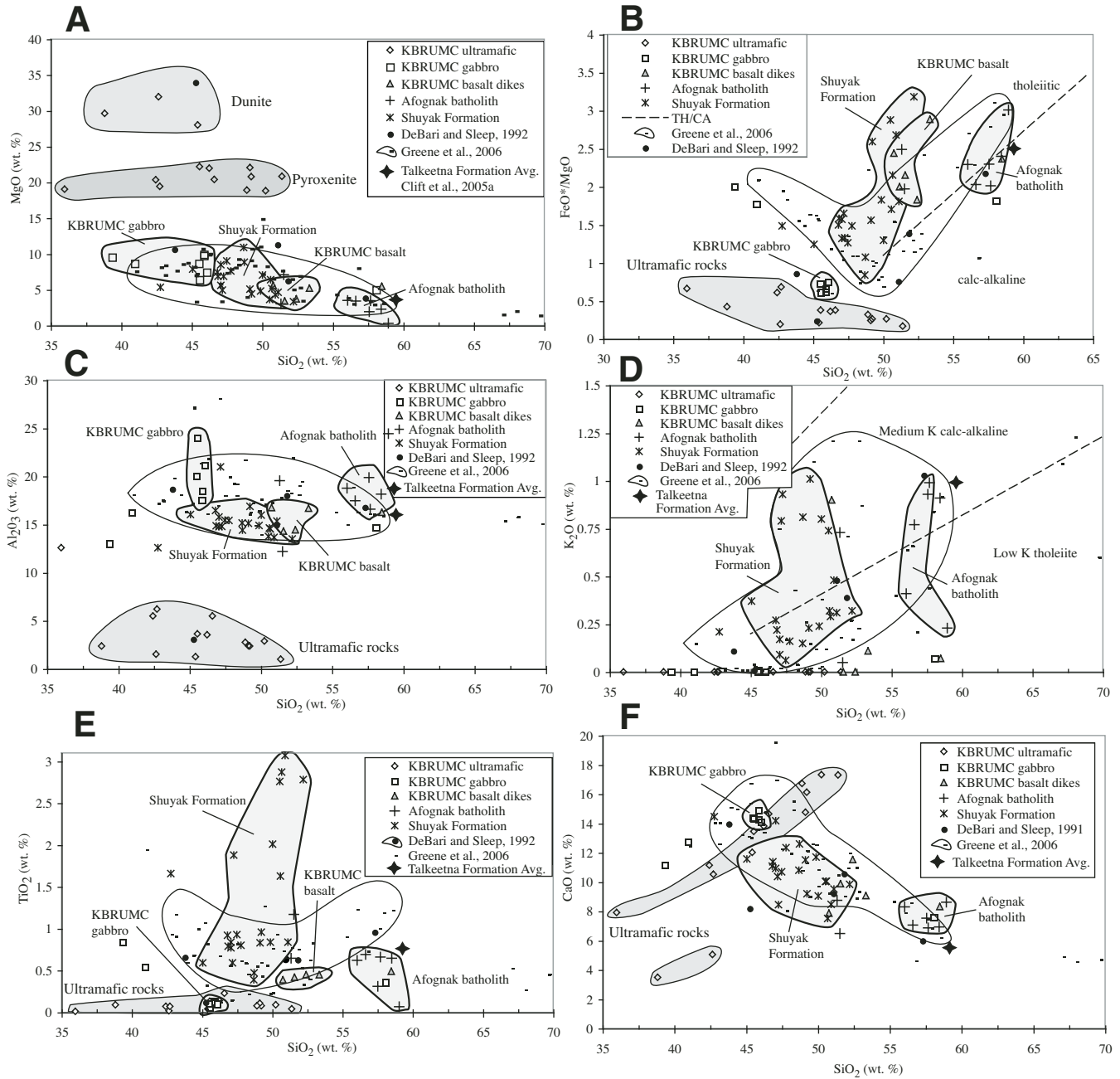


Figure 9. Major-element chemical data from the Kodiak crustal section. Kodiak data from Beyer (1980) and Hill (1979). Eastern Talkeetna data from Greene et al. (2006) and DeBari and Sleep (1991, Tonsina-Nelchina average compositions). Talkeetna Formation average from Clift et al. (2005a). KBRUMC—Kodiak Border Ranges ultramafic-mafic complex. (A) MgO vs. SiO₂, (B) (FeO*/MgO) vs. SiO₂, (C) Al₂O₃ vs. SiO₂, (D) K₂O vs. SiO₂, (E) TiO₂ vs. SiO₂, and (F) CaO vs. SiO₂.

from ultramafic rocks, have Cr concentrations approaching one weight percent. The high Cr compositions are also reflected in the whole-rock data previously discussed. However, Cr compositions in gabbroic rocks are similar in both locations. Another difference between clinopyroxene compositions from the eastern Talkeetna and Kodiak rocks is manifested in the feldspathic wehrlites. They form a linear trend for most major elements and

have compositions that are intermediate between the gabbroic and ultramafic rocks. In the eastern Talkeetna data set, clinopyroxene of this composition are not represented. The lowest Mg # group of clinopyroxenes come from basaltic dikes that intrude the Kodiak Border Ranges ultramafic-mafic complex. These clinopyroxenes form a loose cloud that extends from Mg #s of 75–50 and roughly overlap with the Greene et al. (2006) data, but

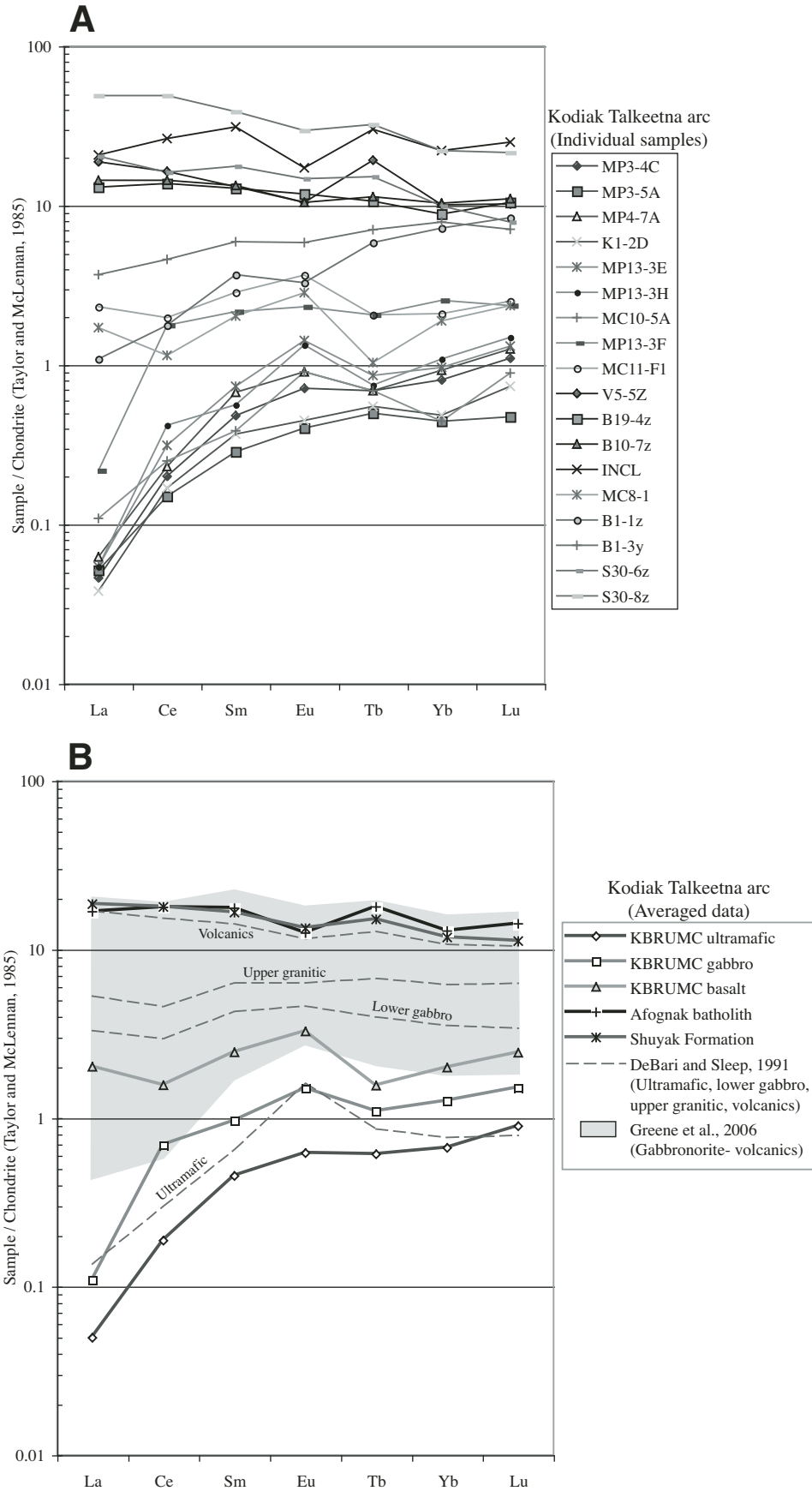


Figure 10. Rare-earth-element data from the Kodiak crustal section. Data is chondrite normalized (Taylor and McLennan, 1985). (A) Individual samples from Kodiak arc. (B) Kodiak data averaged by unit and compared to eastern Talkeetna arc data from Greene et al. (2006) and DeBari and Sleep (1991). KBRUMC—Kodiak Border Ranges ultramafic-mafic complex.

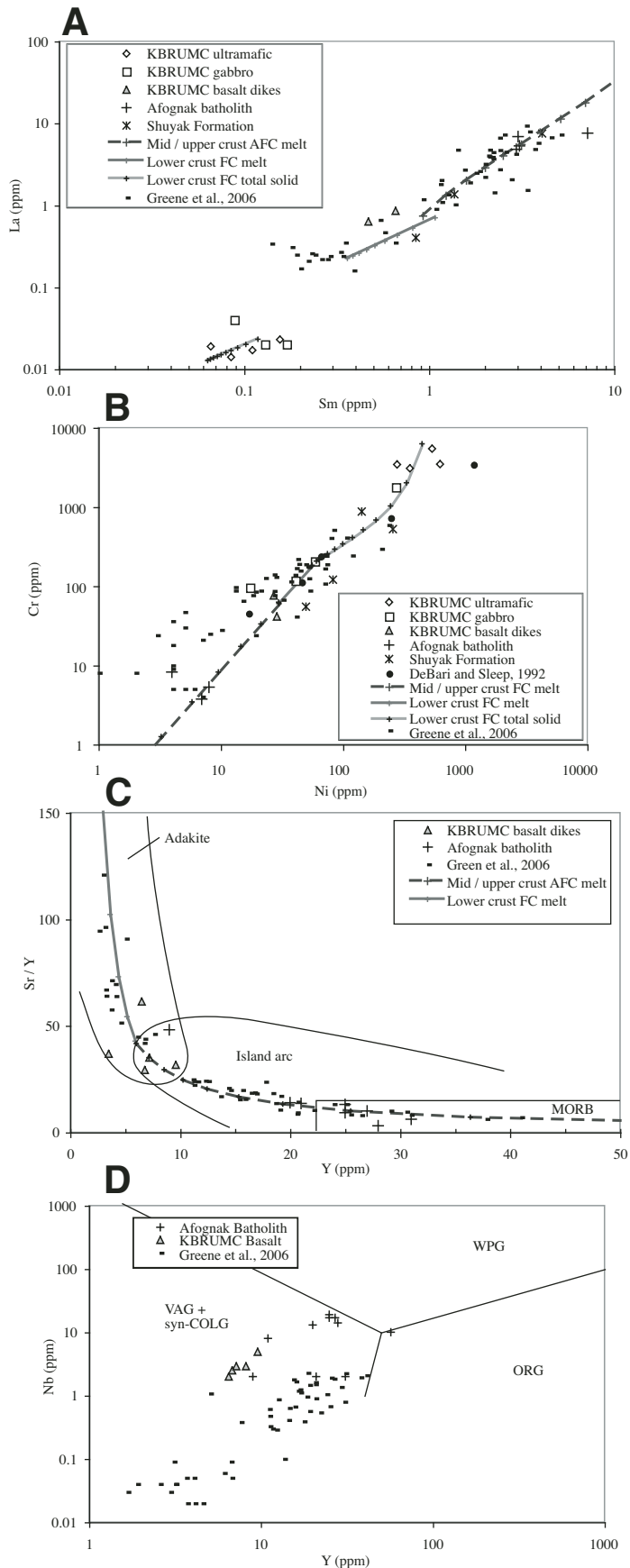


Figure 11. Kodiak trace-element data with model curves. Kodiak data plots dominantly in island-arc compositional fields, and is similar to Greene et al. (2006) with some variations (see text for more detailed discussion). The model curves show the three portions of an integrated geochemical model for the entire crust. Arc mantle root ultramafic rocks are modeled via the total solid component of a fractional crystallization (FC) model, whereas lower crustal gabbroic rocks are from the liquid component. Mid-crustal granitic and upper crustal volcanic rocks are from the liquid component of an assimilation-fractional crystallization model with a starting composition in equilibrium with the lower crustal gabbroic rocks. (A) La (ppm) vs. Sm (ppm); (B) Cr (ppm) vs. Ni (ppm), note that the La/Sm and Cr/Ni compositions evolve in opposite directions; (C) Sr/Y (ppm) vs. Y (ppm), rocks within the adakite field are not adakites, but lower crustal gabbroic rocks; and (D) Nb (ppm) vs. Y (ppm), indicating arc tectonic affinity (Pearce et al., 1984). KBRUMC—Kodiak Border Ranges ultramafic-mafic complex; AFC—assimilation-fractional crystallization; COLG—collisional granite; ORG—ocean-ridge granite; VAG—volcanic arc granite; WPG—within-plate granite.

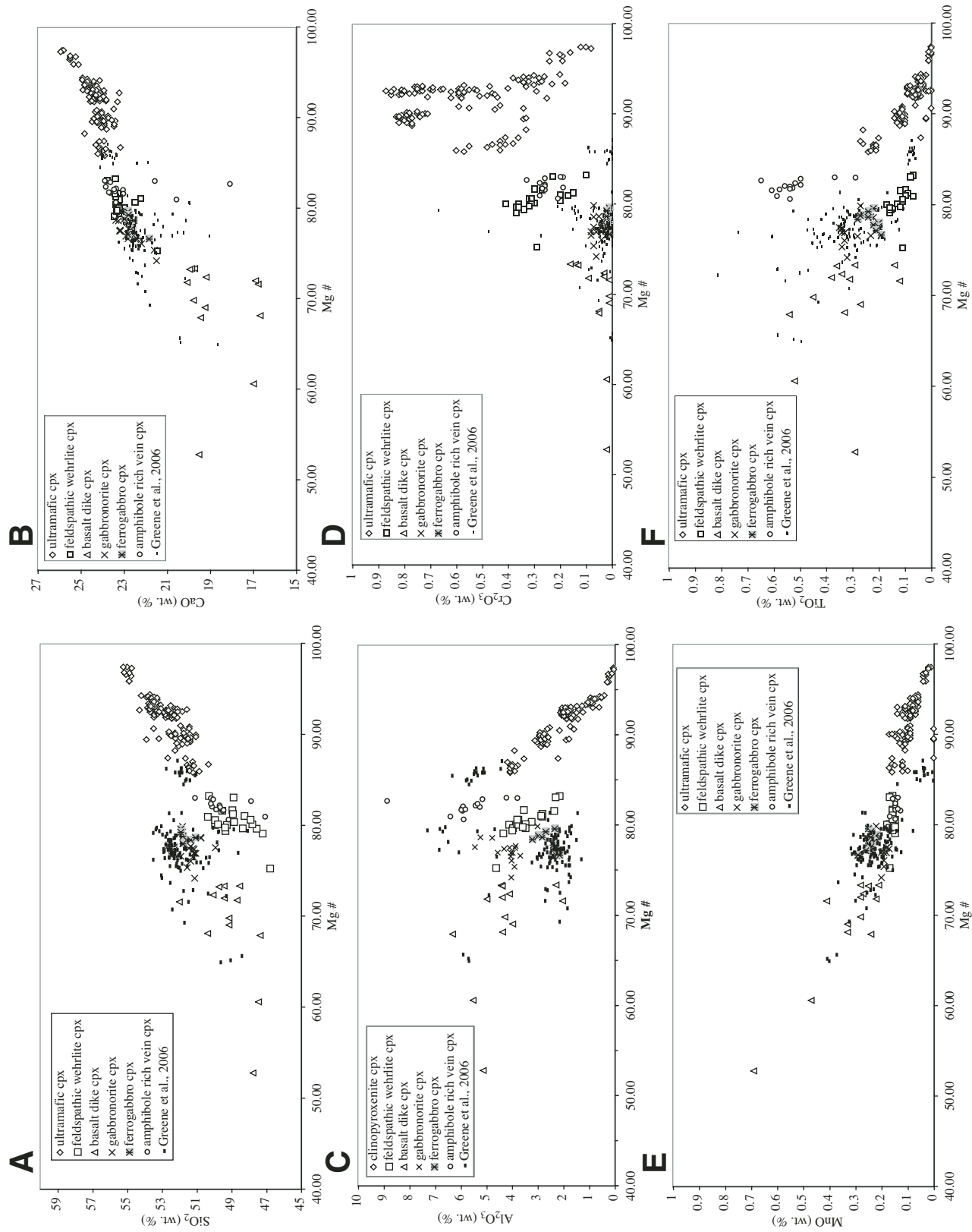


Figure 12. Clinopyroxene mineral chemistry from the Kodiak Border Ranges Ultramafic complex (Beyer, 1980) compared to Greene et al. (2006) data from the eastern Talkeetna arc. Data are broken down by rock type. The largest variations from the eastern Talkeetna data are the high Cr contents, and the greater range of Mg #s (95–60) in the Kodiak data. (A) SiO_2 vs. Mg #, (B) CaO vs. Mg #, (C) Al_2O_3 vs. Mg #, (D) Cr_2O_3 vs. Mg #, (E) MnO vs. Mg #, and (F) TiO_2 vs. Mg #.

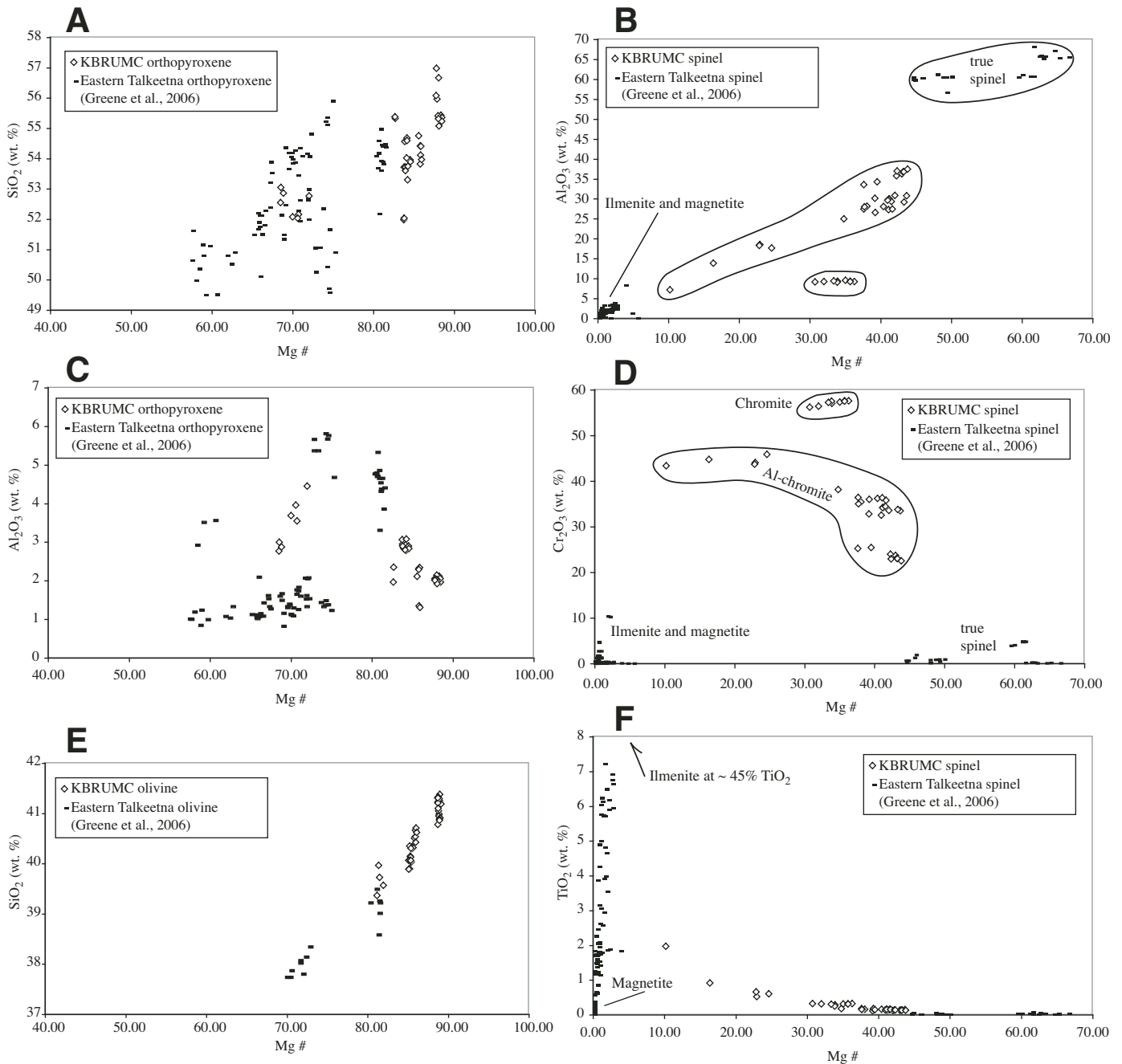


Figure 13. Kodiak Border Ranges ultramafic-mafic complex mineral-chemistry data from orthopyroxene, olivine, and spinel (Beyer, 1980) compared to Greene et al. (2006) data. Kodiak orthopyroxene and olivine in general have higher Mg #s than eastern Talkeetna equivalents, and most spinel from the Kodiak Border Ranges ultramafic-mafic complex is a variety of chromite, whereas the Greene et al. (2006) data are dominated by true spinel and magnetite. KBRUMC—Kodiak Border Ranges ultramafic-mafic complex. (A) Orthopyroxene SiO_2 vs. Mg #, (B) spinel Al_2O_3 vs. Mg #, (C) orthopyroxene Al_2O_3 vs. Mg #, (D) spinel Cr_2O_3 vs. Mg #, (E) olivine SiO_2 vs. Mg #, and (F) spinel TiO_2 vs. Mg #.

are not identical. Overall, clinopyroxenes from Kodiak and the eastern Talkeetna arc have similar compositions when they are from similar rock types, except for Cr. However, the Kodiak data exhibit more linear trends and extend over a much larger range of Mg #s suggesting a greater degree of fractionation, or at least more complete preservation of rocks from the arc root.

Kodiak Border Ranges ultramafic-mafic complex mineral composition data also exist for orthopyroxene, olivine, and spinel (Fig. 13). Due to less abundant data, these have not been broken out by rock type. The orthopyroxene and olivine data lie on trends similar to those found in the eastern Talkeetna, but they, like some of the clinopyroxene data, lie on higher Mg # extensions. In contrast, spinels from the Kodiak Border Ranges ultramafic-mafic complex differ significantly from those analyzed from the eastern Talkeetna. Spinel from Kodiak rocks split into true chromite that contains >50% Cr₂O₃ and Al-chromite that contains between 20%–40% Cr₂O₃, and is enriched in Al₂O₃. In comparison, spinels from the eastern Talkeetna contain very little Cr and are either high Mg # true spinel or form a group consisting chiefly of magnetite with minor ilmenite. Fe-Mg silicates such as olivine and orthopyroxene are similar between Kodiak and the eastern Talkeetna arc, but spinel-group minerals are substantially different. However, Arai et al. (2006) found that high-Cr spinels are common in island arcs.

In addition to major-element mineral data, some REE INAA data exist for clinopyroxenes and plagioclases from Kodiak Border Ranges ultramafic-mafic complex. Figure 14 shows both averaged mineral compositions and the melt in equilibrium with the minerals. Clinopyroxene from ultramafic rocks exhibit HREE values between 0.5 and 1.0 times chondrite with low La values. These values are similar to, but slightly elevated, in comparison to the whole-rock compositions indicating the high abundance of clinopyroxene. Clinopyroxenes from wehrlite have similar REE abundances, but have peaks in Tb and Ce. Melt in equilibrium with the ultramafic clinopyroxene has a similar HREE signature to the gabbroic whole-rock compositions, but is more enriched in LREE. Clinopyroxenes from gabbroic rocks have a REE curve of similar shape to the pyroxenite clinopyroxene, but at elevated abundances. Melt in equilibrium with gabbroic clinopyroxene has values of 2–3 times chondrite, and is used as the initial composition for the evolution of middle- to upper-crustal rocks as discussed in the following section.

Geochemical Modeling

In order to better interpret the Kodiak arc geochemical data, a trace-element model has been constructed (Fig. 15; Table DR4, see footnote 1). The goal of the model is to replicate the average REE compositions from different parts of the arc using realistic degrees of fractionation. In addition to REE, the model has also been applied to Sr, Y, Ni, and Cr data with minor modifications (Fig. 11). The model is split into lower crustal and middle through upper crustal sections. The lower part of the model successfully reproduces the basalt, gabbro, and pyroxenite of the Kodiak

Border Ranges ultramafic-mafic complex via fractional crystallization (Figs. 15A, 15B), whereas the upper part of the model links the Afognak batholith and Shuyak Formation to the Kodiak Border Ranges ultramafic-mafic complex via assimilation-fractional crystallization (Fig. 15D).

In the lower crustal portion of the model, the average gabbro of the Kodiak Border Ranges ultramafic-mafic complex is used as the starting composition. The one exception is for La. Fractionation models are unable to reproduce the La values in basalts of the Kodiak Border Ranges ultramafic-mafic complex without an increase in the La starting composition. The gabbro was chosen because other workers have suggested that primary arc magmas are gabbroic (e.g., Greene et al., 2006), and because the gabbro has an intermediate composition in the Kodiak Border Ranges ultramafic-mafic complex in which melt and solid fractions could be extracted to form basalt and pyroxenites, respectively. Fractional crystallization liquid, and total solid compositions are modeled by:

Fractional crystallization liquid:

$$C_L = C_0 * F^{(D-1)} \quad (1)$$

Fractional crystallization total solid:

$$C_R = C_0 * ((1 - F^D) / (1 - F)) \quad (2)$$

In which C_L is the liquid concentration, C_0 is the initial concentration, C_R is the total residual solid concentration, F is the melt fraction, and D is bulk distribution coefficient (Rollinson, 1998). The fractionating phases in order of abundance are: clinopyroxene, olivine, spinel, and plagioclase. Rare-earth-element curves for the Kodiak Border Ranges ultramafic-mafic complex have a positive Eu anomaly indicative of plagioclase accumulation. To take this into account the plagioclase fraction is negative. This is intended to simulate plagioclase addition, whereas the other phases are subtracted from the melt. The effect of a negative plagioclase mineral fraction on the bulk distribution coefficients is not large, but does make the model better fit the data. The distribution coefficients used are for basaltic melts and are from the geochemical earth reference model (GERM) web page and Rollinson (1998). Overall, the liquid and solid fractions of the model are able to accurately reproduce the Kodiak Border Ranges ultramafic-mafic complex basaltic and pyroxenite compositions, respectively, at melt fractions between 0.4 and 0.6.

Geochemically linking the Afognak batholith and Shuyak Formation to the Kodiak Border Ranges ultramafic-mafic complex initially proved difficult. However, the resulting model accurately reproduces upper-crustal compositions, and provides insight into arc processes. None of the various average whole-rock compositions from the Kodiak Border Ranges ultramafic-mafic complex are appropriate magma compositions for the initial composition for the upper arc. Melt in equilibrium with gabbroic clinopyroxene provided the best fit (Fig. 14A). However, as in the lower-crustal model the initial La composition was increased.

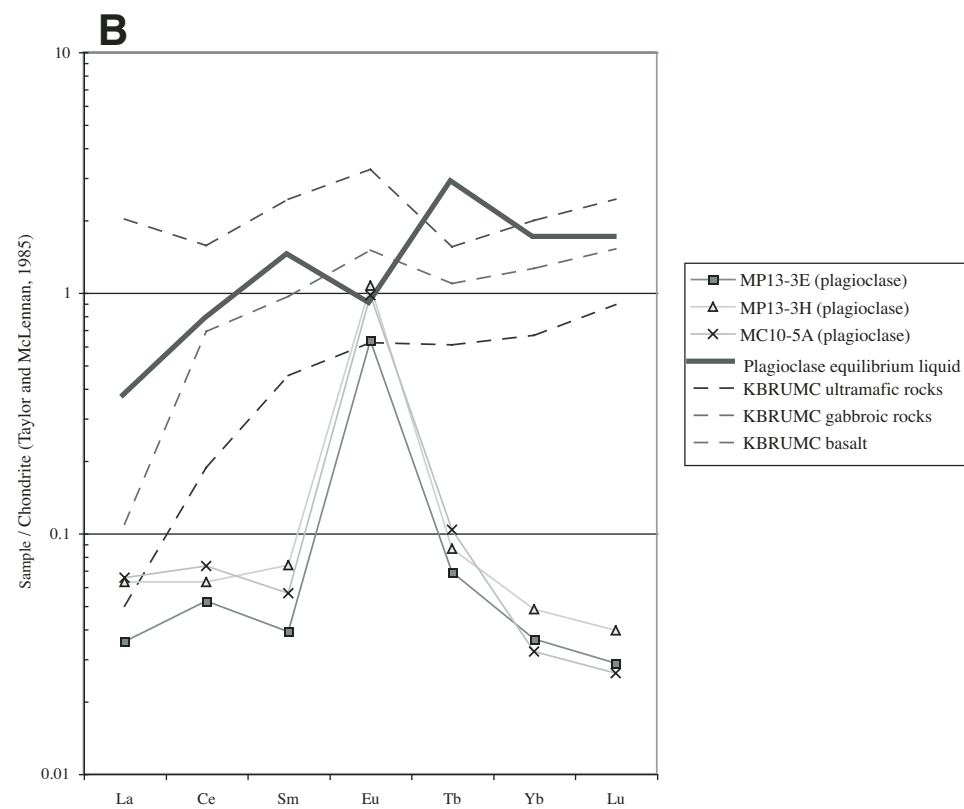
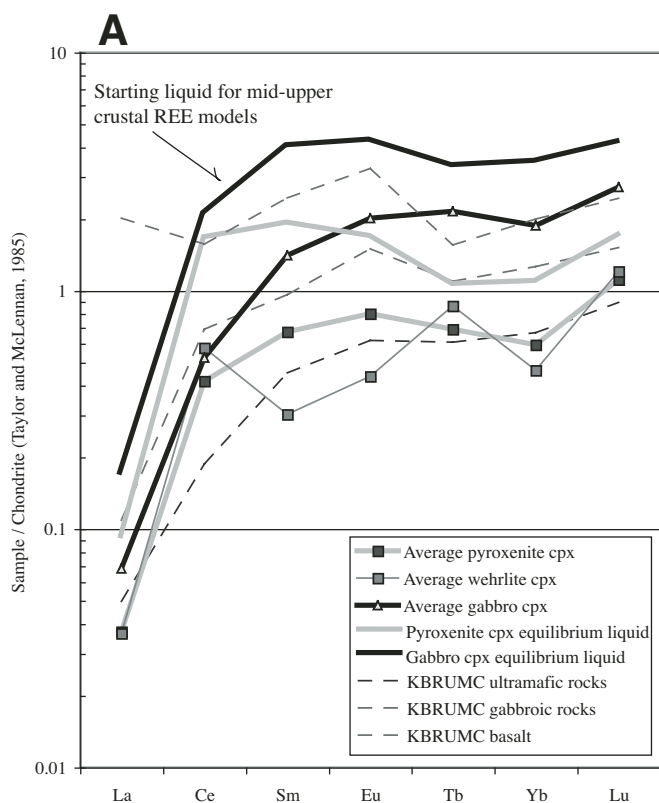


Figure 14. Rare-earth-element, Instrumental Neutron Activation Analysis (INAA) mineral data from the Kodiak Border Ranges ultramafic-mafic complex (Beyer, 1980). Data are chondrite normalized (Taylor and McLennan, 1985). (A) Averaged clinopyroxene compositions for different rock types. Calculated equilibrium liquids also shown. Melt in equilibrium with the gabbro clinopyroxene is used as the starting composition for the mid-upper crustal REE model. (B) Plagioclase REE (rare earth element) data with equilibrium liquid. KBRUMC—Kodiak Border Ranges ultramafic-mafic complex.

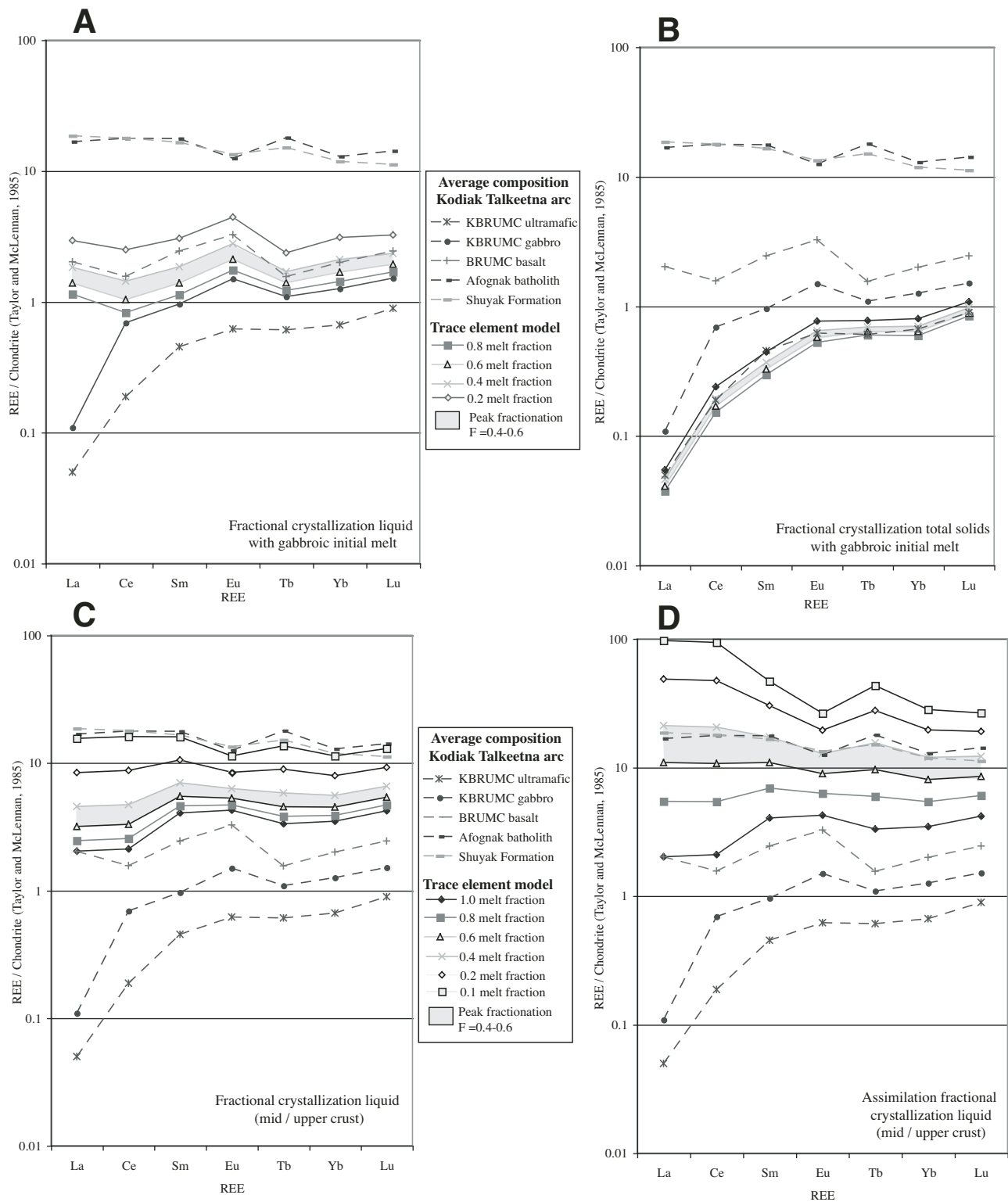


Figure 15. Rare-earth-element (REE) model for the Kodiak crustal section. Model results are chondrite normalized (Taylor and McLennan, 1985). (A) Fractional crystallization model of Kodiak Border Ranges ultramafic-mafic complex melt with average gabbroic rocks as the starting composition. This model reproduces Kodiak Border Ranges ultramafic-mafic complex basalt compositions. (B) Fractional crystallization model of Kodiak Border Ranges ultramafic-mafic complex total solids with average gabbroic rocks as the starting composition. This model reproduces Kodiak Border Ranges ultramafic-mafic complex pyroxenite compositions. (C) Fractional crystallization model of mid-upper crustal melt with gabbroic clinopyroxene equilibrium melt as the starting composition. This model reproduces upper crustal compositions, but requires high ($F = 0.1$) melt fractions. (D) Assimilation-fractional crystallization (AFC) model of mid-upper crustal melt with gabbroic clinopyroxene equilibrium melt as the starting composition. This model reproduces upper-crustal compositions, at reasonable ($F = 0.6-0.4$) melt fractions, and is the preferred upper crustal model. BRUMC—Border Ranges ultramafic-mafic complex; KBRUMC—Kodiak Border Ranges ultramafic-mafic complex.

Melt of that composition can reproduce Afognak batholith and Shuyak Formation compositions purely by fractional crystallization, however, it requires very high melt fractions ($F = 0.1$) that are unrealistic for crustal-scale scenarios (Fig. 15C).

Assimilation-fractional crystallization (AFC) provides a solution that allows melt originating in the lower crustal mafic/ultramafic complexes to reach mid- to upper-crustal compositions. Assimilation fractional crystallization is modeled by:

$$C_L = C_o * [F^{-(r-1+D)/(r-1)} + (r / (r-1 + D)) * (C_A/C_o) * (1 - F^{-(r-1+D)/(r-1)})], \quad (3)$$

in which r is the ratio of assimilation to fractionation, C_A is the concentration of the assimilant, and, C_L , C_o , F , and D are the same as above (DePaolo, 1981; Powell, 1984). The mineral assemblage used in the model was (in decreasing abundance): plagioclase, clinopyroxene, Fe-Ti-Al oxide, quartz, and hornblende with trace apatite and zircon. Basaltic andesite bulk distribution coefficients from the geochemical Earth reference model were used. The assimilant used was the average Shuyak Formation composition. That is geologically realistic because Afognak batholith plutons intrude into the Shuyak Formation and field evidence indicates that at least some incorporation of host rock did occur. The ratio of assimilation/fractionation used in the model is 0.4, which is equivalent to 28% assimilated material, and is similar to estimates from plutonic systems (Paterson et al., 1996; Pignotta and Paterson, 2007; Farris and Paterson, 2007). The AFC model accurately reproduces Afognak batholith and Shuyak Formation REE compositions at melt fractions between 0.6 and 0.4 (Fig. 15D). The higher melt fractions are important because once ~50% crystallization has occurred the crystals form an interlocking framework that make it difficult for additional fractional to occur by standard processes (e.g., Arzi, 1978).

The two-stage arc fractionation model also works for other trace elements (Fig. 11). In terms of Ni and Cr, the residual solid portion of the model reproduces the extremely high whole-rock Cr concentrations found in the ultramafic rocks of the Kodiak Border Ranges ultramafic-mafic complex. This is due to accumulation of both pyroxene and Al-chromite spinel. In the upper part of the arc, the low Afognak batholith Cr and Ni concentrations can be reproduced only if Cr- and Ni-bearing phases from the Shuyak Formation are not assimilated. This is realistic because Cr and Ni are located in the more refractory phases and would not likely be included in AFC process.

For elements such as Sr and Y, the upper and lower crustal models have contrasting behaviors (Fig. 11). Basalt dikes of the Kodiak Border Ranges ultramafic-mafic complex were used as the starting composition. In the lower crustal model, the data require bulk distribution coefficients for $Y > 2$ and $Sr \ll 1$. This generates the high Sr/Y ratio observed in the gabbroic rocks of Greene et al. (2006). Whereas in the upper crustal portion of the model, the Sr bulk D is slightly above 1 and the Y bulk D is $\ll 1$. The upper portion of the model accurately models data from the Afognak batholith.

PRESSURES AND UNIT THICKNESS

Geochemical data in the previous section indicate that the different Kodiak units are part of an island arc, and that all of the units are geochemically related to each other. In the eastern Talkeetna arc, units with similar geochemical and stratigraphic relationships form an arc-crustal section. This suggests that the Kodiak rocks also form an arc-crustal section. To further evaluate this idea, unit thicknesses and depths of formation will be examined in this section. Geochemical data and field relations suggest that the Kodiak Border Ranges ultramafic-mafic complex formed the lower crust and mantle root, the Afognak batholith was emplaced into the middle and upper crust, and the Shuyak Formation formed the upper crust of the arc.

In order to reconstruct the potential arc section, it is important to estimate how much of each unit has been preserved. The simplest method of determining arc paleo-thickness is to sum the thickness of each unit. Along strike the thickness of each unit varies considerably, and so a range of values will be used. The Kodiak Border Ranges ultramafic-mafic complex has a thickness of 1–3 km; the Afognak batholith, 3–5 km; and the Shuyak Formation, 5–8 km, for a total of 9–16 km. Even for an immature island arc, such a range is relatively thin, unless this total represents only partial preservation.

Another method to determine if the Kodiak rocks form a crustal section is to use crystallization pressure for the lower crustal and mantle units. In a crustal section these units should be the deepest. Beyer (1980) estimated a pressure of 7 kb for the Kodiak Border Ranges ultramafic-mafic complex, which are the highest in the Kodiak arc. This estimate is based on clinopyroxene, orthopyroxene, and Al-spinel symplectites at Miner's Point (Beyer, 1980). Pressure estimates based on modern calibrations would make this interpretation more robust, and should be the focus of future studies. However, input of Miner's Point pyroxenite mineral data (clinopyroxene, orthopyroxene, olivine, and spinel) in the QUILF program (Andersen et al., 1993) indicate a pressure of 7 kb at temperatures of 900–1000 °C is reasonable. A 7 kb pressure is equivalent to a crustal depth of ~23–25 km and suggests the Kodiak rocks do form an arc-crustal section, and that a maximum of 35%–70% of the Kodiak arc crust has been preserved.

In comparison to the Tonsina-Nelchina part of the arc, the Kodiak section is substantially thinner. Pressures of up to 10 kb have been calculated in the eastern Talkeetna arc, which correspond to a crustal thickness of ~35 km (DeBari and Coleman, 1989; DeBari and Sleep, 1991; Mehl et al., 2003; Kelemen et al., 2003; Hacker et al., 2005). Also, garnet-bearing gabbro exists in the lower Tonsina-Nelchina crust. Modeling by Jull and Kelemen (2001) and Behn and Kelemen (2006) indicate lower-crustal arc rocks generally need pressures >10 kb to crystallize garnet. In the Kodiak rocks, garnet is not present, which also suggests that the 7 kb pressure estimate is reasonable. Also, the eastern Talkeetna arc contains thicker sections of gabbroic lower crust

(Greene et al., 2006), but on Kodiak thicker pyroxenite sections have been preserved. Overall, the total percentage of crustal preservation in both the eastern Talkeetna and Kodiak portions of the arc is similar at ~50%.

Geochronologic and Cooling Data

A relatively complete set of thermochronologic data exist for several of the units of the Kodiak arc section (Fig. 16; Table DR5, see footnote 1). Others can be dated using paleontological data. The only unit that does not have any direct age control is the Kodiak Border Ranges ultramafic-mafic complex, however, these rocks are geochemically related to rocks in the upper part of the arc for which good age data exist. The two units with the best geochronologic data are the Afognak batholith and Raspberry Schist.

The Afognak batholith on Afognak Island has U-Pb zircon crystallization ages of 218 ± 5 Ma and 216 ± 8 Ma (Roeske et al., 1989). These ages are similar to the Norian fossil age for the Shuyak Formation into which the batholith intrudes (Connelly, 1978). On the adjacent Raspberry Island, there are K-Ar hornblende cooling ages of ca. 190 Ma for the batholith (Carden et al., 1977). On Afognak Island, there is a poorly resolved $^{40}\text{Ar}/^{39}\text{Ar}$ feldspar age of 150–120 Ma (Clendenen et al., 2003), and also lower temperature zircon and apatite fission-track ages of 153 ± 10 Ma and 64 ± 4 Ma, respectively (Clendenen et al., 2003). A cooling curve from these data is shown in Figure 17.

The curve is composed of two straight segments, which indicate periods of constant cooling. From 216 to 153 Ma, the batholith cooled at a rate of $9.5^\circ\text{C}/\text{Ma}$, suggesting mid-crustal conditions, whereas from 153 Ma to the present, the batholith cooled at a rate of $1.2^\circ\text{C}/\text{Ma}$, indicating it was in the upper crust.

The Raspberry Schist exhibits a similar, but not identical cooling history. Its oldest date is a Rb-Sr isochron age of 207 ± 11 Ma (Roeske et al., 1989). Also, close to that age is a U-Pb isochron age of 204 ± 8 Ma. Both the U-Pb and Rb-Sr phengite isochron ages are interpreted to record cooling from peak temperatures of 475°C (Roeske et al., 1989). K-Ar dates on white mica yield ages ca. 190 Ma (Forbes and Lanphere, 1973; Carden et al., 1977), and record cooling through 350°C (Jäger, 1979). Several of the younger ages (193 and 189 Ma) are Rb-Sr whole-rock dates that can be explained by white mica crystallization at temperatures below the Rb-Sr blocking temperature (Hunziker, 1974). The youngest age is a K-Ar crossite date of 173 Ma (Carden et al., 1977). However, crossite may not contain enough potassium to yield an accurate age (Sisson and Onstott, 1986). Zircon and apatite from the schist yielded fission-track ages of 148 ± 14 Ma and 77 ± 10 Ma, respectively, that are identical, within error, to those from the Afognak batholith (Clendenen et al., 2003). Sometime between 190 Ma and 150 Ma, the Afognak batholith and Raspberry Schist obtained identical cooling histories. Some of the ages suggest that it could have happened as early as 190 Ma, however, uncertainty exists due to imprecision of the K-Ar and Rb-Sr ages.

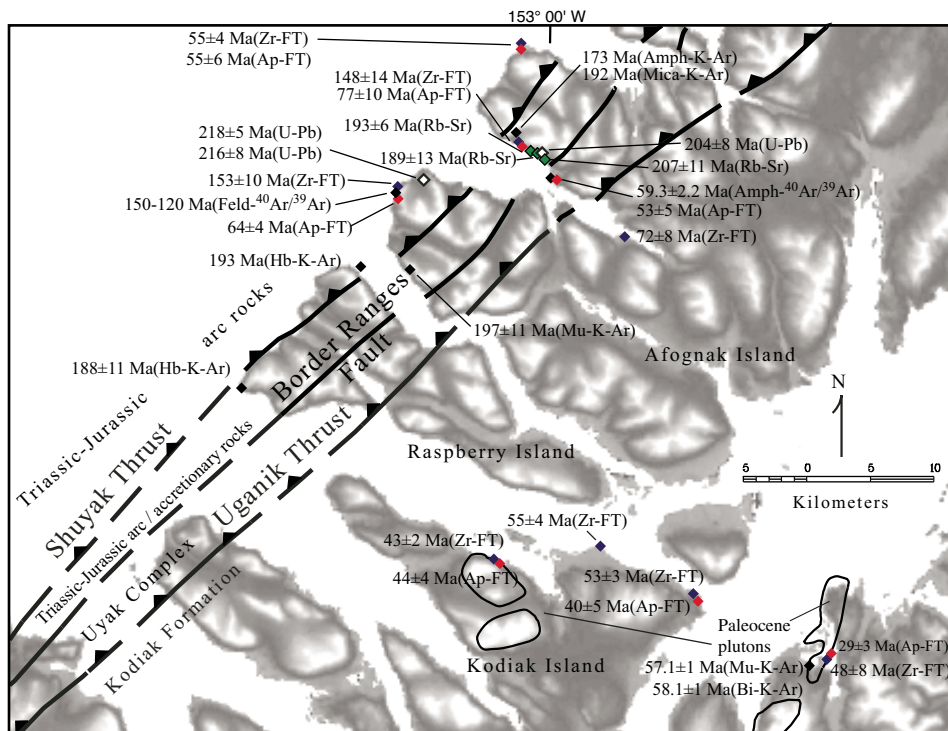


Figure 16. Geologic map showing the location of geochronologic data from the Raspberry Strait region of the Afognak batholith (modified from Farris and Haeussler, in press).

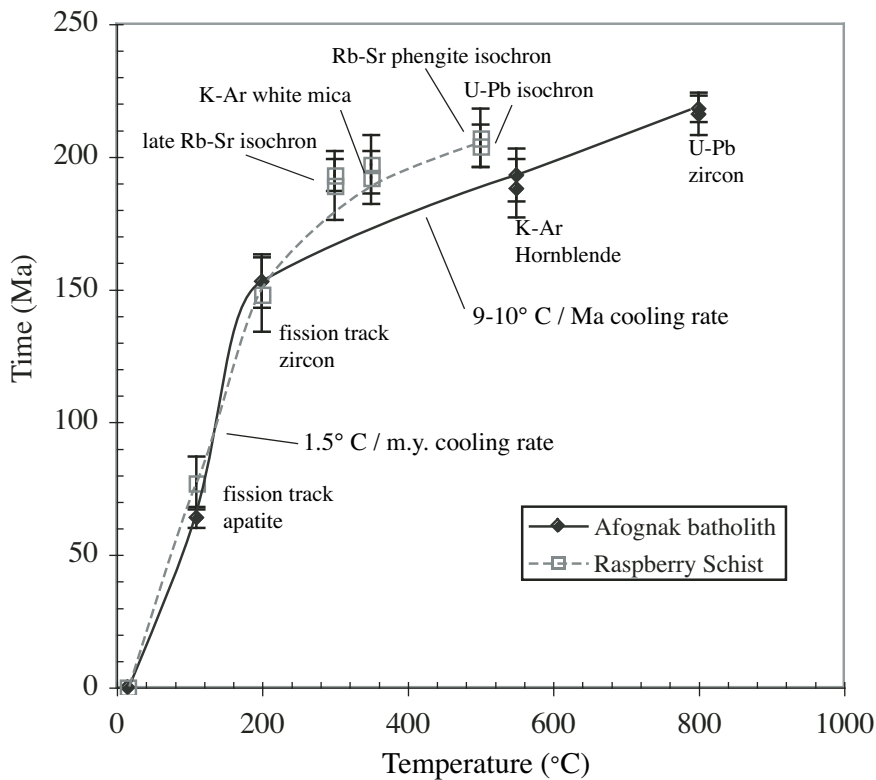


Figure 17. Thermochronologic cooling curves from the Afognak batholith and Raspberry Schist. Note the similarity in thermal evolution between the two adjacent units. By ca. 150 Ma their thermal evolution is identical. Data derived from Carden et al. (1977), Roeske et al. (1989), and Clendenen et al. (2003).

DISCUSSION

Three Different Crustal Levels Are Exposed

The Kodiak crustal section is composed of fault-bounded rock units that make up the upper, middle, and lower crust of an island arc (Fig. 2). The Shuyak Formation, composed chiefly of basaltic flows, basaltic pillow lavas, and volcanoclastic sedimentary rocks, forms the upper crust. The Afognak batholith, composed of dioritic through granitic intrusive rocks, forms the middle crust, and the lower crust and upper mantle are represented by gabbro and pyroxenite of the Kodiak Border Ranges ultramafic-mafic complex.

According to Kodiak unit thickness estimates, the upper 5–8 km of arc crust is composed of tholeiitic to calc-alkaline basaltic and volcanoclastic sedimentary rocks either extruded or deposited on the Earth's surface. However, along strike the thickness of the volcanic pile varies considerably, with the thickest section preserved on the northeast side of Afognak Island (Fig. 2). That location also contains the thinnest section of the Afognak batholith, so a correlation between arc-volcanic section thickness and thickness of the underlying plutonic rocks may exist. Alternatively, covariance of the two units could be related to exposure or crustal thickness changes.

The two Afognak batholith locations examined have geologic relations that suggest they formed at different crustal levels (Figs. 3 and 7). The Afognak batholith rocks exposed on Raspberry and Afognak Islands are tonalitic to dioritic in composition, are surrounded by gneissic metamorphic aureoles, and intrude into the base of a thick volcanic section (Fig. 7). According to unit thickness estimates alone, the emplacement depth of these rocks must have been at least 10–13 km. Metamorphism of the aureole rocks, the slow rate of cooling (Fig. 17), and style of emplacement also suggest mid-crustal depth. In comparison, the following characteristics suggest a shallow upper-crustal emplacement for the Miner's Point Afognak batholith: mutually intrusive plutonic and Shuyak Formation basalt (Fig. 3), discordant and stoped plutonic contacts, and cooling rates fast enough that basaltic melt crystallized as basalt rather than diorite. On Raspberry and Afognak Islands, the Afognak batholith has an estimated emplacement depth of >10–13 km, whereas on the Spiridon Peninsula, emplacement depth is estimated at ~5 km (Fig. 18).

The thickest portion of the Kodiak arc lower crust and mantle (Miner's Point) is only 3 km thick, crystallized at 7 kb pressure, and has an internal structure indicative of a complicated exhumation history. Its basic structure is composed of semi-coherent layered gabbro sandwiched between two layers of sheared

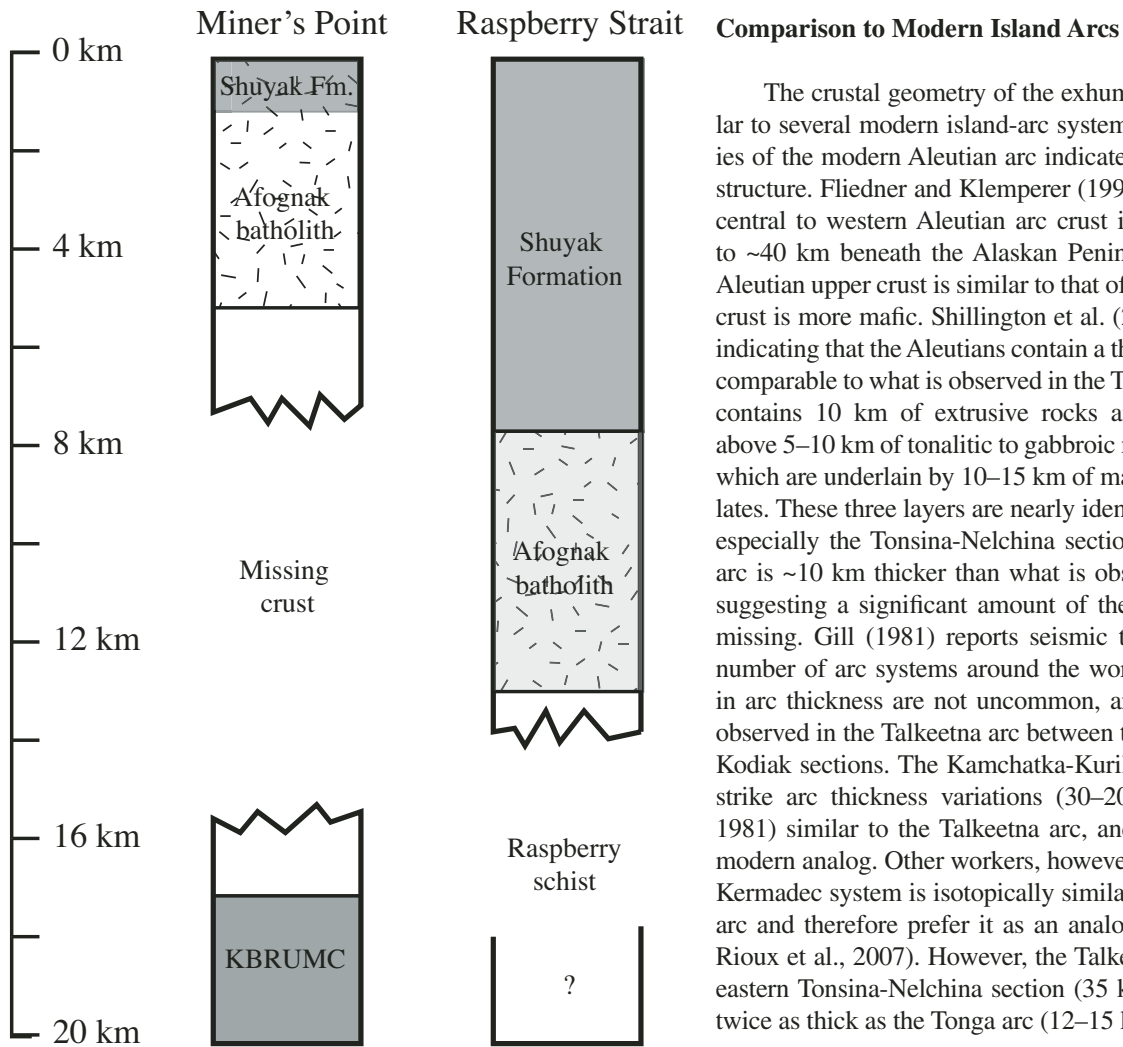


Figure 18. Schematic crustal sections illustrating differences between Miner's Point and Raspberry Strait. Both sections are missing large portions of the gabbroic lower crust. KBRUMC—Kodiak Border Ranges ultramafic-mafic complex.

pyroxenites with minor dunite. According to DeBari and Sleep (1991) and Greene et al. (2006), and the geochemical model in this paper, the layered gabbro should have formed structurally above the pyroxenite. A simple explanation for this geometry would be that during exhumation the ultramafic-mafic section was folded into a synform. That would explain the repeated ultramafic section, however it does not quite agree with the observed structure. Instead, the exterior ultramafic units are both strike parallel and dip to the northwest, and the layered gabbro complex in the middle forms a southwest-plunging antiform (Figs. 3, 4B). This relationship likely formed due to a complex interaction between faulting and folding during exhumation. Apparently, during the exhumation of the Kodiak Border Ranges ultramafic-mafic complex, only a small amount of the lower crust and mantle root was brought to the surface.

The crustal geometry of the exhumed Talkeetna arc is similar to several modern island-arc systems. Detailed seismic studies of the modern Aleutian arc indicate a similar layered crustal structure. Fliedner and Klempner (1999, 2000) indicate that the central to western Aleutian arc crust is ~30 km, and increases to ~40 km beneath the Alaskan Peninsula. They state that the Aleutian upper crust is similar to that of continents, but the lower crust is more mafic. Shillington et al. (2004) report seismic data indicating that the Aleutians contain a three-layer structure that is comparable to what is observed in the Talkeetna arc. Their model contains 10 km of extrusive rocks and upper-crustal plutons above 5–10 km of tonalitic to gabbroic mid-crustal plutons, all of which are underlain by 10–15 km of mafic and ultramafic cumulates. These three layers are nearly identical to the Talkeetna arc, especially the Tonsina-Nelchina section, however, the Aleutian arc is ~10 km thicker than what is observed on Kodiak Island, suggesting a significant amount of the gabbroic lower crust is missing. Gill (1981) reports seismic thickness estimates for a number of arc systems around the world. Along strike changes in arc thickness are not uncommon, and could explain what is observed in the Talkeetna arc between the Tonsina-Nelchina and Kodiak sections. The Kamchatka-Kuriles system exhibits along strike arc thickness variations (30–20 km, respectively; Gill, 1981) similar to the Talkeetna arc, and is therefore a potential modern analog. Other workers, however, have shown the Tonga-Kermadec system is isotopically similar to the eastern Talkeetna arc and therefore prefer it as an analog (Kelemen et al., 2003; Rioux et al., 2007). However, the Talkeetna arc, particularly the eastern Tonsina-Nelchina section (35 km thick), is greater than twice as thick as the Tonga arc (12–15 km; Gill, 1981).

Implications for Arc Processes

One of the most important implications of Kodiak Talkeetna arc rocks for general arc evolution is that all parts of the crust from the mantle to the upper crust are geochemically linked. Major element, REE, trace-element, and mineral-chemistry data indicate clear trends between the upper and lower parts of the arc. Modeling of these data suggest that Kodiak arc evolution occurred in two main stages: (1) A gabbroic initial melt underwent fractional crystallization that produced an ultramafic pyroxenite root and a gabbroic lower crust, and then (2) melt in equilibrium with the gabbroic lower crust underwent assimilation fractional crystallization to produce more silicic mid-crustal plutonic and upper-crustal volcanic rocks. AFC processes allow average mid-to-upper-crustal REE concentrations to be achieved at realistically low ($F = 0.4-0.6$) melt fractions. Otherwise, for a given thickness of upper crustal rocks, the required thickness of the lower crustal and mantle root portions of the arc become unacceptably large.

The Kodiak arc geochemical model suggests maximum melt fractions of 0.4–0.6 for both the lower-crustal and upper-crustal

portions of the model. Consequently, for a given upper-crustal thickness, the thickness of the lower portions of arc crust can be calculated (Fig. 19). The geochemical model does not specify a unit thickness, only the melt fractions to create that composition, so different initial values must be input to ascertain a best fit. Figure 19 depicts calculated crustal columns for upper-crustal thicknesses of 5 and 12 km. Those values were chosen because that is what is preserved at Miner's Point and on Afognak Island, respectively. Also shown are the end-member melt fractions for the model. The effect of AFC versus regular fractional crystallization is to thin the required lower crust (by 5 km) and mantle root (by 13 km). In the fractional crystallization only model (Fig. 15C), melt fractions of $F = 0.1$ are needed to reach average upper-crustal compositions. With a 12-km-thick upper crust, this leads to a mantle root >200 km thick, which is clearly not realistic. Realistic melt fractions need to be adhered to in any model of arc crustal evolution, and using AFC processes in the upper crust is a mechanism that allows this to happen.

Workers in the eastern Talkeetna arc have produced geochemical models that use only fractional crystallization (DeBari and Sleep, 1991; Kelemen et al., 2003; Greene et al., 2006). However, Rouix et al. (2007) presented U-Pb zircon data indicating that at least in the younger portions of the eastern Talkeetna arc assimilation has occurred, and in the older portion of the arc, the

volcanic rocks (i.e., Talkeetna Formation) are the same age as the intruding plutonic rocks and therefore inherited zircons would be difficult to observe. In exposures of the Afognak batholith, partial assimilation of incorporated Shuyak Formation volcanic rocks is observed. Therefore, it is valid to incorporate AFC processes into the model of arc evolution.

The pressure estimate of 7 kb from the Kodiak Border Ranges ultramafic-mafic complex suggests that crustal models 1–3 may be viable for the Kodiak arc section (Figs. 18 and 19). However, at Miner's Point, the thicknesses of the preserved units most closely match model 4, but significant tectonic thinning has occurred, and 10–15 km of mid-upper crust is exposed on Afognak Island. Therefore, the original Kodiak arc section is best approximated by either of the 12 km upper crust models (1–2). With a low melt fraction ($F = 0.4$) a large 45-km-thick ultramafic root is produced. Such a root would extend into the garnet stability field, would be gravitational unstable, and would likely delaminate and sink into the mantle (Kay and Kay, 1993; Ducea, 2001; Saleeby et al., 2003; Greene et al., 2006; Behn and Kelemen, 2006). With a melt fraction of $F = 0.6$ (model 2), a root of only 13 km would be produced. In that scenario, the entire root would be <30 km deep, its center would have a 7 kb pressure, and its preservation potential would be high. The Kodiak Border Ranges ultramafic-mafic complex exposed at Miner's Point is the thickest pyroxenite section in the entire Talkeetna arc, and model 2 would explain why it has been preserved.

Throughout the Talkeetna arc, and most arcs in general, upper- and mid-crustal rocks are preserved to a much higher degree than lower-crustal and mantle rocks. This implies a rheological boundary exists between granitic middle to upper crust and layered gabbroic lower crust and mantle. Above this boundary a near complete crustal section exists, however below it preservation and/or exhumation is incomplete. Most exhumed arcs do not contain any preserved rocks below this boundary (e.g., Ducea, 2001), however, tectonic conditions have led to partial preservation in the Talkeetna arc. Even in the Talkeetna arc, the boundary between mid-crustal granitic rocks and the lower crust is faulted and characterized by missing crust.

One potential explanation for the missing lower crust and mantle root is delamination (Kay and Kay, 1993; Ducea, 2001; Saleeby et al., 2003; Zandt et al., 2004). However, Talkeetna arc mantle rocks have been partially preserved, so this mechanism cannot have been universally effective. Modeling and data from this paper suggest that a combination of total upper-crustal thickness and the degree of fractionation to produce the upper-crust control whether or not a mantle root becomes thick and dense enough to delaminate. In the case of the highest-pressure lower-crustal Talkeetna arc rocks (10 kb garnet gabbro in the Bernard Mountain Tonsina ultramafic complex) only a couple 100 m of pyroxenite is preserved, with the majority of the ultramafic rocks being mantle harzburgite and dunite (Mehl et al., 2003). In this case, the lower crustal gabbro extended to below 35 km depth and would have required a mantle root even thicker than model 1 (Fig. 19). Delamination of such a thick root would have

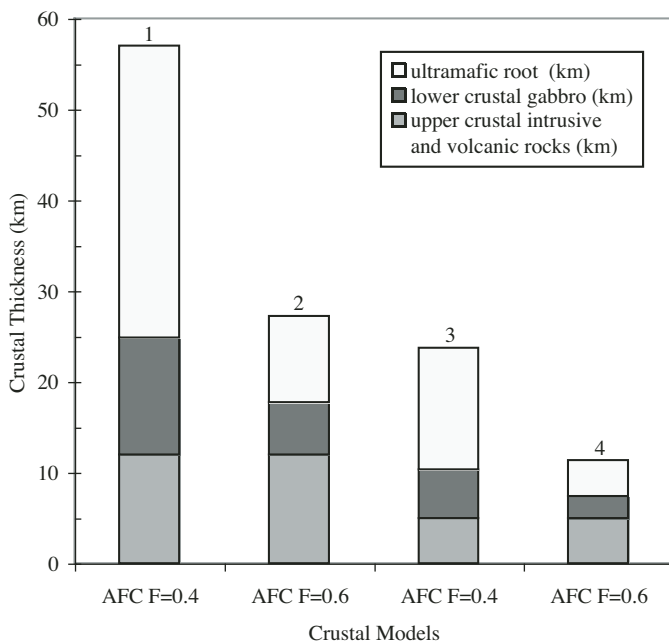


Figure 19. Calculated arc crustal sections. Crustal columns calculated using two-stage AFC (assimilation-fractional crystallization) model previously discussed in text for two different upper crustal thicknesses (12 and 5 km). Use of AFC processes in the upper crust reduces the combined lower crustal and mantle root thicknesses by 18, 7, 5, and 2.5 km for models 1–4, respectively, for similar melt fractions. However, to reach upper crustal compositions by fractional crystallization alone requires lower melt fractions (e.g., $F = 0.1$). Model 2 best approximates the Kodiak crustal section.

been nearly inevitable (Behn and Kelemen, 2006). However, in the Kodiak Talkeetna arc, the mantle root was much thinner, and therefore has been more fully preserved.

Blueschist-Talkeetna Arc Relationship

Between the upper portion of the Talkeetna arc and Chugach accretionary complex to the south, a series of blueschist-facies units (Seldovia, Raspberry, Iceberg Lake, and Liberty Creek Schists) occupy a structural position that is similar to the Border Ranges ultramafic-mafic complexes. Both the blueschist units and Border Ranges ultramafic-mafic complexes occur as large km-scale blocks immediately north of the Border Ranges fault, and to the south as klippen thrust over Cretaceous mélange (Uyak or McHugh Complexes depending on location). Also, both the blueschist and ultramafic-mafic units occur as smaller scale blocks within the mélange itself, such as Red Mountain in the McHugh Complex, Kenai Peninsula, and bodies of the Karluk Border Ranges ultramafic-mafic complexes in the Uyak Complex, western Kodiak Island.

One explanation for the structural relationship between the Talkeetna arc and blueschist units is an episode of subduction erosion (Clift et al., 2005b) coupled with upward and downward motion of crustal blocks within a subduction channel (Shreve and Cloos, 1986). Shreve and Cloos (1986) proposed a model in which a subduction megathrust is not a single surface, but rather is a 0.5–5-km-wide channel of mélange and other subducted materials (Fig. 20). In this model, they defined five different types of subduction channels (types A–E) that depended on the relative flux of incoming trench sediment and the volumetric capacity of the subduction channel. To illustrate end members: Type A subduction channels are those in which the channel capacity is much larger than the incoming sediment load. In such systems, all of the sediment is subducted and subduction erosion results. In the other end member, Type E, the sediment load is much larger than the channel capacity, and significant return flow occurs.

With respect to the Kodiak crustal section, geochronologic data indicate blueschist-facies metamorphism of the Raspberry Schist occurred within 10–15 Ma of Afognak batholith crystallization, and between 200 and 190 Ma both cooled through 500 °C (Fig. 17). Due to the proximity of the schist to the batholith, the entire forearc likely was removed by this time. Therefore, during the time interval, 215–200 Ma, the Kodiak Talkeetna arc must have had a Type A subduction channel. This would have brought the entire arc-crustal section into the forearc. I suggest that at this point subduction changed to a Type D or E subduction channel with return flow. Subduction channel return flow could have removed km-scale blocks from the base of the arc and carried them upwards where they became juxtaposed with the middle to upper crustal portions of the arc. However, in order for that to occur, the volume of sediment flux into the subduction zone must have increased beyond the capacity of the subduction channel. The blueschist-facies rocks themselves could have been part of the increased sediment flux.

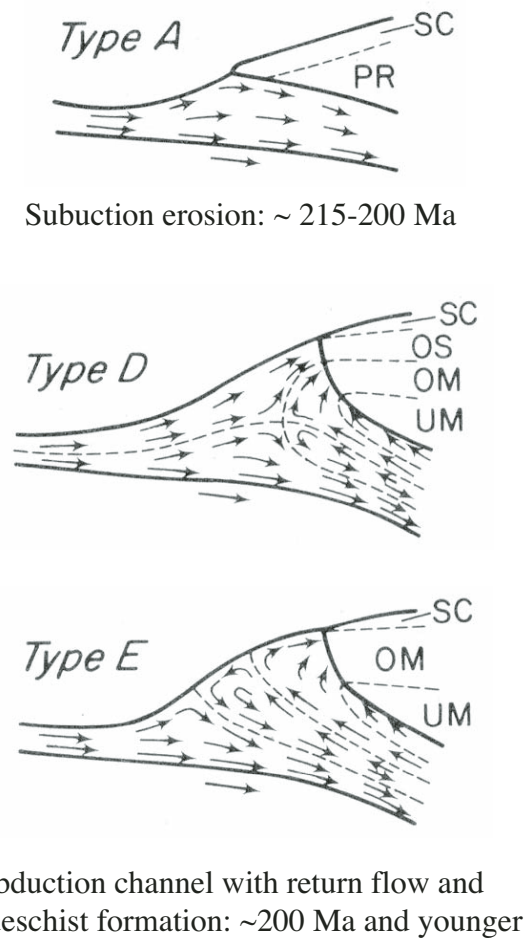


Figure 20. Schematic illustration of different types of subduction channels (from Shreve and Cloos, 1986). Type D and E subduction channels experience return flow. One option for the exhumation of the Kodiak Border Ranges ultramafic-mafic complex is that the subduction zone switched from Type A to Type D or E because of an increased flux of material entering the subduction channel. Abbreviations: slope cover (SC), preexisting rock (PR), offscraped sediment (OS), offscraped mélange (OM), and underplated mélange (UM).

One potential problem with this scenario is that the original Shreve and Cloos (1986) paper modeled the subduction channel contents as relatively low viscosity fluids, such as a mélangé, and in the Talkeetna arc both the blueschist units and Border Ranges ultramafic-mafic complexes form quasi-coherent km-scale blocks. However, other workers have proposed that large, intact crustal blocks can move up and down the subduction interface (e.g., ultra-high pressure terranes, Hacker et al., 2004).

Preferred Tectonic History of Arc Formation, Accretion, and Exhumation

Based on Afognak batholith U-Pb zircon ages, the Kodiak Talkeetna arc was magmatically active between ca. 215 and

185 Ma (Roeske et al., 1989). These dates indicate that the Kodiak segment was the oldest part of the Talkeetna arc and the first to cease activity (Fig. 21). In comparison, Rioux et al. (2007) reports that in the Chugach Mountains of the eastern Talkeetna arc, radiometric ages range from ca. 202–181 Ma. Subsequently, magmatic activity shifted northward into the Talkeetna Mountains, which yield ages from 177.5 to 168.9 Ma, and exhibit an increased crustal component (Rioux et al., 2007).

In the Kodiak Talkeetna arc, magmatism also migrates northward after 180 Ma (Fig. 21). On the Alaskan Peninsula there is a large Jurassic arc batholith (Reed and Lanphere, 1973) that has been interpreted as a western extension of the Talkeetna arc (Hacker et al., 2006; Johnsen et al., 2007). However, Kodiak arc rocks are separated from those on the Alaskan Peninsula by the Shelikof Strait, the modern Aleutian arc, and the Bruin Bay-Castle Mountain fault system, but age and chemistry suggest that both are part of the Talkeetna arc (Johnsen et al., 2007). For the Alaskan Peninsula plutons, Hacker et al. (2006) reports an U-Pb zircon age range of $183.3 \pm 0.6 - 163.9 \pm 0.1$ Ma with cooling

rates constrained by $^{40}\text{Ar}/^{39}\text{Ar}$ biotite ages of 20–100 °C/Ma. This age range is similar to the eastern Talkeetna arc plutons in the Talkeetna Mountains. Therefore, in both the western and eastern Talkeetna arc, magmatism initiated by 200 Ma in the south (Kodiak Island and Chugach Mountains), and then migrated northward after 180 Ma (Alaskan Peninsula batholith and Talkeetna Mountains). However, this northward arc migration occurred several million years earlier in the Kodiak segment.

The separation of the Kodiak Talkeetna arc from its counterpart on the Alaskan Peninsula is largely filled by a >100-km-wide sequence of Jurassic sedimentary rocks upon which the modern Aleutian arc has been built (Beikman, 1980). This sequence of sedimentary rocks narrows substantially in the eastern Talkeetna arc. Two of the major units are the Chitina and Naknek Formations. The Chitina Formation (Callovian, 164–159 Ma) overlaps with the end of Talkeetna arc magmatism and is composed of marine and volcanoclastic sediments, whereas the Naknek Formation (Tithonian–Oxfordian, 159–144 Ma) contains shallow-water and terrestrial sedimentary rocks and Talkeetna arc granitic cobbles (Nokleberg et al., 1994; Trop et al., 2005). The Kodiak and Peninsular portions of the arc must have been separated before or during the deposition of the above rock units. Also, Clift et al. (2005b), and Trop et al. (2005) proposed that arc exhumation and deposition of the Naknek Formation was caused by an intra-oceanic collision between the Peninsular and Wrangellia terranes forming the Wrangellia composite terrane.

On the Kodiak Islands, the timing of blueschist-facies metamorphism provides additional constraints on Talkeetna arc evolution. In the Raspberry Schist, blueschist-facies metamorphism began at 204 Ma (U-Pb isochron) and extends past 190 Ma. These ages fall shortly before the onset of northward arc migration, and correspond with the time period of inferred forearc erosion (e.g., Clift et al., 2005b). However, there is some overlap in the cooling history of the Afognak batholith and Raspberry Schist, but before 150 Ma the two units obtained identical cooling paths, and indicate that the batholithic rocks must have moved into the forearc by this time. These ages also correspond with unroofing of the Talkeetna arc on the Alaskan Peninsula. The earliest date rocks of the batholith and blueschist-facies could have been juxtaposed is ca. 200 Ma however, a younger date seems more likely.

Thermochronologic data from the Kodiak Border Ranges ultramafic-mafic complex are not available. However, due to the continuity of the geochemical trends from the ultramafic-mafic complex through the Afognak batholith and Shuyak Formation, it is considered to have formed synchronously. Also, the shared structural position of it and the Raspberry Schist suggest that the two units have a similar exhumation history. Thermochronologic data also imply that by the time that the blueschist-facies rocks were adjacent to rocks of the Afognak batholith, the Kodiak Border Ranges ultramafic-mafic complex was exhumed to at least a mid-crustal depth. After 150 Ma, zircon and apatite fission-track data (Clendenen et al., 2003) indicate that all of the Kodiak Talkeetna arc units experienced very slow 1.5 °C/Ma cooling, and must have reached upper-crustal levels by this time.

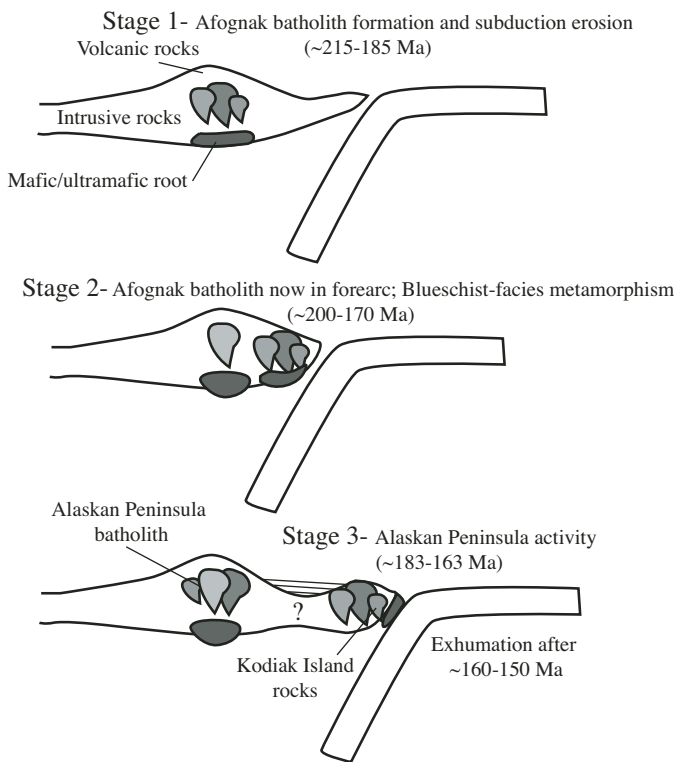


Figure 21. Schematic tectonic history of the Kodiak Talkeetna arc. Stage 1: Island arc formation (ca. 215–185 Ma). Stage 2: Subduction erosion brings initial arc into forearc between ca. 200–170 Ma (after Clift et al., 2005b). Blueschist-facies metamorphism occurs at this time. Stage 3: Arc magmatism migrates northward, and the Alaskan Peninsula batholith is formed (ca. 183–163 Ma) (Hacker et al., 2006). A large forearc basin forms between Kodiak-arc rocks and the Alaskan Peninsula. This basin does not form, or is much smaller, in the eastern Talkeetna arc. Also, upward motion along subduction channel exhumes arc root. Stage 4 (not pictured): ca. 160–150-Ma exhumation event initiates the onset of slow cooling.

Major local tectonic events post-150 Ma include: Early Cretaceous accretion of the Uyak Complex (Connelly, 1978), Late Cretaceous strike-slip motion along the Border Ranges fault (Roeske et al., 2003), Late Cretaceous accretion of the Kodiak and Ghost Rocks Formations (Sample and Moore, 1987), and an early Tertiary spreading-ridge subduction event (Farris et al., 2006). Small fragments of the Kodiak Border Ranges ultramafic-mafic complex occur entirely within the Uyak Complex (e.g., the Karluk bodies). Such blocks could simply have been transferred from the subduction zone hanging-wall into the Uyak Complex during its accretion in the Early Cretaceous.

Roeske et al. (2003) have suggested that upwards of 1000 km of right-lateral displacement occurred along the eastern Border Ranges fault system in the Late Cretaceous. If displacement of a similar magnitude occurred in the Kodiak region it did not significantly disrupt Talkeetna arc stratigraphy. The Kodiak and Tonsina-Nelchina sections are located >500 km apart, and each has uniquely identifiable characteristics across fault-bounded crustal blocks. Therefore, if 100s to 1000s of km of displacement did occur on the western Border Ranges fault, then strands south of the Raspberry Schist accommodated most of the displacement. Alternatively, the magnitude of slip along the Border Ranges fault could be less in western Alaska.

CONCLUSIONS

Arc Processes

- (1) The Kodiak Border Ranges ultramafic-mafic complex, Afognak batholith, and Shuyak Formation together form the lower, middle, and upper crust, respectively of an island-arc crustal section.
- (2) The upper, middle, and lower crust of the Kodiak Talkeetna arc are geochemically linked and can be modeled using (a) a gabbroic initial melt that underwent fractional crystallization producing a pyroxenite root and a gabbroic lower crust, and (b) melt in equilibrium with the gabbroic lower crust that underwent assimilation fractional crystallization to produce mid-crustal plutonic and upper-crustal volcanic rocks.
- (3) The Kodiak Border Ranges ultramafic-mafic complex contains the thickest section of Talkeetna arc pyroxenite. Arc-root preservation was greater in the Kodiak Island region because the root was substantially thinner than in the eastern Talkeetna arc, and did not delaminate back into the mantle. Instead thinning of the Kodiak Border Ranges ultramafic-mafic complex occurred during the exhumation process.

Arc Tectonics

- (4) Kodiak Island region contains the oldest and thinnest portion of the Talkeetna arc.

- (5) In the eastern and western Talkeetna arc, magmatism migrated northward after 180 Ma, likely in response to forearc erosion. Forearc erosion coupled with differential movement within a subduction channel moved middle and lower crustal arc rocks into the trench, causing juxtaposition with blueschist-facies rocks.
- (6) These processes occurred earlier and to a greater degree in the western Talkeetna arc possibly causing the arc to split, separating the Kodiak and Alaskan Peninsula parts of the Talkeetna arc.

ACKNOWLEDGMENTS

I wish to give thanks to Dwight Bradley, Peter Haeussler, and the Slab Windows project of the Minerals Program of the U.S. Geological Survey for logistical and financial support of the fieldwork, and to Susan DeBari and Virginia Sisson for comprehensive reviews that greatly improved the paper.

REFERENCES CITED

- Andersen, D.J., Lindsley, D.H., and Davidson, P.M., 1993, QUILF: A Pascal program to assess equilibria among Fe-Mg-Mn-Ti oxides, pyroxenes, olivine, and quartz: *Computers & Geosciences*, v. 19, p. 1333–1350, doi: 10.1016/0098-3004(93)90033-2.
- Arai, S., Kadoshima, K., and Morishita, T., 2006, Widespread arc-related melting in the mantle section of the northern Oman ophiolite as inferred from detrital chromian spinels: *Journal of the Geological Society*, v. 163, p. 869–879, doi: 10.1144/0016-76492005-057.
- Arzi, A.A., 1978, Critical phenomena in the rheology of partially melted rocks: *Tectonophysics*, v. 44, p. 173–184, doi: 10.1016/0040-1951(78)90069-0.
- Behn, M.D., and Kelemen, P.B., 2006, Stability of arc lower crust: Insights from the Talkeetna arc section, south central Alaska, and the seismic structure of modern arcs: *Journal of Geophysical Research*, v. 111, p. B11207, doi: 10.1029/2006JB004327.
- Beikman, H.M., 1980, Geologic map of Alaska: U.S. Geological Survey, scale 1:2,500,000, 1 sheet.
- Beyer, B.J., 1980, Petrology and geochemistry of ophiolite fragments in a tectonic mélange, Kodiak Islands, Alaska [Ph.D. thesis]: Santa Cruz, University of California, 227 p.
- Brown, M., Rushmer, T., and Sawyer, E.W., 1995, Introduction to special section: Mechanism and consequences of melt segregation from crustal protoliths: *Journal of Geophysical Research*, vol. 100, no. B8, p. 15,551–15,563.
- Burns, L.E., 1985, The Border Ranges ultramafic and mafic complex, south-central Alaska: Cumulate fractionates and island-arc volcanics: *Canadian Journal of Earth Sciences*, v. 22, p. 1020–1038.
- Carden, J.R., Connelly, W., Forbes, R.B., and Turner, D.L., 1977, Blueschists of the Kodiak Islands, Alaska—An extension of the Seldovia schist terrane: *Geology*, v. 5, p. 529–533, doi: 10.1130/0091-7613(1977)5<529:BOTKI A>2.0.CO;2.
- Clark, A.L., and Greenwood, W.R., 1972, Geochemistry and distribution of platinum-group metals in mafic to ultramafic complexes of southern and southeastern Alaska: U.S. Geological Survey Professional Paper 800-C, p. C157–C160.
- Clendenen, W.S., Fisher, D., and Byrne, T., 2003, Cooling and exhumation of the Kodiak accretionary prism, southwest Alaska, *in* Sisson, V.B., Roeske, S.M., and Pavlis, T.L., eds., *Geology of a transpressional orogen developed during ridge-trench interaction along the North Pacific margin*: Geological Society of America Special Paper 371, p. 71–88.
- Clift, P., Draut, A., Kelemen, P.B., Blusztajn, J., and Greene, A.R., 2005a, Stratigraphic and geochemical evolution of an oceanic arc upper crustal section: The Jurassic Talkeetna Volcanic Formation, south-central Alaska: *Geological Society of America Bulletin*, v. 117, p. 902–925, doi: 10.1130/B25638.1.

- Clift, P.D., Pavlis, T., DeBari, S.M., Draut, A.E., Rioux, M., and Kelemen, P.B., 2005b, Subduction erosion of the Jurassic Talkeetna-Bonanza arc and the Mesozoic accretionary tectonics of western North America: *Geology*, v. 33, p. 881–884, doi: 10.1130/G21822.1.
- Connelly, W., 1978, Uyak Complex, Kodiak Islands, Alaska: A Cretaceous subduction complex: *Geological Society of America Bulletin*, v. 89, p. 755–769, doi: 10.1130/0016-7606(1978)89<755:UCKIAA>2.0.CO;2.
- DeBari, S.M., and Coleman, R.G., 1989, Examination of the deep levels of an island arc: Evidence from the Tonsina ultramafic-mafic assemblage, Tonsina, Alaska: *Journal of Geophysical Research*, v. 94, p. 4373–4391.
- DeBari, S.M., and Sleep, N.H., 1991, High-Mg, low-Al bulk composition of the Talkeetna island arc, Alaska: Implications for primary magmas and the nature of arc crust: *Geological Society of America Bulletin*, v. 103, p. 37–47, doi: 10.1130/0016-7606(1991)103<0037:HMLABC>2.3.CO;2.
- DePaolo, D.J., 1981, Trace element and isotopic effects of combined wallrock assimilation and fractional crystallization: *Earth and Planetary Science Letters*, v. 53, p. 189–202.
- Ducea, M.N., 2001, The California arc: Thick granitic batholiths, eclogitic residues, lithospheric-scale thrusting, and magmatic flare-ups: *GSA Today*, v. 11, p. 4–10, doi: 10.1130/1052-5173(2001)011<0004:TCATGB>2.0.CO;2.
- Farris, D.W., and Haeussler, P.J., 2009, Geologic maps of the Kodiak batholith and other Paleocene intrusive rocks, Kodiak Island, Alaska: U.S. Geological Survey Geologic Investigations Series Maps, scale 1:50,000, 1 sheet, 7 plates (in press).
- Farris, D.W., and Paterson, S.R., 2007, Contamination of silicic magmas and fractal fragmentation of xenoliths in Paleocene plutons on Kodiak Island, Alaska: *Canadian Mineralogist*, v. 45, p. 107–129, doi: 10.2113/gscanmin.45.1.107.
- Farris, D.W., Haeussler, P., Friedman, R., Paterson, S.R., Saltus, R.W., and Ayuso, R., 2006, Emplacement of the Kodiak batholith: A consequence of slab-window migration: *Geological Society of America Bulletin*, v. 118, no. 11–12, p. 1360–1376, doi: 10.1130/B25718.1.
- Fliedner, M.M., and Klemperer, S.L., 1999, Structure of an island-arc: Wide-angle seismic studies in the eastern Aleutian Islands, Alaska: *Journal of Geophysical Research*, v. 104, p. 10,667–10,694, doi: 10.1029/98JB01499.
- Fliedner, M.M., and Klemperer, S.L., 2000, Crustal structure transition from oceanic arc to continental arc, eastern Aleutian Islands and Alaska Peninsula: *Earth and Planetary Science Letters*, v. 179, p. 567–579, doi: 10.1016/S0012-821X(00)00142-4.
- Forbes, R.B., and Lanphere, M.A., 1973, Tectonic significance of mineral ages of blueschists near Seldovia, Alaska: *Journal of Geophysical Research*, v. 78, p. 1383–1386, doi: 10.1029/JB078i008p01383.
- Forbes, R.B., and Swainbank, R.C., 1974, Garnet-clinopyroxenite from the Red Mountain pluton, Alaska: *Geological Society of America Bulletin*, v. 85, p. 285–292, doi: 10.1130/0016-7606(1974)85<285:GFTRMP>2.0.CO;2.
- Fountain, D.M., Percival, J., and Salisbury, M.H., 1990, Exposed cross sections of the continental crust—Synopsis, in Salisbury, M.H., and Fountain, D.M., eds., *Exposed cross-sections of the continental crust: Dordrecht, the Netherlands*, Kluwer Academic Publishers, NATO Advanced Study Institute Series C, v. 317, p. 653–662.
- Gill, J.B., 1981, *Orogenic andesites and plate tectonics*: Berlin, Springer-Verlag, 390 p.
- Greene, A.R., DeBari, S.M., Kelemen, P.B., Blusztajn, J., and Clift, P.D., 2006, A detailed geochemical study of island arc crust: The Talkeetna arc section, south-central Alaska: *Journal of Petrology*, v. 47, p. 1051–1093, doi: 10.1093/petrology/eg1002.
- Hacker, B.R., Ratschbacher, L., and Liou, J.G., 2004, Subduction, collision and exhumation in the ultrahigh-pressure Qinling-Dabie orogen, in Malpas, J., Fletcher, C.J.N., Ali, J.R., and Aitchison, J.C., eds., *Aspects of the tectonic evolution of China*: Geological Society of London Special Publication 226, p. 157–175.
- Hacker, B.R., Mehl, L., Kelemen, P.B., Rioux, M., and Greene, A., 2005, Reconstructing the Jurassic Talkeetna intra-oceanic arc of Alaska using thermobarometry: *Eos (Transactions, American Geophysical Union)*, v. 86, p. V51D-1521.
- Hacker, B.R., Kelemen, P.B., Rioux, M., McWilliams, M.O., Gans, P.B., and Reiners, P., 2006, Cooling history of the Talkeetna intra-oceanic arc of Alaska: $^{40}\text{Ar}/^{39}\text{Ar}$ and U-Th/He dating, in *Genesis and evolution of the Jurassic Talkeetna Arc of south-central Alaska*: Geological Society of America Penrose Conference, Arc Genesis and Crustal Evolution, Valdez, Alaska, 9–15 July 2006, Guidebook, p. 41–45.
- Hill, M.D., 1979, Volcanic and plutonic rocks of the Kodiak-Shumagin shelf, Alaska: Subduction deposits and near trench magmatism [Ph.D. thesis]: Santa Cruz, University of California, 279 p.
- Hill, M.D., and Gill, J.B., 1976, Mesozoic greenstones of diverse ages from the Kodiak Islands, Alaska: *Eos (Transactions, American Geophysical Union)*, v. 57, no. 12, p. 1021.
- Hoffman, B.L., 1974, *Geology of the Bernard Mountain area, Tonsina, Alaska* [M.S. thesis]: Fairbanks, University of Alaska, 67 p.
- Hunziker, J.C., 1974, Rb-Sr and K-Ar age determination and the Alpine tectonic history of the Western Alps: *Memorie degli Istituti di Geologia e Mineralogia dell'Università di Padova*, 31, p. 1–54.
- Jackson, J., 2002, Strength of the continental lithosphere: Time to abandon the jelly sandwich?: *GSA Today*, v. 12, no. 9, p. 4–10, doi: 10.1130/1052-5173(2002)012<0004:SOTCLT>2.0.CO;2.
- Jäger, E., 1979, Introduction to geochronology, in Jäger, E., and Hunziker, J.C., eds., *Lectures in isotope geology*: Berlin, Springer-Verlag, p. 2–12.
- Johnsen, M., DeBari, S., and Rioux, M., 2007, The felsic plutonic core of the western Talkeetna island arc crustal section, Alaska: Its formation and implications for crustal growth along continental margins: *Geological Society of America Abstracts with Programs*, v. 39, no. 4, p. 72–73.
- Jull, M., and Kelemen, P.B., 2001, On the conditions for lower crustal convective instability: *Journal of Geophysical Research*, v. 106, p. 6423–6446, doi: 10.1029/2000JB900357.
- Kay, R.W., and Kay, S.M., 1993, Delamination and delamination magmatism: *Tectonophysics*, v. 219, p. 177–189.
- Kelemen, P.B., Hanghøj, K., and Greene, A.R., 2003, One view of the geochemistry of subduction-related magmatic arcs, with emphasis on primitive andesite and lower crust, in Rudnick, R.L., volume ed., *The Crust*, v. 3: *Treatise on Geochemistry* (Holland, H.D., and Turekian, K.K., exec. eds.): Oxford, Elsevier Pergamon, p. 593–659.
- Kohlstedt, D.L., Evans, B., and Mackwell, S.J., 1995, Strength of the lithosphere: Constraints imposed by laboratory experiments: *Journal of Geophysical Research*, v. 100, p. 17,587–17,602, doi: 10.1029/95JB01460.
- Mehl, L., Hacker, B.R., Hirth, G., and Kelemen, P.B., 2003, Arc-parallel flow within the mantle wedge: Evidence from the accreted Talkeetna arc, south central Alaska: *Journal of Geophysical Research*, v. 108, p. 2375, doi: 10.1029/2002JB002233.
- Moore, G.W., 1967, Preliminary geologic map of Kodiak Island and vicinity, Alaska: U.S. Geological Survey Open-File Report OF-67-161, scale 1:250,000.
- Mullen, E.D., 1983, MnO/TiO₂/P₂O₅: A minor element discriminant for basaltic rocks of the oceanic environment and its implications for petrogenesis: *Earth and Planetary Science Letters*, v. 62, p. 53–62, doi: 10.1016/0012-821X(83)90070-5.
- Nokleberg, W.J., Plafker, G., and Wilson, F.H., 1994, Geology of south-central Alaska, in Plafker, G., and Berg, H.C., eds., *The Geology of Alaska: Boulder, Colorado*, Geological Society of America, *Geology of North America*, v. G-1, p. 311–366.
- Paterson, S.R., and Schmidt, K.L., 1999, Is there a close spatial relationship between faults and plutons?: *Journal of Structural Geology*, v. 21, p. 1131–1142, doi: 10.1016/S0191-8141(99)00024-3.
- Paterson, S.R., and Vernon, R.H., 1995, Bursting the bubble of ballooning plutons; a return to nested diapirs emplaced by multiple processes: *Geological Society of America Bulletin*, v. 107, p. 1356–1380, doi: 10.1130/0016-7606(1995)107<1356:BTBOBP>2.3.CO;2.
- Paterson, S.R., Fowler, T.K., Jr., and Miller, R.B., 1996, Pluton emplacement in arcs: A crustal-scale exchange process: *Transactions of the Royal Society of Edinburgh*, v. 87, p. 115–123.
- Pearce, J.A., Harris, N.B.W., and Tindle, A.G., 1984, Trace element discrimination diagrams for the tectonic interpretation of granitic rocks: *Journal of Petrology*, v. 25, p. 956–983.
- Pearcy, L., DeBari, S.M., and Sleep, N.H., 1990, Mass balance calculations of island arc crust and implications for the formation of continents: *Earth and Planetary Science Letters*, v. 96, p. 427–442, doi: 10.1016/0012-821X(90)0018-S.
- Pignotta, G.S., and Paterson, S.R., 2007, Voluminous stoping in the Mitchell Peak granodiorite, Sierra Nevada batholith, California: *Canadian Mineralogist*, v. 45, p. 87–106, doi: 10.2113/gscanmin.45.1.87.

- Plafker, G., Nokleberg, W.J., and Lull, J.S., 1989, Bedrock geology and tectonic evolution of the Wrangellia, Peninsular, and Chugach terranes along the Trans-Alaska Crustal Transect in the Chugach Mountains and southern Copper River basin, Alaska: *Journal of Geophysical Research*, v. 94, B4, p. 4255–4295, doi: 10.1029/JB094iB04p04255.
- Plafker, G., Moore, J.C., and Winkler, G.R., 1994, Geology of the southern Alaska margin, in Plafker, G., and Berg, H.C., eds., *The Geology of Alaska*: Boulder, Colorado, Geological Society of America, *Geology of North America*, v. G-1, p. 389–449.
- Powell, R., 1984, Inversion of the assimilation and fractional crystallization (AFC) equations; characterization of contaminants from isotope and trace element relationships in volcanic suites: *Journal of the Geological Society of London* 141, p. 447–452.
- Reed, B.L., and Lanphere, M.A., 1973, Alaska-Aleutian range batholith: Geochronology, chemistry, and relation to circum-Pacific plutonism: *Geological Society of America Bulletin*, v. 84, p. 2583–2610.
- Rioux, M.E., Mehl, L., Hacker, B.R., Mattinson, J.M., Gans, P., and Wooden, J.L., 2001, Understanding island arc evolution through U/Pb and $^{40}\text{Ar}/^{39}\text{Ar}$ geochronology of the Talkeetna arc, south-central Alaska: *Eos (Transactions, American Geophysical Union)*, v. 82, no. 47, Fall Meeting Supplement, Abstract T41C-0885.
- Rioux, M.E., Kelemen, P.B., Mattinson, J., Hacker, B.R., and Blusztajn, J., 2004, Magmatic differentiation in the accreted Talkeetna arc; south-central Alaska: *Eos (Transactions, American Geophysical Union)*, v. 84, no. 47, Fall Meeting Supplement, abstract V13B-1482.
- Rioux, M.L., Mattinson, J., Hacker, B.R., Kelemen, P., and Blusztajn, J., 2005, Growth and evolution of the Peninsular terrane, southern Alaska: *Geological Society of America Abstracts with Programs*, v. 37, no. 7, p. 82.
- Rioux, M., Hacker, B., Mattinson, J., Kelemen, P., Blusztajn, J., and Gehrels, G., 2007, Magmatic development of an intra-oceanic arc: High precision U-Pb zircon and whole-rock isotopic analyses from the accreted Talkeetna arc, south-central Alaska: *Geological Society of America Bulletin*, v. 119, p. 1168–1184, doi: 10.1130/B25964.1.
- Roeske, S.M., 1986, Field relations and metamorphism of the Raspberry Schist, Kodiak Islands, Alaska, in Evans, B.W., and Brown, E.H., eds., *Blueschists and eclogites*: Geological Society of America Memoir 164, p. 169–184.
- Roeske, S.M., Mattinson, J.M., and Armstrong, R.L., 1989, Isotopic ages of glaucophane schists on the Kodiak Islands, southern Alaska, and their implications for the Mesozoic tectonic history of the Border Ranges fault system: *Geological Society of America Bulletin*, v. 101, p. 1021–1037, doi: 10.1130/0016-7606(1989)101<1021:IAOGSO>2.3.CO;2.
- Roeske, S.M., Snee, L.W., and Pavlis, T.L., 2003, Dextral-slip reactivation of an arc-forearc boundary during Late Cretaceous–Early Eocene oblique convergence in the northern Cordillera, in Sisson, V.B., Roeske, S.M., and Pavlis, T.L., eds., *Geology of a transpressional orogen developed during ridge-trench interaction along the North Pacific Margin*: Geological Society of America Special Paper 371, p. 141–170.
- Rollinson, H., 1998, *Using geochemical data: Evaluation, presentation, interpretation*: Singapore, Longman Group, 352 p.
- Saleeby, J., Ducea, M., and Clemens-Knott, D., 2003, Production and loss of high-density batholithic root, southern Sierra Nevada, California: *Tectonics*, v. 22, no. 6, p. 1064, doi: 10.1029/2002TC001374.
- Sample, J.C., and Moore, J.C., 1987, Structural style and kinematics of an underplated slate belt, Kodiak and adjacent islands, Alaska: *Geological Society of America Bulletin* v. 99, no. 1, p. 7–20.
- Shillington, D.J., Van Avendonk, H.J.A., Holbrook, W.S., Kelemen, P.B., and Hornbach, M.J., 2004, Composition and structure of the central Aleutian island arc from arc-parallel wide-angle seismic data: *Geochemistry Geophysics Geosystems*, v. 5, no. 10, 32 p.
- Shreve, R.L., and Cloos, M., 1986, Dynamics of sediment subduction, melange formation and prism accretion: *Journal of Geophysical Research*, v. 91, p. 10,229–10,245, doi: 10.1029/JB091iB10p10229.
- Sisson, V.B., and Onstott, T.C., 1986, Dating blueschist metamorphism: A combined $^{40}\text{Ar}/^{39}\text{Ar}$ and electron microprobe approach: *Geochimica et Cosmochimica Acta*, v. 50, p. 2111–2117, doi: 10.1016/0016-7037(86)90264-4.
- Taylor, S.R., and McLennan, S.M., 1985, *The continental crust: Its composition and evolution*: Boston, Blackwell Scientific, 312 p.
- Toth, M.L., 1981, Petrology, geochemistry, and origin of the Red Mountain ultramafic body near Seldovia, Alaska: U.S. Geological Survey Open-File Report 81-514, 86 p.
- Trop, J.M., Szuch, D.A., Rioux, M., and Blodgett, R.B., 2005, Sedimentology and provenance of the Upper Jurassic Naknek Formation, Talkeetna Mountains, Alaska: Bearings on the accretionary tectonic history of the Wrangellia composite terrane: *Geological Society of America Bulletin*, v. 117, p. 570–588, doi: 10.1130/B25575.1.
- Zandt, G., Gilbert, H., Owens, T.J., Ducea, M., Saleeby, J., and Jones, C.H., 2004, Active foundering of a continental arc root beneath the southern Sierra Nevada in California: *Nature*, v. 431, p. 41–46, doi: 10.1038/nature02847.

Mid-Cretaceous–Recent crustal evolution in the central Coast orogen, British Columbia and southeastern Alaska

Maria Luisa Crawford*

Department of Geology, Bryn Mawr College, Bryn Mawr, Pennsylvania 19010, USA

Keith A. Klepeis

Department of Geology, University of Vermont, Burlington, Vermont 05405, USA

George E. Gehrels

Department of Geosciences, University of Arizona, Tucson, Arizona 85721, USA

Jennifer Lindline

Department of Natural Sciences, New Mexico Highlands University, Las Vegas, New Mexico 87701, USA

ABSTRACT

The Coast orogen of western coastal British Columbia and southeastern Alaska is one of the largest batholithic belts in the world. This paper addresses the structure and composition of the crust in the central part of this orogen, as well as the history of its development since the mid-Cretaceous. The core of the orogen consists of two belts of metamorphic and plutonic rocks: the western metamorphic and thick-skinned thrust belt comprising 105–90-Ma plutons and their metamorphic country rocks, and the Coast Plutonic Complex on the east, with large volumes of mainly Paleogene magmatic rocks and their high-temperature gneissic host rocks. These two belts are separated by the Coast shear zone, which forms the western boundary of a Paleogene magmatic arc. This shear zone is subvertical, up to 5 km wide, and has been seismically imaged to extend to and offset the Moho. Lithologic units west of the Coast shear zone record contractional deformation and crustal thickening by thrusting and magma emplacement in the mid-Cretaceous. To the east, the Coast Plutonic Complex records regional contraction that evolves to regional extension and coeval uplift and exhumation after ca. 65 Ma. Igneous activity in the Complex formed a Paleogene batholith and gave rise to high crustal temperatures, abundant migmatite and, as a result, considerable strain localization during deformation. In both belts, during each stage of the orogeny, crustal-scale deformation enabled and assisted magma transport and emplacement. In turn, the presence of magma, as well as its thermal effects in the crust, facilitated the deformation. After 50 Ma, the style of crustal evolution changed

*mrcrawfor@brynmawr.edu

Crawford, M.L., Klepeis, K.A., Gehrels, G.E., and Lindline, J., 2009, Mid-Cretaceous–Recent crustal evolution in the central Coast orogen, British Columbia and southeastern Alaska, *in* Miller, R.B., and Snoke, A.W., eds., *Crustal Cross Sections from the Western North American Cordillera and Elsewhere: Implications for Tectonic and Petrologic Processes*: Geological Society of America Special Paper 456, p. 97–124, doi: 10.1130/2009.2456(04). For permission to copy, contact editing@geosociety.org. ©2009 The Geological Society of America. All rights reserved.

to one dominated by periods of extension oriented approximately perpendicular to the orogen. The extension resulted in tilting of large and small crustal blocks as well as intra-plate type magmatic activity across the orogen. Seismic-reflection and refraction studies show that the crust of this orogen is unusually thin, probably due to the periods of orogen-perpendicular stretching. Magmatic activity west of the Coast shear zone in the Late Oligocene and Miocene was related to one period of orogen-parallel transtension along the margin. Small-scale, mafic, mantle-derived volcanic activity continues in the region today. The change from convergence to translation and extension is related to a major plate reorganization in the Pacific that led to a change from subduction of an oceanic plate to northwestward translation of the Pacific plate along the northwest coast of North America. Although it has been proposed that this orogen is the site of major (up to 4000 km) pre-Eocene northward terrane translation, there is little evidence for such large-scale displacement or for the kind of discontinuity in the geological record that such displacement would entail.

INTRODUCTION

In this paper, we summarize ca. 115 million years of post-mid-Cretaceous history of crustal development within the Coast orogen along the western coast of British Columbia and southeastern Alaska. This segment of the northwestern margin of the North American Cordillera was constructed by processes associated with Jurassic accretion of displaced terranes and associated subduction of oceanic lithosphere (Monger *et al.*, 1982). During the Upper Cretaceous and Paleogene two successive and parallel continent-margin arcs were built across the collage of accreted terranes (Hutchison, 1982; Crawford *et al.*, 1999; Hollister and Andronicos, 2000). This period of continental crustal assembly and thickening evolved into an orogen-parallel or nearly parallel extensional regime with related uplift and exhumation of the Paleogene batholith (Andronicos *et al.*, 2003). After 50 Ma, the orogen experienced crustal-scale extension and associated rift-related magmatism as the plate motion along the northwestern margin of the North American plate changed to a transform boundary leading finally to the present strike-slip, slightly transpressional tectonic regime (Hyndman and Hamilton, 1993; Irving *et al.*, 2000). Uplift and erosion of deeper segments of the orogen as a result of post-50-Ma extension exposed the middle crust that had evolved during the previous 60 million years at depths of 15–30 km (Cook and Crawford, 1994; Andronicos *et al.*, 2003; Rusmore *et al.*, 2005). This exhumation history provides the opportunity to observe the features associated with the tectonic thickening and magmatic activity throughout the early convergent to transpressional phase of the orogeny. Reflection and refraction geophysical studies undertaken in connection with the ACCRETE (Morozov *et al.*, 1998) and Slave-Northern Cordilleran Lithosphere Evolution (SNorCLE) (Cook and Erdmer, 2005) geophysical transects supply information on the present character of the crust under the belt.

Features related to crustal evolution elucidated by our studies include:

- 1) The nature of the response of the crust to the overall plate regime throughout the history of the orogen. Based on our observations, we propose links between the features that arose in the evolving crust and the inferred motions between the North American plate and the oceanic plates to the west.
- 2) Temporally and spatially distinctive episodes of igneous activity during the evolution of this continental margin. The igneous rocks constitute a significant component of the crustal section. Their distribution, chemistry, and volume appear closely related to evolving crustal and mantle lithospheric structure, which reflect plate interactions.
- 3) How the style of orogen-scale crustal deformation changed and was partitioned during successive phases of crustal evolution from arc construction and thickening to extension and thinning within the orogen. Much of the nature and distribution of large-scale deformation appears related to contrasts in, and modifications of, crustal rheology due to changing crustal thickness, zones of inherited structural weakness, and crustal weakening mechanisms, including magma emplacement and crustal melting.
- 4) In addition, we evaluate the possible causes of variations in the evolution of the orogen along strike of the area of our detailed studies.

Overview of Plate Motion Related to Orogen History

The Coast orogen, along the western coast of British Columbia and southeastern Alaska, comprises Cretaceous and Paleogene continental margin arcs built across an assemblage of exotic terranes accreted to the northwest margin of North America starting in the Jurassic (Monger *et al.*, 1982). The terrane accretion and associated crustal development is associated with relative motion between the North American plate and various oceanic plates of the northwest Pacific Ocean (Engelbreton *et al.*, 1985).

The Early to Middle Jurassic juxtaposition of outboard oceanic-arc terranes with inboard earlier accreted terranes in a

dextral transpressional regime (van der Heyden, 1992; McClelland and Gehrels, 1990; McClelland et al., 1992c; Gehrels, 2001) was the initial phase of construction of the present northwest edge of the North American continent. During early Cretaceous time, starting ca. 140 Ma, terrane displacement along the continental margin became sinistral (Gehrels and Boghossian, 2000). From the Late Jurassic to mid-Cretaceous, transtensional displacements within the developing marginal arc created a series of within- to back-arc depositional basins along the Cordilleran margin (McClelland et al., 1992c) including the Gravina basin in southeastern Alaska.

According to Engebretson et al. (1985) and Stock and Molnar (1988), the relative motion of the oceanic plates gradually shifted from oblique convergence between the Farallon oceanic plate and North America prior to 110 Ma, to near orthogonal convergence between 110 and 85 Ma. The relative velocity of the plates also increased at this time. At or near 85 Ma the northern part of the Farallon plate, split off to form the Kula plate, leading to a change from near orthogonal convergence to oblique dextral convergence between the oceanic Kula plate and North America. Seafloor magnetic data suggest a major reorganization of the Kula, Pacific, and North American plate boundaries occurred at magnetic anomaly 23r (ca. 52 Ma) (Stock and Molnar, 1988; Lonsdale, 1988; Atwater, 1989). Evidence presented by Tarduno et al. (2003) that the Hawaii-Emperor hot spot was moving south from 80 to 40 Ma suggests less dextral motion during this interval than suggested by the Engebretson et al. (1985) reconstructions. Lonsdale (1988) proposed that Kula plate motion changed from a high angle relative to North America to parallel to the margin by 45 Ma. This change in Kula plate motion was followed by consumption of the subducting plate(s) leading to transcurrent motion of the Pacific plate relative to North America from 45 Ma to Present.

In an alternative model, Haeussler et al. (2003) proposed that another oceanic plate, the Resurrection plate, formed from the eastern side of the Kula plate by least 66 Ma and lay between it and North America. According to this model, arrival of the spreading ridge between the Kula and Resurrection plates at the North American plate margin at 50 Ma terminated subduction across this margin and led to the formation of the Queen Charlotte transform fault, the present North America plate margin. An alternative and more elaborate model for the consumption of the Resurrection plate (Madsen et al., 2006) postulates that plate subduction continued until 40 Ma in the area of this study. The timing of events in the Haeussler et al. (2003) model most closely fits our observations, as reported below. In the last 50 million years northwestward motion of the Pacific plate relative to North America has been transtensional, translational and finally transpressional (Hyndman and Hamilton, 1993; Irving et al., 2000).

Crustal Framework of the Orogen

Three accreted terranes have been identified in the area of this study between the Skeena River in British Columbia and

the Stikine River and Sumner Strait in Alaska (Figs. 1 and 2). Along the eastern side of this segment of the Coast orogen lies the Stikine terrane (Coney et al., 1980), a crustal-scale block assigned to the Intermontane superterrane that comprises Devonian through Jurassic sedimentary and volcanic rocks. The sedimentary and volcanic rocks of Stikinia have primitive Nd isotope ratios (Samson et al., 1989) indicating that the terrane formed in an intra-oceanic setting. These units are overlain by Middle Jurassic to earliest Cretaceous clastic Bowser Lake sedimentary rocks. A U-Pb age of 84.1 ± 0.5 Ma for the Poison pluton that intruded folded Bowser Lake sedimentary rocks indicates that the Bowser Lake units were deformed prior to the latest Cretaceous to form the Skeena fold-and-thrust belt (Fig. 2) (Evenchick and McNicoll, 1993).

West of Stikinia, forming most of the exhumed deep crust of the orogenic belt, are rocks belonging to the Yukon-Tanana terrane (Gehrels et al., 1990; Gareau and Woodsworth, 2000; Boghossian and Gehrels, 2000). These consist of metamorphosed Paleozoic and possibly Neoproterozoic strata with continental-margin affinity (Gehrels et al., 1990) as demonstrated by evolved Nd and Sr isotopic signatures (Samson et al., 1991b) and by detrital zircon data (Gehrels et al., 1991b). Jackson et al. (1991) suggest that the Yukon-Tanana and Stikine terranes were linked by Late Triassic time.

The westernmost units in this area belong to the Alexander terrane, a component of the Insular superterrane. The Paleozoic

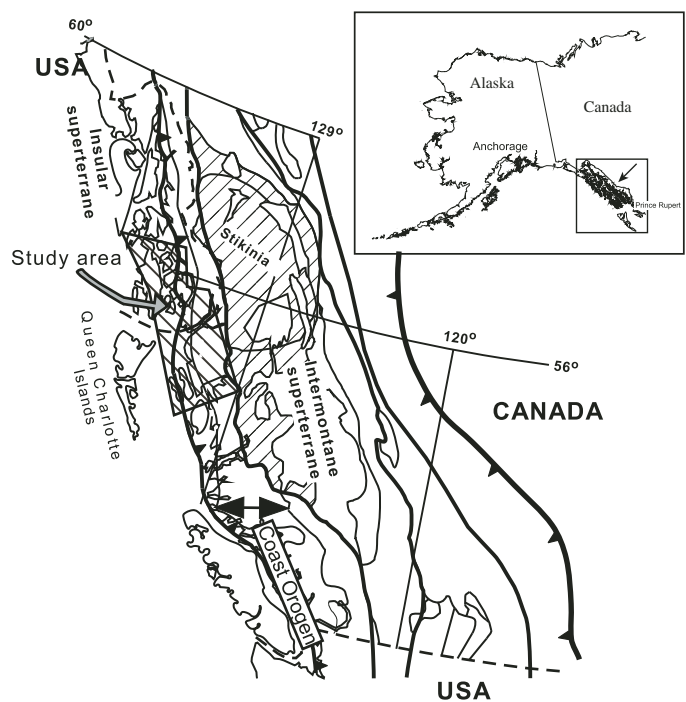


Figure 1. Schematic terrane map for British Columbia and southeastern Alaska, showing the Intermontane and Insular superterranes, Stikinia, Coast orogen, and the location of the study area in the central part of the orogen.

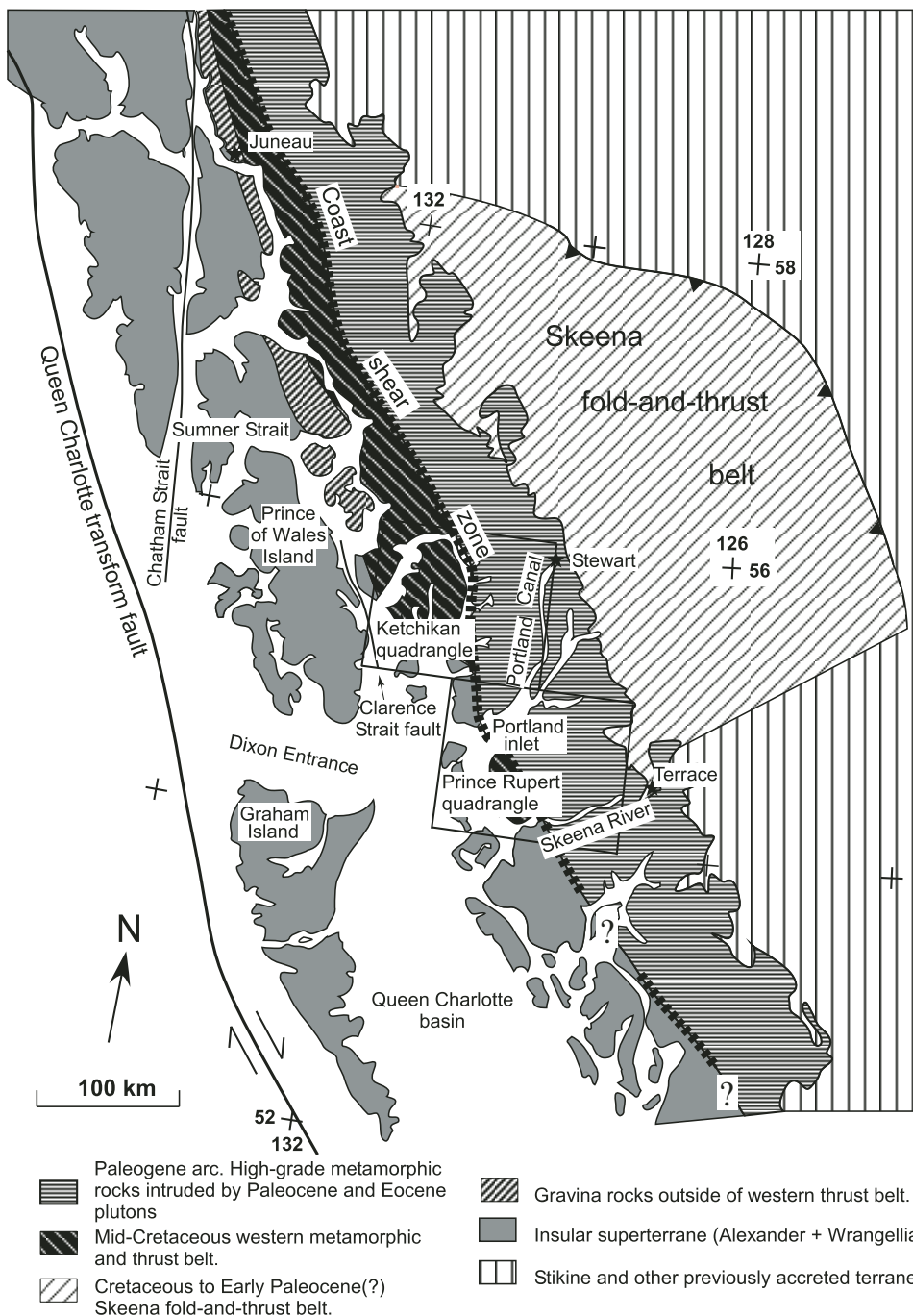


Figure 2. Map of the central part of the Coast orogen showing the major units referred to in the text.

through Triassic history of this terrane is distinctly different from that of Stikinia and Yukon-Tanana terranes (Gehrels and Saleeby, 1987). In the area of this study the Alexander terrane consists of Cambrian, and possibly late Neoproterozoic, through Silurian volcanic and plutonic igneous rocks and associated sedimentary units. The lower Paleozoic igneous rocks represent two successive oceanic volcanic-arc assemblages without evidence for continental crust. Mostly clastic Lower Devonian rocks succeeded by upper Paleozoic oceanic sedimentary rocks, dominated by limestone, overlie these arc rocks. The eastern side of the Alexander

terrane consists of Triassic rift-related sedimentary rocks locally overlain by Middle Jurassic rhyolitic volcanic rocks (Gehrels, 2001). Similar Middle Jurassic volcanic rocks also overlie Yukon-Tanana rocks to the east (Gehrels, 2001), which strongly suggests that the Alexander terrane was accreted to the inboard terranes during or prior to mid-Jurassic time. This juxtaposition of the Alexander and Yukon-Tanana terranes in the Jurassic also is supported by the observations by Gehrels and Boghossian (2000) on the relationship between rocks assigned to these two terranes south of Prince Rupert.

In the study area, the Alexander terrane and Yukon-Tanana terrane are presently separated by rocks of the Gravina sequence deposited in a back-arc or intra-arc pull-apart basin that opened in the Jurassic (McClelland et al., 1992a; Gehrels, 2001). The belt of Gravina sequence rocks is widest between Petersburg and the Alaska-British Columbia border (Figs. 2, 3). Mafic volcanic flows and breccia and graphitic graywacke turbidite sedimentary units of the Gravina sequence (Berg et al., 1972; Rubin and Saleeby, 1991) are thrust southward over the Alexander terrane or, locally, unconformably overlie Triassic rocks of the eastern margin of that terrane (Berg, 1973; Berg et al., 1988). To the east the Gravina units

tectonically underlie the Yukon-Tanana terrane rocks. The oldest Gravina units are Late Jurassic in age (Berg et al., 1972); the youngest, identified near Juneau, north of the area of this study, are Cenomanian (Cohen and Lundberg, 1993). The sedimentary rocks in the western part of the Gravina basin were derived from the Alexander terrane (Cohen and Lundberg, 1993; Kapp and Gehrels, 1998); other Gravina sequence sedimentary rocks contain detrital zircons probably derived from the Yukon-Tanana terrane rocks on the eastern side of the Gravina basin (Gehrels and Kapp, 1998). This evidence of a sedimentologic connection to the older terranes on either side of the Gravina basin supports the conclusion that Alexander

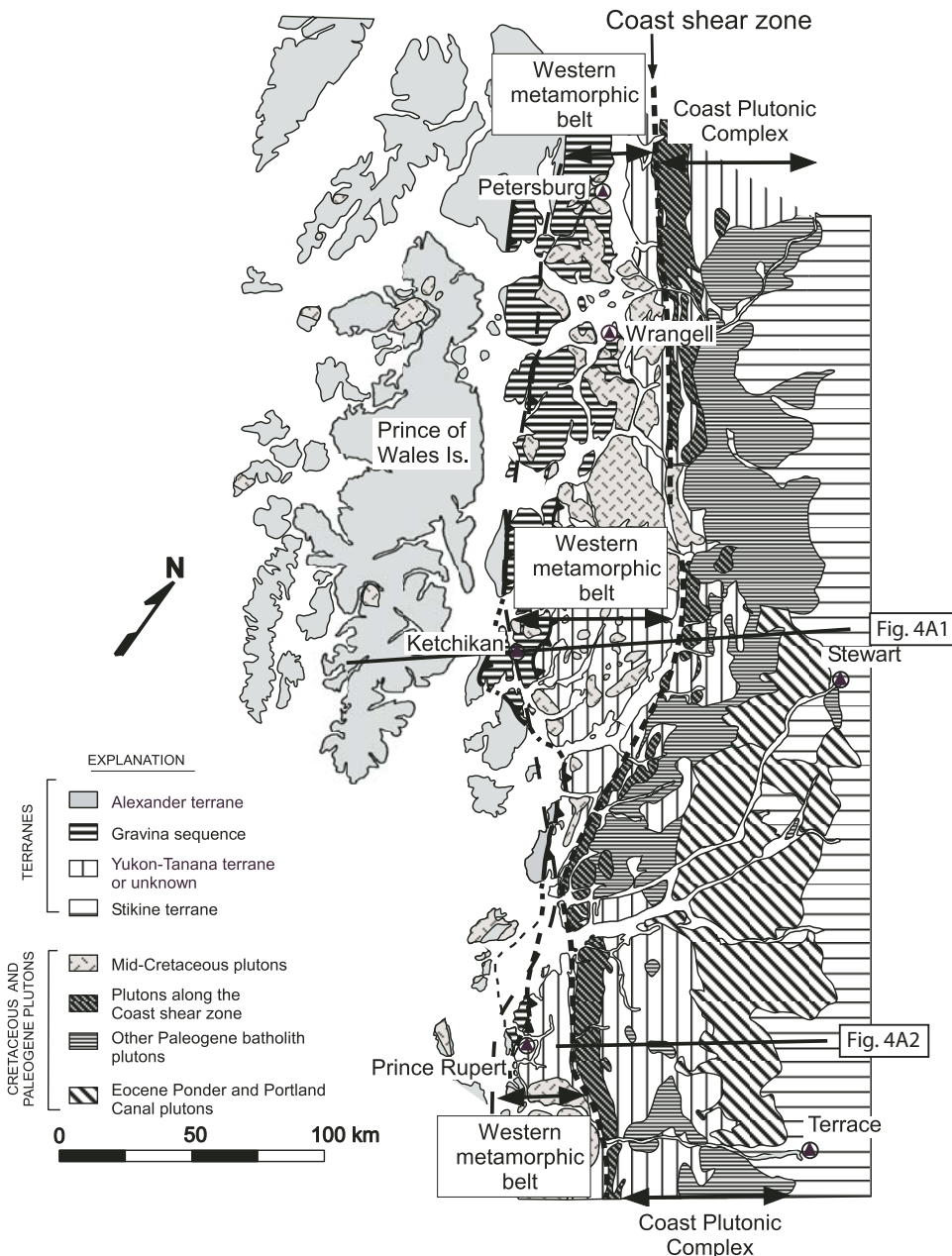


Figure 3. Generalized geological map, Prince Rupert, British Columbia, to Petersburg, Alaska. The main components of the Coast orogen: the western metamorphic belt, Coast shear zone, and Coast Plutonic Complex are indicated as well as the groups of plutons within each belt. The plutons of the Paleogene batholith are patterned to distinguish the belt of narrow and long plutons just east of the Coast shear zone and the 52–50-Ma plutons along the eastern side of the Coast Plutonic Complex. Lines labeled Figures 4A1 and 4A2 correspond to the cross sections shown in Figure 4.

terrane was approximately in its present location relative to the inboard parts of the continental margin prior to Gravina basin formation.

In the area of our study, between Prince Rupert in British Columbia and Wrangell in Alaska, two northwest-trending linear belts of igneous rocks intruded the rocks of these accreted terranes: a mid-Cretaceous plutonic arc on the west and a dominantly Paleogene arc on the east (Fig. 3). These plutonic rocks and their associated metamorphic country rocks form the core of the orogen. A major ductile shear zone, the Coast shear zone, separates the rocks of the two batholithic arcs (McClelland et al., 1991; Ingram and Hutton, 1994; Klepeis et al., 1998; Andronicos et al., 1999; Chardon et al., 1999). Although the specific features of deformation, magma emplacement and thermal history differ

on either side of the Coast shear zone, the rocks of the two belts share features that arise from a close connection between magma emplacement and deformation.

Two sets of overlapping seismic-refraction and wide-angle observations, the ACCRETE data acquired in 1994 (Morozov et al., 1998) and the SNoRCLE line 22 data acquired as part of the Lithoprobe Slave-Northern Cordilleran Lithosphere Evolution (SNoRCLE) studies in 1997 (Hammer et al., 2000), provide information about the crustal structure across the orogen. The lines extend from the Queen Charlotte transform fault along the western edge of the North American plate into the Stikine terrane on the east. The seismic data, summarized in cross sections in Figure 4, show that the crust is divided into three segments by major fault zones. Summary geological cross sections

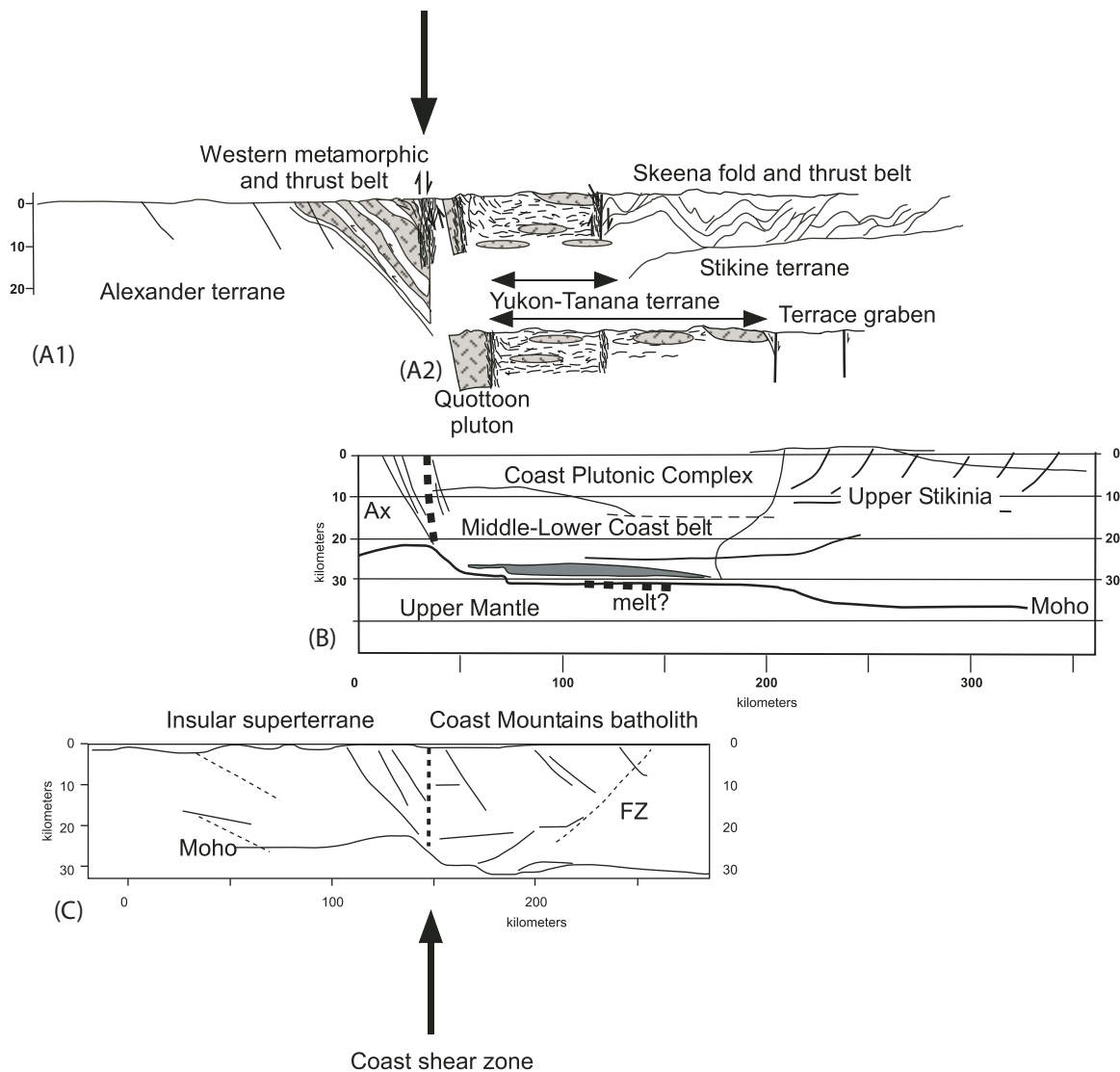


Figure 4. Cross sections across the central part of the Coast orogen. (A1 and A2) Schematic cross sections illustrating the features in the upper part of the crust. Locations of these sections are shown in Figure 3. (B) Interpreted geophysical data from Hammer et al. (2000). (C) Interpreted geophysical data from Morozov et al. (2001). Thin lines—imaged reflecting boundaries; dashed lines—out of section features; FZ—inferred fault zone.

(Fig. 4A) illustrate the major geological features that correlate with these geophysical transects. On the west the units between the Queen Charlotte fault and the Coast shear zone include the rocks of the Alexander terrane and Gravina sequence as well as mid-Cretaceous plutons of the Cretaceous arc. Some of the Yukon-Tanana terrane rocks also lie west of the Coast shear zone. East of the Coast shear zone is the central segment, called the Coast Plutonic Complex, which includes the Paleogene batholith and its country rocks. The country rocks are gneisses, referred to as the Central Gneiss Complex, derived from Yukon-Tanana terrane units (Gehrels et al., 1990; Gareau and Woodsworth, 2000). The eastern side of this central segment is bounded by a series of normal faults that separate it from the Stikine terrane crustal block.

There is a prominent change in depth to the Moho across the faults bounding each of these segments (Figs. 4B, 4C). The crust thins from 35 to 37 km below Stikinia to 30–32 km below the Coast Plutonic Complex (Hammer et al., 2000). This change in crustal thickness, as well as a change in upper-crustal velocity, underlies the mapped eastern side of the Coast Plutonic Complex. Data from the ACCRETE transect (Morozov et al., 2001) show that the crust thins again across the Coast shear zone, from 32 km on the east to 23 km on the west. Farther west, across the Clarence Strait fault (Fig. 2), the depth to the Moho increases slightly, to around 25 km (Fig. 4C). Under the Queen Charlotte Basin and Queen Charlotte Islands average Moho depth is ~27 km.

The three crustal segments also can be distinguished by differences in crustal P- and S-wave velocities. The upper crust of Stikinia, under the Bowser Lake sedimentary rocks, has distinctly lower P-wave velocities (5.7–6.2 km/s) than those observed in the Paleogene batholith of the Coast Plutonic Complex (6.0–6.4 km/s). The average crustal P-wave velocity for Stikinia is 6.25 km/s compared with 6.55 km/s for the crust to the west (Morozov et al., 1998). In the crust under the Coast Plutonic Complex P-wave velocities increase with depth to over 6.4 km/s and, in the central and western part of the Complex, they reach 6.7–6.9 km/s. Morozov et al. (2001) report that Vp/Vs ratios in the central and western part of the Coast Plutonic Complex show a thin upper section with Vp/Vs ratios of 1.74. These ratios increase downward in the middle to lower crust, and reach 1.82 in the lower crust. Laboratory-measured values for seismic velocities through tonalite and diorite agree with the measured values for the upper and middle Coast Plutonic Complex crust (Morozov et al., 2003). These authors note that the higher velocities in the deepest crust may reflect an increase in modal garnet suggesting the presence of mafic garnet granulite. A garnet and sillimanite-bearing restite from crustal melting reported by Hollister and Andronicos (2000), which also has high P-wave velocities and Vp/Vs ratios, may contribute to the high velocities in the deepest crust, although Morozov et al. (2003) concluded that their data do not suggest significant anisotropy in the lower crust as might be expected if there were a considerable thickness of this foliated rock. Hammer et al. (2000) and Morozov et al. (2001) both point out that the velocities under the eastern side of the Coast Plutonic

Complex are more uniform throughout the crust than farther west in the complex. These lower crustal velocities are close to those of Stikinia, and Vp/Vs may actually decrease with depth. This characteristic leads to the suggestion that the eastern part of the Coast Plutonic Complex crust may be part of, or may be tectonically underlain by, the Stikine terrane. This part of the crust is comprised by large volumes of felsic plutons that also may be a cause for this difference in crustal properties.

Hammer et al. (2000) and Hammer and Clowes (2004) note that the thickness of the Coast Plutonic Complex crust is very much less than is typical for orogenic belts. In general it is close to the global average for areas of extended continental crust (Christensen and Mooney, 1995; Mooney et al., 1998). Thin crust would be predicted from the observations of Eocene uplift as well as of Eocene–Miocene and possibly younger extension across the orogen discussed above.

The P-wave velocities of the crust of the Coast Plutonic Complex and that of the Alexander terrane and other crustal units west of the Coast shear zone are similar. However, due to its thin crust, the average P-wave velocities of the Alexander terrane are 0.2–0.4 km/s higher than those of the Coast Plutonic Complex (Hammer et al., 2000). In contrast to P-wave velocities, S-wave velocities change across the Coast shear zone. There is, therefore, a significant contrast in Vp/Vs ratios between the upper and lower crust under the Alexander terrane (Morozov et al., 2001). This lower crustal section shows the highest Vp/Vs ratios, near 1.88, along the ACCRETE transect. These values are close to the average for oceanic crust, providing geophysical evidence that the Alexander terrane has an oceanic island-arc crust.

Within the crust west of the Coast shear zone, Morozov et al. (1998) identified several reflectors that dip northeast at angles of between ~30° and 45°, similar to the observed dip angles of the thrusts in the western metamorphic and thick-skinned thrust belt of the orogen. These reflectors are interpreted to represent those thrust faults. One of these reflectors can be traced to the Moho, whereas others are cut off by the Coast shear zone to the east.

Upper-mantle velocity reported by Morozov et al. (1998) and Hammer et al. (2000) is uniformly low at 7.8–7.9 km/s when compared to the continental average at 8.1 ± 0.2 km/s and is close to that of continental arcs (Christensen and Mooney, 1995). These low velocities are consistent with a very high heat flow (105 ± 22 mW/m²) and estimated uppermost mantle temperatures of 800–1000 °C (Lewis et al., 2003; Hyndman et al., 2005) across the Intermontane region of British Columbia. Sparse data suggest that the high heat flow extends westward to Queen Charlotte Sound. The high heat flow results in a predicted shallow brittle to ductile transition within the crust at ~10–12 km depth. Hammer et al. (2000) speculate that seismic reflections observed at depths of 12–15 km under the Coast Plutonic Complex and Stikinia may arise from this brittle-ductile transition. High heat flow could also result in crystallization of garnet in mafic lower-crustal units as suggested by the high-crustal velocities. Locally sharp impedance contrasts at the base of the central Coast Plutonic Complex reported by Hammer et al. (2000) could be melt lenses. Morozov

et al. (2001) also point out that the sharp Moho with a particularly strong S-wave reflectivity might result from basaltic partial melts at the base of the crust. Small volumes of Recent alkalic mafic volcanic activity support these interpretations.

Orogen Crust West of the Coast Shear Zone— The Mid-Cretaceous Arc

West of the Coast shear zone the Coast orogen consists of the northwest-trending mid-Cretaceous arc and western metamorphic and thick-skinned thrust belt (Fig. 3). This belt comprises 104–90 Ma plutons and their greenschist- to upper amphibolite-facies host rocks of the Gravina sequence on the west and of the Yukon-Tanana terrane on the east (Crawford *et al.*, 1987; Stowell and Crawford, 2000). Folded and faulted Gravina sequence rocks lie along most of the southwestern side of this belt. Southwest-directed thrust faults cut and tectonically thicken the Gravina units and in most places separate the Gravina rocks from those of the Alexander terrane. Within individual thrust slabs Gravina sequence rocks are folded into recumbent, km-scale nappes and outcrop-scale tight to isoclinal folds. On the northeast, Yukon-Tanana terrane rocks overthrust the Gravina units. The resulting imbricated thrust sheets, referred to as the thick-skinned thrust belt (Rubin *et al.*, 1990), juxtapose lithologically distinct crustal slabs that were at different crustal depths prior to thrust imbrication. High-pressure, kyanite-bearing (8.5 kb; Cook and Crawford, 1994) metamorphic assemblages in a pluton contact aureole on the southwestern side of the Gravina belt near Ketchikan indicate these rocks were buried to depths corresponding to ~30 km prior to emplacement of the 104–101-Ma plutons. In contrast, and as discussed further below, rocks to the northeast near Wrangell were buried to only ~10 km or less (McClelland *et al.*, 1991; Himmelberg and Brew, 2004; Himmelberg *et al.*, 2004; Lindline and Crawford, 2005). In the southern part of the area, near and south of the Canada-U.S. border, medium- to high-grade Yukon-Tanana rocks are thrust directly over the rocks of the Alexander terrane with Gravina sequence rocks found only in thin thrust slivers between the two lithotectonic units. In these slivers the Gravina sequence rocks are even more highly folded and deformed than they are to the north resulting in km- to outcrop-scale sheath folds (Crawford *et al.*, 2000; Gehrels, 2001).

The mid-Cretaceous plutons are predominantly quartz diorite, tonalite, and plagioclase-rich leucotonalite; small bodies of granodiorite and mafic to ultramafic hornblende gabbro, hornblende, and dunite/wehrlite also occur (Crawford *et al.*, 2005). Northwest-trending belts of plutons with successively younger ages can be traced across the Alexander terrane and western metamorphic and thick-skinned thrust belt into the Coast Plutonic Complex (Fig. 5). The oldest igneous rocks in the area of focus of this paper, as old as 115 Ma, intrude the very low-grade rocks of the Alexander terrane west of the metamorphic belt. Previously unpublished ages for these plutons along a transect at the latitude of Wrangell are summarized in Table 1, and presented in Table 2 and Figure 6 (on CD-ROM accompanying this volume, or

in the GSA Data Repository¹). East of these rocks and intruded into the easternmost part of the Alexander terrane are the Duke Island (ca. 108 Ma; Saleeby, 1992), and Blashke Island Alaska-type ultramafic complexes (Himmelberg and Loney, 1995). The Union Bay ultramafic body (ca. 101 Ma; Rubin and Saleeby, 1992) intrudes the westernmost part of the Gravina sequence. These mid-Cretaceous ultramafic complexes have initial ⁸⁷Sr/⁸⁶Sr (SIR) values ranging from 0.7026 to 0.7068, with most having SIR of 0.7041–0.7047 (Lanphere, 1968). These values are lower than those of the pre-Mesozoic continental crust which by late Mesozoic mostly exceeded 0.7080 (Arth, 1994) but overlap those of Alexander terrane rocks (0.7028–0.7071) (Samson *et al.*, 1991b). Based on these data these authors inferred that the magmas from which the ultramafic complexes were derived did not interact with significant amounts of older continental crust but may have assimilated Alexander terrane oceanic crustal rocks during ascent or emplacement.

East and northeast of the belt of ultramafic complexes are syntectonic, moderately dipping tabular plutons, sill complexes, and small stocks emplaced between 104 and 90 Ma into the rocks of the western metamorphic belt (Gehrels, 2001; McClelland *et al.*, 1992b; Rubin and Saleeby, 1992; Rubin and Saleeby, 2000; Saleeby, 2000; Figs. 5 and 6). These mid-Cretaceous igneous bodies are located within, or are closely related to, the shear zones that define the imbricate thrusts in this western metamorphic belt. They belong to the calc-alkaline gabbro-tonalite-granodiorite suite with magmatic arc characteristics (Barker and Arth, 1984; Arth *et al.*, 1988; Crawford *et al.*, 2005). They have low Rb and high Sr contents as well as fractionated chondrite-normalized rare earth element (REE) patterns with moderate enrichment in the light to medium REE and relatively flat slopes for the heavy rare earth element (HREE). The REE features suggest a hornblende-rich source lacking garnet. The plutons have SIR values ranging from 0.7043 to 0.7051 (Arth *et al.*, 1988; Lindline, 1997). These chemical characteristics suggest that the plutons originated from mixing of mantle-derived basalt magma, which gave rise to small volume basaltic bodies, with crustal melts derived from partial melting of amphibolite in which plagioclase was rare or melted completely (Lindline, 1997).

Emplacement of the tabular mid-Cretaceous plutons and sill complexes was closely related to, and assisted by, deformation (Hollister and Crawford, 1986). The location of many of the igneous bodies within or adjacent to well-defined shear zones suggests that the magma took advantage of the paths of crustal weakness caused by the crustal-scale deformation for melt transport through the orogen. Others filled spaces created by displacement along syn-magmatic faults and shear zones (e.g., Crawford and Crawford, 1991). Plutons that cut thrust faults juxtaposing Yukon-Tanana terrane rocks against the Gravina sequence (Cook *et al.*, 1991) are younger than those emplaced along the thrusts

¹GSA Data Repository Item 2009156—Figures 6A–6C, 7A–7B, 8, 11, and 12, as well as Tables 2–5 and Appendix (Methods)—is available at www.geosociety.org/pubs/ft2009.htm, or on request from editing@geosociety.org, Documents Secretary, GSA, P.O. Box 9140, Boulder, CO 80301-9140, USA.

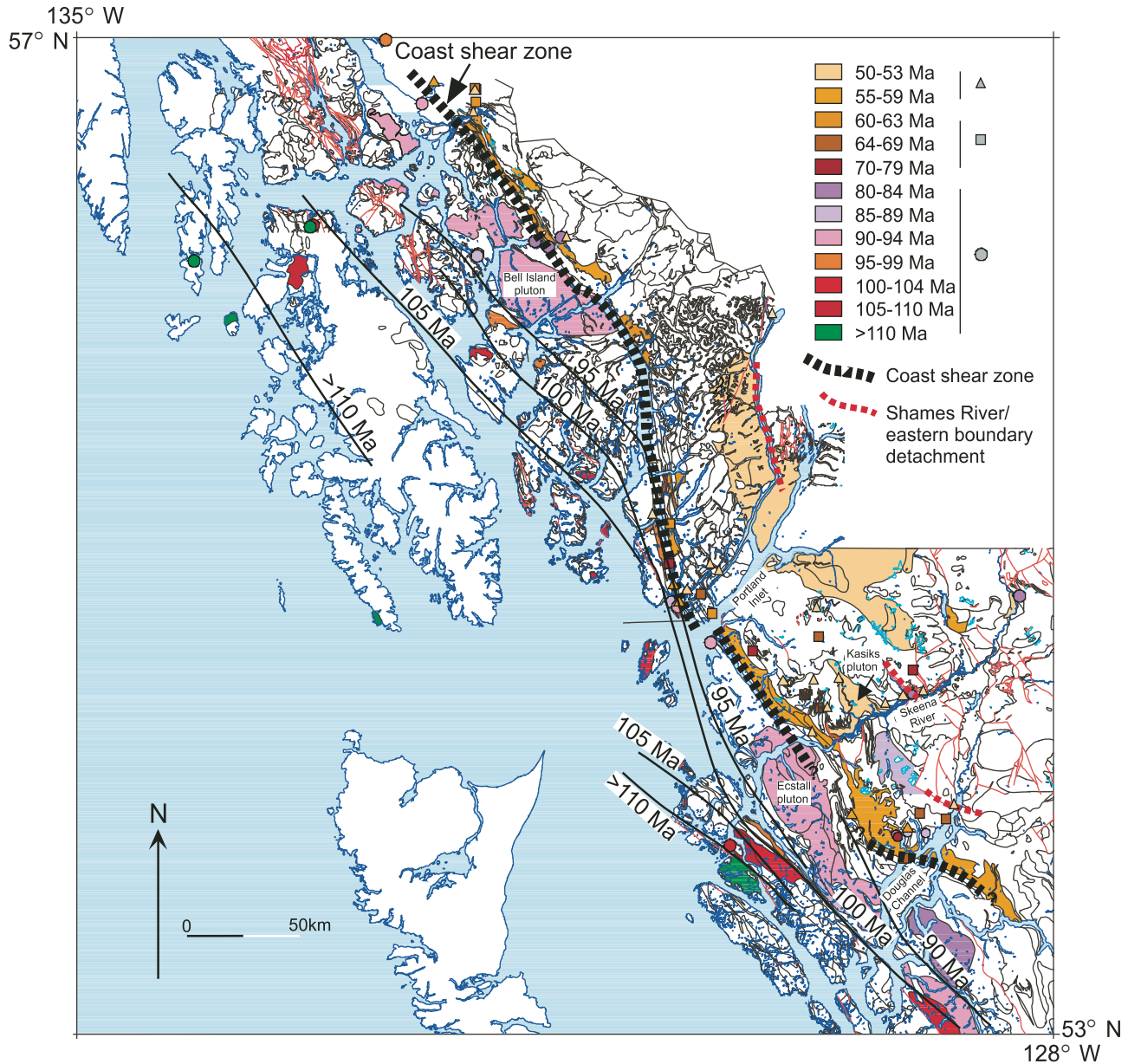


Figure 5. Map showing the ages of plutons in the study area. These include new ages summarized in Table 1 and detailed in Tables 2–5 (on CD-ROM accompanying this volume, or in the GSA Data Repository) as well as previously published data cited in the text. Contours west of the Coast shear zone show the northeasterly progression of decreasing ages across the Alexander terrane and western metamorphic belt. In the Coast Plutonic Complex, east of the Coast shear zone, igneous bodies with ages between 74 and 50 Ma scatter across the belt, however the youngest large plutons are concentrated along the eastern side of that Complex. The plutons are color keyed to their ages as shown in the legend; small bodies such as stocks, dikes, and sills are indicated by the symbols given in the legend.

within the Gravina sequence. The two largest bodies in this part of the orogen, the Bell Island pluton in the Ketchikan quadrangle and Ecstall pluton in the Prince Rupert quadrangle (Figs. 2 and 5), are both ca. 90 Ma (Arth et al., 1988; Butler et al., 2002; Rubin and Saleeby, 1992; Rubin and Saleeby, 2000). These two plutons along the eastern side of the western metamorphic belt also intruded during thrusting. Internally, both are composed of thick, tabular magmatic sheets of relatively uniform composition

with a magmatic foliation (Hutchison, 1982; Cook and Crawford, 1994; Crawford et al., 2002). These sheets currently dip easterly at moderate angles (30–45°). The margins of the plutons show strong solid-state deformation that disappears toward the pluton interior. At the margins, late felsic veins and shear zones filled with leucosome interpreted to have resulted from crustal melting, as well as pegmatite dikes within the plutons, document that the solid-state fabric formed prior to full crystallization of the

TABLE 1. SUMMARY OF NEW U/Pb AGES REPORTED IN THIS PAPER

ZIRCON/SPHENE AGES					
#	Sample name/number	N Latitude (NAD27)	W Longitude (NAD27)	Zircon age (Ma)	Sphene age (Ma)
<u>WRANGELL TRANSECT: Data in Table 2</u>					
1	Kell Bay (KP4)	56.13978	134.15788	115 ± 1.5	
2	Warren Island (KP48)	55.92465	133.92282	111 ± 1.5	
3	El Capitan (KP26)	56.09200	133.36267	108 ± 1.5	
4	Red Bay 1	56.27285	133.32608	113.5 ± 3.8	
5	Red Bay 2	56.27920	133.30374	107.4 ± 2.8	
6	Zarembo West	56.45653	132.87128	90.0 ± 2.2	
7	Zarembo East	56.45611	132.71524	90.7 ± 2.3	91 ± 4.8
8	Woronkofski-1	56.35492	132.52013	93 ± 3	92 ± 3
9	Woronkofski-2	56.41725	132.41833	88 ± 2	88 ± 2
10	Wrangell West	56.27388	132.35052	91.6 ± 2.8	
11	Blake West	56.28521	131.98561	89.1 ± 3.6	90.6 ± 3.6
12	Blake East	56.24869	131.93944	93.3 ± 2.9	87.5 ± 5.3
13	03WT102	56.46693	131.78654	056.6 ± 1.9	51.0 ± 1.9
14	03WT107	56.41381	131.84999	060.4 ± 1.9	53.1 ± 2.4

Notes:

corresponds to location numbers in Figure 6C.

All ages are from plutonic rocks collected during paleomagnetic sampling.

#	Sample name/number	N Latitude (NAD27)	W Longitude (NAD27)	Zircon age (Ma)	Sphene age (Ma)
<u>PALEOGENE BATHOLITH: Data in Table 3</u>					
15	98-148	54.45532	129.9054	193 ± 5	
16	Hidden (98-87)	55.01117	130.2577	187 ± 12 (reset to younger ages)	
17	02-16	54.30565	129.6136	82.0 ± 2.3	
18	01-232	54.83603	130.5977	69.0 ± 1.8	
19	94-36	54.79851	130.5677	65 ± 3	
20	95-114	54.84206	130.4756	65.7 ± 0.8	
17	02-25	54.30399	129.6338	64.4 ± 2.3	
21	01-268	54.73739	130.4456	63.4 ± 1.8	
22	95-130	54.81659	130.525	63.3 ± 0.7	51.0 ± 1.5
23	01-202	54.82213	130.5221	62.9 ± 1.2	
24	01-235	54.81705	130.6268	53.9 ± 0.9	
25	Rousseau (97-123)	55.30999	130.0115	53.3 ± 1	52.7 ± 3.6
26	98-23	55.43583	130.0528	53 ± 3	
27	Halibut (98-42)	55.21367	130.0963	51.7 ± 1.0	51.3 ± 1.0
28	01-208	54.92128	130.462	51.7 ± 1.9	
29	Getukti (97-46)	54.89475	130.3961	51.4 ± 0.8	
30	02-31	54.23917	129.7283	50.6 ± 1.8	

Notes:

corresponds to location numbers in Figure 8.

94-36: Granodiorite sill with melt-present foliation, cut by young top down to the north shear zones.

95-114: Tonalite stock, strong east-plunging mineral lineation.

95-130: Foliated tonalite, foliation similar to country rocks.

Getukti (97-46): Thin, irregular granitic dikes cutting metasedimentary rocks.

Rousseau (97-123): K-feldspar megacrystic granite cut by down to the east shear zones.

98-23: K-feldspar megacrystic granite with igneous foliation.

Halibut (98-42): Undeformed K-feldspar megacrystic granodiorite.

Hidden (98-87): Pluton along Pearse Canal that shows evidence of remelting; melted areas show no fabric.

98-148: Tonalite pluton that appears to be the oldest igneous body in the Khyex sill complex.

01-208: Northern part of E. Filmore Inlet, Prince Rupert quad. Pegmatite sample that provides a youngest age constraint on the country rock fabric.

01-232: Northwestern end of Filmore Inlet, Prince Rupert quad. Strongly deformed tonalite. Older constraint on the fabric.

01-202: East of Regina Cove, Prince Rupert quad. Tonalite with both intense deformation and undeformed parts, sampled the deformed part; deformation probably syn-emplacement.

01-235: West end of Filmore Inlet, Prince Rupert quad. Pegmatite in a young shear that cuts metavolcanic and metasedimentary gneiss.

01-268: South shore of Wales Island, Prince Rupert quad. Mostly undeformed tonalite pluton, constrains the age of down to the north shear zones that cut the pluton.

02-16: Tabular tonalite with contact that cross-cuts country rock foliation.

02-25: Strongly lineated tabular tonalite, cuts another tonalite sill on adjacent ridge. Can be traced to the eastern side of Arden Lake Complex.

02-31: Small granite stock with no fabric that intrudes the contact between gneissic country rocks and the Quottoon pluton along the eastern margin of the pluton. Younger than Quottoon.

(Continued)

TABLE 1. SUMMARY OF NEW U/Pb AGES REPORTED IN THIS PAPER (*Continued*)

ZIRCON/SPHENE AGES (<i>Continued</i>)					
#	Sample name/number	N Latitude (NAD27)	W Longitude (NAD27)	Zircon age (Ma)	Sphene age (Ma)
31	02-KTN	55.3612	131.703	26.5 ± 1.8	
32	Tombstone (97-114)	55.39303	130.0482	22.2 ± 0.8	

Notes:
corresponds to location numbers in Figure 8.
Tombstone (97-114): Undeformed granitic body along the shore just south of Tombstone Bay. Intrudes the larger felsic plutons.
02-KTN: Granitic dike cutting metasedimentary rocks along highway in western Ketchikan; younger than the main deformation.

MONAZITE AGES				
#	Sample number	N Latitude (NAD27)	W Longitude (NAD27)	Monazite age (Ma)
M1	86-43	55.83486	131.5758	101.0 ± 4.4
M2	92-34	55.99	131.956	94.4 ± 7.2
M3	90-157B	54.76644	130.5863	90.0 ± 2.1
M4	86-113	55.97012	132.0058	88.1 ± 2.7
M5	97-134	54.40807	129.7738	76.4 ± 5.5
M3	90-157A	54.76644	130.5863	62.8 ± 1.6
M6	97-27	54.84775	130.5075	54.8 ± 1.6

Notes:
corresponds to location numbers in Figure 8.
86-43: Gedney Pass, Ketchikan quad. Kyanite- and garnet-bearing schist, south of Bell Island pluton.
86-113: Change Island, NE corner of Craig quad. Metasedimentary rocks definitely affected by the Bell Island pluton.
90-157A and 90-157B: Southeasternmost Safa Island NW of Wales Island, Prince Rupert quad. Rock with sillimanite pseudomorphs of kyanite and garnet.
92-34: Santa Anna Inlet, NW corner of Ketchikan quad. Migmatitic pelite screen in Bell Island pluton.
97-27: Edwards Passage, Prince Rupert quad. Nearby tonalite not dated but estimated at 55 Ma based on undeformed appearance.
97-134: Metasedimentary gneiss in Khyex quad. Sillimanite wrapping garnet defines a top to the south shear sense throughout the outcrop.

pluton. These features, as well as a very narrow range of U-Pb zircon ages obtained from these large bodies (90.1 ± 0.8 —Bell Island, 90.4 ± 1.2 —Ecstall), indicate that these plutons formed by rapid syntectonic emplacement of a large volume of magma during convergent deformation (Crawford et al., 2002; Charodon, 2003).

The graywacke and mafic volcanic rocks of the Gravina sequence within the western metamorphic belt record regionally distributed greenschist facies (biotite and garnet grade) mineral assemblages with inferred temperatures of ~ 400 – 500 °C. The exposed widths of the contact metamorphic aureoles with higher temperature mineral assemblages range from a few meters around smaller bodies to ~ 10 km adjacent to the Bell Island and Ecstall plutons (Cook and Crawford, 1994; Stowell and Crawford, 2000). Metamorphic temperatures are also higher in the Yukon-Tanana terrane rocks on the eastern side of the belt. Pressures of 8 kb are recorded by kyanite-bearing rocks along the southwestern side of the belt of Gravina rocks, whereas pressures of 4 kb or less are documented by andalusite in aureoles of the youngest (92–90 Ma) plutons on the northeast side of the belt (Lindline and Crawford, 2005). On the eastern side of the belt a band of 9–10-kb rocks parallel the Coast shear zone (Crawford et al., 1987; McClelland et al., 1991; Cook et al., 1991; Cook and Crawford, 1994; Stowell and Crawford, 2000; Himmelberg and Brew, 2004). K-Ar and $^{40}\text{Ar}/^{39}\text{Ar}$ ages (Smith and Diggles,

1981; Cook et al., 1991) as well as new monazite ages (Tables 1 and 3, on CD-ROM accompanying this volume, or in the GSA Data Repository) date this metamorphism as coeval with the plutons (ca. 101–88 Ma). Mineral overprinting relationships in the contact metamorphic aureoles of the 90-Ma plutons show that burial by tectonic thickening accompanied emplacement of these plutons. A pressure increase from ~ 4 – 6.5 kb, which corresponds to ~ 9 km of crustal thickening, is documented on the west side of the Bell Island pluton where early andalusite is replaced by kyanite+staurolite and, closer to the pluton, by sillimanite (Cook and Crawford, 1994; Stowell and Crawford, 2000). West of the Ecstall pluton pressures increase from 7–8 kb to 8–9 kb as the pluton is approached from the west, accompanied by a temperature increase from around 550 °C to 650 °C. These features document that thrusting and magma emplacement at ca. 90 Ma resulted in significant crustal thickening along the eastern side of the western metamorphic belt.

Evidence that this west-directed thrusting continued after 90 Ma occurs at the mouth of Portland Inlet where post-metamorphic thrust faults cut the country rock schist. The metamorphic isograds are telescoped by displacements on at least two ductile thrust zones. Metamorphic porphyroblasts, surrounded by a sheared matrix, contain inclusion patterns discordant to the penetrative fabric of the matrix. These features all indicate that the deformation occurred after the metamorphic mineral growth,

leading us to conclude that these thrusts may be of similar age to thrusts east of the Coast shear zone discussed below.

Cooling histories for the mid-Cretaceous plutonic rocks that intruded into the western part of the western metamorphic belt and their contact aureoles (Smith and Diggles, 1981; Cook and Crawford, 1994; Stowell and Crawford, 2000) indicate that those plutons and their country rocks did not remain hot for long. Sphene U-Pb ages reported here (Table 1) are within error the same as the zircon. K-Ar and $^{40}\text{Ar}/^{39}\text{Ar}$ ages document that these rocks cooled to 400–300 °C within at most five million years after emplacement. The discordance between hornblende and biotite cooling ages for the plutons is small, also suggesting rapid cooling. The narrow contact aureoles and these cooling rates suggest that the plutons intruded into relatively cold crustal rocks. In contrast, the rocks along the eastern side of the western metamorphic belt and Bell Island pluton, inferred to have been intruded into upper amphibolite-facies rocks at ~10 kb, cooled slowly until ca. 55–50 Ma (Smith and Diggles, 1981; Cook and Crawford, 1994).

Cretaceous-Paleogene Orogen—Eastern Block

East of the Coast shear zone the orogen comprises gneisses and plutons of the Coast Plutonic Complex. The metamorphic rocks of this part of the orogen comprise upper amphibolite- to granulite-facies orthogneiss, semipelite, amphibolite, and rare quartzite and marble. Granodioritic to tonalitic orthogneiss bodies from south of the Skeena River to north of Portland Inlet yield Early Jurassic ages (Gareau, 1991; Gehrels, 2001; Fig. 7A and Table 4A, on CD-ROM accompanying this volume, or in the GSA Data Repository). The gneissic country rocks host latest Cretaceous to Eocene tabular gabbro, tonalite and granodiorite plutons of the Paleogene batholith. Table 1 summarizes previously unpublished ages for these igneous rocks; the data are presented in Table 4 and Figure 7 (see footnote 1); their locations are shown in Figure 8 (see footnote 1). Detrital zircon data from the host metasedimentary rocks as well as inherited zircons in the plutons of the batholith range in age from Paleoproterozoic to mid-Paleozoic (Gehrels *et al.*, 1991a, 1991b). These old zircon ages, as well as evolved Nd isotopic signatures for most of the plutons and $^{87}\text{Sr}/^{86}\text{Sr}$ of 0.70558–0.70664 (Samson *et al.*, 1991a, 1991b), suggest that the rocks of the Coast Plutonic Complex are the easterly extension of the Yukon-Tanana terrane units identified west of the Coast shear zone. Hill *et al.* (1985), however, identified crinoids in rocks on the eastern side of the Coast Plutonic Complex that they used to tentatively correlate the fossil-bearing units with Permian limestone of Stikinia.

The igneous rocks of the Coast Plutonic Complex can be subdivided into several groups on the basis of their age (Fig. 5) and structural relationships. An 88–80-Ma group includes the large Alistair Lake pluton and a scattered group of smaller tonalite-leucotonalite-granodiorite bodies affected by penetrative ductile deformation shared with the country rock. Another group consists of 74–63-Ma small tabular plutons that are some-

what less intensely deformed than this first group. Finally, a group of 63–53-Ma diorite to granite plutons, including the very large Kasiks and Quottoon plutons (Fig. 8, see footnote 1), shows little or no solid-state penetrative deformation. These appear syntectonic with respect to the later stages of deformation of the eastern block. Along the eastern side of the batholith are 52–50-Ma granitic plutons that are associated with orogen uplift and exhumation. These are discussed in the next section. The 88–80-Ma plutons appear to be the eastern and youngest component of the eastward younging Cretaceous magmatic activity that characterizes the western metamorphic belt. South of the area of this study several large plutons of this age lie west of the inferred southern extension of the Coast shear zone (Fig. 5). 84- and 83-Ma plutons also intrude rocks of the Skeena fold-and-thrust belt (Evenchick and McNicoll, 1993; Haggart *et al.*, 2006). On the basis of their ages and emplacement styles, Crawford *et al.* (1999) grouped the 74–53-Ma plutons into the Khyex sill, Arden Lake, and Fillmore complexes, which are composed of latest Cretaceous and Paleocene tonalite and granodiorite bodies; and the earliest Eocene (58–53 Ma) gabbro and tonalite Quottoon and Kasiks plutons (Fig. 9).

Ductile structures within the batholith define four phases of deformation on the basis of cross-cutting fabrics and the ages of the plutons affected by the deformation. The oldest identifiable structural feature in the country rocks is gneissic banding that defines kilometer-scale recumbent nappes in metasedimentary rocks and the associated orthogneissic plutons (Fig. 9A) (Hutchison, 1982; Crawford *et al.*, 1999). All igneous rocks older than ca. 75 Ma are strongly deformed and are approximately concordant with this gneissic fabric in the country rocks. The igneous bodies emplaced between 74 and 53 Ma have compositions that include gabbro, tonalite, leucotonalite, and granodiorite. Most of these plutons are associated with and are bounded by ductile shear zones (Fig. 9) whose formation appears to be closely related to magma emplacement (Klepeis and Crawford, 1999; Crawford *et al.*, 1987; Hollister and Andronicos, 2000; Andronicos *et al.*, 2003). 74–63-Ma plutons show fabrics generally parallel to those in the country rocks; the internal fabrics in these plutons include both solid-state and magmatic textures. Younger, 63–54-Ma bodies are much less deformed; those younger than 59 Ma show only igneous fabrics. In the Khyex sill complex the plutons are tabular and gently to moderately dipping; the Arden Lake and Fillmore complexes, in contrast, comprise narrow steep to vertical tabular igneous bodies (Klepeis and Crawford, 1999; Crawford *et al.*, 1999).

The Khyex sill complex (Fig. 9) is a ~10-km-thick series of sheeted sills and gneissic country rocks that dip 30–45° to the north and northeast (Crawford *et al.*, 1999). The country rocks of this complex, including granodioritic orthogneiss with ages older than 74 Ma, show a penetrative extensional planar fabric, with kinematic indicators recording top down to the south transport parallel to a regional stretching lineation. 74–63-Ma sills have solid state fabrics at their margins that parallel the fabric in the country rocks though, in detail, cross-cutting relations occur. Away from their contacts with host rock, the sills show

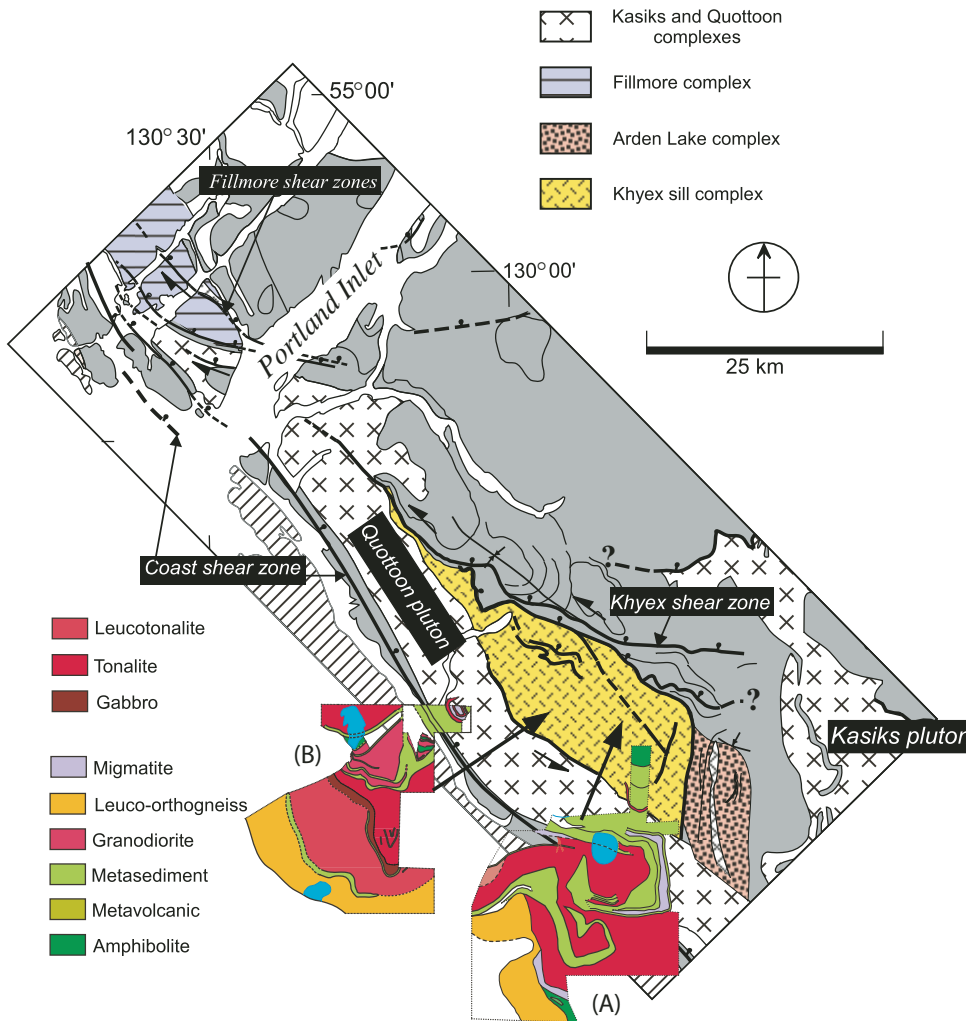


Figure 9. Simplified geological map of the northern part of the Prince Rupert quadrangle showing the igneous complexes discussed in the text as well as the linked steep sinistral and gently north-dipping ductile shear zones that control pluton emplacement and subsequently deform the weakened crust. (A) Outcrop pattern of the earliest ductile nappes. (B) Part of the Khyex sill complex showing the outcrop pattern of gently to moderately dipping tabular, folded plutons and sills. The gabbro-tonalite body in the center of this map is one of the differentiated sills that characterize the Coast Plutonic Complex.

both solid-state and magmatic textures. All fabrics in these sills, including melt-filled shear bands, record top down to the north and northwest extension (see also Klepeis and Crawford, 1999; Andronicos et al., 2003). These textures indicate that deformation in the sill complex occurred prior to full crystallization of the sills and suggest that north to northwesterly extension facilitated the emplacement of the plutons. The gneissic country rocks are migmatitic and have similar melt-filled shear bands suggesting migmatite formation and melt extraction into shears accompanied pluton emplacement. Upright folds with gently north-plunging axes (Fig. 9B) that parallel the north- and north-northwest-plunging stretching lineations in the country rocks and magmatic lineations in the sills reorient the tonalite sills and the foliation. The presence of the folds suggests a constrictional regime with east-west or northeast-southwest contraction that accompanied the top down to the north and northwest extension during this interval.

The Arden Lake and Fillmore complexes (Fig. 9) comprise mainly steeply dipping tabular plutons and sills that measure hundreds of meters in thickness. In the Arden Lake complex

the tabular plutons are up to 500 m thick and are separated by gneissic units with a steep to vertical north-trending foliation. In the Fillmore complex the plutons are associated with, and deformed by, east-side-up reverse ductile shear zones, some of which show a small dextral component (Klepeis et al., 1998). These shear zones lie along the eastern side of the Coast shear zone and, as mentioned above, may be coeval with the post-metamorphic thrusts along the eastern side of the western metamorphic belt at the mouth of Portland Inlet. They are, in turn, cut by steeply dipping north-side-down extensional shear zones and faults. Extensional shear zones with felsic igneous fill, similar to those observed in the Khyex sill complex, suggest that the deformation accompanied magma emplacement. The ages of dikes within these igneous complexes indicate that extensional deformation overlapped in time with crystallization of the plutons (e.g., Crawford et al., 1999; Andronicos et al., 2003).

After 63 Ma, orogen-parallel to oblique extension became the prevailing style of deformation within the arc. This top to the north extension occurred along discrete interconnected strike-slip and extensional shear zones (Figs. 9 and 10) that resulted in

displacements parallel to, or at a low angle to, the arc (Klepeis and Crawford, 1999; Crawford et al., 1999). One of these is a steep shear zone that lies along the eastern side of the Khyex sill complex and separates it from the Arden Lake complex. Another moderately to steeply east-to-northeast-dipping shear zone defines the western side of the Khyex sill complex and separates it from the Quottoon pluton. Linking these steep shear zones, and defining the northern margin of the Khyex sill complex, is a major low angle extensional crustal detachment zone that records top down to the north and northeast displacements (Khyex shear zone, Fig. 9). This shear zone separates the sheeted intrusive rocks and migmatitic gneiss of that complex from overlying migmatite-free amphibolite and metasedimentary rocks intruded by gently dipping sills of unknown age. The sills are folded and appear similar in style and relationship to the country rocks to the 74–63-Ma sills of the Khyex sill complex. Mafic to ultramafic cumulate layers (Douglas, 1986) in some of these sills also resemble cumulate layers we have mapped in the Khyex sill complex (Fig. 9B). One explanation advanced for the high crustal velocities observed in the crust of the Coast Plutonic Complex, as noted in the discussion of geophysical observations, is possible continuation at depth of this type of sill. The rocks above the Khyex shear zone display a strong structural discordance with the detachment zone and with the fabric of the underlying complex. In contrast to the gneisses south of and under the shear zone, the metamorphic rocks to the north experienced little to no melting associated with emplacement of igneous rocks. Thus the shear zone appears to juxtapose crustal blocks of different crustal levels. Fabrics mapped on the north and south shores of Portland Inlet indicate that extensional

shear zones similar to those mapped in the Khyex sill Complex (Fig. 9) cut the rocks on either side of the Inlet.

Klepeis and Crawford (1999) suggest that movement on the shallow and steep shear zones bounding the Khyex sill were kinematically linked and occurred after ca. 63 Ma. Crawford et al. (1999) concluded that displacement on these shear zones accommodated magma emplacement, including the eastern part of the mafic to intermediate 58–55 Ma (Gehrels et al., 1991a; Klepeis et al., 1998; J.B. Thomas, 1999, personal commun.) Quottoon pluton located on either side of Portland Inlet (Fig. 9). This extension also appears to have accommodated the emplacement of some of the steep tabular plutons associated with north-trending vertical shear zones of the Arden Lake complex, of the 53–52-Ma Kasiks pluton (Hollister and Andronicos, 2000; Andronicos et al., 2003), and a number of thin aplite and pegmatite sheet-like bodies oriented perpendicular to the regional stretching lineation. These latter thin granitic sheets all dip more steeply than $\sim 62^\circ$; lower angle shears with a similar orientation also occur but these have no associated igneous rocks. In contrast to the pre-63-Ma plutons, in these post-63-Ma bodies rock fabrics are dominantly magmatic with little or no internal evidence of tectonic strain.

The Quottoon pluton (Fig. 9) is a steeply dipping, tabular body, 10–15 km wide and >100 km long. It trends northwest along the western side of the Coast Plutonic Complex from Portland Inlet to south of Douglas Channel (Fig. 5). This pluton, as originally mapped (Hutchison, 1982), includes two different igneous suites (Thomas and Sinha, 1999). One of these consists of heterogeneous sill shaped bodies that have a pervasive solid-state

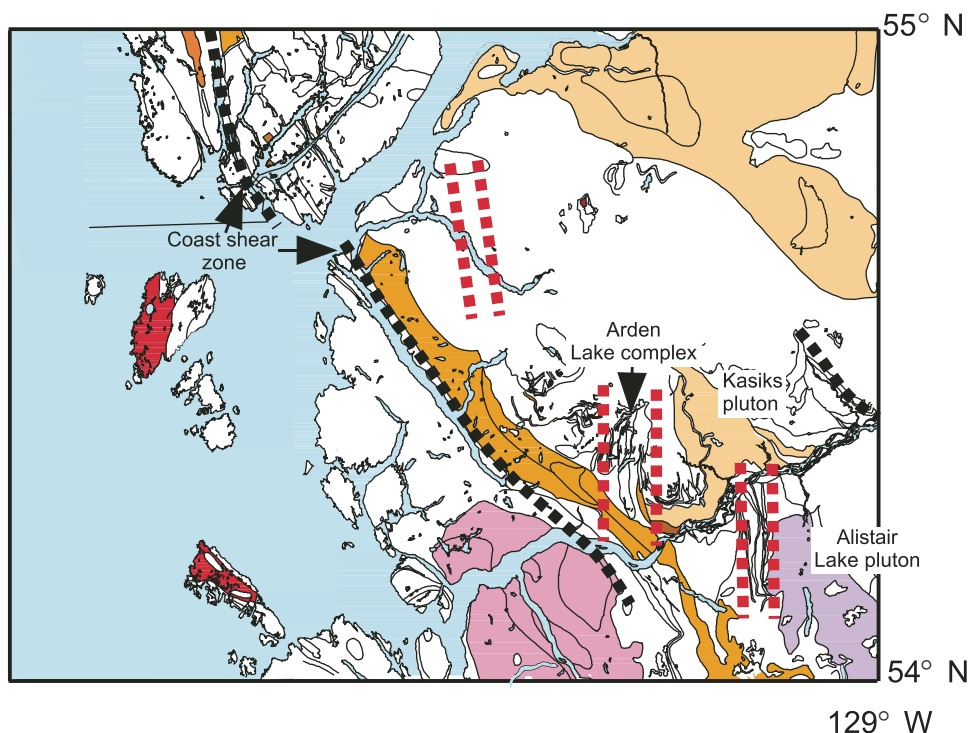


Figure 10. Red dashed lines outline zones in the Coast Plutonic Complex of transposed foliation and layering that document zones of strike-slip, orogen-parallel shearing.

fabric and are older than the western main body of the pluton. This main body, dated by Thomas at ca. 55 Ma (1999, personal commun.) is a homogeneous steep tabular pluton that shows primarily magmatic fabrics. It is one of a number of similar tabular plutons that lie along the orogen east of the Coast Shear zone, between the high temperature metamorphic rocks of this central belt and the lower temperature but higher pressure rocks of the western metamorphic belt (Fig. 3) (Brew and Ford, 1978, 1981; Ingram and Hutton, 1994). The shape of this pluton, its relationships with several generations of extensional shear zones in the Coast Plutonic Complex to the east, its steeply dipping magmatic fabrics and concordant margins, and the lack of evidence of tectonic strain until late in its crystallization history suggest that space for the pluton was created by the orogen parallel sinistral extension (Crawford et al., 1999).

The 53–52-Ma Kasiks pluton (Hollister and Andronicos, 2000) encompasses a 5-km-thick, north-dipping differentiated quartz diorite to tonalite sill with a roof zone consisting of a 5 km complex of thinner tonalite sills and, on the eastern side, a northwest-trending tabular extension similar in thickness and orientation to the young (55 Ma) western part of the Quottoon pluton (Fig. 5). Kinematic indicators within country rocks and orthogneiss adjacent to and within the Kasiks Sill complex are consistent with top-to-the northwest normal shearing during sill emplacement (Andronicos et al., 2003).

The metamorphosed sedimentary and igneous host rocks to the batholith document high temperatures (above 650 °C) at mid-crustal levels (Hollister, 1975; Selverstone and Hollister, 1980; Kenah and Hollister, 1983; Douglas, 1986; Klepeis et al., 1998). Monazite ages of 90.0 ± 2.1 and 91.9 ± 7.6 Ma (Rusmore et al., 2005; Fig. 11C and Table 3, see footnote 1) demonstrate that this oldest documented metamorphism in the Coast Plutonic Complex is the same as the youngest documented metamorphism of the rocks of the western metamorphic belt (Sutter and Crawford, 1985; Stowell and Crawford, 2000; Fig. 11E, Table 3, on CD-ROM accompanying this volume, or in the GSA Data Repository). Relic staurolite and kyanite and pseudomorphs of those minerals in Coast Plutonic Complex paragneiss that yields these mid-Cretaceous monazite ages, as well as at numerous other locations, suggest the pressures and temperatures of the relic assemblages were similar to those observed west of the Coast shear zone. These observations on the metamorphic history of the Paleogene batholith country rocks corroborate the suggestion, based on the 88–80-Ma plutons found in the Coast Plutonic Complex, that the rocks of the Complex record an eastward extension of the mid- to upper Cretaceous events observed in the western metamorphic belt. Subsequent metamorphism coeval with pluton emplacement between ca. 74 and 53 Ma occurred at higher temperatures (650° to 775 °C) and lower pressures (6–7.5 kb) than was the case for the rocks west of the Coast shear zone. Estimates of these metamorphic conditions are based on sillimanite pseudomorphs of the older kyanite and staurolite porphyroblasts and growth of new sillimanite that was subsequently enclosed in younger garnet rims (Crawford et al., 1987; Rusmore et al.,

2005). Monazite grains included in garnet from two sites yield ages of 65.0 ± 2.6 and 62.8 ± 1.6 Ma (Figs. 11D, 11G, Table 3 [see footnote 1], and G.E. Gehrels, 2006, personal commun.), documenting metamorphic mineral growth in the country rocks during 74–63-Ma pluton emplacement. Bordering many of the tonalite and more mafic igneous bodies younger than 65 Ma are zones of migmatite developed in the country rock gneiss or felsic igneous rocks that appear to have formed by crustal melting. Granulite-facies assemblages first reported by Hollister (1975) were identified by the presence of orthopyroxene, commonly replaced by gedrite. These mineral assemblages are found in migmatitic gneiss adjacent to the 53-Ma Kasiks sill and are associated with tabular plutons between the Kasiks sill and Arden Lake complex. The assemblages and quantitative thermobarometry suggest peak metamorphic conditions of 5–6 kb and temperatures as high as 800 °C (Andronicos et al., 2000). The close association of these granulite-facies assemblages and the migmatite in which they occur with the youngest group of plutons indicates their formation was due to heat and fluids advected by the magmas that formed those bodies.

The youngest metamorphism in the Paleogene batholith country rock is also documented by growth of cordierite rims on garnet. The conditions for this event are 5.5 kb at 700 °C (Klepeis et al., 1998) and 4.5 kb, 700 °C (Rusmore et al., 2005). We interpret these low pressures and high temperatures to record decompression without significant cooling during the post–63-Ma extensional deformation.

In summary, the rocks of the Coast Plutonic Complex record deformation that changed from dominantly contractional, as recorded in the western metamorphic belt, to a more oblique to arc parallel transtensional style resulting in ductile strike-slip, and gently and steeply dipping normal extensional faults. The close relationship between coeval low-angle normal faulting and strike-slip faulting represents constrictional deformation that accommodated orogen-parallel extension and vertical thinning. Similar features, associated with gneiss dome complexes that document orogen-parallel extension, were described by Murphy (2002) in Tibet and Nepal. As in the western metamorphic belt, the ductile deformation appears to have played a significant role in controlling pluton emplacement on scales ranging from the outcrop-scale to that of the entire batholith. Shear zones assisted the movement of magma through the crust and ductile extension created dilational sites in which some of the melt accumulated (Klepeis et al., 1998). The relationship between deformation and magma motion and emplacement is observed not only for the larger igneous bodies discussed above, but also for thin sills and dikes formed during migmatite development and crustal melting. In addition, emplacement of igneous rocks apparently played a significant role in modifying crustal ductility thereby producing regional scale shear zones that separate those zones of enhanced ductility from crust with few or no coeval igneous rocks. The thermal history recorded in the metamorphic rocks documents a rise in crustal temperature over time due to the heat introduced by the batholith plutons. The higher temperatures coincided with a

gradual decrease in pressure as the region was uplifted as a result of extension accompanied by continuing magmatic intrusion.

Tectonic Denudation and Exhumation—Earliest Eocene

The final stage of evolution of the Coast Plutonic Complex, between ca. 53–50 Ma, involved rapid (2 mm/year; Hollister, 1982) uplift, decompression and cooling of the mid-crustal metamorphic and plutonic rocks (Andronicos *et al.*, 2003; Rusmore *et al.*, 2005). These events were accompanied by the emplacement of voluminous 52–50-Ma granite and granodiorite plutons of the Ponder pluton/Portland Canal complex along the eastern side of the Coast Plutonic Complex (Figs. 3 and 5, Table 4, see footnote 1). These plutons are post-tectonic with respect to the ductile and penetrative mid-crustal deformation that characterizes the rest of the Complex. The very large volume of felsic magma suggests a significant heat source, possibly mafic melts, derived from the asthenosphere, that underplate the crust. Such mafic melts might be expected as a result of plate detachment related to the arrival of a spreading center between the outboard oceanic (Resurrection/Kula) plate and the edge of the North American accreted terrane belt (Haeussler *et al.*, 2003). The mafic garnet granulite suggested as a possible explanation for the high crustal velocities at depth, observed by the geophysical studies, may represent such underplated basaltic magmas. In addition to the large plutons, coeval smaller granite stocks, and granite and leucotonalite aplite and pegmatite dikes are scattered throughout the batholith (Fig. 5). These felsic bodies, all of which crosscut all the older fabrics and are dated at 51–50 Ma (Crawford *et al.*, 1999; Andronicos *et al.*, 2003), most likely resulted in part from crustal decompression melting during rapid uplift (Hollister, 1982; Crawford and Hollister, 1982; Hollister and Crawford, 1990).

The youngest ductile normal faults observed within the Coast Plutonic Complex are steeper than those associated with 53-Ma and older plutons; the dips are northeast and east dipping rather than north to northwesterly. These younger normal faults deform all the older fabrics as well as the Eocene plutons. Two major shear zones on either side of the Coast Plutonic Complex belong to this group of younger shear faults: on the west the western part of the Coast shear zone dated at 55 Ma and on the east the ca. 52-Ma Shames River/eastern boundary detachment (Heah, 1991; Andronicos *et al.*, 2003; Rusmore *et al.*, 2005). The ductile normal faults, as well as younger steep to vertical brittle faults (Evenchick *et al.*, 1999), segment the crust of the orogen into tens of kilometer wide blocks. North- and northwest-striking vertical shear zones and faults show east-side-down displacement, those that strike east-west show north-side-down displacement. In addition to the normal faults, northeast- to east-northeast-striking faults have strike-slip offset; many of these are eroded to form fjords including Portland Inlet and adjacent fjords to the north and south (Fig. 8, see footnote 1).

The Coast shear zone deforms the western side of the Coast Plutonic Complex. This structure separates the Coast Plutonic Complex gneisses from the lower temperature but higher pressure

rocks of the western metamorphic belt; it also marks the western limit of late Cretaceous to early Tertiary plutons of the Paleogene batholith, including plutons as young as 55 Ma that intrude the eastern side of the shear zone. As noted above, east-side-up reverse motion with a small dextral component dated at between ca. 65 and ca. 57 Ma, lies along the eastern side of the Coast shear zone (Klepeis *et al.*, 1998; Andronicos *et al.*, 1999). In the study area, this phase of deformation was succeeded by east-side down normal displacement, which formed a near vertical, 1.5–4 km-wide zone at the western edge of the batholith. This youngest offset extends from the Skeena River to north of Petersburg (Crawford *et al.*, 1987; Klepeis *et al.*, 1998; McClelland *et al.*, 1992b; McClelland and Mattinson, 2000). The east-side-down displacement is documented by asymmetric sigma clasts, shear bands and offset dikes. It cuts the western edge of the Quottoon pluton just south of Portland Inlet where the pluton was dated at 55 Ma (Thomas, 1999, personal commun.). Undeformed pegmatite bodies within the steep part of the shear zone have ages of 56 ± 3 Ma (Klepeis *et al.*, 1998) and $53 +11/-7$ and $50 +11/-5$ Ma (Saleeby, 2000). The presence of sillimanite stretching lineations and other metamorphic mineral assemblages and textures indicate that the east-side-down shear formed at high temperatures (600°–700 °C) (McClelland *et al.*, 1992b; Klepeis *et al.*, 1998). Motion on this shear zone uplifted the deep crust of the eastern side of the western metamorphic belt. K-Ar and $^{40}\text{Ar}/^{39}\text{Ar}$ ages (Smith and Diggles, 1981; Cook and Crawford, 1994) document cooling of the western metamorphic belt rocks at close to the time of the east side down motion on the Coast shear zone. South of the Skeena River the Coast shear zone becomes less significant. Gareau (1991) was not able to identify this structure east of the Ecstall pluton. As the Coast shear zone cuts the western side of this pluton just north of the Skeena River, it may continue within that pluton to the south. Rusmore *et al.* (2001) identified a narrow zone of west-side-up reverse deformation along the lower (western) boundary of the Quottoon pluton at Douglas Channel; they inferred that this is a southern continuation of the Coast shear zone feature.

The conclusion, based on our geological observations, that the Coast shear zone defines a major crustal discontinuity is supported by the seismic data reported above. Neither the crustal reflectors identified on the west nor those on the east of the shear zone cross to the other side. The location of the cutoffs coincides with a 5 km step in the mantle under the Coast shear zone. These observations led Morozov *et al.* (1998) to suggest that the observed steep to vertical dip of the post-55-Ma east-side-down part of the shear zone continues to and offsets the Moho. The east-side down offset, similar to that of the many other 55 Ma and younger steep normal faults that segment the orogen, suggests this fault was related to approximately east-west extension. The location of the post-55-Ma steep part of the Coast shear zone was likely controlled by a ductility contrast between the older, by this time cold, rocks of the Cretaceous western metamorphic belt (Cook and Crawford, 1994) and the plutons and hot country rocks of the Paleogene batholith. We have found no evidence to suggest that the Coast shear zone is a major strike-slip fault

related to long distance northward transport of outboard Insular belt terranes, as postulated previously (Hollister and Andronicos, 1997; Cowan et al., 1997).

Along the eastern side of the orogen, normal faulting exhumed the high-temperature crust of the Coast Plutonic Complex. North- and northeast-dipping detachment faults, including the ca. 52-Ma moderately dipping Shames River detachment (Heah, 1990, 1991; Andronicos et al., 2003) and the so-called eastern boundary detachment (Rusmore et al., 2005), have been mapped between Douglas Channel and north of the Skeena River (Fig. 5). Rocks of Stikinia form the upper plate of these detachment faults. The seismic data reported by Hammer et al. (2000) and Morozov et al. (2001) show east-dipping reflectors along this eastern side of the high grade part of the orogen that correspond to moderately dipping ductile normal faults mapped at the surface and separate the Coast Plutonic Complex from Stikinia. North of the Skeena River the eastern side of the Shames River detachment is cut by brittle normal faults, the Shames River fault zone (Heah, 1990, 1991). These normal faults juxtapose the high-grade rocks and plutons of the Coast Plutonic Complex with rocks of the Stikine terrane in the Kitselas-Kitsumkalum block (Gareau et al., 1997a). Several plutons in this block were emplaced at approximately the same time as plutons of the Coast Plutonic Complex (Fig. 5) (Gareau et al., 1997a, 1997b). However, the rocks in the graben represent shallower crustal levels than those exposed in the complex to the west. These geological relationships suggest that the fault-bounded Kitselas-Kitsumkalum block represents an intermediate level of crustal uplift between the high-grade metamorphic rocks within the western part of the Coast Plutonic Complex and the near surface rocks of the Stikine terrane. The seismological evidence discussed above shows an increase in crustal thickness of ~5 km crossing into Stikinia on the east from the Coast Plutonic Complex. This increase suggests that the entire crust was involved in the uplift across the fault system.

According to Sisson (1985) the andalusite-bearing metamorphic contact aureole in sediments of the Bowser Lake group adjacent to the Ponder pluton records pressures of 2–3 kb and temperatures of up to 700 °C. Her measurements of fluid inclusions in an undeformed pegmatite that cuts the Coast Plutonic Complex on the west side of the Ponder Pluton give similar pressures. These data suggest ~10 km of vertical displacement based on metamorphic conditions in the Coast Plutonic Complex gneiss prior to uplift and Ponder pluton emplacement. These conditions are inferred by Sisson (1985) to have been ~5.5 kb and 650 °C and by Hollister (1975) 5–6 kb and up to 800 °C.

Farther north, along Portland Canal, moderately to steeply east-dipping ductile fabrics with an east-side-down shear sense cut 53–51-Ma granite plutons. These ductile fabrics are, in turn, cut by steep normal faults that juxtapose the Eocene granite against the low-grade supracrustal rocks of the Stikine terrane on the east. One of these normal faults, with a calculated displacement of at least 0.5 km, offsets a 22-Ma felsic igneous suite (Evenchick et al., 1999). This relationship shows that the faulting on this eastern side of the orogen core continued well into the

Miocene and possibly later. These extensional detachments and steep normal faults represent the last stages of the prolonged history of extension and related exhumation of the Paleogene core of the orogen. The relatively high average crustal P-wave velocities under the Coast Plutonic Complex observed by the geophysical surveys are consistent with removal of 15–25 km of low-density, low-velocity upper crust and exposure at the surface of the relatively high-velocity plutons and associated mid-crustal metamorphic country rocks during the last 50 million years.

Crustal cooling within the Coast Plutonic Complex is recorded by hornblende argon ages that cluster around 51–49 Ma and for biotite around 48 Ma (Smith and Diggles, 1981; Hollister, 1993). U-Pb sphene cooling ages between 53 and 51 (Table 1; Figs. 2C and 4A, see CD-ROM accompanying this volume, or in the GSA Data Repository; Andronicos et al., 2003) are similar to the cooling ages obtained from hornblende. The nearly concordant ages of minerals with different closure temperatures document rapid cooling. Lower-plate cooling ages in the Shames River and eastern boundary detachment systems are similar. Sphene and hornblende ages cluster around 51 Ma, with biotite ages clustering around 48 Ma. As movement on the Shames River detachment was ongoing at 52 Ma (Andronicos et al., 2003) the cooling ages indicate that rapid uplift of the Coast Plutonic Complex was closely associated with the normal faulting along the eastern side of the orogen core.

Eocene to Recent

As noted above, widespread extensional deformation within the batholith after 55 Ma resulted in the formation of discrete crustal blocks separated by normal faults. Petrologic data described below as well as paleomagnetic observations (Butler et al., 2001a, 2002; Butzer et al., 2004) provide constraints on the deformational history of these blocks.

Butler et al. (2001a) obtained paleomagnetic data from plutons with ages between 72.3 and 55 Ma that lie along the east side of the Coast shear zone from the Skeena River to north of Portland Inlet. These authors inferred an Eocene age for the magnetization on the basis of the sphene and K-Ar ages for hornblende in these Paleogene plutons (Smith and Diggles, 1981; Andronicos et al., 2003). The argon closure temperature in hornblende is ~550 °C, which is close to the 580 °C Curie temperature for magnetite. The data on metamorphic temperatures for the host rocks of the plutons discussed above suggest that, prior to the ca. 50-Ma cooling event, the rocks were too hot to acquire the observed characteristic remanent magnetization. The paleomagnetic data show directions that change from mostly concordant relative to the Eocene pole in transects along the Skeena River and along Quottoon Inlet, which lies halfway between the Skeena River and Portland Inlet, to significantly discordant at Portland Inlet and farther to the northwest. Concordant paleomagnetic directions for the 58.6-Ma (Gehrels et al., 1991a) segment of the Quottoon pluton along the Skeena River agree with the paleomagnetic observations reported by Symons (1974) for that pluton. Along each

transect where the data are discordant, the paleomagnetic poles show greater deviation from the expected Eocene geomagnetic field direction for western samples than for eastern samples. This led the authors to conclude that the observed magnetic signature is due to tilting of crustal blocks tens of km-wide about approximately north-northeast oriented axes. As a result of this tilting, magnetization was acquired from west to east across the tilted blocks. The greatest tilt, up to 40°, was inferred for two blocks on the northern side of Portland Inlet. Lesser tilts were identified both to the north and south of the inlet. Faults along the northeast trending fjords in this area are postulated to separate these tilted blocks from each other. This east-side-up tilting of crustal blocks is part of the earliest Eocene extension and uplift of the Coast Plutonic Complex discussed in the previous section. The extension and tilting coincides with the early stages in development of the plate-bounding Queen Charlotte transform fault that lies offshore of the British Columbia-Alaska coast (Fig. 2).

Using pressure estimates derived from petrologic data across the western metamorphic belt, Cook and Crawford (1994) proposed that 14° of east-side-up tilting of the western metamorphic belt crust also occurred at ca. 50 Ma. The postulated mechanism of the tilting is the displacement documented on the youngest part of the Coast shear zone, which forms the eastern margin of the belt. The amount of crustal extension associated with this tilting is hard to determine without knowing the three-dimensional geometry of the tilted blocks. Butler *et al.* (2001a) calculated values of up to 30% extension using the assumption that the blocks slid on a horizontal detachment surface.

After 50-Ma magmatic activity resumed across the entire orogen. Two new ages for this magmatic activity are presented in Tables 5A and 5B and Figure 12 (see footnote 1). A distinctive feature that resulted from this magmatism are swarms of mafic dikes with similar orientations that cut the Eocene and older rocks. On either side of Portland Inlet, these dikes, which generally measure from less than a meter to several meters in width, strike approximately N 60°E. Elsewhere dike strikes cluster close to due north or northwest. Aerial and satellite photographs show lineaments with the same trends. As noted above, faults also show these trends, some carved into fjords or major river valleys by erosion. At some locations felsic dikes occur with the mafic dikes in these swarms, although they are less abundant. Dating these dikes has proven difficult; ages ranging from 42 to 14 Ma have been reported (Evenchick *et al.*, 1999; O'Connell, 2004). Due to dating difficulties it is not possible to ascertain the ages of dikes within the differently oriented clusters.

During the Oligocene and Miocene, this renewed magmatism created the Kuiu-Etolin igneous belt (ca. 25–20 Ma) (Lindline *et al.*, 2000, 2004), other scattered mafic and felsic plutons and stocks, and numerous dikes (Fig. 13). The Kuiu-Etolin igneous complex was emplaced into and onto the Gravina belt and the Alexander terrane units. In contrast to the overall intermediate composition of the Cretaceous to Eocene igneous rocks, the Oligocene and Miocene magmatism is distinctly bimodal. At the southeastern end of the Kuiu-Etolin complex, on Etolin Island and

adjacent areas to the west (Fig. 13), lies the Burnett Inlet igneous complex (Lindline *et al.*, 2000). This consists of three main rock types: granite, alkali granite, and a gabbro–diorite unit consisting of intermingled mafic, hybrid and granitic rocks. Both the mafic and felsic units have intraplate geochemical characteristics, relating the magmatism to an extensional tectonic setting. Metamorphic pressures close to 3.5 kb obtained from contact metamorphic mineral assemblages adjacent to gabbro at the southeastern end of the complex suggest an emplacement depth of 12–13 km (Stowell and Crawford, 2000). Distributions of apatite fission-track lengths and mineral-cooling curves imply that the plutonic rocks cooled to less than 100 °C within less than 5 million years of emplacement (Douglass *et al.*, 1989; Lindline *et al.*, 2000). To the northwest, along the strike of the Kuiu-Etolin igneous complex, the Zarembo Island volcanic suite consists of basalt, andesite, and rhyolite lava flows, which exhibit features that suggest simultaneous eruptions of mafic and felsic lavas (Lindline *et al.*, 2004). Numerous northeast- and northwest-striking basalt and rhyolite dikes cut these flows. Many of the mafic and felsic dikes form composite or sheeted complexes. In the composite dikes, contacts are sharp yet lobate and serrated suggesting the mafic and felsic magmas were coeval. Northwest of Zarembo Island the volume and number of dikes decreases and the rocks are predominantly flows or fragmental volcanic units.

The complex is interpreted to have evolved as one or several shallow-level silicic magma chambers heated by underplated basaltic magma derived from partial melting of enriched upper mantle (Lindline *et al.*, 2000, 2004). We infer the mantle melting resulted from extension related to transtensional deformation along the plate bounding Queen Charlotte fault. Subsequent invasion of the silicic magma chamber by basaltic intrusions induced explosive eruption phases, followed by rapid crystallization and cooling of the entire complex.

The difference in exposed crustal level across the complex from southeast to northwest suggests 8° of tilting of a crustal block ~80 km wide. Butzer *et al.* (2004) obtained paleomagnetic data from mafic dikes related to this complex. East-side-up tilt by 16° about a north-trending (8°) axis explains the discordant declinations observed. Just south of the Kuiu-Etolin igneous complex, an increase in metamorphic grade across Prince of Wales Island (Fig. 13) (Gehrels and Berg, 1992) also suggests east-side-up tilting with a tilt angle of ~8°. Butzer *et al.* (2004) conclude that the greater amount of tilt suggested by the paleomagnetic data may be explained by the presence of smaller tilted blocks within the larger tilted crustal segments.

Also between 25 and 20 Ma, subsidence and tilting in a 150-km-wide zone east of the Queen Charlotte transform fault formed the Queen Charlotte basin. This basin, which extends into Hecate Strait west of Prince Rupert, is characterized by a network of sediment-filled grabens and half-grabens (Rohr and Dietrich, 1992; Dehler *et al.*, 1997). Refraction and gravity data reported by these authors indicate that crustal thickness under the Queen Charlotte basin is 22–28 km and that several kilometers of igneous crust were added to the basin during extension. Seismic reflection

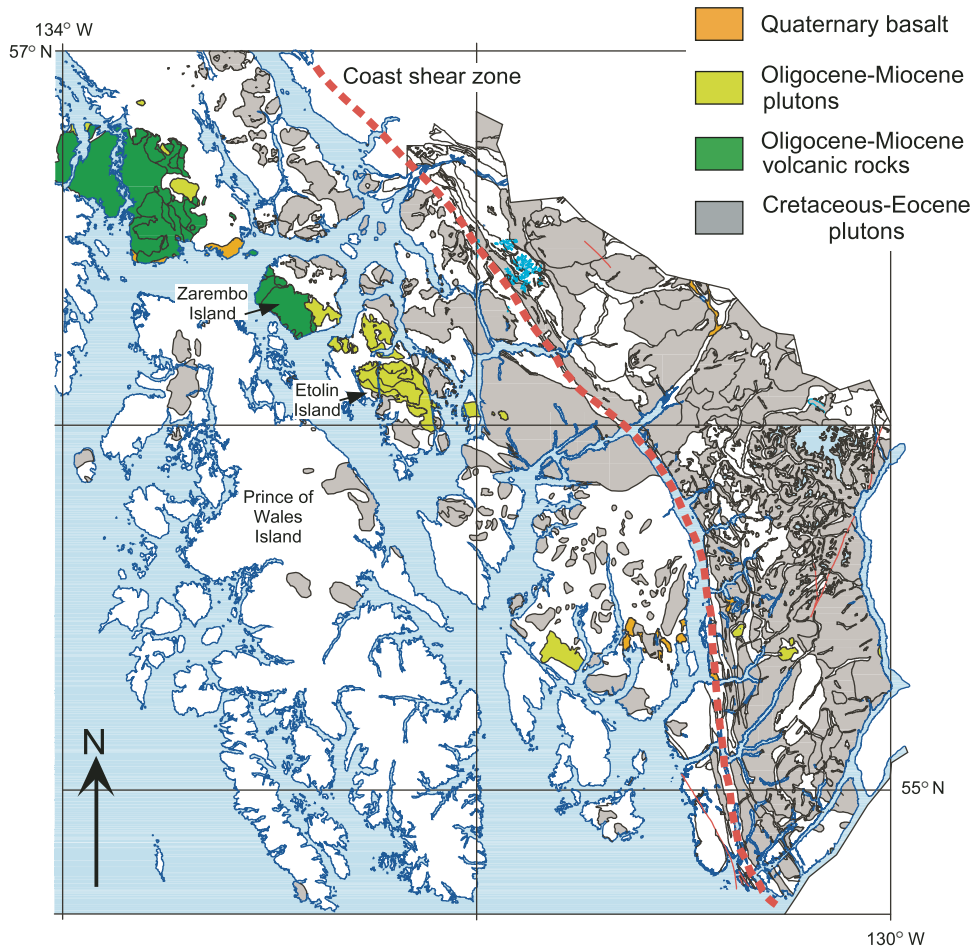


Figure 13. Map highlighting the Miocene to Recent igneous rocks in the study area.

data and drill hole observations in Hecate Strait document post–Middle Miocene northeast-side-up tilts of some crustal blocks by at least 18° (Rohr and Dietrich, 1992). Dehler et al. (1997) concluded that the net lithospheric extension was uniform within the basin, averaging 76%, or ~ 50 km. The Masset volcanic rocks on the Queen Charlotte Islands (Hickson, 1991), dike swarms and small plutons coeval with the volcanic rocks (Souther and Jessop, 1991), and other volcanic rocks located along the western and eastern sides of Hecate Strait (Woodsworth, 1991; Hyndman and Hamilton, 1993), were coeval with this extension and with the emplacement of the Kuiu–Etolin igneous complex. Other Oligocene and Miocene felsic and mafic plutons and stocks occur throughout the region. Among the most notable are the granitic Miocene stocks at Quartz Hill, which are associated with a large porphyry molybdenum deposit (Hudson et al., 1979).

Extension, uplift and associated crustal thinning accompanied by magma emplacement continue to the Present. (U–Th)/He dating in the Coast Mountains (Farley et al., 2001) suggests that exhumation in the orogen east of the Coast shear zone was limited between 30 and 10 Ma, the time of the Miocene extension and magmatic activity to the west however uplift at ~ 0.22 mm/year started at 10 Ma (Farley et al., 2001). These authors document

a higher cooling rate after 4 Ma that may be due to exhumation associated with erosion and rebound following glaciation. Alternatively, it may be due to accelerated cooling as the rocks reached close enough to the surface to interact with cool meteoric water (Dempster and Persano, 2006). Quaternary to Recent alkalic mafic magmatism occurs across the region (Fig. 13) and into the interior of British Columbia (Sutherland-Brown, 1969; Elliott et al., 1981; Crawford et al., 1995; Edwards and Russell, 2000; Crawford et al., 2005; Abraham et al., 2005). These basaltic rocks have initial $^{87}\text{Sr}/^{86}\text{Sr}$ of 0.70322–0.70358 supporting chemical evidence that these igneous rocks are mantle-derived with only minor crustal contamination (Crawford et al., 2005). Observed high heat flow across the region discussed below is probably related to this extension and magmatic activity.

DISCUSSION

Summary of the Key Points of Orogen Evolution

The tectonic evolution of the Coast orogen since the Jurassic occurred in a series of stages. Each of these stages resulted in a distinctive crustal signature that reflects the origin and composition

of the protolith rocks, which were either derived from accreted terranes each with characteristic crustal properties or as rocks deposited in basins superimposed on the terrane collage. The crustal signatures were further modified by the intrusion of successive generations of igneous rocks and, in some areas, by crustal melting as the orogen evolved. The response of the different segments of the orogen to large-scale deformation driven by relative plate motions also played a role in the final crustal characteristics.

The oldest documented events consist of Early to Middle Jurassic accretion of the Alexander and Wrangellia oceanic arc terranes. Subsequently transtensional displacements between the Alexander terrane and the previously accreted Yukon-Tanana terrane created the Gravina basin (McClelland *et al.*, 1992c). In the mid-Cretaceous a change in relative motion between the Farallon oceanic plate and North America, from oblique motion to near-orthogonal convergence and subduction of the oceanic plate, resulted in closure of the Gravina basin and formation of the mid-Cretaceous (post-120-Ma) arc, the west-vergent Cretaceous thick-skinned thrust belt (Rubin *et al.*, 1990), and the western metamorphic belt. Thrust nappes containing Gravina sequence and Yukon-Tanana rocks were emplaced over Alexander terrane rocks. As documented by new ages presented in this paper, Cretaceous subduction-related igneous bodies in the Alexander terrane, Gravina basin, and Yukon-Tanana terrane rocks show a systematic decrease in age from west to east across this western part of the orogen (Fig. 5). The northwest trending and northeast-vergent folds of the Skeena fold-and-thrust belt east of the orogen core (Fig. 2) also formed at this time (Evenchick, 1991). These folds overprinted an older generation of northeast-trending folds that are inferred to have formed during the sinistral plate convergence prior to ca. 110 Ma (Evenchick, 2001). Later stages of thrust-related crustal thickening of the western metamorphic belt coincided with emplacement of voluminous 90-Ma plutons including the Bell Island and Ecstall plutons. Mid-Cretaceous deformation within the Coast Plutonic Complex to the east cannot be specifically identified due to later overprinting; however, there is evidence of moderate pressure (kyanite and staurolite producing) metamorphism at 90 Ma similar to that which characterized the eastern side of the western metamorphic belt at this time.

After ca. 88 Ma, active deformation and igneous activity shifted eastward into the Yukon-Tanana terrane rocks that underlie the Coast Plutonic Complex. This shift coincided with formation of the Kula plate and a related change in relative motion between the outboard oceanic plate and North America to oblique dextral displacement (Engelbreton *et al.*, 1985; Stock and Molnar, 1988). The ensuing transpression across the North American plate margin, accompanied by continuing subduction, generated the Paleogene batholith of the Coast Plutonic Complex. A lack of significant volumes of igneous rock signals an apparent magmatic lull between ca. 80 and 74 Ma. Thereafter, between 74 and 53 Ma, in contrast to the pattern of eastward younging of igneous activity across the western metamorphic belt and thick-skinned thrust belt (Fig. 5), the magmatism was spread across the batholith (Figs. 5, 8). The structural evolution of the Coast Plutonic

Complex–Paleogene batholith crustal block between 63 and 53 Ma was characterized by oblique extension and exhumation of the deeper crust in a transpressional tectonic regime. For most of this history, the crust remained hot as it uplifted, probably due to continuing magmatic input. The rate of exhumation, inferred from the ages of successive generations of metamorphic minerals (Rusmore *et al.*, 2005), gradually increased until rapid uplift associated with extension across the continental margin started after ca. 55 Ma. Emplacement of large plutons including the mafic Quottoon and Kasiks plutons and the felsic plutons of the Ponder pluton/Portland Canal complex accompanied the last stages of orogen development.

The shift from extension nearly along the orogen to orogen perpendicular spreading coincided with final consumption of the Resurrection or Kula plate and formation of the current transform-plate boundary, the Queen Charlotte-Fairweather fault, west of the continental margin. This change in tectonic setting is probably associated with plate detachment (Haeussler *et al.*, 2003). The large volume of 52–50-Ma granitic magmatism possibly represents crustal melting triggered by intrusion of mafic magma into the deeper crust as a consequence of formation of a slab window. It is interesting to speculate whether the large volumes of mafic magma that form the youngest (55 Ma) part of the Quottoon pluton and the 53-Ma Kasiks sill are also related to the arrival of the Resurrection/Kula spreading center at the margin and incipient delamination, both of which would result in high heat flow into the mantle underlying the crust of the orogen.

During the last 50 million years, translation associated with that transform-plate margin has had both transpressional and transtensional phases. Transtension resulted in widespread normal faulting and emplacement of mafic and felsic dikes throughout the orogen. The largest volume of post-Eocene igneous activity occurred during the upper Oligocene–lower Miocene (35–20 Ma). This coincides with a major period of oblique extension across the plate boundary from 36 to 20 Ma proposed by Stock and Molnar (1988). Transpression over the last 5 million years has created large inversion structures and uplifts in the sedimentary sequences in Hecate Strait and has probably caused observed tilting of the Miocene volcanic rocks in the Kuiu-Etolin igneous complex. Quaternary to Recent alkalic mafic magmatism documented at many locations across the region also accompanied this transpression.

In conclusion, the overall orogen evolution reflects the complex interactions involved during accretion of the Insular superterrane to North America and the series of changes in plate motions since the mid-Mesozoic. The details of crustal evolution involve interactions between magmatic activity and crustal deformation, influenced by the pattern imposed by the accretionary processes.

The Coast Shear Zone

The Coast shear zone extends most of the length of the Coast Mountains from near Haines at latitude 59°14'N to Machmell River at latitude 51°40'N, with a total length of at least 1200 km

(Rusmore et al., 2001). Our observations, as well as data from north of the area of this report (Ingram and Hutton, 1994; Stowell and Hooper, 1990) and from the south (Rusmore et al., 2001), show all segments were active from ca. 65–55 Ma. Along its entire length the Coast shear zone shows a protracted period of northeast-side-up dip-slip displacement associated with the formation and early stages of exhumation of the Paleogene Coast Mountains batholith. In addition, from Douglas Channel (Fig. 5) northward, the shear zone marks the western limit of early Tertiary metamorphism and plutonism. Synkinematic plutons found in the shear zone date the deformation.

North of Juneau the northward continuation of the Coast shear zone truncates the northward extension of the western metamorphic belt and associated thrust faults (Gehrels, 2000). The young (ca. 55 Ma) phase of west-side-up displacement, documented between the Skeena River and just north of Petersburg, has not been identified to the north or south of the central part of the belt. Evidence for this conclusion includes the observation that, south of the Skeena River, rocks west of the Quottoon pluton cooled through ~ 350 °C by ca. 70 Ma (Gareau and Woodsworth, 2000) whereas, in the Ketchikan quadrangle (Fig. 2) north of the Skeena, they remained at high temperatures until they were uplifted by displacement on the Coast shear zone at close to 55 Ma (Cook and Crawford, 1994).

Engebretson et al. (1985), Lonsdale (1988), and Haessler et al. (2003) all suggest moderately oblique convergence between the offshore oceanic plate and North America from 66 to 56 Ma with a convergence angle of $\sim 20^\circ$. This angle is likely oblique enough for a transpressional regime resulting in partitioned deformation along strike-slip and contractional faults in the North America plate. The dip-slip displacement of the eastern Coast shear zone records this contractional motion. As noted above in the discussion of the evolution of the Paleogene batholith, strike-slip faults as young as 53 Ma deform the hot rocks of that batholith; both dextral and sinistral motion has been identified on these faults in the study area. The dextral Chatham Strait and Clarence Strait faults (Fig. 2) cutting the Alexander terrane and terranes to the west also formed at this time. Dextral faulting also occurred locally adjacent to the Coast shear zone just south of Juneau (Stowell and Hooper, 1990). Gehrels (2000) reports that splays of the Chatham Strait fault northwest of Juneau offset a pluton dated at ca. 59 Ma but do not cut a nearby 57-Ma pluton. The dextral Denali fault that extends from north of Juneau westward across southern Alaska is also likely early Tertiary (Nokleberg et al., 1985).

The geophysical transect that identified a 5-km step in the Moho at the position of the Coast shear zone (Morozov et al., 2001) crosses the orogen at the mouth of Portland Inlet, where the Alexander terrane is almost directly juxtaposed with the Yukon-Tanana terrane (Fig. 3). At this location it can be argued that the Coast shear zone represents the terrane boundary. To the north, however, this is not the case as the Yukon-Tanana terrane extends a considerable distance west of the Coast shear zone (Fig. 3). This observation of coincidence at Portland Inlet raises the question

as to whether the observed Moho offset can be attributed to the lower Eocene Coast shear zone displacement, or whether it is inherited from the initial terrane accretion along a transpressional boundary between the Alexander and inboard terranes.

Comparison of the Central Coast Orogen with Northern Southeast Alaska

Final juxtaposition of the Alexander terrane and Gravina basin rocks to the previously accreted continental margin terranes occurred at about the same time as in the area of this study as far north as Juneau. Thrust faults that carry Yukon-Tanana rocks over Gravina units in the western metamorphic and thick-skinned thrust belt have been dated at 91 ± 2 Ma at Juneau and 90 Ma near Petersburg based on their relationships with plutons of those ages (Gehrels, 2000; McClelland et al., 1992b). This age of westward thrusting of the Yukon-Tanana terrane is similar to that obtained from plutons near Ketchikan (89–90 Ma) and Prince Rupert (90 Ma) in the area that is the focus of this paper. Neither the thrust faults nor these mid-Cretaceous plutons are recognized north of Juneau. Contact aureoles around ca. 90-Ma plutons north of Wrangell as well as other metamorphic rocks west of the Coast shear zone north of the study area (Stowell and Crawford, 2000) record 6–9 kb pressure metamorphic assemblages similar to those reported from the Ketchikan and Prince Rupert quadrangles (Fig. 2).

Highly elongated and deformed Paleocene plutons with contacts concordant with the shear zone fabrics lie east of the Coast shear zone. Brew and Ford (1978) first described these plutons and their close association with the Coast shear zone. Near Juneau the ages of these elongated plutons decrease eastward from 71.6 Ma on the west to 66.4 Ma on the east (Gehrels et al., 1991a). Klepeis et al. (1998) show a similar pattern of parallel, eastward younging plutons directly east of the Coast shear zone in the southeastern Ketchikan quadrangle (Fig. 2). These pluton ages and styles are similar to those of the plutons within the Coast Plutonic Complex in the study area. As in the Coast Plutonic Complex older plutons are deformed, whereas the youngest show only a flow mineral alignment or lack any fabric.

Comparison of the Central Coast Orogen with Northern Coastal British Columbia

South of the Skeena River the crustal history differs in a number of ways from that to the north. In the south, the Gravina basin rocks are absent. Instead slivers of Alexander terrane rocks tectonically interleaved with ancient metamorphosed continental margin assemblages of the Yukon-Tanana terrane (Gehrels and Boghossian, 2000) lie west of the Coast shear zone. The Yukon-Tanana terrane rocks are intruded by Jurassic and Early Cretaceous plutons. In addition, there are many fewer 105–90-Ma plutons in this part of the Coast orogen. Gareau (1991) was not able to trace the Coast shear zone south of the Skeena River. Farther south however, along and south of Douglas Channel, Rusmore et al.

(2001) identified 2–11-km-thick, steeply northeast-dipping shear zones with reverse motion dated at between 65 and 55 Ma that they correlate with the Coast shear zone. Along Douglas Channel this shear zone forms the southwestern margin of the Quottoon pluton. Farther south, near Bella Coola, the rocks in the upper plate of the shear zone are no longer high-grade gneisses, as they are from Douglas Channel north, but are weakly metamorphosed volcanic rocks interpreted as an Early Cretaceous arc built on Stikinia (Rusmore *et al.*, 2001). Also along Douglas Channel, the field relationships show that the northeastern contact of the Quottoon pluton, here dated at 58.6 Ma, is intrusive. The pluton cuts all rocks fabrics in the country rock and contains stoped blocks of the host gneisses (Rusmore *et al.*, 2005). This situation is different from that observed between the Skeena River and Portland Inlet where the contact is defined by ductile extensional shear zones (Crawford *et al.*, 1999). It is interesting to speculate whether the termination of the Alexander terrane southward plays a role in these changes.

The thermal history of the gneiss in the orogen core, east of the Quottoon pluton, is somewhat better preserved in this transect, possibly due to less igneous activity and therefore less complete overprinting of early mineral assemblages. As in the north, the sequence of metamorphic assemblages are kyanite, in many places replaced by sillimanite, succeeded by newly formed garnet and sillimanite, in places enclosed in garnet rims, and finally cordierite, in part replacing garnet. According to Rusmore *et al.* (2005) the growth of sillimanite occurred after 70 Ma. As in the Coast Plutonic Complex north of the Skeena River, by 52 Ma the rocks had cooled to ~550–600 °C (from ~700 °C), as inferred from U-Pb sphene ages (Table 1). Exhumation of the Coast Plutonic Complex was accomplished by 50–55-Ma crustal extension east of the Coast shear zone (Rusmore *et al.*, 2005). A similar extension has not been observed at Bella Coola or farther south.

About 120 km south of the Skeena River lies a regional-scale, northeast-directed Late Cretaceous (95–85 Ma) thrust belt that marks the western margin of Stikinia (Rusmore and Woodsworth, 1991; Rusmore *et al.*, 2000b). This thrust belt can be traced discontinuously for at least 255 km farther south. In the areas where the affinity of the rocks in the upper plate has been established, they belong to the Yukon-Tanana terrane. Thus, this thrust system defines the boundary between the Yukon-Tanana and Stikinia accreted terranes. From Douglas Channel north, this boundary is obscured by young plutonic rocks. This thrust complex is intersected by the west-vergent Coast shear zone along South Bentinck arm, just south of Bella Coola, British Columbia. Although cross-cutting relationships between the thrust belt and the Coast shear zone have not been observed, motion on the Coast shear zone is younger and thus it likely truncates the mid-Cretaceous thrusts.

The northeast-side-up tilting after ca. 55 Ma that resulted in anomalous paleomagnetic inclinations between Prince Rupert and Petersburg has not been found along Douglas Channel. Rather, between ca. 55–20 Ma, ~50° of counter-clockwise vertical axis rotation of the Quottoon pluton and adjacent rocks formed the

Hawkesbury Warp (Rusmore *et al.*, 2000a). These authors suggest the Eocene to Miocene crustal extension to the north and northwest may have caused the warp. This suggestion for the origin of the Hawkesbury Warp may also explain the observed offset of the Coast shear zone across Portland Inlet (Figs. 5 and 9). As noted above, Butler *et al.* (2001a) inferred significantly greater tilt and hence greater extension on the northern side of Portland Inlet, possibly associated with a fault under the inlet.

Comparison with Other Areas

This central part of the Coast orogen displays many features in common with structures described for other major Cordilleran batholiths that have evolved through cycles of contraction and extension. One example is the Chelan block in the core of the Cascades in northwestern Washington. This area experienced Late Cretaceous to Eocene evolution very similar in broad terms to that described above (Paterson *et al.*, 2004). According to these authors, late Cretaceous (>96–73 Ma) contraction in the Cascades was followed by dextral transpression from 73 to 55 Ma and then transtension. As in the Coast orogen, exhumation accompanied each of these stages. Cretaceous uplift of deeper crustal units by thrusting was followed by top north arc-oblique shearing that initially occurred during melt present conditions. In the Cascades the early stages of top north ductile shearing, associated with ongoing contraction, is inferred to have started at 73 Ma, sooner than in the Coast Plutonic Complex. In both areas the shearing oblique to the orogen resulted in high-temperature decompression followed by cooling recorded by the metamorphic rocks. Paterson *et al.* (2004) suggest that after 55 Ma further deformation resulted from transtension across the orogen but this stage is not well documented in the rocks of their study.

In Fiordland, New Zealand, the Median batholith (Mortimer *et al.*, 1999) records a history of Early Mesozoic subduction-related magmatism and intra-arc deformation that resulted in the formation of a crustal-scale, subvertical shear zone called the Indecision Creek shear zone (Klepeis *et al.*, 2004; Marcotte *et al.*, 2005). Like the Coast shear zone, the Indecision Creek shear zone is composed of a steep zone of ductile, upper amphibolite-facies foliations that formed along the boundary between two blocks of arc crust of different ages. Significant elements of both the Coast and Indecision Creek shear zones evolved following a major phase of arc magmatism and assisted in the transport magma vertically and horizontally through the crust. In both cases, the shear zones continued to be active during the waning stages of arc magmatism as regional contraction and transpression declined. Deformation in the two shear zones outlasted arc magmatism, resulting in steep zones up to 5 km-wide that mostly comprise subsolidus fabrics with down-dip mineral lineations. These similarities suggest that major subvertical shear zones that bound crustal blocks displaying dissimilar histories are common to continental arcs.

In addition to these similarities, shear zones in Fiordland display several major differences from those in the Coast ranges.

Unlike the Coast shear zone, Khyex shear zone, and other extensional shear zones in the Coast Mountains batholith, the Indecision Creek shear zone does not record deformation during a period extension that followed an older phase of intra-arc contraction. Instead, large extensional shear zones in Fiordland post-date the Indecision Creek shear zone. Although these extensional shear zones appear to have initiated in areas of the lower crust that were weakened by magma and heat, the extension was not accompanied by the emplacement of large volumes of magma at the crustal levels that are currently exposed (Klepeis et al., 2004; Scott and Cooper, 2006; Klepeis and King, this volume). The cause of these differences, and especially the different relationships between extension and magma emplacement, is uncertain. Nevertheless, the large crustal-scale shear zones in both settings form a fundamental part of the structure of the batholiths, with the late stages of motion resulting in the tectonic denudation and exhumation of the deep crust following a prolonged period of subduction, convergence, and magmatism.

Evaluation of Proposed Large-Magnitude Translation

Major sinistral shear zones southwest of Prince Rupert, including the Kitkatla, Principe Laredo, and Grenville Channel faults, cut 160–120-Ma plutons (Gehrels and Boghossian, 2000; Mansfield and Andronicos, 2004). Based on this evidence Gehrels and Boghossian (2000) suggested that, starting ca. 140 Ma, sinistral displacement of the Alexander terrane occurred along the continental margin. This had ceased by the time of thrusting in the Gravina belt units and emplacement of the oldest mid-Cretaceous plutons at ca. 115 Ma.

There has been considerable discussion, based on paleomagnetic data, concerning whether significant orogen-parallel dextral displacement occurred along the Insular-Intermontane superterrane boundary after the Late Cretaceous (e.g., Irving et al., 1996; Butler et al., 2001b; Hollister and Andronicos, 1997; Cowan et al., 1997). As others who have worked in the area, we take the view that post–mid-Cretaceous but pre-Eocene dextral coastwise translation of rocks within and west of the Coast orogen has been limited. We base this on the field evidence reported by geologists working in the area who have been unable to identify any major structure coincident with that boundary that records strike-slip motion and who have traced Yukon-Tanana stratigraphy across the Coast shear zone (McClelland et al., 1992a; Rusmore et al., 2000b; Crawford et al., 2000; Gehrels, 2001). Also, Butler and coworkers (Butler et al., 2001a, 2001b, 2002; Butzer et al., 2004), suggest their paleomagnetic data, which clearly document discordant paleopole positions that might suggest translation, should be interpreted as due to tilting rather than translation.

The dextral Denali-Chatham Strait fault system offsets Insular superterrane rocks north and west of the area of this paper. There is no evidence for pre-Eocene motion on the strand of the Denali fault north of the area of this study (Miller et al., 2002), although these authors suggest movement as old as 85 Ma in western Alaska. Age constraints on the Chatham Strait and Clarence

Strait faults also suggest the dextral motion on those faults is likely early Tertiary (Gehrels, 2000). The temporal coincidence between the crustal extension by tilting at and after ca. 55 Ma with these dextral strike-slip systems suggest those strike-slip and normal faults are related to the large-scale changes in plate motion at this time.

The argument that pre-Eocene dextral translation did take place but that evidence for translation has been overprinted and thus obliterated invites a comparison with other major intra-arc strike-slip shear zones where significant trench-parallel displacements have occurred. One well-studied example is the Liquiñe-Ofqui fault of southern Chile. This is an active 1000 km-long, dextral strike-slip fault zone that cuts through the Patagonian batholith and modern volcanic arc of the southern Andes for ~1000 km. This major fault is nearly vertical, parallels the Peru-Chile trench, and accommodates the trench-parallel component of oblique convergence between the Pacific and Nazca plates (Cembrano et al., 2000, 2002). The oblique convergence, presently oriented at an angle of ~26° from the orthogonal to the trench, has resulted in translation of arc crust parallel to the Peru-Chile trench and has formed a 300–400-km wide transpressional orogen. Exhumation, involving the erosion of at least 7 km of rock during the last 4 m.y., accompanied the transpressional deformation (Cembrano et al., 2002). Despite millions of years of plutonic activity and exhumation, the oblique subduction driven, trench-parallel displacements generated well-preserved structures inside the Patagonian batholith that document that translation. The absence of similar structures that record pre-Eocene strike-slip displacements along the Coast shear zone suggests such structures were not present.

Summary

The segment of the Coast orogen along the northernmost coast of British Columbia and southeastern Alaska discussed in this paper records a history of Jurassic terrane accretion and basin formation followed by evolution of the orogen starting in mid-Cretaceous time. This evolution was influenced by changes in the relative motion between oceanic plates located west of the orogen. These changes involved translation along the margin prior to the mid-Cretaceous associated with terrane transport followed by a shift to convergent plate motion at around 115–110 Ma. The crustal rocks of the orogen responded to these plate motions first by forming an intra-arc basin along southeastern Alaska and into northernmost British Columbia during and shortly after terrane accretion, followed by a thick-skinned thrust belt that deformed the Late Jurassic to mid-Cretaceous sedimentary and volcanic rocks deposited in that basin as well as older rocks to the east. Thrusting was accompanied by formation of a 110–83-Ma batholith.

Relative plate motion changed to transpression in the Late Cretaceous. Rocks in the hot middle crust of the eastern part of the orogen responded to the changes in plate motion by a gradual change from formation of large-scale recumbent thrust nappes

resulting from orogen normal compressional deformation to upright folding accompanied by extension on low-angle ductile shear zones to predominantly extensional deformation at a low angle to the long dimension of the orogen. This Paleogene extension led to crustal thinning and uplift of mid-crustal rocks across the orogen. Increasingly oblique subduction between ca. 85 and 50 Ma probably caused this extension. Arc magmatism between 75 and 52 Ma resulted in the emplacement of a Paleogene batholithic complex currently separated from the pre-90-Ma plutons of the mid-Cretaceous batholith on the west by the crustal-scale Coast shear zone. We speculate that the pervasive nature and relatively long duration of this deformation resulted from enhanced crustal ductility due to the combined effects of emplacement of large volumes of magma and crustal thermal weakening as a consequence of the magma emplacement. This weakening produced strain localization, especially as the crust began to cool during uplift.

After ca. 55 Ma, plate motion changed back to translation along the margin. Likely related to this change was foundering of the subducting slab when the spreading center between the Pacific Ocean plate and the oceanic plate(s) to the east (Resurrection/Kula) approached and/or reached the continental margin (Haeussler *et al.*, 2003). Formation of a slab-window as a result of this detachment and final subduction of the oceanic plate probably resulted in the emplacement of basaltic magma under the orogen producing the large volume of melting in the overlying crust starting at ca. 51 Ma. Intervals of transtensional motion on the dextral transform plate boundary led to orogen-normal extension by block tilting; the extension gave rise to rift related magmatic activity across the orogen through the Tertiary. Much of this interpretation can be extended north along the orogen to Juneau. To the south, the differences in history that become greater southward may reflect termination of the Alexander terrane crustal block west of the orogen in that direction.

There has been much discussion of the interpretation of structural observations in various parts of the orogen discussed here with apparently conflicting conclusions as to large-scale crustal displacements along the western side of North America. We suggest that many of these conflicts can be resolved by acknowledging the complexities involved in formation of the orogen. These include the change from terrane accretion by margin-parallel translation to formation of a convergent and generally thickening ductile orogenic crust in turn followed by extension and accompanied by significant crustal thinning. This evolutionary history has led to partitioned deformation with locally opposing senses of displacement. Care must be taken in scale of observations as differences in details may lead to erroneous interpretations unless they are viewed in the context of the overall orogen evolution in both space and time.

ACKNOWLEDGMENTS

This work was funded by NSF grants EAR 92-18489, EAR-9527395, and EAR-0207586 to M.L. Crawford and NSF grant

EAR-0309885 to George Gehrels. Over many years numerous colleagues have assisted with fieldwork and with discussions of the results; these contributed significantly to our research and our analysis and understanding of the features observed. We appreciate reviews by Harold Stowell and an anonymous individual as well as the encouragement and persistence of the editors of this volume.

REFERENCES CITED

- Abraham, A.C., Francis, D., and Polvé, M., 2005, Origin of Recent alkaline lavas by lithospheric thinning beneath the northern Canadian Cordillera: *Canadian Journal of Earth Sciences*, v. 42, p. 1073–1095, doi: 10.1139/e04-092.
- Aleinikoff, J.N., Schenck, W.S., Plank, M.O., Srogi, L., Fanning, C.M., Kamo, S.L., and Bosbyshell, H., 2006, Deciphering igneous and metamorphic events in high-grade rocks of the Wilmington Complex, Delaware: Morphology, cathodoluminescence and backscattered electron zoning, and SHRIMP U-Pb geochronology of zircon and monazite: *Geological Society of America Bulletin*, v. 118, p. 39–64, doi: 10.1130/B25659.1.
- Andronicos, C.L., Hollister, L.S., Davidson, C., and Chardon, D., 1999, Kinematics and tectonic significance of transpressive structures within the Coast Plutonic Complex, British Columbia: *Journal of Structural Geology*, v. 21, p. 229–243, doi: 10.1016/S0191-8141(98)00117-5.
- Andronicos, C.L., Rusmore, M.E., Chardon, D.H., Hollister, L.S., Davidson, C., and Woodsworth, G.J., 2000, Eocene crustal extension within the Coast Plutonic Complex, British Columbia: *Geological Society of America Abstracts with Programs*, v. 32, no. 6, p. 2.
- Andronicos, C.L., Chardon, D., Hollister, L.S., Gehrels, G.E., and Woodsworth, G.J., 2003, Strain partitioning in an obliquely convergent orogen, plutonism, and synorogenic collapse: Coast Mountains Batholith, British Columbia, Canada: *Tectonics*, v. 22, p. 1012, doi: 10.1029/2001TC001312.
- Arth, J.G., 1994, Isotopic composition of the igneous rocks of Alaska, *in* Plafker, G., and Berg, H.C., eds., *The Geology of Alaska: Boulder, Colorado*, Geological Society of America, *Geology of North America*, vol. G-1, p. 781–795.
- Arth, J.G., Barker, F., and Stern, T.W., 1988, Coast batholith and Taku plutons near Ketchikan, Alaska; petrography, geochronology, geochemistry, and isotopic character: *American Journal of Science*, v. 288-A, p. 461–489.
- Atwater, T., 1989, Plate tectonic history of the northeast Pacific and western North America, *in* Winterer, E.L., Hussong, D.M., and Decker, R.W., eds., *The eastern Pacific Ocean and Hawaii: Boulder, Colorado*, Geological Society of America, *Geology of North America*, v. N, p. 21–72.
- Barker, F., and Arth, J.G., 1984, Preliminary results, Central Gneiss Complex of the Coast Range Batholith, southeastern Alaska; the roots of a high-K, calc-alkaline arc?: *Physics of the Earth and Planetary Interiors*, v. 35, p. 191–198, doi: 10.1016/0031-9201(84)90042-6.
- Berg, H.C., 1973, *Geology of Gravina Island, Alaska*: U.S. Geological Survey Bulletin 1373, 41 p.
- Berg, H.C., Jones, D.L., and Richter, D.H., 1972, Gravina-Nutzotin belt—Tectonic significance of an upper Mesozoic sedimentary and volcanic sequence in southern and southeastern Alaska: U.S. Geological Survey Professional Paper 800-D, p. D1–D24.
- Berg, H.C., Elliott, R.L., and Koch, D., 1988, Geologic map of the Ketchikan and Prince Rupert quadrangles, southeastern Alaska: U.S. Geological Survey Miscellaneous Investigations Series I-1807, 1 sheet, scale 1:250,000 with 27 p. text.
- Boghossian, N.D., and Gehrels, G.E., 2000, Nd isotopic signature of metasedimentary pendants in the Coast Mountains between Prince Rupert and Bella Coola, British Columbia, *in* Stowell, H.H., and McClelland, W.C., eds., *Tectonics of the Coast Mountains, southeastern Alaska and British Columbia*: Geological Society of America Special Paper 343, p. 77–87.
- Brew, D.A., and Ford, A.B., 1978, Megalineament in southeastern Alaska marks southwest edge of Coast Range batholithic complex: *Canadian Journal of Earth Sciences*, v. 15, p. 1763–1772.
- Brew, D.A., and Ford, A.B., 1981, The Coast Plutonic Complex sill, southeastern Alaska, *in* Albert, N.R., and Hudson, T., eds., *U.S. Geological Survey in Alaska; accomplishments during 1979*: U.S. Geological Survey Circular C823-B, p. 96–99.

- Butler, R.F., Gehrels, G.E., Crawford, M.L., and Crawford, W.A., 2001a, Paleomagnetism of the Quotton plutonic complex in the Coast Mountains of British Columbia and southeastern Alaska: Evidence for tilting during uplift: *Canadian Journal of Earth Sciences*, v. 38, p. 1367–1384, doi: 10.1139/cjes-38-9-1367.
- Butler, R.F., Gehrels, G.E., and Kodama, K.P., 2001b, A moderate translation alternative to the Baja British Columbia hypothesis: *GSA Today*, v. 11, no. 6, p. 4–10.
- Butler, R.F., Gehrels, G.E., Baldwin, S.L., and Davidson, C., 2002, Paleomagnetism and geochronology of the Ecstall pluton in the Coast Mountains of British Columbia; evidence for local deformation rather than large-scale transport: *Journal of Geophysical Research*, v. 107 (B1), 13 p., doi: 10.1029/2001JB000270.
- Butzer, C., Butler, R.F., Gehrels, G.E., and Davidson, C., O'Connell, K., and Crawford, M.L., 2004, Neogene tilting of crustal panels near Wrangell, Alaska: *Geology*, v. 32, p. 1061–1064.
- Cembrano, J., Schermer, E., Lavenu, A., and Sanhueza, A., 2000, Contrasting nature of deformation along an intra-arc shear zone, the Liquiñe-Ofqui fault zone, southern Chilean Andes: *Tectonophysics*, v. 319, p. 129–149, doi: 10.1016/S0040-1951(99)00321-2.
- Cembrano, J., Lavenu, A., Reynolds, P., Arancibia, G., Lopez, G., and Sanhueza, A., 2002, Late Cenozoic transpressional ductile deformation north of the Nazca–South America–Antarctica triple junction: *Tectonophysics*, v. 354, p. 289–314, doi: 10.1016/S0040-1951(02)00388-8.
- Chardon, D., 2003, Strain partitioning and batholith emplacement at the root of a transpressive magmatic arc: *Journal of Structural Geology*, v. 25, p. 91–107, doi: 10.1016/S0191-8141(02)00015-9.
- Chardon, D., Andronicos, C.L., and Hollister, L.S., 1999, Large-scale transpressive shear zone patterns and displacements within magmatic arcs; the Coast Plutonic Complex, British Columbia: *Tectonics*, v. 18, p. 278–292, doi: 10.1029/1998TC900035.
- Christensen, N.I., and Mooney, W.D., 1995, Seismic velocity structure and composition of the continental crust: A global view: *Journal of Geophysical Research*, v. 100, p. 9761–9788, doi: 10.1029/95JB00259.
- Cohen, H.A., and Lundberg, N., 1993, Detrital record of the Gravina arc, southeastern Alaska: Petrology and provenance of Seymour Canal Formation sandstones: *Geological Society of America Bulletin*, v. 105, p. 1400–1414, doi: 10.1130/0016-7606(1993)105<1400:DROTGA>2.3.CO;2.
- Coney, P.J., Jones, D.L., and Monger, J.W.H., 1980, Cordilleran suspect terranes: *Nature*, v. 288, p. 329–333, doi: 10.1038/288329a0.
- Cook, F.A., and Erdmer, P., 2005, An 1800-km cross section of the lithosphere through the northwestern North American plate: Lessons from 4.0 billion years of Earth's history: *Canadian Journal of Earth Sciences*, v. 42, p. 1295–1311, doi: 10.1139/e04-106.
- Cook, R.D., and Crawford, M.L., 1994, Exhumation and tilting of the western metamorphic belt of the Coast orogen in southeastern Alaska: *Tectonics*, v. 13, p. 528–537, doi: 10.1029/93TC03152.
- Cook, R.D., Crawford, M.L., Omar, G.I., and Crawford, W.A., 1991, Magmatism and deformation, southern Revillagigedo Island, southeastern Alaska: *Geological Society of America Bulletin*, v. 103, p. 829–841, doi: 10.1130/0016-7606(1991)103<0829:MADSRI>2.3.CO;2.
- Cowan, D.S., Brandon, M.T., and Garver, J.I., 1997, Geologic tests of hypotheses for large coastwise displacement—A critique illustrated by the Baja British Columbia controversy: *American Journal of Science*, v. 297, p. 117–173.
- Crawford, M.L., and Crawford, W.A., 1991, Magma emplacement in a convergent tectonic orogen, southern Revillagigedo Island, southeastern Alaska: *Canadian Journal of Earth Sciences*, v. 28, p. 929–936.
- Crawford, M.L., and Hollister, L.S., 1982, Contrast of metamorphic and structural histories across the Work Channel lineament, Coast Plutonic Complex, British Columbia: *Journal of Geophysical Research*, v. 87, p. 3849–3860, doi: 10.1029/JB0871B05p03849.
- Crawford, M.L., Hollister, L.S., and Woodsworth, G.J., 1987, Crustal deformation and metamorphism across a terrane boundary, Coast Plutonic Complex, British Columbia: *Tectonics*, v. 6, p. 343–361, doi: 10.1029/TC006i003p00343.
- Crawford, M.L., Klepeis, K.A., Gehrels, G.E., and Isachsen, C., 1999, Batholith emplacement at mid-crustal levels and its exhumation within an obliquely convergent margin: *Tectonophysics*, v. 312, p. 57–78, doi: 10.1016/S0040-1951(99)00170-5.
- Crawford, M.L., Crawford, W.A., and Gehrels, G.E., 2000, Terrane assembly and structural relationships in the eastern Prince Rupert quadrangle, British Columbia, in Stowell, H.H., and McClelland, W.C., eds., *Tectonics of the Coast Mountains, Southeastern Alaska and British Columbia*: Geological Society of America Special Paper 343, p. 1–21.
- Crawford, M.L., Lindline, J., Crawford, W.A., and Sinha, A.K., 2002, Syntectonic tonalite magma emplacement during crustal thickening, the Bell Island Pluton, SE Alaska: *Geological Society of America Abstracts with Programs*, v. 34, no. 6, p. 44.
- Crawford, M.L., Crawford, W.A., and Lindline, J., 2005, 105 million years of igneous activity, Wrangell, Alaska, to Prince Rupert, British Columbia: *Canadian Journal of Earth Sciences*, v. 42, p. 1097–1116, doi: 10.1139/e05-022.
- Crawford, W.A., Crawford, M.L., and Sinha, K.A., 1995, Evolutionary paths of members of the late Cenozoic alkaline olivine basalt family of Southeastern Alaska: *Geological Association of Canada Annual Meeting Program with Abstracts*, v. 20, p. 21.
- Dehler, S.A., Keen, C.E., and Rohr, K.M.M., 1997, Tectonic and thermal evolution of Queen Charlotte Basin: Lithospheric deformation and subsidence models: *Basin Research*, v. 9, p. 243–261, doi: 10.1046/j.1365-2117.1997.00043.x.
- Dempster, T.J., and Persano, C., 2006, Low-temperature thermochronology; resolving geotherm shapes or denudation histories?: *Geology*, v. 34, p. 73–76, doi: 10.1130/G21980.1.
- Douglas, B.J., 1986, Deformational history of an outlier of metasedimentary rocks, Coast Plutonic Complex, British Columbia, Canada: *Canadian Journal of Earth Sciences*, v. 23, p. 813–826.
- Douglass, S.L., Webster, J.H., Burrell, P.D., Lanphere, M.A., and Brew, D.A., 1989, Major-element chemistry, radiometric ages, and locations of samples from the Petersburg and parts of the Port Alexander and Sumdum quadrangles, southeastern Alaska: *U.S. Geological Survey Open-File Report 89-0527*, 66 p.
- Edwards, B.R., and Russell, J.K., 2000, Distribution, nature, and origin of Neogene–Quaternary magmatism in the northern Cordilleran volcanic province, Canada: *Geological Society of America Bulletin*, v. 112, p. 1280–1295, doi: 10.1130/0016-7606(2000)112<1280:DNAOON>2.3.CO;2.
- Elliott, R.L., Koch, R.D., and Robinson, S.W., 1981, Age of basalt flows in the Blue River Valley, Bradfield Canal quadrangle: *U.S. Geological Survey Circular 823-B*, p. 115–116.
- Engelbreton, D.C., Cox, A., and Gordon, R.G., 1985, Relative motions between oceanic and continental plates in the Pacific Basin: *Geological Society of America Special Paper 206*, 59 p.
- Evenchick, C.A., 1991, Geometry, evolution and tectonic framework of the Skeena fold belt, north central British Columbia: *Tectonics*, v. 10, p. 527–546, doi: 10.1029/90TC02680.
- Evenchick, C.A., 2001, Northeast-trending folds in the western Skeena fold belt, northern Canadian Cordillera; a record of Early Cretaceous sinistral plate convergence, in White, J.C., Bleeker, W., and Elliott, C., eds., *Evolution of structures in deforming rocks, in honour of Paul F. Williams*: *Journal of Structural Geology*, v. 23, p. 1123–1140.
- Evenchick, C.A., and McNicoll, V.J., 1993, U-Pb ages for Late Cretaceous and early Tertiary plutons in the Skeena fold belt, north-central British Columbia, in Radiogenic age and isotopic studies: Ottawa, Ontario, Geological Survey of Canada Report 7, Geological Survey of Canada Paper 93-2, p. 99–106.
- Evenchick, C.A., Crawford, M.L., McNicoll, V.J., Currie, L.D., and O'Sullivan, P.B., 1999, Early Miocene or younger normal faults and other Tertiary structures in west Nass River map area, northwest British Columbia, and adjacent parts of Alaska, in *Current Research, part A*: Ottawa, Ontario, Geological Survey of Canada Paper 99-1A, p. 1–11.
- Farley, K.A., Rusmore, M.E., and Bogue, S.W., 2001, Post–10 Ma uplift and exhumation of the northern Coast Mountains, British Columbia: *Geology*, v. 29, p. 99–102, doi: 10.1130/0091-7613(2001)029<0099:PMUAE0>2.0.CO;2.
- Gareau, S.A., 1991, The Scotia-Quaal metamorphic belt; a distinct assemblage with pre-early Late Cretaceous deformational and metamorphic history, Coast Plutonic Complex, British Columbia: *Canadian Journal of Earth Sciences*, v. 28, p. 870–880.
- Gareau, S.A., and Woodsworth, G.J., 2000, Yukon-Tanana terrane in the Scotia-Quaal Belt, Coast Plutonic Complex, central-western British Columbia, in Stowell, H.H., and McClelland, W.C., eds., *Tectonics of the Coast Mountains, Southeastern Alaska and British Columbia*: Geological Society of America Special Paper 343, p. 23–43.

- Gareau, S.A., Woodsworth, G.J., and Friedman, R.M., 1997a, Late Cretaceous to Eocene plutonism and deformation near Terrace, British Columbia: Geological Society of America Abstracts with Programs, v. 29, no. 6, p. 84.
- Gareau, S.A., Friedman, R.M., Woodsworth, G.J., and Childe, F., 1997b, U-Pb dates from the northeastern quadrant of Terrace map area, west-central British Columbia: Ottawa, Ontario, Current Research Part A, Geological Survey of Canada Paper 1997-1A, p. 31–40.
- Gehrels, G.E., 2000, Reconnaissance geology and U-Pb geochronology of the western flank of the Coast Mountains between Juneau and Skagway, southeastern Alaska, in Stowell, H.H., and McClelland, W.C., eds., Tectonics of the Coast Mountains, Southeastern Alaska and British Columbia: Geological Society of America Special Paper 343, p. 213–233.
- Gehrels, G.E., 2001, Geology of the Chatham Sound region, southeast Alaska and coastal British Columbia: Canadian Journal of Earth Sciences, v. 38, p. 1579–1599, doi: 10.1139/cjes-38-11-1579.
- Gehrels, G.E., and Berg, H.C., 1992, Geologic map of southeastern Alaska: U.S. Geological Survey Miscellaneous Investigations Map I-1867, scale 1:600,000, 1 sheet.
- Gehrels, G.E., and Boghossian, N.D., 2000, Reconnaissance geology and U-Pb geochronology of the west flank of the Coast Mountains between Bella Coola and Prince Rupert, coastal British Columbia, in Stowell, H.H., and McClelland, W.C., eds., Tectonics of the Coast Mountains, Southeastern Alaska and British Columbia: Geological Society of America Special Paper 343, p. 61–75.
- Gehrels, G.E., and Kapp, P.A., 1998, Detrital zircon geochronology and regional correlation of metasedimentary rocks in the Coast Mountains, southeastern Alaska: Canadian Journal of Earth Sciences, v. 35, p. 269–279, doi: 10.1139/cjes-35-3-269.
- Gehrels, G.E., and Saleeby, J.B., 1987, Geologic framework, tectonic evolution, and displacement history of the Alexander terrane: Tectonics, v. 6, p. 151–173, doi: 10.1029/TC006i002p00151.
- Gehrels, G.E., McClelland, W.C., Samson, S.D., Patchett, P.J., and Jackson, J.L., 1990, Ancient continental margin assemblage in the Coast Mountains, southeast Alaska and northwest Canada: Geology, v. 18, p. 208–211.
- Gehrels, G.E., McClelland, W.C., Samson, S.D., and Patchett, P.J., 1991a, U-Pb geochronology of Late Cretaceous and early Tertiary plutons in the northern Coast Mountains batholith: Canadian Journal of Earth Sciences, v. 28, p. 899–911.
- Gehrels, G.E., McClelland, W.C., Samson, S.D., and Patchett, P.J., 1991b, U-Pb geochronology of detrital zircons from a continental margin assemblage in the northern Coast Mountains, southeastern Alaska: Canadian Journal of Earth Sciences, v. 28, p. 1285–1300.
- Haeussler, P.J., Bradley, D.C., Wells, R.E., and Miller, M.L., 2003, Life and death of the Resurrection plate: Evidence for its existence and subduction in the northwestern Pacific in Paleocene-Eocene time: Geological Society of America Bulletin, v. 115, p. 867–880, doi: 10.1130/0016-7606(2003)115<0867:LADOTR>2.0.CO;2.
- Haggart, J.W., Woodsworth, G.J., and McNicoll, V.J., 2006, Uranium-lead geochronology of two intrusions in the southern Bowser Basin, British Columbia: Current Research, Ottawa, Ontario, Geological Survey of Canada Current Research 2006-F2, 6 p.
- Hammer, P.T.C., and Clowes, R.M., 2004, Accreted terranes of northwestern British Columbia, Canada: Lithospheric velocity structure and tectonics: Journal of Geophysical Research, v. 109, B06305, doi: 10.1029/2003JB002749.
- Hammer, P.T.C., Clowes, R.M., and Ellis, R.M., 2000, Crustal structure of N.W. British Columbia and S.E. Alaska from seismic wide-angle studies: Coast Plutonic Complex to Stikinia: Journal of Geophysical Research, v. 105, p. 7961–7981, doi: 10.1029/1999JB900378.
- Heah, T.S.T., 1990, Eastern margin of the Central Gneiss Complex in the Shames River area, Terrace, British Columbia: Current Research E, Ottawa, Ontario, Geological Survey of Canada Paper 90-1E, p. 159–169.
- Heah, T.S.T., 1991, Mesozoic ductile shear and Paleogene extension along the eastern margin of the Central Gneiss Complex, Coast Belt, Shames River area near Terrace, British Columbia [M.S. thesis]: Vancouver, University of British Columbia, 155 p.
- Hickson, C.J., 1991, The Masset Formation on Graham Island, Queen Charlotte Islands, British Columbia, in Woodsworth, G.J., ed., Evolution and hydrocarbon potential of the Queen Charlotte Basin, British Columbia: Ottawa, Ontario, Geological Survey of Canada Paper 90-10, p. 305–324.
- Hill, M.L., Woodsworth, G.J., and van der Heyden, P., 1985, The Coast Plutonic Complex near Terrace, B.C.; a metamorphosed western extension of Stikinia: Geological Society of America Abstracts with Programs, v. 17, no. 6, p. 362.
- Himmelberg, G.R., and Brew, D.A., 2004, Thermobarometric constraints on mid-Cretaceous to Late Cretaceous metamorphic events in the western metamorphic belt of the Coast Mountains complex, near Petersburg, southeastern Alaska: U.S. Geological Survey Professional Paper 1709-C, p. 1–18.
- Himmelberg, G.R., and Loney, R.A., 1995, Characteristics and petrogenesis of Alaskan-type ultramafic-mafic intrusions, southeastern Alaska: U.S. Geological Survey Professional Paper 1564, 47 p.
- Himmelberg, G.R., Haeussler, P.J., and Brew, D.A., 2004, Emplacement, rapid burial, and exhumation of 90-Ma plutons in Southeastern Alaska: Canadian Journal of Earth Sciences, v. 41, p. 87–102, doi: 10.1139/e03-087.
- Hollister, L.S., 1975, Granulite facies metamorphism in the Coast Range crystalline belt: Canadian Journal of Earth Sciences, v. 12, p. 1953–1955.
- Hollister, L.S., 1982, Metamorphic evidence for rapid (2 mm/yr) uplift of a portion of the Central Gneiss Complex, Coast Mountains, British Columbia: Canadian Mineralogist, v. 30, p. 319–332.
- Hollister, L.S., 1993, The role of melt in the uplift and exhumation of orogenic belts: Chemical Geology, v. 108, p. 31–48, doi: 10.1016/0009-2541(93)90316-B.
- Hollister, L.S., and Andronicos, C., 1997, A candidate for the Baja British Columbia fault system in the Coast Plutonic Complex: GSA Today, v. 7, no. 11, p. 1–7.
- Hollister, L.S., and Andronicos, C., 2000, The Central Gneiss Complex, Coast Mountains, British Columbia, in Stowell, H.H., and McClelland, W.C., eds., Tectonics of the Coast Mountains, Southeastern Alaska and British Columbia: Geological Society of America Special Paper 343, p. 45–59.
- Hollister, L.S., and Crawford, M.L., 1986, Melt-enhanced deformation—A major tectonic process: Geology, v. 14, p. 558–561, doi: 10.1130/0091-7613(1986)14<558:MDAMTP>2.0.CO;2.
- Hollister, L.S., and Crawford, M.L., 1990, Crustal formation at depth during continental collision, in Salisbury, M.H., and Fountain, D.M., eds., Exposed Cross-Sections of the Continental Crust: Dordrecht, the Netherlands, Kluwer Academic Publishers, p. 215–226.
- Hudson, T., Smith, J.G., and Elliott, R.L., 1979, Petrology, composition, and age of intrusive rocks associated with the Quartz Hill molybdenite deposit, southeastern Alaska: Canadian Journal of Earth Sciences, v. 16, p. 1805–1822.
- Hutchison, W.W., 1982, Geology of the Prince-Rupert-Skeena map area, British Columbia: Geological Survey of Canada Memoir 394, 116 p.
- Hyndman, R.D., and Hamilton, T.S., 1993, Queen Charlotte area Cenozoic tectonics and volcanism and their association with relative plate motions along the northeastern Pacific margin: Journal of Geophysical Research, v. 98, p. 14,257–14,277, doi: 10.1029/93JB00777.
- Hyndman, R.D., Flück, P., Mazzotti, S., Lewis, T.J., Ristau, J., and Leonard, L., 2005, Constraints on current tectonics of the northern Canadian Cordillera: Canadian Journal of Earth Sciences, v. 42, p. 1117–1136, doi: 10.1139/e05-023.
- Ingram, G.M., and Hutton, D.H.W., 1994, The Great Tonalite Sill: Emplacement into a contractional shear zone and implications for Late Cretaceous to early Eocene tectonics in southeastern Alaska and British Columbia: Geological Society of America Bulletin, v. 106, p. 715–728, doi: 10.1130/0016-7606(1994)106<0715:TGTSEI>2.3.CO;2.
- Irving, E., Wynne, P.J., Thorkelson, D.J., and Schiarizza, P., 1996, Large (1000 to 4000 km) northward movements of tectonic domains in the northern Cordillera, 83 to 45 Ma: Journal of Geophysical Research, v. 101, p. 17,901–17,916, doi: 10.1029/96JB01181.
- Irving, E., Baker, J., Wynne, P.J., Hamilton, T.S., and Wingate, M.T.D., 2000, Evolution of the Queen Charlotte Basin; further paleomagnetic evidence of Tertiary extension and tilting, in Housen, B., Heller, F., and Mpodozis, C., eds., Advances in paleomagnetism and tectonics of active margins; in honor of retirement of Myrl E. Beck, Jr.: Tectonophysics, v. 326, p. 1–22.
- Jackson, J.L., Gehrels, G.E., and Patchett, P.J., 1991, Stratigraphic and isotopic link between the northern Stikine terrane and an ancient continental margin assemblage, Canadian Cordillera: Geology, v. 19, p. 1177–1180.
- Kapp, P.A., and Gehrels, G.E., 1998, Detrital zircon constraints on the tectonic evolution of the Gravina belt, southeastern Alaska: Canadian Journal of Earth Sciences, v. 35, p. 253–268, doi: 10.1139/cjes-35-3-253.

- Kenah, C., and Hollister, L.S., 1983, Anatexis in the Central Gneiss Complex, British Columbia, in Atherton, M.P., and Gribble, C.D., eds., *Migmatites, melting and metamorphism*: Nantwich, UK, Shiva Publishing, p. 142–162.
- Klepeis, K.A., and Crawford, M.L., 1999, High-temperature arc-parallel normal faulting and transtension at the roots of an obliquely convergent orogen: *Geology*, v. 27, p. 7–10, doi: 10.1130/0091-7613(1999)027<0007:HTAPNF>2.3.CO;2.
- Klepeis, K.A., Crawford, M.L., and Gehrels, G., 1998, Strain field patterns and structural history of the high temperature Coast shear zone near Portland Canal, southeast Alaska and British Columbia: *Journal of Structural Geology*, v. 20, p. 883–904, doi: 10.1016/S0191-8141(98)00020-0.
- Klepeis, K.A., Clarke, G.L., Gehrels, G.E., and Vervoort, J.D., 2004, Processes controlling vertical coupling and decoupling between the upper and lower crust of orogens; results from Fiordland, New Zealand: *Journal of Structural Geology*, v. 26, p. 765–791, doi: 10.1016/j.jsg.2003.08.012.
- Lanphere, M.A., 1968, Sr-Rb-K and Sr isotopic relationships in ultramafic rocks, southeastern Alaska: *Earth and Planetary Science Letters*, v. 4, p. 185–190, doi: 10.1016/0012-821X(68)90033-2.
- Lewis, T.J., Hyndman, R.D., and Flück, P., 2003, Heat flow, heat generation, and crustal temperatures in the northern Canadian Cordillera: Thermal control of tectonics: *Journal of Geophysical Research*, v. 108 (B6, 2316): doi: 10.1029/2002JB002090.
- Lindline, J., 1997, Magmatic history of the southeastern Petersburg quadrangle, Alaska [Ph.D. thesis]: Bryn Mawr, Pennsylvania, Bryn Mawr College, 272 p.
- Lindline, J., and Crawford, M.L., 2005, Resolving mechanisms of mid-Cretaceous orogeny around central Admiralty-Revillagigedo belt granitoids, Wrangell, Alaska: *Geological Society of America Abstracts with Programs*, v. 37, no. 7, p. 81.
- Lindline, J., Crawford, W.A., Crawford, M.L., and Omar, G.I., 2000, Post-accretion magmatism within the Kuiu-Etolin igneous belt, southeastern Alaska: *Canadian Mineralogist*, v. 38, p. 951–974, doi: 10.2113/gscanmin.38.4.951.
- Lindline, J., Crawford, W.A., and Crawford, M.L., 2004, A bimodal volcanic-plutonic system, the Zarembo Island extrusive suite and the Burnett Inlet intrusive complex: *Canadian Journal of Earth Sciences*, v. 41, p. 355–375, doi: 10.1139/e04-009.
- Lonsdale, P.F., 1988, Paleogene history of the Kula plate; offshore evidence and onshore implications: *Geological Society of America Bulletin*, v. 100, p. 733–754, doi: 10.1130/0016-7606(1988)100<0733:PHOTKP>2.3.CO;2.
- Ludwig, K.R., 2003, *Isoplot 3.00*: Berkeley Geochronology Center, Special Publication 4, 70 p.
- Madsen, J.K., Thorkelson, D.J., Friedman, R.M., and Marshall, D.D., 2006, Cenozoic to Recent plate configurations in the Pacific Basin: Ridge subduction and slab window magmatism in western North America: *Geosphere*, v. 2, p. 11–34, doi: 10.1130/GES00020.1.
- Mansfield, M.L., and Andronicos, C.L., 2004, Metamorphic pressure-temperature conditions during transpression within the roots of a transpressive magmatic arc: *Geological Society of America Abstracts with Programs*, v. 36, no. 5, p. 343–344.
- Marcotte, S.B., Klepeis, K.A., Clarke, G.L., Gehrels, G.E., and Hollis, J.A., 2005, Intra-arc transpression in the lower crust and its relationship to magmatism in a Mesozoic magmatic arc: *Tectonophysics*, v. 407, p. 135–163, doi: 10.1016/j.tecto.2005.07.007.
- McClelland, W.C., and Gehrels, G.E., 1990, Geology of the Duncan Canal shear zone: Evidence for Early-Middle Jurassic deformation of the Alexander terrane, southeastern Alaska: *Geological Society of America Bulletin*, v. 102, p. 1378–1392, doi: 10.1130/0016-7606(1990)102<1378:GOTDCS>2.3.CO;2.
- McClelland, W.C., and Mattinson, J.M., 2000, Cretaceous-Tertiary evolution of the western Coast Mountains, central southeastern Alaska, in Stowell, H.H., and McClelland, W.C., eds., *Tectonics of the Coast Mountains, Southeastern Alaska and British Columbia*: Geological Society of America Special Paper 343, p. 159–182.
- McClelland, W.C., Anovitz, L.M., and Gehrels, G.E., 1991, Thermobarometric constraints on the structural evolution of the Coast Mountains batholith, central southeastern Alaska: *Canadian Journal of Earth Sciences*, v. 28, p. 912–928.
- McClelland, W.C., Gehrels, G.E., Samson, S.D., and Patchett, P.J., 1992a, Protonolith relations of the Gravina Belt and Yukon-Tanana Terrane in central southeastern Alaska: *The Journal of Geology*, v. 100, p. 107–123.
- McClelland, W.C., Gehrels, G.E., Samson, S.D., and Patchett, P.J., 1992b, Structural and geochronologic relations along the western flank of the Coast Mountains batholith: Stikine River to Cape Fanshaw, central SE Alaska: *Journal of Structural Geology*, v. 14, p. 475–489, doi: 10.1016/0191-8141(92)90107-8.
- McClelland, W.C., Gehrels, G.E., and Saleeby, J.B., 1992c, Upper Jurassic-lower Cretaceous basinal strata along the Cordilleran margin: Implications for the accretionary history of the Alexander-Wrangellia-Peninsular terrane: *Tectonics*, v. 11, p. 823–835, doi: 10.1029/92TC00241.
- Miller, M.L., Bradley, D.C., Bundtzen, T.K., and McClelland, W., 2002, Late Cretaceous through Cenozoic strike-slip tectonics of southwestern Alaska: *The Journal of Geology*, v. 110, p. 247–270, doi: 10.1086/339531.
- Monger, J.W.H., Price, R.A., and Tempelman-Kluit, J.D., 1982, Tectonic accretion and the origin of the two major metamorphic and plutonic belts in the Canadian Cordillera: *Geology*, v. 10, p. 70–75, doi: 10.1130/0091-7613(1982)10<70:TAATOO>2.0.CO;2.
- Mooney, W.D., Laske, G., and Masters, T.G., 1998, CRUST 5.1: A global crustal model at 5° × 5°: *Journal of Geophysical Research*, v. 103, p. 727–747, doi: 10.1029/97JB02122.
- Morozov, I.B., Smithson, S.B., Hollister, L.S., and Diebold, J.B., 1998, Wide-angle seismic imaging across accreted terranes, southeastern Alaska and western British Columbia: *Tectonophysics*, v. 299, p. 281–296, doi: 10.1016/S0040-1951(98)00208-X.
- Morozov, I.B., Smithson, S.B., Chen, J., and Hollister, L.S., 2001, Generation of new continental crust and terrane accretion in southeastern Alaska and western British Columbia from P- and S-wave wide-angle seismic data (ACCURETE): *Tectonophysics*, v. 341, p. 49–67, doi: 10.1016/S0040-1951(01)00190-1.
- Morozov, I.B., Christensen, N.I., Smithson, S.B., and Hollister, L.S., 2003, Seismic and laboratory constraints on crustal formation in a former continental arc (ACCURETE, southeastern Alaska and western British Columbia): *Journal of Geophysical Research*, v. 108, doi: 10.1029/2001JB001740.
- Mortimer, N., Tulloch, A.J., Spark, R.N., Walker, N.W., Ladley, E., Allibone, A., and Kimbrough, D.L., 1999, Overview of the Median batholith, New Zealand; a new interpretation of the geology of the Median Tectonic Zone and adjacent rocks: *Journal of African Earth Sciences*, v. 29, p. 257–268, doi: 10.1016/S0899-5362(99)00095-0.
- Murphy, M.A., 2002, Orogen-parallel extension as expressed by the development of gneiss domes; an example from the Himalaya: *Geological Society of America Abstracts with Programs*, v. 34, no. 6, p. 108.
- Nokleberg, W.J., Jones, D.L., and Silberling, N.J., 1985, Origin and tectonic evolution of the Maclaren and Wrangellia terranes, eastern Alaska Range, Alaska: *Geological Society of America Bulletin*, v. 96, p. 1251–1270, doi: 10.1130/0016-7606(1985)96<1251:OATEOT>2.0.CO;2.
- O’Connell, K., 2004, Ages, geochemistry, and field relationships of mafic dikes along the Wrangell transect, southeast Alaska [Senior paper]: Northfield, Minnesota, Carleton College, 37 p.
- Paterson, S.R., Miller, R.B., Alsleben, H., Whitney, D.L., Valley, P.M., and Hurlow, H., 2004, Driving mechanisms for >40 km of exhumation during contraction and extension in a continental arc, Cascades core, Washington: *Tectonics*, v. 23, doi: 10.1029/2002TC001440.
- Rohr, K.M.M., and Dietrich, J.R., 1992, Strike-slip tectonics and development of the Tertiary Queen Charlotte Basin, offshore western Canada: Evidence from seismic reflection data: *Basin Research*, v. 4, p. 1–19, doi: 10.1111/j.1365-2117.1992.tb00039.x.
- Rubin, C.M., and Saleeby, J.B., 1991, The Gravina sequence: Remnants of a mid-Mesozoic oceanic arc in southern southeast Alaska: *Journal of Geophysical Research*, v. 96, p. 14,551–14,568, doi: 10.1029/91JB00591.
- Rubin, C.M., and Saleeby, J.B., 1992, Tectonic history of the eastern edge of the Alexander terrane, southeast Alaska: *Tectonics*, v. 11, p. 586–602, doi: 10.1029/91TC02182.
- Rubin, C.M., and Saleeby, J.B., 2000, U-Pb geochronology of mid-Cretaceous and Tertiary plutons along the western edge of the Coast Mountains, in Stowell, H.H., and McClelland, W.C., eds., *Tectonics of the Coast Mountains, Southeastern Alaska and British Columbia*: Geological Society of America Special Paper 343, p. 145–157.
- Rubin, C.M., Saleeby, J.B., Cowan, D.S., Brandon, M.T., and McGroder, M.F., 1990, Regionally extensive mid-Cretaceous west-vergent thrust system

- in the northwestern Cordillera: Implications for continental margin tectonism: *Geology*, v. 18, p. 276–280, doi: 10.1130/0091-7613(1990)018<0276:REMCWV>2.3.CO;2.
- Rusmore, M.E., and Woodsworth, G.J., 1991, Coast Plutonic Complex: A mid-Cretaceous contractional orogen: *Geology*, v. 19, p. 941–944, doi: 10.1130/0091-7613(1991)019<0941:CPCAMC>2.3.CO;2.
- Rusmore, M.E., Bogue, S.W., Farley, K.A., and Dodson, K.E., 2000a, Cenozoic deformation and exhumation, Douglas Channel, Coast Mountains, British Columbia: *Geological Society of America Abstracts with Programs*, v. 32, no. 6, p. 65–66.
- Rusmore, M.E., Woodsworth, G.J., and Gehrels, G.E., 2000b, Late Cretaceous evolution of the eastern Coast Mountains, Bella Coola, British Columbia, in Stowell, H.H., and McClelland, W.C., eds., *Tectonics of the Coast Mountains, Southeastern Alaska and British Columbia*: Geological Society of America Special Paper 343, p. 89–105.
- Rusmore, M.E., Gehrels, G.E., and Woodsworth, G.J., 2001, Southern continuation of the Coast shear zone and Paleocene strain partitioning in British Columbia-southeast Alaska: *Geological Society of America Bulletin*, v. 113, p. 961–975, doi: 10.1130/0016-7606(2001)113<0961:SCOTCS>2.0.CO;2.
- Rusmore, M.E., Woodsworth, G.J., and Gehrels, G.E., 2005, Two-stage exhumation of midcrustal arc rocks, Coast Mountains, British Columbia: *Tectonics*, v. 24, p. TC5013, doi: 10.1029/2004TC001750.
- Saleeby, J.B., 1992, Age and tectonic setting of the Duke Island intrusive complex, southern southeast Alaska: *Canadian Journal of Earth Sciences*, v. 29, p. 506–522.
- Saleeby, J.B., 2000, Geochronologic investigations along the Alexander-Taku terrane boundary, southern Revillagigedo Island to Cape Fox areas, southeast Alaska, in Stowell, H.H., and McClelland, W.C., eds., *Tectonics of the Coast Mountains, Southeastern Alaska and British Columbia*: Geological Society of America Special Paper 343, p. 107–143.
- Samson, S.D., McClelland, W.C., Patchett, P.J., Gehrels, G.E., and Anderson, R.G., 1989, Evidence from neodymium isotopes for mantle contributions to Phanerozoic crustal genesis in the Canadian Cordillera: *Nature*, v. 337, p. 705–709, doi: 10.1038/337705a0.
- Samson, S.D., Patchett, P.J., McClelland, W.C., and Gehrels, G.E., 1991a, Nd isotopic characterization of metamorphic rocks in the Coast Mountains, Alaskan and Canadian Cordillera; ancient crust bounded by juvenile terranes: *Tectonics*, v. 10, p. 770–780, doi: 10.1029/90TC02732.
- Samson, S.D., Patchett, P.J., McClelland, W.C., and Gehrels, G.E., 1991b, Nd and Sr isotopic constraints on the petrogenesis of the west side of the northern Coast Mountains batholith, Alaskan and Canadian Cordillera: *Canadian Journal of Earth Sciences*, v. 28, p. 939–946.
- Scott, J.M., and Cooper, A.F., 2006, Early Cretaceous extensional exhumation of the lower crust of a magmatic arc; evidence from the Mount Irene shear zone, Fiordland, New Zealand: *Tectonics*, v. 25, p. 3018, doi: 10.1029/2005TC001890.
- Selverstone, J., and Hollister, L.S., 1980, Cordierite-bearing granulites from the Coast Ranges, British Columbia: *P-T conditions of metamorphism*: *Canadian Mineralogist*, v. 18, p. 119–129.
- Sisson, V.B., 1985, Contact metamorphism and fluid evolution associated with the intrusion of the Ponder Pluton, Coast Plutonic Complex, British Columbia, Canada [Ph.D. thesis]: Princeton, New Jersey, Princeton University, 345 p.
- Smith, J.G., and Diggles, M.F., 1981, Potassium-argon determinations in the Ketchikan and Prince Rupert quadrangles, southeastern Alaska: U.S. Geological Survey Open-File Report 78-73N, 16 p.
- Souther, J.G., and Jessop, A.M., 1991, Dyke swarms in the Queen Charlotte Islands, British Columbia, and implications for hydrocarbon exploration, in Woodsworth, G.J., ed., *Evolution and hydrocarbon potential of the Queen Charlotte Basin, British Columbia*: Ottawa, Ontario, Geological Survey of Canada Paper 90-10, p. 465–487.
- Stacey, J.S., and Kramers, J.D., 1975, Approximation of terrestrial lead isotope evolution by a two-stage model: *Earth and Planetary Science Letters*, v. 26, p. 207–221, doi: 10.1016/0012-821X(75)90088-6.
- Stock, J., and Molnar, P., 1988, Uncertainties and implications of the Late Cretaceous and Tertiary position of North America relative to the Farallon, Kula, and Pacific plates: *Tectonics*, v. 7, p. 1339–1384, doi: 10.1029/TC007i006p01339.
- Stowell, H.H., and Crawford, M.L., 2000, Metamorphic history of the Coast Mountains orogen, western British Columbia and southeastern Alaska, in Stowell, H.H., and McClelland, W.C., eds., *Tectonics of the Coast Mountains, Southeastern Alaska and British Columbia*: Geological Society of America Special Paper 343, p. 257–283.
- Stowell, H.H., and Hooper, R.J., 1990, Structural development of the western metamorphic belt adjacent to the Coast Plutonic Complex, southeastern Alaska: Evidence from Holkham Bay: *Tectonics*, v. 9, p. 391–407, doi: 10.1029/TC009i003p00391.
- Sutherland-Brown, A., 1969, Aiyansh lava flow, British Columbia: *Canadian Journal of Earth Sciences*, v. 6, p. 1460–1468.
- Sutter, J.F., and Crawford, M.L., 1985, Timing of metamorphism and uplift in the vicinity of Prince Rupert, British Columbia and Ketchikan, Alaska: *Geological Society of America Abstracts with Programs*, v. 17, no. 6, p. 411.
- Symons, D.T.A., 1974, Age and tectonic implications of paleomagnetic results from plutons near Prince Rupert, British Columbia: *Journal of Geophysical Research*, v. 79, p. 2690–2697, doi: 10.1029/JB079i017p02690.
- Tarduno, J.A., Duncan, R.A., Scholl, D.W., Cottrell, R.D., Steinberber, B., Thordarson, T., Kerr-Bryan, C., Neal, C.R., Frey, F.A., Torii, M., and Carvallo, C., 2003, The Emperor Seamounts; southward motion of the Hawaiian Hotspot plume in Earth's mantle: *Science*, v. 301, p. 1064–1069, doi: 10.1126/science.1086442.
- Thomas, J.B., and Sinha, A.K., 1999, Field, geochemical, and isotopic evidence for magma mixing and assimilation and fractional crystallization processes in the Quottoon Igneous Complex, northwestern British Columbia and southeastern Alaska: *Canadian Journal of Earth Sciences*, v. 36, p. 819–831, doi: 10.1139/cjes-36-5-819.
- van der Heyden, P., 1992, A Middle Jurassic to Early Tertiary Andean-Sierran arc model for the Coast Belt of British Columbia: *Tectonics*, v. 11, p. 82–97, doi: 10.1029/91TC02183.
- Woodsworth, G.J., 1991, Neogene to Recent volcanism along the east side of Hecate Strait, British Columbia, in Woodsworth, G.J., ed., *Evolution and hydrocarbon potential of the Queen Charlotte Basin, British Columbia*: Ottawa, Ontario, Canada, Geological Survey of Canada Paper 90-10, p. 325–335.

Plutonism at different crustal levels: Insights from the ~5–40 km (paleodepth) North Cascades crustal section, Washington

Robert B. Miller*

Department of Geology, San José State University, San José, California 95192-0102, USA

Scott R. Paterson

Department of Earth Sciences, University of Southern California, Los Angeles, California 90089, USA

Jennifer P. Matzel†

Berkeley Geochronology Center, 2455 Ridge Road, Berkeley, California 94709, USA

ABSTRACT

The crystalline core of the North Cascades preserves a Cretaceous crustal section that facilitates evaluation of pluton construction, emplacement, geometry, composition, and deformation at widely variable crustal levels (~5–40-km paleodepth) in a thick (≥ 55 km) continental magmatic arc. The oldest and largest pulse of plutonism was focused between 96 and 89 Ma when fluxes were a minimum of 3.9×10^{-6} km³/yr/km of arc length, but the coincidence with regional crustal thickening and underthrusting of a cool outboard terrane resulted in relatively low mid- to deep-crustal temperatures for an arc. A second, smaller peak of magmatism at 78–71 Ma (minimum of 8.2×10^{-7} km³/yr/km of arc length) occurred during regional transpression. Tonalite dominates at all levels of the section. Intrusions range from large plutons to thin (<50 m) dispersed sheets encased in metamorphic rocks that record less focused magmatism. The percentage of igneous rocks increases systematically from shallow to middle to deep levels, from ~37% to 55% to 65% of the total rock volume. Unfocused magmas comprise much higher percentages (~19%) of the total plutonic rock at deep- and mid-crustal depths, but only ~1% at shallower levels, whereas the largest intrusions were emplaced into shallow crust. Plutons have a range of shapes, including: asymmetric wedges to funnels; subhorizontal tabular sheets; steep-sided, blade-shaped bodies with high aspect ratios in map view; and steep-sided, vertically extensive (≥ 8 km) bodies shaped like thick disks and/or hockey pucks. Sheeted intrusions and gently dipping tabular bodies are more common with depth. Some of these plutons fit the model that most intrusions are subhorizontal and tabular, but many do not, reflecting the complex changes in rock type and rheology in arc crust undergoing regional shortening. The steep-sheeted plutons partly represent magma transfer zones that fed the large shallow

*rmiller@geosun.sjsu.edu

†Current address: Physical and Life Sciences Directorate, Lawrence Livermore National Laboratory, Livermore, California 94550, USA.

Miller, R.B., Paterson, S.R., and Matzel, J.P., 2009, Plutonism at different crustal levels: Insights from the ~5–40 km (paleodepth) North Cascades crustal section, Washington, in Miller, R.B., and Snoke, A.W., eds., *Crustal Cross Sections from the Western North American Cordillera and Elsewhere: Implications for Tectonic and Petrologic Processes*: Geological Society of America Special Paper 456, p. 125–149, doi: 10.1130/2009.2456(05). For permission to copy, contact editing@geosociety.org. ©2009 The Geological Society of America. All rights reserved.

plutons, which were sites of intermittent magma accumulation for up to 5.5 m.y. Downward movement of host rocks by multiple processes occurred at all crustal levels during pluton emplacement. Ductile flow and accompanying rigid rotation were the dominant processes; stoping played an important secondary role, and magma wedging and regional deformation also aided emplacement. Overall, there are some striking changes with increasing depth, but many features and processes in the arc are similar throughout the crustal section, probably reflecting the relatively small differences in peak temperatures between the middle and deep crust. Such patterns may be representative of thick continental magmatic arcs constructed during regional shortening.

INTRODUCTION

Vertically extensive crustal sections through magmatic arcs are excellent natural laboratories to evaluate the physical and chemical properties of magmatic bodies and processes acting to form plutons at different crustal levels. It has long been recognized that styles of pluton emplacement, associated metamorphism, and fabric development in intrusions may vary substantially with depth, as illustrated by the classic concept of epizonal, mesozonal, and catazonal bodies (Buddington, 1959). For example, during pluton emplacement the operation of different host rock material transfer processes, such as ductile flow, roof uplift, and stoping are commonly inferred to vary with depth (e.g., Buddington, 1959; Pitcher, 1979; Paterson et al., 1996). Most studies, however, focus on emplacement of individual plutons or suites of plutons intruded at similar crustal levels in an orogen, and there have been few attempts to explore material transfer processes active during emplacement of many plutons from a wide range of paleodepths in the same crustal cross section. Similarly, the relationships of magmatism and pluton emplacement to faulting and regional deformation are complicated and presumably vary with depth.

Related topics that have been the focus of many recent studies, such as the geometries of plutons, are also amenable to evaluation by examination of crustal sections. A current widely cited model is that most plutons are subhorizontal tabular bodies that approximate laccoliths in the shallow crust and lopoliths at mid-crustal levels (e.g., Hamilton and Meyers, 1967; McCaffrey and Petford, 1997; Cruden, 1998, 2006; Wiebe and Collins, 1998; Brown and McClelland, 2000). These bodies are constructed from melts that ascend through dikes (e.g., Petford, 1996) and/or fracture networks (Weinberg, 1999; Brown, 2004), and are trapped at the brittle-ductile transition and/or level of neutral buoyancy (e.g., Collins and Sawyer, 1996; Brown and Solar, 1999). These models predict that the roofs and floors of plutons are commonly preserved in thick crustal sections and the deep crust consists of metamorphic rocks cut by dikes and/or pervasive networks of thin granitoids that represent channels for magma ascent. An inference of this model is that the volume of plutonic rock may decrease with depth (e.g., Collins and Sawyer, 1996). Alternatively, others have proposed that some plutons are vertically extensive, steep-sided bodies (e.g., Buddington, 1959;

Pitcher and Berger, 1972; Hutton, 1992; Paterson et al., 1996). Large elliptical to “blob-like” plutons in the shallow to mid-crust may pass downward into broad zones of steep sheeted plutons that represent magma conduits and transfer zones (e.g., Miller and Paterson, 2001a; Matzel et al., 2006).

The overall composition of plutons and the crust in general becomes more mafic with depth (e.g., Saleeby, 1990; Christensen and Mooney, 1995; Rudnick and Fountain, 1995; Ducea et al., 2003). Another widespread observation is that normally zoned tonalite to granite plutons are common in continental magmatic arcs. Most classic zoned intrusions were emplaced into the mid- to upper crust, such as in the Sierra Nevada batholith (e.g., Bateman and Chappell, 1979; Bateman, 1992), and their presence and/or characteristics at deeper crustal levels are less certain. An interpretation from this observation is that in some plutons the emplacement of early mafic magmas with a significant mantle component is followed by larger volume, more silicic magmas with a greater crustal component (e.g., Pitcher et al., 1985). It is not clear whether such temporal relations are preserved at all crustal levels, or only in upper-crustal sites of magma accumulation and pluton construction.

A final general point is that many classical crustal sections (e.g., Ivrea-Verbano zone, Kohistan, Talkeetna), as summarized in Percival et al. (1992) and Miller and Snoke (this volume), are from extensional terranes, oceanic arcs, and continental arcs of relatively normal crustal thickness. Relatively few studied crustal sections are of thick continental magmatic arcs, such as may represent analogues for the modern central Andes.

We evaluate these and other issues in the following analysis of an oblique crustal section through a mid-Cretaceous to Eocene continental magmatic arc represented by the crystalline core of the North Cascades (Cascades core), Washington and southwest British Columbia (Figs. 1 and 2) (Miller and Paterson, 2001b). This crustal section comprises oceanic and arc terranes that were metamorphosed to amphibolite facies and intruded by ca. 96–45-Ma plutons (e.g., Tabor et al., 1989). The Cretaceous part of the crustal section contains intrusions emplaced at paleodepths of <5 km to ≥ 35 km (e.g., Brown and Walker, 1993; Dawes, 1993; Miller and Paterson, 2001b). It thus represents some of the deepest exposed crustal levels in the Cordilleran arcs. It exposes rocks deeper than those in many lower-crustal sections (e.g., Percival et al., 1992), and may represent an analogue for

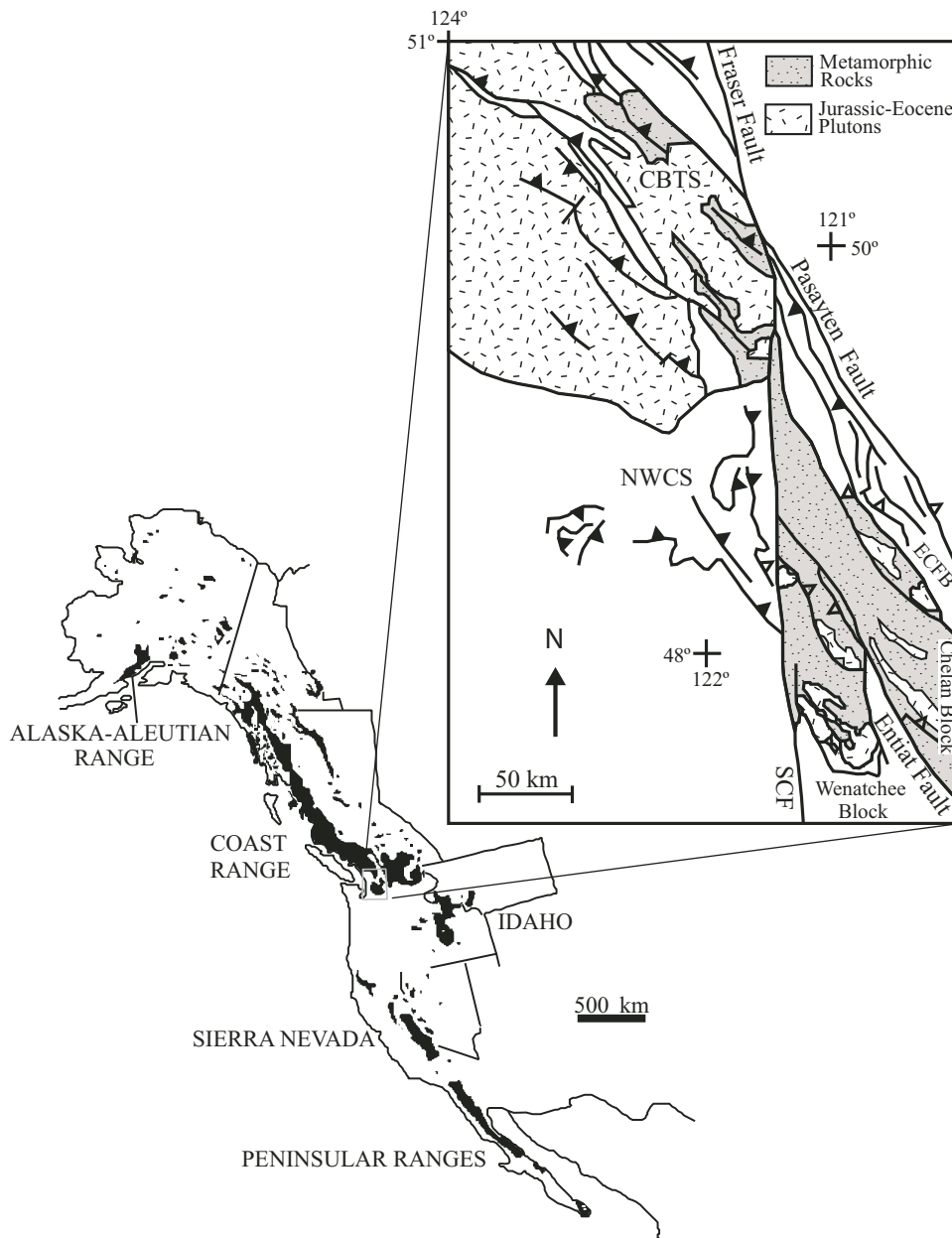


Figure 1. Sketch map of Mesozoic and Paleogene arc plutons in the western North American Cordillera. Inset emphasizes distribution of metamorphic rocks and plutons in the Cascades core and southern Coast belt of Washington and southwest British Columbia. Cretaceous thrust faults in the Cascades core, Coast belt thrust system (CBTS), and lower-grade rocks of the Eastern Cascades fold belt (ECFB) and Northwest Cascades system (NWCS) are also shown. The dextral Fraser–Straight Creek (SCF) fault offsets the Cascades core from the main part of the Coast belt. The Entiat fault and Pasayten fault are other major high-angle faults; the Entiat fault divides the Cascades into the Wenatchee and Chelan blocks, which have different thermal histories.

other thick continental arcs, such as the central Andes (Miller and Paterson, 2001b; Whitney et al., 2004). As such, it is an excellent natural laboratory for structural, metamorphic, magmatic, and thermochronologic studies of arcs.

A crustal section was synthesized by Miller and Paterson (2001b) utilizing structural, thermobarometric, and geochronologic data from the southern part of the Cascades core where more than 15 km of structural relief is exposed through large, km-scale upright folds (Fig. 3) and northeast-side-up tilt. Miller and Paterson (2001b) restored the crustal section by “unfolding” the large upright folds and restoring slip on a regional shear zone. Barometric data from metamorphic and plutonic rocks were used to constrain appropriate depths during the Late Cretaceous. In

this paper, we build on the model of Miller and Paterson (2001b), which emphasized the gross architecture and rheology of the crustal section, and focus on plutonism.

In discussing crustal sections, a common approach is to refer to lower, middle, and upper crust. These subdivisions, which are commonly defined by seismic velocities and compositions, are approximate. Standard average thicknesses for continental crust are from ~0–12 km for the upper crust, 12–23 km for middle crust, and 23–40 km for lower crust (e.g., Rudnick and Fountain, 1995; Gao et al., 1998; Rudnick and Gao, 2005). The Cretaceous crustal thickness of the Cascades arc, however, was probably ≥ 55 km (see below) (Miller and Paterson, 2001b), and we refer to rocks with paleodepths of >23 km as deep crust.

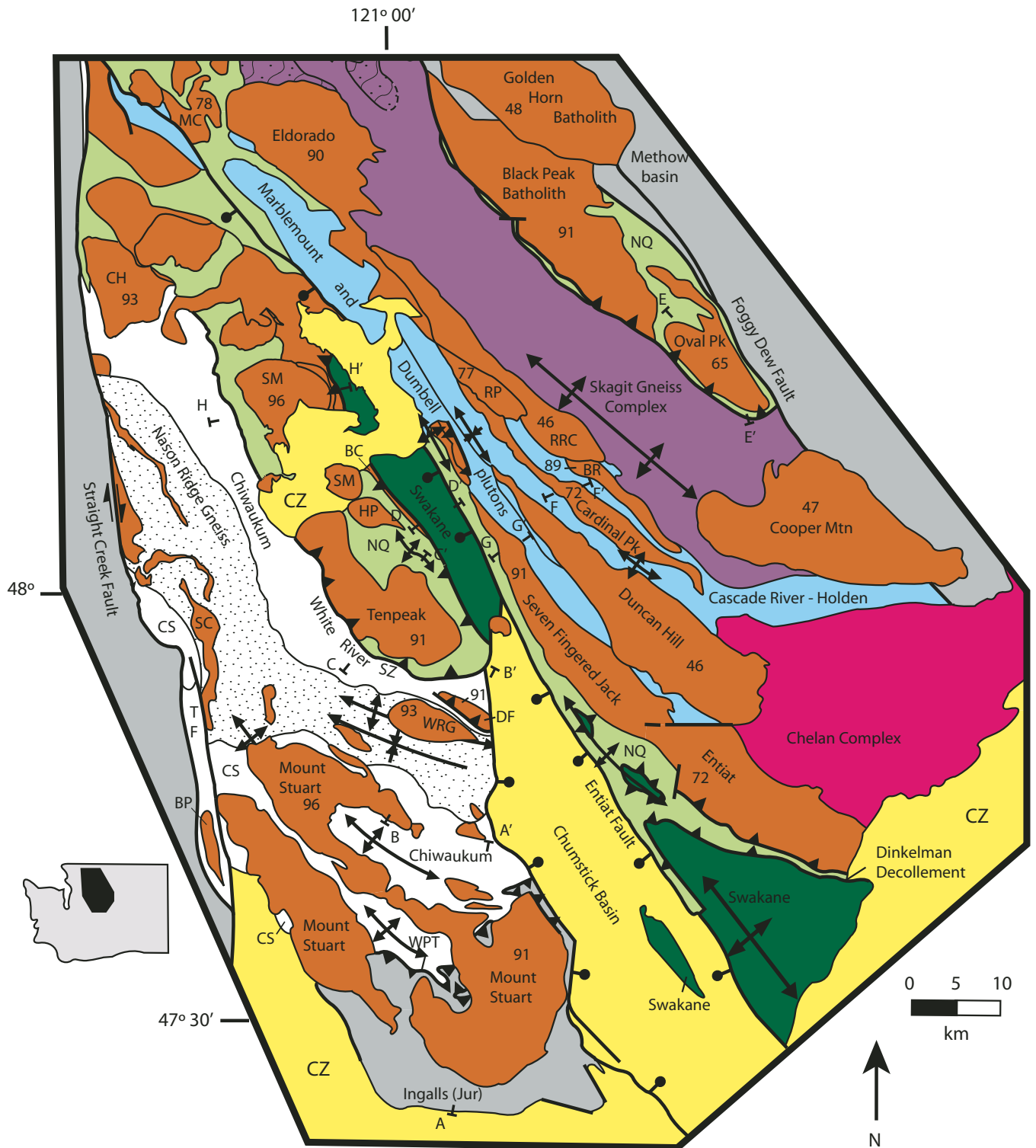


Figure 2. Simplified geologic map emphasizing the Cascades core. Plutons are colored orange and numbers are crystallization ages. BC—Buck Creek Pass pluton; BP—Beckler Peak stock; BR—Bearcat Ridge Orthogneiss; CH—Chaval pluton; CS—Chiwaukum Schist; CZ—Cenozoic undifferentiated (mid-Eocene to Quaternary); DF—Dirtyface pluton; HP—High Pass pluton; MC—Marble Creek pluton; NQ—Napeequa unit; NWCS—Northwest Cascades system; RP—Riddle Peaks pluton; RRC—Railroad Creek pluton; SC—Sloan Creek plutons; SM—Sulphur Mountain pluton; SZ—shear zone; TF—Tonga Formation; WPT—Windy Pass thrust; WRG—Wenatchee Ridge Gneiss. Also shown are regional fold axial traces and the lines of cross sections in Figures 3 and 6. The Ingalls ophiolite, Methow basin, and rocks west of the Straight Creek fault (parts west of the Northwest Cascades system) are shown with the same color, emphasizing their Cretaceous and/or older age, and low-grade to non-metamorphic rocks. Inset shows Washington State and location of the geologic map. Sources are described in the text.

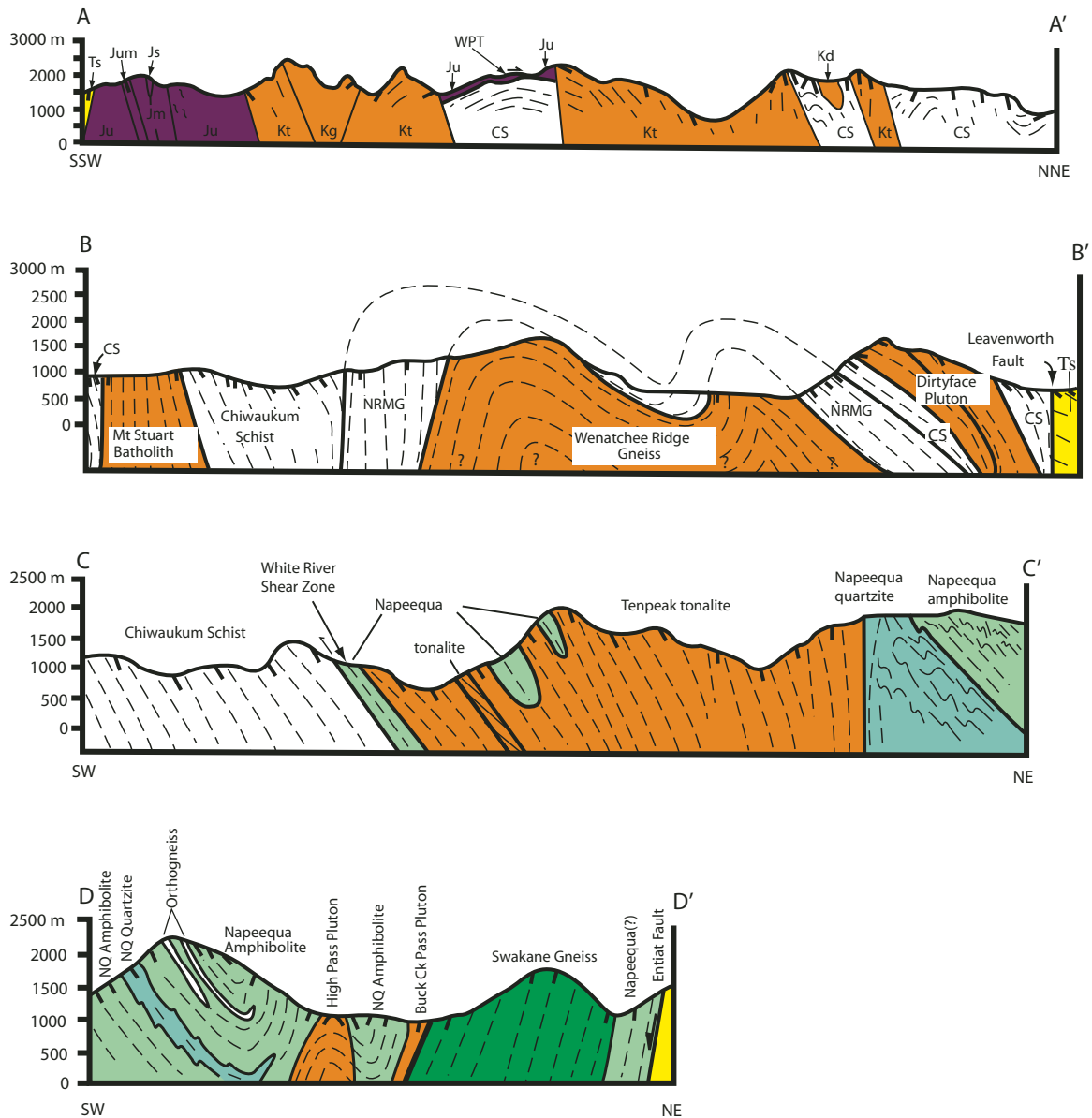


Figure 3. Cross sections through the Wenatchee block [arranged from southwest and shallow levels (A–A′) to northeast and deep levels (D–D′)]. Dashes are inferred foliation traces. Squiggles—foliation in sheared serpentinite. Note that foliation and some contacts define large, southwest-vergent folds. CS—Chiwaukum Schist; Kd—Mount Stuart diorite and gabbro; Kg—Mount Stuart granodiorite; Kt—Mount Stuart tonalite; Jm—Ingalls Complex mafic rock; Js—Ingalls Complex sedimentary rock; Ju—Ingalls Complex ultramafic rock; Jum—Ingalls Complex serpentinite mélange; NQ—Napeequa unit; NRMG—Nason Ridge Migmatite Gneiss; Ts—Tertiary sandstone; WPT—Windy Pass thrust. The Napeequa-Swakane fault contact is a Tertiary structure. Modified from Miller et al. (2006).

GEOLOGIC SETTING

The crystalline core of the North Cascades (Cascades core) is the southernmost extension of the >1500-km-long Coast belt of the Northwest Cordilleran orogen (Fig. 1), which underwent major crustal shortening and metamorphism during final suturing of the Insular superterrane to North America in the mid-Cretaceous (Monger et al., 1982; Rubin et al., 1990; Journeay

and Friedman, 1993). The Cascades core includes oceanic, island-arc, and clastic-dominated terranes that were mostly juxtaposed prior to the peak of mid-Cretaceous amphibolite-facies metamorphism, arc-normal shortening, and ca. 96–45-Ma magmatism (e.g., Tabor et al., 1989). Regional shortening resulted in crustal thickening and burial of supracrustal rocks to depths of 25 to ≥40 km in many parts of the orogen (Whitney et al., 1999; Valley et al., 2003).

In the mid-Cretaceous, shallow-level (<10 km) rocks flanking the Cascades core were deformed by southwest-directed thrusting (e.g., Misch [1966]; Brandon et al. [1988]; but see Brown [1987] for a different interpretation). At deeper levels, ductile deformation during amphibolite-facies metamorphism was dominated by multiple cycles of folding and cleavage development, modest southwest-directed reverse shear in ductile shear zones, and sub-horizontal, orogen-parallel stretching (Miller et al., 2006). Miller and Paterson (2001b) inferred that the recorded pressures were achieved when the dominant mesoscopic structures formed, but predate, or are synchronous with, many of the regional upright folds of the dominant foliation, although some folding occurred earlier. Unfolding the high-amplitude regional folds suggests that early structures and terrane boundaries were initially subhorizontal to moderately dipping.

The steep, post-metamorphic Entiat fault divides the Cascades core into a southwestern Wenatchee block and northeastern Chelan block (Figs. 1 and 2) (Tabor et al., 1989). The Cascades crustal section (Fig. 4) is largely based on relationships in the Wenatchee block and southwestern Chelan block. In the Wenatchee block, K-Ar and ⁴⁰Ar/³⁹Ar cooling ages (Engels et al., 1976; Tabor et al., 1982, 1987; Evans and Davidson, 1999; Matzel, 2004) temporally overlap 96–84-Ma plutons and ductile structures indicating that deformation predominantly occurred in the mid-Cretaceous (e.g., Tabor et al., 1989; Paterson et al., 1994; Miller and Paterson, 2001b). The Chelan block was also deformed at this time, but records additional shortening coincident with ca. 78–65-Ma magmatism and subsequent orogen-parallel stretching during Eocene magmatism and exhumation (Haugerud et al., 1991; Hurlow, 1992; Paterson et al., 2004; Miller et al., 2006).

Cascades Crustal Section

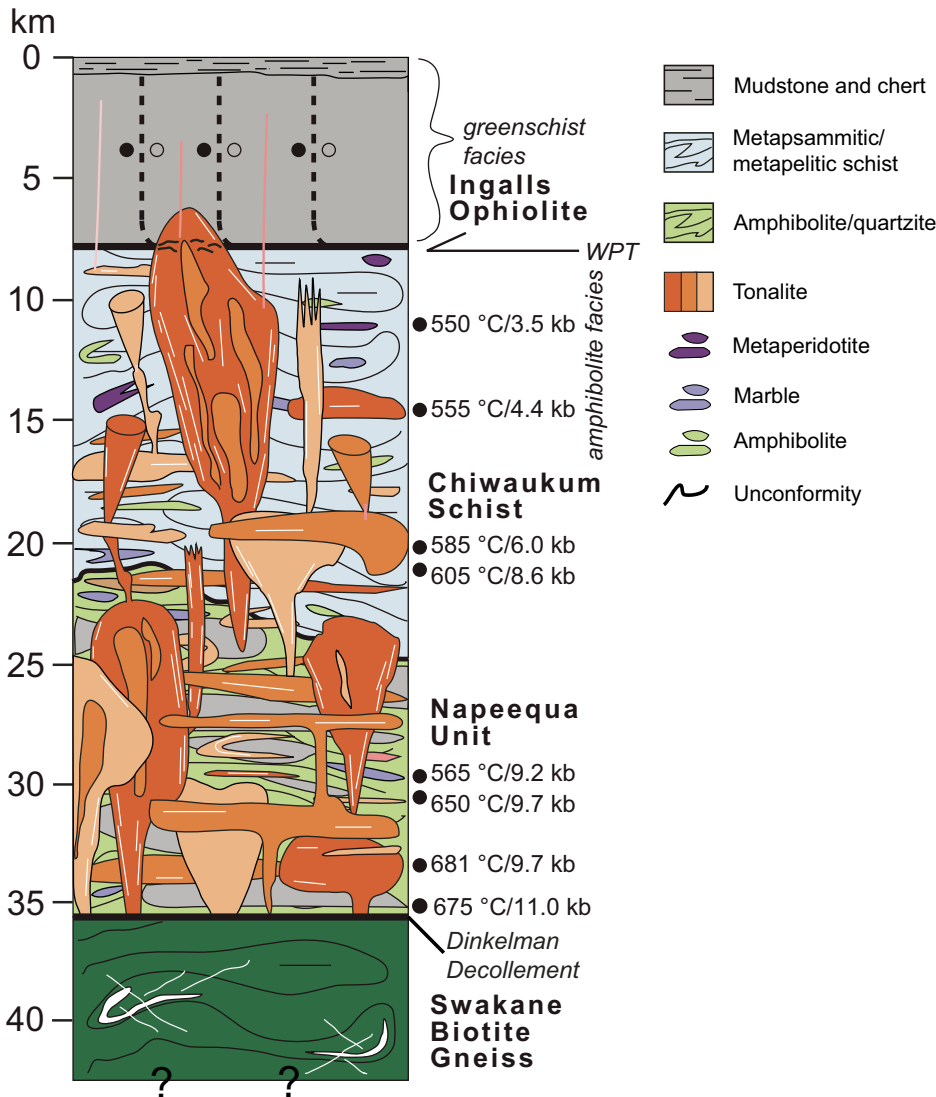


Figure 4. Diagram schematically summarizing major rock types, particularly the distribution and shapes of plutons, and *P-T* conditions in the Cascades crustal section (Miller and Paterson, 2001b). Plutons are in orange. Vertical dashed lines are faults in Ingalls ophiolite, and only a few other major faults are shown. WPT—Windy Pass thrust. Representative temperatures and pressures used to help construct the section are shown in appropriate position on right side of section. See text for references to sources of data.

Cretaceous magmatic bodies are distributed throughout the crustal section. Plutons are dominantly tonalite (Misch, 1966; Cater, 1982; Dawes, 1993). Diorite and gabbro are subordinate components of most intrusions; granodiorite is found in variable amounts, and is the main constituent of many of the youngest (Eocene) plutons (Misch, 1966). Dawes (1993) and DeBari (DeBari et al., 1998; Miller et al., 2000) infer from geochemical data that the dominant tonalites formed by variable mixing of mantle-derived mafic magmas with lower-crustal melts (felsic tonalite, trondhjemite, granodiorite). ϵ_{Nd} values of +6.3 to +1.5 also likely record mixing of mantle-derived melt with melt formed by partial anatexis of isotopically juvenile terranes (Matzel et al., 2008). Rare-earth-element (REE) patterns indicate a garnet-bearing mafic source for the crustal melts (Miller et al., 2000), and pressures of ~15–16 kb are inferred for melting (De Bari et al., 1998; Miller et al., 2000).

HOST ROCK FRAMEWORK OF CRUSTAL SECTION

Cretaceous plutons that intrude the Wenatchee block and southwestern Chelan block are hosted by dominantly meta-supracrustal rocks. Metamorphic grade ranges from greenschist- to amphibolite-facies conditions (Misch, 1966; Brown and Walker, 1993; Whitney et al., 1999). The base of the section represents paleodepths of ~40 km (Miller and Paterson, 2001b). There is little control on what was beneath the section in the Cretaceous; Miller and Paterson (2001b) inferred that mafic plutonic and metamorphic rocks were likely important components.

The shallowest level of the crustal section is represented by the Jurassic Ingalls ophiolite complex. It consists of Early Jurassic within-plate basalts and a more voluminous Late Jurassic supra-subduction-zone ophiolite deformed in an oceanic fracture zone represented in part by steeply dipping serpentinite-matrix mélange (Miller, 1985; Metzger et al., 2002; MacDonald et al., 2008). The ophiolite is dominated by ultramafic mantle tectonites, has a thin crustal mafic intrusive and volcanic section, and is overlain by mainly mudstone and chert (Miller, 1985; Miller and Mogk, 1987; MacDonald et al., 2008). Metamorphic grade ranges from prehnite-pumpellyite facies in the south, to amphibolite facies near the mid-Cretaceous Windy Pass thrust (Fig. 2), which forms the lower boundary of the ophiolite (Miller, 1985). In general, the time-averaged brittle-ductile transition corresponds to the transition from greenschist- to amphibolite-facies assemblages (Fig. 4) (Miller and Paterson, 2001b).

In the footwall of the Windy Pass thrust, the Chiwaukum Schist and related Tonga Formation and Nason Ridge Migmatitic Gneiss form the Nason terrane (Fig. 2). The Chiwaukum Schist predominantly comprises pelitic and psammitic schist, and lesser amphibolite and ultramafic lenses (e.g., Plummer, 1980; Tabor et al., 1987; Paterson et al., 1994). The schist protoliths may have been mixed in an accretionary wedge prior to arc magmatism and metamorphism (Paterson et al., 1994). The Tonga Formation, which was deposited in the Early Cretaceous (Brown and

Gehrels, 2007), has the same protoliths as the schist, but differs in that primary sedimentary structures are well preserved (Duggan and Brown, 1994). The Chiwaukum Schist grades structurally downward into the Nason Ridge Migmatitic Gneiss, which consists of schist and paragneiss that resemble Chiwaukum rocks, but is also extensively intruded by tonalitic sheets (e.g., Tabor et al., 1987, 1993; Magloughlin, 1993; Paterson et al., 1994). In all of the units, mid-Cretaceous folds are the dominant structures and the strain pattern reflects superposition of upright folds on gently inclined to recumbent folds (Paterson et al., 1994; Miller et al., 2006; Jensen et al., 2007).

The lowermost exposed contact of the Nason Ridge gneiss is a folded intrusive contact with the >1-km-thick Wenatchee Ridge Gneiss (Fig. 3), a ca. 93-Ma orthogneiss (Tabor et al., 1987; Miller and Paterson, 2001b). Metamorphic pressures are lowest at the southern end of the Chiwaukum Schist and increase from ~3 kb to 9 kb at temperatures of ~540–700 °C over an ~10 km distance northeast from the Mount Stuart batholith. Schist near the batholith underwent an increase in pressure soon after batholith emplacement (e.g., Evans and Berti, 1986; Brown and Walker, 1993; Paterson et al., 1994; Stowell and Tinkham, 2003; Stowell et al., 2007).

The Nason Ridge Migmatitic Gneiss and Wenatchee Ridge Gneiss most likely were underlain by the Napeequa complex (Napeequa Schist of Cater and Crowder [1967]) prior to reverse-slip on the White River shear zone (Figs. 2–4) (Miller and Paterson, 2001b; Brown and Dragovich, 2003; Miller et al., 2003). The Napeequa unit consists mainly of amphibolite, quartzite, and biotite schist; minor metaperidotite and marble are also present, and the protoliths indicate an oceanic origin. These rocks were metamorphosed to ~8–11 kb (Brown and Walker, 1993; Valley et al., 2003), and were deformed by tight to isoclinal, gently inclined to recumbent folds and subsequent outcrop- to map-scale, open to tight, upright to overturned folds (Cater and Crowder, 1967; Miller et al., 2006).

The base of the Napeequa complex is the Dinkelman décollement, which places the unit over the meta-psammitic Swakane Gneiss (Fig. 3) (Paterson et al., 2004). Swakane rocks were underthrust beneath the Napeequa unit between ca. 72–68 Ma to depths corresponding to pressures reaching 12 kb (Valley et al., 2003; Matzel et al., 2004). The Napeequa and Swakane units are also exposed in the Chelan block, where the décollement records primarily Paleogene top-to-north shear during exhumation (Paterson et al., 2004). The Swakane Gneiss is only intruded by small leucogranite bodies (Boysun, 2004) and Neogene plutons. It postdates much of the time frame discussed in this manuscript and is not further considered.

Another major component of the Chelan block is the Cascade River unit-Holden assemblage (Fig. 2), which has a Triassic arc protolith and consists mainly of hornblende-rich metavolcanic and metaclastic rocks that are associated with Late Triassic arc plutons (e.g., Misch, 1966; Tabor et al., 1989). Metamorphic pressures reach ~8 kb in the assemblage (Miller et al., 1993a; Brown et al., 1994). The relationship of these arc rocks to other

units of the crustal section is not clear (cf. Tabor et al., 1989; Brown et al., 1994; Miller et al., 1994).

PLUTONS IN THE CASCADES CRUSTAL SECTION

In the following, we describe Late Cretaceous magmatic bodies in the crustal section. Emphasis is placed on the Wenatchee block, but well-studied 91–65-Ma plutons in the southwest part of the Chelan block and Ross Lake fault zone are also considered. We emphasize features most relevant to the issues raised in the introduction that are well suited to study in crustal sections. Details on the plutons are included in Table 1.

TABLE 1. PLUTONS IN CRUSTAL SECTION

Plutons	Age	Sq km	*P-emp (kb)
Beckler Peak	91	20	2
Mt. Stuart	96	194	2–4
Mt. Stuart	94	78	2–4
Mt. Stuart	91	208	2–4
Mt. Stuart—SW	93	231	
Sulphur Mountain	96	130	7–9
Tenpeak	92	197	8–9
Dirtyface	91	15	7
High Pass	88	15	9–10
Clark Mountain	85	3	9
Buck Creek	84	1	8–9
Wenatchee Ridge	93	52	>8
Sloan Creek	90	71	3–5
<u>Other plutons—NE of crustal section</u>			
Seven-Fingered-Jack	92	240	6–8
Black Peak	91–89	336	1–5(?)
Chaval	92	70	
Eldorado	90	231	
Knapp Coulee	78	23	
Bearcat Ridge	89	37	
Riddle Peaks	78	30	6–8
Cardinal Peak	78–72	62	6–8
Entiat	73–71	246	6–8
Hidden Lake	75	17	
Jordan Lakes	74	65	
Oval Peak	65	129	6
<u>Unfocused magmas</u>			
Napeequa Sheets—Deep Crust	88–84	117	7–10
Napeequa Sheets—Mid-Crust	90–71	53	6–8
Cascade River Sheets	90–72	35	
Nason Terrane Sheets	90	130	4–8
Ingalls Sheets	93–91	2	≤2

*P-emp—emplacement pressure.

Note: Sources for ages and pressures are cited in text.

Deepest Plutons in Crustal Section

Compatible metamorphic and igneous barometry, widespread magmatic epidote, and structural position suggest that the deepest intrusions in the crustal section intrude the Napeequa unit at paleodepths of ~25–35 km in an ~10-km-wide, orogen-parallel belt between the White River shear zone and Entiat fault (Zen, 1988; Brown and Walker, 1993; Dawes, 1993; Miller and Paterson, 2001b) (Figs. 2 and 5). These intrusions range from ca. 96–84 Ma. They include thin, sheeted plutons, broadly elliptical plutons consisting of sheets and more homogeneous masses, and 10s-of-cm- to 10s-of-m-thick sheets.

Tenpeak Pluton

The best-studied deep intrusion is the 92.3–89.7-Ma Tenpeak pluton (e.g., Cater, 1982; Dawes, 1993; Miller and Paterson, 1999; Matzel et al., 2006). This 7–10-kb pluton is broadly elliptical in map view (Fig. 5), and has a nearly vertical northeast contact and moderately to steeply inward-dipping southwest and southern margins. The contacts define an asymmetrical wedge-shaped body, and extrapolated downward from the present erosional surface imply an apparent vertical extent of ≥9.5 km. The southwest margin in part corresponds to the scissor-like, White River shear zone (Figs. 3 and 5) (Van Diver, 1967; Magloughlin, 1993; Miller and Paterson, 1999; Raszewski, 2005), along which reverse slip decreases to the northwest. This shear zone forms the boundary between the Chiwaukum Schist and Napeequa unit; the pluton locally intrudes the schist in this zone, but is mostly hosted by Napeequa rocks.

A generally <500-m-wide, discontinuous heterogeneous zone of mingled and sheeted gabbro, tonalite, and hornblende forms the margin of the Tenpeak pluton (Fig. 5) (Cater, 1982; Miller et al., 2000). Inward from this mafic zone is voluminous tonalite and, in the north, diorite and mafic tonalite. Within the tonalite, a ca. 92.2-Ma phase overlaps in age with the mafic zone. Less than 0.3 m.y. later, sheets were injected in an internal zone that contains numerous m-scale inclusions of Napeequa unit (Matzel et al., 2006). Tonalitic magmatism continued at 91.3 Ma in the northeast margin and at 90.6 Ma in the north end (Fig. 5), and was followed by an apparent hiatus before intrusion at 89.7 Ma of distinctive coarser-grained tonalite that truncated the sheeted zones (Miller and Paterson, 1999; Matzel et al., 2006). Matzel et al. (2006) concluded that magma flux was broadly distributed during the 2.6 m.y. of pluton construction.

Abundant inclusions of Napeequa amphibolite, schist, and metaperidotite range from <5-cm long to km-scale. They are concentrated in the margins and internal sheeted zone; map-scale bodies are mostly enclosed by the older tonalite phase (Fig. 5). Foliation and lithological contacts in the smaller Napeequa inclusions are commonly rotated relative to each other and the host magmatic and solid-state foliation.

Margin-parallel foliation and lineation with moderate to steep pitches typify the pluton (Miller and Paterson, 1999). Fabrics in much of the pluton interior are magmatic, although

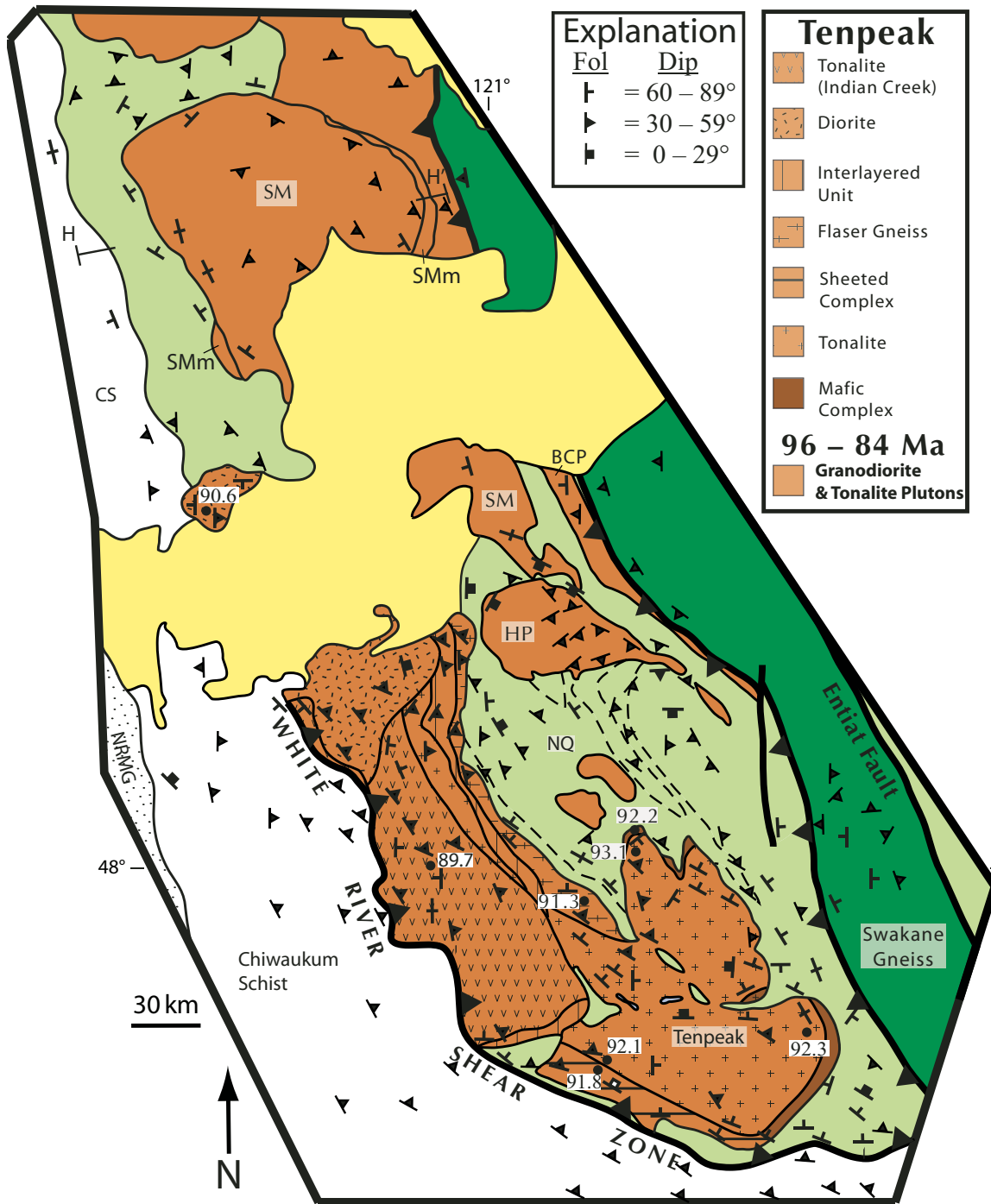


Figure 5. Map of the deep-crustal domain between the White River shear zone and Entiat fault. Units and U-Pb zircon ages (Matzel et al., 2006) of the Tenpeak pluton are emphasized. Dashed lines in the Napeequa unit are traces of internal contacts between quartzite, amphibolite, and biotite schist dominated units. BCP—Buck Creek Pass pluton; CS—Chiwaukum Schist; HP—High Pass pluton; NQ—Napeequa unit; NRMG—Nason Ridge Migmatitic Gneiss; SM—Sulphur Mountain; SMm—Sulphur Mountain marginal heterogeneous zone. H–H' is line of cross section shown on Figure 6.

weak high-temperature solid-state deformation is common and increases in intensity in the White River shear zone. Features typical of undeformed plutons are well preserved and include compositional layering and enclave swarms where enclaves display delicate magma mingling features.

Emplacement of the Tenpeak pluton was dominated by vertical material transfer processes and subhorizontal wedging (cf. Weinberg and Searle, 1998; Weinberg, 1999), as discussed by Miller and Paterson (1999). Ductile flow is recorded in narrow (500 m–1 km) structural aureoles and by downward deflection of the Napeequa-Chiwaukum contact. Stopping is indicated by the rotated host-rock xenoliths.

Sulphur Mountain Pluton

The 96-Ma Sulphur Mountain pluton is separated by the Quaternary Glacier Peak volcano into a larger northwest, “head-shaped” body and a southeast, “tail-like” domain (Fig. 5). The pluton is mainly granodiorite and tonalite (Crowder et al., 1966; Cater, 1982); discontinuous, ~300-m-wide contact zones in the eastern and western margins of the larger body are marked by tonalite intercalated with schist, gneiss, and hornblende (Crowder et al., 1966), and ~50-cm-wide xenoliths to m-scale rafts of Napeequa unit are common in the tail region. White et al. (1988) interpreted $\delta^{18}\text{O}$ isotope values of >10 to indicate involvement of metasedimentary or altered volcanic rocks in the petrogenesis of the intrusion.

The tail region of the Sulphur Mountain pluton is broadly sheet-like. Mostly concordant meter-scale sheets adjacent to the eastern contact intrude Napeequa host rocks and dip 20° to $\geq 60^\circ$ northeast, reflecting at least in part the regional folding best seen in the Napeequa unit. The sheets and tail display high-temperature subsolidus foliation and lineation coincident with that of the host rocks.

The northwestern “head” region is relatively homogeneous outside of the contact zones and displays weaker solid-state deformation than the tail. Foliation strikes parallel to the pluton margin (Fig. 5), both in the pluton and a >1 -km-wide structural aureole in the host rocks where contacts are also concordant to foliation (Tabor et al., 2002). The foliation and map pattern imply that the northern part of the pluton has an asymmetric, wedge-like to funnel shape (Fig. 6, section H–H’); a moderately west-dipping eastern contact and steep western margin can be traced over a minimum of 750 m of topographic relief.

The Sulphur Mountain pluton may have undergone modest southeast-end-up tilt, as metamorphic isobars constructed by Brown and Walker (1993) from limited data suggest a northwest plunge for the block between the White River shear zone and Entiat fault. Such tilt is compatible with the greater subsolidus deformation of the tail region, and with feeding of the larger “head domain” by deeper sheets that are part of a frozen magma conduit.

Emplacement of the pluton was accommodated by multiple processes. The structural aureole around the head is evidence for ductile flow of host rock. Xenoliths, including dense amphibolite,

imply that stopping also aided emplacement. The oxygen isotope data are compatible with assimilation of stopped blocks, although the depth of any assimilation is unconstrained. Finally, sheeting in the tail region probably wedged aside Napeequa rafts.

High Pass Pluton, Buck Creek Pass Pluton, and Thin Intrusive Sheets in Napeequa Unit

Broadly related thin sheets and small plutons of leucocratic biotite granodiorite and tonalite, the largest of which are the High Pass and Buck Creek Pass plutons, intrude the Napeequa unit (Fig. 5) (Cater, 1982). The ca. 88-Ma (J.P. Matzel, personal observation) High Pass pluton in map view is weakly elliptical with a 500-m-wide tail extending to the east-southeast. Its orientation in part reflects regional folding (Fig. 5), and the pluton tail lies along the crest of an antiform in the Napeequa unit (Cater, 1982). The northern and western parts of the pluton display only weak foliation, but foliation intensity and solid-state deformation increase to the south and east (Cater, 1982). Contacts of the pluton are partly concordant and partly discordant to lithological contacts within the host rocks. The overall geometry of the pluton is broadly sheet-like, to wedge-shaped and synformal with a moderate southeast plunge; we estimate a thickness of ~2.5 km. Abundant concordant and discordant sheets, and irregularly shaped masses intrude the Napeequa unit and Sulphur Mountain pluton for distances of up to 100s of m from the main pluton contact. Host rock xenoliths are common near contacts (Cater, 1982, and our observations).

The ca. 84-Ma Buck Creek Pass pluton (Fig. 5; Hurlow, 1992) was mapped by Cater and Crowder (1967) as consisting of an ~600-m-thick body and isolated thinner sheets intruding the Napeequa unit. These rocks display moderate- to high-temperature solid-state foliation and lineation parallel to equivalent structures in their host rocks. The Buck Creek Pass pluton is made up of m- to 10s of m-thick sheets distinguished by generally small differences in grain size and color index. The western contact is relatively sharp, whereas the eastern margin grades into a zone of alternating intrusive sheets and Napeequa amphibolite. Overall, the pluton is a concordant, moderately to steeply southwest-dipping, tabular body (Fig. 3, D–D’).

Dispersed thin (<50 m), dominantly concordant intrusive sheets probably make up $\geq 30\%$ of the Napeequa outcrop belt. They record moderate- to high-temperature recrystallization, and share many of the structural features of the host rocks.

The initial orientations of the plutons and thinner sheets, and host-rock material transfer processes during emplacement, have been partially obscured by the penetrative regional deformation. Most of the sheets probably intruded concordantly to host-rock foliation and lithological contacts, although some may have been rotated into near-parallelism by strong deformation. We infer that most of the sheets and the Buck Creek Pass pluton were intruded subhorizontally before latest upright folding. Emplacement of the more geometrically complex, broadly sheet-like High Pass pluton probably involved wedging of host rocks. The numerous host rock inclusions and truncation of contacts by the southern margin of the High Pass pluton indicate at least limited stopping.

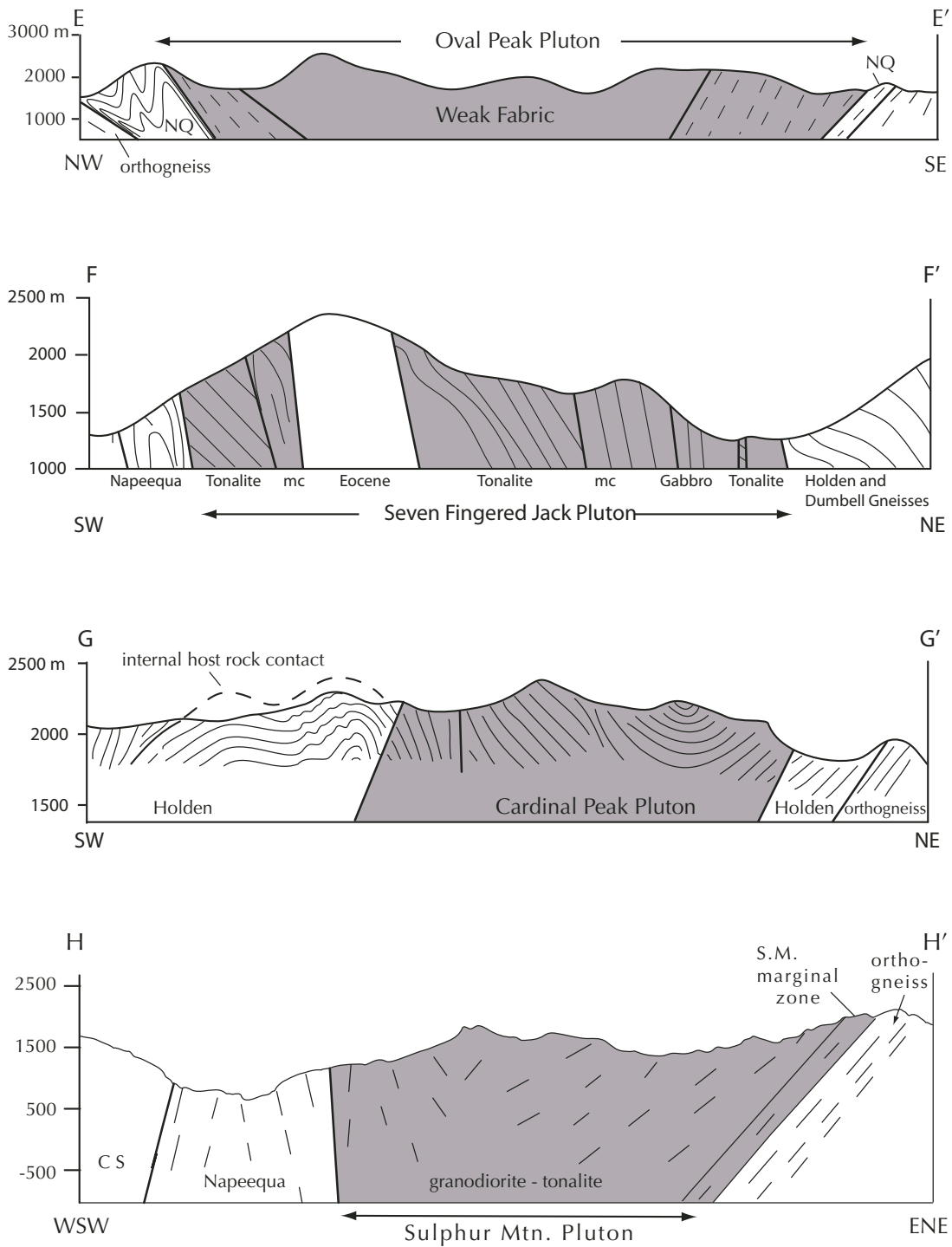


Figure 6. Cross sections emphasizing geometry of selected plutons. Sections arranged from shallowest (Oval Peak pluton) to deepest pluton (Sulphur Mountain pluton). Location of E-E', F-F', and G-G' is on Figure 2, and H-H' is on Figure 5. CS—Chiwaukee Schist; mc—mafic complex; NQ—Napeequa unit; S.M.—Sulphur Mountain.

Deep Mid-Crustal Plutons

Three domains that are probably only slightly shallower than, and may overlap in paleodepth with, the Tenpeak domain are marked by plutons and sheets that crystallized at ~6–8 kb. One domain is in the northeastern part of the Nason terrane, another is in the western part of the Chelan block, and the third is in the Ross Lake fault zone.

Northeastern Nason Terrane

The deepest part of the Nason terrane includes discrete plutons, such as the ~7 kb, 91-Ma Dirtyface pluton (Hurlow, 1992) and ca. 93-Ma Wenatchee Ridge Gneiss, and a multitude of thinner sheets that intruded the Nason Ridge Migmatitic Gneiss and Chiwaukum Schist (Fig. 2) (Brown and Walker, 1993; Magloughlin, 1993; Miller et al., 2000, 2003; Stowell and Tinkham, 2003; Stowell et al., 2007).

The ~1-km-thick, 91-Ma Dirtyface pluton consists of alternating sheets of hornblende-biotite quartz diorite and felsic two-mica granitoid, some of which are separated by rafts of Chiwaukum Schist. Sheets are moderately dipping (35–55°) and conformable to host-rock foliation along the southwest margin of the pluton, become thicker, dip steeper (50–70°), and are more discordant to host-rock structure as the northeast contact is approached. The overall shape of the body is thus an inclined wedge. The quartz diorite sheets are compositionally homogeneous and are similar geochemically to sheeted units in the Tenpeak pluton (Miller et al., 2000). The two-mica granitoid sheets are petrographically similar to sheeted units in the Wenatchee Ridge Gneiss.

Sheets in the Dirtyface pluton have strong magmatic and locally subsolidus foliation and steeply pitching lineation, all of which cut sheet contacts and are continuous with host-rock structures. Subsolidus deformation intensifies toward the southwest margin where S-C fabrics and asymmetrical tails on grains give reverse, top-to-southwest sense of shear.

The Wenatchee Ridge Gneiss is the structurally deepest body that intrudes the Nason terrane. It is largely muscovite- and biotite-bearing trondhjemite and leucotonalite, and may represent another largely sheeted intrusion (Magloughlin, 1993; Paterson et al., 1994). Sheets range from 10s of cm to many meters in thickness and are separated by local zones of schist and metaperidotite blocks. Sheets appear to thicken, and the body is probably more homogeneous with depth, suggesting that the exposed levels are the top of a large intrusion. The mineral content and presence of widespread ultramafic blocks make this a unique intrusion in the Cascades core.

Intrusive sheets, which range from <10 cm to 10s of m in thickness, make up ~30% of the exposed outcrop area of the Nason Ridge Migmatitic Gneiss and northeastern part of the Chiwaukum Schist. The dominantly tonalitic to two-mica granite sheets show a wide range of compositions and textures, are commonly concordant with the dominant foliation in the interlayered Chiwaukum Schist, and display strong magmatic and/or

subsolidus fabric (Getsinger, 1978; Magloughlin, 1993; Miller and Paterson, 2001b).

Emplacement of the extensively sheeted Dirtyface and Wenatchee intrusions, and the dispersed sheets in the Nason Ridge Migmatitic Gneiss, was at least in part by magma wedging. Wedging does not explain, however, the steep discordant northeast margin of the Dirtyface pluton.

Chelan Block

A 20-km-wide, orogen-parallel zone in the southwest part of the Chelan block contains ca. 92–70-Ma plutons that are constructed largely of steep, cm- to km-scale sheets and crystallized at ~20–25 km (Fig. 2) (e.g., Hurlow, 1992; Dawes, 1993; Paterson and Miller, 1998a; Miller and Paterson, 2001a; Matzel, 2004). The contiguous 92–90-Ma Seven-Fingered Jack pluton in the northwest and 73–71-Ma Entiat pluton (*sensu stricto*) in the southeast represent a <10-km-wide plutonic complex that extends for >80 km, and the nearby 78–72-Ma Cardinal Peak pluton is ~35 km by 3 km in map view (Fig. 2). These plutons intrude the Napeequa complex and hornblende gneiss, schist, amphibolite, and calc-silicate rock of the Holden assemblage. We have described these plutons in detail elsewhere (Paterson and Miller, 1998a; Miller and Paterson, 2001a; Matzel, 2004), and only briefly summarize major features, treating the three intrusions together in the following discussion.

Heterogeneous mafic rocks are mingled with tonalite in the margins of the plutons and northwest tips of the Seven Fingered Jack and Cardinal Peak intrusions. Inward from the marginal, thinly sheeted zones are thicker sheets and less elongate masses of tonalite, which dominate the intrusions. Rafts and xenoliths of host rocks are abundant between and within marginal sheets of the plutons, and throughout the Cardinal Peak pluton.

Gently to moderately dipping magmatic and less widespread high-temperature subsolidus foliations of moderate to strong intensity are continuous with host-rock foliation, but commonly discordant to sheet and pluton contacts (Fig. 6, section G–G'). Foliation has been deformed into outcrop- to map-scale folds that are subparallel to host-rock folds, and magmatic lineation is similarly subparallel to host-rock fabrics. The magmatic structures thus record regional shortening during intermittent, prolonged pluton construction (92–70 Ma) (Paterson and Miller, 1998a; Paterson et al., 1998; Miller and Paterson, 2001a).

Narrow structural aureoles next to the three plutons display dramatic along-strike variability (Paterson and Miller, 1998a; Miller and Paterson, 2001a). Vertical and largely downward ductile flow is recorded next to some pluton segments by deflection of regional gently to moderately dipping host-rock markers into subparallelism with steep pluton contacts in structural aureoles that reach 1 km in width. Emplacement of sheet tips along axial surfaces of upright, gently plunging folds (Paterson and Miller, 1998a), and the folding of magmatic foliation, are compatible with regional deformation aiding emplacement (cf. Weinberg and Mark, 2008). Several sharply discordant segments of pluton contacts (Fig. 6, section G–G') and rotated xenoliths support stoping.

We utilized these and other relationships to hypothesize that early magmatic sheets wedged aside host rock, then coalesced to isolate host rock pieces, which finally led to detachment and vertical downward movement of host rock through magma and formation of relatively large, inclusion-poor bodies (cf. Miller and Paterson, 2001a). This model is further supported by Matzel's (2004) age data, which demonstrate that: the Seven-Fingered Jack and Entiat intrusions were each constructed over 2–3-m.y. intervals; zircon inheritance patterns reflect incorporation of host rock near the level of emplacement; and early sheets were partially mixed with slightly younger sheets.

Other less extensively sheeted plutons intrude the Napeequa and Cascade River-Holden units in the Chelan block. These include the ca. 77.5-Ma Riddle Peaks pluton (Fig. 2), which is the largest (~30 km²) mafic body in the arc and intruded synchronously with the mafic complex of the adjacent Cardinal Peak pluton (Cater, 1982; McPeck et al., 2002). Much of this hornblende gabbro is layered on the cm- to m-scale and displays strong magmatic foliation. The pluton contains numerous inclusions of amphibolite, schist, and marble of the Holden assemblage, which range up to 100s of m across (Cater, 1982; McPeck et al., 2002). Inclusions are dispersed throughout the intrusion, but are most common near an internal contact between layered and non-layered rocks. Cater (1982) infers from dips and grading of layers, and distribution of the largest host-rock inclusions that this contact is the roof of the layered phase. He assumes that the northeast-dipping layering and pluton were initially subhorizontal, and that the pluton has been tilted to moderate dips. The estimated pluton thickness is 2.5 km (Cater, 1982).

Host-rock inclusions range from slabby to blocky, and from concordant to discordant to layering in the gabbro. The blocky varieties are especially likely to be discordant. Cater (1982) notes that inclusions of all sizes are encased by contaminated and hybrid rocks, and infers that the similar densities of gabbroic magma and inclusions led to prolonged assimilation. These abundantly rotated, partially assimilated xenoliths are strong evidence for stoping. Evidence for other material transfer processes during emplacement has been largely obscured by intrusion of younger plutons.

The ~6-kb, 65-Ma Oval Peak pluton intrudes the lowest-grade rocks of the Napeequa unit in the eastern part of the Chelan block in the Ross Lake fault system (Miller and Bowring, 1990). This weakly elliptical tonalite, which has a narrow northern tail (Fig. 2), has the shape of an elongate, truncated funnel, as defined by its moderately inward dipping contacts (Fig. 6, section E–E'); the northeast boundary is a major post-emplacement shear zone (Miller and Bowring, 1990; Miller and Paterson, 1999). Downward projection of observed contact dips from the present erosional level implies a minimum vertical extent of 6 km. Magmatic foliation is overprinted by high-temperature subsolidus foliation in a 1–2-km-wide marginal zone in the south and west. Adjacent to this zone is a 200 m–2 km-wide structural aureole marked by deflection of host-rock markers and rotation of regional subhorizontal lineation into a down-dip orientation (Miller and Bowring,

1990). This rotation, and pluton-side-up kinematic indicators in the pluton and aureole, document downward flow of host rock during emplacement.

In addition to the plutons in the western half of the Chelan belt, thin 90–70-Ma sheets (Hurlow, 1992; Matzel, 2004) extensively intrude the Napeequa and Cascade River-Holden units. These dominantly leucotonalite sheets are typically of m-scale thickness and vary in abundance. Unpublished detailed mapping near the Entiat pluton by Paterson indicates that sheets make up at least 30% of the Napeequa outcrop belt.

Shallow Crustal Levels (<5–12 km)

The two large-volume, relatively shallow plutons in the Cascades core are the Mount Stuart and Black Peak batholiths (Fig. 2). These plutons overlap in age and are similar in many respects (Misch, 1966). The better-studied Mount Stuart batholith is tied to the crustal section, and the Black Peak batholith also provides insights into magmatism at shallow levels of the arc.

Mount Stuart Batholith

The 96.3–90.8-Ma Mount Stuart batholith, which consists of a larger (~480 km²) northeast body and smaller southwest body (not mentioned further), is the largest intrusion in the North Cascades. The map pattern of the ~2–4 kb northeast body has been considered in terms of a southeastern “mushroom-shaped” region, the stem of which extends into a central sheet-like segment, and a northwestern “hook-shaped” region (Fig. 2). The “hook” consists of granodiorite which grades to the southeast into tonalite that also makes up the central sheet-like segment. In the mushroom-shaped region, tonalite dominates, grades into granodiorite in the center, and surrounds two-pyroxene gabbro and diorite to the east (Erikson, 1977; Tabor et al., 1987; Paterson et al., 1994).

Matzel et al. (2006) divided the batholith into four age groups. The oldest rocks are 96.3–95.4 Ma, and are in the hook region and a gabbro outlier. The next age group is tonalite in the sheet-like region, followed by tonalite in the “stem” of the mushroom-shaped region (Matzel et al., 2006). The youngest (90.9–90.8 Ma) and most voluminous age domain consists of gabbro, tonalite, and granodiorite of the mushroom region. Matzel et al. (2006) concluded from these age data that the batholith was constructed by short periods of high magma flux separated by magmatic lulls. They also demonstrated that a minimum of 500 km³ of magma was intruded over an interval of ~200 k.y. and that a large magma reservoir existed at this time.

Magmatic foliation in the Mount Stuart batholith defines complex patterns (Paterson and Miller, 1998b). Foliation in the hook-like region delineates dm- to km-scale folds that mimic the shape of the hook and folds in the host Chiwaukum Schist (Paterson and Miller, 1998b; Benn et al., 2001). Strong foliation in the sheet-like domain defines magmatic folds that are parallel to host rock folds, as is subhorizontal lineation, thus demonstrating that some of the host-rock folding occurred at ca. 94–92 Ma (Miller

and Paterson, 1994). An intense flat-lying magmatic foliation with a weak subsolidus overprint near the Windy Pass thrust probably records latest thrust-related strain. In the mushroom region, foliation largely parallels contacts, forming “onion-skin” patterns and records internal magmatic processes (Paterson and Miller, 1998b).

The shape of the batholith is similarly complex. The hook-shaped region is probably a folded, initially subhorizontal to moderately dipping sheet (Paterson and Miller, 1998b). The sheet-like domain dips steeply to the north (Fig. 3) (Tabor et al., 1987), but rolls over into a roof flap (Paterson et al., 1996; Paterson and Miller, 1998b). The roof-wall join is sharp, ranging from subhorizontal to subvertical over ~100 m. Rotated xenoliths are abundant for 200 m vertically below the roof and are locally found >1 km below the roof. In contrast to the older sheet-like phase, the mushroom-shaped region is weakly elliptical in map view, and its southern and southeastern contacts largely dip steeply inward (Fig. 3) where the batholith overlies the Ingalls ophiolite. A km-thick, subhorizontal body of schist, displaying intense subhorizontal foliation, is encased by the batholith below the Windy Pass thrust, and the northeast margin is overprinted by a steep southwest-directed reverse shear zone that has the Ingalls ophiolite in the hanging wall.

Paterson and Miller (1998b) reasoned that the batholith was emplaced by multiple material transfer processes. We briefly summarize their conclusions and refer the reader to their paper for documentation. Ductile flow operated in 1–2-km-wide structural aureoles in the Chiwaukum Schist and eastern part of the Ingalls ophiolite (cf. Albertz et al., 2005) and provided perhaps as much as 50% of the needed material transfer. Crustal thickening by folding, foliation formation, and displacement on reverse shear zones resulted in flow of magma into fold hinges and fractures, and probably accommodated ~15% of the necessary material transfer. Stopping was another significant mechanism, as demonstrated by the xenoliths and truncation of host-rock markers next to segments of the batholith contact. Paterson and Miller (1998b) concluded from structural relationships of deformed markers next to contacts and particularly in the roof that vertical downward transfer of host rock dominated during emplacement.

Small ($\leq 20 \text{ km}^2$) ca. 94–91-Ma satellite bodies (e.g., Becker Peak stock; Fig. 2) that are loosely related to the nearby Mount Stuart batholith intrude the Tonga Formation and Ingalls ophiolite (Southwick, 1962; Duggan and Brown, 1994; Harper et al., 2003), which are the shallowest part of the crustal section. Intrusions into the Ingalls ophiolite include a network of m-scale leucogranite sills fed by dikes just above the Windy Pass thrust (Miller, 1985) and hornblende-phyric dacite to tonalite dikes and stocks that intrude biotite- and sub-biotite-zone rocks of the ophiolite (Southwick, 1962).

Black Peak Batholith

The ca. 91–89-Ma Black Peak batholith intruded across the boundary between the Cascades core and weakly metamorphosed rocks of the Methow basin, and was deformed by Paleogene

shear zones of the Ross Lake fault system (Fig. 2) (Misch, 1966; Kriens and Wernicke, 1990; Miller, 1994). This elliptical-shaped batholith consists dominantly of tonalite and granodiorite. Diorite, gabbro, and hornblende are exposed in a narrow, discontinuous belt along the eastern margin of the batholith, a leuco-tonalite body forms the southern part of the batholith, and there is a transition from hornblende-bearing rocks in the north to hornblende-absent granitoids in the south (Adams, 1964; Miller, 1987). Field relations suggest an age progression from most mafic to felsic rocks (Dragovich et al., 1997).

The eastern contact of the batholith with Methow strata is steep, irregularly shaped in map view, and largely discordant to host rock structures. Host-rock xenoliths are abundant in the outer 50 m of the intrusion next to this contact. The westward protruding flap of greenschist- to lower-amphibolite-facies host rocks equivalent to the Napeequa unit (Fig. 2) is part of the roof (Adams, 1961). These rocks are extensively injected by diorite dikes, and detached and rotated xenoliths ranging from <10 cm to >10 m across are abundant in the adjacent pluton (Adams, 1961, and our observations). In places, it is difficult to recognize a single contact. The western margin of the batholith is a tectonically modified intrusive contact with the higher-grade Napeequa unit.

Hornblende barometry indicates that the eastern part of the batholith crystallized at ~1–3 kb (D.L. Whitney and R.B. Miller, unpublished data from 4 samples), in accord with the weak metamorphism and preservation of sedimentary structures in the host rock (Adams, 1964; Miller et al., 1994). In contrast, amphibolite-facies host rocks on the west record pressures of 6–8 kb (Miller et al., 1993a, 1993b). The higher pressures in the west probably in part record differential loading of the batholith after emplacement (Miller et al., 1993a, 1993b). Nevertheless, regional gradients in metamorphism imply different paleo-depths across the intrusion, and we infer that the vertical extent of the intrusion is probably >8 km.

Complex structural patterns in the Black Peak batholith reflect variable overprinting of magmatic foliation and lineation by solid-state fabrics related to different strands of the Ross Lake fault system and Cretaceous to Eocene regional deformation (e.g., Miller, 1994; Dragovich et al., 1997). This solid-state deformation, which is mostly much younger than crystallization, hinders interpretation of emplacement mechanisms. The rotated xenoliths described above and discordant contacts are evidence of stopping. An ~200-m-wide structural aureole east of the inferred roof is marked by gentle deflection of bedding and cleavage in host rocks into sub-parallelism with the contact and indicates at least limited ductile deformation. No strong solid-state strain, however, is developed in the pluton or host rocks next to this segment of the contact.

Cretaceous Volcanism

A comparison with other continental magmatic arcs implies that the Cretaceous plutons were associated with volcanic rocks, which have been almost entirely removed by erosion. The Cenomanian–Turonian andesitic volcanic rocks, which are

intercalated with clastic rocks of the Methow basin (Barksdale, 1975; McGroder, 1989), are the only mid-Cretaceous arc volcanic rocks adjacent to the Cascades core. These volcanic rocks are roughly coeval with the nearby Black Peak batholith (cf. Kriens and Wernicke, 1990).

Indirect evidence for volcanism comes from the shallow, 91-Ma phase of the Mount Stuart batholith. It represents a large ($\geq 520 \text{ km}^3$), low crystallinity magma reservoir, and records a short period of high magma flux on time scales similar to those of young, high-volume volcanic systems (Matzel et al., 2006; Lipman, 2007).

DISCUSSION

In the following, we return to questions and interpretations about magmatism raised in the “Introduction” of this article that may be addressed by studies of crustal sections, such as that of the North Cascades. Some of these questions involve overall processes operating in magmatic systems, and others deal with potential changes with paleodepth. We focus on more controversial issues and/or on features and processes that are well displayed in the Cascades core.

Changes in Deformation with Depth

The coupling between fabrics in plutons and host rocks increases with depth in the crustal section. Magmatic foliation, lineation, and folds in the mid- to deep-crustal plutons (e.g., Seven-Fingered Jack, Cardinal Peak) are mostly parallel to equivalent structures in host rocks (Fig. 6, sections F–F' and G–G'). These magmatic structures typically record regional shortening. In shallower plutons, particularly the “mushroom-part” of the Mount Stuart batholith, fabrics are partially decoupled from host-rock structures and record internal magmatic processes (e.g., Paterson and Miller, 1998b). These differences with depth probably reflect the slower cooling of deeper plutons and decreasing rheological contrasts between plutons and increasingly hot host rocks.

Solid-state deformation of plutons increases with depth. This is compatible with the smaller rheological contrast between intrusions and host rocks at deeper levels, and the expected slower cooling after reaching the solidus also results in plutons that are weak for longer periods than comparable-sized bodies at shallower depths. Nevertheless, the interiors of several deep plutons (Tenpeak, Sulphur Mountain, High Pass) record only weak solid-state deformation and preserve many igneous features, such as enclaves with crenulate margins, schlieren and other compositional layers typical of mid- to shallow-crustal plutons. The only sizeable orthogneiss that is penetratively deformed in the solid state is the Wenatchee Ridge Gneiss.

Pluton Shapes

A conclusion of recent compilations of pluton shapes inferred from interpretation of gravity data and to a lesser extent

geological mapping is that intrusions are commonly subhorizontal tabular bodies or are wedge shaped (McCaffrey and Petford, 1997; Cruden and McCaffrey, 2001; Cruden, 2006). These analyses probably underestimate the number of steep-sided, vertically extensive ($\geq 10 \text{ km}$) plutons because of the generally insufficient topographic and/or structural relief in most orogens to preserve both the roofs and floors of such plutons. The structural relief of the Cascades crustal section facilitates evaluation of pluton shapes, but for many of the plutons the roof and/or floor is not preserved. Structural complications and poor outcrop in some areas further hinder determination of pluton geometry and we are commonly forced to assume that dips of contacts do not change significantly when projected upward or downward.

Despite these problems, plutons in the Cascades core can be generalized into four broad categories: (1) asymmetric wedges to funnels that are elliptical in map view; (2) subhorizontal tabular bodies; (3) steep-sided, blade-shaped bodies with high aspect ratios in map view; and (4) steep-sided, vertically extensive ($\geq 8 \text{ km}$) bodies that are complexly shaped to elliptical in map view.

The wedge-shaped intrusions include the deep Tenpeak and Sulphur Mountain plutons, which have subvertical contacts for segments of their boundaries and moderately to steeply inward dips along other segments (Figs. 3, section C–C', and 6, section H–H'). The Oval Peak pluton is an elongate funnel (Fig. 6, section E–E'). These intrusions have topographic relief of $\geq 2 \text{ km}$, and simple downward projection of contacts leads to inferred minimum (no roof exposed) vertical extents of ~ 6 – 11.5 km . These plutons range from 21 km to 37 km in length in map view; crude estimates of length-to-thickness ratios range from 1.8 to 4.7. The Dirtyface pluton has a different type of wedge-like geometry; it has a moderately (25 – 50°) dipping floor and moderately to steeply (60 – 80°) dipping, discordant “roof.”

Intrusions that were emplaced as subhorizontal tabular bodies include the 600-m-thick Buck Creek Pass pluton and thinner associated sheets in the Napeequa unit, and some of the sheeted bodies in the Nason Ridge Migmatitic Gneiss. The folded High Pass pluton and hook-like region of the Mount Stuart batholith were probably emplaced as subhorizontal to moderately dipping bodies, and the Riddle Peaks Gabbro may be a tilted, initially subhorizontal sheet.

Steep sheet-like intrusions in the Cascades core are typified by the Seven-Fingered Jack, Entiat, and Cardinal Peak plutons. These intrusions have high aspect ratios in map view (up to 11.5:1), steep contacts that are in part discordant to host rock contacts and structures in cross-sectional view (Fig. 6, sections F–F' and G–G'), and are exposed over $\geq 1.8 \text{ km}$ of topographic relief. The overall shape approximates a knife blade with a horizontal long axis.

Moderately to steeply dipping contacts bound large parts of the Mount Stuart (Fig. 3) and Black Peak batholiths, the two largest intrusions of the Cascades core. Both have locally preserved segments of roofs. Steep contacts of the “mushroom-like” part of the Mount Stuart batholith have a vertical topographic extent of 2.5 km, and host rocks of the Ingalls ophiolite on the south are of

lower grade and probably pressure than elsewhere. Interpretation of hornblende barometry from the Mount Stuart batholith is controversial (cf. Ague and Brandon, 1996, and Anderson, 1997), but is compatible with emplacement depths of different parts of the batholith varying by ~6 km. These observations suggest that the intrusion is vertically extensive (>8 km). Similarly, major differences in metamorphic pressures between host rocks on the east and west sides of the Black Peak batholith imply that it also has a structural relief of >8 km. These vertically extensive plutons are nearly spherical (Mount Stuart “mushroom”) to elliptical (Black Peak) in map view, and extend for 20 km and 50 km, respectively. Their overall geometry probably resembles a thick disk or hockey puck.

Some Cascades intrusions fit the model proposed from compilations that most plutons are subhorizontal and tabular, or wedge-shaped (see above). There is considerable diversity, however, in the geometry of Cascades plutons. Many have minimum vertical extents of 5 km, and have high aspect ratios in map view. Thin (<5 km) subhorizontal tabular bodies are more common with depth and are best represented at depths of >20 km; however, steep sheeted (blade-shaped) bodies and wedge-shaped plutons are also present at these levels.

In the compilations and our analysis, plutons have been considered as isolated entities. We note, however, that many of these plutons are probably thicker “trapped” parts of continuous magma plumbing systems. We envision that many of the plutons pass upward and downward into both thicker and thinner magmatic bodies, and complex lateral changes may also be present. For example, the vertically extensive mushroom region of the Mount Stuart batholith is connected along strike by an older, moderately to steeply dipping, sheet-like mass into a gently to moderately dipping fold-shaped body (Fig. 2).

The detailed high-precision geochronological data from the Mount Stuart batholith and Tenpeak pluton summarized above also indicate that both large blobby plutons and more elongate, partly sheet-like bodies grow over relatively long time periods (2.7–5.6 m.y.) (Matzel et al., 2006). The shapes represented by magmas of individual time intervals may differ significantly from the final geometry of the composite pluton.

We conclude that plutons in the Cascades core display much diversity in geometry, which probably reflects the complex changes in rock type and rheology in arc crust undergoing regional shortening, vertical thickening, and orogen-parallel stretching. This crust is characterized by metamorphosed supracrustal and plutonic rocks with widely varying strengths, and the heterogeneous distribution of magmatism leads to further spatially and temporally variable rheology, all of which influence pluton geometry.

Percentages of Plutonic and Host Rocks with Depth

We have quantitatively estimated accumulation of Cretaceous magmas at shallow, middle, and deep levels in the Cascades core (Table 2). The area considered does not include the

TABLE 2. PLUTON VOLUMES

	Pluton (% of total rock volume)	Unfocused (% of total pluton)
Shallow	37.1	1
Mid-crust	54.6	19
Deep	65.3	18

voluminous Skagit Gneiss Complex (and plutons to the east in the Ross Lake fault zone) because of the uncertainty of crystallization ages of orthogneiss protoliths, nor does it include areas north of where we have conducted research. Areas of discrete plutons are easy to calculate using standard GIS tools, but it is more difficult to determine the amount of intrusive rock represented by the thin sheets (unfocused magmas) that intrude the Napeequa unit, Cascade River-Holden unit, and Nason terrane. Our best estimates of the percentage of the latter types of intrusive rocks from areas we have studied in detail are extrapolated throughout the panel of rock under consideration, and are probably accurate to within 10%.

This analysis indicates that plutonic rocks are volumetrically significant at all crustal levels. The percentage of intrusive rocks increases systematically from shallow, to middle, to deep crustal levels; from ~37% to 55% to 65%, respectively. Focused magmatism defined by discrete plutons and unfocused (dispersed) magmatism represented by typically <50 m-thick sheet-like and irregularly shaped bodies encased by metamorphic host rocks are present at all crustal levels, but are unevenly distributed. Unfocused magmas comprise ~18% of the total plutonic rock in the deep crust and 19% at mid-crustal depths, but <1% at shallower levels (Table 2). The two largest intrusions, the Mount Stuart and Black Peak batholiths, were emplaced at relatively shallow depths.

In some contractional arcs, such as the Arunta inlier of central Australia (Collins and Sawyer, 1996) and the Proterozoic of the southwest United States (e.g., Karlstrom and Williams, 2006), the deep crust is envisioned as a site of rapid melt segregation and migration, either by dikes, or by a pervasive network of mostly meter-scale channels. Magmas generated near the base of the crust are thought to migrate rapidly through deep (25–30 km) crust until they reach a level of neutral buoyancy and accumulate to form batholiths at shallow (10–20 km) levels (Fig. 7) (Collins and Sawyer, 1996). In the Arunta inlier, granitoids make up <10% of the deep crust and >80% of the upper crust (Collins and Sawyer, 1996), and Karlstrom and Williams (2006) reach similar conclusions for the southwest United States. Collins and Sawyer (1996) conclude that large plutons do not form in the deep crust in arcs undergoing compressional deformation.

The Cretaceous contractional arc of the North Cascades clearly differs substantially from observations and models from the arcs described above. Overall, sizeable volumes of magmas accumulated at a very wide range of crustal levels (5–35 km). The percentage of plutonic rock increases, rather than decreases with

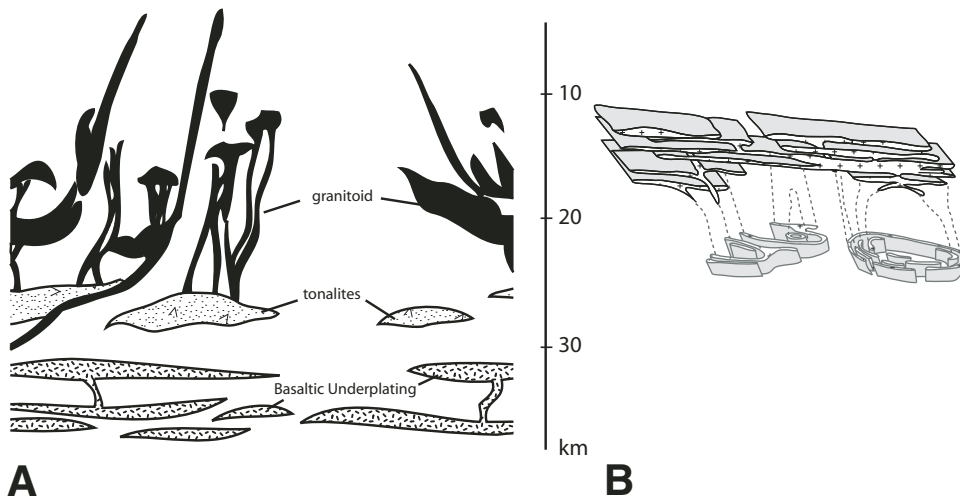


Figure 7. Schematic sections through other contractional arcs emphasizing melt generation in the lower crust and accumulation in upper crust. (A) Proterozoic of southwest United States after Karlstrom and Williams (2006). (B) Arunta inlier of Central Australia after Collins and Sawyer (1996). Vertical scale applies to both sections. See text for discussion.

depth. Much magma accumulated at paleodepths of 25–35 km and formed plutons with minimum volumes of 400 km³. Narrow, widely separated dikes or magma networks cutting long distances through metamorphic rocks are not recognized in the Cascades crustal section. Instead, probable magma transfer zones are represented in the mid- to deep crust by steep-sided sheeted intrusions, such as the Cardinal Peak, Seven-Fingered Jack, and Entiat plutons.

The increase in percentage of plutonic rocks with depth, at least to 25–30 km, is probably typical of other Cordilleran arcs. Such an increase is well-displayed by the Sierra Nevada batholith (e.g., Saleeby, 1990; Saleeby et al., 2003) and Salinian block (Ducea et al., 2003; Kidder et al., 2003).

Magma Fluxes

The compilation of pluton areas, combined with geochronological data, enables evaluation of minimum magma fluxes during construction of the Cretaceous Cascades arc. Minimum fluxes were estimated by multiplying the pluton area times the average topographic relief, which is ≥1.6 km. These calculations indicate that by far the greatest flux of magma in the crustal section and adjacent areas of the Cascades core occurred between 96 and 89 Ma. A minimum of 3586 km³ of magma intruded over an arc length of 130 km, the length for which we have significant geochronological control in the Washington segment of the arc. This corresponds to an average minimum flux of 3.9 × 10⁻⁶ km³/yr/km of arc length during this 7 Ma interval (Table 3). If more realistic thicknesses of 5 km (still probably an underestimate) are used,

then fluxes of 1.2 × 10⁻⁵ km³/yr/km of arc length are obtained (Table 3). Much higher rates are likely over shorter time periods. For example, Matzel et al. (2006) calculated a minimum flux of 3.1 × 10⁻³ km³/yr (assuming minimum thickness of 2.5 km) over the maximum 300,000 year construction of the 91 Ma phase (~208 km²) of the Mount Stuart batholith.

There is little documented magmatism between 88 and 79 Ma, and the other sizeable pulse of Cretaceous plutonism is from ca. 78–71 Ma. Dated plutons of the latter age interval are restricted to the deep mid-crust (6–8 kb). For this latter interval, a minimum of 750 km³ of magma was intruded, which yields an average minimum flux of 8.2 × 10⁻⁷ km³/yr/km of arc length, assuming a thickness of 1.6 km, and 2.6 × 10⁻⁶ km³/yr/km of arc length, assuming a thickness of 5 km. These fluxes are <25% of those from 96 to 89 Ma, and indicate that the greatest magmatic flux occurred during the height of regional mid-Cretaceous shortening of the Coast belt. Reduced magmatism from 88 to 71 Ma was synchronous with an interval of inferred regional transpression (Miller and Bowring, 1990; Hurlow, 1992). We did not extend this analysis to younger time intervals, as the major locus of Eocene magmatism is northeast of the crustal section in the Chelan block (Haugerud et al., 1991), and crystallization ages of protoliths of large volumes of orthogneiss in the Skagit Gneiss Complex are poorly known.

The calculated values for the North Cascades are broadly similar to, or lower than, those estimated for other arcs. For example, Francis and Rundle (1976) calculated values of 2.9 × 10⁻⁶ km³/yr/km of arc length for the Peruvian Coastal batholith and 8.9 × 10⁻⁶ km³/yr/km of arc length for the Cordillera Blanca

TABLE 3. MAGMA FLUXES (130-km-SEGMENT OF ARC)

	Area (km ²)	Flux (1.6 km thick)/km arc length	Flux (5 km thick)/km arc length
96–89 Ma	2241	3.9 × 10 ⁻⁶ km ³ /yr	1.2 × 10 ⁻⁵ km ³ /yr
78–71 Ma	469	8.2 × 10 ⁻⁷ km ³ /yr	2.6 × 10 ⁻⁶ km ³ /yr

batholith, assuming average pluton thicknesses of 5 km. Ducea (2001) utilizing a plutonic thickness of 30 km estimated rates of 1×10^{-2} km³/yr/km of arc length for the entire duration (Triassic-Cretaceous) of the Sierra Nevada batholith. Rates were dramatically higher during the main pulse of Cretaceous magmatism in the batholith, reaching 8.5×10^{-2} km³/yr/km (Ducea, 2001).

Petrology and Geochemistry

Tonalites dominate at all levels of the crustal section, and there are only relatively minor differences in rock types between deep and shallow plutons. Granodiorites are subsidiary components of most of the major plutons. Gabbros and diorites are also subordinate, but not rare. The 30 km², 6–8 kb Riddle Peaks pluton is entirely gabbro, and diorite and gabbro comprise ~75 km² of the large northeast body of the Mount Stuart batholith. Mafic rocks make up a small percentage of several other plutons considered in this study; we estimate that they represent ~2% of the volume of studied plutons.

It is more difficult to quantify the percentage of individual rock types in the thin sheets that intrude the Napeequa, Nason Ridge, and Cascade River-Holden units. Unfocused magmatism represented by sheets formed rocks with lower color index than the isolated plutons, and gabbro sheets are rare. The unfocused magmas may represent a greater degree of locally transported partial melt than in the discrete plutons.

Simple zoned plutons are rare in the Cascades core, particularly compared to another large Mesozoic Cordilleran arc, the Sierra Nevada batholith (e.g., Bateman, 1992). The same temporal sequence, however, of early mafic magmas followed by more felsic magma, and accompanying overall inward increase in SiO₂, as typifies normally zoned plutons, is observed in many of the Cascades plutons. This sequence is illustrated by mid- to deep-crustal, steep sheet-like (Cardinal Peak, Entiat, Seven Fingered Jack) and wedge-shaped (Tenpeak, Sulphur Mountain) intrusions where early marginal, heterogeneous mafic complexes yield inward to tonalite and/or granodiorite (Cater, 1982; Dawes, 1993; Miller and Paterson, 2001a). In the shallower Mount Stuart batholith, mafic rocks were emplaced during both the earliest (96.5 Ma) and latest (91 Ma) magmatic pulses (Matzel et al., 2006). The latter, high-volume pulse resulted in an asymmetric, normally zoned pattern from gabbro/diorite through tonalite to granodiorite and back to tonalite.

In arcs, and continental crust as a whole, plutons and host rocks are more mafic with depth. We have not attempted to systematically examine host-rock geochemical composition with depth in the crustal section, but as for the plutons, host-rock chemistry does not appear to vary systematically with depth. The shallowest part of the section is ultramafic-dominated ophiolitic rock. On average, the mid-crust is mainly pelitic and psammitic schist. Mafic rocks (amphibolite) make up perhaps 30%–60% of the deep-crustal Napeequa unit, but the rest are high-silica rocks (quartzite and biotite schist). We have speculated previously (Miller and Paterson, 2001b) on the constituents of the

unexposed deepest crust. By analogy with other crustal sections, migmatites should be present below exposed crustal levels. Mafic rocks, such as gabbro, mafic gneiss, amphibolite, and granulite, are likely components, particularly given the generally felsic composition of the exposed Cascades crust. Mafic rocks make up the lowermost 10–15 km of crust in the on-strike continuation of the Cascades core according to seismic reflection and refraction data collected in southwest British Columbia (Clowes et al., 1995, 1997; Zelt et al., 1996). Petrological and geochemical data from tonalitic plutons in the Cascades suggest derivation in part from partial melting of deep-crustal (~18 kb, ~55–60 km) garnet amphibolite (Dawes, 1993; DeBari et al., 1998).

Emplacement

Interpretations of emplacement mechanisms for individual plutons have been presented in the appropriate sections above, and we have published detailed observations relevant to emplacement of individual plutons elsewhere (e.g., Miller and Bowring, 1990; Paterson et al., 1996; Paterson and Miller, 1998a, 1998b; Miller and Paterson, 1999, 2001a). In the following, we briefly summarize our conclusions on emplacement at different crustal levels.

Multiple material transfer processes operated during emplacement at all crustal levels. The relative importance of different processes changes with depth, but there are no appreciable differences in mechanisms with crustal level. The following features are common to most Cascades plutons.

1. Narrow (≤ 1 km wide) structural aureoles are typical, as displayed by one of the deepest plutons, the Tenpeak pluton, and one of the shallowest plutons, the Mount Stuart batholith. Segments of contacts of some intrusions are sharply discordant, as illustrated by parts of the 6–8 kb, Cardinal Peak pluton (Fig. 6, G–G'). Overall, structural aureoles are slightly wider (normalized to body radii) for the deep plutons.
2. Heterogeneous vertical ductile flow dominated in the structural aureoles, and deflection of host rock markers and the kinematics of non-coaxial shear indicate that host rock dominantly was transported downward relative to the adjacent pluton (Figs. 3 and 6). Brown and McClelland (2000) reached similar conclusions for the emplacement of several plutons in the northernmost part of the North Cascades in southwest British Columbia.
3. Stopping occurred during emplacement at the deepest (Sulphur Mountain, Tenpeak), intermediate (Riddle Peaks, Cardinal Peak), and shallowest (Mount Stuart, Black Peak) structural levels. Stopping may have transferred relatively limited amounts of host rock, probably <30% of the necessary material (cf. Paterson et al., 2008), but if it removed parts of inner structural aureoles, then it partially obscured potential emplacement mechanisms (Paterson et al., 1996; Gerbi et al., 2004). Stopping was thus an important mechanism throughout the arc section,

contrary to assertions that stoping is an insignificant process (Glazner and Bartley, 2006).

4. There is little to no evidence that dilation in or across fault zones was a significant material transfer process during emplacement. Many of the plutons in the Cascades core are not associated spatially with map-scale faults or shear zones (Fig. 2). Syn-emplacement, southwest-directed reverse shear zones that developed along segments of the margins of the Mount Stuart batholith, Dirtyface pluton, and Tenpeak pluton (Fig. 2) do not extend beyond the plutons and thus did not act as a regional anisotropy that controlled emplacement. Instead, these structures were likely localized by the rheological contrast between the solidified plutons and weaker host rocks (Miller and Paterson, 2001b). In the Ross Lake fault zone, the Black Peak batholith is cut by shear zones (Fig. 2), but these are >20 m.y. younger than emplacement. The southwest and southern margins of the Oval Peak pluton coincide with a reverse-slip shear zone active during transpression in the Ross Lake fault zone; this may represent the closest relationship between pluton emplacement and faulting. In short, active faults probably affected the local stress field near some plutons, and thus indirectly influenced magma ascent, but there was little direct relationship between emplacement and faulting.
5. Folding and heterogeneous ductile regional deformation occurred during magmatism, and folding was intimately linked to emplacement of several plutons. This is illustrated by the fold-like shapes of the hook-like region of the Mount Stuart batholith and High Pass pluton, which mimic folds in the enclosing host rock, and the position of the tips of sheets of the Seven-Fingered Jack and Entiat plutons along axial surfaces of host-rock folds (Paterson and Miller, 1998a). Further, 10-cm- to m-scale-thick bodies locally form saddle reefs in smaller host rock folds (Miller and Paterson, 2001b; Alibert et al., 2005). We suggest that the genetic link between folding and emplacement is through effects on the stress field, as growth of folds is typically slow compared to magma transport rates (e.g., Paterson and Tobisch, 1992).
6. Roof uplift and cauldron subsidence, which are important material transfer processes for shallow-level magma bodies, have not been recognized in the crustal section. This may reflect the only minor preservation of very shallow levels of the Cretaceous crust.
7. As with most studies of individual plutons, it is difficult to find field evidence for the amount of needed material transfer to accommodate the large-volume magmatism. We infer that ductile flow and bending of rocks in narrow aureoles, combined with stoping and magma wedging, can account for much of the needed material transfer.

The conclusions listed above, particularly the widespread evidence for vertical ductile flow and stoping, indicate that host rock was dominantly transported vertically and not laterally during

emplacement. This vertical transport probably records return flow (e.g., Saleeby, 1990; Paterson et al., 1996; Tobisch et al., 2000; Paterson and Farris, 2008) and/or floor sinking (Cruden, 1998, 2006; Brown and McClelland, 2000). Ductile flow occurred in a narrow zone between undeformed (by emplacement) host rock and the pluton wall. This zone typically widened slightly downward, and persisted into the deep crust despite the presumably smaller thermal gradients between plutons and host rocks (cf. Paterson and Farris, 2008).

Stoping, a brittle process that is commonly considered a shallow-level mechanism, occurred at all crustal levels. We infer that this largely reflects the high flux rates during growth of large magma chambers relative to ductile strain rates of host rocks. Thermal heating, regional strain, and diking all may cause host rock to break apart, and in the Cascades core the commonly relatively denser host rocks (e.g., amphibolite) may have collapsed into rheologically weaker magmas (Paterson and Farris, 2008). Magma fluxes probably varied widely during the construction of individual plutons. For example, the vertically sheeted plutons (e.g., Cardinal Peak) were constructed initially by low-volume sheets, during which wedging and ductile flow probably occurred in the structural aureole; as subsequent, larger-volume bodies were emplaced, other mechanisms such as stoping and rigid rotations are inferred to have increased in importance.

The downward transport of host rock associated with emplacement largely occurred during major orogen-normal shortening and burial of supracrustal rocks in the North Cascades core. Regional deformation and vertical host rock transport thus contributed to crustal thickening and formation of a crustal root in the orogen (cf. Saleeby, 1990; Tobisch et al., 2000; Paterson and Farris, 2008).

Geothermal Gradient of the Crustal Section

The architecture and rheology of an arc, and depths at which different processes operate, are strongly influenced by the paleogeothermal gradient. The gradient in the upper crust of the Cascades arc was relatively steep, as recorded in the Ingalls ophiolite which grades from lower-greenschist to upper-amphibolite facies over ~11 km in map view. Amphibolite-facies assemblages in the highest-grade part of the ophiolite, near the 2–4 kb Mount Stuart batholith, indicate that upper-crustal gradients exceeded 40 °C/km for at least a short time interval. In contrast, in the middle to deep crust of the arc, thermobarometry from the Nason terrane and Napeequa unit indicates that temperatures did not exceed 700 °C at depths reaching ≥35 km, corresponding to a gradient of ~20 °C/km. The high gradients in the upper crust are typical of continental magmatic arcs, but there were relatively small differences (~555° to <700 °C) between peak temperatures at paleodepths of 15–35 km. This range in peak temperatures in the middle to deep crust is much lower than that commonly cited for this interval based on numerical models and typical metamorphic field gradients (e.g., Barton and Hanson, 1989; Rothstein and Manning, 2003).

The relatively low temperatures of the mid- to deep-crustal rocks probably reflect the interplay between advection of heat by magmatism and crustal thickening by regional deformation. Rapid crustal thickening presumably reduced the geothermal gradient. We also speculate that mid-Cretaceous underthrusting of relatively cool Wrangellian terrane beneath at least part of the North Cascades orogen had a chilling effect, although deep-seated melting continued during shortening. The impingement of Wrangellia beneath the arc may have also led to the near cessation of magmatism at ca. 88 Ma. Moreover, the position of the Cascades core at the termination of the arc likely further contributed to the relatively low temperatures. The higher temperatures in the deep crust of many other contractional arcs may in part reflect a combination of less crustal thickening, higher magma fluxes, and/or lack of underthrusting of cold crust.

The relatively low temperatures in the mid- to deep crust probably explains some of the differences between the Cascades arc and other thinner arc crustal sections. For example, plutons with weak to modest solid-state deformation at ~25–35 km paleodepths in the Cascades core contrast with the strongly deformed orthogneisses that typify some crustal sections at equivalent paleodepths (cf. Percival et al., 1992). Further, there is no widespread migmatization and/or mafic-rich zones of melting, assimilation, storage, and homogenization (MASH) at these levels in the Cascades core, in contrast to many other arc sections.

Summary Model

The much greater abundance of unfocused magma at mid- and deep-crustal levels, and presence of the largest plutons at shallow levels have interesting implications. Many lower-volume pulses of magma apparently stall at depths that range from ≥ 35 to ~18 km. These magmas commonly intrude subhorizontally at the level of emplacement, as represented by the thin sill-like sheets and small irregularly shaped masses. Other magmas accumulated in the deep crust in higher volumes and coalesced to form discrete plutons. Some of these plutons also intruded subhorizontally (e.g., High Pass, Buck Creek Pass), but in other sites at equivalent depths, plutons with steep contacts formed (e.g., Tenpeak, Sulphur Mountain). In the shallow crust, the batholith-sized intrusions and limited unfocused bodies in the shallowest crust imply that significant volumes of magma were able to rise efficiently to higher crustal levels along the same pathways. Such intrusions remained sites of large-volume accumulations for extended time intervals, as demonstrated by the ca. 5.5 m.y. for construction of the Mount Stuart batholith.

The relatively big intrusions at deeper crustal levels, such as the Tenpeak and Seven-Fingered Jack pluton, are constructed of magma sheets and larger, more elliptical masses of distinct composition and texture with little evidence of homogenization between magma pulses. In contrast, the shallow-level Mount Stuart batholith shows apparently gradational contacts between magma pulses of differing composition and significantly different

ages (Matzel et al., 2006). These differences may reflect construction by distinct lower-volume magma batches emplaced episodically, such as in the Tenpeak pluton, versus short-lived, higher-flux magmatism such as in the Mount Stuart batholith (Matzel et al., 2006). Alternatively, if the mid- to lower-crustal intrusions represent conduits between lower crustal zones of magma generation and mixing, and upper crustal zones of large, relatively homogenous intrusions such as the Mount Stuart batholith, then the sharp internal contacts in deeper plutons may record the last magma to ascend through the system, and thus represent a “snapshot” of ascending magmas (Miller and Paterson, 2001a).

We interpret these relationships in terms of the following model (Fig. 8). Magmas encompassing variable proportions of mantle-derived mafic melt and crustal melt from a garnet-bearing source in the lower crust below the exposed Cretaceous crustal section rose to a wide range of crustal levels. These magmas ascended in broadly arc-parallel, magma transfer zones during regional shortening. The elongate, vertically sheeted, deep- to mid-crustal bodies oriented at high angles to the regional shortening direction do not fit classic brittle diking mechanisms. We contend that it is more likely that magmas ascended through a network of channels (e.g., Weinberg, 1999; Brown, 2004) and/or as multiple pulses of narrow, elongate visco-elastic diapirs (Paterson and Miller, 1998a; Miller and Paterson, 1999, 2001a). Early mafic sheets crystallized along the walls of the plutonic system. These rocks were intruded by wider tonalite sheets, and a larger “chamber” eventually formed in the interior of the system (Fig. 8). The amount of crustal melt presumably increased with time. The vertically sheeted, partially molten bodies aided the ascent of subsequent magmas to higher crustal levels (e.g., Mount Stuart) where larger volumes of magma became more thoroughly hybridized, which led to gradational contacts. The final product is a complex three-dimensional system of variably connected plutonic bodies with a wide range of shapes and sizes.

CONCLUSIONS AND MAJOR REMAINING QUESTIONS

1. The Cascades core provides an opportunity to examine Cretaceous magmatic systems from ~5–40 km paleodepth.
2. The volume of trapped magmas increases with depth.
3. Pluton shapes and sizes vary widely at all crustal levels, and include: asymmetric wedges to elongate funnels that are elliptical in map view; subhorizontal tabular bodies; steep-sided blade-shaped intrusions that have high aspect ratios in map view; and steep-sided, vertically extensive (≥ 10 km) bodies that are probably shaped like thick disks or hockey pucks.
4. The largest magmatic bodies occur at shallow levels, whereas small, unfocused bodies are abundant at mid- to deep-crustal levels. The focused and unfocused bodies are probably parts of complex magma plumbing systems.

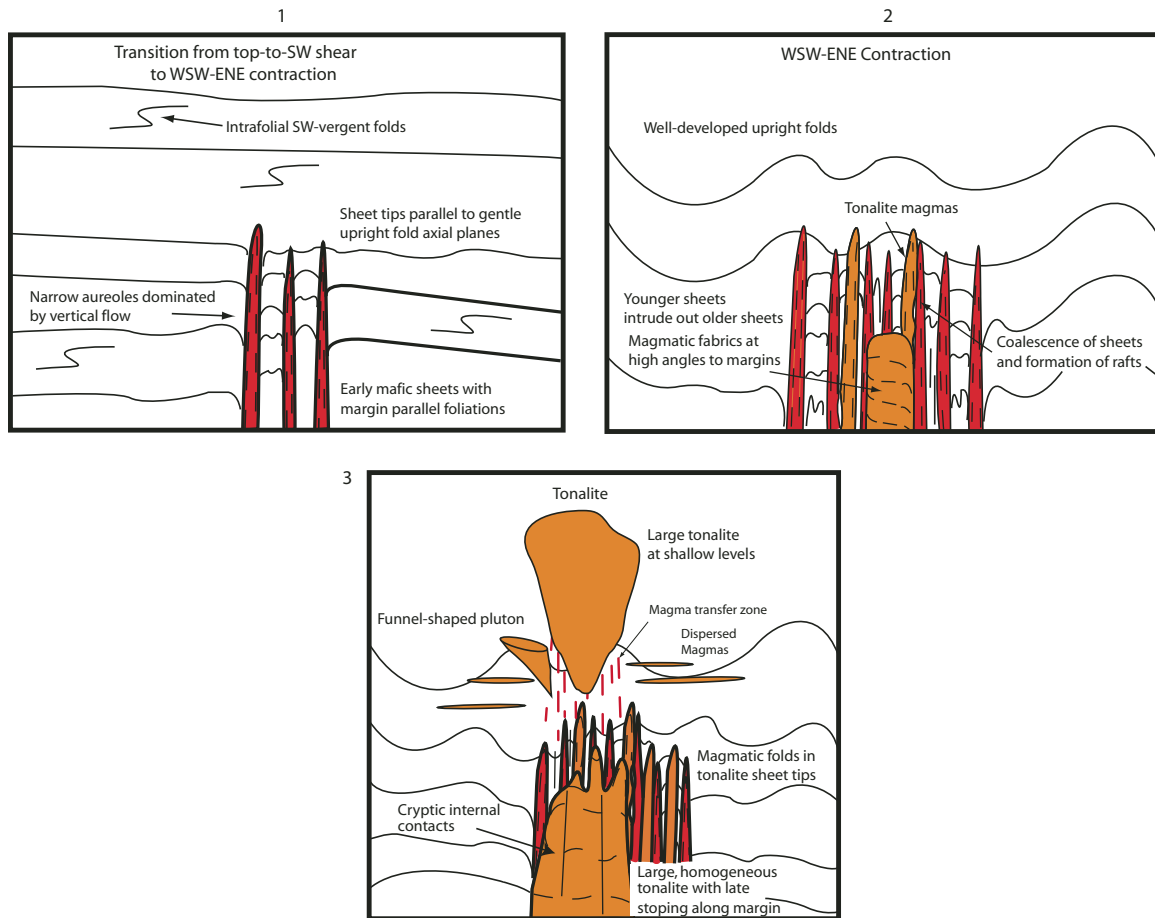


Figure 8. Cartoon illustrating hypothesized development of sheeted plutons and possible role as magma transfer zones for larger and more homogeneous plutons in the shallow crust. The cartoon illustrates representative shapes of plutons (see text for discussion).

5. The Cascades core is part of an episodic, but at times high flux continental magmatic arc system with its maximum peak at 96–89 Ma, and a smaller peak at 78–71 Ma. Such episodic patterns are likely representative of Cordilleran systems in general.
6. Many plutonic systems in the arc are composite and form over millions of years (e.g., 2.5 m.y. for Tenpeak pluton and 5.5 m.y. for Mount Stuart batholith).
7. Downward movement of host rock by multiple processes occurred at all crustal levels during emplacement. Ductile deformation and accompanying rigid rotations probably dominated and stoping played an important secondary role. Magma wedging and regional deformation also aided emplacement.
8. Peak metamorphic temperatures in the mid- to deep crust were low for magmatic arcs, perhaps reflecting rapid crustal thickening by regional deformation and underthrusting of cold crust of the Wrangellian terrane. These low temperatures may explain several differences between the Cascades core and thinner arc sections, including the

only modest solid-state deformation of tonalitic plutons and lack of migmatization of host rocks in the deep (30–35 km) crust.

A number of unanswered questions are raised by our synthesis.

1. What causes major variations in magmatic fluxes?
2. Are Cordilleran arcs dramatically different than arcs elsewhere, and if so, why?
3. Are there major differences between magmatic systems in the deep crust with some dominated by metamorphic host rocks and others by downward increasing volumes of magma?
4. What is the most important material transfer process during emplacement? Does downward movement dominate? What are the roles of stoping and faulting? It is also important to consider that with incrementally constructed magma systems, “host rock” includes earlier magmatic pulses in the system.
5. What is the duration of growth of magma chambers at different crustal levels and in bodies of different shapes?

6. How are larger, apparently more homogeneous, and in some cases zoned bodies formed at shallower levels if magma is passing through complex plumbing systems at depth?

ACKNOWLEDGMENTS

We thank Lawford Anderson, Cal Barnes, Sam Bowring, Ned Brown, Sue DeBari, Jonathan Miller, Harold Stowell, and Donna Whitney for helpful discussions. This research was supported by National Science Foundation Grants EAR-9980623 to S. Bowring, EAR-9218741 and EAR-9614521 to Paterson, and EAR-9980662 and EAR-0511062 to Miller. Ned Brown and co-editor Art Snoko provided thorough and very helpful reviews.

REFERENCES CITED

- Adams, J.B., 1961, Petrology and structure of the Stehekin-Twisp Pass area, North Cascades, Washington [Ph.D. thesis]: Seattle, University of Washington, 171 p.
- Adams, J.B., 1964, Origin of the Black Peak Quartz Diorite, northern Cascades, Washington: *American Journal of Science*, v. 262, p. 290–306.
- Ague, J.L., and Brandon, M.T., 1996, Regional tilt of the Mount Stuart batholith, Washington, determined using aluminum-in-hornblende barometry: Implications for the northward translation of Baja British Columbia: *Geological Society of America Bulletin*, v. 108, p. 471–488, doi: 10.1130/0016-7606(1996)108<0471:RTOTMS>2.3.CO;2.
- Albertz, M., Paterson, S.R., and Okaya, D., 2005, Fast strain rates during pluton emplacement: Magmatically folded leucocratic dikes in aureoles of the Mount Stuart batholith, Washington and Tuolumne Intrusive Suite, California: *Geological Society of America Bulletin*, v. 117, p. 450–465, doi: 10.1130/B25444.1.
- Anderson, J.L., 1997, Regional tilt of the Mount Stuart batholith, Washington, determined using aluminum-in-hornblende barometry: Implications for the northward translation of Baja British Columbia: Discussion and reply: *Geological Society of America Bulletin*, v. 109, p. 1223–1227, doi: 10.1130/0016-7606(1997)109<1223:RTOTMS>2.3.CO;2.
- Barksdale, J.D., 1975, Geology of the Methow Valley, Okanogan County, Washington: Washington Division of Geology and Earth Resources Bulletin 68, 72 p.
- Barton, M.D., and Hanson, R.B., 1989, Magmatism and the development of low-pressure metamorphic belts: Implications from the western United States and thermal modeling: *Geological Society of America Bulletin*, v. 101, p. 1051–1065, doi: 10.1130/0016-7606(1989)101<1051:MATDOL>2.3.CO;2.
- Bateman, P.C., 1992, Plutonism in the central part of the Sierra Nevada batholith, California: U.S. Geological Survey Professional Paper 1483, 186 p.
- Bateman, P.C., and Chappell, B.W., 1979, Crystallization, fractionation, and solidification of the Tuolumne Intrusive Series, Yosemite National Park, California: *Geological Society of America Bulletin*, v. 90, p. 465–482, doi: 10.1130/0016-7606(1979)90<465:CFASOT>2.0.CO;2.
- Benn, K., Paterson, S.R., Lund, S.P., Pignotta, G.S., and Kruse, S., 2001, Magmatic fabrics in batholiths as markers of regional strains and plate kinematics: Example of the Cretaceous Mt. Stuart batholith: *Physics and Chemistry of the Earth: Solid Earth and Geodesy*, v. 26, p. 343–354, doi: 10.1016/S1464-1895(01)00064-3.
- Boysun, M.A., 2004, Partial melting, melt collection and transport in the Swakane Gneiss, North Cascades crystalline core, WA [M.S. thesis]: Los Angeles, University of Southern California, 86 p.
- Brandon, M.T., Cowan, D.S., and Vance, J.A., 1988, The Late Cretaceous San Juan thrust system, San Juan Islands, Washington: *Geological Society of America Special Paper* 221, 81 p.
- Brown, E.H., 1987, Structural geology and accretionary history of the Northwest Cascades system, Washington and British Columbia: *Geological Society of America Bulletin*, v. 99, p. 201–214, doi: 10.1130/0016-7606(1987)99<201:SGAAHO>2.0.CO;2.
- Brown, E.H., and Dragovich, J.D., 2003, Tectonic elements and evolution of northwest Washington: Washington Division of Geology and Earth Resources, Geologic Map GM-52, scale 1:625,000.
- Brown, E.H., and Gehrels, G.E., 2007, Detrital zircon constraints on terrane ages and affinities and timing of orogenic events in the San Juan Islands and North Cascades, Washington: *Canadian Journal of Earth Sciences*, v. 44, p. 1375–1396, doi: 10.1139/E07-040.
- Brown, E.H., and McClelland, W.C., 2000, Pluton emplacement by sheeting and vertical ballooning in part of the southeast Coast Plutonic Complex, British Columbia: *Geological Society of America Bulletin*, v. 112, p. 708–719, doi: 10.1130/0016-7606(2000)112<0708:PEBSAV>2.3.CO;2.
- Brown, E.H., and Walker, N.W., 1993, A magma-loading model for Barrovian metamorphism in the southeast Coast Plutonic Complex, British Columbia and Washington: *Geological Society of America Bulletin*, v. 105, p. 479–500, doi: 10.1130/0016-7606(1993)105<0479:AMLMBF>2.3.CO;2.
- Brown, E.H., Carey, J.A., Dougan, B.E., Dragovich, J.D., Fluke, S.M., and McShane, D.P., 1994, Tectonic evolution of the Cascades crystalline core in the Cascade River area, Washington: Washington Division of Geology and Earth Resources Bulletin, v. 80, p. 93–113.
- Brown, M., 2004, The mechanism of melt extraction from lower continental crust of orogens: *Transactions of the Royal Society of Edinburgh: Earth Sciences*, v. 95, p. 35–48, doi: 10.1017/S026359330000900.
- Brown, M., and Solar, G.S., 1999, The mechanism of ascent and emplacement of granite magma during transpression: A syntectonic granite paradigm: *Tectonophysics*, v. 312, p. 1–33, doi: 10.1016/S0040-1951(99)00169-9.
- Buddington, A.F., 1959, Granite emplacement with special reference to North America: *Geological Society of America Bulletin*, v. 70, p. 671–747, doi: 10.1130/0016-7606(1959)70[671:GEWSRT]2.0.CO;2.
- Cater, F.W., 1982, Intrusive rocks of the Holden and Lucerne quadrangles, Washington; the relation of depth zones, composition, textures, and emplacement of plutons: U.S. Geological Survey Professional Paper 1220, 108 p.
- Cater, F.W., and Crowder, D.F., 1967, Geologic map of the Holden Quadrangle, Snohomish and Chelan Counties, Washington: U.S. Geological Survey Map GQ-646, scale 1:62,500.
- Christensen, N.I., and Mooney, W.D., 1995, Seismic velocity structure and composition of the continental crust: A global view: *Journal of Geophysical Research*, v. 100, p. 9761–9788, doi: 10.1029/95JB00259.
- Clowes, R.M., Zelt, C.A., Amor, J.R., and Ellis, R.M., 1995, Lithospheric structure in the southern Canadian Cordillera from a network of seismic refraction lines: *Canadian Journal of Earth Sciences*, v. 32, p. 1485–1513.
- Clowes, R.M., Baird, D.J., and Dehler, S.A., 1997, Crustal structure of the Cascadia subduction zone, southwestern British Columbia, from potential field and seismic studies: *Canadian Journal of Earth Sciences*, v. 34, p. 317–335.
- Collins, W.J., and Sawyer, E.W., 1996, Pervasive magma transfer through the lower-middle crust during non-coaxial compressional deformation: An alternative to dyking: *Journal of Metamorphic Geology*, v. 14, p. 565–579, doi: 10.1046/j.1525-1314.1996.00442.x.
- Crowder, D.F., Tabor, R.W., and Ford, A.B., 1966, Geologic map of the Glacier Peak Quadrangle, Snohomish and Chelan Counties, Washington: U.S. Geological Survey Map, GQ-473, scale 1:62,500.
- Cruden, A.R., 1998, On the emplacement of tabular granites: *Journal of the Geological Society of London*, v. 155, p. 853–862, doi: 10.1144/gsjgs.155.5.0853.
- Cruden, A.R., 2006, Emplacement and growth of plutons: Implications for rates of melting and mass transfer in continental crust, in Brown, M., and Rushmer, T., eds., *Evolution and differentiation of continental crust*: Cambridge, UK, Cambridge University Press, p. 455–519.
- Cruden, A.R., and McCaffrey, K.J.W., 2001, Growth of plutons by floor subsidence: Implications for rates of emplacement, intrusion spacing and melt-extraction mechanisms: *Physics and Chemistry of the Earth. Part A: Solid Earth and Geodesy*, v. 26, p. 303–315, doi: 10.1016/S1464-1895(01)00060-6.
- Dawes, R.L., 1993, Mid-crustal Late Cretaceous plutons of the North Cascades: Petrogenesis and implications for the growth of continental crust [Ph.D. thesis]: Seattle, University of Washington, 272 p.
- DeBari, S.M., Miller, R.B., and Paterson, S.R., 1998, Genesis of tonalitic plutons in the Cretaceous magmatic arc of the North Cascades; mixing of mantle-derived mafic magmas and melts of a garnet-bearing lower crust:

- Geological Society of America Abstracts with Programs, v. 30, no. 5, p. 257–258.
- Dragovich, J.D., Norman, D.K., Haugerud, R.A., and Miller, R.B., 1997, Geologic map and bedrock history of the Gilbert 7.5-minute Quadrangle, Chelan and Okanogan Counties, Washington: Washington Division of Geology and Earth Resources Geologic Map GM-46, 67 p.
- Ducea, M., 2001, The California arc: Thick granitic batholiths, eclogitic residues, lithospheric-scale thrusting, and magmatic flare-ups: *GSA Today*, v. 11, no. 11, p. 4–10, doi: 10.1130/1052-5173(2001)011<0004:TCATGB>2.0.CO;2.
- Ducea, M.N., Kidder, S., and Zandt, G., 2003, Arc composition at mid-crustal depths: Insights from the Coast Range belt, Santa Lucia Mountains, California: *Geophysical Research Letters*, v. 30, doi: 10.1029/2002GL016297.
- Duggan, K.M., and Brown, E.H., 1994, Correlation of the Tonga Formation and Chiwaukum Schist, North Cascades, Washington: *Tectonics*, v. 13, p. 1411–1424, doi: 10.1029/94TC02019.
- Engels, J.C., Tabor, R.W., Miller, F.K., and Obradovich, J.D., 1976, Summary of K-Ar, Rb-Sr, U-Pb, Pb-alpha, and fission-track ages of rocks from Washington State prior to 1975 (exclusive of Columbia Plateau basalts): U.S. Geological Survey Miscellaneous Field Studies, Map MF-710.
- Erikson, E.H., 1977, Petrology and petrogenesis of the Mt. Stuart batholith—Plutonic equivalent of the high-alumina basalt association?: Contributions to Mineralogy and Petrology, v. 60, p. 183–207, doi: 10.1007/BF00372281.
- Evans, B.W., and Berti, J.W., 1986, Revised metamorphic history for the Chiwaukum Schist, North Cascades, Washington: *Geology*, v. 14, p. 695–698, doi: 10.1130/0091-7613(1986)14<695:RMHFTC>2.0.CO;2.
- Evans, B.W., and Davidson, G.F., 1999, Kinetic control of metamorphic imprint during synplutonic loading of batholiths: An example from Mount Stuart, Washington: *Geology*, v. 27, p. 415–418, doi: 10.1130/0091-7613(1999)027<0415:KCOMID>2.3.CO;2.
- Francis, P., and Rundle, C.C., 1976, Rates of production of the main magma types in the central Andes: *Geological Society of America Bulletin*, v. 87, p. 474–480, doi: 10.1130/0016-7606(1976)87<474:ROPOTM>2.0.CO;2.
- Gao, S., Zhang, B.R., Jin, Z.M., Kern, H., Luo, T.C., and Zhao, Z.D., 1998, How mafic is the lower continental crust?: *Earth and Planetary Science Letters*, v. 161, p. 101–117, doi: 10.1016/S0012-821X(98)00140-X.
- Gerbi, C.C., Johnson, S.E., and Paterson, S.R., 2004, Implications of rapid, dike-fed pluton growth for host-rock strain rates and emplacement mechanisms: *Journal of Structural Geology*, v. 26, p. 583–594, doi: 10.1016/j.jsg.2003.08.008.
- Getsinger, J.S., 1978, A structural and petrologic study of the Chiwaukum Schist on Nason Ridge, northeast of Stevens Pass, North Cascades, Washington [M.S. thesis]: Seattle, University of Washington, 151 p.
- Glazner, A.F., and Bartley, J.M., 2006, Is stoping a volumetrically significant pluton process?: *Geological Society of America Bulletin*, v. 118, p. 1185–1195, doi: 10.1130/B25738.1.
- Hamilton, W., and Meyers, W.B., 1967, The nature of batholiths: U.S. Geological Survey Professional Paper 554, p. 1–30.
- Harper, G.D., Miller, R.B., MacDonald, J.H., Miller, J.S., and Mlinarevic, A.N., 2003, Evolution of a polygenetic ophiolite: The Jurassic Ingalls ophiolite, Washington Cascades, in Swanson, T.W., ed., *Western Cordillera and adjacent areas*: Geological Society of America Field Guide 4, p. 251–265.
- Haugerud, R.A., van der Heyden, P., Tabor, R.W., Stacey, J.S., and Zartman, R.E., 1991, Late Cretaceous and Early Tertiary plutonism and deformation in the Skagit Gneiss Complex, North Cascade Range, Washington and British Columbia: *Geological Society of America Bulletin*, v. 103, p. 1297–1307, doi: 10.1130/0016-7606(1991)103<1297:LCAETP>2.3.CO;2.
- Hurlow, H.A., 1992, Structural and U/Pb geochronologic studies of the Pasayten fault, Okanogan Range batholith, and southeastern Cascades crystalline core, Washington [Ph.D. thesis]: Seattle, University of Washington, 180 p.
- Hutton, D.H.W., 1992, Granite sheeted complexes: Evidence for the dyking ascent mechanism: *Transactions of the Royal Society of Edinburgh: Earth Sciences*, v. 83, p. 377–382.
- Jensen, L., Lebit, H., Paterson, S.R., Miller, R.B., and Vernon, R.H., 2007, Regional inverted metamorphism in the coaxially refolded Tonga Formation: Evidence for Mesozoic accretional tectonics in the Cascades crystalline core: *Geological Society of America Abstracts with Programs*, v. 39, no. 4, p. 14.
- Journeay, J.M., and Friedman, R.M., 1993, The Coast Belt thrust system: Evidence of Late Cretaceous shortening in southwest British Columbia: *Tectonics*, v. 12, p. 756–775, doi: 10.1029/92TC02773.
- Karlstrom, K.E., and Williams, M.L., 2006, Nature and evolution of the middle crust: Heterogeneity of structure and process due to pluton-enhanced tectonism, in Brown, M., and Rushmer, T., eds., *Evolution and differentiation of continental crust*: Cambridge, UK, Cambridge University Press, p. 268–295.
- Kidder, S., Ducea, M., Gehrels, G., Patchett, P.J., and Vervoort, J., 2003, Tectonic and magmatic development of the Salinian Coast Ridge belt, California: *Tectonics*, v. 23, doi: 10.1029/2002TC001409.
- Kriens, B., and Wernicke, B., 1990, Nature of the zone between the North Cascades crystalline core and the Methow Sequence in the Ross Lake area, Washington: Implications for Cordilleran tectonics: *Tectonics*, v. 9, p. 953–981, doi: 10.1029/TC009i005p0953.
- Lipman, P.W., 2007, Incremental assembly and prolonged consolidation of Cordilleran magma chambers: Evidence from the southern Rocky Mountain volcanic field: *Geosphere*, v. 3, p. 42–70, doi: 10.1130/GES00061.1.
- MacDonald, J.H., Harper, G.D., Miller, R.B., Miller, J.S., Mlinarevic, A.N., and Schultz, C., 2008, Geochemistry of the polygenetic Ingalls ophiolite complex, in Wright, J.E., and Shervais, J.W., eds., *Ophiolites, arcs, and batholiths: A tribute to Cliff Hopson*: Geological Society of America Special Paper 438, p. 133–159, doi: 10.1130/2008.2438(04).
- Magloughlin, J.F., 1993, A Nason terrane trilogy: I, Nature and significance of pseudotachylite: II, Summary of the structural and tectonic history: III, Major and trace element geochemistry and strontium and neodymium isotope geochemistry of the Chiwaukum Schist, amphibolite, and metatonalite gneiss of the Nason terrane [Ph.D. thesis]: University of Minnesota, 325 p.
- Matzel, J.P., 2004, Rates of tectonic and magmatic processes in the North Cascades continental magmatic arc [Ph.D. thesis]: Cambridge, Massachusetts Institute of Technology, 249 p.
- Matzel, J.P., Bowring, S.A., and Miller, R.B., 2004, Protolith age of the Swakane Gneiss, North Cascades, Washington: Evidence of rapid underthrusting of sediments beneath an arc: *Tectonics*, v. 23, doi: 10.1029/2003TC001577.
- Matzel, J.P., Bowring, S.A., and Miller, R.B., 2006, Timescales of pluton construction at differing crustal levels: Examples from the Mount Stuart and Tenpeak intrusions, North Cascades, Washington: *Geological Society of America Bulletin*, v. 118, p. 1412–1430, doi: 10.1130/B25923.1.
- Matzel, J.P., Bowring, S.A., and Miller, R.B., 2008, Spatial and temporal variations in Nd isotopic signatures across the crystalline core of the North Cascades, WA, in Wright, J.E., and Shervais, J.W., eds., *Ophiolites, arcs, and batholiths: A tribute to Cliff Hopson*: Geological Society of America Special Paper 438, p. 499–516, doi: 10.1130/2008.2438(18).
- McCaffrey, K.J.W., and Petford, N., 1997, Are granitic intrusions scale-invariant?: *Journal of the Geological Society of London*, v. 154, p. 1–4, doi: 10.1144/gsjgs.154.1.0001.
- McGroder, M.F., 1989, Structural geometry and kinematic evolution of the eastern Cascades foldbelt, Washington and British Columbia: *Canadian Journal of Earth Sciences*, v. 26, p. 1586–1602.
- McPeck, S.L., Miller, R.B., Miller, J.S., and Matzel, J.P., 2002, Significance of fabric development in the gabbroic Riddle Peaks pluton, North Cascades, Washington: *Geological Society of America Abstracts with Programs*, v. 34, no. 5, p. A-96.
- Metzger, E.P., Miller, R.B., and Harper, G.D., 2002, Geochemistry and tectonic setting of the ophiolitic Ingalls Complex, North Cascades, Washington: Implications for correlations of Jurassic Cordilleran ophiolites: *The Journal of Geology*, v. 110, p. 543–560, doi: 10.1086/341759.
- Miller, R.B., 1985, The ophiolitic Ingalls Complex, North Central Cascade Mountains, Washington: *Geological Society of America Bulletin*, v. 96, p. 27–42, doi: 10.1130/0016-7606(1985)96<27:TOICNC>2.0.CO;2.
- Miller, R.B., 1987, Geology of the Twisp River-Chelan Divide region, North Cascades, Washington: Washington Division of Geology and Earth Resources Open-File Report 87-17, 12 p.
- Miller, R.B., 1994, A mid-crustal contractional shear zone in a strike-slip system, North Cascades, Washington: *Journal of Structural Geology*, v. 16, p. 47–60, doi: 10.1016/0191-8141(94)90017-5.
- Miller, R.B., and Bowring, S.A., 1990, Structure and chronology of the Oval Peak batholith and adjacent rocks: Implications for the Ross Lake fault zone, North Cascades, Washington: *Geological Society of America Bulletin*, v. 102, p. 1361–1377, doi: 10.1130/0016-7606(1990)102<1361:SACOTO>2.3.CO;2.

- Miller, R.B., and Mogk, D.W., 1987, Ultramafic rocks of a fracture-zone ophiolite, North Cascades, Washington: *Tectonophysics*, v. 142, p. 261–289, doi: 10.1016/0040-1951(87)90127-2.
- Miller, R.B., and Paterson, S.R., 1994, The transition from magmatic to high-temperature solid-state deformation: Implications from the Mount Stuart batholith, Washington: *Journal of Structural Geology*, v. 16, p. 853–865, doi: 10.1016/0191-8141(94)90150-3.
- Miller, R.B., and Paterson, S.R., 1999, In defense of magmatic diapirs: *Journal of Structural Geology*, v. 21, p. 1161–1173, doi: 10.1016/S0191-8141(99)00033-4.
- Miller, R.B., and Paterson, S.R., 2001a, Construction of mid-crustal sheeted plutons: Examples from the North Cascades, Washington: *Geological Society of America Bulletin*, v. 113, p. 1423–1442, doi: 10.1130/0016-7606(2001)113<1423:COMCSP>2.0.CO;2.
- Miller, R.B., and Paterson, S.R., 2001b, Influence of lithological heterogeneity, mechanical anisotropy, and magmatism on the rheology of an arc, North Cascades, Washington: *Tectonophysics*, v. 342, p. 351–370, doi: 10.1016/S0040-1951(01)00170-6.
- Miller, R.B., and Snoke, A.W., 2009, this volume, The utility of crustal cross sections in the analysis of orogenic processes in contrasting tectonic settings, in Miller, R.B., and Snoke, A.W., eds., *Crustal cross sections from the western North American Cordillera and elsewhere: Implications for tectonic and petrologic processes*: Geological Society of America Special Paper 456, doi: 10.1130/2009.2456(01).
- Miller, R.B., Brown, E.H., McShane, D.P., and Whitney, D.L., 1993a, Intra-arc crustal loading and its tectonic implications, North Cascades crystalline core, Washington and British Columbia: *Geology*, v. 21, p. 255–258, doi: 10.1130/0091-7613(1993)021<0255:IACLA1>2.3.CO;2.
- Miller, R.B., Whitney, D.L., and Geary, E.E., 1993b, Tectonostratigraphic terranes and the metamorphic history of the northeastern part of the Cascades crystalline core—Evidence from the Twisp Valley Schist: *Canadian Journal of Earth Sciences*, v. 30, p. 1306–1323.
- Miller, R.B., Haugerud, R.A., Murphy, F., and Nicholson, L.S., 1994, Tectonostratigraphic framework of the northeastern Cascades: Washington Division of Geology and Earth Resources Bulletin, v. 80, p. 73–92.
- Miller, R.B., Paterson, S.R., DeBari, S.M., and Whitney, D.L., 2000, North Cascades Cretaceous crustal section: Changing kinematics, rheology, metamorphism, pluton emplacement and petrogenesis from 0 to 40 km depth, in Woodsworth, G.J., Jackson, J.L.E., Nelson, J.L., and Ward, B.C., eds., *Guidebook for geological field trips in southwestern British Columbia and northern Washington*: Vancouver, Geological Association of Canada, p. 229–278.
- Miller, R.B., Matzel, J.P., Paterson, S.R., and Stowell, H., 2003, Cretaceous to Paleogene Cascades arc: Structure, metamorphism, and timescales of magmatism, burial, and exhumation of a crustal section, in Swanson, T.W., ed., *Western Cordillera and adjacent areas*: Geological Society of America Field Guide 4, p. 107–135.
- Miller, R.B., Paterson, S.R., Lebit, H., Alsleben, H., and Lüneburg, C., 2006, Significance of composite lineations in the mid- to deep crust: A case study from the North Cascades, Washington: *Journal of Structural Geology*, v. 28, p. 302–322, doi: 10.1016/j.jsg.2005.11.003.
- Misch, P., 1966, Tectonic evolution of the Northern Cascades of Washington State: A west-Cordilleran case history, in Gunning, H.C., ed., *Symposium on the tectonic history and mineral deposits of the western Cordillera in British Columbia and neighboring parts of United States*: Canadian Institute of Mining and Metallurgy, Special Volume 8, p. 101–148.
- Monger, J.W.H., Price, R.A., and Tempelman-Kluit, D.J., 1982, Tectonic accretion and the origin of the two major metamorphic and plutonic belts in the Canadian Cordillera: *Geology*, v. 10, p. 70–75, doi: 10.1130/0091-7613(1982)10<70:TAATOO>2.0.CO;2.
- Paterson, S.R., and Farris, D.W., 2008, Downward host rock transport and the formation of rim monoclines during the emplacement of Cordilleran batholiths: *Transactions of the Royal Society of Edinburgh: Earth Sciences; Special Issue, Plutons and Batholiths (Wallace Pitcher Memorial Volume)*, v. 97, p. 397–413.
- Paterson, S.R., and Miller, R.B., 1998a, Mid-crustal magmatic sheets in the Cascades Mountains, Washington: Implications for magma ascent: *Journal of Structural Geology*, v. 20, p. 1345–1363, doi: 10.1016/S0191-8141(98)00072-8.
- Paterson, S.R., and Miller, R.B., 1998b, Magma emplacement during arc-perpendicular shortening: An example from the Cascades crystalline core, Washington: *Tectonics*, v. 17, p. 571–586, doi: 10.1029/98TC01604.
- Paterson, S.R., and Tobisch, O.T., 1992, Rates of processes in arcs: Implications for timing and nature of pluton emplacement and wall rock deformation: *Journal of Structural Geology*, v. 14, p. 291–300, doi: 10.1016/0191-8141(92)90087-D.
- Paterson, S.R., Miller, R.B., Anderson, J.L., Lund, S.P., Bendixen, J., Taylor, N., and Fink, T., 1994, Emplacement and evolution of the Mt. Stuart batholith, in Swanson, D.A., and Haugerud, R.A., eds., *Geologic field trips in the Pacific Northwest: 1994 Geological Society of American Annual Meeting*, Geological Society of America, p. 2F1–2F47.
- Paterson, S.R., Fowler, T.K., and Miller, R.B., 1996, Pluton emplacement in arcs: A crustal-scale exchange process: *Transactions of the Royal Society of Edinburgh: Earth Sciences*, v. 87, p. 115–123.
- Paterson, S.R., Fowler, T.K., Jr., Schmidt, K.L., Yoshinobu, A.A., Yuan, E.S., and Miller, R.B., 1998, Interpreting magmatic fabric patterns in plutons: *Lithos*, v. 44, p. 53–82, doi: 10.1016/S0024-4937(98)00022-X.
- Paterson, S.R., Miller, R.B., Alsleben, H., Whitney, D.L., Valley, P.M., and Hurlow, H., 2004, Driving mechanisms for >40 km of exhumation during contraction and extension in a continental arc, Cascades core, Washington: *Tectonics*, v. 23, doi: 10.1029/2002TC001440.
- Paterson, S.R., Pignotta, G.S., Farris, D., Memeti, V., Miller, R.B., Vernon, R.H., and Zák, J., 2008, Is stopping a volumetrically significant pluton emplacement process? Discussion: *Geological Society of America Bulletin*, v. 120, p. 1075–1079, doi: 10.1130/B26148.1.
- Percival, J.A., Fountain, D.M., and Salisbury, M.H., 1992, Exposed crustal cross sections as windows on the lower crust, in Kay, R.A., Arculus, R.J., and Fountain, D.M., eds., *Lower continental crust*: Amsterdam, Elsevier, p. 317–362.
- Petford, N., 1996, Dykes and diapirs?: *Transactions of the Royal Society of Edinburgh: Earth Sciences*, v. 87, p. 105–114.
- Pitcher, W.S., 1979, The nature, ascent, and emplacement of granitic magmas: *Journal of the Geological Society of London*, v. 136, p. 627–662, doi: 10.1144/gsjgs.136.6.0627.
- Pitcher, W.S., and Berger, A.R., 1972, *The geology of Donegal: A study of granite emplacement and unroofing*: New York, Wiley, 435 p.
- Pitcher, W.S., Atherton, M.P., Cobbing, E.J., and Beckinsale, R.D., 1985, Magmatism at a plate edge: The Peruvian Andes: Glasgow, Blackie, 328 p.
- Plummer, C.C., 1980, Dynamothermal contact metamorphism superposed on regional metamorphism in the pelitic rocks of the Chiwaukum Mountains area, Washington Cascades: Summary: *Geological Society of America Bulletin*, v. 91, p. 386–388, doi: 10.1130/0016-7606(1980)91<386:DCMSOR>2.0.CO;2.
- Raszewski, D.A., 2005, *Metamorphism, lithologic relations, and structural architecture of the White River shear zone, North Cascade Mountains, Washington* [M.S. thesis]: Fort Collins, Colorado State University, 256 p.
- Rothstein, D.A., and Manning, C.E., 2003, Geothermal gradients in continental magmatic arcs: Constraints from the eastern Peninsular Ranges batholith, Baja California, Mexico, in Johnson, S.E., Paterson, S.R., Fletcher, J.M., Girty, G.H., Kimbrough, D.L., and Martin-Barajas, A., eds., *Tectonic evolution of northwestern Mexico and the southwestern USA*: Geological Society of America Special Paper 374, p. 337–354.
- Rubin, C.M., Saleeby, J.B., Cowan, D.S., Brandon, M.T., and McGroder, M.F., 1990, Regionally extensive mid-Cretaceous west-vergent thrust system in the northwestern Cordillera: Implications for continent-margin tectonism: *Geology*, v. 18, p. 276–280, doi: 10.1130/0091-7613(1990)018<0276:REMCWV>2.3.CO;2.
- Rudnick, R.L., and Fountain, D.M., 1995, Nature and composition of the continental crust: a lower crustal perspective: *Reviews of Geophysics*, v. 33, p. 267–309, doi: 10.1029/95RG01302.
- Rudnick, R.L., and Gao, S., 2005, Composition of the continental crust, in Rudnick, R.L., ed., *The crust, Treatise on Geochemistry*, v. 3: Amsterdam, Elsevier, p. 1–64.
- Saleeby, J.B., 1990, Progress in tectonic and petrogenetic studies in an exposed cross-section of young (~100 Ma) continental crust, southern Sierra Nevada, California, in Salisbury, M.H., and Fountain, D.M., eds., *Exposed cross-sections of the continental crust*: Dordrecht, the Netherlands, Kluwer Academic, NATO Advanced Studies Institute, p. 137–158.
- Saleeby, J.B., Ducea, M., and Clemens-Knott, D., 2003, Production and loss of high-density batholithic root, southern Sierra Nevada, California: *Tectonics*, v. 22, doi: 10.1029/2002TC001374.
- Southwick, D.L., 1962, *Mafic and ultramafic rocks of the Ingalls-Peshastin area, Washington, and their geologic setting* [Ph.D. thesis]: Baltimore, Johns Hopkins University, 287 p.

- Stowell, H.H., and Tinkham, D.K., 2003, Integration of phase equilibria modelling and garnet Sm-Nd chronology for construction of P-T-t paths: Examples from the Cordilleran Coast Plutonic Complex, USA, *in* Vance, D., Muller, W., and Villa, I., eds., *Geochronology: Linking the isotopic record with petrology and textures*: Geological Society of London Special Publication 220, p. 119–145.
- Stowell, H.H., Bulman, G.R., Zuluaga, C.A., Tinkham, D.K., Miller, R.B., and Stein, E., 2007, Mid-crustal Late Cretaceous metamorphism in the Nason terrane, Cascades crystalline core, Washington, USA: Implications for tectonic models, *in* Hatcher, R.D., Jr., Carlson, M.P., McBride, J.H., and Martinez-Catalan, J.R., eds., *4-D framework of continental crust*: Geological Society of America Memoir 200, p. 211–232, doi: 10.1130/2007.1200(12).
- Tabor, R.W., Waitt, R.B., Jr., Frizzell, V.A., Jr., Swanson, D.A., Byerly, G.R., and Bentley, R.D., 1982, Geologic map of the Wenatchee 1:100,000 Quadrangle, central Washington: U.S. Geological Survey Map I-1311, scale 1:100,000.
- Tabor, R.W., Frizzell, V.A., Jr., Whetten, J.T., Waitt, R.B., Jr., Swanson, D.A., Byerly, G.R., Booth, D.B., Hetherington, M.J., and Zartman, R.E., 1987, Geologic map of the Chelan 30- by 60-minute Quadrangle, Washington: U.S. Geological Survey, scale 1:100,000.
- Tabor, R.W., Haugerud, R.A., and Miller, R.B., 1989, Overview of the geology of the North Cascades, International Geologic Congress Trip T307: Washington, American Geophysical Union, 62 p.
- Tabor, R.W., Frizzell, V.A., Jr., Booth, D.B., Waitt, R.B., Whetten, J.T., and Zartman, R.E., 1993, Geologic map of the Skykomish River 30- by 60-minute quadrangle, Washington: U.S. Geological Survey Map I-1963, scale 1:100,000.
- Tabor, R.W., Booth, D.B., Vance, J.A., and Ford, A.B., 2002, Geologic map of the Sauk River 30- by 60-minute quadrangle, Washington: U.S. Geological Survey Map I-2592, scale 1:100,000.
- Tobisch, O.T., Fiske, R.S., Sorenson, S.S., Saleeby, J.B., and Holt, E., 2000, Steep tilting of metavolcanic rocks by multiple mechanisms, central Sierra Nevada, California: *Geological Society of America Bulletin*, v. 112, p. 1043–1058, doi: 10.1130/0016-7606(2000)112<1043:STOMRB>2.3.CO;2.
- Valley, P.M., Whitney, D.L., Paterson, S.R., Miller, R.B., and Alsleben, H., 2003, Metamorphism of the deepest exposed arc rocks in the Cretaceous to Paleogene Cascades belt, Washington: Evidence for large-scale vertical motion in a continental arc: *Journal of Metamorphic Geology*, v. 21, p. 203–220, doi: 10.1046/j.1525-1314.2003.00437.x.
- Van Diver, B.B., 1967, Contemporaneous faulting-metamorphism in Wenatchee Ridge area, Northern Cascades, Washington: *American Journal of Science*, v. 265, p. 132–150.
- Weinberg, R.F., 1999, Mesoscale pervasive felsic magma migration: Alternatives to dyking: *Lithos*, v. 46, p. 393–410, doi: 10.1016/S0024-4937(98)00075-9.
- Weinberg, R.F., and Mark, G., 2008, Magma migration, folding and disaggregation of migmatites in the Karakoram shear zone, Ladakh, NW India: *Geological Society of America*, v. 120, p. 994–1009, doi: 10.1130/B26227.1.
- Weinberg, R.F., and Searle, M.P., 1998, The Pangong injection complex, Indian Karakoram: A case of pervasive granite flow through hot viscous crust: *Journal of the Geological Society of London*, v. 155, p. 883–891, doi: 10.1144/gsjgs.155.5.0883.
- White, L.D., Maley, C.A., Barnes, I., and Ford, A.B., 1988, Oxygen isotopic data for plutonic rocks and gneisses of the Glacier Peak Wilderness and vicinity, northern Cascades, Washington: U.S. Geological Survey Open-File Report 86-76, 35 p.
- Whitney, D.L., Miller, R.B., and Paterson, S.R., 1999, P-T-t evidence for mechanisms of vertical tectonic motion in a contractional orogen: Northwestern US and Canadian Cordillera: *Journal of Metamorphic Geology*, v. 17, p. 75–90, doi: 10.1046/j.1525-1314.1999.00181.x.
- Whitney, D.L., Paterson, S.R., Schmidt, K.L., Glazner, A.F., and Kopf, C., 2004, Growth and demise of continental arcs and orogenic plateaux in the North American Cordillera: From Baja to British Columbia, *in* Grotcott, J., McCaffrey, K.J.W., Taylor, G., and Tikoff, B., eds., *Vertical coupling and decoupling in the lithosphere*: Geological Society of London Special Publication 227, p. 167–176.
- Wiebe, R.A., and Collins, W.J., 1998, Depositional features and stratigraphic sections in granitic plutons: Implications for the emplacement and crystallization of granitic magma: *Journal of Structural Geology*, v. 20, p. 1273–1289, doi: 10.1016/S0191-8141(98)00059-5.
- Zelt, B.C., Ellis, R.M., Clowes, R.M., and Hole, J.A., 1996, Inversion of three-dimensional wide-angle seismic data from the southwestern Canadian Cordillera: *Journal of Geophysical Research*, v. 101, p. 8503–8529, doi: 10.1029/95JB02807.
- Zen, E-an, 1988, Tectonic significance of high-pressure plutonic rocks in the western Cordillera of North America, *in* Ernst, W.G., ed., *Metamorphic and crustal evolution of the western United States: Rubey Volume VII*: Englewood Cliffs, New Jersey, Prentice-Hall, p. 41–67.

Granulite- to amphibolite-facies metamorphism and penetrative deformation in a disrupted ophiolite, Klamath Mountains, California: A deep view into the basement of an accreted oceanic arc

Sarah R. Garlick

Department of Geology and Geophysics, Department 3006, 1000 East University Avenue, University of Wyoming, Laramie, Wyoming 82071, USA

L. Gordon Medaris Jr.

Department of Geology and Geophysics, University of Wisconsin, 1215 West Dayton Street, Madison, Wisconsin 53706, USA

Arthur W. Snoke

Joshua J. Schwartz

Susan M. Swapp

Department of Geology and Geophysics, Department 3006, 1000 East University Avenue, University of Wyoming, Laramie, Wyoming 82071, USA

ABSTRACT

Neogene doming in the north-central Klamath Mountains, California, tilted the Rattlesnake Creek terrane, chiefly an ophiolitic *mélange*, exposing an oblique cross section through disrupted and metamorphosed oceanic crust and mantle. The deepest section of the tilted terrane, in the Kangaroo Mountain area near Seiad Valley, contains tectonic slices of ultramafic, mafic, and sedimentary rocks that were penetratively deformed and metamorphosed under upper-amphibolite- to granulite-facies conditions. This section, called the Seiad complex, is the ophiolitic basement of an accreted Mesozoic island arc, and its polygenetic history reflects the magmatic and tectonic processes that occur during island-arc construction and evolution.

The presence of metarodinite and metaserpentine, and the concordance of structural elements and metamorphic grade among all units of the Seiad complex, indicate that initial tectonic disruption of the ophiolitic suite occurred in the upper crust and subsequent penetrative deformation and metamorphism occurred under high-temperature conditions in the deep crust. Crustal granulite-facies metamorphism is indicated by two-pyroxene metagabbroic bodies and two-pyroxene metasedimentary paragneiss. Geothermobarometric data from garnet amphibolite and granulite-facies metagabbro within the ophiolitic suite yielded pressure and temperature conditions of ~5–7 kb and ~650–750 °C. Geochemical data from samples of granulite, amphibolite, and leucotrochilite suggest a supra-subduction origin, although there is significant variation among the amphibolite samples, indicating multiple magma types.

Crosscutting, radiometrically dated plutons and the regional geologic context suggest that high-grade metamorphism and deformation of these disrupted ophiolitic rocks occurred in the Middle Jurassic (ca. 172–167 Ma). This time interval broadly corresponds with contraction along several regional thrust faults in the Klamath Mountains province and juxtaposition of the Rattlesnake Creek terrane with terranes to the east. A U-Pb zircon age of 152.7 ± 1.8 Ma on a sample of a crosscutting leucotrochmalitic dike swarm and published $^{40}\text{Ar}/^{39}\text{Ar}$ hornblende age spectra of ca. 150 ± 2 Ma from amphibolite indicate that magmatism and an accompanying thermal flux continued to affect this region into the Late Jurassic.

Compared with the deep-crustal sections of the well-studied Kohistan and Talaiketna arc complexes, the widespread *mélange* character of the Rattlesnake Creek terrane (including the Seiad complex) is unique. However, ophiolitic rocks, including mantle ultramafic rocks, are common components in the basal parts of these classic arc crustal sections. Hornblende gabbro/diorite and clinopyroxenite in the Seiad complex may be small-scale melt conduits that fed middle- and upper-crustal components of the arc, analogous to the relationship seen in Kohistan between deep-crustal ultramafic-mafic bodies and mid-crustal magma chambers.

INTRODUCTION

Accretion of oceanic rocks to an active continental margin is a fundamental process in the lateral growth of continental crust (e.g., Hamilton, 1969; Irwin, 1972; Coney et al., 1980; Samson and Patchett, 1991; Dickinson, 2008). A hallmark of this process is a structural geometry of stacked and imbricated units that represent different components of oceanic supra-subduction complexes (e.g., Irwin and Dennis, 1978; Irwin, 1981; Saleeby et al., 1982; Mortimer, 1985; Wright and Fahan, 1988; Saleeby and Harper, 1993; Ernst, 1999; Yule et al., 2006). These components include: arc volcanic and plutonic rocks; accretionary-prism complexes; back-arc, fore-arc, and trench-slope sedimentary rocks; and oceanic crust and upper mantle rocks that range from complete ophiolite sequences to ophiolitic *mélange* (e.g., Saleeby, 1979, 1992; Moores, 1998; Hawkins, 2003). Detailed studies of accreted terranes have thus contributed not only to our understanding of the processes of continental growth, but also to our knowledge of the basic architecture and evolution of oceanic lithosphere (e.g., Gansser, 1974; Saleeby, 1979; Raymond, 1984; Maekawa, 1989; Meschede et al., 1999; Dilek and Newcomb, 2003; Robertson, 2004). This study focuses on a metamorphosed disrupted ophiolite (i.e., ophiolitic *mélange*) in the north-central Klamath Mountains of California (Fig. 1) that forms the basement of an accreted Mesozoic arc (Donato, 1987; Donato et al., 1996). Neogene doming in the Klamath Mountains has tilted the disrupted ophiolite such that an oblique cross section through the terrane is exposed, providing an unusually deep view into the basement of an island arc (Mortimer and Coleman, 1985; Jachens et al., 1986; Barnes et al., 1990). Here, large ultramafic massifs, oceanic sedimentary rocks, and mafic volcanic and volcanoclastic rocks have been penetratively deformed and metamorphosed together under upper-amphibolite- to granulite-facies conditions (Medaris, 1966).

This study investigates the multi-stage history recorded in these rocks in order to better understand the magmatic and tectonic processes that occur during the construction and evolution of an oceanic supra-subduction complex. The unusually deep view provided by the study area allows us to consider these processes in an arc-basement setting as well as to investigate the granulite-facies metamorphism first described by Medaris (1966). Evidence for granulite-facies metamorphism in accreted terranes is uncommon and its presence in the Klamath Mountains may be an important key to understanding the orogenic history of the province.

REGIONAL GEOLOGIC SETTING

The Klamath Mountains province is a region of glacially sculpted ridgelines and deep river valleys that straddles the boundary between northwest California and southwest Oregon (Figs. 1, 2). This geologic province lies in the fore-arc of the modern-day Cascadia subduction zone, just north of the Mendocino triple junction. For more than four decades, geoscientists have recognized that the Klamath Mountains province is a classic example of successive lateral accretion of oceanic rocks along an active continental margin (e.g., Irwin, 1960, 1981, 1994; Hamilton, 1969; Davis et al., 1978; Snoke and Barnes, 2006). The mode of this accretion, although the subject of controversy, is considered to be subduction-related, reflecting the development of several supra-subduction complexes since the early Paleozoic (e.g., Saleeby et al., 1982; Harper and Wright, 1984; Wright and Fahan, 1988; Wright and Wyld, 1994; Hacker et al., 1995; Ernst, 1999).

A long-held and still leading tectonic model for the Klamath Mountains involves east-directed accretion by episodic underthrusting of oceanic rocks along a west-facing subduction zone, marginal to the western edge of the North American continent (e.g., Davis et al., 1978; Harper and Wright, 1984; Donato, 1987; Wright and Fahan, 1988; Burchfiel et al., 1992; Hacker

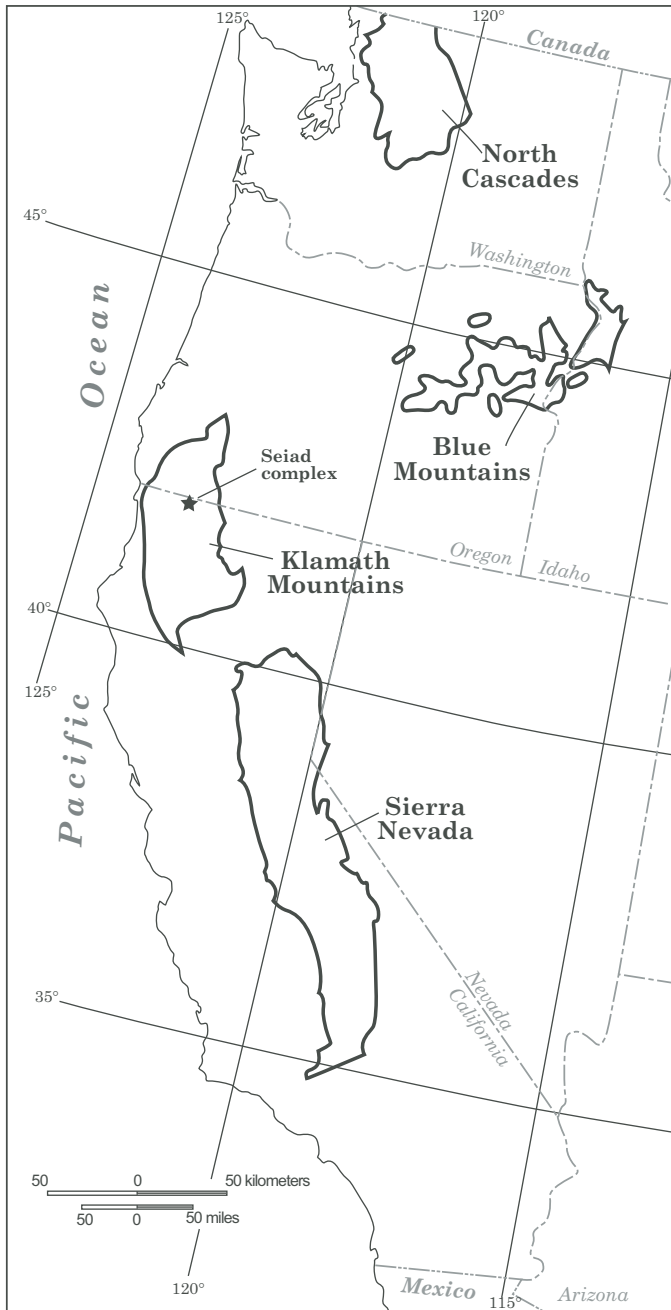


Figure 1. Geologic sketch map of a part of the western North American Cordillera showing the position of the Klamath Mountains province with respect to the Sierra Nevada (central California), Blue Mountains (northeast Oregon), and North Cascades (north-central Washington State). Adapted from King ([1967] 1970).

et al., 1995; Ernst, 1999). This model predicts the overall tectonic geometry of the province, where terranes are generally younger to the west and separated by east-rooted thrust faults, forming a distinctive belt-like pattern in map view (Irwin, 1994). The episodic underthrusting model also predicts the overall metamorphic history of the province, where widespread, low-grade mineral

assemblages indicate low-to-moderate pressures and temperatures of metamorphism, suggesting imbrication in shallow levels of the crust (Coleman et al., 1988). However, in many regions of the Klamath Mountains province, these generalizations are problematic. Considerable tectonic overprinting, including regional uplift and the reactivation of thrust faults as normal faults, has obscured primary relationships between terranes (e.g., Mortimer and Coleman, 1985; Barrow and Metcalf, 2006) and there are well-documented regions of high-grade metamorphic rocks that suggest synchronous crustal thickening and heating (e.g., Medaris, 1966; Barrows, 1969). Furthermore, there is isotopic evidence for cryptic, “hidden terranes” in the subsurface (Allen and Barnes, 2006), suggesting that the exposed geologic record in the province is far from complete.

Some of these complications can be viewed in the north-central part of the Klamath Mountains, where a domical, fault-bounded window disrupts the characteristic belt geometry of the province (Fig. 2) (Mortimer and Coleman, 1984, 1985; Irwin, 1994). The hanging-wall rocks that frame the window are part of the heterogeneous, Late Triassic–Early Jurassic Rattlesnake Creek terrane, chiefly an ophiolitic *mélange* (Rawson and Petersen, 1982; Norman et al., 1983; Mortimer, 1985; Wright and Wyld, 1994). The footwall rocks of the window are the composite Condrey Mountain terrane (Helper, 1986; Saleeby and Harper, 1993; Irwin, 1994), consisting of an upper, fault-bounded, greenschist-facies unit of metavolcanic-metasedimentary rocks and an underlying greenschist–blueschist-facies unit of graphitic quartz-white mica schist, subordinate blueschist-facies rocks, and metaserpentinite (Hotz, 1979; Helper, 1986 [see his figures 2 and 4]; Saleeby and Harper, 1993).

This study focuses on the west side of the Condrey Mountain window near Seiad Valley, California, where the Rattlesnake Creek terrane exhibits the highest-grade rocks reported in the Klamath Mountains (Medaris, 1966, 1975; Lundquist, 1983; Grover, 1984; Grover and Rice, 1985; Lieberman and Rice, 1986; Snoke and Barnes, 2006). One of the principal goals of this study is to document the nature of the high-grade deformation and metamorphism in the Rattlesnake Creek terrane. We also use new whole-rock major-, trace- and rare-earth-element abundances of these high-grade rocks to understand their pro-tolith origins; compositional data of Cr-spinel to compare the ultramafic rocks of the map area to oceanic abyssal peridotites and ophiolitic suites exposed in the Klamath Mountains province, and geochronological analysis of a crosscutting dike swarm to provide a minimum age constraint on ductile deformation and metamorphism. Finally, we use these new conclusions and our regional understanding of the Klamath Mountains province to develop a model for the magmatic and tectonic evolution of this accreted supra-subduction complex.

STUDY AREA AND PREVIOUS WORK

The study area is a ~40 km² region within the Kangaroo Mountain 7.5 min quadrangle, just south of the California–Oregon

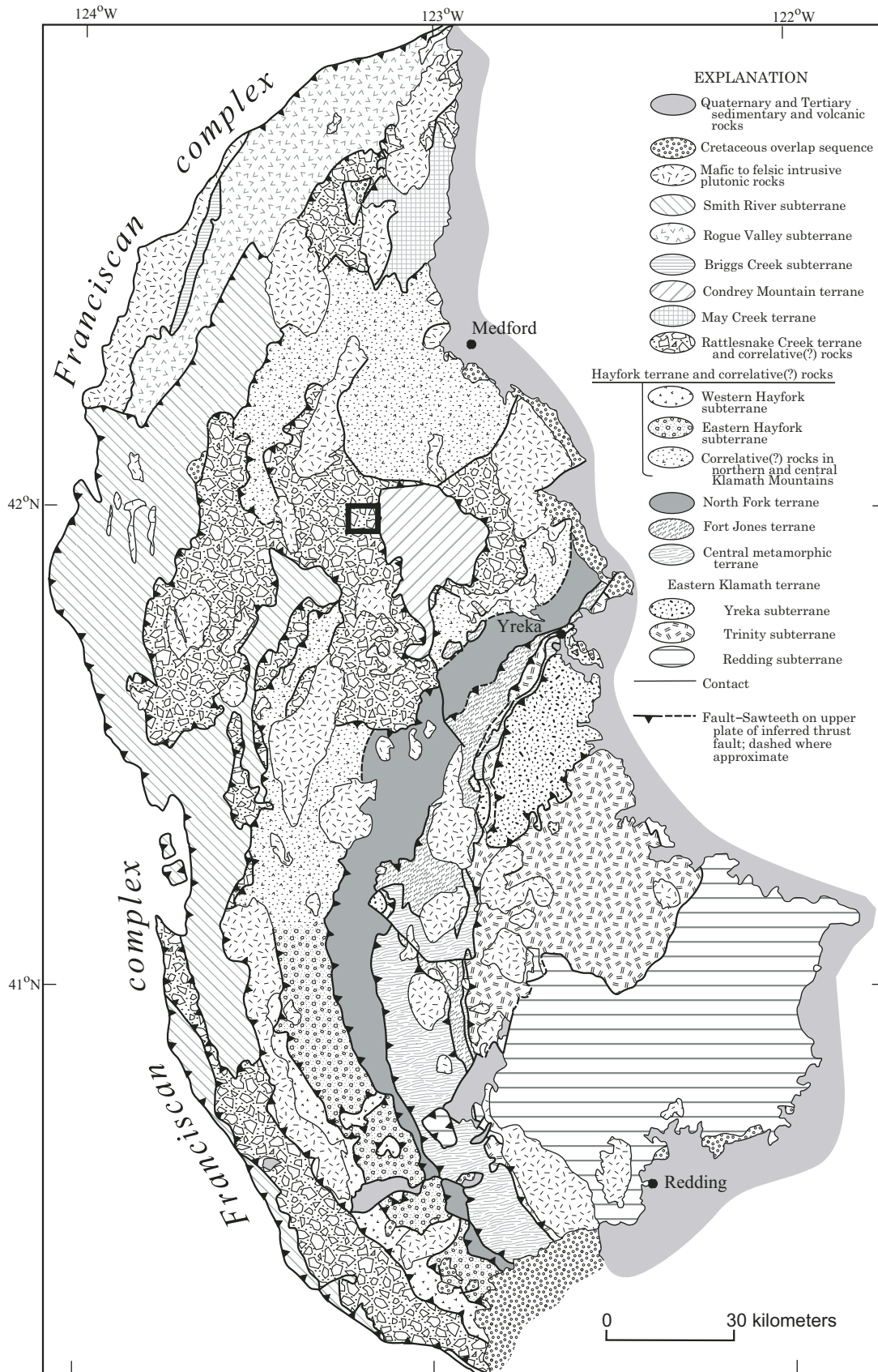


Figure 2. Geologic map of the Klamath Mountains province, California and Oregon (after Irwin, 1994, and Snoko and Barnes, 2006). Map area of Figure 3 and Plate 1 (Appendix 1 on the CD-ROM accompanying this volume) is outlined in black rectangle.

border (Figs. 3 and 4). The study area is dominated by two large ultramafic massifs that are separated by a sequence of metasedimentary and metavolcanic rocks and surrounded by a region of amphibolite and amphibole gneiss (see Appendix 1 on the CD-ROM accompanying this volume and in the GSA Data Repository¹). The rocks of this area, termed the Seiad complex by Medaris (1966), are oceanic in character and have been described by previous workers as either a disrupted, incomplete ophiolite or a metamorphosed ophiolitic mélange (e.g., Lundquist, 1983; Cannat, 1985).

Medaris (1966) completed the first detailed study of this region, which focused on the petrology of the ultramafic rocks and documented the presence of two-pyroxene, granulite-facies rocks in the complex. Other important studies on the Seiad complex include: Loomis and Gottschalk (1981), Lundquist (1983), Grover (1984), Grover and Rice (1985), Cannat (1985), and Lieberman and Rice (1986).

ROCK UNITS

Introduction

Key field relations and petrographic observations for the rock units in the Seiad complex are summarized below. Additional detailed petrographic descriptions are also summarized in the "Explanation" on Appendix 1 (see CD-ROM accompanying this volume or the GSA Data Repository). A self-guided Geologic Field Trip Guide has been prepared to provide future workers with an overview of the field relations that support interpretations made in this report (Appendix 2; CD-ROM accompanying this volume).

West Fork Ultramafic Body

The West Fork unit is a ~3-km-thick slab of ultramafic rock that occupies the structurally deepest part of the Seiad complex in the eastern part of the map area (Fig. 3; Appendix 1). Its eastern boundary is the Condrey Mountain fault, an inferred original thrust fault that was subsequently overprinted by a Tertiary(?) subvertical, normal fault that separates a hanging-wall block of Rattlesnake Creek terrane from a footwall block consisting of the greenschist-facies metavolcanic-metasedimentary unit of the Condrey Mountain terrane. The West Fork body is the largest and most heterogeneous ultramafic massif in the Seiad complex. It is composed of dunite and spinel lherzolite, with minor wehrlite, harzburgite, and chromitite (Fig. 5A). It also contains elongate, lenticular bodies of websterite and granulite-facies mafic gneiss/metagabbro (see individual descriptions below).

The ultramafic rocks in this unit are remarkably fresh and unaltered, with serpentine-group minerals constituting less than 5 mod%. The degree of serpentinization increases with proximity to the Condrey Mountain fault. Between the easternmost websterite body and Condrey Mountain fault, the unit is dominantly tectonic spinel lherzolite. Structurally above the spinel lherzolite and separating it from a body of dunite are a lens of granulite-facies metagabbro and the easternmost body of websterite. Dunite dominates the rest of the massif, accounting for over 75% of the unit. In the structurally highest and westernmost part of the slab, there are zones of interlayered dunite-wehrlite with minor harzburgite.

Spinel lherzolite is distinguished in hand sample by tan-brown orthopyroxene, pale green clinopyroxene, and dark-green pargasitic amphibole. The spinel lherzolite has a strong foliation defined by aligned pyroxenes and amphibole and trains of fine-grained spinel (metallic black in hand sample and olive-brown in thin section). Thin sections of spinel lherzolite show pronounced grain-size reduction compared with thin sections of surrounding ultramafic rocks (Fig. 6A). Dunite varies from regions of 100% olivine to zones that contain thin layers and/or segregations of chromite. These chromite layers are commonly isoclinally folded, providing one of the most obvious mesoscopic fabric elements in the rock (Fig. 5A). Olivine is fine grained and appears not to have a distinguishable grain-shape fabric, yielding an equigranular, sugary texture. Thin sections of dunite contain a mosaic equigranular microstructure, with medium-sized (~0.5–1 mm) olivine grains that are equant to slightly elongate and an even distribution of equant chromite grains (Fig. 6B).

Along the western border of the West Fork body, near the contact with amphibolite to the south and near the contact with the metasedimentary-metavolcanic unit to the north, lies strongly tectonic harzburgite, perhaps indicating strain partitioning and shear-zone development along the external contacts of the body. These rocks are dominantly harzburgite L-S tectonites (L>S), with the fabric defined by alignment of orthopyroxene, pargasitic amphibole, and chromite.

Chromitite exists as isoclinally folded layers and irregular masses of podiform chromitite within dunite (Fig. 5A). The West Fork ultramafic unit contains dikes of clinopyroxenite and numerous monomineralic amphibole veins varying in composition from green pargasitic amphibole to white tremolite. These dikes and veins vary in orientation from concordant to discordant to the foliation. Some clinopyroxenite dikes are boudinaged.

Kangaroo Mountain Peridotite

The Kangaroo Mountain peridotite, ~1 km in structural thickness, is a thinner slab than the West Fork ultramafic massif, and also more homogeneous. This unit is dominantly harzburgite with minor amounts of dunite. The Kangaroo Mountain peridotite is a resistant unit, defining the double peaks of Red Butte and broad summit of Kangaroo Mountain (Fig. 4). Alignment

¹GSA Data Repository Item 2009157, Appendix 1: Geologic Map of the Seiad Complex, Kangaroo Mountain Area, Klamath Mountains, California, by Sarah R. Garlick and L. Gordon Medaris Jr., 2009, and Appendix 2: Field-trip guide to the Seiad complex, Kangaroo Mountain area, by Sarah R. Garlick and Arthur W. Snoke, is available at www.geosociety.org/pubs/ft2009.htm, or on request from editing@geosociety.org, Documents Secretary, GSA, P.O. Box 9140, Boulder, CO 80301-9140, USA.

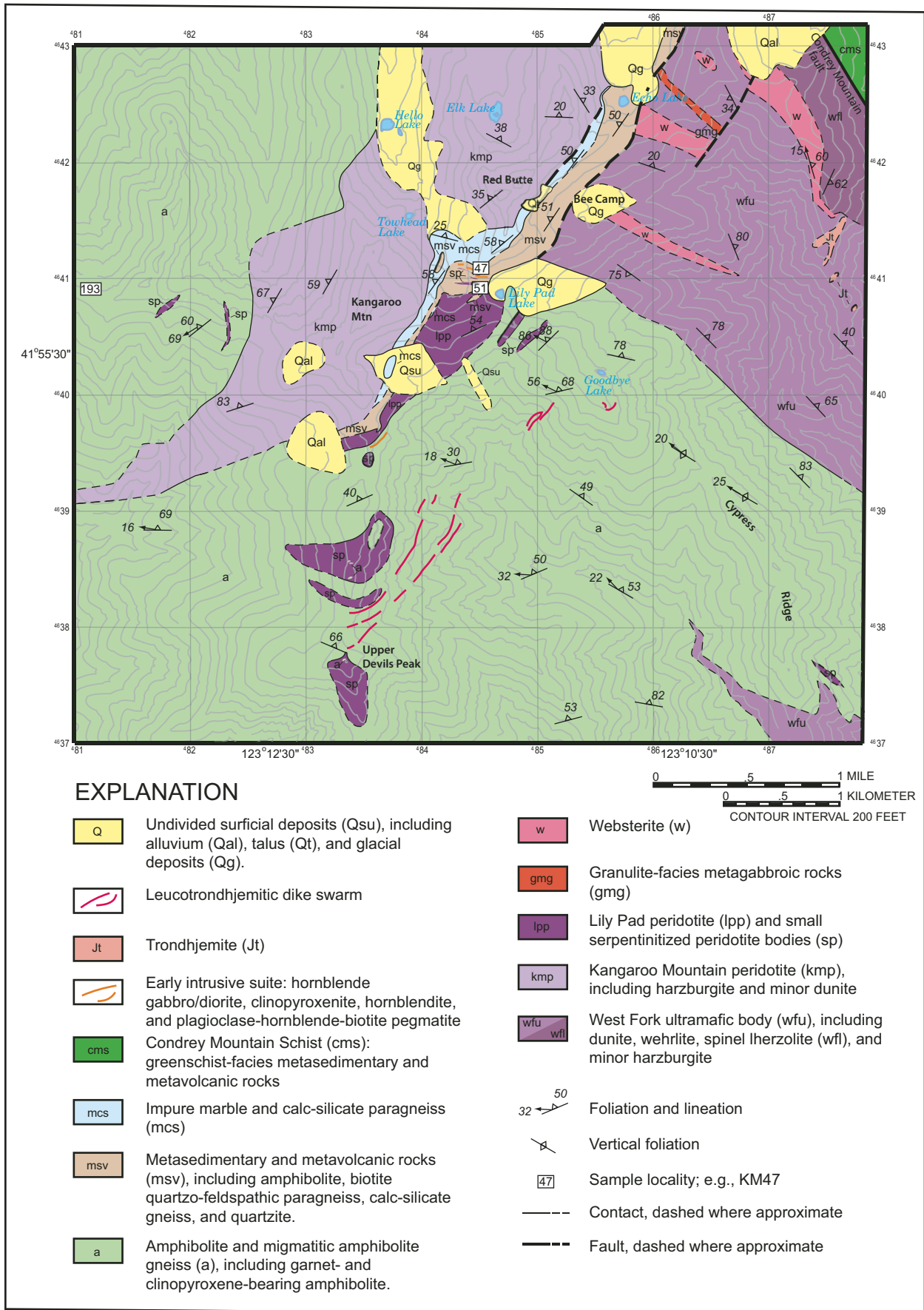


Figure 3. Simplified geologic map of the Seiad complex, Klamath Mountains, California.

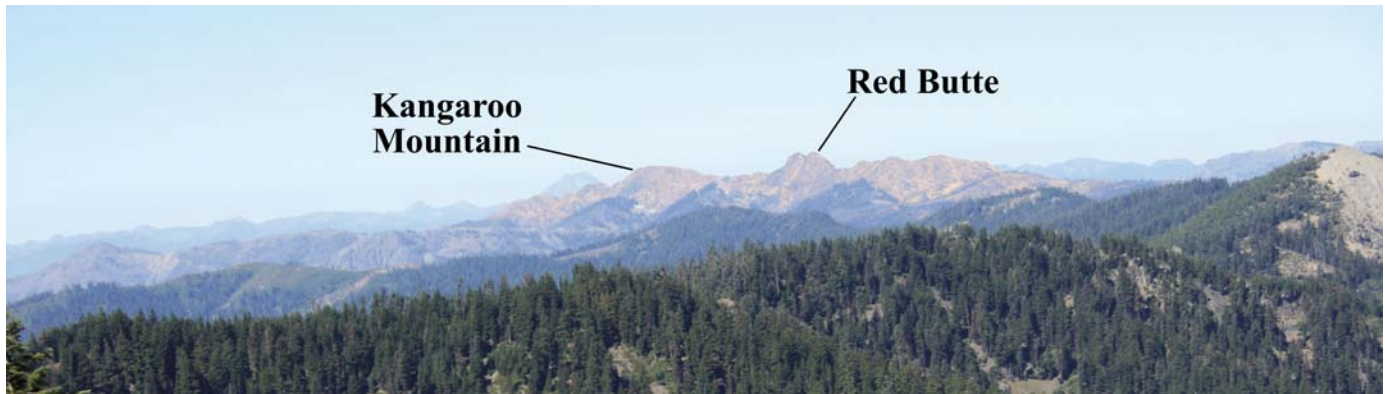


Figure 4. View of the Kangaroo Mountain–Red Butte area from the southwest flank of Scraggy Mountain in the Condrey Mountain dome. View to the west-southwest.

of cm-scale orthopyroxene porphyroclasts and smaller bright green amphibole grains defines a variable foliation and lineation in this unit. Outcrops range from containing a strong, visible mineral fabric to containing no measurable features other than joint surfaces or veins. Harzburgite and dunite are related in cm-scale compositional layers as well as in diffuse, irregular pyroxene-rich and -poor zones (Fig. 5C). The orthopyroxene porphyroclasts are more resistant to weathering than the surrounding olivine grains, giving the harzburgite a knobby texture in outcrop (Fig. 5C). In thin section, harzburgite commonly has a porphyroclastic microstructure, with bimodal grain size in olivine and orthopyroxene. Both of these phases appear to have undergone recrystallization (Fig. 6C; Table 1).

The Kangaroo Mountain peridotite contains scattered occurrences of dark, fine-grained, dike-like dunite bodies. These “dikes” are made up of elongate olivine grains with abundant ultrafine-grained magnetite inclusions (Figs. 6D, 6E). These textures are indications of metamorphic olivine growing after serpentine-group minerals (Frost, 1975). The “dikes” are interpreted as relict fracture zones where fluids infiltrated the peridotite, causing local intense serpentinization. Prograde metamorphism subsequently altered the serpentinite to (meta)dunite.

Lily Pad Peridotite and Small Serpentinized Peridotite Bodies

The Lily Pad peridotite is a small slab of tectonic harzburgite west of Lily Pad Lake. It sits structurally between the Kangaroo Mountain and West Fork ultramafic massifs. There are also numerous tectonic slivers of peridotite within the amphibolite unit and metasedimentary-metavolcanic unit. These slivers range from tectonic, serpentinized harzburgite to 100% serpentinite in composition and are variable in size and shape (Fig. 3; Appendix 1, see CD-ROM accompanying this volume and footnote 1). Amphibole-chlorite blackwalls commonly occur along the boundaries of these units. Some metaserpentinite slivers surround lensoid bodies of metaroddingite.

Granulite-Facies Metagabbroic Rocks

This unit comprises two lenticular bodies of mafic gneiss within the West Fork ultramafic body. The unit is primarily granulite-facies mafic gneiss with the assemblage: clinopyroxene + orthopyroxene + plagioclase ± hornblende ± biotite + accessory rutile. The unit also contains subordinate amphibolite (hornblende + plagioclase) and hornblendite (hornblende ± plagioclase).

As observed in the well-exposed western lens, granulite-facies gneiss grades to amphibolite along narrow (<2 cm) boundaries. Thin (2–4 cm) seams of amphibolite in granulite-facies gneiss suggest former cracks along which fluids entered and hydrated the surrounding rock, altering two-pyroxene gneiss to amphibolite (Fig. 5B). The granulite-facies gneiss contains L>S tectonic fabrics defined by orientation of pyroxene grains. The lineation (L_1) has a shallow (<15°) plunge and trends parallel to the long axis of the body.

The small eastern lens of granulite-facies mafic gneiss lies between the spinel lherzolite to the east and a websterite body to the west (see Appendix 2, Field-trip STOP 1). This lens displays strong compositional layering defined by variations in proportions of plagioclase and pyroxene. Thin sections of samples from the eastern lens are extensively retrograded to fine-grained amphibole, saussurite, and epidote-group minerals.

The dike-like shape of these bodies and the relatively coarse (~0.5–1 mm), equigranular textures of the rocks suggest a gabbro protolith. The contact between these rocks and the surrounding West Fork ultramafic rocks is poorly exposed.

Websterite

The websterite unit crops out as three elongate, lenticular bodies within the West Fork ultramafic unit. The websterite is made up of orthopyroxene + clinopyroxene + hornblende ± olivine + accessory Fe-Ti oxides. In the field, websterite is a dark, tough, medium- to coarse-grained rock that commonly has a rusty-orange weathering rind typical of ultramafic rocks. Individual

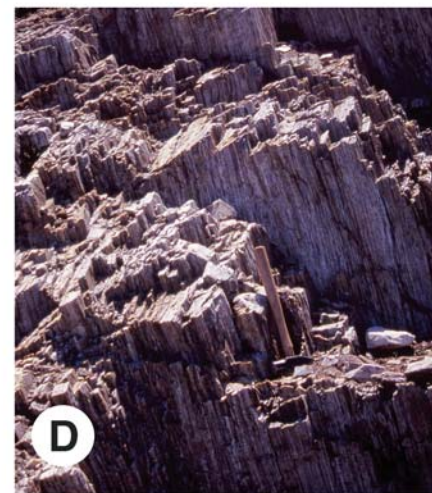
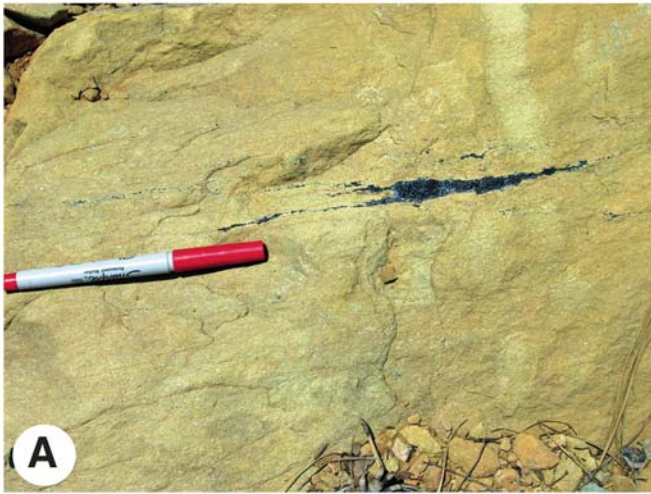


Figure 5. Photographs of some representative rock types from the Seiad complex. (A) Isoclinally folded chromite segregation in dunite, part of the West Fork ultramafic body. (B) Outcrop showing the transition from granulite-facies mafic gneiss to amphibolite in the granulite-facies metagabbro unit. The tan-colored rock at the base of the outcrop near the hammer is granulite-facies mafic gneiss. The dark gray rock in the upper right half of the photograph is amphibolite. (C) Irregular concentrations of orthopyroxene porphyroclasts within Kangaroo Mountain harzburgite, orthopyroxene fabric subparallel to the pen. (D) Flaggy, strongly lineated quartzite (original protolith was impure chert), part of the metasedimentary-metavolcanic unit. Lineation plunges steeply down the foliation. (E) Irregular leucosome layer crosscutting the fabric of the host amphibolite, part of the metasedimentary-metavolcanic unit. (F) Relict fragmental texture in amphibolite, part of the amphibolite and migmatitic amphibole gneiss unit.

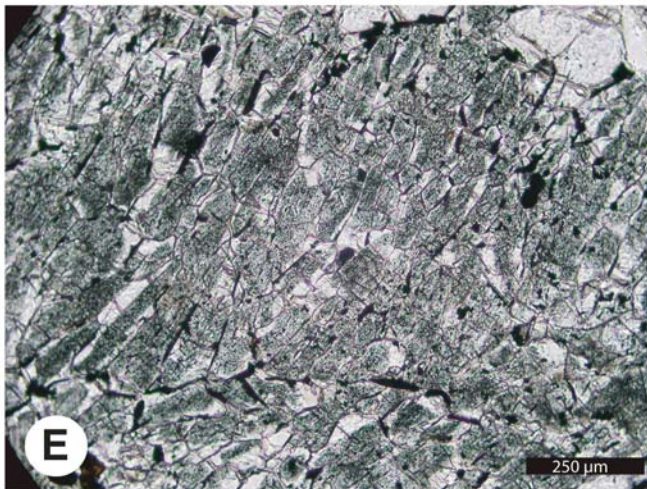
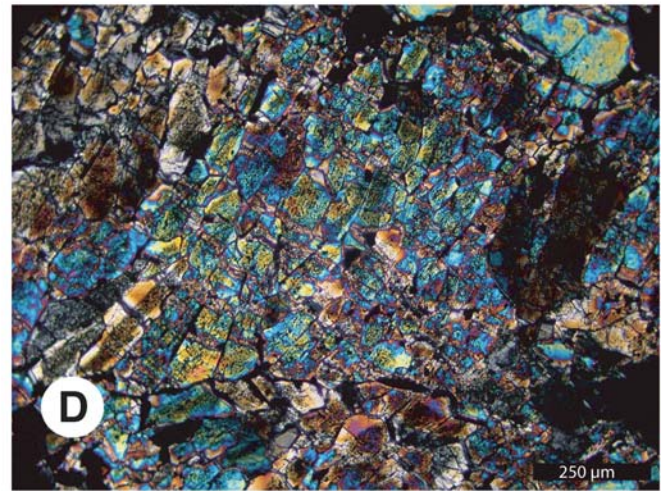
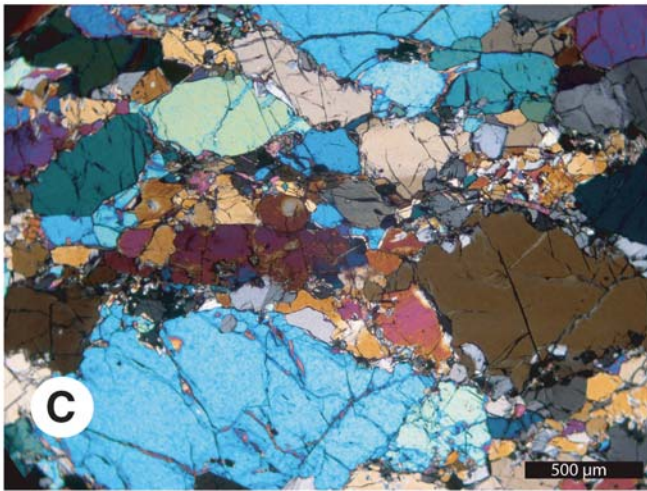
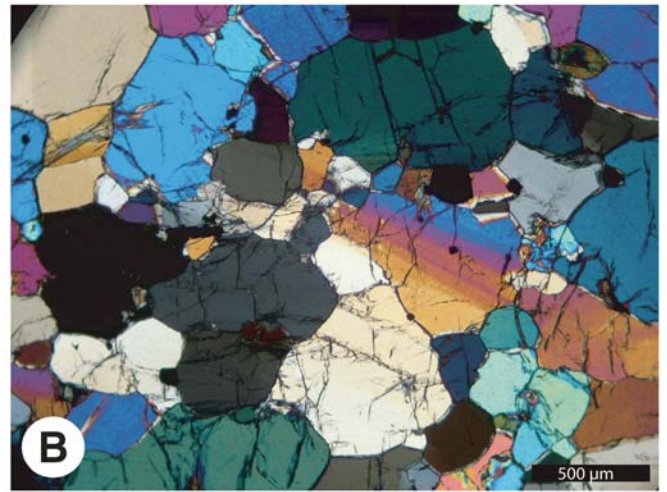


Figure 6. Photomicrographs of some representative ultramafic rocks from the Seiad complex. (A) Spinel lherzolite from the easternmost part of the West Fork ultramafic unit. Field of view consists of irregularly shaped olivine and orthopyroxene grains. A large orthopyroxene porphyroblast occupies the center top edge of the photomicrograph. (B) Dunite from the West Fork ultramafic unit. Field of view is entirely made up of olivine grains, with the exception of small, equant, opaque chromite grains. (C) Porphyroclastic harzburgite from the Kangaroo Mountain peridotite unit. Large colorful grains are olivine and gray grains are typically orthopyroxene. The finer-grained phases include olivine, orthopyroxene, chlorite, and clino-amphibole. (D) Metaserpentinite from the Kangaroo Mountain peridotite unit. Field of view consists of elongate metamorphic olivine grains with abundant ultra-fine inclusions of magnetite. (E) Same image in plane polarized light.

TABLE 1. SUMMARY OF STRUCTURAL ELEMENTS, SEIAD COMPLEX

Event	Description	Foliation/Layering	Lineation	Folds
D ₀	Protolith formation	S ₀ : primary sedimentary and volcanic bedding; primary layering in ultramafic rocks	N/A	N/A
Pre-D ₁	Tectonic mixing of distinct lithologic units	N/A	N/A	N/A
D ₁₋₂	Progressive penetrative deformation synchronous with high-T/moderate-P metamorphism	S ₁ : planar orientation of metamorphic minerals	L ₁₋₂ : elongation direction of metamorphic minerals, parallel to hinge lines of F ₂ folds in amphibolite	F ₁ : isoclinal folding of S ₀ F ₂ : isoclinal folding of S ₁ and metamorphic minerals
D ₃	Open, upright meter- and kilometer-scale folding of S ₁ and F ₂	N/A	N/A	F ₃ : open, upright folds of S ₁
Post-D ₃	Brittle faulting along lithologic contacts	N/A	N/A	N/A

tan-brown orthopyroxene grains are visible in outcrop. Outcrops of websterite vary from strongly deformed, with obvious lineation and foliation defined by elongate and flattened pyroxenes and hornblende, to equigranular varieties with a faint to absent fabric. In the easternmost websterite body, a block of granulite-facies mafic gneiss (orthopyroxene + clinopyroxene + hornblende [pale tan in thin section] + olivine + plagioclase + accessory spinel [green in thin section]) occurs as a lens within the websterite (see Appendix 2, Field-trip STOP 1). A thin (2–4 cm) dikelet of websterite crosscuts the lens. Also, a strong solid-state lineation and foliation pass uninterrupted across the boundary between the lens and surrounding websterite. These relationships indicate that the mafic lens is older than the websterite and that it was incorporated into the intrusive websterite prior to deformation and granulite-facies metamorphism.

Amphibolite and Migmatitic Amphibole Gneiss

The ultramafic massifs and metasedimentary rocks of the Seiad complex are surrounded by an extensive body of amphibolite and migmatitic amphibole gneiss that continues beyond the map area of this study. This is a heterogeneous unit of texturally and compositionally variable amphibolite and migmatitic amphibole gneiss. Tectonic slivers of metaperidotite are common in the unit. Rocks range from fine-grained, salt-and-pepper textured amphibolite to medium- and coarse-grained amphibole gneiss with abundant segregations of plagioclase and hornblende layers. Leucosomes of plagioclase ± quartz ± hornblende exist as discontinuous veinlets and lenses that both crosscut and are deformed with the host amphibolite fabric, suggesting syntectonic partial melting of amphibolite (Fig. 5E). Amphibolite consists predominantly of amphibole and plagioclase, but compositional varieties include clinopyroxene-bearing amphibolite and garnet-bearing amphibolite. Garnet amphibolite was found only in one outcrop near Rattlesnake Mountain (locality KM193, Fig. 3; Appendix 1, see footnote 1). Primary textures and structures throughout the unit have almost everywhere been transposed or obliterated by deformation and metamorphism. One exception, however, is an outcrop of amphibolite along Cypress Ridge that contains a

distinctive lenticular fragmental texture, suggesting an original volcanoclastic protolith (Fig. 5F).

Metasedimentary-Metavolcanic Unit

The metasedimentary-metavolcanic unit is a suite of isoclinally infolded amphibolite, biotite quartzo-feldspathic paragneiss, calc-silicate paragneiss, and quartzite (metachert) that lies with the marble unit (see below) between the two large ultramafic massifs. Primary depositional surfaces in this unit have been transposed into the dominant foliation (S₁) by isoclinal folding. This unit also hosts numerous tectonic slivers of metaperidotite that are commonly surrounded by blackwall and rodingite metasomatic reaction zones (see individual descriptions below).

Amphibolite in this unit is texturally and compositionally variable. Textures vary from fine- to medium-grained varieties with an equal distribution of plagioclase and hornblende to segregated varieties with heterogeneous, foliation-parallel layers of plagioclase and hornblende. Leucosomes of plagioclase + quartz ± hornblende exist as discontinuous veinlets and segregations that both crosscut and are deformed with the amphibolite fabric. These relationships suggest local derivation of the leucosomes by syntectonic partial melting of the amphibolite gneiss. Garnet-bearing amphibolite is scarce in the Seiad complex; only one layer of garnet amphibolite (hornblende + plagioclase + garnet + quartz) was found in the metasedimentary-metavolcanic unit (locality KM47, Fig. 3; Appendix 1).

Calc-silicate paragneiss forms m-scale zones interlayered with amphibolite and biotite quartzo-feldspathic paragneiss, and also occurs as cm-scale boudinaged layers within amphibolite. Calc-silicate paragneiss contains the assemblage plagioclase + clinopyroxene + garnet + titanite ± hornblende ± clinozoisite/epidote.

Biotite quartzo-feldspathic paragneiss is less abundant than amphibolite and calc-silicate paragneiss and consists of garnet-bearing varieties and two-pyroxene-bearing varieties. The two-pyroxene varieties contain the assemblage quartz + plagioclase + orthopyroxene + clinopyroxene + biotite + graphite, and indicate granulite-facies metamorphic conditions in the metasedimentary-metavolcanic unit.

Quartzite crops out in a ~5-m-thick layer along the southeast slope of Kangaroo Mountain. Quartzite is strongly foliated and lineated, resulting in a flaggy outcrop appearance (Fig. 5D). In thin sections cut parallel to lineation and perpendicular to foliation, asymmetric garnet, muscovite, and feldspar grains indicate dominant down-lineation (top down to the northwest) sense of shear. Quartz grains show a high-temperature microstructure of serrated grain boundaries and chessboard subgrains.

Marble and Calc-Silicate Paragneiss

This unit is dominantly marble with minor calc-silicate paragneiss. The marble unit forms a thick layer that is locally infolded with layers in the bordering metasedimentary-metavolcanic unit. The white marble forms conspicuous contacts where juxtaposed against the dun-colored ultramafic rocks of the Kangaroo Mountain peridotite.

The marble is relatively pure calcite \pm dolomite, with fine black graphite plates aligned in a foliation. Subtle compositional layers are isoclinally folded parallel to the foliation. The calc-silicate paragneisses form thin, parallel layers along the contact between the marble and quartz-rich rocks of the metasedimentary-metavolcanic unit. The calc-silicate paragneisses are made up of garnet + clinozoisite + clinopyroxene + plagioclase + titanite + calcite + quartz. In thin section, an elongate shape fabric in most phases defines a slight foliation. Plagioclase grains have fine serrated boundaries, indicative of grain-boundary migration recrystallization. Titanite grains are common and are relatively coarse ~500 μ m, wedge-shaped prisms.

Early Intrusive Suite

This unit encompasses a broad suite of hornblende gabbro/diorite, hornblende, and clinopyroxenite that apparently intruded the metasedimentary-metavolcanic and amphibolite units during the early stages of penetrative deformation. Because of similar mineral assemblages, hornblende gabbro/diorite can be difficult to distinguish from host amphibole gneiss. However, a coarser grain size and lack of compositional segregation are distinguishing characteristics of this suite. Additionally, these rocks commonly make up boudinaged layers within host gneisses. Crosscutting relationships with host gneisses are also preserved, indicating an intrusive origin for the suite (Figs. 7A, 7B).

Hornblende gabbro/diorite and clinopyroxenite intrusions (meter- to decameter-scale) are variably deformed, with dikes that show little or no evidence for internal deformation and dikes that are brecciated, boudinaged, or folded. Dikes commonly contain plagioclase-rich leucocratic layers that surround boudins and fill in space between boudin necks (Fig. 7B). In thin section, the dike rocks are dominantly clinopyroxene + hornblende \pm olivine \pm plagioclase. Clear to pale-green hornblende grains commonly overgrow coarse clinopyroxene grains, sometimes in a patchy alteration texture. Olivine is usually altered to brown iddingsite.

In addition to these rocks, we mapped a single, thick (~4 m) pegmatitic biotite-hornblende diorite dike as part of the early intrusive suite. The pegmatitic diorite locally crosscuts the foliation of the host amphibolite (in the metasedimentary-metavolcanic unit), although the contact is warped and not sharp, suggesting syndeformational emplacement (Fig. 7C). The pegmatitic diorite is predominantly plagioclase with large elongate hornblende grains (up to 22 cm) that are sometimes bent and appear to be hollow and cored by plagioclase. The pegmatitic diorite contains xenoliths of amphibolite that are similar to the surrounding amphibolite (Fig. 7D).

Leucotrochjemitic Dike Swarm

A swarm of leucotrochjemitic dikes crosses the amphibolite unit in a northeast-southwest strike. These rocks contain the assemblage plagioclase + quartz \pm hornblende \pm biotite + accessory apatite and zircon. The dikes range in width from <4 cm to >1 m and do not appear to be internally deformed (Fig. 8A). The dikes broadly parallel the strike of the host amphibolite foliation, though in detail, most dike boundaries are crosscutting. Thin dikelets associated with otherwise undeformed, crosscutting dikes are tightly folded with axial surfaces parallel to the host amphibolite foliation and fold hinge zones thicker than limbs (Fig. 8B). These relationships indicate a component of flattening strain when the dikelet was still relatively hot and mobile. See geochronology section below for more discussion.

Metamorphosed Blackwall and Rodingite

In the Seiad complex, zones of amphibole and/or chlorite commonly rim tectonic slivers of peridotite found within the mafic gneisses of the metasedimentary-metavolcanic unit and amphibolite unit. These are blackwall rocks, formed by metasomatism during simultaneous metamorphism of juxtaposed ultramafic and mafic rocks (e.g., Frost, 1975; Sanford, 1982), reflecting the incompatibility of olivine and plagioclase under medium-grade, hydrous metamorphic conditions. In the Seiad complex, these contact zones are commonly weathered, and it is rare to find an uninterrupted transition from amphibolite to peridotite. In the metasedimentary-metavolcanic unit, blackwall zones are commonly ~10–50-cm thick bands of monomineralic, bright-green amphibole rock. Amphibole alignment defines a faint fabric. In thin section, the amphibole is a clear, clin amphibole with prismatic habit. In the amphibolite unit along the ridge leading to Upper Devil peak, the monomineralic zones around peridotite slivers are dominantly fine-grained chlorite schist.

Another type of metasomatic rock found in the Seiad complex is rodingite (now metamorphosed), a calcium-enriched rock that develops along the boundaries of juxtaposed mafic and ultramafic rocks during serpentinization (e.g., Coleman, 1967; Frost, 1975). The metarodingite contains a strong foliation defined by alignment of clinopyroxene. Lundquist (1983) confirmed that these rocks are metarodingites by bulk-composition chemical analyses



Figure 7. Field photographs of some representative rock types from the early intrusive suite. (A) Deformed hornblende layers subparallel to host amphibole gneiss. (B) Deformed intrusive body of clinopyroxenite (lower right half of the photograph) within interlayered amphibolite and metaserpentinite (upper left half of the photograph). Clinopyroxenite body is brecciated and plagioclase-rich leucosomes surround the fragments of clinopyroxenite. (C) Diffuse contact between leucocratic amphibole gneiss of the metasedimentary-metavolcanic unit and pegmatitic biotite-hornblende diorite. (D) Xenolith of amphibolite in pegmatitic biotite-hornblende diorite. Prismatic hornblende grains, which reach ~20 cm in length, rim the xenolith.

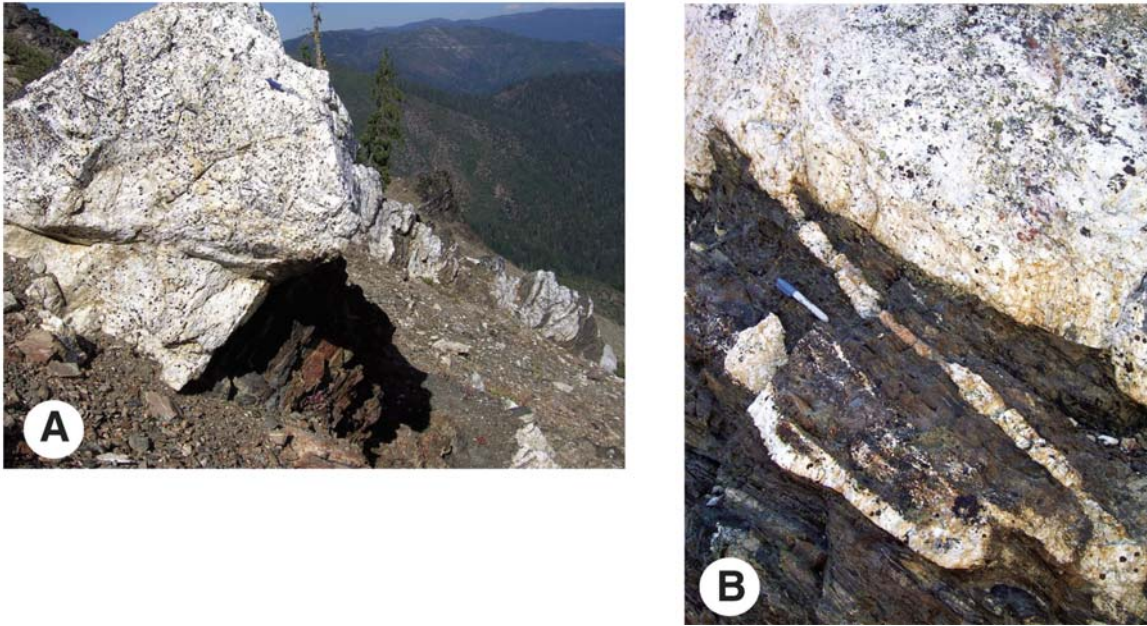


Figure 8. (A) Field photograph of a trondhjemitic dike in the amphibolite and migmatitic amphibole gneiss unit. Dikes of this swarm generally strike subparallel to the foliation of the host rock amphibolite, although local crosscutting relationships are common. The dikes are internally undeformed. (B) Dikelet of leucotrandhjemite isoclinally folded with axial surface subparallel to the host amphibolite foliation.

that showed depletion of SiO_2 and Na_2O and enrichment in Al_2O_3 and CaO . The most common mineral assemblage in metarodingite of the Seiad complex is grossularite + clinopyroxene + epidote + chlorite \pm vesuvianite \pm spinel. Some peridotite slivers surround lensoid masses of metarodingite, suggesting the former existence of a mafic block surrounded by serpentinite (Fig. 9) (see “Metamorphic History” section later in this chapter).

STRUCTURAL ANALYSIS

Structural elements throughout the study area are remarkably subparallel and the resultant map pattern indicates that the peridotite massifs, interleaved metasedimentary and metavolcanic rocks, and surrounding amphibolites were penetratively deformed and folded together, after juxtaposition and mélangé formation. All primary layering within units and tectonic contacts between units have been transposed by this primary deformation event. The large-scale structure of the Seiad complex is a northwest-plunging antiform (Fig. 10). Discordance of foliation in adjacent rock units with regard to the northeast–southwest strike of the metasedimentary-metavolcanic unit (Fig. 3 and Appendix 1 on the CD-ROM accompanying this volume) indicates localized, late brittle deformation along lithologic contacts, and possibly localized shear in the metasedimentary-metavolcanic unit during the primary deformation event. These northeast–southwest-striking faults are inferred to continue to the southwest in the field area, although they are not delineated on the geologic maps



Figure 9. Lens of metarodingite (white), consisting chiefly of grossularite, clinopyroxene, Ca-amphibole, clinozoisite, and chlorite surrounded by serpentinite.

(Fig. 3 and Appendix 1) because they become concordant to the dominant foliation in a southwesterly direction. A northeast–southwest-striking brittle fault is mapped in the West Fork ultramafic body, indicated by truncated bodies of websterite and granulite-facies mafic gneiss.

The structural elements of the study area can be classified into three distinct events: D_0 , D_{1-2} , and D_3 (Table 1). Two additional events, labeled pre- D_1 and post- D_3 on Table 1, are inferred

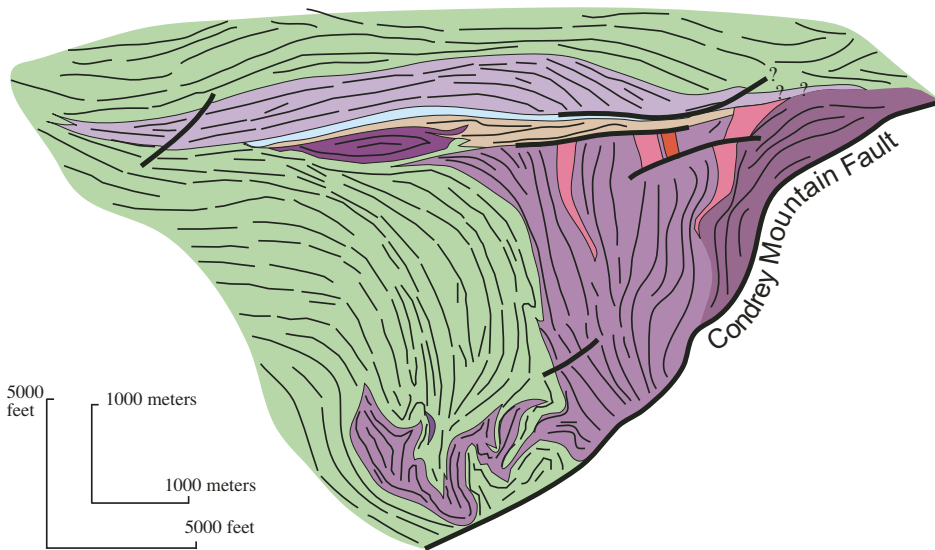

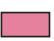










Figure 10. Axial-plunge diagram viewed in a northward direction showing the structure of the Seiad complex. Based on an unpublished map and diagram by L.G. Medaris Jr.

EXPLANATION

	Impure marble and calc-silicate paragneiss (mcs)		Websterite (w)
	Metasedimentary and metavolcanic rocks (msv)		Granulite-facies metagabbroic rocks (gmg)
	Amphibolite and migmatitic amphibolite gneiss (a)		Lily Pad peridotite (lpp) and small serpentinitized peridotite bodies (sp)
	West Fork ultramafic body (wfu), including spinel lherzolite (wfl)		Kangaroo Mountain peridotite (kmp)
	Fault		
	Trace of dominant foliation (S ₁)		

by overall structural relationships within the map area. D_0 is the protolith-forming history and is characterized by S_0 primary sedimentary and volcanic layering. Although most contacts in the field area are tectonic, some of these are transposed S_0 surfaces; e.g., the marble-metasedimentary unit contact.

After protolith formation and before the main penetrative deformation event (pre- D_1), the different lithologic units of the field area were tectonically intercalated into an ophiolitic mélangé. Based on the presence of metamorphosed rodingite, this mixing took place at shallow crustal levels in the presence of seawater. Sedimentary processes, e.g., submarine landsliding associated with the development of steep carbonate and/or volcanic platforms or intra-oceanic fault scarps, could have also contributed to the development of the primary mélangé (e.g., Saleeby, 1984). However, the presence of large peridotite massifs, as well as contacts between ocean-floor rocks (marble and metachert) and upper-mantle rocks (harzburgite), strongly indicate an important tectonic component to mélangé formation.

Blocks incorporated into the mélangé may have carried with them a fabric of a prior tectonic event (e.g., Gorman, 1985; Coleman et al., 1988), and previous workers have found evidence for locally preserved upper-mantle fabrics in the ultramafic massifs

(Lundquist, 1983; Cannat, 1985). However, the concordance of D_{1-2} fabrics and similarities of metamorphic facies across lithologic contacts are evidence that any prior structures or metamorphic mineral assemblages were completely overprinted or transposed after development of the mélangé.

D_{1-2} represents the main tectonic event that affected the rocks in the study area. Based on the presence of two distinct, yet subparallel generations of folding (F_1 and F_2), we interpret D_{1-2} structures as forming during a single, progressive deformational event. Mineral flattening and elongation directions define the dominant measured foliation and lineation (S_1 and L_{1-2}). Lineations are given the subscript 1–2 because in amphibolite they are typically parallel to hinge lines of isoclinal folds that fold S_1 fabric (i.e., F_2 folds). F_1 isoclinal folds primary layering and have axial surfaces parallel to S_1 . The axial surfaces of F_2 folds are also subparallel to S_1 .

Orientation of anisotropic minerals—typically amphibole and/or biotite—defines S_1 and L_1 in amphibolite and metasedimentary gneisses. Shape fabric in quartz and transposed primary layering define S_1 in quartzite; the axial surfaces of F_1 isoclinal folds and transposed primary layering define S_1 in marble. Flattened and elongate orthopyroxene and Ca-amphibole porphyroclasts

define S_1 and L_1 in hornblende harzburgite of the Kangaroo Mountain peridotite, Lily Pad peridotite, and harzburgite sections of the West Fork body. Within the West Fork body, alignment of chromite grains define S_1 and L_1 in dunite, whereas aligned pyroxenes and trains of fine-grained spinel define S_1 and L_1 in spinel lherzolite. Chromitite stringers commonly exhibit spectacular isoclinal folds with thinned limbs and thickened hinge zones (Fig. 5A).

D_3 represents regional folding that resulted in open F_3 folds at the outcrop and map scale. All previous structural elements are folded by this event. F_3 folds range from broad, m-scale warping at the outcrop to map-scale antiforms and synforms. Foliation measurements and map patterns indicate a shallowly north-northwest-plunging antiform and synform pair in the metasedimentary unit and a broad northwest-plunging antiform in the amphibolite unit (Figs. 3 and 10). Concordance of fabrics and contacts around these folds indicate that all units were folded together.

METAMORPHIC HISTORY

The multi-stage history recorded by the structures of the Seiad complex is also evident in the metamorphic features of the rocks. These features include early rodingite development, subsequent prograde metamorphism of the entire complex to upper amphibolite to granulite facies, and widespread retrograde metamorphism.

We did not identify systematic changes in mineral assemblages in the map area that allowed the delineation of isograds. Grover (1984) and Grover and Rice (1985) identified isograds in ultramafic rocks to the west of this map area, where the enstatite-in isograd is just west of Rattlesnake Mountain (~1 km west of the western map border) and the spinel-in isograd is along the western border of the map area.

Representative mineral assemblages from the major rock units in the Seiad complex are presented together in Table 2. Four separate rock types contain prograde granulite-facies assemblages: spinel lherzolite (olivine + orthopyroxene + clinopyroxene + Al-spinel \pm pargasite), websterite (orthopyroxene + clinopyroxene \pm hornblende), mafic gneiss/metagabbro (orthopyroxene + clinopyroxene + plagioclase \pm hornblende), and biotite quartzofeldspathic paragneiss (quartz + plagioclase + clinopyroxene + orthopyroxene + biotite). The spinel lherzolite, websterite, and metagabbro outcrops occur in the structurally deepest section of the study area and are all within the West Fork ultramafic block (Fig. 3). The biotite two-pyroxene quartzofeldspathic paragneiss crops out in the metasedimentary-metavolcanic unit near Lily Pad Lake (site KM51, Fig. 3).

In contrast to these four rock types, the rocks of the Seiad complex contain upper amphibolite-facies mineral assemblages. The large ultramafic massifs contain rocks with the stable, prograde assemblage olivine + orthopyroxene + pargasitic amphibole + spinel, indicative of upper amphibolite-facies metamorphism (Evans, 1977). In mafic amphibolites, the common presence of stable clinopyroxene with hornblende and plagioclase suggest

dehydration melting under water-poor conditions (Beard and Lofgren, 1991). Also, the generation of both deformed and cross-cutting leucosomes with the assemblage of plagioclase + quartz \pm hornblende indicate syntectonic partial melting of amphibolite at $T > 700$ °C (Beard, 1990, 1995; Beard and Lofgren, 1991).

Blackwall compositions and the mineral assemblage in metamorphosed rodingite also indicate amphibolite-facies metamorphic conditions. Blackwall rocks are highly variable, depending on the composition of the juxtaposed rock types. However, during amphibolite-facies metamorphism, blackwalls that develop between peridotite and mafic rocks are typically made up of hornblende and chlorite (Sanford, 1982). In the Seiad complex, typical blackwall between peridotite and amphibolite is made up of monomineralic aluminous amphibole. Lieberman and Rice (1986, p. 184) also report blackwalls that contain the assemblage olivine + orthopyroxene + chlorite + spinel, corresponding to the reaction between chlorite and spinel at ~700 °C (Frost, 1975). The metarodingite assemblage in the Seiad complex also indicates high-grade metamorphism (Frost, 1975).

In addition to information about the conditions of metamorphism, blackwall and metarodingite rocks provide key evidence for the relative timing of mélangé formation and peak metamorphism. The presence of rodingite in the field area indicates that the ultramafic units must have undergone at least partial serpentinization during mélangé formation and juxtaposition with mafic blocks, requiring relatively low pressures and temperatures and the presence of seawater.

Thus, the metamorphic relationships in rocks of the Seiad complex suggest a history of imbrication in the upper crust, where ultramafic rocks were partially serpentinized, and subsequent burial and heating during penetrative deformation, resulting in upper amphibolite- to granulite-facies mineral assemblages that contain tectonite fabrics.

The presence of granulite-facies assemblages in metaperidotite, metapyroxenite, metagabbro, and metasedimentary rocks, as well as the concordance of structural elements throughout the complex, make it highly unlikely that these assemblages are relict features of blocks in a mélangé (cf. Coleman et al., 1988). Rather, the high-grade dynamothermal metamorphism that is evident in all of the units of the Seiad complex locally reached granulite-facies conditions.

Despite the preservation of granulite- and upper amphibolite-facies prograde mineral assemblages, there are also widespread effects of retrograde metamorphism in the Seiad complex. Harzburgite samples contain phases from several of the stages of retrograde mineral assemblages in peridotite, including olivine + Ca-amphibole + anthophyllite + chlorite and olivine + tremolite + talc + chlorite (Table 2). Also, saussuritization is widespread in all of the plagioclase-bearing units. There is field evidence for granulite-facies metagabbro altering to amphibolite along a retrograde path (Fig. 5B; see Appendix 2, Field-trip STOP 2), and in thin section, the aligned pyroxenes of the granulite are in places pseudomorphosed by aggregates of randomly oriented, fine-grained amphibole.

TABLE 2. REPRESENTATIVE METAMORPHIC MINERAL ASSEMBLAGES, SEIAD COMPLEX
<p>Amphibolite and Migmatitic Amphibole Gneiss hornblende + plagioclase ± quartz + accessory titanite hornblende + plagioclase + quartz + garnet hornblende + clinopyroxene + plagioclase + accessory titanite plagioclase + hornblende + clinopyroxene + biotite + accessory titanite</p>
<p>Kangaroo Mountain Peridotite (harzburgite) olivine + orthopyroxene + Ca-amphibole + Cr-spinel olivine + orthopyroxene + Ca-amphibole + chlorite olivine + Ca-amphibole + anthophyllite + chlorite olivine + tremolite + talc + chlorite</p>
<p>West Fork Ultramafic Body olivine + orthopyroxene + clinopyroxene + Ca-amphibole + Al-spinel (spinel lherzolite) olivine + orthopyroxene + Ca-amphibole + Cr-spinel (harzburgite) olivine + orthopyroxene + Ca-amphibole + chlorite (harzburgite) olivine + Cr-spinel (dunite) clinopyroxene + olivine + Ca-amphibole (wehrlite)</p>
<p>Websterite orthopyroxene + clinopyroxene + hornblende ± olivine + accessory Fe-Ti oxides</p>
<p>Metagabbroic Rocks hornblende ± plagioclase orthopyroxene + clinopyroxene + plagioclase ± hornblende ± biotite + accessory rutile</p>
<p>Lily Pad Peridotite and Small Serpentinized Peridotite Bodies olivine + orthopyroxene + Ca-amphibole + Cr-spinel olivine + orthopyroxene + Ca-amphibole + chlorite olivine + Ca-amphibole + anthophyllite + chlorite olivine + tremolite + talc + chlorite</p>
<p>Metasedimentary-Metavolcanic Unit quartz + plagioclase + orthopyroxene + clinopyroxene + biotite + graphite hornblende + plagioclase + biotite + quartz + garnet clinopyroxene + clinozoisite + hornblende + plagioclase + titanite + calcite + garnet plagioclase + hornblende + accessory titanite, rutile, monazite, apatite hornblende + plagioclase + clinopyroxene + accessory titanite, chromite quartz + plagioclase + biotite + garnet + perthitic K-feldspar + graphite + accessory monazite, zircon quartzite (metachert): quartz + muscovite + biotite + garnet + plagioclase ± K-feldspar ± chlorite</p>
<p>Marble and Calc-Silicate Paragneiss calcite + dolomite + graphite + muscovite + quartz + titanite garnet + clinozoisite + clinopyroxene + plagioclase + titanite + calcite + quartz</p>
<p>Metamorphosed Rodingite grossularite + clinopyroxene + epidote + chlorite ± vesuvianite ± spinel Ca-amphibole + clinopyroxene + chlorite + clintonite + clinozoisite + hercynite plagioclase + clinozoisite + Ca-amphibole + clinopyroxene + chlorite</p>
<p>Metamorphosed Blackwall Ca-amphibole ± chlorite Ca-amphibole + chlorite + talc + magnetite Na-amphibole + hornblende + chlorite + ilmenite</p>

GEO THERMOBAROMETRY

Introduction and Methods

The temperature of peak metamorphism in the Seiad complex is relatively well constrained by diagnostic mineral assemblages of several different rock types (see above) and by previously published geothermometry to ≥ 700 °C (Medaris, 1975; Loomis and Gottschalk, 1981; Lieberman, 1983; Grover, 1984; Grover and Rice, 1985; Liebermann and Rice, 1986).

Pressure conditions, however, are not well constrained, as most mineral assemblages in the complex are generally not conducive to geobarometry. Grover (1984) and Grover and Rice (1985) estimated ~7 kb based on the intersection of the quartz + zoisite breakdown curve in calc-silicate rocks with the anthophyllite + forsterite breakdown curve in ultramafic rocks. Lieberman and Rice (1986) estimated 7–8 kb based on the calc-silicate assemblage grossularite + wollastonite + quartz and the chloritic blackwall assemblage olivine + orthopyroxene + chlorite + spinel.

To refine these estimates, we collected two samples of scarce garnet-bearing amphibolite in the Seiad complex for geothermobarometry, one from the amphibolite unit (KM193a) and one from the metasedimentary-metavolcanic unit (KM47). Both samples contain the mineral assemblage hornblende + plagioclase + garnet + quartz and are thus appropriate for the geothermobarometric methods of Kohn and Spear (1989).

Additionally, to better understand the granulite-facies metagabbro and further test our interpretation that all of the units of the Seiad complex experienced the same dynamothermal metamorphism, we obtained temperature estimates for granulite-facies metagabbro by application of two two-pyroxene geothermometers (Brey and Köhler, 1990; Taylor, 1998).

Sample localities for geothermometry, geobarometry, geochemistry, and geochronology (see below) are shown in Figure 11; and electron microprobe analytical conditions are given in Table 3.

Results

Table 3 shows representative mineral compositions for samples of garnet amphibolite and granulite and summarizes results of our thermobarometric calculations. Geothermobarometric calculations for garnet amphibolite sample KM47 from the metasedimentary-metavolcanic unit yield temperature and pressure conditions of 713 ± 76 °C and 7.3 ± 0.9 kb. Sample KM193a, from the amphibolite and migmatitic amphibole gneiss unit, ~2 km structurally above sample KM47, yields temperature and pressure conditions of $\sim 661 \pm 18$ °C and 4.9 ± 0.7 kb. These estimates confirm the results of previous studies and of field and petrographic evidence for relatively high temperatures and moderately high-pressure conditions during metamorphism in the Seiad complex (Grover, 1984; Grover and Rice, 1985; Lieberman and Rice, 1986).

The granulite-facies metagabbro (granulite) contains a mineral assemblage of enstatite ($\text{Ca}_{1.3-2.2}\text{Mg}_{64.6-70.2}\text{Fe}_{28.4-33.4}$) + diopside ($\text{Ca}_{46.3-46.7}\text{Mg}_{41.0-43.2}\text{Fe}_{9.6-12.0}$) + plagioclase (An_{66-92}) + rutile \pm amphibole \pm biotite. Pyroxenes in granulite are largely devoid of exsolution lamellae and are relatively homogeneous in composition. Application of the Taylor (1998) two-pyroxene geothermometer to six samples of granulite yields an average 743 ± 52 °C (calculated at $P = 7$ kb), and the Brey and Köhler (1990) geothermometer yields a similar result, 706 ± 38 °C. Such results confirm the granulite-facies conditions for the Seiad granulite and are consistent with temperatures inferred for the granulite-facies assemblages in spinel lherzolite and websterite.

MAJOR-, TRACE-, AND RARE-EARTH-ELEMENT CONCENTRATIONS

Introduction and Methods

Although a comprehensive geochemical investigation of the Seiad complex is beyond the scope of this study, major- and

trace-element compositions have been determined for selected samples of lherzolite, harzburgite, websterite, granulite, and amphibolite. Such analyses provide a more complete characterization of high-grade rocks in the complex and yield insights into their petrogeneses and tectonic settings. Analyses were performed by the GeoAnalytical Laboratory at Washington State University, where major elements were determined by X-ray fluorescence (XRF) techniques and trace elements by Inductively Coupled Plasma–Mass Spectrometry (ICP–MS).

Spinel Lherzolite and Harzburgite

Relative to primitive mantle, spinel lherzolite in the West Fork unit has higher MgO contents and is depleted in incompatible elements, such as Ti, Al, Ca, and Na (Fig. 12; Table 4). The elevated Na_2O content in one lherzolite sample is likely due to the mobility and introduction of Na during metamorphism. The depleted nature of spinel lherzolite is also seen in rare-earth-element (REE) patterns normalized to primitive mantle (Fig. 13A), in which light rare-earth elements (LREE) are reduced relative to heavy rare-earth elements (HREE), and normalized values for the HREE are less than 1.0. An extended trace-element plot for lherzolite sample SV10 (Fig. 13B) is relatively flat at a level ~ 0.2 – 0.7 times that of primitive mantle, with slight negative anomalies for K and Zr, and a small positive anomaly for Pb. In contrast, a comparable plot for lherzolite SV11B1, which occurs adjacent to a 1-cm-thick pyroxenite vein, shows a pronounced positive anomaly for Pb and prominent negative anomalies for Nb, Ta, and K.

Two samples of harzburgite from the Kangaroo Mountain peridotite and one sample of harzburgite from the West Fork body contain lower amounts of MgO (44.6%–47.5%), CaO (<0.6%), and TiO_2 (0.01%), compared to spinel lherzolite (Fig. 12; Table 4). Al_2O_3 contents in two samples of harzburgite are similar to those in the spinel lherzolite and reflect the presence of spinel. Elevated amounts of Na_2O and K_2O (not shown) in two harzburgite samples are probably due to introduction of these constituents during metamorphism, as thought to be the case in spinel lherzolite. Harzburgite KM201 was analyzed for trace elements, but the concentrations are extremely low, near the detection limits of the ICP–MS procedure; because of this situation, the results are given in Table 4 but not included in Figure 13B.

The chemical distinction between lherzolite and harzburgite is also revealed by the composition of spinel, which is primarily a function of bulk-rock composition and, secondarily, of equilibration conditions. Disseminated spinel in lherzolite is markedly aluminous, with Cr-numbers ranging from 10 to 25 (Fig. 14), which lie at the Al-rich end of the spinel compositional array for abyssal peridotite. In contrast, spinel in harzburgite, dunite, and podiform chromite is more Cr-rich, with Cr-numbers ranging from 50 to 80 (Fig. 14), similar to that in the cumulate portions of ophiolite complexes and stratiform basic complexes (Irvine, 1967). By comparison, spinel in the Josephine peridotite (Dick and Bullen, 1984) spans the same range of composition as that in the Seiad suite, although the Cr-rich Josephine spinel has a higher

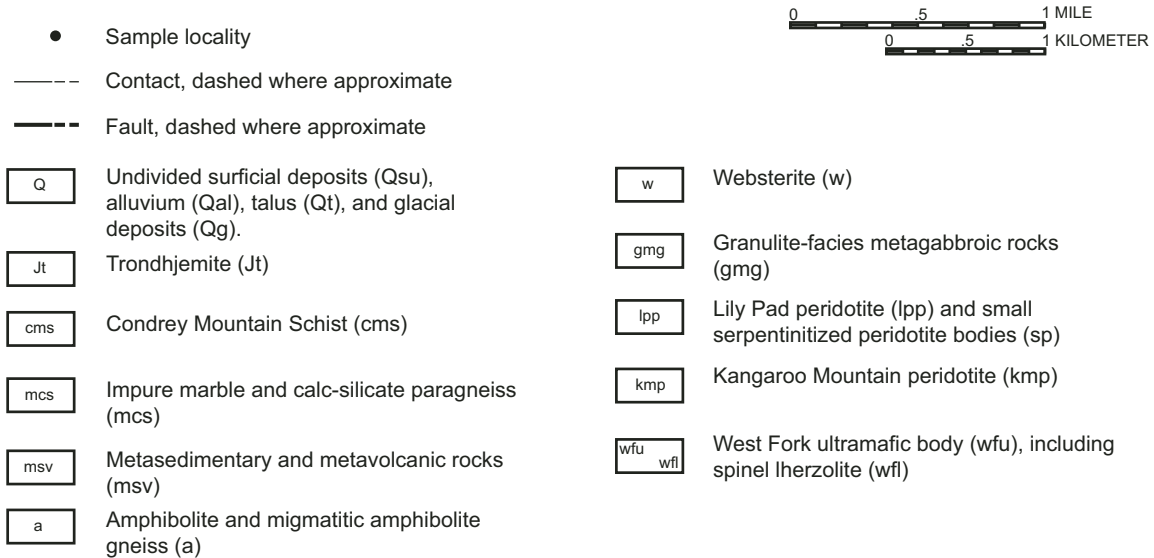
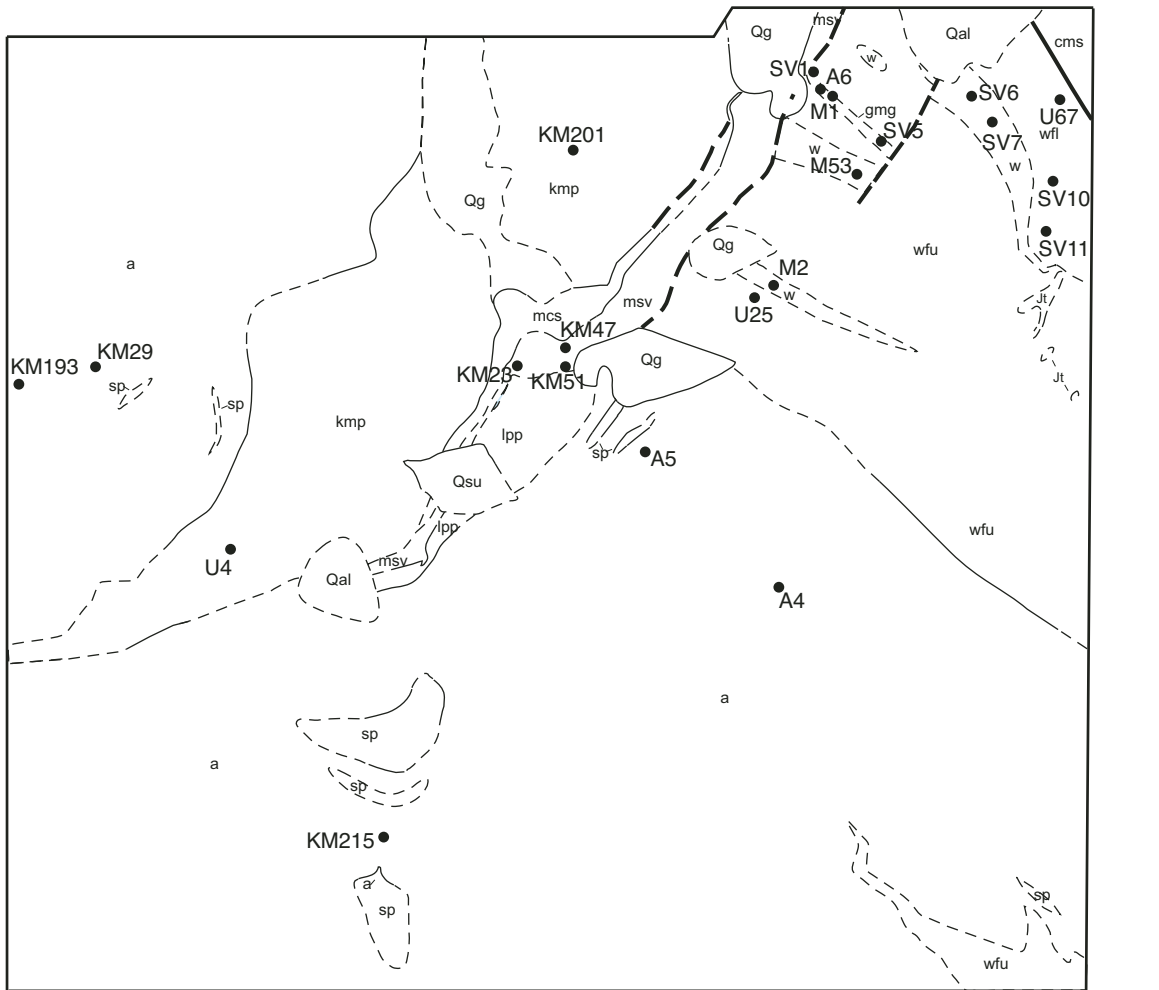


Figure 11. Sketch map of the Seiad complex showing sample localities.

TABLE 3A. REPRESENTATIVE MINERAL COMPOSITIONS AND THERMOBAROMETRIC RESULTS FOR KM193a

#	1	2	3	4	5	6	7	8	9	10	11	mean	std
T(°C)	635	655	669	677	682	676	684	669	638	664	674	661	18
P(Kb)	4.8	5.0	4.8	5.1	4.7	5.2	5.1	5.4	4.5	4.2	4.9	4.9	0.3
Garnet													
Sample # / Analysis #	2/2	2/3	2/4	2/5	2/6	1/1	1/3	1/4	1/5	1/6	1/7		
SiO ₂	37.686	37.606	37.466	37.623	37.317	37.372	37.367	37.308	37.269	37.490	37.201		
Al ₂ O ₃	20.895	20.846	20.686	20.830	20.857	20.874	20.811	20.816	20.817	20.890	20.824		
Cr ₂ O ₃	0.017	0.006	0.021	0.010	0.026	0.009	0.009	0.003	0.004	0.009	0.005		
MgO	4.221	4.003	4.126	4.199	3.919	4.422	4.473	4.161	4.069	4.520	4.614		
FeO	31.475	30.403	30.491	31.635	30.881	31.399	30.501	30.170	30.656	31.238	31.118		
MnO	1.663	1.895	1.792	1.526	2.068	1.363	1.504	1.758	1.705	1.446	1.397		
CaO	4.278	4.367	4.322	4.363	4.264	3.973	3.912	4.460	4.419	3.639	3.565		
Total	100.236	99.125	98.904	100.186	99.331	99.411	98.577	98.676	98.939	99.232	98.725		
Cations: 12 oxygen basis													
Si	2.996	3.014	3.011	2.994	2.995	2.991	3.006	3.002	2.997	3.001	2.993		
Al	1.958	1.969	1.959	1.954	1.973	1.969	1.973	1.974	1.973	1.971	1.975		
Cr	0.001	0.000	0.001	0.001	0.002	0.001	0.001	0.000	0.000	0.001	0.000		
Mg	0.500	0.478	0.494	0.498	0.469	0.528	0.536	0.499	0.488	0.539	0.553		
Fe	2.092	2.037	2.049	2.106	2.073	2.102	2.052	2.030	2.062	2.091	2.094		
Mn	0.112	0.129	0.122	0.103	0.141	0.092	0.103	0.120	0.116	0.098	0.095		
Ca	0.365	0.375	0.372	0.372	0.367	0.341	0.337	0.385	0.381	0.312	0.307		
Total	8.025	8.002	8.009	8.028	8.018	8.024	8.007	8.011	8.016	8.013	8.019		
Hornblende													
Sample # / Analysis #	2/3	2/4	2/5	2/6	2/8	1/1	1/3	1/4	1/5	1/6	1/7		
SiO ₂	43.023	43.062	42.856	42.707	43.114	42.937	43.307	43.072	43.845	42.956	42.978		
TiO ₂	0.727	0.864	0.953	0.877	0.945	0.884	0.842	0.819	0.830	0.886	0.883		
Al ₂ O ₃	14.977	14.692	14.570	14.595	14.159	14.851	14.431	14.931	13.212	14.638	15.038		
Cr ₂ O ₃	0.001	0.024	0.001	0.010	0.001	0.000	0.005	0.002	0.007	0.043	0.015		
FeO	17.378	18.307	18.431	18.682	18.361	18.164	18.127	17.886	19.046	18.133	17.645		
MnO	0.165	0.170	0.211	0.150	0.230	0.141	0.171	0.158	0.250	0.150	0.154		
MgO	9.067	9.108	9.084	9.091	9.123	9.234	9.397	9.268	9.744	9.217	9.174		
CaO	10.988	10.786	10.470	9.981	10.290	10.557	10.520	10.812	9.502	10.677	10.933		
Na ₂ O	1.725	1.753	1.785	1.676	1.736	1.792	1.723	1.734	1.651	1.771	1.773		
K ₂ O	0.229	0.243	0.245	0.221	0.203	0.198	0.233	0.232	0.210	0.242	0.211		
F	0.000	0.014	0.007	0.007	0.009	0.020	0.000	0.004	0.007	0.008	0.007		
Cl	0.001	0.003	0.000	0.007	0.020	0.000	0.009	0.013	0.002	0.031	0.010		
Total	98.280	99.021	98.612	98.000	98.180	98.766	98.760	98.925	98.303	98.743	98.815		

(Continued)

TABLE 3A. REPRESENTATIVE MINERAL COMPOSITIONS AND THERMOBAROMETRIC RESULTS FOR KM193a (Continued)

Hornblende (Continued)												
Sample # / Analysis #	2/3	2/4	2/5	2/6	2/8	2/avg	1/1	1/3	1/4	1/5	1/6	1/7
No.	17.667	23.500	30.000	35.400	47.000	52.500	64.500	70.750	77.000	84.000	89.500	
Si	6.367	6.352	6.352	6.364	6.409	6.340	6.392	6.345	6.510	6.350	6.334	
Ti	0.081	0.096	0.106	0.098	0.106	0.098	0.094	0.091	0.093	0.098	0.098	
Al	2.613	2.555	2.545	2.564	2.480	2.585	2.511	2.593	2.312	2.551	2.613	
Cr	0.000	0.003	0.000	0.001	0.000	0.000	0.001	0.000	0.001	0.005	0.002	
Fe	2.151	2.259	2.285	2.329	2.282	2.243	2.238	2.204	2.365	2.242	2.175	
Mn	0.021	0.021	0.027	0.019	0.029	0.018	0.021	0.020	0.031	0.019	0.019	
Mg	2.001	2.003	2.007	2.019	2.022	2.032	2.068	2.035	2.157	2.031	2.015	
Ca	1.743	1.705	1.663	1.593	1.639	1.670	1.664	1.707	1.512	1.691	1.726	
Na	0.495	0.502	0.513	0.484	0.500	0.513	0.493	0.495	0.475	0.508	0.507	
K	0.043	0.046	0.046	0.042	0.038	0.037	0.044	0.044	0.040	0.046	0.040	
F	0.000	0.007	0.003	0.003	0.004	0.009	0.000	0.002	0.003	0.004	0.003	
Cl	0.000	0.001	0.000	0.002	0.005	0.000	0.002	0.003	0.001	0.008	0.002	
Total	15.514	15.547	15.548	15.519	15.515	15.545	15.527	15.538	15.499	15.551	15.534	
Plagioclase												
Sample # / Analysis #	2/3	2/4	2/7	2/1	2/avg	1/1	1/3	1/5	1/6	1/7	1/8	
SiO ₂	52.969	53.510	52.179	54.021	53.472	55.175	54.723	54.533	52.891	52.910	55.162	
Al ₂ O ₃	29.460	29.368	30.158	28.877	29.328	28.451	28.581	28.907	30.041	30.160	28.394	
Fe ₂ O ₃	0.088	0.044	0.108	0.122	0.081	0.086	0.044	0.185	0.091	0.183	0.068	
CaO	10.987	10.900	11.802	10.372	10.818	9.784	9.919	10.250	11.450	11.760	9.761	
Na ₂ O	5.110	5.210	4.642	5.463	5.220	5.936	5.795	5.627	4.916	4.874	5.897	
K ₂ O	0.025	0.024	0.027	0.033	0.035	0.026	0.050	0.035	0.043	0.027	0.036	
Total	98.639	99.056	98.916	98.887	98.954	99.460	99.111	99.537	99.430	99.914	99.317	
Cations: 8 oxygen basis												
Si	2.423	2.436	2.386	2.460	2.437	2.494	2.483	2.467	2.403	2.396	2.496	
Al	1.589	1.576	1.625	1.550	1.575	1.516	1.529	1.541	1.609	1.609	1.514	
Total	4.012	4.012	4.011	4.010	4.012	4.009	4.012	4.008	4.012	4.005	4.010	
Fe	0.003	0.002	0.004	0.004	0.003	0.003	0.002	0.006	0.003	0.006	0.002	
Ca	0.539	0.532	0.578	0.506	0.528	0.474	0.482	0.497	0.558	0.571	0.473	
Na	0.453	0.460	0.412	0.482	0.461	0.520	0.510	0.494	0.433	0.428	0.517	
K	0.001	0.001	0.002	0.002	0.002	0.002	0.003	0.002	0.002	0.002	0.002	
Total	0.996	0.994	0.995	0.995	0.994	0.999	0.996	0.999	0.996	1.006	0.995	
AN	0.542	0.536	0.583	0.511	0.533	0.476	0.485	0.500	0.561	0.571	0.477	
AB	0.456	0.463	0.415	0.487	0.465	0.523	0.512	0.498	0.436	0.428	0.521	
OR	0.001	0.001	0.002	0.002	0.002	0.002	0.003	0.002	0.002	0.002	0.002	

TABLE 3B. REPRESENTATIVE MINERAL COMPOSITIONS AND THERMOBAROMETRIC RESULTS FOR KM47

#	1	2	3	4	5	6	7	8	9	10	11	12	13	14	mean	std
T(°C)	761	760	688	677	695	782	768	622	577	741	833	589	735	758	713	76
P(Kb)	7.4	7.4	6.8	6.6	6.9	8.1	8.4	7.4	6.9	7	7.7	6.6	7	7.3	7.3	0.5
Garnet																
Sample # / Analysis #	y/2	y/2	y/1	y/1	y/2	bx/avg.	bx/2	bx/4	bx/3	z/1	z/4	z/2	z/3	z/2		
SiO ₂	37.597	37.597	37.346	37.346	37.597	37.313	37.382	37.471	37.216	37.499	37.373	37.392	37.685	37.392		
Al ₂ O ₃	20.752	20.752	20.851	20.851	20.752	20.479	20.346	20.717	20.310	20.794	20.542	20.655	20.662	20.655		
MgO	2.761	2.761	2.941	2.941	2.761	2.364	2.134	2.754	1.987	2.564	2.705	2.696	2.854	2.696		
FeO	31.281	31.281	31.697	31.697	31.281	32.044	32.297	32.288	31.956	30.958	31.453	31.419	31.679	31.419		
MnO	2.801	2.801	2.363	2.363	2.801	2.361	2.215	2.131	2.420	2.864	2.643	2.701	2.492	2.701		
CaO	5.483	5.483	5.230	5.230	5.483	5.665	6.020	5.399	5.954	5.697	5.488	5.460	5.433	5.460		
Total	100.674	100.674	100.426	100.426	100.674	100.226	100.394	100.758	99.841	100.376	100.204	100.323	100.805	100.323		
Cations: 12 oxygen basis																
Si	3.000	3.000	2.987	2.987	3.000	3.001	3.006	2.992	3.008	3.000	2.999	2.997	3.003	2.997		
Al	1.952	1.952	1.965	1.965	1.952	1.941	1.928	1.950	1.935	1.951	1.943	1.951	1.941	1.951		
Mg	0.328	0.328	0.351	0.351	0.328	0.283	0.256	0.328	0.239	0.306	0.324	0.322	0.339	0.322		
Fe	2.087	2.087	2.120	2.120	2.087	2.155	2.172	2.156	2.160	2.071	2.111	2.106	2.111	2.106		
Mn	0.189	0.189	0.160	0.160	0.189	0.161	0.151	0.144	0.166	0.194	0.180	0.183	0.168	0.183		
Ca	0.469	0.469	0.448	0.448	0.469	0.488	0.519	0.462	0.516	0.488	0.472	0.469	0.464	0.469		
Total	8.025	8.025	8.031	8.031	8.025	8.029	8.031	8.033	8.024	8.020	8.029	8.028	8.026	8.028		
Hornblende																
Sample # / Analysis #	y/6	y/6	y/3	y/4	y/5	bx/2	bx/3	bx/5	bx/4	z/2	z/1	z/4	z/6	z/5		
SiO ₂	39.285	39.285	39.785	40.871	40.243	39.289	39.060	39.575	39.554	40.271	40.234	40.223	40.353	39.590		
TiO ₂	1.608	1.608	2.159	2.399	2.378	1.410	1.285	1.422	1.970	1.559	1.000	2.016	2.431	1.823		
Al ₂ O ₃	14.404	14.404	13.443	13.164	13.746	13.907	14.848	14.808	14.345	13.982	15.265	13.977	12.702	13.970		
FeO	22.745	22.745	22.175	21.273	21.156	23.140	23.353	21.497	21.438	22.208	22.321	20.052	21.650	22.428		
MnO	0.311	0.311	0.227	0.199	0.349	0.291	0.261	0.180	0.229	0.308	0.269	0.197	0.330	0.327		
MgO	6.032	6.032	6.975	6.714	6.248	5.067	4.818	7.285	5.971	5.732	5.128	7.212	6.010	5.799		
CaO	10.245	10.245	9.200	10.267	10.622	10.918	10.391	9.005	10.929	11.107	11.669	10.811	10.789	10.876		
Na ₂ O	1.488	1.488	1.632	1.726	1.561	1.617	1.598	1.739	1.772	1.582	1.488	1.681	1.552	1.430		
K ₂ O	1.191	1.191	1.214	1.329	1.364	1.320	1.408	1.101	1.389	1.248	1.206	1.403	1.364	1.322		
F	0.031	0.031	0.032	0.018	0.007	0.000	0.081	0.032	0.039	0.000	0.023	0.099	0.025	0.025		
Cl	0.013	0.013	0.010	0.008	0.015	0.019	0.015	0.004	0.005	0.010	0.010	0.010	0.021	0.004		
Total	97.351	97.351	96.852	97.969	97.690	96.978	97.117	96.648	97.640	98.007	98.613	97.680	97.227	97.594		

(Continued)

TABLE 3B. REPRESENTATIVE MINERAL COMPOSITIONS AND THERMOBAROMETRIC RESULTS FOR KM47 (Continued)

Hornblende (Continued)												
Sample # / Analysis #	y/6	y/3	y/4	y/5	bx/2	bx/3	bx/5	bx/4	z/2	z/1	z/4	z/5
Cations: 23 oxygen basis												
Si	6.101	6.179	6.259	6.192	6.165	6.107	6.122	6.110	6.207	6.156	6.155	6.141
Ti	0.187	0.252	0.276	0.275	0.166	0.151	0.165	0.229	0.181	0.115	0.232	0.212
Al	2.641	2.463	2.376	2.493	2.572	2.737	2.705	2.612	2.540	2.754	2.521	2.555
Fe	2.960	2.884	2.725	2.723	3.037	3.054	2.789	2.770	2.863	2.857	2.566	2.911
Mn	0.041	0.030	0.026	0.046	0.039	0.035	0.024	0.030	0.040	0.035	0.026	0.043
Mg	1.398	1.616	1.533	1.433	1.185	1.123	1.683	1.375	1.317	1.170	1.645	1.341
Ca	1.703	1.530	1.685	1.751	1.836	1.741	1.487	1.809	1.834	1.913	1.772	1.807
Na	0.447	0.491	0.513	0.466	0.492	0.485	0.520	0.531	0.473	0.442	0.499	0.430
K	0.235	0.240	0.260	0.268	0.264	0.281	0.217	0.274	0.245	0.236	0.274	0.261
F	0.015	0.015	0.009	0.003	0.000	0.040	0.015	0.019	0.000	0.011	0.048	0.012
Cl	0.003	0.003	0.002	0.004	0.005	0.004	0.001	0.001	0.003	0.003	0.003	0.001
Total	15.732	15.703	15.663	15.653	15.761	15.756	15.729	15.758	15.702	15.691	15.739	15.715
Plagioclase												
Sample # / Analysis #	y/4	y/5	y/5	y/5	bx/2	bx/avg.	bx/avg.	bx/4	z/2	z/1	z/avg	z/avg
SiO ₂	57.125	56.814	56.814	56.814	58.500	58.454	58.454	57.216	56.355	56.818	56.586	56.586
Al ₂ O ₃	27.469	27.442	27.442	27.442	26.133	25.562	25.562	26.852	27.223	26.450	26.836	26.836
Fe ₂ O ₃	0.040	0.024	0.024	0.024	0.126	0.224	0.224	0.077	0.175	0.014	0.094	0.094
CaO	8.348	8.388	8.388	8.388	7.241	6.981	6.981	8.097	8.790	8.178	8.484	8.484
Na ₂ O	6.528	6.496	6.496	6.496	7.105	7.208	7.208	6.653	6.305	6.610	6.458	6.458
K ₂ O	0.145	0.099	0.099	0.099	0.182	0.154	0.154	0.209	0.168	0.130	0.149	0.149
Total	99.654	99.262	99.262	99.262	99.286	98.582	98.582	99.104	99.016	98.198	98.607	98.607
Cations: 8 oxygen basis												
Si	2.564	2.560	2.560	2.560	2.628	2.643	2.643	2.582	2.552	2.588	2.570	2.570
Al	1.453	1.458	1.458	1.458	1.384	1.362	1.362	1.428	1.453	1.420	1.436	1.436
Total	4.017	4.018	4.018	4.018	4.011	4.006	4.006	4.011	4.005	4.007	4.006	4.006
Cations: 23 oxygen basis												
Fe	0.001	0.001	0.001	0.001	0.004	0.008	0.008	0.003	0.006	0.000	0.003	0.003
Ca	0.402	0.405	0.405	0.405	0.348	0.338	0.338	0.392	0.427	0.399	0.413	0.413
Na	0.568	0.568	0.568	0.568	0.619	0.632	0.632	0.582	0.554	0.584	0.569	0.569
K	0.008	0.006	0.006	0.006	0.010	0.009	0.009	0.012	0.010	0.008	0.009	0.009
Total	0.979	0.979	0.979	0.979	0.982	0.987	0.987	0.989	0.996	0.991	0.993	0.993
AN	0.411	0.414	0.414	0.414	0.356	0.345	0.345	0.397	0.431	0.403	0.417	0.417
AB	0.581	0.580	0.580	0.580	0.633	0.646	0.646	0.591	0.559	0.590	0.575	0.575
OR	0.008	0.006	0.006	0.006	0.011	0.009	0.009	0.012	0.010	0.008	0.009	0.009

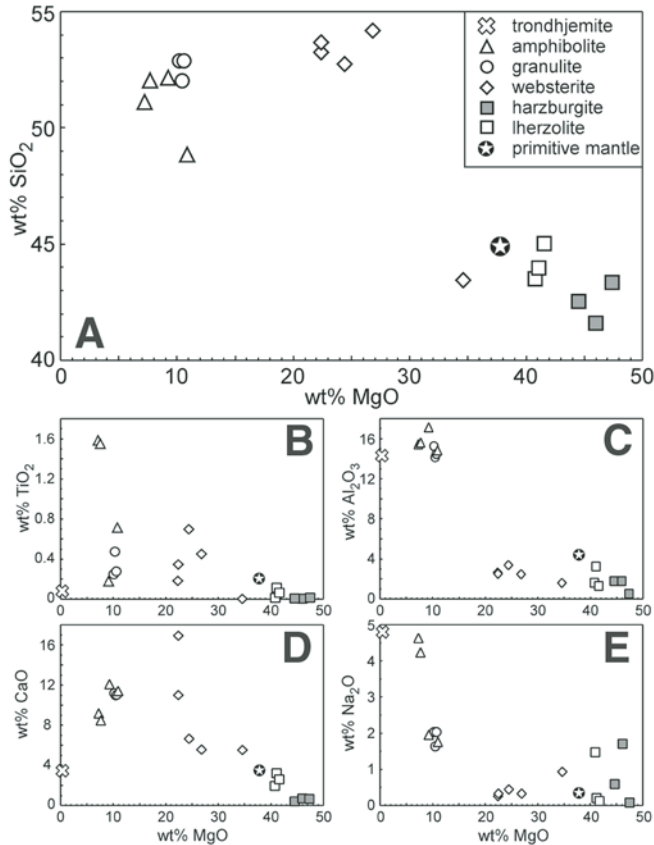


Figure 12. Major-element variation diagrams: (A) SiO_2 versus MgO ; (B) TiO_2 versus MgO ; (C) Al_2O_3 versus MgO ; (D) CaO versus MgO ; and (E) Na_2O versus MgO .

Mg-number than does Seiad Cr-rich spinel. Because olivine compositions in the Seiad and Josephine peridotites largely overlap, the lower Mg-numbers for Cr-rich Seiad spinel may be attributed to recrystallization under granulite- to upper-amphibolite-facies conditions in the Seiad complex, in contrast to the relict mantle compositions in the Josephine peridotite (i.e., for a given olivine composition, the Mg-number in coexisting spinel shifts to lower values with a decrease in temperature).

Websterite

Five samples of websterite from the West Fork body were analyzed for major elements, including a thin vein (SV11B2) in lherzolite, two samples (SV6B and SV7) from the eastern websterite lens, an olivine websterite (M53) from the intermediate lens, and a fifth sample (M2) from the western lens (Fig. 11). Among the five samples, olivine websterite (M53) has the highest MgO content (34%), reflecting the presence of olivine, and the pyroxenite vein (SV11B2) has the highest CaO content (16.8%), due to a high proportion of clinopyroxene (Fig. 12; Table 4). Among the remaining three samples, there is notable

scatter in TiO_2 and CaO contents, and all samples have relatively low amounts of Al_2O_3 and Na_2O . Such features suggest that the websterites do not represent melt compositions, but are the products of crystal accumulation \pm trapped melt.

The REE patterns for the pyroxenite vein in lherzolite and two websterites (SV6B and SV7) show LREE depletion and relatively flat HREE at ~ 1.5 – 3 times that of primitive mantle (Fig. 13A; Table 4). In addition, the two websterites have a small negative Eu anomaly, which may signify the presence of plagioclase in the source from which the websterite melts were derived. With respect to extended trace elements (Figs. 13B, 13C), the pyroxenite veinlet is similar to the two websterites in having negative P, Zr, Hf, and Ti anomalies, but differs in having negative Nb and Ta anomalies (absent in websterites) and a positive Pb anomaly, whereas the websterites have a negative Pb anomaly, which is accompanied by negative Th and U anomalies.

Granulite and Amphibolite

Three samples of granulite and four of amphibolite are generally basic in composition, with SiO_2 contents ranging from 47 to 53% and MgO from 7 to 11% (Fig. 12). The scatter in plots of MgO versus SiO_2 , TiO_2 , CaO , and, to a lesser extent, Al_2O_3 in these seven samples may arise from the effects of cumulate processes, thereby precluding their classification by volcanic terminology and tectonic assignment via discrimination diagrams, which are based on melt compositions.

The REE patterns for two samples of granulite are similar in shape to that of E-MORB, but at much lower levels of concentration (Fig. 15A). The REE pattern for amphibolite KM29 has a similar shape to those for granulite, but at even lower overall concentrations. All three samples have positive Eu anomalies, which suggest that plagioclase accumulation may have played a role in their petrogenesis. Extended trace-element patterns for the two granulites and single amphibolite are similar, all showing positive anomalies for the LILE (light lithophile elements), Pb, and Sr, and negative anomalies for Nb, Ta, P, Zr, Hf, and Ti (Fig. 15B).

Leucotrandhjemite

Leucotrandhjemite is similar to plagiogranite (Coleman and Peterman, 1975) in its high concentration of SiO_2 (75%), low amounts of FeO (0.47%), MgO (0.32%), and K_2O (0.33%), and high contents of sialic normative constituents, which comprise 97% of the total norm in the proportion, Q:Or:Ab:An = 38:2:41:17. The REE contents of leucotrandhjemite are unusually low, being 0.05–0.3 times that of N-MORB and ~ 10 times less than that of plagiogranite in the Josephine ophiolite (Fig. 16A). The pronounced positive Eu anomaly is likely due to plagioclase accumulation. An extended trace-element plot reveals positive anomalies for the LILE, Pb, Sr, Zr, and Hf and negative anomalies for Nb and Ta, unlike the Josephine plagiogranite, in which such anomalies are absent (Fig. 16B). Accumulation of plagioclase

TABLE 4. WHOLE-ROCK MAJOR-, TRACE-, AND RARE-EARTH-ELEMENT CONCENTRATIONS, SEIAD COMPLEX

Unit	Kangaroo peridotite										West Fork complex															
	Sample	KM201 ¹	U4 [*]	harz	lherz	U67 [*]	SV10 ¹	SV11B1 ¹	SV11B2 ¹	pxite lens	U25 [*]	M53 [*]	SV6B ¹	SV7 ¹	M2 [*]	M1 [*]	SV1 ¹	SV5A ¹	A4 [*]	A5 [*]	A6 [*]	KM29 ¹	KM47B ¹	KM215 ¹	Relative SD% ¹	
Lithology	harz	harz	harz	lherz	lherz	lherz	lherz	pxite lens	pxite lens	harz	hb-ol pxite	hb pxite	hb pxite	hb pxite	hb pxite	gran	gran	gran	amph	amph	amph	amph	amph	grt	trond	Relative SD% ¹
wt% oxides																										
SiO ₂	41.67	40.75	42.45	43.62	44.75	52.84	52.84	0.18	0.18	40.52	42.55	53.95	52.59	53.39	50.85	52.76	52.39	49.36	50.43	47.19	52.05	45.22	75.35	0.38		
TiO ₂	0.01	0.00	0.01	0.11	0.06	0.18	0.18	0.18	0.18	0.00	0.00	0.44	0.69	0.34	0.46	0.24	0.27	1.53	1.50	0.69	0.17	2.74	0.08	0.67		
Al ₂ O ₃	0.42	1.63	1.52	3.16	1.20	2.58	2.58	0.23	0.23	1.69	1.53	2.39	3.33	2.46	13.88	15.31	14.43	15.02	15.21	14.42	17.23	19.37	14.27	0.41		
Cr ₂ O ₃	0.47	0.42	0.43	0.43	0.39	0.23	0.23	0.39	0.23	0.42	0.34	0.35	0.31	0.32	0.06	0.07	0.08	0.00	0.02	0.00	0.01	0.05	0.00	0.88		
FeO	7.25	9.05	9.77	7.65	8.86	4.02	4.02	8.86	4.02	7.39	12.92	9.62	11.09	9.06	9.70	7.72	8.11	10.00	9.57	10.64	6.92	13.74	0.41	0.74		
MnO	0.12	0.19	0.14	0.12	0.15	0.11	0.11	0.11	0.11	0.11	0.19	0.24	0.26	0.22	0.18	0.18	0.18	0.17	0.12	0.19	0.14	0.29	0.01	0.75		
MgO	45.72	42.84	40.01	40.93	41.50	22.26	22.26	16.79	16.79	44.99	33.95	26.75	24.41	22.35	10.28	10.24	10.62	7.02	7.44	10.58	9.22	2.61	0.32	0.54		
CaO	0.52	0.29	1.81	3.10	2.50	0.27	0.27	1.67	1.67	0.55	5.36	5.49	6.58	10.93	10.67	11.11	10.88	8.82	8.18	11.01	12.04	8.27	3.53	0.41		
Na ₂ O	0.09	0.58	1.45	0.21	0.14	0.02	0.02	0.02	0.02	1.67	0.93	0.34	0.47	0.34	1.61	2.03	2.02	4.47	4.11	1.71	1.96	3.54	4.79	1.26		
K ₂ O	0.00	0.14	0.17	0.00	0.00	0.02	0.02	0.02	0.02	0.23	0.29	0.02	0.04	0.14	0.14	0.22	0.19	0.20	0.26	0.14	0.08	1.93	0.33	1.16		
P ₂ O ₅	0.00	0.09	0.01	0.00	0.00	0.00	0.00	0.00	0.00	0.01	0.01	0.02	0.01	0.01	0.03	0.02	0.02	0.08	0.12	0.15	0.01	0.58	0.01	0.64		
H ₂ O [*]	na	2.79	1.62	na	na	na	na	na	na	0.23	1.50	na	na	0.36	1.47	na	na	2.20	2.09	1.89	na	0.75	na	na		
H ₂ O-	na	1.20	0.49	na	na	na	na	na	na	1.75	0.51	na	na	0.40	0.25	na	na	0.55	0.67	0.58	na	na	na	na		
Sum	96.27	99.97	99.88	99.34	99.56	99.32	99.32	99.56	99.32	99.56	100.08	99.62	99.78	100.32	99.58	99.91	99.18	99.42	99.72	99.19	99.85	99.09	99.09	99.09		
ppm																										
Sc	7.4	16.1	17.6	65.8	38.4	48.3	47.8	49.9	41.9	49.8	1.2	3.9	1.2	3.9	1.2	3.9	1.2	3.9	1.2	3.9	1.2	3.9	1.2	3.9	1.7	
V	28	74	73	208	249	326	220	240	183	286	5	0.5	0.5	0.5	0.5	0.5	0.5	0.5	0.5	0.5	0.5	0.5	0.5	0.5	0.5	
Cr	3228	2946	2654	1556	2381	2148	473	517	98	356	10	0.9	0.9	0.9	0.9	0.9	0.9	0.9	0.9	0.9	0.9	0.9	0.9	0.9	0.9	
Ni	2508	1964	2272	2237	604	2200	786	314	67	120	10	1.7	1.7	1.7	1.7	1.7	1.7	1.7	1.7	1.7	1.7	1.7	1.7	1.7	1.7	
Cu	6	3	45	47	21	42	23	2	23	182	8	0.8	0.8	0.8	0.8	0.8	0.8	0.8	0.8	0.8	0.8	0.8	0.8	0.8	0.8	
Zn	48	45	60	16	81	73	72	78	57	154	7	1.2	1.2	1.2	1.2	1.2	1.2	1.2	1.2	1.2	1.2	1.2	1.2	1.2	1.2	
Ga	1	3	3	4	5	7	15	14	14	24	12	1.0	1.0	1.0	1.0	1.0	1.0	1.0	1.0	1.0	1.0	1.0	1.0	1.0	1.0	
Rb	0.06	0.20	0.15	0.56	0.51	0.49	1.60	0.66	0.63	41.0	6.96	8.0	8.0	8.0	8.0	8.0	8.0	8.0	8.0	8.0	8.0	8.0	8.0	8.0	8.0	
Sr	2	5	4	19	13	20	303	282	182	637	229	1.7	1.7	1.7	1.7	1.7	1.7	1.7	1.7	1.7	1.7	1.7	1.7	1.7	1.7	

(Continued)

TABLE 4. WHOLE-ROCK MAJOR-, TRACE-, AND RARE-EARTH-ELEMENT CONCENTRATIONS, SEIAD COMPLEX (Continued)

Unit	Kangaroo peridotite	West Fork complex																				
Sample	KM201 [†]	U4*	U67*	SV10 [†]	SV11B1 [†]	SV11B2 [†]	U25*	M53*	SV6B [†]	SV7 [†]	M2*	M1*	SV1 [†]	SV5A [†]	A4*	A5*	A6*	KM29 [†]	KM47B [†]	KM215 [†]	Relative SD% [†]	
Lithology	harz	harz	lherz	lherz	pxite lens	harz	hb-ol pxite	hb pxite	hb pxite	hb pxite	hb pxite	gran	gran	gran	amph	amph	amph	amph	amph	grt amph	trond	
Y	0.05		2.56	1.25	6.03			10.44	14.04				8.06	8.98				4.48	64.48	1.91	2.3	
Zr	0.3		2.2	1.3	5.6			9.3	10.4				7.5	8.7				7.1	176	99.8	1.6	
Nb	0.06		0.16	0.03	0.06			0.33	0.38				0.19	0.17				0.22	11.14	0.12	4.5	
Cs	0.003		0.01	0.01	0.04			0.03	0.02				0.03	0.03				0.05	1.14	0.15	8.6	
Ba	0.5		2	4	6			24	15				137	125				22	2023	86	2.3	
Hf	0.01		0.11	0.06	0.24			0.41	0.52				0.32	0.35				0.27	4.66	2.16	2.3	
Ta	0.002		0.011	0.002	0.005			0.022	0.024				0.013	0.012				0.009	0.73	0.009	5.9	
Pb	0.07		0.10	0.21	0.51			0.11	0.15				1.32	1.33				0.41	3.59	2.08	7.6	
Th	0.02		0.02	0.02	0.03			0.01	0.01				0.06	0.04				0.05	0.62	0.08	8.3	
U	0.01		0.01	0.01	0.01			0.01	0.00				0.02	0.01				0.02	0.31	0.07	6.5	
La	0.051		0.17	0.10	0.41			0.51	0.47				2.07	2.26				1.50	13.61	0.83	2.5	
Ce	0.099		0.46	0.26	1.30			2.11	2.08				4.33	4.84				3.48	29.70	1.15	1.6	
Pr	0.011		0.08	0.04	0.26			0.44	0.47				0.65	0.75				0.47	5.05	0.12	2.2	
Nd	0.037		0.44	0.22	1.52			2.66	3.04				3.21	3.65				2.08	24.44	0.50	1.9	
Sm	0.004		0.20	0.10	0.64			1.06	1.30				1.04	1.18				0.57	7.43	0.12	1.9	
Eu	0.008		0.08	0.03	0.24			0.30	0.41				0.56	0.60				0.34	2.76	0.20	2.1	
Gd	0.002		0.33	0.15	0.89			1.50	1.97				1.28	1.44				0.71	9.20	0.18	2.1	
Tb	0.001		0.07	0.03	0.18			0.29	0.39				0.23	0.26				0.13	1.64	0.03	1.9	
Dy	0.009		0.45	0.23	1.18			1.93	2.64				1.51	1.68				0.87	10.76	0.23	1.4	
Ho	0.002		0.11	0.05	0.26			0.42	0.59				0.33	0.37				0.19	2.27	0.06	1.8	
Er	0.005		0.30	0.15	0.70			1.20	1.66				0.94	1.04				0.52	6.37	0.19	1.7	
Tm	0.001		0.05	0.02	0.10			0.18	0.24				0.14	0.15				0.08	0.90	0.03	1.7	
Yb	0.013		0.29	0.14	0.61			1.15	1.53				0.87	0.97				0.49	5.58	0.21	1.2	
Lu	0.004		0.05	0.03	0.09			0.19	0.24				0.14	0.16				0.08	0.88	0.05	2.1	

Note: Lherz—lherzolite; harz—harzburgite; pxite—pyroxenite; hb-ol pxite—hornblende olivine pyroxenite; hb pxite—hornblende pyroxenite; gran—granulite; amph—amphibolite; trond—trondhjemite.

*Previous XRF (X-ray fluorescence) analyses for major elements, Cr and Ni.

[†]XRF for major elements; ICP-MS (Inductively Coupled Plasma-Mass Spectrometry) for trace elements; Washington State University GeoAnalytical Laboratory.

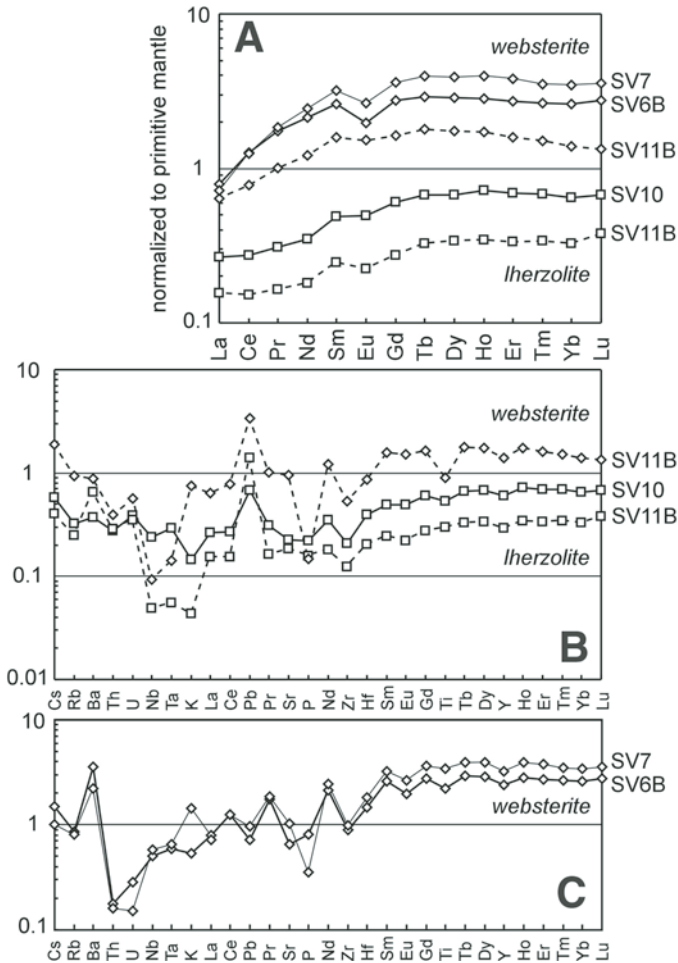


Figure 13. (A) Rare-earth-element diagram for ultramafic rocks of the Seiad complex, normalized to primitive mantle values (McDonough and Sun, 1995). (B) Extended trace-element diagram for samples SV11B and SV10, normalized to primitive mantle values (McDonough and Sun, 1995). (C) Extended trace-element diagram for samples SV7 and SV6B, normalized to primitive mantle values (McDonough and Sun, 1995).

and zircon can generate the positive anomalies in the leucotrochondjemite pattern, but not the negative Nb and Ta anomalies.

GEOCHRONOLOGY

Introduction and Methods

In order to understand the structural, metamorphic, and geochemical characteristics of the Seiad complex in a regional plate-tectonic framework, geochronological data are required. Unfortunately there are few obvious targets within the Seiad complex for geochronological analysis, with the exception of the zircon-bearing leucotrochondjemite unit. Leucotrochondjemitic dikes

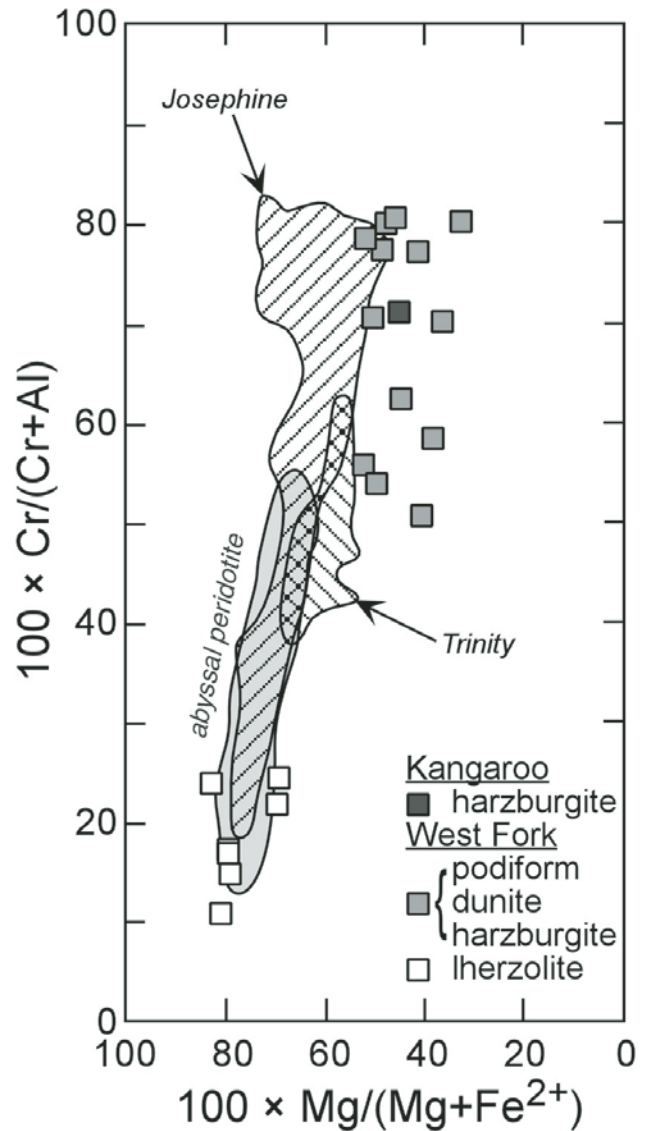


Figure 14. The composition of spinel in peridotites of the Seiad complex. Fields for abyssal peridotite (after Dick and Bullen, 1984), Josephine ophiolite (after Dick and Bullen [1984] and Harper [2003]), and Trinity peridotite (after Quick, 1981).

crosscut the amphibolite unit and are internally undeformed, although narrow stringers are sometimes folded parallel to host foliation (see discussion below); thus the igneous age of these rocks should provide a minimum limit for the age of deformation and metamorphism in the surrounding rocks. With this goal in mind, we obtained a sample of leucotrochondjemite (KM215) (Fig. 11) for U-Pb geochronological analysis.

Zircon fractions of the leucotrochondjemite were hand picked to obtain optically clear, colorless grains free or largely free of mineral and fluid inclusions. Analytical methods followed those of Krogh (1973, 1982). One fraction was annealed at 800 °C for 36 h prior to dissolution, and then chemically abraded following methods of Mattinson (2005). Initial Pb corrections were

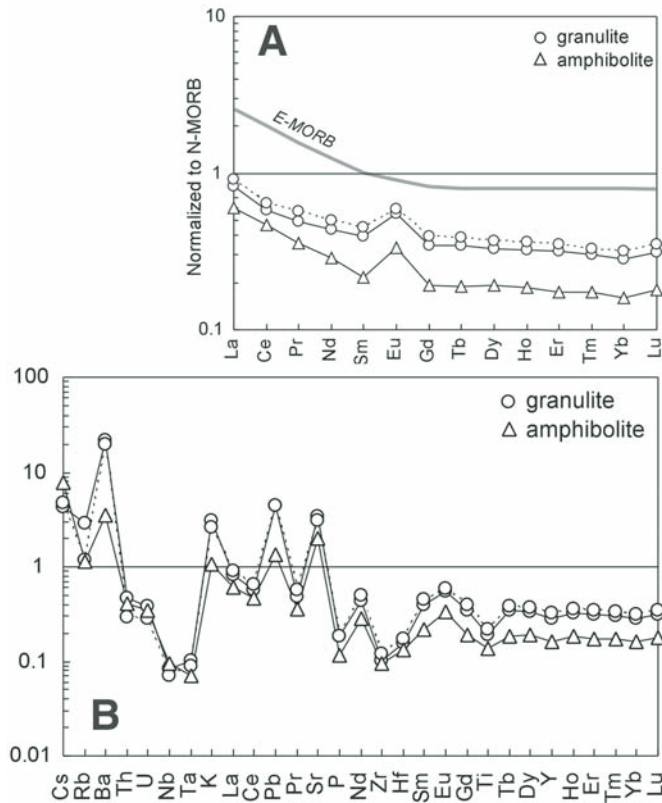


Figure 15. (A) Rare-earth-element diagram for granulite and amphibolite in the Seiad complex, normalized to N-MORB values (Sun and McDonough, 1989). (B) Extended trace-element diagram for granulite and amphibolite in the Seiad complex, normalized to N-MORB values (Sun and McDonough, 1989).

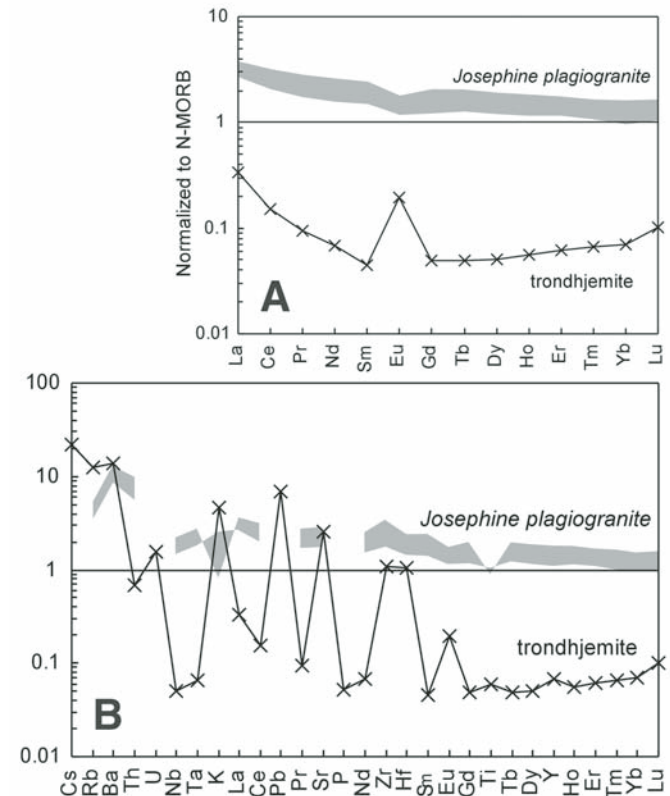


Figure 16. (A) Rare-earth-element diagram for leucotondhjemite in the Seiad complex, normalized to N-MORB values (Sun and McDonough, 1989). The shaded field represents plagiogranite from the Josephine ophiolite (Harper, 2003). (B) Extended trace-element diagram for leucotondhjemite in the Seiad complex, normalized to N-MORB values (Sun and McDonough, 1989). The shaded field represents plagiogranite from the Josephine ophiolite (Harper, 2003).

made using an age-appropriate Pb isotopic composition (Stacey and Kramers, 1975). All U-Pb ages are calculated using PBDAT (Ludwig, 1988) and are reported at 95% confidence limits. Crystallization ages are calculated from the weighted average of the $^{206}\text{Pb}/^{238}\text{U}$ age.

Results

U-Pb zircon geochronological data from KM 215 show evidence for both older inherited zircons as well as Pb loss (Table 5). Multigrain fractions are plotted on a Concordia diagram in Figure 17. Two multi-grain fractions from KM 215 are concordant, two fractions are slightly reversely discordant, and one fraction is strongly discordant. The slightly reversely discordant analyses may be attributed to incorrect assignment of common Pb composition, exacerbated by a low $^{206}\text{Pb}/^{204}\text{Pb}$ value. The two concordant and one slightly reversely discordant zircon fractions yield a weighted average $^{206}\text{Pb}/^{238}\text{U}$ age of 152.7 ± 1.8 Ma (MSWD = 2.3), which is interpreted as the crystallization age. One fraction is

affected by a younger Pb-loss event and gives a slightly reversely discordant age of 141.3 ± 2.0 Ma ($^{206}\text{Pb}/^{238}\text{U}$ age). This age is interpreted as a maximum age for the timing of Pb loss. The presence of older inherited zircons is indicated by one strongly discordant analysis, which gives a $^{207}\text{Pb}/^{206}\text{Pb}$ age of 368.7 Ma.

Discussion of New and Existing Geochronological Data

The 152.7 ± 1.8 -Ma age that we obtained for the leucotondhjemitic dike overlaps with the only other direct date obtained from the Seiad complex, a 153.0 ± 2.2 -Ma $^{40}\text{Ar}/^{39}\text{Ar}$ date on metamorphic hornblende from amphibolite reported by Hacker et al. (1995). This age matches numerous $^{40}\text{Ar}/^{39}\text{Ar}$ results for amphibole and mica from rocks throughout the northern and central Klamath Mountains that demonstrate widespread cooling of the province at ca. 150 ± 2 Ma (Hacker et al., 1995). However, the penetrative deformation and high-grade metamorphism in the Seiad complex must be older than these dates because of regional overprinting relationships that are discussed below.

TABLE 5. U-Pb ZIRCON ISOTOPIC ANALYSES AND AGES

Mineral properties*	Concentrations [†]			Atomic ratios [‡]			Ages (Ma)	
	Weight (mg)	U (ppm)	Pb (ppm)	²⁰⁶ Pb/ ²⁰⁴ Pb (measured)	²⁰⁶ Pb/ ²³⁸ U (err abs)	²⁰⁷ Pb/ ²³⁵ U (err abs)	²⁰⁶ Pb/ ²³⁸ U	²⁰⁷ Pb/ ²³⁵ Pb
<i>Trondhjemite (KM215): 152.7 ± 1.8 Ma[§]</i>								
7 zr, 3:1-4:1, clr, c, eu, an, CA	0.10	110.2	3.22	225	0.02420 ± 33	0.1678 ± 64	154.1 ± 2.1	208.3 ± 78.4
30 zr, 3:1-4:1, clr, c, eu	0.10	268.8	6.90	439	0.02401 ± 11	0.1634 ± 17	152.9 ± 0.7	164.7 ± 21.7
35 zr, 3:1-4:1, clr, c, eu	0.10	407.9	9.46	1233	0.02384 ± 16	0.1568 ± 26	151.9 ± 1.0	84.9 ± 33.2
40 zr, 3:1-4:1, clr, c, eu	0.10	615.0	13.24	1399	0.02216 ± 32	0.1473 ± 27	141.3 ± 2.0	108.9 ± 25.5
40 zr, 3:1-4:1, clr, c, eu	0.10	646.9	14.67	2808	0.02348 ± 21	0.1746 ± 24	149.6 ± 1.3	368.7 ± 22.5

*zr—zircon; aspect ratio; clr—clear; c—colorless; eu—euhedral; an—annealed; CA—chemically abraded; err abs—absolute error.

[†]Weights are estimated and subject to large uncertainties.

[‡]U/Pb ratios corrected for total blanks of Pb = 0.10 ± 0.05 ng; U = 0.002 ng; mass fractionation = 0.08 ± 0.06 percent/amu; and initial Pb (Stacey and Kramers, 1975).

Errors reported at 2σ level and refer to last digits.

[§]Age calculated from weighted average of ²⁰⁶Pb/²³⁸U ages. The last two analyses are not included in age calculation due to inheritance and/or open system behavior.

Errors reported at 2σ level and refer to last digits.

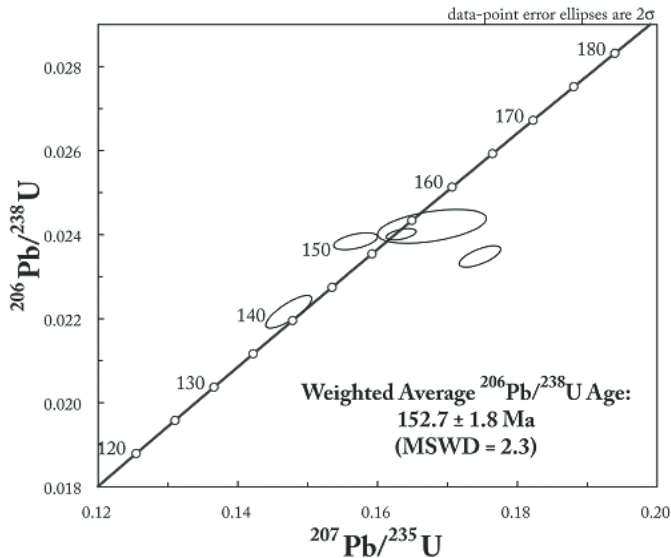


Figure 17. Concordia plot of U-Pb (zircon) data from leucotrochondrite sample from the Seiad complex. MSWD—mean square of weighted deviations.

The structural location of the Seiad complex—in the deepest exposed section of the Rattlesnake Creek terrane—as well as the ophiolitic and imbricate character of the complex, support a direct correlation of the complex with surrounding Rattlesnake Creek terrane rocks, including lower-amphibolite-facies rocks of the Marble Mountains (Donato, 1987, 1989) and sub-greenschist-facies serpentinite-matrix *mélange* of the southern Klamath Mountains (Wright and Wyld, 1994). Previous studies suggested this correlation (e.g., Rawson and Petersen, 1982; Norman et al., 1983; Mortimer, 1985; Donato, 1987) and the regional extent and concentric pattern of high-grade Rattlesnake Creek rocks around the Condrey Mountain dome indicate significant vertical and horizontal metamorphic gradients within the terrane.

If the metamorphic history of the Seiad complex is correlative with the regional metamorphic history of the Rattlesnake Creek terrane, then the timing of deformation and metamorphism in these rocks should be relatively synchronous. Regional geochronological data bracket penetrative deformation and high-grade metamorphism in the Rattlesnake Creek terrane to 172–167 Ma (Table 6). The limits of this time interval are the inferred igneous age of metaplagiogranite of the China Peak complex that intrudes the Rattlesnake Creek terrane (Saleeby and Harper, 1993, samples 5 and 6 in their Table 1) and the age of the Vesa Bluffs pluton that crosscuts and contact-metamorphosed high-grade Rattlesnake Creek terrane rocks (Mortimer, 1985; Allen and Barnes, 2006). However, considering the possibility for regional variation in the timing of orogenic events, as well as the likelihood that deformation and metamorphism were somewhat protracted (e.g., Hacker et al., 1995), we regard the 172–167-Ma time interval as simply an estimate of Middle Jurassic orogenesis.

DEVELOPMENTAL HISTORY OF THE SEIAD COMPLEX

Introduction

As part of the Rattlesnake Creek terrane, the Seiad complex provides a deep view into the basement of an oceanic arc that initially developed in early Mesozoic time (Late Triassic?), was likely accreted to western North America during the Middle Jurassic, was then intruded by a suite of post-accretion calc-alkaline magmas, and subsequently became tilted and uplifted during Neogene tectonics related to the Cascadia subduction zone. The evolutionary history of the partial crustal cross-section now exposed in the Kangaroo Mountain area near Seiad Valley therefore is a product of multiple magmatic and tectonic events and records the early Mesozoic through late Tertiary history of the Klamath Mountains province.

Evidence of Mantle Processes Overprinted by Deep-Crustal Metamorphism

Relicts of an early high-temperature history, presumably in the upper mantle, are preserved in the ultramafic rocks of the Seiad complex. These relict features include lithologic variations such as chromitite layers, podiform chromite, websterite layers, cross-cutting websterite and clinopyroxenite dikes, and locally dunite-harzburgite; as well as whole-rock and mineral-chemical characteristics (Medaris, 1975; Lundquist, 1983; Cannat, 1985). The spinel lherzolite, harzburgite, and dunite may represent depleted mantle rocks from which basaltic magmas were extracted, but subsequently these ultramafic rocks were strongly overprinted by crustal metamorphism that locally reached granulite-facies conditions. Evidence of the role of fluids in the history of these ultramafic rocks is indicated by unusually high Na_2O contents for such rocks and the presence of metarodinite along contacts between mafic and ultramafic rocks. The presence of metarodinite indicates that portions of the ultramafic massifs were serpentinized at upper-crustal levels before an overprinting episode of deeper-crustal metamorphism.

Possible Development of the Seiad Ophiolitic *Mélange* in a Fore-Arc Setting

The Seiad complex has many classic earmarks of a dismembered ophiolitic suite (i.e., an ophiolitic *mélange* as described by Gansser [1974] and many other geologists), including a variety of ultramafic and mafic rock types, relict upper-mantle features (lithologic, mineralogical, and geochemical), a polygenetic history developed at various crustal levels, and an association with supracrustal metavolcanic and metasedimentary rocks. Many rock types in the Seiad complex, including peridotite (adjacent to pyroxenite), pyroxenite, granulite, and amphibolite, show prominent negative anomalies for the high-field-strength elements in extended trace-element plots. Because depletion in the

TABLE 6. COMPILATION OF GEOCHRONOLOGICAL DATA RELATED TO THE SEIAD COMPLEX

Age and method	Sample	Interpreted significance	Reference
Devonian(?) corals, Carboniferous-Permian fusulinids	Limestone blocks from the RCt, southern Klamath Mountains	Inferred original depositional age of blocks in the mélange; mélange formation post-dates fossil ages in the blocks.	Irwin (1972)
Late Triassic-Early Jurassic radiolarians	Chert blocks from the RCt, southern Klamath Mountains	Age of blocks in the mélange; minimum age for mélange formation.	Irwin et al. (1977, 1982, 1985)
207–193 Ma (U-Pb zircon)	Intrusive bodies in the RCt mélange and cover sequence, southern Klamath Mountains	Mélange formation and eruptive/depositional history of the cover sequence must predate and/or be coeval with this intrusive suite.	Wright and Wyld (1994)
Ca. 190 Ma ($^{40}\text{Ar}/^{39}\text{Ar}$, hornblende)	Gneissic amphibolite block in the RCt mélange	Metamorphic cooling age for a block in the mélange; suggests an older, cryptic episode of metamorphism.	Gorman (1985)
170 ± 4 Ma (U-Pb zircon)	Metaplagiogrinite from amphibolite-facies mafic dike complex of the RCt, south of Seiad Valley	Igneous age of a metamorphosed plagiogrinite in the RCt; maximum age of amphibolite-facies metamorphism and associated deformation.	Saleeby and Harper (1993)
167.1 ± 1.8 Ma (U-Pb zircon)	Vesa Bluffs pluton	The Vesa Bluffs pluton intruded and contact metamorphosed the North Fork terrane, eHt, and RCt; thus its radiometric age provides a minimum constraint on the tectonic amalgamation of these terranes.	Mortimer (1985); Wright and Fahan (1988); Allen and Barnes (2006)
165, 167 Ma (discordant $^{207}\text{Pb}/^{206}\text{Pb}$ zircon ages)	Folded, amphibolite-facies metatonalite dike in the ophiolitic mélange of the Applegate Group, northeast boundary of the Condrey Mountain dome, southwestern Oregon	Igneous age of crosscutting, deformed and metamorphosed tonalite dike in the ophiolitic mélange correlated as high-grade RCt. A maximum(?) age of amphibolite-facies metamorphism and deformation in the ophiolitic mélange.	Donato et al. (1996)
Ca. 162 Ma (U-Pb zircon)	Slinkard pluton	The Slinkard pluton cuts penetrative foliation associated with amphibolite-facies metamorphism; also contains xenoliths of amphibolite, thus provides a minimum age of amphibolite-facies metamorphism and deformation.	Reported by Allen et al. (1982); Barnes et al. (1986a); listed in Hill (1985).
Ca. 163 Ma (U-Pb zircon)	Thompson Ridge pluton	Cross cuts metamorphic rocks of the upper and lower units of the Applegate Group, interpreted as the wHt and RCt, respectively. Minimum age of metamorphism in these terranes.	Donato et al. (1996)
151–149 Ma (K-Ar hornblende)	Amphibolite from the RCt, east of the Condrey Mountain dome	Cooling age of metamorphic hornblende; age at which these rocks cooled below ~500 °C.	Lanphere et al. (1968)
153 ± 2.2 Ma ($^{40}\text{Ar}/^{39}\text{Ar}$ hornblende)	Amphibolite at Seiad Valley	Cooling age of metamorphic hornblende in amphibolite from the Seiad complex; age at which these rocks cooled below ~500 °C.	Hacker et al. (1995)

* RCt—Rattlesnake Creek terrane; wHt—western Hayfork terrane; eHt—eastern Hayfork terrane

high-field-strength elements is a characteristic chemical feature of supra-subduction zone ophiolites (Hawkins, 2003), the presence of such depletion in the Seiad complex may signify its development in a supra-subduction setting. In the southern Klamath Mountains where the Rattlesnake Creek terrane was first defined (Irwin, 1972), the mélangé character of this lithotectonic unit has been interpreted to represent dismemberment of oceanic lithosphere in an oceanic fracture zone that subsequently served as basement for the development of a Late Triassic–Early Jurassic intra-oceanic arc (Wright and Wyld, 1994). The contact between the serpentinite-matrix mélangé component of the Rattlesnake Creek terrane and the younger oceanic-arc rocks is either not exposed or strongly overprinted by late brittle deformation. Nonetheless, this contact has been interpreted as a significant unconformity within the development of the Rattlesnake Creek terrane. The possible presence of supra-subduction rocks in the Seiad complex, the deepest known part of the Rattlesnake Creek terrane, however, introduces the prospect that some segments of the Rattlesnake Creek terrane may have developed in a supra-subduction setting. By this interpretation, mélangé development may be an artifact of fore-arc structural imbrication during the subduction process as argued by Donato (1987).

Establishment of an Oceanic Basement for the Middle Jurassic Western Hayfork Island Arc

The western Hayfork terrane is a Middle Jurassic (ca. 177–169 Ma) volcanic arc terrane (Wright, 1982; Wright and Fahan, 1988) that lies structurally above the Rattlesnake Creek terrane along a faulted, depositional contact (Fig. 18) (Donato, 1987; Wright and Fahan, 1988; Donato et al., 1996). The western Hayfork terrane is thus interpreted as an oceanic island arc and volcanoclastic apron built upon a disrupted ophiolitic basement of the Rattlesnake Creek terrane (Wright and Wyld, 1994).

Metamorphism and Penetrative Deformation during Middle Jurassic Time

Upper-amphibolite- to granulite-facies metamorphism manifested in the deep exposures of the Rattlesnake Creek terrane as exposed in the north-central Klamath Mountains are in stark contrast to the lower-greenschist-facies conditions that characterize broad tracts of this terrane in the southern Klamath Mountains (Wright and Fahan, 1988; Wright and Wyld, 1994). The age of the high-grade metamorphism in the north-central Klamath Mountains has never been directly dated, but crosscutting plutons that impose contact-metamorphic effects on the regional metamorphic rocks provide a lower limit on the age of the earlier high-grade metamorphism. A critical intrusion in this relative chronology is the Vesa Bluffs pluton, which has been dated by U-Pb (zircon) techniques at ca. 167 Ma (Mortimer, 1985; Allen and Barnes, 2006, see their figure 1 and Table 1). The upper limit of the age of regional metamorphism is based on the igneous protolith age of a felsic dike from the China Peak complex, which

yielded an U-Pb (zircon) age of 170 ± 4 Ma (Saleeby and Harper, 1993, their Table 1, p. 69). Wright and Fahan (1988) attempted to define the age interval of the Middle Jurassic orogenic history in the southern Klamath Mountains and suggested a time interval of ca. 169–161 Ma. Both of these estimates indicate that the age of the dynamothermal amphibolite- to granulite-facies metamorphism that affected the deep portions of the Rattlesnake Creek terrane is Middle Jurassic (ca. 170 ± 4 Ma) in age.

A Middle Jurassic age of orogenesis broadly corresponds with the timing of contraction along several regional thrust faults and juxtaposition of the Rattlesnake Creek terrane with accreted terranes to the east. Contraction along the faulted contact between the western Hayfork terrane and Rattlesnake Creek terrane is bracketed as within the interval ca. 169–162 Ma, based on cross-cutting plutons (Wright and Fahan, 1988; Allen and Barnes, 2006). Contraction along the thrust fault between the western Hayfork terrane and the overlying terrane to the east (Figs. 2 and 18) is tightly bracketed to ca. 170–169 Ma, also by intrusive plutonic field relations (Wright and Fahan, 1988; Barnes et al., 2006a).

Juxtaposition of the Rattlesnake Creek terrane with the terranes to the west began with contraction along the Condrey Mountain fault, which separates the Rattlesnake Creek terrane from the upper unit of the composite Condrey Mountain terrane (Figs. 2 and 18). This juxtaposition locally upgraded greenschist-facies rocks of the Condrey Mountain terrane to upper amphibolite facies (Barrows, 1969; Hanks, 1981). Metamorphic hornblende from the dynamothermal aureole yielded an $^{40}\text{Ar}/^{39}\text{Ar}$ age of ca. 157 ± 2 Ma (M. Grove, 2007, personal comm.).

Post-Orogenic Tectonic History: Uplift, Extension, and Cooling

Evidence for widespread retrograde metamorphism in the Seiad complex (e.g., post-kinematic replacement of pyroxene by hornblende in granulite-facies metagabbro and widespread saussuritization of plagioclase) and mineral cooling ages of ca. 150 ± 2 Ma from a broad region of the north-central Klamath Mountains, including the Seiad complex, reported by Hacker et al. (1995), indicate that these rocks stayed relatively hot (and possibly deep) until the Late Jurassic, after peak metamorphic conditions were achieved. The isoclinal folding of an offshoot of the ca. 152-Ma trondhjemite intrusion in the Seiad complex (Fig. 8B) is further evidence of the relatively high-temperature conditions thereby facilitating ductile flow during Late Jurassic time.

The maintenance of moderately high temperatures (>500 °C) after Middle Jurassic deformation and peak metamorphism likely reflects the rapid renewal of arc magmatism in the Klamath Mountains province after terrane accretion, manifested by voluminous late Middle Jurassic calc-alkaline plutons (Barnes et al., 1986b; Allen and Barnes, 2006). Following this time, during the Late Jurassic, renewed contraction brought the western Klamath terrane (marginal ocean basin and arc rocks) beneath the now amalgamated terranes to the east (Fig. 18) during the “Nevadan orogeny.” The underthrusting of cold material disrupted the thermal

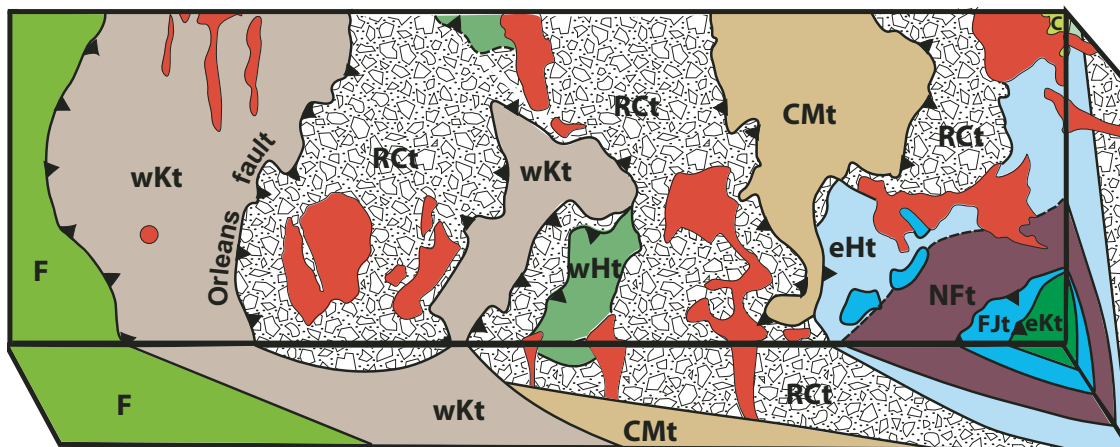


Figure 18. Block diagram showing schematic relationships among terranes and plutons in the north-central Klamath Mountains province, modified from Hill (1985), Coleman et al. (1988), and Snoke and Barnes (2006). **CMt**—Condrey Mountain terrane; **eHt**—eastern Hayfork terrane; **eKt**—eastern Klamath terrane and Central Metamorphic terrane; **F**—Franciscan complex; **FJt**—Fort Jones terrane; **NFt**—North Fork terrane; **RCt**—Rattlesnake Creek terrane; **wHt**—western Hayfork terrane; and **wKt**—western Klamath terrane.

architecture of the amalgamated terranes (including the Rattlesnake Creek terrane), causing rapid cooling of a broad region of the Klamath Mountains province at ca. 150 ± 2 Ma (Hacker et al., 1995). Underthrusting of the western Klamath terrane also likely caused some uplift of terranes to the east, although the final exhumation of the high-grade Rattlesnake Creek terrane did not occur until the late Tertiary uplift of the Klamath Mountains province (Mortimer and Coleman, 1985).

Regional Uplift Related to Neogene Tectonics Associated with the Cascadia Subduction System

Tilting of the Rattlesnake Creek terrane and exposure of the Seiad complex occurred during regional uplift of the Klamath Mountains province and the development of the Condrey Mountain dome (Mortimer and Coleman, 1985). Although these events are beyond the scope of this study, they represent the important final chapter of the developmental history of the Rattlesnake Creek terrane and thus we present a brief review.

The Condrey Mountain dome is a structural enigma in regard to the belt-like pattern of the lithotectonic units that comprise the Klamath Mountains province (Irwin, 1994). Coleman and Helper (1983) initially noted the potential significance of this structural dome and identified a group of radially oriented, high-angle faults that cut the low-angle fault system inferred to frame the window that exposes the Condrey Mountain terrane. Subsequently, Mortimer and Coleman (1984, 1985) expanded on these initial observations and developed a model of Neogene doming related to underthrusting of subducted material and shortening in the fore-arc region of the Cascade Volcanic Arc. Mortimer and Coleman (1985) noted that the tilting of plutons (e.g., Barnes and Rice, 1983, and subsequently documented in detail in Barnes

et al., 1986a, 1986b) away from the Condrey Mountain dome is a manifestation of the regional doming characteristic of this part of the Klamath Mountains province. In the context of this article, it is important that highest-grade rocks of the Rattlesnake Creek terrane surround the Condrey Mountain terrane, including the Seiad complex (Medaris, 1966) on the west, Tom Martin Peak area (Barrows, 1969) on the southwest, and Observation Peak area on the northeast (Kays and Ferns, 1980).

CONCLUSIONS

The structural, metamorphic, and geochemical features of the Seiad complex reveal a multi-stage history that includes ophiolitic mélangé formation, possibly in a supra-subduction zone, followed by penetrative deformation and upper amphibolite- to granulite-facies metamorphism in the deep crust, and a subsequent episode of retrograde mineral growth and intrusion of crosscutting, arc-related leucotondhjemitic dikes. Geothermobarometry indicates penetrative deformation and metamorphism occurred at high temperatures (>700 °C) and moderately high pressures (~ 7 kb), and regional field relationships and geochronological data constrain this event as Middle Jurassic.

The implications of our study bear upon regional issues regarding the geologic history of the Klamath Mountains province in general, as well as issues regarding the tectonic and magmatic processes that occur during the inception, development, and accretion of oceanic supra-subduction rocks. For the Klamath Mountains province, the rocks of the Seiad complex further confirm previous reports of significant, province-wide, contractional deformation and regional metamorphism during the Middle Jurassic. The specific plate-tectonic setting for this orogenesis and how it relates to the tectonic events of the Late Jurassic

(i.e., the rapid opening and closing of an oceanic basin; e.g., see Yule et al. [2006] and Snoke and Barnes [2006]) are still unclear. However, any tectonic model for the Mesozoic development of the Klamath Mountains province must account for synchronous penetrative deformation and regional metamorphism under high-temperature and moderately high-pressure conditions, locally reaching granulite-facies conditions. Although this high-grade dynamothermal metamorphism and accompanying anatexis of metabasic rocks may seem at odds with tectonic accretion associated with a long-lived convergent margin, the leading tectonic model of the Klamath Mountains province, Phanerozoic granulites are commonly associated with the deep roots of magmatic arcs (e.g., Windley, 1981; Miller and Snoke, this volume).

Beyond the tectonic history of the Klamath Mountains province, our study documents the complex geology of a disrupted and highly metamorphosed ophiolitic suite that is exposed in a partial crustal cross section. These geologic relationships provide insight into the multi-stage and complicated nature of the basement rocks upon which oceanic arcs are built. We view the multi-stage history of the Seiad complex as including: (1) the structural juxtaposition of upper-mantle rocks and oceanic supracrustal rocks in a fore-arc setting (*mélange* formation); (2) the transition from upper-amphibolite to granulite-facies conditions within a variable suite of ultramafic and mafic rocks (deep-crustal metamorphism); (3) the development of chemical reaction zones between ultramafic and mafic rocks during serpentinization (<500 °C) and high-temperature metamorphism (>700 °C); and (4) syndeformational anatexis, segregation, and mobilization of melt in metabasic rocks in the roots of an island-arc terrane.

Finally, we can compare the geologic evolution manifested in the Seiad complex to other deep exposures of oceanic-arc crust. The best known and most widely recognized deep-crustal sections through an ancient oceanic-arc complex are the Kohistan complex of northwest Pakistan and the Talkeetna arc of south-central Alaska (see Miller and Snoke, this volume, for detailed descriptions of these oceanic-arc crustal sections). A detailed comparative anatomy of these classic oceanic-arc crustal sections with the Seiad complex and related parts of the Klamath Late Triassic–Middle Jurassic oceanic-arc section is beyond the scope of this paper. Nonetheless, several important differences are noted below and provide insights into apparent variations among oceanic-arc sections.

Ophiolitic rocks, including mantle ultramafic rocks, are part of the lower parts of both the Kohistan and Talkeetna arc crustal sections. However, the widespread ophiolitic *mélange* character of the Klamath section is unique in comparison to the classic sections. Although ophiolitic *mélange* exists near the base of the Kohistan arc section, it is associated with the Main Mantle thrust, the westward extension of the Indus-Tsango suture zone (Gansser, 1964). The Talkeetna arc section includes residual mantle rocks, chiefly harzburgite and dunite, but the bulk of the ultramafic-mafic rocks are interpreted as arc cumulates crystallized at the base of an intra-oceanic island arc (Burns, 1985; DeBari and Coleman, 1989). Ophiolitic *mélange* is commonly associated

with other Cordilleran oceanic-arc sections such as the Canyon Mountain (northeast Oregon) section (Bishop, 1995) and Late Jurassic Rogue-Chetco volcanic-plutonic arc (western Klamath Mountains, southwestern Oregon) (Yule et al., 2006).

In the Kohistan section, Jagoutz et al., (2006) have interpreted km-scale, zoned ultramafic-mafic complexes as potential melt conduits that fed mid-crustal magma chambers such as the Chilas gabbro-norite sequence. In the Seiad complex, we speculate that the numerous intrusive bodies of hornblende gabbro/diorite and clinopyroxenite are analogous melt channels that fed middle- to upper-crustal magma chambers that formed the plutonic core of the Late Triassic–Middle Jurassic arc. However, the Seiad intrusive rocks occur as numerous small-scale bodies (meter- to decameter-scale) and suggest a more pervasive (dike-like) intrusive pattern rather than focused melt channels (Jagoutz et al., 2006).

The abundance of granulite-facies rocks is another variable among these inferred oceanic-arc sections. In the Talkeetna arc, garnet granulite forms a transition from mantle rocks to lower-crustal cumulates (DeBari, 1997), whereas in the Kohistan arc, granulite-facies metamorphic conditions are widespread in both the Chilas and Jijal complexes. In the Seiad complex, amphibolite-facies rocks greatly predominate, although granulite-facies mineral assemblages occur in ultramafic rocks as well as in scattered metagabbro and paragneiss localities. Both the Kohistan and Talkeetna arc section are intruded by massive calc-alkaline batholiths that indicate the transition from oceanic crust to continental crust. In the Seiad complex *sensu stricto*, late calc-alkaline plutons are not present, although a Late Jurassic leucotondhjemite dike swarm (152.7 ± 1.8 Ma) may be the harbinger of the widespread “western Klamath plutonic suite,” a group of composite plutons, ranging in composition from ultramafic to silicic, that intruded various terranes of the Klamath Mountains province between ca. 151–144 Ma (Barnes et al., 2006b).

ACKNOWLEDGMENTS

We are grateful to the following sources that provided financial support for this project: U.S. Geological Survey EDMAP program (Award 05HQAG0051 and 06HQAG0073), Geological Society of America Penrose Fund, Gregg Ranch Foundation, University of Wyoming College of Arts and Sciences, the Roy J. Shlemon Fellowship, and the Department of Geology and Geophysics at the University of Wyoming. SRG especially thanks her two intrepid field assistants, Esther Kingsbury and Jakob Wartman, for their positive attitudes, hard work, and keen insights during the summer field seasons of 2005 and 2006. Several geologists spent time in the field with us studying the Seiad complex, and we greatly appreciate their ideas, suggestions, and enthusiasm: Calvin G. Barnes, Edward D. Ghent, and Walter A. “Bill” Sullivan. A recent field trip with Mark A. Helper and Marty Grove clarified many aspects of the development of the Condrey Mountain terrane for AWS. Phyllis A. Ranz provided expert help on the initial phases of the computer

drafting the geologic map (scale 1:12,000) that is Appendix 1 (see the CM-ROM that accompanies this volume and footnote 1). Finally, Calvin G. Barnes, W. Gary Ernst, and Robert B. Miller provided us with many comments and suggestions that were helpful in preparing the final version of this chapter.

REFERENCES CITED

- Allen, C.M., and Barnes, C.G., 2006, Ages and some cryptic sources of Mesozoic plutonic rocks in the Klamath Mountains, California and Oregon, *in* Snoke, A.W., and Barnes, C.G., eds., Geological studies in the Klamath Mountains province, California and Oregon: A volume in honor of William P. Irwin: Geological Society of America Special Paper 410, p. 223–246.
- Allen, C.M., Barnes, C.G., Kays, M.A., and Saleeby, J.B., 1982, Comagmatic nature of the Wooley Creek batholith and the Slinkard pluton and age constraints on tectonic and metamorphic events in the western Paleozoic and Triassic belt, Klamath Mountains, northern California: Geological Society of America Abstracts with Programs, v. 14, no. 4, p. 145.
- Barnes, C.G., and Rice, J.M., 1983, Tilted plutons in the Klamath Mountains: Geological Society of America Abstracts with Programs, v. 15, no. 5, p. 314.
- Barnes, C.G., Rice, J.M., and Gribble, R.F., 1986a, Tilted plutons in the Klamath Mountains of California and Oregon: Journal of Geophysical Research, v. 91, p. 6059–6071, doi: 10.1029/JB091iB06p06059.
- Barnes, C.G., Allen, C.M., and Saleeby, J.B., 1986b, Open- and closed-system characteristics of a tilted plutonic system, Klamath Mountains, California: Journal of Geophysical Research, v. 91, p. 6073–6090, doi: 10.1029/JB091iB06p06073.
- Barnes, C.G., Allen, C.M., Hoover, J.D., and Brigham, R.H., 1990, Magmatic components of a tilted plutonic system, Klamath Mountains, California, *in* Anderson, J.L., ed., The nature and origin of Cordilleran magmatism: Geological Society of America Memoir 174, p. 331–346.
- Barnes, C.G., Mars, E.V., Swapp, S., and Frost, C.D., 2006a, Petrology and geochemistry of the Middle Jurassic Ironside Mountain batholith: Evolution of potassic magmas in a primitive arc setting, *in* Snoke, A.W., and Barnes, C.G., eds., Geological studies in the Klamath Mountains province, California and Oregon: A volume in honor of William P. Irwin: Geological Society of America Special Paper 410, p. 199–221.
- Barnes, C.G., Snoke, A.W., Harper, G.D., Frost, C.D., McFadden, R.R., Bushey, J.C., and Barnes, M.A.W., 2006b, Arc plutonism following regional thrusting: Petrology and geochemistry of syn- and post-Nevadan plutons in the Siskiyou Mountains, Klamath Mountains province, California, *in* Snoke, A.W., and Barnes, C.G., eds., Geological studies in the Klamath Mountains province, California and Oregon: A volume in honor of William P. Irwin: Geological Society of America Special Paper 410, p. 357–376.
- Barrow, W.M., and Metcalf, R.V., 2006, A reevaluation of the paleotectonic significance of the Paleozoic Central Metamorphic terrane, eastern Klamath Mountains, California: New constraints from trace element geochemistry and ⁴⁰Ar/³⁹Ar thermochronology, *in* Snoke, A.W., and Barnes, C.G., eds., Geological studies in the Klamath Mountains province, California and Oregon: A volume in honor of William P. Irwin: Geological Society of America Special Paper 410, p. 393–410.
- Barrows, A.G., 1969, Geology of the Hamburg-McGuffey Creek area, Siskiyou County, California, and petrology of the Tom Martin ultramafic complex, California [Ph.D. thesis]: Los Angeles, University of California, 301 p.
- Beard, J.S., 1990, Dehydration melting of amphibolite at 1–7 kilobars: Eos (Transactions, American Geophysical Union), v. 71, no. 43, p. 1714.
- Beard, J.S., 1995, Experimental, geological, and geochemical constraints on the origins of low-K silicic magmas in oceanic arcs: Journal of Geophysical Research, v. 100, p. 15,593–15,600, doi: 10.1029/95JB00861.
- Beard, J.S., and Lofgren, G.E., 1991, Dehydration melting and water-saturated melting of basaltic and andesitic greenstones and amphibolites at 1, 3, and 6.9 kb: Journal of Petrology, v. 32, p. 365–401.
- Bishop, E.M., 1995, Mafic and ultramafic rocks of the Baker terrane, eastern Oregon, and their implications for terrane origin, *in* Vallier, T.L., and Brooks, H.C., eds., Geology of the Blue Mountains region of Oregon, Idaho, and Washington—Petrology and tectonic evolution of pre-Tertiary rocks of the Blue Mountains region: U.S. Geological Survey Professional Paper 1438, p. 221–245.
- Brey, G.P., and Köhler, T., 1990, Geothermobarometry in four-phase lherzolites: II. New thermobarometers and practical assessment of existing thermobarometers: Journal of Petrology, v. 31, p. 1352–1378.
- Burchfiel, B.C., Cowan, D.S., and Davis, G.A., 1992, Tectonic overview of the Cordilleran orogen in the western United States, *in* Burchfiel, B.C., Lipman, P.W., and Zoback, M.L., eds., The Cordilleran orogen: Conterminous U.S.: Boulder, Colorado, Geological Society of America, Geology of North America, v. G-3, p. 407–479.
- Burns, L.E., 1985, The Border Ranges ultramafic-mafic complex, south-central Alaska: Cumulate fractionates of island-arc volcanics: Canadian Journal of Earth Sciences, v. 22, p. 1020–1038.
- Cannat, M., 1985, Tectonics of the Seiad massif, northern Klamath Mountains, California: Geological Society of America Bulletin, v. 96, p. 15–26, doi: 10.1130/0016-7606(1985)96<15:TOTSMN>2.0.CO;2.
- Coleman, R.G., 1967, Low-temperature reaction zones and alpine ultramafic rocks of California, Oregon and Washington: U.S. Geological Survey Bulletin 1247, 49 p.
- Coleman, R.G., and Helper, M.A., 1983, The significance of the Condrey Mountain dome in the evolution of the Klamath Mountains, California and Oregon: Geological Society of America Abstracts with Programs, v. 15, no. 5, p. 294.
- Coleman, R.G., and Peterman, Z.E., 1975, Oceanic plagiogranite: Journal of Geophysical Research, v. 80, p. 1099–1108, doi: 10.1029/JB080i008p01099.
- Coleman, R.G., Manning, C.E., Mortimer, N., Donato, M.M., and Hill, L.B., 1988, Tectonic and regional metamorphic framework of the Klamath Mountains and adjacent Coast Ranges, California and Oregon, *in* Ernst, W.G., ed., Metamorphism and crustal evolution of the western United States—Rubey Volume VII: Englewood Cliffs, New Jersey, Prentice Hall, p. 1061–1097.
- Coney, P.J., Jones, D.L., and Monger, J.W.H., 1980, Cordilleran suspect terranes: Nature, v. 288, p. 329–333, doi: 10.1038/288329a0.
- Davis, G.A., Monger, J.W.H., and Burchfiel, B.C., 1978, Mesozoic construction of the Cordilleran “collage,” central British Columbia to central California, *in* Howell, D.G., and McDougall, K.A., eds., Mesozoic paleogeography of the western United States, Pacific Coast Paleogeography Symposium 2: Los Angeles, Pacific Section, Society of Economic Paleontologists and Mineralogists, p. 1–32.
- DeBari, S.M., 1997, Evolution of magmas in continental and oceanic arcs: The role of the lower crust: Canadian Mineralogist, v. 35, p. 501–519.
- DeBari, S.M., and Coleman, R.G., 1989, Examination of the deep levels of an island arc: Evidence from the Tonsina ultramafic-mafic assemblage, Tonsina, Alaska: Journal of Geophysical Research, v. 94, p. 4373–4391, doi: 10.1029/JB094iB04p04373.
- Dick, H.J.B., and Bullen, T., 1984, Chromian spinel as a petrogenetic indicator in abyssal and alpine-type peridotites and spatially associated lavas: Contributions to Mineralogy and Petrology, v. 86, p. 54–76, doi: 10.1007/BF00373711.
- Dickinson, W.R., 2008, Accretionary Mesozoic–Cenozoic expansion of the Cordilleran continental margin in California and adjacent Oregon: Geosphere, v. 4, no. 2, p. 329–353, doi: 10.1130/GES00105.1.
- Dilek, Y., and Newcomb, S., eds., 2003, Ophiolite concept and the evolution of geologic thought: Geological Society of America Special Paper 373, 504 p.
- Donato, M.M., 1987, Evolution of an ophiolitic tectonic mélange, Marble Mountains, northern California Klamath Mountains: Geological Society of America Bulletin, v. 98, p. 448–464, doi: 10.1130/0016-7606(1987)98<448:EOAOTM>2.0.CO;2.
- Donato, M.M., 1989, Metamorphism of an ophiolitic tectonic mélange, northern California, Klamath Mountains, U.S.A.: Journal of Metamorphic Geology, v. 7, p. 515–528, doi: 10.1111/j.1525-1314.1989.tb00614.x.
- Donato, M.M., Barnes, C.G., and Tomlinson, S.L., 1996, The enigmatic Applegate Group of southwestern Oregon: Age, correlation, and tectonic affinity: Oregon Geology, v. 58, p. 79–91.
- Ernst, W.G., 1999, Mesozoic petrotectonic development of the Sawyers Bar suprasubduction-zone arc, central Klamath Mountains, northern California: Geological Society of America Bulletin, v. 111, p. 1217–1232, doi: 10.1130/0016-7606(1999)111<1217:MPDOTS>2.3.CO;2.

- Evans, B.W., 1977, Metamorphism of alpine peridotite and serpentinite: Annual Review of Earth and Planetary Sciences, v. 5, p. 397–447, doi: 10.1146/annurev.ea.05.050177.002145.
- Frost, B.R., 1975, Contact metamorphism of serpentinite, chloritic blackwall and rodingite at Paddy-Go-Easy Pass, central Cascades, Washington: Journal of Petrology, v. 16, p. 272–313.
- Gansser, A., 1964, Geology of the Himalayas: New York, Interscience Publishers, 289 p.
- Gansser, A., 1974, The ophiolitic mélange, a world-wide problem on Tethyan examples: Eclogae Geologicae Helvetiae, v. 67, p. 479–507.
- Gorman, C.M., 1985, Geology, geochemistry and geochronology of the Rattlesnake Creek terrane, west-central Klamath Mountains, California [M.S. thesis]: Salt Lake City, University of Utah, 111 p.
- Grover, T.W., 1984, Progressive metamorphism west of the Condrey Mountain dome, north-central Klamath Mountains, northern California [M.S. thesis]: Eugene, University of Oregon, 129 p.
- Grover, T.W., and Rice, J.M., 1985, A progressive metamorphic sequence west of the Condrey Mountain dome, north-central Klamath Mountains, California: Geological Society of America Abstracts with Programs, v. 17, no. 6, p. 358.
- Hacker, B.R., Donato, M.M., Barnes, C.G., McWilliams, M.O., and Ernst, W.G., 1995, Timescales of orogeny: Jurassic construction of the Klamath Mountains: Tectonics, v. 14, p. 677–703, doi: 10.1029/94TC02454.
- Hamilton, W., 1969, Mesozoic California and the underflow of Pacific mantle: Geological Society of America Bulletin, v. 80, p. 2409–2430, doi: 10.1130/0016-7606(1969)80[2409:MCATUO]2.0.CO;2.
- Hanks, C.L., 1981, The emplacement history of the Tom Martin ultramafic complex and associated metamorphic rocks, north-central Klamath Mountains, California [M.S. thesis]: Seattle, University of Washington, 112 p.
- Harper, G.D., 2003, Tectonic implications of boninite, arc tholeiite, and MORB magma types in the Josephine ophiolite, California–Oregon, in Dilek, Y., and Robinson, P.T., eds., Ophiolites in Earth history: Geological Society of London Special Publication 218, p. 207–230.
- Harper, G.D., and Wright, J.E., 1984, Middle to Late Jurassic tectonic evolution of the Klamath Mountains, California–Oregon: Tectonics, v. 3, p. 759–772, doi: 10.1029/TC003i007p00759.
- Hawkins, J.W., 2003, Geology of supra-subduction zones; implications for the origin of ophiolites, in Dilek, Y., and Newcomb, S., eds., Ophiolite concept and the evolution of geological thought: Geological Society of America Special Paper 373, p. 227–268.
- Helper, M.A., 1986, Deformation and high P/T metamorphism in the central part of the Condrey Mountain window, north-central Klamath Mountains, California and Oregon, in Evans, B.W., and Brown, E.H., eds., Blueschists and eclogites: Geological Society of America Memoir 164, p. 125–141.
- Hill, L.B., 1985, Metamorphic, deformational and temporal constraints on terrane assembly, northern Klamath Mountains, California, in Howell, D.G., ed., Tectonostratigraphic terranes of the Circum-Pacific region: Houston, Texas, Circum-Pacific Council Energy and Mineral Resources, Earth Sciences Series 1, p. 173–186.
- Hotz, P.E., 1979, Regional metamorphism in the Condrey Mountain quadrangle, north-central Klamath Mountains, California: U.S. Geological Survey Professional Paper 1086, 25 p.
- Irvine, T.N., 1967, Chromian spinel as a petrogenetic indicator; Part 2, Petrologic applications: Canadian Journal of Earth Sciences, v. 4, p. 71–103.
- Irwin, W.P., 1960, Geologic reconnaissance of the northern Coast Ranges and Klamath Mountains, California, with a summary of the mineral resources: San Francisco, California, Division of Mines and Geology Bulletin 179, 80 p.
- Irwin, W.P., 1972, Terranes of the western Paleozoic and Triassic belt in the southern Klamath Mountains, California: U.S. Geological Survey Professional Paper 800-C, p. C103–C111.
- Irwin, W.P., 1981, Tectonic accretion of the Klamath Mountains, in Ernst, W.G., ed., The geotectonic development of California—Rubey Volume I: Englewood Cliffs, New Jersey, Prentice Hall, p. 29–49.
- Irwin, W.P., 1994, Geologic map of the Klamath Mountains, California and Oregon: U.S. Geological Survey Miscellaneous Investigation Series Map I-2148, scale 1:500,000, 2 sheets.
- Irwin, W.P., and Dennis, M.D., 1978, Geologic structure section across southern Klamath Mountains, Coast Ranges, and seaward to Point Delgada, California: Boulder, Colorado, Geological Society of America Map and Chart Series MC-28D, 1 sheet, scale 1:250,000.
- Irwin, W.P., Jones, D.L., and Pessagno, E.A., Jr., 1977, Significance of Mesozoic radiolarians from the pre-Nevadan rocks of the southern Klamath Mountains, California: Geology, v. 5, p. 557–562.
- Irwin, W.P., Jones, D.L., and Blome, C.D., 1982, Map showing sampled radiolarian localities in the western Paleozoic and Triassic belt, Klamath Mountains, California: U.S. Geological Survey Miscellaneous Field Studies Map MF-1399, scale 1:250,000.
- Irwin, W.P., Yule, J.D., Court, B.L., Snoke, A.W., Stern, L.A., and Copeland, W.B., 1985, Reconnaissance geologic map of the Dubakella Mountain quadrangle, Trinity, Shasta, and Tehama Counties, California: U.S. Geological Survey Miscellaneous Field Studies Map MF-1808, scale 1:62,500.
- Jachens, R.C., Barnes, C.G., and Donato, M.M., 1986, Subsurface configuration of the Orleans fault: Implications for deformation in the western Klamath Mountains, California: Geological Society of America Bulletin, v. 97, p. 388–395, doi: 10.1130/0016-7606(1986)97<388:SCOTOF>2.0.CO;2.
- Jagoutz, O., Müntener, O., Burg, J.-P., Ulmer, P., and Jagoutz, E., 2006, Lower continental crust formation through focused flow in km-scale melt conduits: The zoned ultramafic bodies of the Chilas Complex in the Kohistan island arc (NW Pakistan): Earth and Planetary Science Letters, v. 242, p. 320–342, doi: 10.1016/j.epsl.2005.12.005.
- Kays, M.A., and Ferns, M.L., 1980, Geologic field trip guide through the north-central Klamath Mountains: Oregon Geology, v. 42, p. 23–35.
- King, P.B., [1967] 1970, Tectonic features, in The national atlas of the United States: Washington, D.C., U.S. Department of the Interior, Geological Survey, p. 70–71, scale 1:7,500,000.
- Kohn, M.J., and Spear, F.S., 1989, Empirical calibration of geobarometers for the assemblage garnet + hornblende + plagioclase + quartz: The American Mineralogist, v. 74, p. 77–84.
- Krogh, T.E., 1973, A low-contamination method for hydrothermal decomposition of zircon and extraction of U and Pb for isotopic age determinations: Geochimica et Cosmochimica Acta, v. 37, p. 485–494, doi: 10.1016/0016-7037(73)90213-5.
- Krogh, T.E., 1982, Improved accuracy of U-Pb zircon dating by the creation of more concordant systems using air abrasion technique: Geochimica et Cosmochimica Acta, v. 46, p. 637–649, doi: 10.1016/0016-7037(82)90165-X.
- Lanphere, M.A., Irwin, W.P., and Hotz, P.E., 1968, Isotopic age of the Nevada orogeny and older plutonic and metamorphic events in the Klamath Mountains, California: Geological Society of America Bulletin, v. 79, p. 1027–1057.
- Lieberman, J.E., 1983, Petrology and petrogenesis of marble and peridotite, Seiad Valley complex [M.S. thesis]: Eugene, University of Oregon, 119 p.
- Lieberman, J.E., and Rice, J.M., 1986, Petrology of marble and peridotite in the Seiad ultramafic complex, northern California, USA: Journal of Metamorphic Geology, v. 4, p. 179–199, doi: 10.1111/j.1525-1314.1986.tb00346.x.
- Loomis, T.P., and Gottschalk, R.R., 1981, Hydrothermal origin of mafic layers in Alpine-type peridotites: Evidence from the Seiad ultramafic complex, California, USA: Contributions to Mineralogy and Petrology, v. 76, p. 1–11, doi: 10.1007/BF00373677.
- Ludwig, K.R., 1988, PBDAT for MS-DOS, a computer program for IBM-PC compatibles for processing raw Pb-U-Th isotope data, version 1.24: Reston, Virginia, U.S. Geological Survey Open-File Report 88-542, 32 p.
- Lundquist, S.M., 1983, Deformation history of the ultramafic and associated metamorphic rocks of the Seiad complex, Seiad Valley, California [M.S. thesis]: Seattle, University of Washington, 167 p.
- Maekawa, H., 1989, Two modes of mixing of Biei ophiolitic mélange, Kamuikotan blueschist belt, Japan: The Journal of Geology, v. 97, p. 93–108.
- Mattinson, J.M., 2005, Zircon U-Pb chemical abrasion (“CA-TIMS”) method: Combined annealing and multi-step partial dissolution analysis for improved precision and accuracy of zircon ages: Chemical Geology, v. 220, p. 47–66, doi: 10.1016/j.chemgeo.2005.03.011.
- McDonough, W.F., and Sun, S.-s., 1995, The composition of the Earth: Chemical Geology, v. 120, p. 223–253, doi: 10.1016/0009-2541(94)00140-4.
- Medaris, L.G., Jr., 1966, Geology of the Seiad Valley area, Siskiyou County, California, and petrology of the Seiad ultramafic complex [Ph.D. thesis]: Los Angeles, University of California, Los Angeles, 333 p.
- Medaris, L.G., Jr., 1975, Coexisting spinel and silicates in alpine peridotites of the granulite facies: Geochimica et Cosmochimica Acta, v. 39, p. 947–958, doi: 10.1016/0016-7037(75)90040-X.

- Meschede, M., Zweigel, P., Frisch, W., and Voelker, D., 1999, Mélange formation by subduction erosion; the case of the Osa mélange in southern Costa Rica: *Terra Nova*, v. 11, p. 141–148, doi: 10.1046/j.1365-3121.1999.00237.x.
- Miller, R.B., and Snoke, A.W., 2009, this volume, The utility of crustal cross sections in the analysis of orogenic processes in contrasting tectonic settings, in Miller, R.B., and Snoke, A.W., eds., *Crustal cross sections from the western North American Cordillera and elsewhere: Implications for tectonic and petrologic processes: Geological Society of America Special Paper 456*, doi: 10.1130/2009.2456(01).
- Moore, E.M., 1998, Ophiolites, the Sierra Nevada, “Cordillera,” and orogeny along the Pacific and Caribbean margins of North and South America: *International Geology Review*, v. 40, p. 40–54.
- Mortimer, N., 1985, Structural and metamorphic aspects of Middle Jurassic terrane juxtaposition, northeastern Klamath Mountains, California, in Howell, D.G., ed., *Tectonostratigraphic terranes of the Circum-Pacific region: Houston, Texas, Circum-Pacific Council Energy and Mineral Resources, Earth Sciences Series 1*, p. 201–214.
- Mortimer, N., and Coleman, R.G., 1984, A Neogene structural dome in the Klamath Mountains, California and Oregon, in Nilsen, T.H., ed., *Geology of the Upper Cretaceous Hornbrook Formation, Oregon and California: Los Angeles, Pacific Section, Society of Economic Paleontologists and Mineralogists*, v. 42, p. 179–186.
- Mortimer, N., and Coleman, R.G., 1985, A Neogene structural dome in the Klamath Mountains, California and Oregon: *Geology*, v. 13, p. 253–256, doi: 10.1130/0091-7613(1985)13<253:ANSDIT>2.0.CO;2.
- Norman, E.A., Gorman, C.M., and Harper, G.D., 1983, Northern extension of the Rattlesnake Creek terrane: *Geological Society of America Abstracts with Programs*, v. 15, no. 5, p. 314.
- Quick, J.E., 1981, Petrology and petrogenesis of the Trinity peridotite, an upper mantle diapir in the eastern Klamath Mountains, northern California: *Journal of Geophysical Research*, v. 86, p. 11,837–11,863, doi: 10.1029/JB086iB12p11837.
- Rawson, S.A., and Petersen, S.W., 1982, Structural and lithologic equivalence of the Rattlesnake Creek terrane and high-grade rocks of the Western Paleozoic and Triassic belt, north central Klamath Mountains, California: *Geological Society of America Abstracts with Programs*, v. 14, no. 4, p. 226.
- Raymond, L.A., 1984, The mélange problem—A review, in Raymond, L.A., ed., *Mélanges: Their nature, origin, and significance: Geological Society of America Special Paper 198*, p. 1–3.
- Robertson, A., 2004, Development of concepts concerning the genesis and emplacement of Tethyan ophiolites in the Eastern Mediterranean and Oman regions: *Earth-Science Reviews*, v. 66, p. 331–387, doi: 10.1016/j.earscirev.2004.01.005.
- Saleeby, J.B., 1979, Kaweah serpentinite mélange, southwest Sierra Nevada foothills, California: *Geological Society of America Bulletin*, v. 90, p. 29–46, doi: 10.1130/0016-7606(1979)90<29:KSMSSN>2.0.CO;2.
- Saleeby, J.B., 1984, Tectonic significance of serpentinite mobility and ophiolitic mélange, in Raymond, L.A., ed., *Mélanges: Their nature, origin, and significance: Geological Society of America Special Paper 198*, p. 153–168.
- Saleeby, J.B., 1992, Petrotectonic and paleogeographic settings of U.S. Cordilleran ophiolites, in Burchfiel, B.C., Lipman, P.W., and Zoback, M.L., eds., *The Cordilleran orogen: Conterminous U.S.: Boulder, Colorado, Geological Society of America, Geology of North America*, v. G-3, p. 653–682.
- Saleeby, J.B., and Harper, G.D., 1993, Tectonic relations between the Galice Formation and the Condrey Mountain Schist, Klamath Mountains, northern California, in Dunne, G.C., and McDougall, K.A., eds., *Mesozoic paleogeography of the Western United States-II: Los Angeles, Pacific Section, Society of Economic Paleontologists and Mineralogists*, v. 71, p. 61–80.
- Saleeby, J.B., Harper, G.D., Snoke, A.W., and Sharp, W.D., 1982, Time relations and structural-stratigraphic patterns in ophiolite accretion, west-central Klamath Mountains, California: *Journal of Geophysical Research*, v. 87, p. 3831–3848, doi: 10.1029/JB087iB05p03831.
- Samson, S.D., and Patchett, P.J., 1991, The Canadian Cordillera as a modern analogue of Proterozoic crustal growth: *Australian Journal of Earth Sciences*, v. 38, p. 595–611, doi: 10.1080/08120099108727994.
- Sanford, R.F., 1982, Growth of ultramafic reaction zones in greenschist to amphibolite facies metamorphism: *American Journal of Science*, v. 282, p. 543–616.
- Snoke, A.W., and Barnes, C.G., 2006, The development of tectonic concepts for the Klamath Mountains province, California and Oregon, in Snoke, A.W., and Barnes, C.G., eds., *Geological studies in the Klamath Mountains province, California and Oregon: A volume in honor of William P. Irwin: Geological Society of America Special Paper 410*, p. 1–30.
- Stacey, J.S., and Kramers, J.D., 1975, Approximation of terrestrial lead isotope evolution by a two-stage model: *Earth and Planetary Science Letters*, v. 26, p. 207–221, doi: 10.1016/0012-821X(75)90088-6.
- Sun, S.-s., and McDonough, W.F., 1989, Chemical and isotopic systematics of oceanic basalts: Implications for mantle composition and processes, in Saunders, A.D., and Norry, M.J., eds., *Magmatism in the ocean basins: Bath, UK, Geological Society of London Special Publication 42*, p. 313–345.
- Taylor, W.R., 1998, An experimental test of some geothermometer and geobarometer formulations for upper mantle peridotites with application to the thermobarometry of fertile lherzolite and garnet websterite: *Neues Jahrbuch für Mineralogie-Abhandlungen*, v. 172, p. 381–408.
- Windley, B.F., 1981, Phanerozoic granulites: *Journal of the Geological Society*, v. 138, p. 745–751, doi: 10.1144/gsjgs.138.6.0745.
- Wright, J.E., 1982, Permo-Triassic accretionary subduction complex, southwestern Klamath Mountains, Northern California: *Journal of Geophysical Research*, v. 87, p. 3805–3818, doi: 10.1029/JB087iB05p03805.
- Wright, J.E., and Fahan, M.R., 1988, An expanded view of Jurassic orogenesis in the Western United States Cordillera: Middle Jurassic (pre-Nevadan) regional metamorphism and thrust faulting within an active arc environment, Klamath Mountains, California: *Geological Society of America Bulletin*, v. 100, p. 859–876, doi: 10.1130/0016-7606(1988)100<859:AEVOJO>2.3.CO;2.
- Wright, J.E., and Wyld, S.J., 1994, The Rattlesnake Creek terrane, Klamath Mountains, California: An early Mesozoic volcanic arc and its basement of tectonically disrupted oceanic crust: *Geological Society of America Bulletin*, v. 106, p. 1033–1056, doi: 10.1130/0016-7606(1994)106<1033:TRCTKM>2.3.CO;2.
- Yule, J.D., Saleeby, J.B., and Barnes, C.G., 2006, A rift-edge facies of the Late Jurassic Rogue–Chetco arc and Josephine ophiolite, Klamath Mountains, Oregon, in Snoke, A.W., and Barnes, C.G., eds., *Geological studies in the Klamath Mountains province, California and Oregon: A volume in honor of William P. Irwin: Geological Society of America Special Paper 410*, p. 53–76.

Mesozoic magmatism in an upper- to middle-crustal section through the Cordilleran continental margin arc, eastern Transverse Ranges, California

Sarah K. Needy*

Department of Earth Sciences, Indiana University–Purdue University Indianapolis, Indianapolis, Indiana 46202, USA

J. Lawford Anderson

Department of Earth Sciences, University of Southern California, Los Angeles, California 90089, USA

Joseph L. Wooden

R.J. Fleck

U.S. Geological Survey, 345 Middlefield Road, Menlo Park, California 94025, USA

Andrew P. Barth

Department of Earth Sciences, Indiana University–Purdue University Indianapolis, Indianapolis, Indiana 46202, USA

Scott R. Paterson

Valbone Memeti

Department of Earth Sciences, University of Southern California, Los Angeles, California 90089, USA

Geoffrey S. Pignotta[†]

Department of Earth Sciences, University of Southern California, Los Angeles, California 90089, USA

ABSTRACT

The eastern Transverse Ranges provide essentially continuous exposure for >100 km across the strike of the Mesozoic Cordilleran orogen. Thermobarometric calculations based on hornblende and plagioclase compositions in Mesozoic plutonic rocks show that the first-order distribution of rock units resulted from differential Laramide exhumation. Mesozoic supracrustal rocks are preserved in the relatively little exhumed eastern part of the eastern Transverse Ranges and south-central Mojave Desert, and progressively greater rock uplift and exhumation toward the west exposed rocks originating at mid-crustal depths. The eastern Transverse Ranges thus constitute a tilted, nearly continuously exposed crustal section of the Mesozoic magmatic arc and framework rocks from subvolcanic levels to paleodepths as great

*sneedy@iupui.edu

[†]Current address: Department of Geology, University of Wisconsin, Eau Claire, Wisconsin 54702, USA.

as ~22 km. The base of this tilted arc section is a moderately east-dipping sheeted magmatic complex >10 km in width by 70 km in length, constructed structurally beneath, yet synchronous with Late Jurassic and Cretaceous upper-crustal plutons. Geochronology and regional structural relations thus suggest that arc magmas generated in the lower crust of this continental arc interacted in a complex mid-crustal zone of crystallization and mixing; products of this zone were parental magmas that formed relatively homogeneous upper crustal felsic plutons and fed lavas and voluminous ignimbrites.

INTRODUCTION

Depth-dependent changes in structural style and magmatic character in convergent-margin orogenic belts are difficult to assess because of the lack of three-dimensional control. For this reason, tilted arc crustal sections are invaluable settings in which to better understand magmatic and geodynamic aspects of convergent margin evolution (Saleeby, 1990; Kidder et al., 2003; Behn and Kelemen, 2006). In this report, we document a tilted crustal section in the eastern Transverse Ranges of southern California, where it was exhumed across the strike of the Mesozoic Cordilleran orogenic belt. This crustal section extends from volcanic and sedimentary units in the east to ~22 km paleodepth in the west, where it is truncated by the San Andreas fault. The character of upper-crustal magmatism includes surficial flows and pyroclastic rocks underlain by relatively homogeneous granodioritic to granitic plutons. The base of the crustal section, at 15–22 km paleodepth, is a magmatic sheeted complex that records coeval but compositionally and structurally distinct mid-crustal magmatism.

Regionally extensive magmatic sheeted complexes have characteristics that make them unique from single sheeted plutons and from adjacent and coeval magmatic belts, especially the sheet-like and dike-like to sill-like shapes of magma bodies with a dramatic range in composition over relatively short distances, and with well-developed magmatic and/or solid-state fabrics indicative of the presence of long-lived or recurrent deviatoric stress in the cores of active orogens. Cordilleran sheeted complexes include the Great Tonalite Sill (a collection of sills or dikes) in the Coast Plutonic Complex (Brew and Ford, 1981; Ingram and Hutton, 1994; Stowell and Pike, 2000; Hollister and Andronicos, 2000), the Skagit Gneiss Complex and other units in the Washington Cascades crystalline core (Misch, 1966, 1968; Miller et al., 1989; Haugerud et al., 1991; Miller and Paterson, 2001), sheeted complexes in the Idaho suture zone (Lund and Snee, 1988; Manduca et al., 1993), and a central sheeted complex in the core of the Peninsular Ranges batholith (Todd et al., 1988; Thomson and Girty, 1994; Schmidt and Paterson, 2002; Shaw et al., 2003; Fig. 1). These sheeted complexes have been interpreted as the deeper parts of magma plumbing systems that fed elliptical chambers at shallower levels (e.g., Skagit Gneiss Complex), as magma emplacement controlled by active faults (e.g., Great Tonalite Sill), as magmatism along lithospheric-scale

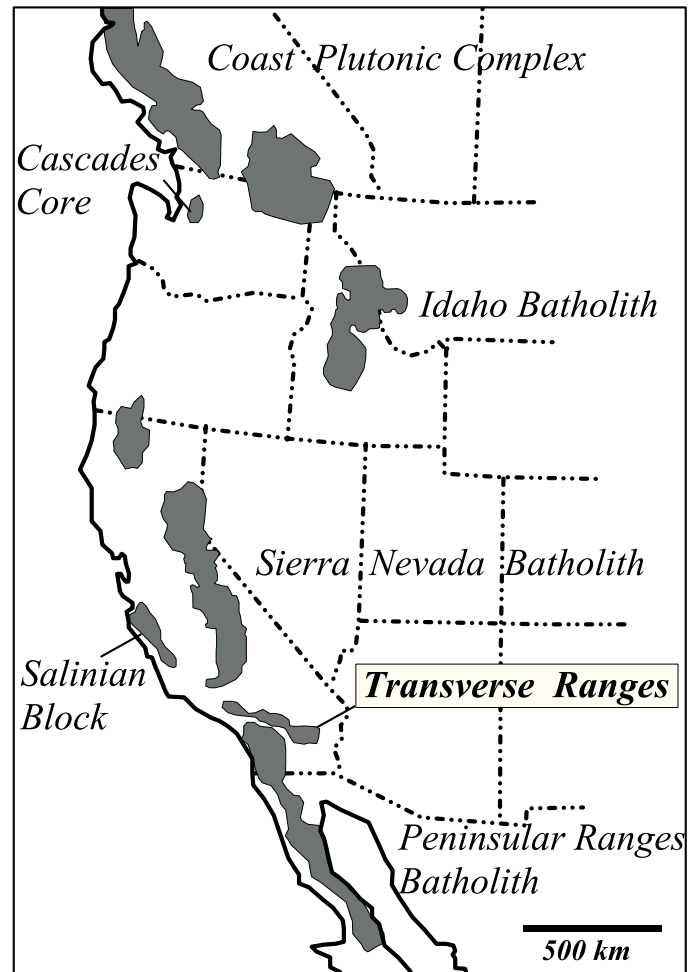


Figure 1. Major convergent margin plutonic belts of the Cordillera.

boundaries that may or may not have been active faults (e.g., Idaho suture zone and Peninsular Ranges batholith), and as dike swarms controlled by a regional stress field.

Many of these models for formation of sheeted complexes are difficult to apply because of the lack of three-dimensional control. Below we characterize a regional-scale sheeted complex at the base of the tilted crustal section in the eastern Transverse Ranges, as an initial step to evaluating the significance of Cordilleran sheeted complexes in general. We build on the initial

regional data set of Anderson et al. (1992) to focus on rapid change in calculated emplacement depths of plutons east of the San Andreas fault in the eastern Transverse Ranges (Fig. 2). We then relate the timing to the physical framework of Mesozoic magmatism to emplacement depth, and compare our results to observations in other tilted sections through Cordilleran arc crust constructed in distinct framework rocks.

GEOLOGIC FRAMEWORK

The eastern Transverse Ranges is composed of Paleoproterozoic basement rocks, Mesozoic volcanic and sedimentary rocks, and a variety of Mesozoic plutons (Miller, 1946; Rogers, 1954; Dibblee, 1967, 1968; Hope, 1969), extending eastward from southern San Andreas fault to the northwest-trending ranges of the southeastern Mojave Desert. As such, the eastern Transverse Ranges is a well-exposed crystalline terrain extending more than 100 km across the strike of the Mesozoic Cordilleran orogen. Powell (1981) developed a hypothesis for the structural evolution of the Transverse Ranges, based on the concept of suspect (or exotic) tectonostratigraphic terranes. Several subsequent studies have identified chronologic and petrologic ties between these inferred suspect terranes and concluded that local Proterozoic basement is not exotic, but is part of the Mojave crustal province forming the North American craton edge in the southwestern Cordillera (Bennett and DePaolo, 1987; Anderson et al., 1990; 1992; Bender et al., 1993; Barth et al., 2001a). As an alternative view of the crustal structure and structural evolution of this region, we suggest that the first-order distribution of rock units across the eastern Transverse Ranges results principally from differential Laramide exhumation of the Mesozoic orogen. Laramide uplift

resulted in little exhumation of Mesozoic rocks in the far eastern part of the eastern Transverse Ranges. Progressively greater uplift to the west exhumed rocks from mid-crustal depths (Fig. 3; Anderson et al., 1992; Mayo et al., 1998). The eastern Transverse Ranges thus also constitute a tilted, nearly continuously exposed crustal section of the Cordilleran orogen, from subvolcanic levels to mid-crustal paleodepths.

The eastern part of the crustal section exposes Jurassic volcanic and hypabyssal rocks (Fig. 3), in part correlative with the Dome Rock sequence of Tosdal et al. (1989), and sedimentary rocks of the medial Cretaceous, fluvial McCoy Mountains Formation (Harding and Coney, 1985; Stone and Pelka, 1989; Fackler-Adams et al., 1997; Barth et al., 2004). These Jurassic volcanic and Cretaceous sedimentary rocks were weakly thermally metamorphosed and intruded by Jurassic and Late Cretaceous plutons. Calzia (1982) inferred that hornfels facies rocks along the southern margin of the Late Cretaceous pluton in the Coxcomb Mountains (Fig. 3) formed at ≤ 2 kb. Mayo et al. (1998) estimated that Jurassic plutonic rocks in the Eagle Mountains were emplaced at ~ 6 km (Fig. 1), consistent with the shallow crustal nature of the enclosing stratigraphic sequences and the generally low metamorphic grade in this region.

The central core of the eastern Transverse Ranges is distinguished by plutons of Triassic, Jurassic, and Late Cretaceous age (Fig. 3) that intruded a Paleoproterozoic gneissic framework, and by the lack of Mesozoic supracrustal rocks. The gneisses include a variety of rock types overlapped by an upright sequence of weakly deformed and recrystallized Mesoproterozoic sedimentary rocks (Coleman et al., 2002). Plutons in the central region are discordant, typically forming sharp intrusive contacts truncating moderately to steeply east- or west-dipping foliation in

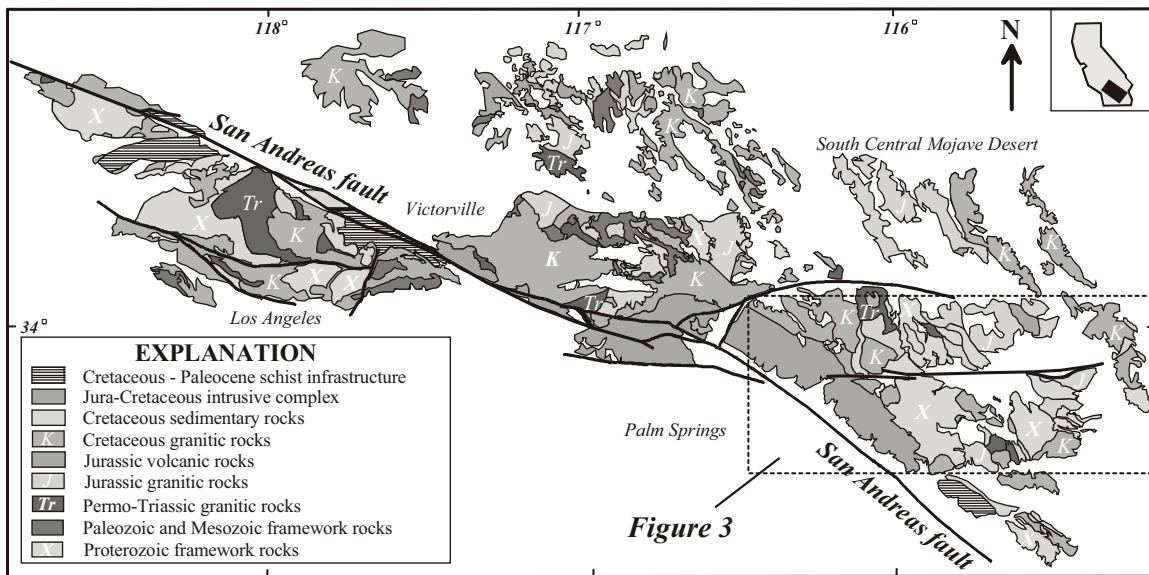


Figure 2. Geologic map of the Transverse Ranges and adjacent parts of the southern Mojave Desert. Box outlines the location of the eastern Transverse Ranges.

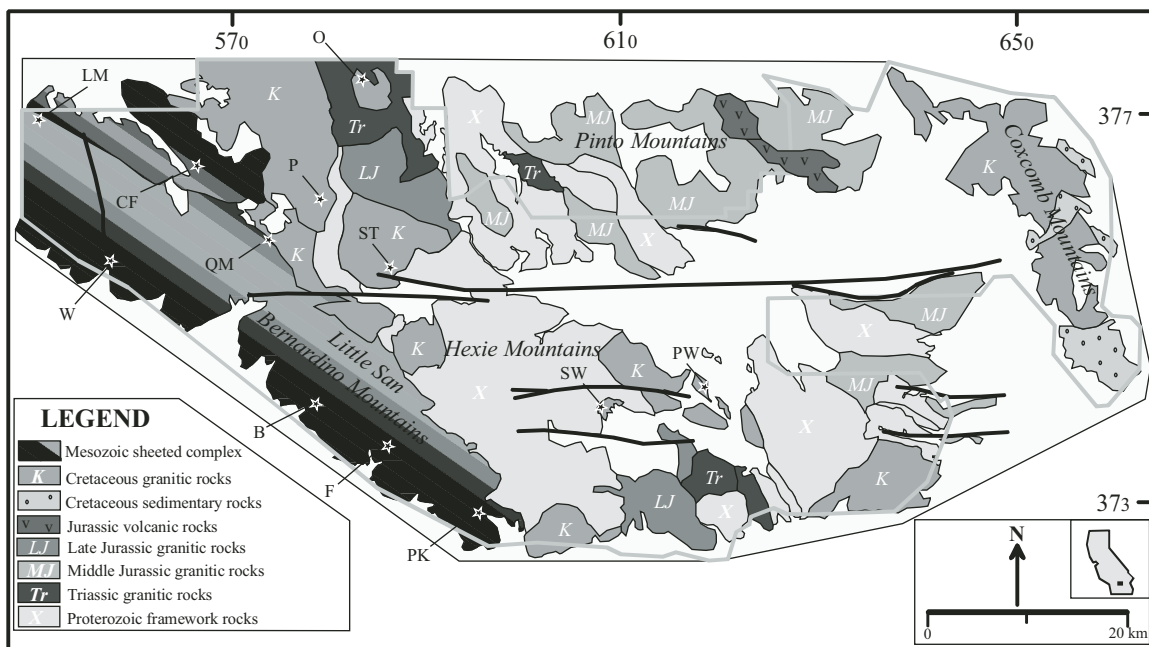


Figure 3. Geologic map showing the locations (stars) of plutons sampled for geochronology in the Little San Bernardino, Pinto, and Hexie Mountains, eastern Transverse Ranges. See Table 2 for abbreviations and calculated ages.

Paleoproterozoic gneisses. Regional intrusive sequences of Mesozoic plutonic rocks in this central region were originally inferred by Powell (1981), Brand (1985), James (1989), Mayo et al. (1998), and Howard (2002). Recent geochemical and geochronologic work indicates that quartz monzonitic to granitic rocks, locally porphyritic, are of Early Triassic age (Barth and Wooden, 2006). Monzodioritic to granitic rocks of Middle Jurassic age are part of their regional Kitt Peak–Trigo Peaks superunit, which extends southeastward into Arizona and northern Sonora and northward into the Mojave Desert and eastern Sierra Nevada (Tosdal et al., 1989); granites of Late Jurassic age are exposed in a northwest-trending belt west of, and subparallel to this belt of Middle Jurassic plutons, recording the outboard migration of Jurassic magmatism in Late Jurassic time (Barth et al., 2008). Anderson et al. (1992) estimated that Early Triassic plutons were emplaced at a depth of ~15 km in the central part of the eastern Transverse Ranges, consistent with our result for a Jurassic pluton in the same area (Fig. 4), and consistent with the greater exhumation inferred from the lack of preserved Mesozoic supracrustal stratigraphic sequences in the central eastern Transverse Ranges.

Along the western fringe of the eastern Transverse Ranges, Paleoproterozoic gneissic rocks give way, across a relatively abrupt boundary, to a northwest-trending terrain of layered crystalline rocks lacking discrete mappable Mesozoic plutons. This western terrain was originally mapped as Precambrian(?) gneissic rocks, and later interpreted as a largely late Mesozoic gneissic complex with pervasive brittle deformation (Powell, 1981). More recent geochronologic work (Wooden et al., 1994, 2001) suggested that this terrain is largely composed of Jurassic

and Cretaceous foliated igneous rocks. Our mapping suggests that this terrain is characterized by plutonic rocks that preserve an intrusive geometry of concordant to slightly discordant, meter- to decimeter-thick sheets. The sheets typically dip moderately north and east, though tilting as documented below suggests the original average dip was more gentle. Younger, commonly more felsic sheets intrude older plutonic sheets; recognizable Proterozoic gneisses occur locally, but usually comprise less than 10–20% of any outcrop area, primarily as interlayered septa. Reconnaissance petrographic work suggests that plutonic sheets record a broad compositional spectrum, but that the volumetrically dominant components are tonalite – granodiorite and biotite + muscovite ± garnet granite. Foliations in the intrusive sheets are typically magmatic, with a weak solid-state overprint at low to moderate temperatures (300–450 °C; Brown et al., 2006). Similarly layered complexes are exposed for an additional 100 km to the northwest of the area shown in Figure 3 (Powell, 1993; Barth et al., 2001b).

In succeeding sections, we describe geobarometry which indicates that the sheeted complex is more deeply exhumed than, and thus underlies discordant plutons throughout this part of the orogen. We next describe ages for discordant plutons in the eastern and central parts of the study region, coupled with a review of previous age assignments. We conclude that the study region comprises segments of regionally extensive Permo-Triassic, Middle to Late Jurassic, and Late Cretaceous arcs. Finally, we describe ages of components of the western sheeted complex, demonstrating that construction was contemporaneous with emplacement of discordant upper-crustal plutons now exposed to the east.

GEOBAROMETRY

Electron microprobe analyses were completed on 14 tonalite to granodiorite samples to estimate solidus pressures and temperatures. Three additional samples with calculated pressures were reported by Anderson et al. (1992) and Mayo et al. (1998), giving a total of 17 samples from which pressure estimates are available (Table 1). Samples were examined in thin section for euhedral to subhedral hornblende grains in direct contact with quartz and plagioclase, with associated alkali feldspar, biotite, sphene and magnetite. Where possible, three analyses were made transecting from the rim of the hornblende grain touching quartz, through the interior, and onto the center of the hornblende grain to examine compositional zonation. In other cases, the hornblende sections were too thin to sensibly do this, and only rim and center analyses were obtained. Analyses of hornblende and plagioclase rims were completed on the Cameca electron microprobe at Indiana University operating at 15 kV and 20 nA with a 2 μ m beam diameter.

Total Al content of amphibole rims was used to calculate solidus pressure conditions using the equation P (kb) = $4.76 * Al^{tot} - 3.01$ (Schmidt, 1992). The resulting pressures range from 2 to 6 kb. Using the amphibole–plagioclase thermometer of Holland and Blundy (1994), several of the samples yielded solidus temperatures significantly higher than the experimental temperatures used by Schmidt (1992). Therefore, we recalculated crystallization pressures using the thermobarometer of Anderson and Smith (1995), which incorporates the effect of higher temperature on the total Al content of amphibole coexisting with plagioclase and quartz.

Paleodepths of crystallization were calculated from solidus pressures by applying average crustal density. The calculated paleodepths are highly correlated with geographic position; correlation of paleodepth to UTM easting coordinate is $depth$ (km) = $-0.000137 * UTM\ E$ (m) + 94.779 ($R^2 = 0.74$; Fig. 4). There is no significant correlation with northing coordinates. If the crustal section behaved as a coherent block, the angle of tilt (α) necessary to uplift and exhume these rocks is $\sim 8^\circ$, about a north-trending axis. However, the data are fit equally well by a simple polynomial function, indicating that the structure may also be represented as the eastern limb of a broad regional antiform. Given the map pattern in Figure 3 and our sample distribution, these data may be equally well described by a northwest-trending antiform.

GEOCHRONOLOGY

Zircon U–Pb isotopic compositions were analyzed in thirty samples of igneous rocks collected across the tilted crustal section. Additional bulk fraction U–Pb ages of zircon and $^{40}Ar/^{39}Ar$ ages of biotite and hornblende for a subset of these samples were described by Wooden et al. (2001). Zircon grains from samples of granite, granodiorite, tonalite and diorite were separated, imaged using cathodoluminescence (CL) microscopy, and analyzed by ion microprobe on the U.S. Geological Survey SHRIMP-RG (sensitive high-resolution ion microprobe–reverse geometry)

housed at Stanford University, using techniques described in Barth and Wooden (2006). SHRIMP-RG data were reduced using the SQUID program (Ludwig, 2002), with isotope ratios standardized against Braintree Complex zircon R33 (419 Ma; Black et al., 2004). Errors on calculated crystallization ages reported in the text and in Tables 2 and 3 are reported at the 95% confidence level. Errors on measured ages of each individual grain are reported in Table 3 at one sigma. It has been demonstrated that ion microprobe analysis yields precise and accurate crystallization ages in Mesozoic monogenetic and polygenetic zircon suites (Black et al., 2004; Barth and Wooden, 2006; Barth et al., 2008).

Geochronology of Cretaceous Plutons in the Hexie and Pinto Mountains

Existing U–Pb zircon ages indicate that episodic plutonism occurred from Early Triassic to Late Cretaceous time at higher structural levels in the central and eastern part of the study area (Barth et al., 2004, 2008; Barth and Wooden, 2006). In this study, we report additional ages for Cretaceous plutons, which allow us to better characterize migratory Late Cretaceous plutonism and the nature of the compositional and age relationships between these plutons and the sheeted complex in the western, structurally deeper part of the study area.

The granite of Smoke Tree Well (SW in Fig. 3) intrudes Proterozoic gneiss in the eastern Hexie Mountains, and was originally mapped as part of the Late Jurassic granite of Cottonwood by Powell (2001); our mapping suggests it is a petrographically distinct unit comprised of porphyritic biotite granite with euhedral to subhedral alkali feldspar phenocrysts up to 2 cm in long dimension. Zircons from a sample of this porphyritic granite are equant

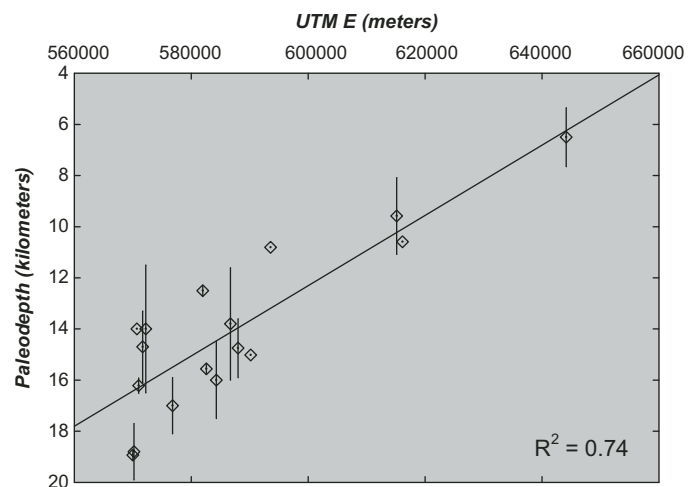


Figure 4. East to west variation in emplacement depth, estimated from hornblende Al^I barometry of Mesozoic plutons [additional data from Anderson et al. (1992) and Mayo et al. (1998)]. The high correlation coefficient of these data supports a model of $\sim 8^\circ$ west-side-up block tilting of the crust about a north-trending axis, following emplacement of Late Cretaceous plutonic rocks at 14–19 km paleodepth in the Little San Bernardino Mountains.

TABLE 1. HORNBLende AND PLAGIOCLASE CHEMISTRY FOR GRANITIC ROCKS OF THE EASTERN TRANSVERSE RANGES

	<i>jw-178</i>	<i>jw-194</i>	<i>jw-195</i>	<i>jw-198</i>	<i>jw-219</i>	<i>01-330</i>	<i>04-523</i>	<i>04-529</i>	<i>04-531</i>	<i>04-534</i>	<i>04-548</i>
	grd 2rim	grd 1rim	ton 18rim	grd 8rim	grd 1rim	grd 3rim	grd 2rim	gr 2rim	grd 3rim	grd 2rim	ton 5rim
SiO ₂	44.08	42.74	44.79	43.16	48.65	47.80	44.30	44.76	43.21	43.33	41.63
TiO ₂	1.40	1.36	1.09	1.51	1.114	0.77	0.68	1.31	0.57	0.84	1.21
Al ₂ O ₃	8.74	10.07	9.4	9.83	7.316	6.43	9.52	8.57	10.08	10.34	10.97
FeO*	17.55	18.04	17.22	18.44	15.763	15.57	17.26	16.34	19.03	19.36	18.66
MgO	11.19	10.60	11.16	10.63	13.297	12.77	10.90	11.78	10.69	9.74	10.24
MnO	0.60	0.52	0.45	0.66	0.49	0.80	0.84	0.83	0.53	0.53	0.47
CaO	11.89	11.89	12.63	11.66	11.391	11.67	11.73	11.60	11.89	11.89	11.92
Na ₂ O	1.11	1.06	1.02	1.10	1.251	0.97	0.95	1.33	1.03	1.00	1.19
K ₂ O	1.07	1.21	0.95	1.22	0.666	0.63	1.04	0.81	0.96	1.15	1.39
sum	97.63	97.49	98.71	98.21	99.94	97.42	97.22	97.33	97.99	98.17	97.69
Si	6.666	6.501	6.673	6.404	6.983	6.933	6.703	6.740	6.550	6.565	6.359
Al	1.557	1.806	1.650	1.720	1.238	1.319	1.698	1.520	1.800	1.847	1.976
Ti	0.159	0.155	0.122	0.169	0.120	0.108	0.077	0.150	0.065	0.095	0.139
Fe ⁺²	2.220	2.295	2.145	2.274	1.892	1.901	2.184	2.060	2.412	2.454	2.384
Mn	0.077	0.067	0.057	0.083	0.060	0.083	0.107	0.110	0.068	0.068	0.061
Mg	2.523	2.404	2.479	2.350	2.845	2.832	2.459	2.640	2.416	2.199	2.331
Ca	1.927	1.938	2.016	1.855	1.906	1.870	1.901	1.870	1.931	1.930	1.951
Na	0.324	0.313	0.295	0.317	0.348	0.359	0.279	0.390	0.301	0.293	0.352
K	0.207	0.236	0.181	0.230	0.122	0.151	0.201	0.160	0.186	0.222	0.270
sum	15.660	15.715	15.618	15.402	15.514	15.556	15.609	15.640	15.729	15.673	15.823
Ab (pl)	0.64	0.66	0.60	0.70	0.78	0.68	0.68	0.72	0.58	0.58	0.61
An (pl)	0.36	0.33	0.38	0.29	0.21	0.31	0.31	0.27	0.40	0.41	0.38
UTM E	593545	590145	584277	586695	616152	615140	576797	581951	572206	570981	571669
UTM N	66213	32109	35555	44798	44786	44282	54024	57815	59613	61145	56692
T[C] [†]	765(11)	755(12)	703	756(28)	669	720(21)	708(17)	689(31)	785(15)	752(4)	786(11)
D[km] [†]	10.8	15(0.5)	16(1.5)	13.8(2.1)	10.6	9.6(1.5)	17(1.1)	12.5(0.2)	14(2.5)	16.2(0.3)	14.7(1.4)

(Continued)

TABLE 1. HORNBLende AND PLAGIOCLASE CHEMISTRY FOR GRANITIC ROCKS OF THE EASTERN TRANSVERSE RANGES (Continued)

	04-565		05-598		05-608		j2		j82		EM10	
	grd 1rim	grd 2rim	grd 2rim	grd 2rim	grd 2rim	grd A1	grd B2	grd A1	grd B2	grd B2	mzd 2	
SiO ₂	44.232	43.10	42.61	44.55	44.82	44.82	44.82	44.82	44.82	44.82	48.11	
TiO ₂	0.899	0.88	0.92	0.50	0.63	0.50	0.63	0.50	0.63	0.63	1.04	
Al ₂ O ₃	9.182	10.54	10.25	8.80	8.92	8.80	8.92	8.80	8.92	8.92	5.97	
FeO*	17.882	19.11	18.31	18.02	17.35	18.02	17.35	18.02	17.35	17.35	13.96	
MgO	11.32	9.57	9.75	10.38	11.15	10.38	11.15	10.38	11.15	11.15	14.14	
MnO	0.516	0.61	0.67	1.18	0.90	1.18	0.90	1.18	0.90	0.90	0.57	
CaO	12.059	11.54	11.59	11.52	11.87	11.52	11.87	11.52	11.87	11.87	12.12	
Na ² O	0.978	1.35	1.17	1.50	1.42	1.50	1.42	1.50	1.42	1.42	0.80	
K ₂ O	0.926	1.39	1.29	1.08	1.10	1.08	1.10	1.08	1.10	1.10	0.62	
sum	97.99	98.08	96.55	97.53	98.16	97.53	98.16	97.53	98.16	98.16	97.33	
Si	6.502	6.545	6.555	6.766	6.735	6.766	6.735	6.766	6.735	6.735	7.106	
Al	1.776	1.886	1.858	1.575	1.580	1.575	1.580	1.575	1.580	1.580	1.039	
Ti	0.126	0.100	0.107	0.057	0.071	0.057	0.071	0.057	0.071	0.071	0.115	
Fe ⁺²	2.422	2.427	2.356	2.289	2.181	2.289	2.181	2.289	2.181	2.181	1.724	
Mn	0.065	0.078	0.087	0.152	0.115	0.152	0.115	0.152	0.115	0.115	0.071	
Mg	2.363	2.166	2.236	2.351	2.498	2.351	2.498	2.351	2.498	2.498	3.114	
Ca	1.927	1.877	1.911	1.875	1.911	1.875	1.911	1.875	1.911	1.911	1.917	
Na	0.366	0.397	0.348	0.442	0.414	0.442	0.414	0.442	0.414	0.414	0.229	
K	0.237	0.269	0.252	0.209	0.211	0.209	0.211	0.209	0.211	0.211	0.117	
sum	15.784	15.745	15.710	15.716	15.716	15.716	15.716	15.716	15.716	15.716	15.432	
Ab (pl)	0.67	0.68	0.68	0.77	0.77	0.77	0.77	0.77	0.77	0.77	0.65	
An (pl)	0.32	0.31	0.30	0.23	0.22	0.23	0.22	0.23	0.22	0.22	0.33	
UTM E	570700	569997	570193	582564	587990	582564	587990	582564	587990	587990	644143	
UTM N	54469	67549	65598	74120	72034	74120	72034	74120	72034	72034		
T[C] [†]	741(20)	725(3)	718(7)	692(4)	695(20)	692(4)	695(20)	692(4)	695(20)	695(20)	709(33)	
D(km) [†]	14.0	18.9(0.2)	18.8(1.1)	15.6(0.2)	14.7(1.1)	15.6(0.2)	14.7(1.1)	15.6(0.2)	14.7(1.1)	14.7(1.1)	6.5(1.2)	

Notes: Values in parentheses are standard deviation of multiple mineral pairs.

*Total Fe as FeO; †depth calculated from Anderson and Smith (1995), corrected for temperature from Holland and Blundy (1994).

TABLE 2. LOCATIONS AND AGES FOR JURASSIC AND CRETACEOUS IGNEOUS ROCKS OF THE EASTERN TRANSVERSE RANGES

Map label	Rock unit	Sample #	Rock type	Age (Ma)	References
<u>Plutons</u>					
SW	Granite of Smoke Tree Well	03-456	Granite	75 ± 1.4	1
PW	Granodiorite of Porcupine Wash	JW219	Granodiorite	75 ± 2	1
ST	Granite of Squaw Tank	529	Granite	79.5 ± 1.1	2
P	Granite of Palms	561	Granite	77.2 ± 0.6	2, 3
O	Granite of Oasis	03-508	Granite	103 ± 1	3
<u>Sheeted Complex</u>					
<u>Diorite</u>					
CF	Diorite of Covington Flat	JW264	Diorite	78 ± 3	
<u>Granodiorite</u>					
F	Fargo Canyon	JW195	Granodiorite	75.4 ± 0.8	
B	Berdoo Canyon	JW198	Granodiorite	82 ± 1	
B	Berdoo Canyon	JW199	Granodiorite	76.9 ± 1.0	
W	Wide Canyon	JW216	Gneissic granodiorite	82 ± 1	
	Indian Cove boulder	JW222	Granodiorite	78 ± 1	3
B	Berdoo Canyon	JW256	Foliated granodiorite	79 ± 2	
LM	Upper Little Morongo Canyon	JW259	Foliated granodiorite	152 ± 1	
LM	Upper Little Morongo Canyon	JW260	Foliated tonalite	150 ± 2	
QM	Granodiorite of Quail Mountain complex	537	Granodiorite	81.1 ± 1.2	4
QM	Granodiorite of Bighorn complex	548	Granodiorite	81.8 ± 1.4	4
<u>Granite</u>					
PK	Lower Pinkham Canyon	JW193	Granite	74 ± 2	
F	West fork, Fargo Canyon	JW196	Granite	150 ± 2	
LM	Little Morongo Canyon	JW215	Gneissic granite	81 ± 1	
W	Wide Canyon	JW217	Granite	74 ± 2	
	West park entrance station	JW221	Granite	79 ± 1	3
	West of Indian Cove	JW224	Granite	81 ± 1	3

(Continued)

TABLE 2. LOCATIONS AND AGES FOR JURASSIC AND CRETACEOUS IGNEOUS ROCKS OF THE EASTERN TRANSVERSE RANGES (Continued)

Map label	Rock unit	Sample #	Rock type	Age (Ma)	References
<i>Granite (Continued)</i>					
B	Berdoo Canyon	JW257	Granite	153 ± 2	
B	Lower Berdoo Canyon	JW258	Granite	83 ± 2	
CF	Covington Flat	JW262	Foliated granite	80 ± 1	
QM	Stubbe Springs	544	Granite	76 ± 4	4
QM	Granite of Bighorn complex	549	Granite	NC	4
<i>Granite Dikes</i>					
B	Upper Berdoo Canyon	JW197	Granite	NC	
LM	Upper Little Morongo Canyon	JW261	Granite	75 ± 2	
CF	Covington Flat	JW263	Granite	75 ± 1	

Note: NC—no age calculated; References: 1—Powell (2001), 2—Rogers (1954), 3—Brand (1985), and 4—Paterson et al. (2006).

TABLE 3. SHRIMP-RG ZIRCON U-Pb DATA FOR IGNEOUS ROCKS OF THE EASTERN TRANSVERSE RANGES

	U (ppm)	Th (ppm)	$^{238}\text{U}/^{206}\text{Pb}$	$^{207}\text{Pb}/^{206}\text{Pb}$	$^{206}\text{Pb}^*/^{238}\text{U}$ age (Ma)	$^{207}\text{Pb}^*/^{206}\text{Pb}$ age (Ma)
<u>Granite of lower Pinkham Canyon</u>						
			33.68419*	115.965	74 ± 2 [†]	
JW193-1	189	125	88.70	1.7	72.2	1.3
JW193-2	361	106	4.22	1.1	1350.8	14.5
JW193-3	689	290	84.50	1.3	75.7	1.0
JW193-4	385	289	90.37	1.4	70.9	1.0
JW193-5	435	291	86.15	1.4	74.3	1.0
JW193-6	989	276	86.67	1.2	73.8	0.9
JW193-7	201	140	87.20	1.6	73.6	1.2
<u>Granodiorite of Fargo Canyon</u>						
			33.75847	116.0898	75.4 ± 0.8	
JW195-1	709	321	85.57	1.2	74.8	0.9
JW195-2	562	197	85.35	1.3	75.1	1.0
JW195-3	1682	327	3.39	1.0	1665.3	16.5
JW195-4	912	303	84.83	1.2	75.5	0.9
JW195-5	551	213	83.05	1.3	76.9	1.0
JW195-6	396	141	85.84	1.4	74.5	1.1
JW195-7	407	141	84.78	1.4	75.7	1.1
<u>Leucogranite of west fork of Fargo Canyon</u>						
			33.78764	116.1069	150 ± 2	
JW196-1	307	259	43.13	1.3	147.4	1.9
JW196-2	1047	880	42.64	1.1	149.5	1.6
JW196-3	292	224	42.93	1.3	147.9	2.0
JW196-4	785	780	41.53	1.1	153.4	1.7
JW196-5	432	470	43.97	1.2	145.0	1.8
JW196-6	198	240	42.05	1.5	151.2	2.2
JW196-7	232	389	41.58	1.4	153.0	2.1
<u>Garnet granite dike of upper Berdoo Canyon</u>						
			33.82994	116.1065		
JW197-1	220	122	4.31	1.1	1341.4	14.9
JW197-2	776	96	73.21	1.2	87.3	1.0
JW197-3	523	382	3.42	1.1	1655.2	17.2
JW197-4	58	81	42.28	2.5	150.3	3.8
JW197-5	141	171	89.63	2.0	71.1	1.4
JW197-6	480	315	84.13	1.3	76.3	1.0
JW197-7	1601	114	27.01	1.2	232.0	2.7

(Continued)

TABLE 3. SHRIMP-RG ZIRCON U-Pb DATA FOR IGNEOUS ROCKS OF THE EASTERN TRANSVERSE RANGES (Continued)

	U (ppm)	Th (ppm)	$^{238}\text{U}/^{206}\text{Pb}$	$^{207}\text{Pb}/^{206}\text{Pb}$	$^{206}\text{Pb}^*/^{238}\text{U}$ age (Ma)	$^{207}\text{Pb}/^{206}\text{Pb}^*$ age (Ma)
<u>Garnet granite dike of upper Berdoo Canyon (Continued)</u>						
JW197-8	71	63	41.79	0.0516	6.6	152.0 3.2
JW197-9	303	90	26.30	0.0522	2.5	240.2 3.0
JW197-10	271	156	81.40	0.0461	4.8	78.9 1.3
JW197-11	571	80	27.65	0.0512	1.8	228.9 2.6
<u>Granodiorite of Berdoo Canyon</u>			33.83989	116.0634	82 ± 1	
JW198-5	92	91	79.06	0.0507	6.5	80.7 1.7
JW198-6	124	152	77.75	0.0518	5.5	82.0 1.5
JW198-7	405	37	3.85	0.1023	0.5	1471.3 6.0 1656.5 10.1
JW198-8	82	85	80.68	0.0484	7.3	79.3 1.8
JW198-9	120	125	78.91	0.0517	5.8	80.8 1.5
JW198-10	180	142	78.08	0.0508	4.7	81.7 1.3
JW198-11	146	158	77.88	0.0496	5.3	82.0 1.4
JW198-12	133	120	76.94	0.0497	6.3	83.0 1.5
JW198-13	92	104	74.87	0.0488	6.8	85.4 1.9
JW198-14	74	90	78.43	0.0412	8.7	82.3 2.0
<u>Granodiorite of Berdoo Canyon</u>			33.82947	116.0973	76.9 ± 1.0	
JW199-5	529	228	83.36	0.0509	3.6	76.5 0.7
JW199-6	417	153	84.06	0.0490	3.3	76.1 0.8
JW199-7	400	119	86.05	0.0495	3.4	74.3 0.8
JW199-8	472	126	83.71	0.0507	3.0	76.3 0.9
JW199-9	433	108	81.07	0.0471	3.2	79.1 0.8
JW199-10	429	151	83.86	0.0493	3.2	76.3 0.8
JW199-11	988	580	82.25	0.0479	2.1	77.9 0.5
JW199-12	403	200	3.24	0.1072	0.5	1729.9 8.2 1749.2 8.7
JW199-13	383	138	83.70	0.0480	3.4	76.5 0.8
JW199-14	514	222	82.71	0.0479	3.0	77.4 0.7
<u>Gneissic granite of Little Morongo Canyon</u>			34.00069	116.5178	81 ± 1	
JW215-1	155	197	79.41	0.0482	6.1	80.6 1.5
JW215-2	252	227	79.83	0.0457	4.8	80.4 1.3
JW215-3	133	148	79.91	0.0481	6.9	80.1 1.6

(Continued)

TABLE 3. SHRIMP-RG ZIRCON U-Pb DATA FOR IGNEOUS ROCKS OF THE EASTERN TRANSVERSE RANGES (Continued)

		U (ppm)	Th (ppm)	$^{238}\text{U}/^{206}\text{Pb}$	$^{207}\text{Pb}/^{206}\text{Pb}$	$^{206}\text{Pb}^*/^{238}\text{U}$ age (Ma)	$^{207}\text{Pb}^*/^{206}\text{Pb}^*$ age (Ma)
<u>Gneissic granite of Little Morongo Canyon (Continued)</u>							
JW215-4	181	266	78.94	1.8	0.0488	81.0	1.4
JW215-5	52	52	76.61	2.8	0.0668	81.7	2.4
JW215-6	186	156	78.63	1.7	0.0511	81.1	1.4
<u>Gneissic granodiorite of Wide Canyon</u>				33.93144	116.3768	82 ± 1	
JW216-1	135	156	77.40	1.9	0.0490	82.6	1.6
JW216-2	129	159	78.55	2.0	0.0479	81.5	1.7
JW216-3	152	182	77.60	1.9	0.0503	82.3	1.6
JW216-4	134	161	76.83	2.0	0.0476	83.4	1.7
JW216-5	175	191	80.26	1.8	0.0491	79.7	1.4
JW216-6	852	97	76.57	1.2	0.0478	83.6	1.0
JW216-7	554	599	77.03	1.3	0.0467	83.3	1.1
JW216-8	278	258	79.79	1.6	0.0570	79.3	1.3
JW216-9	319	129	87.04	1.6	0.0513	73.3	1.2
JW216-10	857	82	83.99	1.3	0.0494	76.1	1.0
JW216-11	308	118	87.04	1.6	0.0460	73.8	1.2
JW216-12	439	228	76.62	1.4	0.0494	83.4	1.2
<u>Leucogranite of Wide Canyon</u>				33.9325	116.3878	74 ± 2	
JW217-1	771	257	88.91	1.2	0.0486	72.0	0.9
JW217-2	268	145	69.31	1.5	0.0505	92.0	1.4
JW217-3	1501	72	77.96	1.1	0.0512	81.8	0.9
JW217-4	1787	133	81.55	1.1	0.0469	78.6	0.9
JW217-5	457	228	66.27	1.3	0.0485	96.5	1.3
JW217-6	350	110	89.10	1.5	0.0496	71.7	1.1
JW217-7	513	106	74.10	1.3	0.0486	86.3	1.1
JW217-8	627	305	69.06	1.2	0.0461	92.9	1.2
JW217-9	944	166	86.78	1.2	0.0489	73.7	0.9
JW217-10	416	248	67.02	1.4	0.0485	95.4	1.3
JW217-11	444	139	86.87	1.4	0.0492	73.6	1.1
JW217-12	514	175	84.85	1.4	0.0504	75.3	1.0

(Continued)

TABLE 3. SHRIMP-RG ZIRCON U-Pb DATA FOR IGNEOUS ROCKS OF THE EASTERN TRANSVERSE RANGES (Continued)

		U (ppm)	Th (ppm)	$^{238}\text{U}/^{206}\text{Pb}$	$^{207}\text{Pb}/^{206}\text{Pb}$	$^{206}\text{Pb}*/^{238}\text{U}$ age (Ma)	$^{207}\text{Pb}*/^{206}\text{Pb}$ age (Ma)
<u>Leucogranite of Wide Canyon (Continued)</u>							
JW217-13		1212	73	84.61	1.2	0.0472	2.6
JW217-14		426	281	66.87	1.3	0.0451	3.6
<u>Granodiorite of Porcupine Wash</u>				33.83694	115.7447		75 ± 2
JW219-1		323	191	86.66	1.1	0.0507	4.4
JW219-2		486	334	83.21	0.9	0.0462	3.7
JW219-3		214	124	85.99	1.4	0.0492	5.4
JW219-4		226	59	86.72	1.4	0.0476	5.5
JW219-5		260	168	85.26	1.3	0.0482	5.0
JW219-6		291	185	87.27	1.2	0.0466	4.8
<u>Granite of west entrance station</u>				34.09008	116.2664		79 ± 1
JW221-1		201	76	3.16	0.5	0.1081	0.7
JW221-2		372	51	24.85	0.6	0.0540	2.0
JW221-3		1070	337	81.40	0.5	0.0469	2.2
JW221-4		545	25	78.36	0.7	0.0489	3.0
JW221-5		947	447	79.58	0.6	0.0478	2.3
JW221-6		214	134	83.55	1.2	0.0511	4.8
JW221-7		285	228	81.70	1.0	0.0457	4.2
JW221-8		557	21	3.56	0.4	0.0991	3.3
JW221-9		966	592	81.42	0.7	0.0484	2.7
JW221-10		201	54	83.14	1.2	0.0479	5.0
<u>Granodiorite, Indian Cove stream boulder</u>				34.08411	116.1353		78 ± 1
JW222-5		193	169	82.81	1.5	0.0522	4.8
JW222-6		252	243	82.63	1.4	0.0497	4.2
JW222-7		105	30	3.25	0.9	0.1009	1.0
JW222-8		154	146	78.50	1.7	0.0517	5.3
JW222-9		155	145	80.93	1.8	0.0461	6.0
JW222-10		80	108	86.55	2.4	0.0494	7.3
JW222-11		350	302	81.36	1.1	0.0483	3.5
JW222-12		98	173	81.36	2.2	0.0526	7.4
							1762.0
							12.4
							9.3
							1.5
							0.4
							0.6
							0.5
							0.9
							0.8
							8.2
							61.7
							1596.7
							78.6
							0.5
							77.0
							1.0
							78 ± 1
							76.9
							1.2
							77.3
							1.1
							1740.9
							14.6
							1613.3
							22.9
							81.2
							1.4
							79.3
							1.5
							73.9
							1.8
							78.7
							0.9
							1165.0
							51.0
							0.9
							78.2
							1.7

(Continued)

TABLE 3. SHRIMP-RG ZIRCON U-Pb DATA FOR IGNEOUS ROCKS OF THE EASTERN TRANSVERSE RANGES (Continued)

	U (ppm)	Th (ppm)	$^{238}\text{U}/^{206}\text{Pb}$	$^{207}\text{Pb}/^{206}\text{Pb}$	$^{206}\text{Pb}*/^{238}\text{U}$ age (Ma)	$^{207}\text{Pb}*/^{206}\text{Pb}$ age (Ma)
<u>Granite west of Indian Cove</u>						
			34.12075	116.1963	81 ± 1	
JW224-1	595	161	3.40	0.4	1660.1	6.0
JW224-2	114	60	80.56	1.6	78.9	1.3
JW224-3	1084	1545	79.29	0.5	80.9	0.4
JW224-4	248	272	79.35	1.1	80.7	0.9
JW224-5	660	596	79.28	0.7	81.0	0.6
JW224-6	766	371	3.02	0.3	1851.2	6.0
JW224-7	917	1175	79.22	0.6	80.8	0.5
JW224-8	166	91	80.03	1.4	80.0	1.1
JW224-9	473	648	80.11	0.8	79.8	0.7
JW224-10	1096	126	3.15	0.3	1784.9	4.9
JW224-11	415	190	2.53	0.4	2166.6	8.5
<u>Foliated granodiorite of Berdoo Canyon</u>						
			33.83079	116.1376	79 ± 2	
JW256-1	665	276	82.09	0.7	78.0	0.5
JW256-2	372	123	81.26	0.9	78.9	0.8
JW256-3	478	215	79.25	0.8	81.0	0.7
JW256-4	503	179	81.98	0.8	78.1	0.7
JW256-5	401	131	79.35	1.0	80.7	0.8
JW256-6	448	176	77.30	0.9	82.8	0.8
JW256-7	521	222	83.50	0.8	76.5	0.6
JW256-8	394	149	79.49	0.9	80.5	0.8
<u>Granite of Berdoo Canyon</u>						
			33.84001	116.1288	153 ± 2	
JW257-1	544	361	42.49	0.6	149.9	0.9
JW257-2	512	296	40.06	0.7	159.0	1.1
JW257-3	619	325	41.27	0.7	154.2	1.1
JW257-4	598	327	41.27	0.6	154.5	1.0
JW257-5	322	444	41.76	0.8	152.4	1.3
JW257-6	428	509	42.25	0.8	150.4	1.2
JW257-7	987	515	41.56	0.5	153.3	0.7
JW257-8	216	312	42.49	1.0	149.1	1.5

(Continued)

TABLE 3. SHRIMP-RG ZIRCON U-Pb DATA FOR IGNEOUS ROCKS OF THE EASTERN TRANSVERSE RANGES (Continued)

Granite of Berdoo Canyon (Continued)		U (ppm)	Th (ppm)	$^{238}\text{U}/^{206}\text{Pb}$	$^{207}\text{Pb}/^{206}\text{Pb}$	$^{206}\text{Pb}/^{238}\text{U}$ age (Ma)	$^{207}\text{Pb}/^{206}\text{Pb}$ age (Ma)
JW257-9	205	320	41.83	1.0	0.0469	152.7	1.6
JW257-10	557	878	41.39	0.6	0.0496	153.8	1.0
<u>Granite of lower Berdoo Canyon</u>			33.82312	116.1625		83 ± 2	
JW258-1	236	289	76.98	1.1	0.0479	83.2	1.0
JW258-1.2	199	221	73.88	1.8	0.0568	85.7	1.6
JW258-2	138	211	75.97	1.4	0.0510	83.9	1.2
JW258-3	330	309	77.11	1.4	0.0507	82.7	1.2
JW258-4	170	136	80.09	2.0	0.0560	79.1	1.7
JW258-5	1174	719	76.17	0.7	0.0502	83.8	0.6
JW258-6	2797	792	77.55	0.5	0.0478	82.6	0.4
JW258-7	210	146	75.56	1.7	0.0512	84.4	1.5
JW258-8	2420	1030	71.58	0.5	0.0483	89.4	0.5
JW258-9	243	264	76.80	1.5	0.0502	83.1	1.3
JW258-10	465	480	13.85	0.6	0.0861	433.0	3.5
JW258-11	455	446	79.13	1.1	0.0472	81.0	1.0
JW258-12	364	222	77.45	1.2	0.0503	82.4	1.1
<u>Foliated granodiorite of upper Little Morongo Canyon</u>			34.05278	116.5111		152 ± 1	
JW259-1	83	135	44.82	1.6	0.0507	141.9	2.4
JW259-2	71	120	44.15	1.8	0.0482	144.5	2.6
JW259-3	17	26	41.53	3.7	0.0622	150.9	5.7
JW259-4	421	543	41.53	0.7	0.0500	153.2	1.2
JW259-5	49	79	41.37	2.2	0.0503	153.8	3.5
JW259-6	136	48	43.20	1.3	0.0518	147.0	2.0
JW259-7	273	322	42.43	0.9	0.0506	149.9	1.4
JW259-7.2	231	271	41.86	1.2	0.0527	151.5	1.9
JW259-8	121	156	42.04	1.4	0.0516	151.1	2.1
JW259-9	384	518	41.02	0.8	0.0494	155.2	1.3
JW259-10	93	145	43.41	2.0	0.0643	144.0	3.0
JW259-11	405	611	42.45	0.9	0.0508	149.8	1.4
JW259-12	342	354	41.06	1.0	0.0490	155.1	1.6

(Continued)

TABLE 3. SHRIMP-RG ZIRCON U-Pb DATA FOR IGNEOUS ROCKS OF THE EASTERN TRANSVERSE RANGES (Continued)

	U (ppm)	Th (ppm)	$^{238}\text{U}/^{206}\text{Pb}$	$^{207}\text{Pb}/^{206}\text{Pb}$	$^{206}\text{Pb}^*/^{238}\text{U}$ age (Ma)	$^{207}\text{Pb}^*/^{206}\text{Pb}$ age (Ma)
<u>Foliated granodiorite of upper Little Morongo Canyon (Continued)</u>						
JW259-13	41	62	43.66	2.9	142.9	4.3
JW259-14	302	480	41.49	1.1	152.5	1.7
JW259-15	376	501	41.71	1.0	152.1	1.5
JW259-16	264	192	46.04	1.2	138.9	1.7
JW259-17	269	408	42.33	1.1	150.1	1.8
JW259-1	52	90	43.12	2.2	145.0	3.4
JW259-2	178	1	42.42	1.1	149.8	1.7
JW259-3	97	158	42.92	1.5	148.1	2.3
JW259-4	367	328	41.44	0.8	153.6	1.2
JW259-5	248	278	42.57	1.1	150.0	1.7
JW259-6	292	569	41.75	0.9	152.1	1.4
JW259-7	392	822	41.78	0.8	152.0	1.2
JW259-8	93	160	40.91	1.6	153.9	2.5
JW259-9	553	557	40.43	0.6	156.9	1.0
JW259-10	111	3	73.90	1.8	86.1	1.6
JW259-11	13	11	39.34	3.3	149.5	5.6
JW259-12	57	7	61.16	2.0	98.4	2.2
JW259-13	29	19	46.66	2.5	132.4	3.5
JW259-14	234	442	43.56	1.2	145.6	1.7
JW259-15	91	157	42.88	1.6	146.0	2.7
JW259-16	464	7	55.22	1.8	115.4	2.0
JW259-16C	418	545	41.72	0.9	152.3	1.3
JW259-17	55	110	41.10	2.0	151.0	3.2
JW259-18	261	454	40.25	1.0	148.6	1.9
<u>Foliated tonalite of upper Little Morongo Canyon</u>			34.05328	116.5119	150 ± 2	
JW260-1	76	149	42.45	2.2	148.0	3.6
JW260-2	358	307	42.60	1.0	149.2	1.6
JW260-3	120	231	42.26	1.7	148.8	2.6
JW260-4	669	91	87.90	1.0	72.8	0.7
JW260-5	746	286	42.57	0.7	149.4	1.0

(Continued)

TABLE 3. SHRIMP-RG ZIRCON U-Pb DATA FOR IGNEOUS ROCKS OF THE EASTERN TRANSVERSE RANGES (Continued)

	U (ppm)	Th (ppm)	$^{238}\text{U}/^{206}\text{Pb}$	$^{207}\text{Pb}/^{206}\text{Pb}$	$^{206}\text{Pb}/^{238}\text{U}$ age (Ma)	$^{207}\text{Pb}/^{206}\text{Pb}$ age (Ma)
<u>Foliated tonalite of upper Little Morongo Canyon (Continued)</u>						
JW260-6	458	93	87.93	0.0510	4.6	72.6
JW260-7	198	128	41.69	0.0475	4.9	153.1
JW260-8	109	252	42.28	0.0480	6.6	150.9
JW260-9	72	135	42.62	0.0615	7.0	147.2
JW260-10	70	141	42.13	0.0503	7.7	151.0
<u>Granite dike of upper Little Morongo Canyon</u>			34.05274	116.511	75 ± 2	
JW261-1	479	219	88.68	0.0559	3.5	71.5
JW261-2	741	28	4.05	0.0906	0.6	1421.9
JW261-3	282	113	3.82	0.1010	0.7	1484.9
JW261-4	759	43	85.84	0.0481	2.6	74.6
JW261-5	503	334	3.97	0.0906	0.5	1449.7
JW261-6	432	223	3.19	0.1064	0.5	1758.1
JW261-7	1323	914	84.46	0.0484	2.0	75.8
JW261-8	1361	929	84.23	0.0468	2.1	76.2
JW261-9	1068	1030	85.12	0.0470	2.3	75.3
JW261-10	390	124	3.42	0.1036	0.9	1649.3
<u>Foliated granite of Covington Flat</u>			34.08029	116.341	80 ± 1	
JW262-1	7481	811	69.38	0.0477	1.0	92.3
JW262-2	191	186	74.71	0.0517	6.3	85.3
JW262-3	274	203	79.61	0.0486	5.8	80.4
JW262-4	234	164	78.59	0.0598	5.6	80.3
JW262-5	57	122	77.82	0.0565	11.5	81.4
JW262-6	227	172	80.60	0.0553	5.9	78.7
JW262-7	2083	186	80.00	0.0584	1.8	79.0
JW262-8	92	146	78.22	0.0563	8.9	81.0
JW262-9	2371	289	78.53	0.0503	1.9	81.3
<u>Granite dike at Covington Flat</u>			34.07896	116.3402	75 ± 1	
JW263-1	1513	454	86.48	0.0473	1.9	74.1
JW263-1.2C	345	51	4.32	0.0877	0.8	1341.1
JW263-2.1R	213	55	84.09	0.0495	4.8	76.0
						1685.8
						1435.3
						1642.5
						1434.1
						1736.6
						10.1
						8.6
						15.8
						1368.4
						16.2

(Continued)

TABLE 3. SHRIMP-RG ZIRCON U-Pb DATA FOR IGNEOUS ROCKS OF THE EASTERN TRANSVERSE RANGES (Continued)

		U (ppm)		Th (ppm)	$^{238}\text{U}/^{206}\text{Pb}$		$^{207}\text{Pb}/^{206}\text{Pb}$		$^{206}\text{Pb}*/^{238}\text{U}$ age (Ma)	$^{207}\text{Pb}*/^{206}\text{Pb}$ age (Ma)
<u>Granite dike at Covington Flat (Continued)</u>										
JW263-2.2C	41	23	87.96	3.5	0.0560	10.5	72.1	2.6		
JW263-3.1C	19	24	37.36	3.7	0.0529	10.4	169.5	6.2		
JW263-4.1R	781	209	84.88	0.8	0.0488	2.5	75.4	0.6		
JW263-4.2C	82	47	3.25	1.0	0.1040	1.1	1733.7	17.3	1719.5	23.4
JW263-5.1C	21	26	45.69	3.8	0.0683	9.8	136.3	5.3		
JW263-5.2R	1187	942	87.64	0.7	0.0497	2.0	72.9	0.5		
JW263-6.1R	353	79	84.15	1.2	0.0477	3.8	76.1	0.9		
JW263-6.2C	245	221	67.72	1.3	0.0492	4.1	94.4	1.3		
JW263-7.1C	19	29	40.67	3.6	0.0616	9.6	154.2	5.7		
JW263-8.1R	40	60	5.23	1.7	0.0880	2.1	1112.8	18.7	1425.4	58.5
JW263-9.1	31	20	45.92	3.1	0.0519	9.6	138.4	4.3		
JW263-10.1	89	162	83.95	2.3	0.0542	15.3	75.7	1.9		
JW263-11.1C	124	57	4.72	0.8	0.0902	1.1	1224.6	10.1	1420.4	22.5
JW263-11.1R	384	275	4.26	0.5	0.0880	0.6	1358.6	6.3	1378.4	11.9
JW263-12.1C	87	173	39.99	1.7	0.0502	5.0	159.0	2.8		
JW263-13.1C	418	58	3.15	0.4	0.1060	0.5	1781.6	8.0	1729.3	8.8
JW263-14.1C	204	136	86.34	1.6	0.0502	4.8	74.0	1.2		
JW263-15.1	1029	370	83.21	0.8	0.0482	2.3	76.9	0.6		
JW263-16.1	678	354	81.51	0.9	0.0496	2.7	78.4	0.7		
JW263-17.1C	1127	355	4.03	0.3	0.1042	0.3	1402.1	5.2	1698.9	6.0
JW263-18.1R	948	231	85.60	0.7	0.0476	2.3	74.9	0.5		
JW263-18.2C	56	114	4.15	1.2	0.0893	1.6	1389.5	16.8	1377.3	38.4
JW263-19.1C	349	313	43.73	1.8	0.0495	2.6	145.7	2.6		
JW263-19.2R	54	71	40.76	2.3	0.0535	6.5	155.4	3.6		
JW263-20.1	55	98	83.19	3.1	0.0603	8.7	75.8	2.4		
JW263-21.1C	313	16	84.41	1.3	0.0459	4.1	76.1	1.0		
JW263-22.1C	717	41	3.29	0.4	0.1051	0.4	1710.6	6.6	1718.4	6.8
JW263-23.1C	96	114	3.38	0.9	0.1029	1.0	1669.6	15.3	1685.5	19.2
JW263-24.1C	2092	199	3.76	0.2	0.0952	1.1	1517.0	3.9	1531.8	19.8

(Continued)

TABLE 3. SHRIMP-RG ZIRCON U-Pb DATA FOR IGNEOUS ROCKS OF THE EASTERN TRANSVERSE RANGES (Continued)

	U (ppm)	Th (ppm)	$^{238}\text{U}/^{206}\text{Pb}$	$^{207}\text{Pb}/^{206}\text{Pb}$	$^{206}\text{Pb}^*/^{238}\text{U}$ age (Ma)	$^{207}\text{Pb}^*/^{206}\text{Pb}$ age (Ma)
<u>Granite dike at Covington Flat (Continued)</u>						
JW263-25.1C	1145	239	83.21	0.0492	2.1	76.8 0.5
JW263-26.1C	753	131	28.14	0.0491	1.6	225.5 1.4
<u>Dioritic gneiss of Covington Flat</u>			34.08118	116.3443		78 ± 3
JW264-1	1807	3341	84.02	0.0474	2.0	76.0 0.4
JW264-2	1747	3103	82.20	0.0475	2.0	77.7 0.4
JW264-3	257	256	78.86	0.0481	5.0	80.6 1.1
JW264-4	1394	2921	81.30	0.0461	2.3	78.8 0.4
<u>Granite of Squaw Tank</u>			581951	3757815		79.5 ± 1.1
529Z-1	529	288	79.19	0.0486	4.0	80.8 0.9
529Z-2	270	354	76.66	0.0581	5.0	82.4 1.2
529Z-3	3014	849	47.86	0.0537	1.2	132.5 0.5
529Z-4	87	141	82.27	0.0675	8.2	75.9 3.2
529Z-5	937	538	79.90	0.0510	3.5	79.8 0.6
529Z-6	402	204	82.72	0.0514	4.3	77.1 0.9
529Z-7	504	326	79.49	0.0508	3.4	80.3 0.8
529Z-8	687	298	80.05	0.0495	3.0	79.8 0.7
529Z-9	369	183	80.25	0.0527	4.0	79.3 0.9
529Z-10	570	277	82.09	0.0523	3.6	77.6 0.7
<u>Granodiorite of Quail Mountain</u>			570845	3761991		81.1 ± 1.2
537Z-1	774	414	78.10	0.0484	2.6	81.9 0.6
537Z-2	378	237	77.81	0.0483	3.8	82.3 0.8
537Z-3	396	172	81.88	0.0504	3.7	78.0 0.8
537Z-4	426	216	78.23	0.0502	3.4	81.6 0.8
537Z-5	1317	3519	78.32	0.0472	2.0	81.8 0.5
537Z-6	682	203	41.79	0.0740	1.7	147.7 1.1
537Z-7	587	150	4.19	0.0889	0.5	1377.8 4.9
537Z-8	321	158	3.32	0.1088	0.6	1687.0 8.1
537Z-9	300	119	80.63	0.0492	4.2	79.3 0.9
537Z-10	171	183	77.05	0.0576	5.2	82.1 1.2
537Z-11	329	224	75.43	0.0496	4.7	84.7 0.9

(Continued)

TABLE 3. SHRIMP-RG ZIRCON U-Pb DATA FOR IGNEOUS ROCKS OF THE EASTERN TRANSVERSE RANGES (Continued)

	U (ppm)	Th (ppm)	$^{238}\text{U}/^{206}\text{Pb}$	$^{207}\text{Pb}/^{206}\text{Pb}$	$^{206}\text{Pb}^*/^{238}\text{U}$ age (Ma)	$^{207}\text{Pb}^*/^{206}\text{Pb}$ age (Ma)
<u>Granodiorite of Quail Mountain (Continued)</u>						
537Z-12	102	70	80.44	0.0555	6.7	1.6
537Z-13	734	494	79.61	0.0488	2.6	0.6
537Z-14	398	184	77.24	0.0502	3.3	0.8
537Z-15	822	337	80.35	0.0489	2.4	0.5
537Z-16	142	292	87.02	0.0512	6.2	1.3
<u>Granite of Stubbe Springs</u>			572719	3758168	76 ± 4	
544-1	1519	133	28.38	0.0519	1.1	0.8
544-1.2	141	62	3.56	0.1023	1.0	11.4
544-2	139	107	88.33	0.0548	6.5	1.3
544-3	1352	1699	41.25	0.0500	1.5	0.7
544-4	165	144	70.36	0.1424	5.5	2.1
544-5	2175	52	3.51	0.1037	0.5	1609.9
544-6	722	401	78.06	0.0498	2.7	81.8
544-7	66	48	82.92	0.0594	8.4	76.1
544-8	912	86	3.55	0.1046	0.6	1589.9
544-9	485	158	4.74	0.1027	0.6	1204.3
544-10	152	196	84.01	0.0560	5.6	75.5
544-11	5832	7035	79.76	0.0475	1.0	80.3
544-12	125	305	43.34	0.0524	4.9	146.4
544-13	514	280	3.25	0.1076	0.5	1724.6
544-14	73	48	75.44	0.2044	4.4	68.2
544-15	52	37	89.89	0.0666	9.3	69.6
544-16	901	88	3.58	0.1012	0.6	1580.6
544-17	200	126	3.17	0.1110	0.7	1759.7
544-18	423	193	3.38	0.1044	0.5	1667.5
544-19	131	86	42.26	0.0492	4.7	150.7
544-20	366	358	87.28	0.0476	4.2	73.4
<u>Tonalite of Bighorn</u>			571669	3756692	82.0 ± 1.6	
548-1	203	143	79.71	0.0507	5.1	80.1
548-2	89	89	76.23	0.0549	7.2	83.3

(Continued)

TABLE 3. SHRIMP-RG ZIRCON U-Pb DATA FOR IGNEOUS ROCKS OF THE EASTERN TRANSVERSE RANGES (Continued)

Tonallite of Bighorn (Continued)		U (ppm)	Th (ppm)	$^{238}\text{U}/^{206}\text{Pb}$	$^{207}\text{Pb}/^{206}\text{Pb}$	$^{206}\text{Pb}^*/^{238}\text{U}$ age (Ma)	$^{207}\text{Pb}^*/^{206}\text{Pb}$ age (Ma)				
548-3	102	109	76.39	1.9	0.0568	6.5	82.9	1.6			
548-4	34	66	78.03	3.3	0.0650	10.7	80.3	2.8			
548-5	212	202	75.27	1.5	0.0495	6.7	84.9	1.3			
548-6	117	42	3.26	0.8	0.1075	1.0	1722.3	13.6	1750.2	17.8	
548-7	156	57	3.23	0.8	0.1078	1.3	1737.9	13.9	1760.5	25.0	
548-8	72	76	60.18	2.0	0.1564	4.3	91.8	2.8			
548-9	106	111	78.30	1.9	0.0512	6.9	81.4	1.6			
548-11	75	90	78.97	2.3	0.0620	7.6	79.6	1.9			
548-10	49	70	70.78	2.7	0.0648	8.8	88.5	2.5			
548-12	233	99	78.09	1.3	0.0527	4.6	81.5	1.1			
548-13	68	64	79.11	2.4	0.0581	8.4	79.9	2.0			
548-14	533	27	3.89	0.4	0.0998	0.5	1464.2	5.5	1616.4	9.3	
548-15	2226	76	3.27	0.2	0.1059	0.2	1718.8	3.2	1727.4	4.2	
548-16	406	96	4.52	0.4	0.1057	0.6	1257.6	6.8	1703.3	13.2	
548-17	1252	1062	3.03	0.3	0.1069	0.3	1850.2	4.9	1740.9	5.6	
548-18	810	89	3.44	0.4	0.1044	1.1	1638.7	6.0	1701.6	19.9	
<u>Granite of Bighorn</u>				571317	3756774						
549-1	425	203	3.22	0.5	0.1073	0.5	1739.7	8.2	1748.4	9.4	
549-2	1396	64	3.51	0.3	0.1025	0.4	1611.6	4.4	1669.6	6.6	
549-3	319	80	4.46	0.5	0.0884	0.9	1297.0	6.5	1392.0	17.3	
549-4	179	302	41.88	1.2	0.0512	3.9	151.7	1.8			
549-5	973	215	3.50	0.3	0.1040	1.4	1612.0	5.3	1691.0	26.3	
549-6	1523	40	3.83	0.3	0.1025	0.3	1481.8	4.1	1666.9	6.0	
549-7	831	57	82.97	0.7	0.0509	2.6	76.9	0.6			
549-8	480	151	3.45	0.4	0.1061	0.5	1629.8	6.7	1729.3	9.8	
549-9	694	11	5.73	0.5	0.0958	1.3	1010.6	6.0	1548.2	23.9	
549-10	1210	190	3.35	0.3	0.1037	0.9	1685.6	5.0	1688.3	16.6	
549-11	1549	193	3.40	0.3	0.1031	0.3	1659.2	4.2	1680.7	5.1	
549-12	932	43	4.76	0.3	0.0897	0.5	1217.4	4.2	1424.1	9.9	

(Continued)

TABLE 3. SHRIMP-RG ZIRCON U-Pb DATA FOR IGNEOUS ROCKS OF THE EASTERN TRANSVERSE RANGES (Continued)

	U (ppm)	Th (ppm)	$^{238}\text{U}/^{206}\text{Pb}$	$^{207}\text{Pb}/^{206}\text{Pb}$	$^{206}\text{Pb}^*/^{238}\text{U}$ age (Ma)	$^{207}\text{Pb}^*/^{206}\text{Pb}^*$ age (Ma)
<u>Granite of Palms</u>						
			579493	3761737	77.2 ± 0.6	
561Z-1	933	1107	83.14	0.7	76.9	0.5
561Z-2	383	297	82.18	1.1	77.9	0.8
561Z-3	744	1189	82.13	0.8	78.1	0.6
561Z-4	380	363	93.60	1.1	66.7	0.8
561Z-5	885	1006	84.39	0.7	75.7	0.5
561Z-6	1087	1394	82.34	0.7	77.3	0.6
561Z-7	1901	4332	82.49	0.5	77.8	0.4
561Z-8	755	976	83.08	0.7	77.0	0.6
561Z-9	263	295	83.34	1.2	76.3	1.0
561Z-10	928	1176	82.93	0.7	77.2	0.5
<u>Granite of Smoke Tree Well</u>						
			607221	3740214	75.0 ± 1.4	
03456-1	285	171	88.0	1.5	72.7	1.1
03456-2	294	209	85.5	1.5	74.8	1.2
03456-3	301	227	84.5	1.5	75.6	1.2
03456-4	293	196	84.0	1.6	76.5	1.2
03456-5	988	1165	3.2	0.7	1775.4	12.7
03456-6	371	230	83.8	1.4	76.4	1.1
03456-7	480	361	84.3	1.3	76.1	1.0
03456-8	409	167	87.0	1.3	73.5	1.0
03456-9	621	37	12.7	0.8	472.2	3.9
03456-10	416	134	9.9	0.9	598.8	5.7
<u>Granite of Oasis</u>						
			582629	3774034	103 ± 1	
03508-1	6613	971	61.9	0.2	103.2	0.3
03508-2	5136	727	62.3	0.3	102.6	0.3
03508-3	1413	534	58.1	0.5	108.3	0.6
03508-4	58	42	63.6	2.3	99.6	2.3
03508-5	4940	640	63.1	0.3	101.3	0.3
03508-6	757	897	95.0	0.9	66.3	0.6
03508-7	8216	1493	65.8	0.2	93.3	0.3

(Continued)

TABLE 3. SHRIMP-RG ZIRCON U-Pb DATA FOR IGNEOUS ROCKS OF THE EASTERN TRANSVERSE RANGES (Continued)

Granite of Oasis (Continued)		U (ppm)	Th (ppm)	$^{238}\text{U}/^{206}\text{Pb}$	$^{207}\text{Pb}/^{206}\text{Pb}$	$^{206}\text{Pb}^*/^{238}\text{U}$ age (Ma)	$^{207}\text{Pb}^*/^{206}\text{Pb}^*$ age (Ma)
03508-8	5784	788	62.3	0.3	0.0	102.7	0.3
03508-9	608	48	3.4	3.3	0.1	1679.8	54.1
03508-10	6134	715	62.4	0.3	0.1	102.1	0.3
03508-11	4715	610	61.8	0.3	0.0	103.5	0.3
03508-12	5279	783	61.7	0.3	0.0	103.6	0.3
03508-13	927	461	64.0	0.6	0.0	99.8	0.6
03508-14	258	123	3.3	0.6	0.1	1684.5	9.9
03508-15	611	508	41.9	0.6	0.1	150.9	1.0
03508-16	289	227	41.5	0.9	0.1	151.9	1.5

*Locations in latitude and longitude, or in UTM NAD27.

†Interpreted crystallization age.

SHRIMP-RG—sensitive high-resolution ion microprobe—reverse geometry.

to prismatic, up to 200 μm in longest dimension, and many contain prominent pre-magmatic cores overgrown by oscillatory-zoned magmatic zircon rims. Three analyzed pre-magmatic cores yielded discordant Proterozoic ages; excluding these, seven oscillatory-zoned zircons yielded a weighted mean $^{206}\text{Pb}^*/^{238}\text{U}$ age of 75.0 ± 1.4 Ma (MSWD [mean square of weighted deviations] = 1.8; Fig. 5A).

The granodiorite of Porcupine Wash [PW in figure 3; part of Pinto Basin granodiorite of Powell (2001)] is a sphene-hornblende-biotite granodiorite that intrudes Proterozoic gneiss just northeast of the granite of Smoke Tree Well. Zircons from a sample of this granodiorite are euhedral and prismatic, up to 250 μm in long dimension, display oscillatory zoning and lack evidence of pre-magmatic cores. Excluding one significantly younger grain, nine grains yield a weighted mean $^{206}\text{Pb}^*/^{238}\text{U}$ age of 75 ± 2 (MSWD = 3.5; Fig. 5B). This age is in good agreement with a second sample of this pluton that yielded an age of 76.1 ± 1.4 Ma (MSWD = 0.8; Barth et al., 2004), and suggests the granodiorite is contemporaneous with the granite of Smoke Tree Well.

To the northwest, the granite of Squaw Tank (ST in Fig. 3) occupies the southern half of the granite originally mapped as granite of White Tank by Rogers (1954), but our observations suggest it is a texturally distinct, seriate metaluminous to weakly peraluminous hornblende biotite granite (Palmer, 2005). Zircons are euhedral and prismatic, with oscillatory zoned interiors that range from generally CL-bright cores to CL-dark, U-enriched rims. Excluding one exceedingly U-rich, significantly older grain, nine grains yield a weighted mean $^{206}\text{Pb}^*/^{238}\text{U}$ age of 79.5 ± 1.1 (MSWD = 3.1; Fig. 5C). This age confirms the distinction of this granite body from the allanite biotite granite of White Tank to the northeast, which yielded a Late Jurassic U-Pb zircon age (Barth et al., 2008).

Still farther to the northwest, the granite of Palms (P in Fig. 3) was originally mapped by Rogers (1954) as both granite of Palms and granite of White Tank, but was correlated with the White Tank by Dibblee (1968) and Brand (1985); our observations suggest it is a texturally distinct, weakly peraluminous sphene biotite granite (Palmer, 2005). Geochronology confirms this distinction, and so we retain the name granite of Palms as originally assigned to part of this pluton by Rogers (1954) as a means to distinguish it from the Late Jurassic granite of White Tank. A sample of this granite yielded subhedral, broken prismatic zircons up to 500 μm in long dimension with CL-dark, oscillatory zoned interiors. About 15% of zircon grains contain anhedral, irregularly zoned cores that were avoided in our analyses. Excluding one significantly younger grain, nine grains yield a weighted mean $^{206}\text{Pb}^*/^{238}\text{U}$ age of 77.2 ± 0.6 (MSWD = 1.8; 5D). This age is in agreement with the 75.5 ± 1.6 Ma age of relatively mafic granite from the interior of the Palms pluton (Barth et al., 2004).

The granite of Oasis (O in Fig. 3; Brand, 1985) is a texturally distinct, fine-grained peraluminous garnet muscovite granite intruding older Triassic granite. Zircons are of two texturally distinct types; euhedral to anhedral, oscillatory zoned zircons and

zircon cores, and CL-dark, exceedingly U-rich zircon grains and rims on oscillatory zoned cores. Four oscillatory zoned zircon grains and cores yielded older ages, including two concordant Paleoproterozoic ages, two Late Jurassic ages identical to the age of the White Tank granite to the south, and one Early Cretaceous age. All CL-dark zircons and rims and two oscillatory-zoned cores yield medial to Late Cretaceous ages. Nine grains yield a weighted mean age of 103 ± 1 Ma (MSWD = 8.4; Fig. 5E). Excess scatter in these data may indicate some additional Pb loss but this has little effect on the calculated age. We conclude that the Oasis granite has an age of ca. 103 Ma, older and compositionally distinct from metaluminous to weakly peraluminous biotite granodiorite and granite that comprises the bulk of Late Cretaceous plutons in the study area.

In summary, Cretaceous granites in the central and eastern part of the study area include mid-Cretaceous peraluminous garnet granite and many relatively homogeneous, metaluminous to weakly peraluminous biotite granodiorite to granite plutons of Late Cretaceous age. Combining the ages reported here with those reported by Barth et al. (2004), we conclude that Late Cretaceous plutons range in age from ca. 82–76 Ma in the eastern Transverse Ranges to ca. 74–73 Ma to the east in adjacent parts of the south-central Mojave Desert (Fig. 2).

Geochronology of Sheeted Plutonic Bodies in the Little San Bernardino Mountains

We analyzed a reconnaissance sample set consisting of diorite, granodiorite and granite to assess the age of components of the magmatic sheeted complex along its entire length in the Little San Bernardino Mountains. Results suggest the complex includes Late Jurassic and Late Cretaceous igneous components whose crystallization ages are comparable to Late Jurassic and Late Cretaceous upper-crustal granodiorite to granite plutons exposed to the east. No components of the sheeted complex have yet been identified that overlap in age with the Triassic and Middle Jurassic plutons, although these older plutons typically outcrop somewhat farther to the east than the Late Jurassic and Late Cretaceous plutons.

The most mafic sample examined is a foliated diorite from Covington Flat (CF in Fig. 3) in the northern part of the complex. Zircons in this sample are subhedral, complexly zoned and partially resorbed, with CL-bright overgrowths up to ~20 μm thick. Four zircon interiors range from 81 to 76 Ma, and yield an estimated age of 78 ± 3 Ma.

Mafic tonalite to granodiorite sheets are a volumetrically dominant component of the sheeted complex regionally, as well as locally where we have mapped it at 1:24,000 scale. We analyzed ten samples of tonalite and granodiorite collected along the length of the sheeted complex. Data for all samples are summarized in Table 2 and all analyses are reported in Table 3; Concordia plots for representative samples are shown in Figure 6. The majority of the samples contain premagmatic zircons of Paleoproterozoic age as well as oscillatory-zoned magmatic zircon

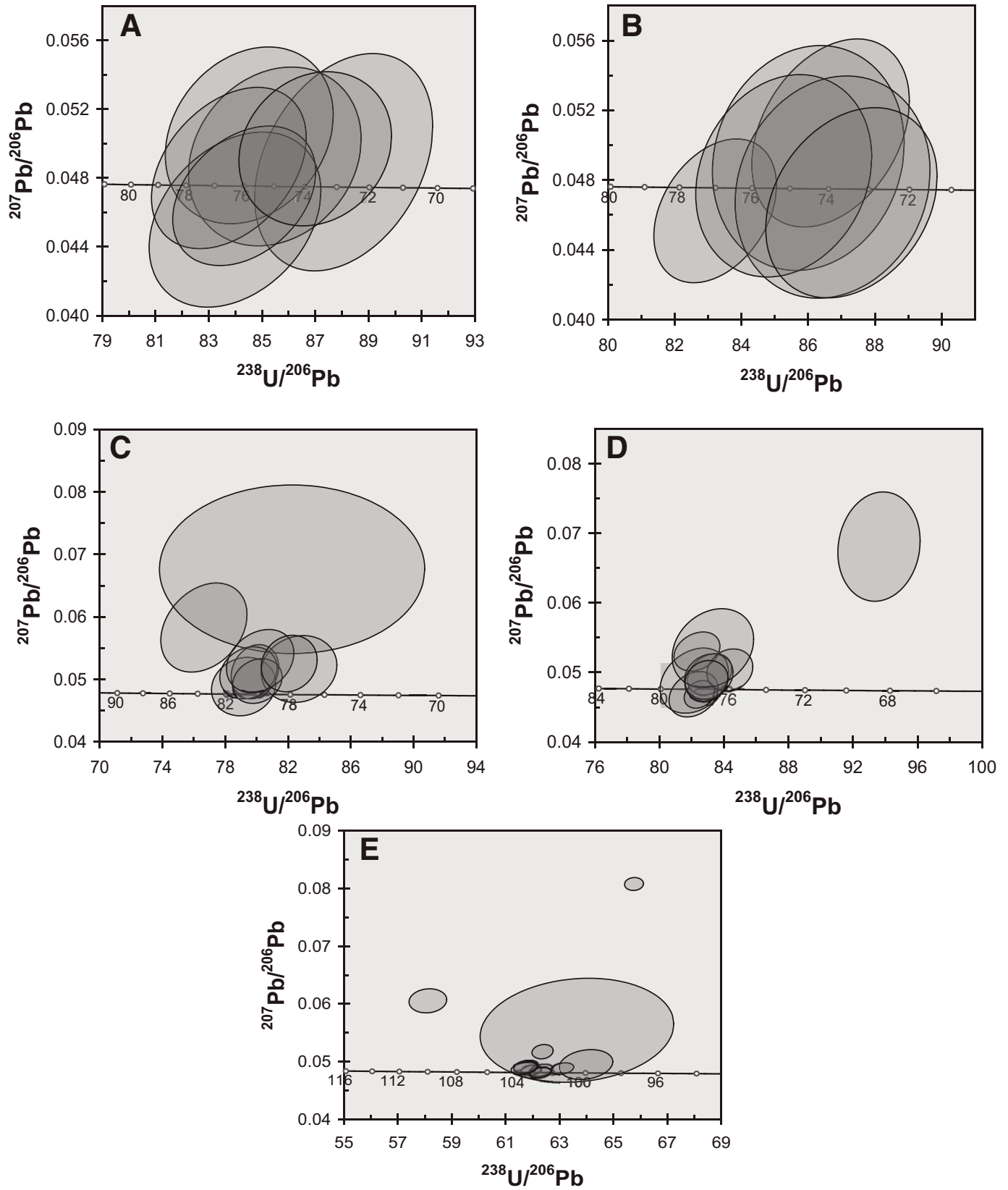


Figure 5. Concordia diagrams for Cretaceous plutons in the Hexie and Pinto Mountains. (A) granite of Smoke Tree Well; (B) granodiorite of Porcupine Wash; (C) granite of Squaw Tank; (D) granite of Palms; (E) granite of Oasis. See Figure 3 for locations.

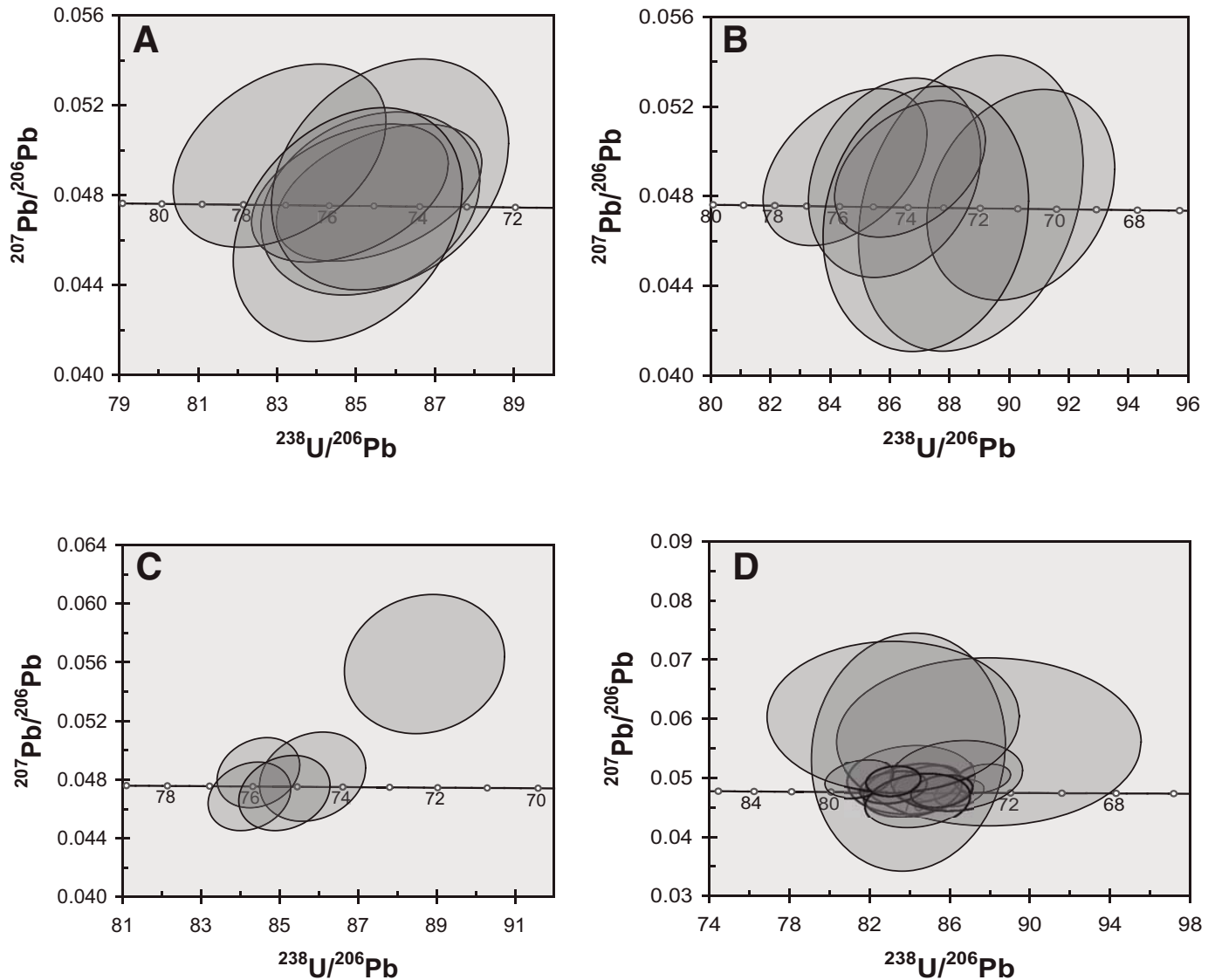


Figure 6. Concordia diagrams for the youngest Cretaceous components of the sheeted complex in the Little San Bernardino Mountains. (A) Granodiorite of Fargo Canyon; (B) granite of lower Pinkham Canyon; (C) granite dike of upper Little Morongo Canyon; (D) granite dike at Covington Flat. See Figure 3 for locations.

and magmatic overgrowths. Two samples, a foliated tonalite and a foliated granodiorite from the northern end of the complex in Little Morongo Canyon (LM in Fig. 3) yielded Late Jurassic ages of 152 ± 1 (MSWD = 3.8) and 150 ± 2 Ma (MSWD = 0.6); each sample has a few younger grains, whose ages were excluded from the calculation because we infer that they were affected by loss of radiogenic Pb during reheating by younger magmatism. Eight additional samples from throughout the complex, after excluding pre-magmatic grain ages, yielded inferred crystallization ages from 82 Ma to the youngest well-defined age of 75.4 ± 0.8 Ma (MSWD = 0.7; Fig. 6A).

We also analyzed eleven samples of granite from the same localities along the length of the sheeted complex (Table 2 and

Fig. 3). Two samples of granite from the southern end of the complex in Fargo Canyon and Berdoo Canyon (F and B in Fig. 3) yielded Late Jurassic ages of 153 ± 3 (MSWD = 3.1) and 150 ± 2 Ma (MSWD = 1.8), which are indistinguishable in age from the older group of granodiorites. Nine additional granites from throughout the complex, after excluding pre-magmatic grain ages, yielded inferred crystallization ages from 83 Ma to the youngest well-defined ages of 74 ± 2 Ma (MSWD = 2.6; Fig. 6B) and 74 ± 2 Ma (MSWD = 2.9). Thus, the range in crystallization ages of granites completely overlaps the ages of diorite and granodiorite.

Granite dikes range in dip from gentle to steep and cut the moderately dipping foliation in sheeted diorite, granodiorite and granite. Three samples have abundant pre-magmatic zircon with

Mesoproterozoic and Paleoproterozoic ages and magmatic zircon overgrowths. One sample yielded scattered Late Cretaceous ages for magmatic zircon that did not give a precise crystallization age, but two other samples yield ages of ca. 75 Ma (Figs. 6C and 6D). The ages of these dikes are thus indistinguishable from the age of the youngest granodiorites and granites. They provide the best estimate of the minimum age for magmatism and final development of the moderately east-dipping fabric in the sheeted complex.

Summary of Regional Intrusive Chronology

New ion microprobe results reported here, when combined with recently reported ages across the broader region, yield a clear picture of episodic, migratory plutonism across southeastern California and through a range of crustal depths within the upper and middle crust (Fig. 2). Mesozoic magmatism commenced with plutonism which migrated from northwest to southeast across the region in Permo-Triassic to Late Triassic time (Barth and Wooden, 2006). Following a 25 Ma hiatus, Jurassic magmatism commenced with volcanism at 181 Ma (Schermer et al., 2002; Fohey et al., 2005). No plutonism synchronous with the initial volcanism is recognized, but Middle and Late Jurassic plutonism and volcanism were synchronous across the region, apparently migrating from east to west between ca. 167 and 149 Ma (Barth et al., 2008). Following a second hiatus of ca. 25 Ma duration, plutonism and volcanism commenced ca. 125 Ma in western California in the Sierra Nevada–Salinia region (e.g., Bateman, 1992; Kistler and Champion, 2001); magmatism continued while slowly migrating eastward until ca. 85 Ma, when it migrated rapidly eastward across southeastern California between ca. 82 Ma and 72 Ma. Late Jurassic and Late Cretaceous episodes of plutonism at upper-crustal levels in the eastern Transverse Ranges were associated with construction of the underlying sheeted complex in the Little San Bernardino Mountains.

No plutons have been recognized in the study area younger than ca. 73 Ma, and the youngest components of the mid-crustal sheeted complex are 74 Ma. $^{40}\text{Ar}/^{39}\text{Ar}$ ages from the sheeted complex indicate that cooling of mid-crustal rocks began immediately after final emplacement. Hornblende ages of Jurassic and Cretaceous mafic intrusive rocks from Little Morongo Canyon, Covington Flats, and Berdoo Canyon (Fig. 3) range from 76.3 Ma to 72.9 Ma (Wooden et al., 2001). Biotite ages of these same rocks and associated Jurassic and Cretaceous granite sheets and two Late Cretaceous granite dikes yielded cooling ages from 71 to 66.5 Ma.

DISCUSSION

Regional structural relationships in central and southern California provide a framework for understanding tilting and exhumation of the eastern Transverse Ranges crustal section, because regional arc evolution, underthrusting by ensimatic schist terranes, and regional crustal cooling progressed from northwest

to southeast in Late Cretaceous to Eocene time (Grove et al., 2003). Northwest of the Transverse Ranges, Late Cretaceous magmatism ended and cooling of arc crust began ca. 80 Ma, essentially synchronous with emplacement and metamorphism of the Rand and Portal Ridge schists and the correlative Schist of Sierra de Salinas in the Salinian block (Barth et al., 2003; Grove et al., 2003). Emplacement of the Orocopia schist now exposed in the Orocopia Mountains immediately to the southeast of the eastern Transverse Ranges occurred by underthrusting between ca. 68 and 56 Ma (Jacobson et al., 2000, 2007). U-Pb ages in this study indicate that magmatism in the intervening region of the Transverse Ranges continued until ca. 72 Ma, and $^{40}\text{Ar}/^{39}\text{Ar}$ ages of biotite indicate that regional cooling of the arc crust had begun by 71 Ma. These data do not allow us to discern whether regional crustal cooling resulted directly from exhumation of the tilted section, from refrigeration of the crust by underthrusting of schists, or from a combination of these effects. Further low-temperature geochronologic data are needed to evaluate the relative significance of refrigeration and exhumation-related cooling. Nevertheless, in a regional context it appears likely that the tilting and exhumation of this crustal section is directly related to arc extinction and schist underplating during Laramide orogenesis.

Our thermobarometric results are consistent with west-side-up block tilting as a mechanism to exhume the arc section. However, our sample set is not sufficiently dense to evaluate the significance of syn-exhumation faulting within the tilted section. Postlethwaite (1988) and Howard (2002) suggested that Late Mesozoic and/or Cenozoic top-to-the-east normal faulting played a role in exhuming lower plate rocks in the western part of the study area. Thermochronologic data are needed to evaluate the timing of movement across these structures and their relative significance in contributing to exhumation of the eastern Transverse Ranges.

In addition to its significance in understanding the regional progression of arc extinction and Laramide underthrusting in southern California, the tilted eastern Transverse Ranges crustal section is significant because it provides an oblique window into depth-dependent changes in structural style and magmatic character in the Cordilleran continental margin arc. The eastern, upper-crustal part of the section is primarily composed of Late Jurassic and Cretaceous, relatively homogeneous, granodioritic to granitic plutons emplaced into Paleoproterozoic and older Mesozoic wallrocks. However, the base of the tilted crustal section in the Little San Bernardino Mountains is a moderately dipping sheeted magmatic complex, at least 5 km thick, constructed synchronously, but structurally beneath these upper crustal plutons and their associated volcanoes. The scale of this tilted section suggests that the geometric and compositional features of the arc exposed here may be fundamental features of the Cordilleran arc where it was constructed on thick Paleoproterozoic crust (Fig. 7). The discrete mid-crustal sheeted magmatic complex we have described is in some ways reminiscent of geometry predicted to occur in the middle crust on theoretical geophysical grounds (Glazner and Ussler, 1988; Meissner and Mooney, 1998), and is

broadly similar to features described to the northwest in Salinian block arc rocks (Ducea et al., 2003), but is unique in its moderate to shallow dip and intra-cratonic setting.

The origin of the sheeted middle-crustal zone is unclear; it may represent a density boundary not conducive to transport of hydrous mafic magmas into the upper crust, a rheological boundary that controlled the style of pluton inflation, favoring thin sheets rather than more homogeneous plutons, or a décollement associated with relative motion between the arc superstructure and an actively shortening lower lithosphere. We tested the first hypothesis by developing a density and P-wave velocity (V_p) model for the crustal section in the eastern Transverse Ranges, using density measurements on surface samples (Fig. 8). Density measurements were converted to V_p at appropriate depths using the paleodepth relation derived above and the density-velocity relation and average heat flow model of Christensen and Mooney (1995; Zoback and Mooney, 2003). This model corresponds to a geothermal gradient of ~ 15 °C/km, which we take to be reasonable for crust outside the active plutonic zone in this long-lived, migratory arc setting. Higher heat flow, corresponding to a gradient of ~ 25 °C/km and more appropriate to times of active plutonism, would result in a 1%–2% decrease in computed V_p , which is insignificant compared to the lithologic variation in the exposed arc section. Our resulting V_p model is approximated by a homogeneous upper crust with an average V_p of 6.2 km/sec (density ~ 2750 kg/m³). This result is broadly similar to the global average continental arc structure derived by Christensen and

Mooney (1995) from refraction surveys, and to the upper-crustal structure of parts of the southern Mojave Desert and eastern Transverse Ranges, which experienced minimal Laramide and younger exhumation (Hauksson, 2000). There is some suggestion in these data that the sheeted complex lies in a region of the middle crust where higher density (and computed V_p) framework rocks are more common (ca. 15 km paleodepth; Fig. 8). However, we caution that the ages of these dense, garnetiferous gneisses found along the margin of the sheeted complex at this depth are not known, and computed V_p could be misleading if their densities increased by metamorphic dehydration associated with assembly of the underlying sheeted complex (e.g., Barboza and Bergantz, 2000). We conclude from these data that the 6.2 km/sec upper crust in this region is typical of continental arc settings worldwide, and so the sheeted middle crust may be as well. We can also conclude that, if buoyancy forces play an important role in magma ascent, hydrous mafic magmas may have been able to ascend through more dense lower and middle crust of the arc but been impeded from transiting ~ 2750 kg/m³ upper crust without further differentiation and/or mixing with felsic magmas.

A second hypothesis is that rheological boundaries may preferentially trap magmas in the mid-crust (Pitcher, 1979; Hogan et al., 1998). These rheological boundaries may reflect a stress boundary (either a maximum or minimum) and/or a material strength boundary that somehow interferes with the rise of magma as a function of its ascent mechanism. For example, magmas ascending in dikes along cracks may have the propagation of

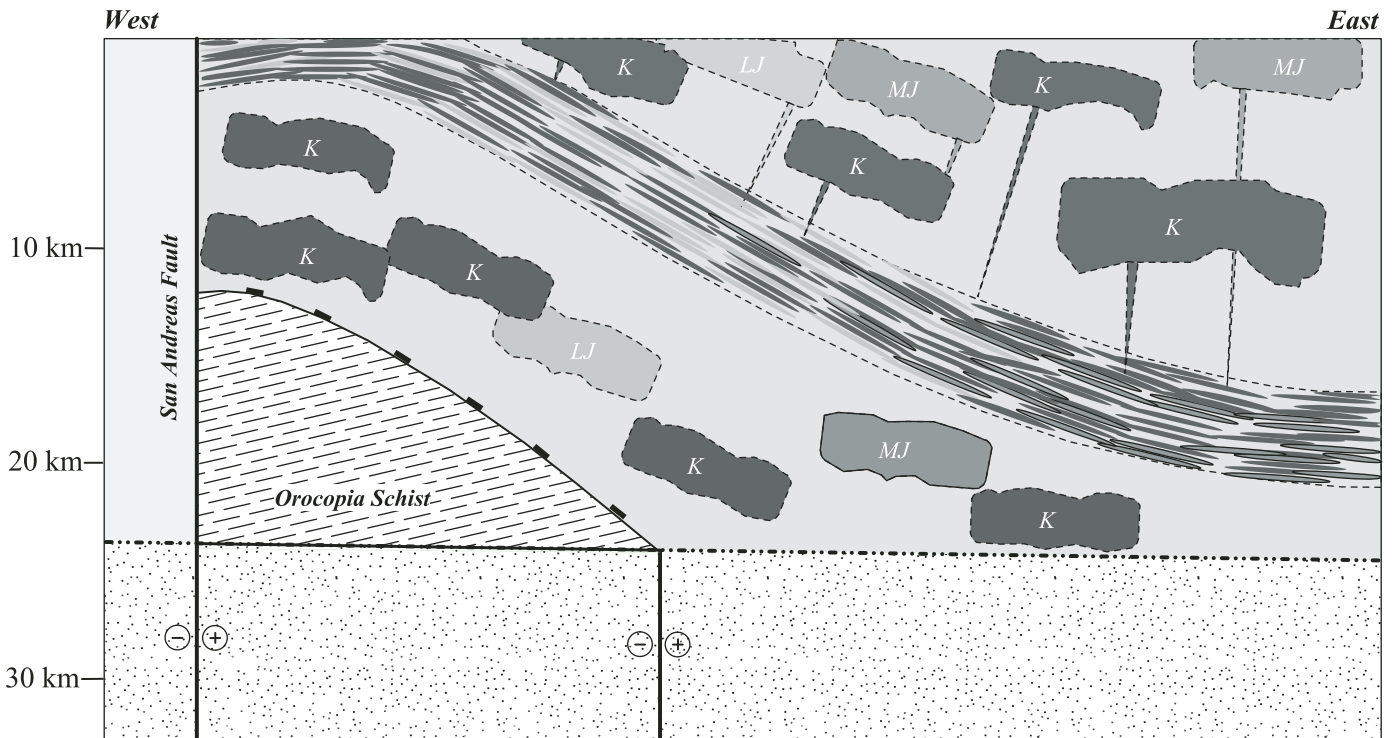


Figure 7. Schematic cross section of the eastern Transverse Ranges crustal section. See Figure 3 for map unit abbreviations.

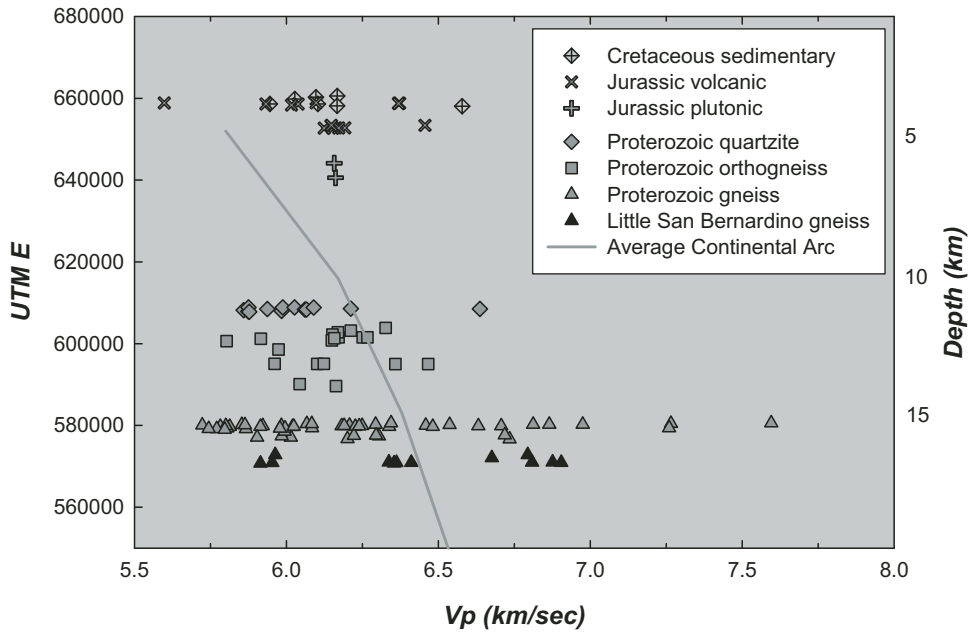


Figure 8. Model crustal Vp structure for the eastern Transverse Ranges. Vp calculated from density using the average heat flow model of Christensen and Mooney (1995). Depth calculated from easting coordinates based on the regression in Figure 4. Global average continental arc Vp from Christensen and Mooney (1995).

the crack tips influenced by the stress or strength characteristics of the host rock. Magma ascending in diapirs may require greater energy to “process” colder, stronger host rocks at such a rheological boundary.

There are a number of issues that concern us about these hypotheses. One is the observation (including in the Cascades core; e.g., Miller et al., 2003, this volume) that many plutons, both diapir-like and dike-like, do make it across these boundaries and are now emplaced at higher crustal levels, or even made it to the surface and fed volcanoes. Another concern is our view that partially crystallized magma bodies have sufficient heat and buoyancy to continue to process host rock by either ductile or brittle processes, such as thermal softening and flow or thermal cracking and stoping (Marsh, 1982). In the eastern Transverse Ranges crustal section many shallow-crustal plutons indicate that magma of the same ages as that in the sheeted complex did rise higher into the crustal section. So the sheeted complex at best was not a dramatic rheology boundary and magma trap. This conclusion is consistent with our preliminary field studies, which indicate that fairly similar rock types and structures occur both below and above the sheeted complex. However, additional work is required to assess whether less obvious changes exist across this boundary that preferentially trapped at least some of the rising magmas.

If arc and retroarc deformation are coupled with (and ultimately driven by) subduction processes, then one or more mid-crustal or basal crustal detachments may have linked retroarc shortening to the convergent margin in Mesozoic time (Oldow et al., 1989). The southern Sevier, East Sierran, and Maria foreland fold-and-thrust belts, and associated sediments in the southern Sevier and Maria foreland basins record foreland shortening contemporaneous with Late Jurassic and medial Cretaceous

magmatism (Fleck et al., 1994; Walker et al., 1995, 2002; Barth et al., 2004). However, there is presently little evidence for pervasive ductile deformation within the mid-crustal part of the section, but our observations are limited by the small quantity of remaining host rocks in the areas we have thus far mapped in detail.

Further work in this tilted section will focus on the density and velocity structure of the crustal section, to evaluate the role of possible density contrast in determining pluton emplacement style. The geochemical diversity of the heterogeneous sheeted complex and a comparative analysis of the homogeneous or zoned upper-crustal plutons will provide a unique view of depth-dependent changes in composition during magma transfer through, and emplacement within, the Proterozoic host rocks of the arc. Finally, understanding variations in structure and petrofabric in the sheeted complex as a function of composition and time will allow evaluation of the role of magmatic differentiation and synchronous strain in evolution of arc middle crust.

ACKNOWLEDGMENTS

The National Science Foundation (EAR-0106881, -0408730, and -0809003), the National Geographic Society (7214-02), the U.S. Geological Survey, the Southern California Earthquake Center, and the Joshua Tree National Park Association provided support for this research. We are grateful to the staff at Joshua Tree National Park who have continually supported and encouraged our fieldwork, and to Kenneth Brown, Nicole Fohey, Kristin Hughes, Emerson Palmer, and Kelly Probst who assisted with sample collections. We thank Brad Ito for his continuing efforts to keep the SHRIMP-RG in shape, and Frank Mazdab for assistance with the ion microprobe laboratory work. We thank Chusi Li for assistance with the electron microprobe

work, and Christina Forbes and Laqueshia Curry for providing invaluable help with laboratory measurements. Carl Jacobson and Dee Trent provided very helpful discussions, and Calvin Miller, Keith Howard, and Bob Miller provided constructive and thoughtful reviews.

REFERENCES CITED

- Anderson, J.L., and Smith, D.R., 1995, The effect of temperature and oxygen fugacity on Al-in-hornblende barometry: *The American Mineralogist*, v. 80, p. 549–559.
- Anderson, J.L., Barth, A.P., Bender, E.E., Davis, M.J., Farber, D.L., Hayes, E.M., Johnson, K.A., Young, E.D., Wooden, J.L., and Tosdal, R.M., 1990, San Gabriel (Tujunga) terrane—Coming home to Mojave: *Geological Society of America Abstracts with Programs*, v. 22, no. 7, p. A303.
- Anderson, J.L., Barth, A.P., Young, E.D., Bender, E.E., Davis, M.J., Farber, D.L., Hayes, E.M., and Johnson, K.A., 1992, Plutonism across the Tujunga-North American terrane boundary: A middle to upper crustal view of two juxtaposed magmatic arcs, *in* Bartholomew, M.J., Hyndman, D.W., Mogk, D.W., and Mason, R., eds., *Basement tectonics 8: Characterization and comparison of ancient and Mesozoic continental margins*: Kluwer, Dordrecht, *Proceedings of the Eighth International Conference on Basement Tectonics*, p. 205–230.
- Barboza, S.A., and Bergantz, G.W., 2000, Metamorphism and anatexis in the Mafic Complex contact aureole, Ivrea zone, Northern Italy: *Journal of Petrology*, v. 41, p. 1307–1327, doi: 10.1093/ptrology/41.8.1307.
- Barth, A.P., and Wooden, J.L., 2006, Timing of magmatism following initial convergence at a passive margin, southwestern U.S. Cordillera, and ages of lower crustal magma sources: *The Journal of Geology*, v. 114, p. 231–245, doi: 10.1086/499573.
- Barth, A.P., Wooden, J.L., and Coleman, D.S., 2001a, SHRIMP-RG U-Pb zircon geochronology of Mesoproterozoic metamorphism and plutonism in the southwesternmost United States: *The Journal of Geology*, v. 109, p. 319–327, doi: 10.1086/319975.
- Barth, A.P., Jacobson, C.E., Coleman, D.S., and Wooden, J.L., 2001b, Construction and tectonic evolution of Cordilleran continental crust: Examples from the San Gabriel and San Bernardino Mountains, *in* Dunne, G., and Cooper, J., eds., *Geologic excursions in the California desert and adjacent Transverse Ranges*: Pacific Section, Society of Economic Paleontologists and Mineralogists, Book 88, p. 17–53.
- Barth, A.P., Wooden, J.L., Grove, M., Jacobson, C.E., and Dawson, J.P., 2003, U-Pb geochronology of rocks in the Salinas Valley region of California: A reevaluation of the crustal structure and origin of the Salinian block: *Geology*, v. 31, p. 517–520, doi: 10.1130/0091-7613(2003)031<0517:UZGORI>2.0.CO;2.
- Barth, A.P., Wooden, J.L., Jacobson, C.E., and Probst, K., 2004, U-Pb geochronology and geochemistry of the McCoy Mountains Formation, southeastern California: A Cretaceous retroarc foreland basin: *Geological Society of America Bulletin*, v. 116, p. 142–153, doi: 10.1130/B25288.1.
- Barth, A.P., Wooden, J.L., Howard, K.A., and Richards, J.L., 2008, Late Jurassic plutonism in the southwest U.S. Cordillera, *in* Wright, J.E., and Shervais, J.W., eds., *Arcs, ophiolites and batholiths: A tribute to Cliff Hops*: Geological Society of America Special Paper 438, p. 379–396, doi: 10.1130/2008.2438(13).
- Bateman, P.C., 1992, Plutonism in the central part of the Sierra Nevada batholith: U.S. Geological Survey Professional Paper 1483, 186 p.
- Behn, M.D., and Kelemen, P.B., 2006, Stability of arc lower crust: Insights from the Talkeetna arc section, south central Alaska, and the seismic structure of modern arcs: *Journal of Geophysical Research*, v. 111, doi: 10.1029/2006JB004327.
- Bender, E.E., Morrison, J., Anderson, J.L., and Wooden, J.L., 1993, Early Proterozoic ties between two suspect terranes and the Mojave crustal block of the southwestern U.S.: *The Journal of Geology*, v. 101, p. 715–728.
- Bennett, V.C., and DePaolo, D.J., 1987, Proterozoic crustal history of the western United States as determined by neodymium isotopic mapping: *Geological Society of America Bulletin*, v. 99, p. 674–685, doi: 10.1130/0016-7606(1987)99<674:PCHOTW>2.0.CO;2.
- Black, L.P., Kamo, S.L., Allen, C.M., Davis, D.W., Aleinikoff, J.N., Valley, J.W., Mundil, R.M., Campbell, I.H., Korsch, R.J., Williams, I.S., and Foudoulis, C., 2004, Improved $^{206}\text{Pb}/^{238}\text{U}$ microprobe geochronology by the monitoring of a trace-element-related matrix effect: SHRIMP, ID-TIMS, ELA-ICP-MS, and oxygen isotope documentation for a series of zircon standards: *Chemical Geology*, v. 205, p. 115–140, doi: 10.1016/j.chemgeo.2004.01.003.
- Brand, J.H., 1985, Mesozoic alkalic quartz monzonite and peraluminous monzogranites of the northern portion of Joshua Tree National Monument, southern California [M.S. thesis]: Los Angeles, University of Southern California, 187 p.
- Brew, D.A., and Ford, A.B., 1981, The Coast Plutonic Complex sill, southeastern Alaska: U.S. Geological Survey Circular 823-B, p. 96–99.
- Brown, K.L., Paterson, S.R., and Barth, A.P., 2006, Changing melt-migration geometries with crustal depth: An example from the eastern Transverse Ranges [abs. V23D-0661]: *Eos (Transactions, American Geophysical Union)*.
- Calzia, J.P., 1982, Geology of granodiorite in the Coxcomb Mountains, southeastern California, *in* Frost, E.G., and Martin, D.L., eds., *Mesozoic–Cenozoic tectonic evolution of the Colorado River region, California, Arizona, and Nevada*: San Diego, California, Cordilleran Publishers, p. 173–180.
- Christensen, N.I., and Mooney, W.D., 1995, Seismic velocity structure and composition of the continental crust: A global view: *Journal of Geophysical Research*, v. 100, p. 9761–9788, doi: 10.1029/95JB00259.
- Coleman, D.S., Barth, A.P., and Wooden, J.L., 2002, Early to Middle Proterozoic construction of the Mojave province, southwestern United States: *Gondwana Research*, v. 5, p. 75–78, doi: 10.1016/S1342-937X(05)70890-X.
- Dibblee, T.W., 1967, Geologic map of the Joshua Tree quadrangle, San Bernardino and Riverside Counties, California: U.S. Geological Survey Map I-516, scale 1:62,500.
- Dibblee, T.W., 1968, Geologic map of the Twentynine Palms quadrangle, San Bernardino and Riverside Counties, California: U.S. Geological Survey Map I-561, scale 1:62,500.
- Ducea, M.N., Kidder, S., and Zandt, G., 2003, Arc composition at mid-crustal depths: Insights from the Coast Ridge belt, Santa Lucia Mountains, California: *Geophysical Research Letters*, v. 30, p. 1703, doi: 10.1029/2002GL016297.
- Fackler-Adams, B.N., Busby, C.J., and Mattinson, J.M., 1997, Jurassic magmatism and sedimentation in the Palen Mountains, southeastern California: Implications for regional tectonic controls on the Mesozoic continental arc: *Geological Society of America Bulletin*, v. 109, p. 1464–1484, doi: 10.1130/0016-7606(1997)109<1464:JMASIT>2.3.CO;2.
- Fleck, R.J., Mattinson, J.M., Busby, C.J., Carr, M.D., Davis, G.A., and Burchfiel, B.C., 1994, Isotopic complexities and the age of the Delfonte volcanic rocks, eastern Mescal Range, southeastern California: Stratigraphic and tectonic implications: *Geological Society of America Bulletin*, v. 106, p. 1242–1253, doi: 10.1130/0016-7606(1994)106<1242:ICATAO>2.3.CO;2.
- Fohey, N., Wooden, J.L., and Barth, A.P., 2005, A comparison of ignimbrites of the Sidewinder Volcanic Series to exposed plutons, southern California: *Geological Society of America Abstracts with Programs*, v. 37, no. 7, p. 288.
- Glazner, A.F., and Ussler, W., 1988, Trapping of magma at mid-crustal density discontinuities: *Geophysical Research Letters*, v. 15, p. 673–675, doi: 10.1029/GL015i007p00673.
- Grove, M., Jacobson, C.E., Barth, A.P., and Vucic, A., 2003, Temporal and spatial trends of Late Cretaceous–Early Tertiary underplating of Pelona and related schist beneath southern California and southwestern Arizona, *in* Johnson, S.E., Paterson, S.R., Fletcher, J.M., Girty, G.H., Kimbrough, D.L., and Martín-Barajas, A., eds., *Tectonic evolution of Northwestern Mexico and Southwestern USA*: Geological Society of America Special Paper 374, p. 381–406.
- Harding, L.E., and Coney, P.J., 1985, The geology of the McCoy Mountains Formation, southeastern California and southwestern Arizona: *Geological Society of America Bulletin*, v. 96, p. 755–769, doi: 10.1130/0016-7606(1985)96<755:TGOTMM>2.0.CO;2.
- Haugerud, R.A., Van der Heyden, P., Tabor, R.W., Stacey, J.S., and Zartman, R.E., 1991, Late Cretaceous and early Tertiary plutonism and deformation in the Skagit gneiss complex, North Cascade Range, Washington and British Columbia: *Geological Society of America Bulletin*, v. 103, p. 1297–1307, doi: 10.1130/0016-7606(1991)103<1297:LCAETP>2.3.CO;2.
- Hauksson, E., 2000, Crustal structure and seismicity distribution adjacent to the Pacific and North America plate boundary in southern California:

- Journal of Geophysical Research, v. 105, p. 13,875–13,903, doi: 10.1029/2000JB900016.
- Hogan, J., Price, J., and Gilbert, M., 1998, Magma traps and driving pressure: Consequences for pluton shape and emplacement in an extensional regime: *Journal of Structural Geology*, v. 20, p. 1155–1168, doi: 10.1016/S0191-8141(98)00063-7.
- Holland, T., and Blundy, J., 1994, Non-ideal interactions in calcic amphiboles and their bearing on amphibole-plagioclase thermometry: *Contributions to Mineralogy and Petrology*, v. 116, p. 433–447, doi: 10.1007/BF00310910.
- Hollister, L.S., and Andronicos, C., 2000, The Central Gneiss Complex, Coast Mountains, British Columbia, *in* Stowell, H.H., and McLelland, W.C., eds., *Tectonics of the Coast Mountains, Southeastern Alaska and British Columbia*: Geological Society of America Special Paper 343, p. 45–59.
- Hope, R.A., 1969, The Blue Cut fault, southeastern California: U.S. Geological Survey Professional Paper, v. 650-D, p. D116–D121.
- Howard, K.A., 2002, Geologic map of the Sheep Hole Mountains 30 × 60 quadrangle, San Bernardino and Riverside Counties, California: U.S. Geological Survey Miscellaneous Field Studies Map MF-2344, scale 1:100,000.
- Ingram, G.M., and Hutton, D.H.W., 1994, The Great Tonalite Sill: Emplacement into a contractional shear zone and implications for Late Cretaceous to early Eocene tectonics in southeastern Alaska and British Columbia: *Geological Society of America Bulletin*, v. 106, p. 715–728, doi: 10.1130/0016-7606(1994)106<0715:TGTSEI>2.3.CO;2.
- Jacobson, C.E., Barth, A.P., and Grove, M., 2000, Late Cretaceous protolith age and provenance of the Pelona and Orocochia schists, southern California: Implications for evolution of the Cordilleran margin: *Geology*, v. 28, p. 219–222, doi: 10.1130/0091-7613(2000)28<219:LCPAAP>2.0.CO;2.
- Jacobson, C.E., Grove, M., Vucic, A., Pedrick, J.N., and Ebert, K.A., 2007, Exhumation of the Orocochia schist and associated rocks of southeastern California: Relative roles of erosion, synsubduction tectonic denudation, and middle Cenozoic extension, *in* Cloos, M., Carlson, W.D., Gilbert, M.C., Liou, J.G., Rumble, D., and Sorensen, S.S., eds., *Convergent margin terranes and associated regions*: Geological Society of America Special Paper 419, p. 1–37.
- James, E.W., 1989, Southern extension of the Independence dike swarm of eastern California: *Geology*, v. 17, p. 587–590, doi: 10.1130/0091-7613(1989)017<0587:SEOTID>2.3.CO;2.
- Kidder, S., Ducea, M., Gehrels, G., Patchett, P.J., and Vervoort, J., 2003, Tectonic and magmatic development of the Salinian Coast Ridge belt, California: *Tectonics*, v. 22, doi: 10.1029/2002TC001409.
- Kistler, R.W., and Champion, D.E., 2001, Rb-Sr whole-rock and mineral ages, K-Ar, ⁴⁰Ar/³⁹Ar, and U-Pb mineral ages, and strontium, lead, neodymium, and oxygen isotopic compositions for granitic rocks from the Salinian composite terrane, California: U.S. Geological Survey Open-File Report 01-453, 84 p.
- Ludwig, K.R., 2002, Squid: Berkeley Geochronology Center Special Publication 2, and Isoplot/Ex, a geochronology toolkit for Microsoft Excel: Berkeley Geochronology Center Special Publication 1.
- Lund, K., and Snee, L.W., 1988, Metamorphism, structural development, and age of the continent-island arc juncture in west-central Idaho, *in* Ernst, W.G., ed., *Metamorphism and crustal evolution of the western United States*, Rubey Vol. VII: Englewood Cliffs, New Jersey, Prentice-Hall, p. 296–331.
- Manduca, C.A., Kuntz, M.A., and Silver, L.T., 1993, Emplacement and deformation history of the western margin of the Idaho batholith near McCall, Idaho: Influence of a major terrane boundary: *Geological Society of America Bulletin*, v. 105, p. 749–765, doi: 10.1130/0016-7606(1993)105<0749:EADHOT>2.3.CO;2.
- Marsh, B.D., 1982, On the mechanics of igneous diapirism, stoping and zone melting: *American Journal of Science*, v. 282, p. 808–855.
- Mayo, D.P., Anderson, J.L., and Wooden, J.L., 1998, Isotopic constraints on the petrogenesis of Jurassic plutons, southeastern California: *International Geology Review*, v. 40, p. 421–442.
- Meissner, R., and Mooney, W., 1998, Weakness of the lower continental crust: a condition for delamination, uplift and escape: *Tectonophysics*, v. 296, p. 47–60, doi: 10.1016/S0040-1951(98)00136-X.
- Miller, R.B., and Paterson, S.R., 2001, Construction of mid-crustal sheeted plutons: Examples from the North Cascades, Washington: *Geological Society of America Bulletin*, v. 113, p. 1423–1442, doi: 10.1130/0016-7606(2001)113<1423:COMCSP>2.0.CO;2.
- Miller, R.B., Bowring, S.A., and Hoppe, W.J., 1989, Paleocene plutonism and its tectonic implications, North Cascades, Washington: *Geology*, v. 17, p. 846–849, doi: 10.1130/0091-7613(1989)017<0846:PPAITI>2.3.CO;2.
- Miller, R.B., Matzel, J.P., Paterson, S.R., and Stowell, H.H., 2003, Cretaceous to Paleogene Cascades arc: Structure, metamorphism, and timescales of magmatism, burial, and exhumation of a crustal section, *in* Swanson, T., ed., *Western Cordillera and adjacent areas*: Geological Society of America Field Guide 4, p. 107–135.
- Miller, R.B., Paterson, S.R., and Matzel, J.P., 2009, this volume, Plutonism at different crustal levels: Insights from the ~5–40 km (paleodepth) North Cascades crustal section, Washington, *in* Miller, R.B., and Snoke, A.W., eds., *Crustal cross sections from the western North American Cordillera and elsewhere: Implications for tectonic and petrologic processes*: Geological Society of America Special Paper 456, doi: 10.1130/2009.2456(05).
- Miller, W.J., 1946, Crystalline rocks of southern California: *Geological Society of America Bulletin*, v. 57, p. 457–542, doi: 10.1130/0016-7606(1946)57[457:CROSC]2.0.CO;2.
- Misch, P., 1966, Tectonic evolution of the northern Cascades of Washington State—A west-Cordilleran case history, *in* Gunning, H.C., ed., *Proceedings of a symposium on the tectonic history of mineral deposits of the western Cordillera in British Columbia and neighboring parts of the United States*: Canadian Institute of Mining and Metallurgy Special Volume 8, p. 101–148.
- Misch, P., 1968, Plagioclase compositions and non-anatectic origin of migmatitic gneisses in Northern Cascade Mountains of Washington State: *Contributions to Mineralogy and Petrology*, v. 17, p. 1–70, doi: 10.1007/BF00371809.
- Oldow, J.S., Bally, A.W., Avé Lallemand, H.G., and Leeman, W.P., 1989, Phanerozoic evolution of the North American Cordillera: United States and Canada, *in* *The Geology of North America—An overview*: Boulder, Colorado, Geological Society of America, *Geology of North America*, v. A, p. 139–232.
- Palmer, E.F., 2005, Five distinct plutons of north-central Joshua Tree National Park, California [B.S. thesis]: Indianapolis, Indiana University–Purdue University, 44 p.
- Paterson, S.R., Barth, A.P., Wooden, J.L., Pignotta, G.S., and Memeti, V., 2006, Bedrock geologic map of the Keys View 7.5 minute quadrangle, Riverside County, California: United States National Park Service, scale 1:24,000.
- Pitcher, W.S., 1979, The nature, ascent and emplacement of granitic magmas: *Journal of the Geological Society*, v. 136, p. 627–662, doi: 10.1144/gsjgs.136.6.0627.
- Postlethwaite, C.E., 1988, The structural geology of the Red Cloud thrust system, southern eastern Transverse Ranges, California [Ph.D. thesis]: Ames, Iowa State University, 135 p.
- Powell, R.E., 1981, Geology of the crystalline basement complex, Eastern Transverse Ranges, southern California: Constraints on regional tectonic interpretation [Ph.D. thesis]: Pasadena, California Institute of Technology, 441 p.
- Powell, R.E., 1993, Balanced palinspastic reconstruction of pre-late Cenozoic paleogeology, southern California: Geologic and kinematic constraints on evolution of the San Andreas fault system, *in* Powell, R.E., Weldon, R.J., and Matti, J.C., eds., *The San Andreas fault system*: Geological Society of America Memoir 178, p. 1–106.
- Powell, R.E., 2001, Geologic map and digital database of the Porcupine Wash 7.5 minute quadrangle, Riverside County, California: U.S. Geological Survey Open-File Report 01-030, scale 1:24,000.
- Rogers, J.J.W., 1954, Geology of a portion of Joshua Tree National Monument, Riverside County: California Division of Mines and Geology Bulletin, v. 170, Map Sheet 24, scale ~1:85,000.
- Saleeby, J.B., 1990, Progress in tectonic and petrogenetic studies in an exposed cross-section of young (~100 Ma) continental crust, southern Sierra Nevada, California, *in* Salisbury, M.H., and Fountain, D.M., eds., *Exposed cross-sections of the continental crust*: Dordrecht, Kluwer Academic, p. 137–157.
- Schermer, E.R., Busby, C.J., and Mattinson, J.M., 2002, Paleogeographic and tectonic implications of Jurassic sedimentary and volcanic sequences in the central Mojave block, *in* Glazner, A.F., Walker, J.D., and Bartley, J.M., eds., *Geologic evolution of the Mojave Desert and Southwestern Basin and Range*: Geological Society of America Memoir 195, p. 93–115.
- Schmidt, K.L., and Paterson, S.R., 2002, A doubly vergent, fan structure in the Peninsular Ranges batholith: Transpression or complex flow along a crustal-scale discontinuity?: *Tectonics*, v. 21, p. 14-1 to 14-19.

- Schmidt, M.W., 1992, Amphibole composition in tonalite as a function of pressure: An experimental calibration of the Al-in-hornblende barometer: *Contributions to Mineralogy and Petrology*, v. 110, p. 304–310, doi: 10.1007/BF00310745.
- Shaw, S.E., Todd, V.R., and Grove, M., 2003, Jurassic peraluminous gneissic granites in the axial zone of the Peninsular Ranges, southern California, in Johnson, S.E., Paterson, S.R., Fletcher, J.M., Girty, G.H., Kimbrough, D.L., and Martín-Barajas, A., eds., *Tectonic evolution of Northwestern Mexico and Southwestern USA: Geological Society of America Special Paper 374*, p. 157–184.
- Stone, P., and Pelka, G.J., 1989, Geologic map of the Palen-McCoy Wilderness Study Area, and vicinity, Riverside County, California: United States Geological Survey Map MF-2092, scale 1:62,500.
- Stowell, H.H., and Pike, M.A., 2000, One-dimensional thermal models of metamorphism resulting from the Coast Plutonic complex sill, northern Coast Mountains, southeastern Alaska, in Stowell, H.H., and McLelland, W.C., eds., *Tectonics of the Coast Mountains, Southeastern Alaska and British Columbia: Geological Society of America Special Paper 343*, p. 183–192.
- Thomson, C.N., and Girty, G.H., 1994, Early Cretaceous intra-arc ductile strain in Triassic-Jurassic and Cretaceous continental margin arc rocks, Peninsular Ranges, California: *Tectonics*, v. 13, p. 1108–1119, doi: 10.1029/94TC01649.
- Todd, V.R., Erskine, B.G., and Morton, D.M., 1988, Metamorphic and tectonic evolution of the northern Peninsular Ranges batholith, in Ernst, W.G., ed., *Metamorphism and crustal evolution of the western United States*, Rubey Vol. VII: Englewood Cliffs, New Jersey, Prentice-Hall, p. 894–937.
- Tosdal, R.M., Haxel, G.B., and Wright, J.E., 1989, Jurassic geology of the Sonoran Desert region, southern Arizona, southeast California, and northernmost Sonora: Construction of a continental margin magmatic arc: *Arizona Geological Society Digest*, v. 17, p. 397–434.
- Walker, J.D., Burchfiel, B.C., and Davis, G.A., 1995, New age controls on initiation and timing of foreland belt thrusting in the Clark Mountains, southern California: *Geological Society of America Bulletin*, v. 107, p. 742–750, doi: 10.1130/0016-7606(1995)107<0742:NACOIA>2.3.CO;2.
- Walker, J.D., Martin, M.W., and Glazner, A.F., 2002, Late Paleozoic to Mesozoic development of the Mojave Desert and environs, California, in Glazner, A.F., Walker, J.D., and Bartley, J.M., eds., *Geological evolution of the Mojave Desert and Southwestern Basin and Range: Geological Society of America Memoir 195*, p. 1–18.
- Wooden, J.L., Tosdal, R.M., Howard, K.A., Powell, R.E., Matti, J.C., and Barth, A.P., 1994, Mesozoic intrusive history of parts of the eastern Transverse Ranges, California: Preliminary U-Pb zircon results: *Geological Society of America Abstracts with Programs*, v. 26, no. 2, p. 104.
- Wooden, J.L., Fleck, R.J., Matti, J.C., Powell, R.E., and Barth, A.P., 2001, Late Cretaceous intrusive migmatites of the Little San Bernardino Mountains, California: *Geological Society of America Abstracts with Programs*, v. 33, no. 3, p. A65.
- Zoback, M.L., and Mooney, W.D., 2003, Lithospheric buoyancy and continental intraplate stresses: *Geological Society of America International Book Series*, v. 7, p. 367–390.

MANUSCRIPT ACCEPTED BY THE SOCIETY 24 FEBRUARY 2009

Perspectives on the architecture of continental crust from integrated field studies of exposed isobaric sections

Michael L. Williams*

Department of Geosciences, University of Massachusetts, Amherst, Massachusetts 01003, USA

Karl E. Karlstrom

Department of Earth and Planetary Sciences, University of New Mexico, Albuquerque, New Mexico 87131, USA

Gregory Dumond†

Department of Geosciences, University of Massachusetts, Amherst, Massachusetts 01003, USA

Kevin H. Mahan§

Division of Geological & Planetary Sciences, California Institute of Technology, Pasadena, California 91125, USA

ABSTRACT

Depth-dependent variations in the structure and composition of continental crust can be studied via integrated investigations of isobaric terranes. In this contribution, we summarize three isobaric terranes in Archean to Proterozoic crust. In western Canada, 35–45-km-deep lower crust is exposed over an area of more than 20,000 km². The Upper Granite Gorge of Grand Canyon, Arizona, provides a transect of 20–25-km-deep middle crust. The Proterozoic basement of central Arizona represents an isobaric exposure of 10–15-km-deep middle crust. Isobaric terranes yield a conceptual image of continental crust that can be compared to seismic images, xenolith data, and drill core data to clarify rheology, coupling/decoupling of crustal levels, and the interplay between deformation, metamorphism, and plutonism. General observations include: (1) The crust is heterogeneous at all levels and cannot be accurately modeled as a simple progression from quartz-rich to feldspar-rich lithologies or from felsic to mafic bulk compositions. (2) The crust is segmented into foliation domains that alternate between steeply dipping and shallowly dipping. (3) Magmatism is expressed differently at different depths due to different background temperatures and a general upward distillation from mafic to felsic composition, and may be the most important control on crustal architecture and rheology. The strength of continental crust (and its potential for low-viscosity flow) is not simply a function of temperature, depth, and compositional layering, but is controlled by the size and distribution of rheological domains. The rheological character of a particular layer can vary in space and time at any crustal level.

*mlw@geo.umass.edu

†Current address: Department of Earth, Atmospheric, and Planetary Sciences, Massachusetts Institute of Technology, Cambridge, Massachusetts 02139, USA.

§Current address: Department of Geological Sciences, University of Colorado–Boulder, Boulder, Colorado 80309, USA.

Williams, M.L., Karlstrom, K.E., Dumond, G., and Mahan, K.H., 2009, Perspectives on the architecture of continental crust from integrated field studies of exposed isobaric sections, *in* Miller, R.B., and Snoke, A.W., eds., *Crustal Cross Sections from the Western North American Cordillera and Elsewhere: Implications for Tectonic and Petrologic Processes*: Geological Society of America Special Paper 456, p. 219–241, doi: 10.1130/2009.2456(08).

INTRODUCTION

Knowledge of the deep structure of continental crust relies on geophysical data combined with direct observations from xenoliths and crystalline rocks that have been exhumed from deep levels. Considerable attention has been paid to exposed crustal cross sections—tilted slices of crust exposed at the surface (e.g., Salisbury and Fountain, 1990; Percival et al., 1992). These can provide cross-sectional views of depth-dependent variations in composition as well as processes. Examples such as the Ivrea-Verbano zone (Burke and Fountain, 1990; Rutter et al., 1999), Fiordland (Klepeis et al., 2004), and the Kapuskasing uplift (Percival and Card, 1983; Percival and West, 1994) have provided information on the character and degree of coupling or decoupling across crustal boundaries, including the Moho. Although important insights have arisen from these sections, by their nature, they provide less information about lateral variation in physical properties and/or rheological behavior.

In contrast to crustal cross sections, *isobaric terranes* are here defined as regions that were laterally contiguous at a specific depth in the crust during part of their geologic history, commonly including the time of peak metamorphism. The degree to which a region can be defined as an isobaric terrane depends on the spatial and temporal scales over which pressures were nearly constant and on the questions being asked. Isobaric terranes provide rich field laboratories for evaluating the spatial heterogeneity of material and processes at particular crustal levels. For example, these terranes provide the most directly observable data regarding the degree of strain partitioning (e.g., Butler et al., 2002), bulk rheology (e.g., Handy and Zingg, 1991; Metzger, 1992; Rutter and Brodie, 1992; Klepeis et al., 2003, 2004), and nature of crustal flow (e.g., Williams and Jiang, 2005). Understanding such processes through map-view geologic images of particular crustal levels provides the necessary regional context to accurately interpret seismic and xenolith data.

In this contribution, we present three examples of regions we define as isobaric terranes, each representing a different crustal level; one from the western Canadian Shield and two from Proterozoic provinces in Arizona. Our purpose is to discuss and compare isobaric terranes as a tool for understanding crustal architecture, and in particular, lateral variations in characteristics such as composition, structure, and rheological properties that may be difficult to constrain from remote seismic observations or tilted two-dimensional cross sections.

BACKGROUND—ISOBARICALLY COOLED AND ISOBARIC TERRANES

Metamorphic terranes have traditionally been classified into broad groups based on the style of P - T - t (pressure-temperature-time) history. Perhaps the most familiar are terranes characterized by near-isothermal decompression during or immediately after orogenesis. These Alpine or Himalayan-type terranes are interpreted to have evolved within a tectonically thickened (or

overthickened) crust that underwent thermal relaxation due to syn-orogenic extension or orogenic collapse (England and Thompson, 1984; Platt, 1986; Harley, 1989; Percival et al., 1992). A second common type includes *isobarically cooled terranes* (Harley, 1989; Percival, 1989; Rudnick and Fountain, 1995). These are metamorphic terranes that record one or more tectonic events during residence at a particular level of the crust for an extended period of time (Ellis, 1987; Harley, 1989). These regions achieved isostatic stability at some time after orogenesis; i.e., they cooled to a normal geotherm and thus offer a more direct view of a particular crustal level in a stable or steady-state environment (Harley, 1989; Percival et al., 1992). Exhumation commonly involves tectonic events unrelated to those that led to initial burial and prograde metamorphism. The first type of terrane is typically described by “clockwise” P - T paths and the latter by “anti-clockwise” P - T paths, on a pressure-up P - T diagram. Both types, however, can have overall clockwise looping P - T paths (Williams and Karlstrom, 1996).

Isobaric terranes, as discussed here, are relatively large terranes that preserve nearly constant metamorphic pressures. These regions underwent peak deformation and metamorphism at some specific crustal level prior to exhumation to shallower crustal levels. It must be determined if the region was exhumed as a single block or if sub-domains or blocks were exhumed separately by similar amounts and juxtaposed again near the surface. The key point is that the components of these isobaric terranes were present at one specific depth during a tectonic event, and thus can reveal some of the variability in rock types and processes at that particular crustal level. Unlike the *isobarically cooled terranes*, not all isobaric terranes represent isostatically stable crust, but significant insights can still be gained. Of the three examples discussed below, two (Athabasca granulite terrane and Proterozoic basement of central Arizona) are isobarically cooled terranes. The Upper Granite Gorge of the Grand Canyon is an ~0.7 GPa isobaric terrane that decompressed to 0.3–0.4 GPa late in the orogenic cycle. In addition to the isobaric terranes described here, there are numerous examples from the literature that could be considered. These include the central Sierra Nevada (0.2–0.3 GPa; Ague and Brimhall, 1988), central Otago schist terrane (~0.8 GPa; Mortimer, 2000), western Maine (0.3–0.4 GPa; Guidotti and Cheney, 1989; Guidotti and Johnson, 2002), and the Napier complex, Antarctica (~1.0 GPa; Sheraton and Black, 1983; Harley and Black, 1997). Our purpose here is to draw attention to these regions as an underutilized source of information about geologic processes and lateral heterogeneity within the crust.

EXAMPLES OF ISOBARIC TERRANES

Numerous maps and publications exist on the three isobaric terranes discussed below. A brief introduction and overview is presented here, but we refer readers to the cited literature for more detail. Our goal is to compare and contrast certain features and processes, especially those for which new insights about crustal

processes come from the isobaric nature of the terranes. We focus on: (1) the interplay between early sub-horizontal and later sub-vertical fabrics in all three regions, and (2) the character of igneous rocks and advective heating in the three regions. Admittedly, the three terranes evolved in different places at generally different times, but we suggest that important insights and conclusions may be drawn from the comparison. Ultimately, these observations provide a framework for integrating and comparing additional isobaric terranes. Generalized P-T-t paths for the three terranes summarized here are shown in Figure 1.

Athabasca Granulite Terrane, Saskatchewan, Canada (1.0–1.2 GPa; 35–45 km Depths)

The region northeast of Lake Athabasca, northern Saskatchewan, is underlain by more than 20,000 km² of high-pressure granulites (1.0 to >1.5 GPa). They occur at the eastern margin of the Rae domain in the western Churchill cratonic province of the Canadian Shield (Fig. 2). A fundamental characteristic of this region is its segmented architecture, with 10- to 50-km-scale, structurally bounded domains that differ from each other in composition and tectonic history. Three domains (Chipman,

Northwestern, and Southern) make up the East Athabasca mylonite triangle (Fig. 3A) (Hanmer et al., 1994; Williams and Hanmer, 2006). The Chipman domain is dominated by the Mesoarchean (>3.0 Ga) Chipman tonalite gneiss with a voluminous 1.9 Ga mafic dike swarm that intruded at conditions of 1.0–1.2 GPa and 750–850 °C, i.e., while the rocks resided in the lower continental crust (Williams et al., 1995; Flowers et al., 2006a). The Northwestern domain is dominated by ca. 2.6 Ga plutonic rocks including the Mary batholith (granite to granodiorite) and the Bohica mafic complex (Hanmer, 1997) that record metamorphic conditions of 1.0 GPa and 750–800 °C (Williams et al., 2000). The felsic to intermediate plutonic rocks were emplaced into the deep crust and preserve a record of the structural and metamorphic evolution from igneous Opx- and Hb-bearing granitoids to gneissic garnet granulites (Williams et al., 2000). The Northwestern domain is separated from the Chipman domain by the Cora Lake shear zone. The Southern domain is dominated by Grt-rich felsic granulite (“white gneiss”) interpreted as the restitic product of extreme anatexis (Snoeyenbos et al., 1995; Baldwin et al., 2006). The white gneiss is interlayered with meter- to kilometer-thick mafic granulite sills that may represent underplating or intraplating of mafic magma in the deep crust. The domain

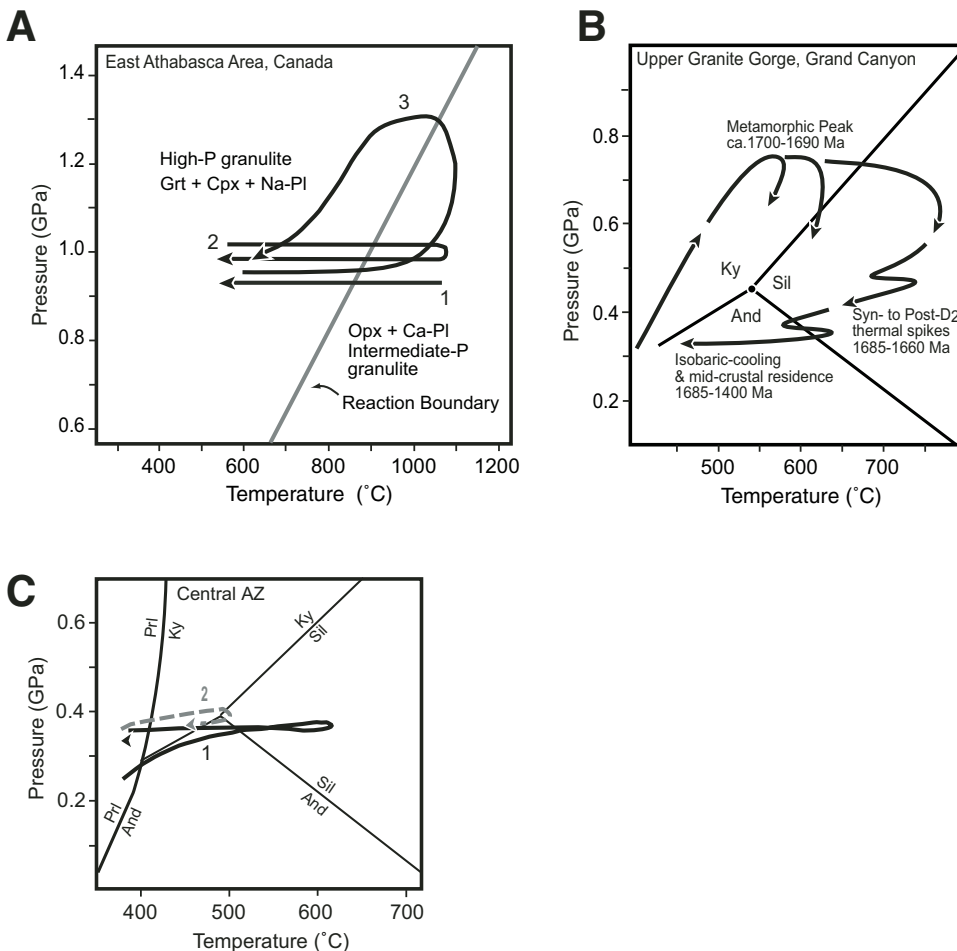


Figure 1. Representative *P-T* paths from the three isobaric terranes discussed here. (A) Paths from the East Athabasca granulite terrane. Path-1 represents igneous rocks emplaced at 1.0 GPa and cooled. Path-2 shows rocks that experienced a thermal event while resident in the deep crust. Path-3 experienced a transient period of high-P metamorphism (see Baldwin et al., 2003). Reaction Boundary shows the approximate phase boundary between intermediate-pressure (Opx) and high-pressure (Grt-Cpx) granulites (Williams et al., 2000). (B) Composite *P-T* path from the Upper Gorge of the Grand Canyon. Essentially all rocks experienced 0.7 GPa metamorphism during the 1.7–1.68 Ga Yavapai orogeny and then were decompressed to ~0.4 GPa (Dumond et al., 2007a). (C) Generalized *P-T* paths representative of much of the central Arizona (AZ) Proterozoic basement, the lower gorge of Grand Canyon, and Proterozoic basement of northern New Mexico.

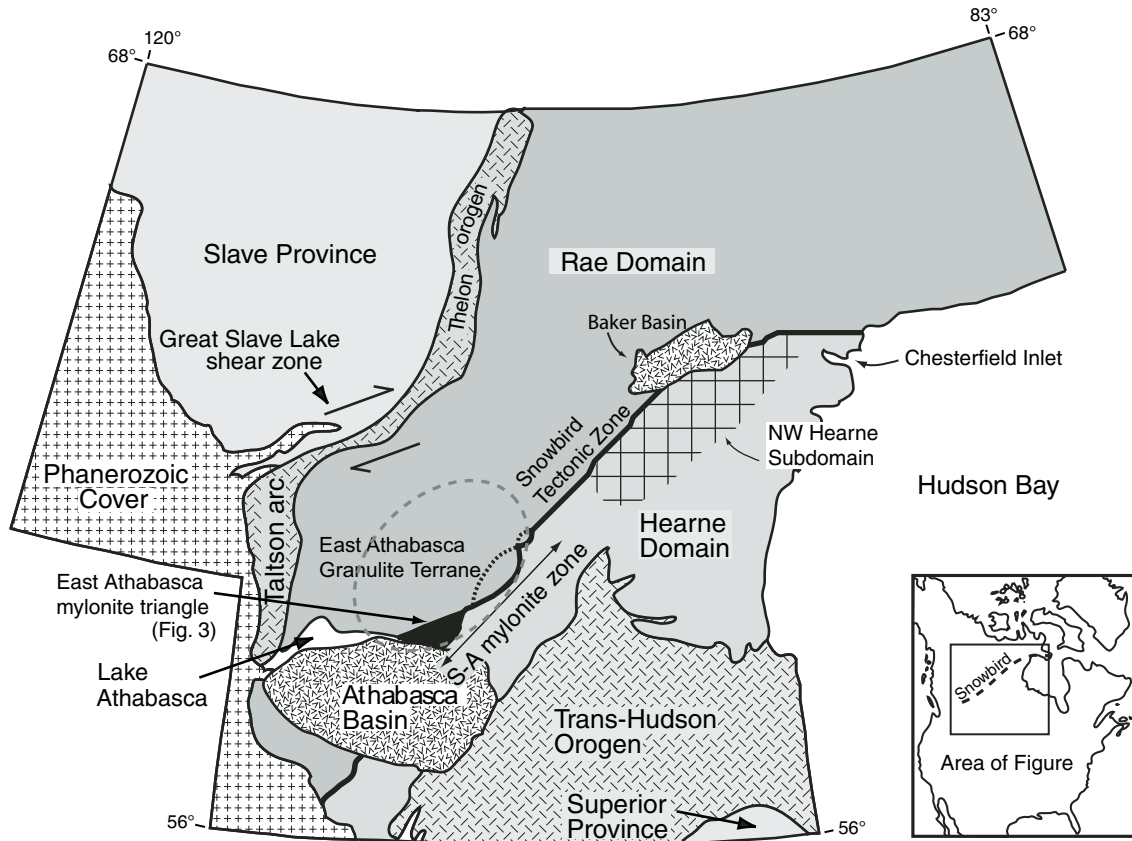


Figure 2. Location of the Snowbird tectonic zone and East Athabasca granulite terrane within northern Saskatchewan and Northwest Territories, Canada. Dashed oval shows approximate extent of East Athabasca granulite terrane.

also hosts minor eclogite, and all rocks record an early event of higher peak pressures of ~ 1.5 GPa at 750–1000 °C (Snoeyenbos et al., 1995; Baldwin et al., 2003, 2004, 2007). A large portion of the Rae domain to the west (Figs. 2 and 3) also experienced ~ 1.0 GPa pressure and is included with the East Athabasca mylonite triangle as the near-isobaric Athabasca granulite terrane.

Two main generations of deformation have been identified throughout many portions of the Athabasca granulite terrane, although multiple periods of reactivation have been documented along the high-strain zone boundaries (e.g., Legs Lake shear zone: Mahan et al., 2003; Grease River shear zone: Lafrance and Sibbald, 1997; Dumond et al., 2008). Early structures include sub-horizontal- to northwest-striking gneissic fabrics (S_1) and recumbent isoclinal folds of compositional layering (e.g., Slimmon, 1989; Kopf, 1999; Card, 2002; Mahan and Williams, 2005; Dumond et al., 2005a, 2005b; Martel, 2005). Later structures include open- to isoclinal folds of S_1 and transposition of older folds and fabrics into sub-vertical, northeast-striking mylonitic foliations (Hanmer et al., 1995; Hanmer, 1997; Mahan et al., 2003; Mahan and Williams, 2005; Martel, 2005). The eastern boundary of the high-pressure terrane is marked by the Legs Lake shear zone, part of a ~ 500 -km-long contractional fault system that accommodated more than 20 km of vertical displacement

(Mahan et al., 2003; Mahan and Williams, 2005; Mahan et al., 2006a, 2006b) (Fig. 3B). The Hearne domain to the east records maximum peak pressures of 0.5 GPa (Mahan et al., 2003).

Rocks in the Northwestern, Southern, and Chipman domains underwent high-pressure (~ 1.0 GPa) metamorphism at 2.6–2.55 Ga and again at 1.9 Ga. We suggest that the rocks resided in the deep crust from 2.6 Ga to 1.9 Ga, and thus essentially constituted lower continental crust in the region during that period of time (Williams and Hanmer, 2006; Flowers et al., 2008). Although the thickness of the crust at that time is unconstrained, the alternative interpretation that the rocks resided within the middle levels of an overthickened crust seems unlikely because of the long duration (700 Ma) of essentially constant pressures and the lack of geologic evidence for decompression to shallower crustal levels between ca. 2.6 Ga and 1.9 Ga. High-pressure conditions (0.8–1.0 GPa, ~ 900 °C) were recorded at 1.9 Ga in a large area of the Rae domain west of the Grease River shear zone (Figs. 2 and 3) (Kopf, 1999; Krikorian, 2002; Williams and Hanmer, 2006). However, these rocks show little or no record of high-grade 2.6–2.55 Ga metamorphism with abundant evidence for prograde metamorphism and decompression at ca. 1.92–1.9 Ga (Kopf, 1999; Williams and Jercinovic, 2002; Martel et al., 2008). Thus, the two lower crustal domains may have been juxtaposed at

1.9 Ga. Collectively, the region north of Lake Athabasca preserves a large and heterogeneous exposure of the lower continental crust at 1.9 Ga, with parts of the region having existed in the deep crust from 2.6 Ga to 1.9 Ga. Although some of the segmentation and block juxtaposition may have originated during exhumation, at least some of the domain boundaries apparently existed when the rocks resided in the deep crust (Flowers et al., 2006b).

The tectonic setting of the Athabasca granulite terrane is not completely established. It is clear that by 2.62–2.6 Ga, thick continental crust existed in the region (Snoeyenbos et al., 1995; Williams et al., 2000; Flowers et al., 2008). We suspect that the events recorded in the deep crust between 2.62 Ga and 2.55 Ga represent the final phases of an (accretionary) orogenic event. The event represents the addition of new crustal components and the juxtaposition of older Archean components. The final stages of the evolution apparently left a laterally extensive area in a state of near-isostatic equilibrium with little to no post-orogenic decompression recorded. Events at ca. 1.9 Ga are interpreted to reflect a limited amount of rifting with mafic underplating, intraplate, and diking (Flowers et al., 2006a) followed by shortening involving large-scale thrusting, smaller-scale folding, cleavage formation, and exhumation (see Baldwin et al., 2003, 2004, and Berman et al., 2007, for alternative interpretation). The shortening is likely related to the continental collision of the Slave province to the northwest followed by the Trans-Hudson orogeny to the southeast, both consistent with regional shortening and dextral shearing in the Athabasca area (e.g., Mahan and Williams, 2005; Dumond et al., 2008).

Proterozoic Basement of the Southwest United States (0.3–0.4 GPa, 10–15 km Depths)

Proterozoic rocks across a large area in central Arizona and northern New Mexico preserve nearly constant peak metamorphic pressures of 0.3–0.4 GPa (Fig. 4). These rocks have been interpreted to have resided within the middle crust from ca 1.7 Ga to at least 1.4 Ga and locally much longer, thus providing an exceptional view of middle crustal processes (Williams and Karlstrom, 1996; Karlstrom and Williams, 2006). The region is divided into tens-of-km-scale tectonic blocks that are bounded by sub-vertical shear zones (Karlstrom and Bowring, 1988). The blocks record markedly different temperatures of metamorphism (400–650 °C) with only moderate differences in pressure. This isobaric terrane provides a view of the 10–15-km-deep level of an accretionary orogen (Karlstrom et al., 2001; Whitmeyer and Karlstrom, 2007). The following description is taken mainly from central Arizona, specifically the Big Bug block (Karlstrom and Bowring, 1988; Karlstrom and Williams, 1995), because a number of descriptive publications are available and because this region is characteristic of much of the Proterozoic basement of central Arizona and northern New Mexico (Figs. 5A and 5B).

Supracrustal rocks in the Big Bug block are dominated by metamorphosed arc-related volcanic and immature (turbidite) sedimentary rocks, and ~50% of the exposed region is composed

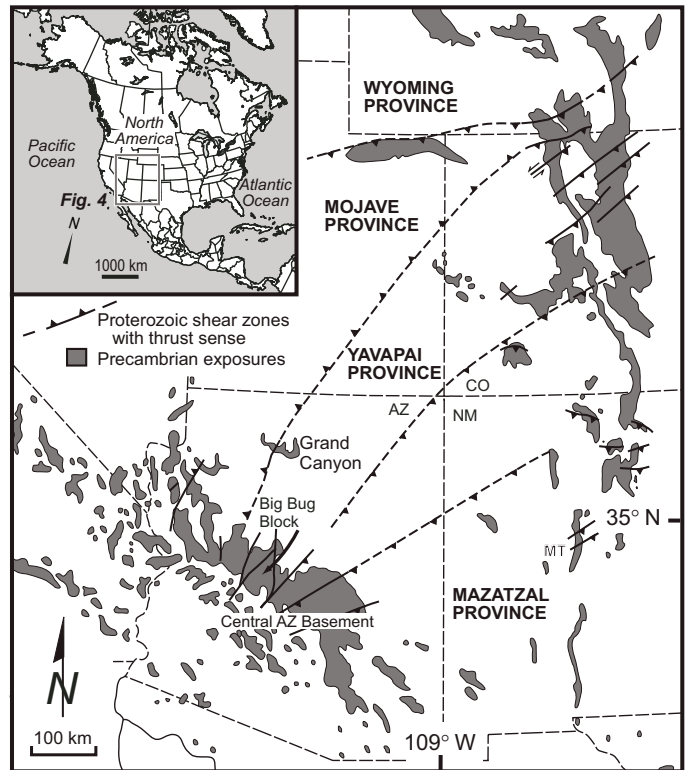


Figure 4. Location of Proterozoic rocks in southwestern Laurentia. The Big Bug block, in the central Arizona (AZ) Proterozoic basement, is highlighted in text. CO—Colorado; NM—New Mexico.

of granitoids. Although a number of early, arc-related plutons are present, these are intruded by a suite of ca. 1.7–1.65 Ga syn-tectonic granites. The rocks preserve evidence of two deformational events or cycles. The earliest event (D_1) is marked by layer-parallel foliation with shallow dip, generally $<30\text{--}40^\circ$. The later event is characterized by upright folds with sub-horizontal enveloping surfaces and sub-vertical foliation in the form of locally intense axial-planar cleavage. Although metamorphic pressures are relatively constant across the terrane, temperatures and D_2 fabric intensity increase toward the margins of the syn-tectonic plutons. Three such plutons have been studied in some detail: the 1.7 Ga Crazy Basin monzogranite batholith (Karlstrom and Williams, 1995), the 1.68 Ga Horse Mountain granite, and an unnamed ca. 1.66 Ga granite to the south (Fig. 5B) (Burr, 1991). During regional metamorphism, pluton-related heating led to weakening, fabric development, and higher metamorphic temperatures (Burr, 1991; Williams, 1991; Karlstrom and Williams, 1995, 2006). Thus, the predominant upright, northeast-trending S_2 foliation does not represent a single “tectonic event”, but rather strain accumulated in different localities at different times over a period of contraction that lasted 50 Ma or more. We call this “pluton-enhanced tectonism” to emphasize the critical role of magmatism in localizing deformation and metamorphism.

Rocks in the Big Bug block are interpreted to have existed at 0.3 GPa to 0.35 GPa (10–15 km depths) during the period of

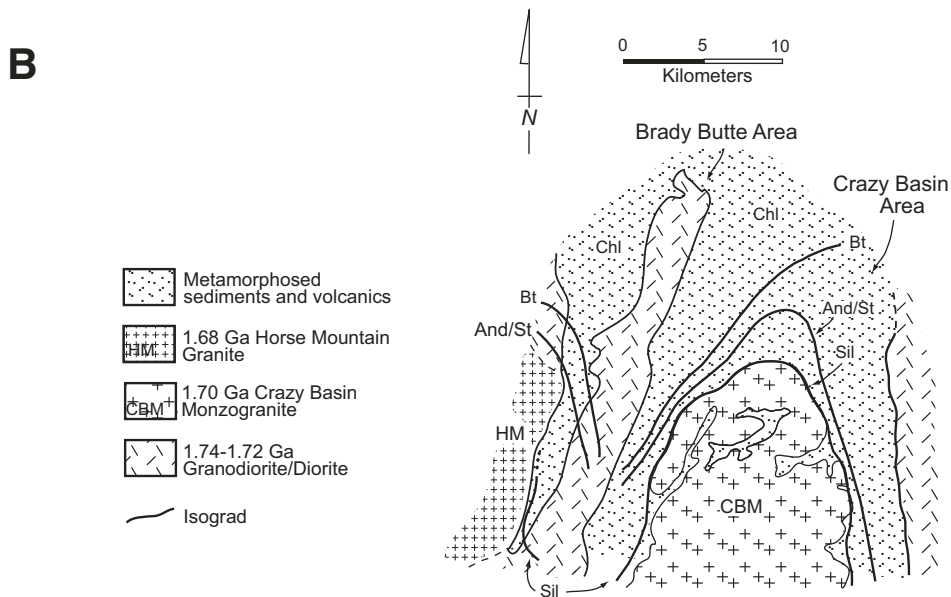
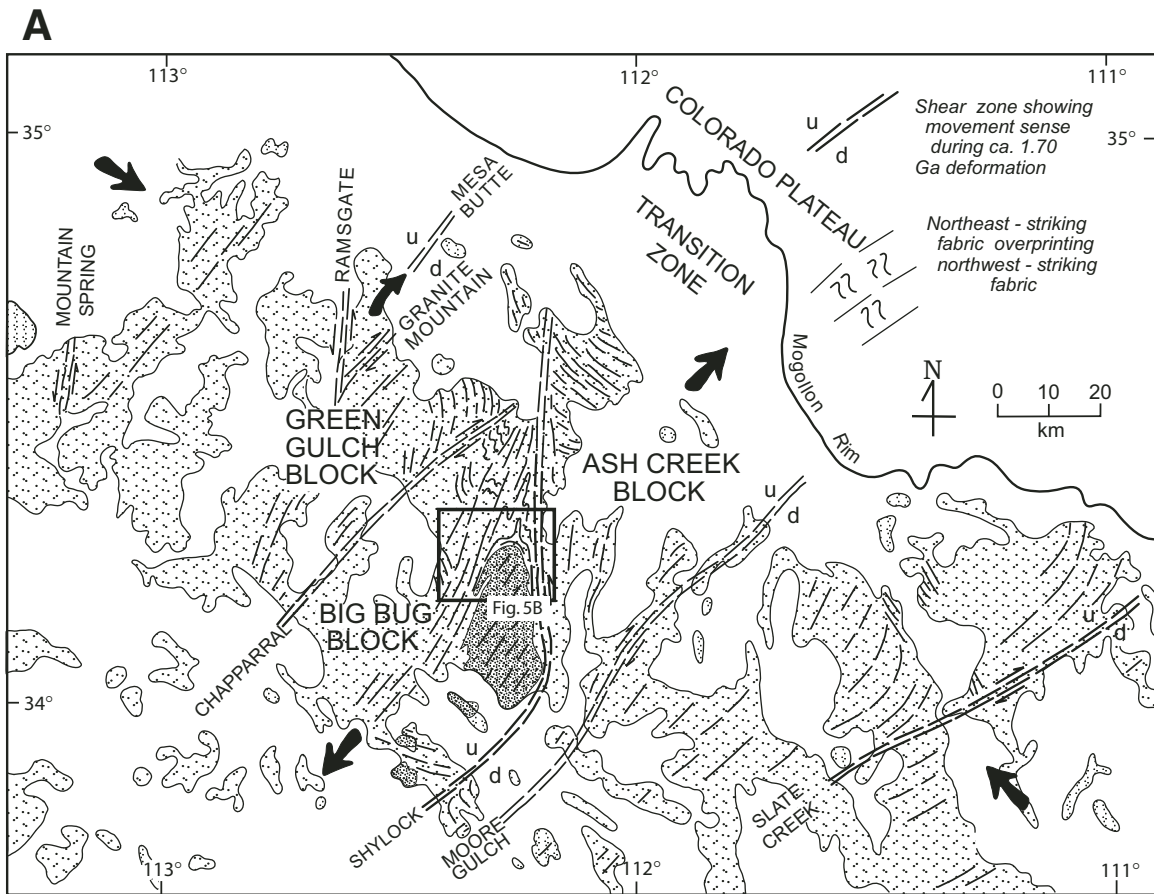


Figure 5. (A) General tectonic model showing tectonic blocks and high-strain D_2 shear zones in Proterozoic rocks in the central Arizona Proterozoic basement (modified from Bergh and Karlstrom, 1992). Arrows represent general motion vectors during 1.71–1.65 Ga tectonism. Inset shows area of Figure 5B. (B) Detail of the northern end of the Crazy Basin quartz monzonite and location of major metamorphic isograds (modified from Karlstrom and Williams, 1995).

syn-tectonic plutonism from 1.7 to at least 1.65 Ga (Williams, 1994; Karlstrom and Williams, 1995). Regional thermo-tectonic events between ca. 1.48 Ga and 1.35 Ga are also recorded at pressures near 0.3–0.4 GPa, and thus it is suggested that large parts of the Proterozoic terrane were in the mid-crust for the intervening 200 Ma. Exhumation occurred in some areas soon after the ca. 1.4 Ga event, but much later in other areas. Thus, as with much of the Proterozoic terrane of the southwestern United States, the Big Bug block is an isobarically cooled terrane that preserves a view of the lateral heterogeneity in the shallow mid-crust over several hundred millions of years.

Tectonic models for Proterozoic basement of the southwestern United States involve arc accretion, assembly, and stabilization that resulted in addition of new continental lithosphere along a long-lived active margin (Bowring and Karlstrom, 1990; Karlstrom et al., 2001; Whitmeyer and Karlstrom, 2007). Some of the arcs may have developed outboard of the continent, followed by assembly during arc-continent collisions. On a regional scale, these isobaric terranes generally represent first-cycle formation and stabilization of normal thickness continental crust from thinner oceanic fragments (Bowring and Karlstrom, 1990). The long-term residence of these rocks in the middle crust has been interpreted in terms of isostatically stable lithosphere and slow cooling, which was perturbed by the 1.48–1.35 Ga tectono-magmatic episode. The isobaric character of the metamorphic terrane has been interpreted in terms of an orogenic plateau with steep thermal gradients, perhaps above a ca. 1.4 Ga magma-fluid layer (at times of elevated temperature), analogous to the Tibetan plateau (Shaw et al., 2005).

Proterozoic Basement of the Grand Canyon (0.6–0.7 GPa; 20–25 km)

The Upper Granite Gorge of the Grand Canyon (Figs. 4 and 6) represents an important exception to the 0.3–0.4 GPa peak pressures that characterize much of the Proterozoic basement of the southwestern United States. The volcanic and immature sedimentary rocks, and the structural styles are similar to those across the region, but peak pressures of 0.6–0.7 GPa (20–25 km depths) are recorded. The region also preserves a similar block-type crustal architecture, consisting of multi-km-scale blocks characterized by relatively homogeneous deformation and metamorphism bounded by sub-vertical high-strain zones (Fig. 6B). Variations in metamorphic conditions along the Upper Granite Gorge transect are primarily thermal in nature and include differences in: the temperature of the prograde history (i.e., early andalusite versus kyanite), peak temperature, and the intensity of late-stage thermal spikes due to the local emplacement of plutons and dike swarms. High-precision ΔPT “relative” thermobarometry confirms lateral temperature variations on the order of 100–250 °C with little to no variation in pressure (Dumond et al., 2007a). The Upper Granite Gorge thus represents a sub-horizontal section of lowermost middle continental crust (~0.7 GPa) at least at the time of peak metamorphism. The entire ~70 km-long transect

apparently decompressed from ~0.7 GPa to ~0.3–0.4 GPa levels (back to the regional middle crustal level) as one large coherent block immediately after tectonism in the Paleoproterozoic (Dumond et al., 2007a).

Tectonic models for this region are similar to models proposed for other parts of the southwestern United States, involving stabilization of dominantly juvenile Proterozoic crust during arc collisions. One shear zone within the Upper Gorge isobaric terrane has been interpreted as a suture zone between different arcs (Ilg et al., 1996). Hence, this isobaric terrane, like the others, probably includes juxtaposition of different crustal levels, but the peak pressures are interpreted to record stabilization of an accretionary “duplex system” at 20–25 km depths near the end of the convergent process (~1.7–1.69 Ga; Ilg et al., 1996). Exhumation of this terrane to 10–15-km levels at ca. 1.68 Ga may reflect continued syn-shortening exhumation (thrusting plus erosion or fault-removal of overlying material) of a large isobaric region within the same orogenic cycle before long-term residence (1.68–1.4 Ga) at ~10–15 km depths (Dumond et al., 2007a). Extensional collapse of overthickened crust might also have been active, but syn-decompressional extensional structures have not been identified at exposed crustal levels.

During this same time interval, rocks southeast of the Big Bug block, called the “Mazatzal block,” appear to preserve a region that was at shallow crustal levels. The Mazatzal block consists of the 1.73 Ga Payson ophiolite as basement (Dann and Bowring, 1997) to ca. 1.70 Ga quartzites that were deposited at the same time as the 1.70 Ga emplacement of the Crazy Basin batholith. The deformational architecture of the quartzites is that of a shallow-level fold-thrust belt (Doe and Karlstrom, 1991). Although the timing and movement history on the shear zones that juxtapose this level with the 10 km isobaric terrane of the Big Bug block remain incompletely understood (Karlstrom et al., 1987), this snapshot of upper-crustal levels can be integrated with the isobaric sections in terms of a schematic whole-crustal column, and reinforces the importance of understanding the mechanisms of juxtaposition and ultimate preservation of different crustal levels within an orogenic system (e.g., Klepeis et al., 2007).

OBSERVATIONS AND COMPARISONS

Lateral Heterogeneity

A first-order characteristic of each of the isobaric terranes discussed above is their heterogeneity of rock types, structures, fabrics, and metamorphic assemblages. Because each of the regions is interpreted to represent either a contiguous or disrupted but reconstructable isobaric terrane, it is possible to appreciate the extreme lateral variation in almost all of the characteristics that control rheology. Rocks vary from mafic to felsic, massive to layered, regular to contorted, highly strained to relatively undeformed, porphyroblast-rich to porphyroblast-poor, and relatively wet to relatively dry. Even the scale of heterogeneity is variable. It would certainly not be possible to assign a single rock type,

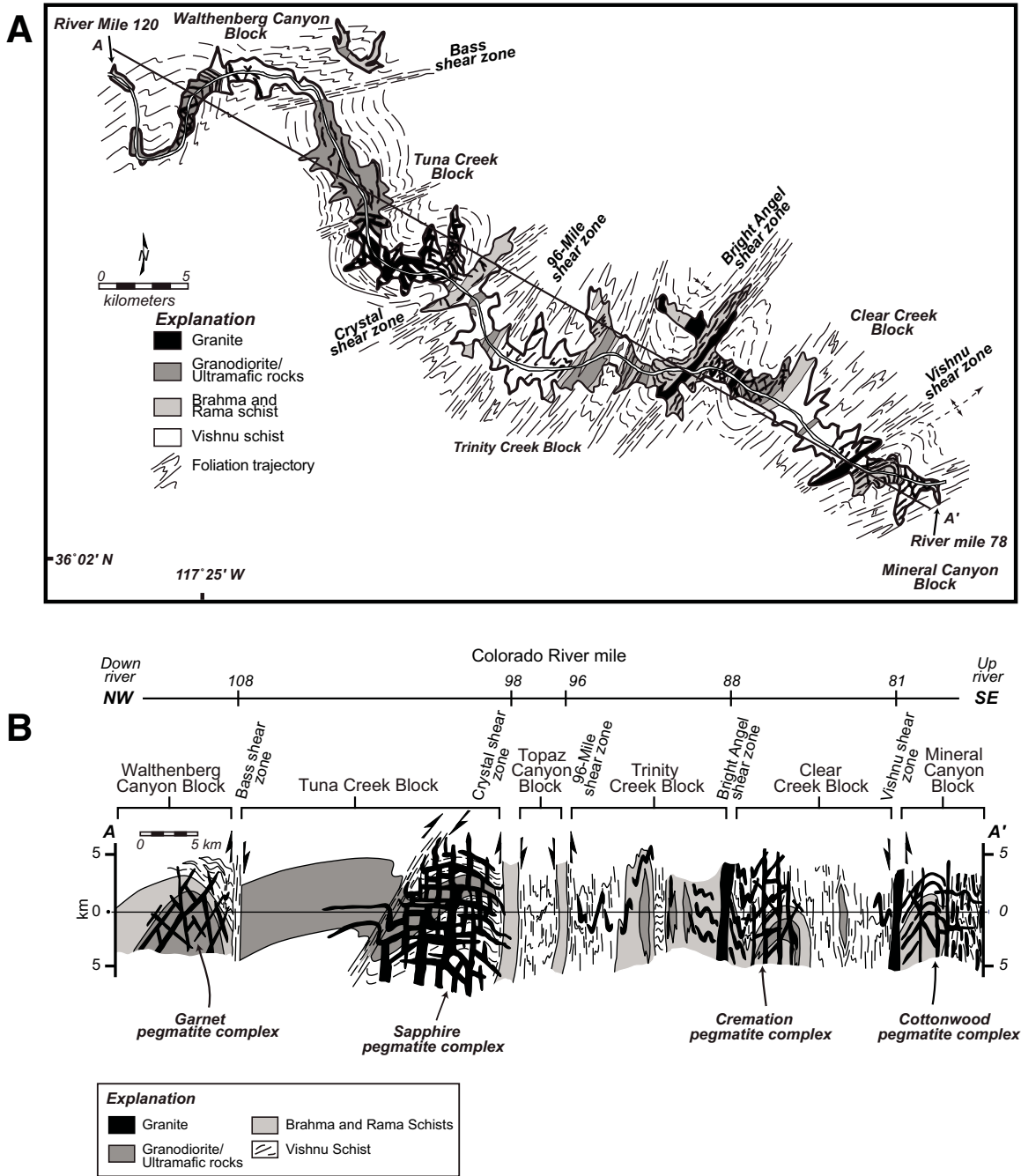


Figure 6. Generalized geologic map (A) and cross section (B) of the Upper Gorge of the Grand Canyon (modified from Ilg et al., 1996; Dumond et al., 2007a). See text for discussion.

reology, or set of physical properties to any of these crustal levels. Interpreting geophysical images and crustal rheology must involve understanding the nature, evolution, and implications of this heterogeneity at all scales, as emphasized (but not yet achieved) by recent thermal-mechanical numerical modeling efforts (Jamieson et al., 2007; Groome et al., 2008).

Lateral compositional heterogeneity also evolves; i.e., it can be enhanced or reduced during the orogenic process and/or

during long-term residence at a given crustal level. Mafic underplating and intraplating significantly changes bulk density, rheology, and thermal structure as do metamorphic reactions (particularly those involving growth or dissolution of garnet). This is particularly relevant for interpreting geophysical data. It is important to correlate seismic images with data about the history of the particular crust being imaged (Rutter et al., 1999; Magnani et al., 2004; Karlstrom et al., 2005). This record of

evolution through time can, in some cases, provide a template that may be used to help interpret the dynamics of modern orogens that are imaged geophysically (e.g., Mahan, 2006). For example, seismic images of Magnani et al. (2004) show strong deep-crustal reflections that are interpreted to be of vastly different ages. Prominent but somewhat diffuse bands of reflectivity are interpreted as a Proterozoic bivergent collisional system, and these reflections are cross-cut by sharper bright reflectors interpreted to be mafic sills emplaced during much later (either 1.1 Ga or Miocene) magmatism.

Shallow and Steep Fabrics

Despite the differences in crustal level, a number of structural characteristics are shared by each of the isobaric terranes investigated here. These include (1) the presence of early sub-horizontal or shallowly dipping deformation fabrics (S_1) and later, variably intense, upright structures and fabrics (S_2); (2) a resulting block-type architecture that reflects the distribution of zones or domains with minimal overprinting by S_2 fabric and those with intense transposition and S_2 fabric development; and (3) the scale of this structural heterogeneity, best developed on the 10 km scale, but expressed from micrometers to tens of kilometers. In each region, domains dominated by shallowly dipping and gently folded S_1 fabric are separated by domains of steep intense S_2 fabric. In some areas, the high-strain S_2 domains can be classified as shear zones across which rock types and structures cannot be readily correlated, but others are zones with only slight offset of earlier markers (Ilg et al., 1996). There is evidence for more than one generation of folds and cleavage within the overall shallow and steep fabric domains (i.e., S_{1a} , S_{1b} , S_{2a} , S_{2b} , etc.), but it is commonly difficult to break out regionally correlative fabric-producing sub-events. This may suggest that the transition from shallow to steep deformation reflects not just a new pulse of deformation, but a more fundamental change in rock properties and bulk strain.

Timing issues are critical and can be extremely difficult to resolve. One of the first-order questions concerning the significance of the block-type architecture is the extent to which the block geometry was established when the domains existed at depth in the crust (perhaps inheriting even earlier D_1 accretionary boundaries), if it was established during progressive crustal shortening (D_2), and/or during exhumation. A further complication is that block-bounding shear zones commonly get reactivated during even later (post- D_2) more localized movements. These later movements span the ductile and brittle strain regimes and typically coincide with exhumation of the region.

The steep fabrics, structures, and strain gradients are typically the most apparent features, especially on geologic maps and cross sections, although perhaps not on seismic images (e.g., reflection seismic transparency of vertical anisotropy: Levander et al., 1994). These might be initially taken as the dominant structures representing the dominant tectonic event(s). However, in each area, closer inspection reveals that the earlier fabrics

are more penetrative and pervasive, at least outside of intense block-bounding shear zones. These early sub-horizontal fabrics represent fundamental components of the tectonic history, and are critical for understanding the crustal evolution and crustal processes in general. The less reoriented shallow fabrics would be preferentially imaged in reflection seismic profiles and thus, domains of strong versus weak reflectivity may correspond to domains where predominantly shallow versus steep fabrics are preserved. Thus, domains of weak reflectivity may correspond to vertically foliated crust rather than zones of low signal/noise in the seismic data acquisition process.

P-T Context of Steep and Shallow Fabric Development

Understanding the significance of the steep and shallow fabrics involves understanding the depth and timing of deformation events, i.e., the *P-T-t*-deformation history, of the block-bounding shear zones relative to the history of the blocks themselves. Recent work in the Upper Granite Gorge of the Grand Canyon (Dumond et al., 2007a) illustrates some of the methods and challenges associated with constraining these structures. Thermobarometric (*P-T*) calculations, and the ability to date metamorphic fabrics via geochronology, generally have large uncertainties, making it difficult to recognize pressure differences across structures. Techniques such as relative *P-T* calculations can provide better resolution but it can be difficult to separate thermal and baric effects (Hodges and McKenna, 1987; Worley and Powell, 2000; Dumond et al., 2007a).

All three terranes discussed here contain both earlier shallow and later steep fabrics (Fig. 7), but there are important differences with respect to the timing of fabric development and its relationship to metamorphism. In the Athabasca granulite terrane, early shallow fabrics generally coincide with the highest-temperature metamorphic conditions. Hundreds of km² areas of early fabrics are associated with intense melting followed by isobaric-cooling and $L \gg S$ to L -tectonite development (Dumond et al., 2005a, 2006). Where evidence for melting is lacking, early high-temperature (>700 °C) sub-horizontal fabric development is synchronous with lower-crustal emplacement and cooling of granitoid plutons and batholiths (Dumond et al., 2005a, 2005b) and syn-metamorphic recrystallization (Williams et al., 2000). It has generally not been possible to identify even earlier, prograde, fabric elements that may pre-date the oldest plutons because most of the rocks probably originated as deep-crustal plutonic rocks. Steep fabrics in the deep crustal rocks are generally more discrete and commonly indicate lower temperature conditions.

In contrast, the shallowly dipping S_1 fabric in both Proterozoic terranes of the southwestern United States apparently initiated at lower grade and is interpreted to reflect prograde metamorphic conditions. Peak conditions were generally associated with the D_2 events (Williams, 1994; Karlstrom and Williams, 1995; Ilg et al., 1996; Dumond et al., 2007a). However, an additional characteristic of the Upper Granite Gorge is that the shallow fabrics locally preserve composite histories where

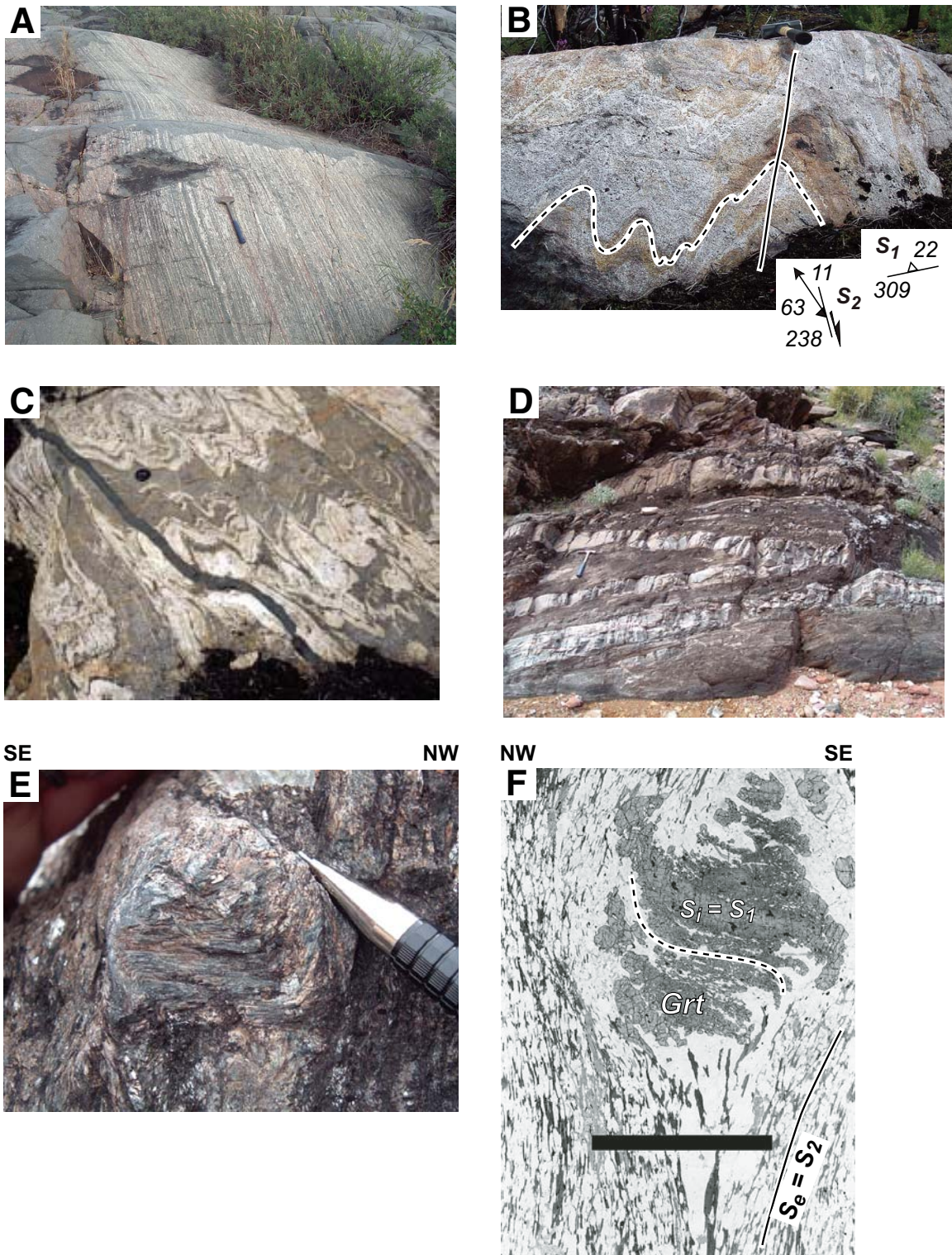


Figure 7. Photos showing early shallow (S_1) and steep (S_2) fabrics in East Lake Athabasca and the Grand Canyon. (A) Shallow S_1 surface, northwestern domain, East Lake Athabasca with strong lineation parallel to hammer. (B) S_2 -overprinting of S_1 migmatite/restite “white gneiss”, Southern domain, East Lake Athabasca granulite terrane. (C) S_2 -overprinting of S_1 in tonalitic orthogneiss, eastern Chipman domain, East Athabasca. Dike is interpreted to represent a syn- S_2 Chipman dike. Camera lens cap for scale. (D) Large early intrafolial fold with S_1 defining the axial plane, mile-102, Grand Canyon. (E) Andalusite crystal with S_1 inclusion trails and S_2 external foliation, mile 84, Grand Canyon. (F) S_1 - S_2 relationships from sub-vertical thin section cut normal to S_2 foliation and parallel to lineation in Grt-Bt-Ms-Pl-Qtz schist from Upper Granite Gorge, Grand Canyon (scale ~3 mm: modified from Ilg and Karlstrom, 2000).

the S_1 fabric initially formed during prograde metamorphism but was reactivated and modified during peak metamorphism and D_2 deformation (Fig. 8).

Differences in timing relationships, especially with respect to metamorphism, have led to differences in the interpretations and implications of the fabric transition in the deep and mid-crustal examples. In the former (Athabasca), the shallow fabrics are interpreted to result from weakness of the deep crust possibly involving flow due to differential lithostatic load (e.g., Royden, 1996) or mantle dynamics (Tikoff et al., 2004). In the middle crust of the southwestern United States, the early fabrics are interpreted to represent collisional fabrics, perhaps shear zones related to early thrust sheets that formed during crustal thickening (Karlstrom and Williams, 2006). These differences have important implications (discussed below) for interpretations of rheology and seismic images.

Absolute Timing Constraints

Absolute timing constraints are critical for interpreting and correlating fabrics in any poly-metamorphic and poly-deformed terrane, particularly the isobaric terranes discussed here. By their nature, these terranes spend an extended period of time at some level of crust, and thus generally preserve fabrics that formed during several, perhaps widely separated, deformation events. Traditionally, ages of fabrics are constrained by dating igneous units that either contain or cross-cut the fabric. However, it can be difficult to isolate the age of one particular fabric in a multiply deformed rock, strain-partitioning can lead to difficulty in determining if an igneous rock was or was not affected by a particular deformation, and fabrics commonly develop diachronously and hence cannot be used as time markers.

U-Pb monazite geochronology, and especially in situ monazite dating, is proving to be a useful tool for constraining the age of metamorphic reactions and deformational fabrics (Hawkins and Bowring, 1999; Williams and Jercinovic, 2002). Under

the right circumstances, monazite itself can be a fabric-forming mineral, an inclusion in a fabric-forming mineral, or a product in a reaction that occurred during a fabric-forming event (Shaw et al., 2001; Williams and Jercinovic, 2002; Mahan et al., 2006b). Monazite overgrowths can grow on earlier grains in the extensional quadrants of the strain ellipsoid; and as such can be used to directly date a deformation event or pulse (Dumond et al., 2008). Further, monazite trace elements can be balanced into metamorphic reactions and thus used to directly date a segment of the P - T path and associated deformation (e.g., Pyle and Spear, 2003; Foster et al., 2004; McFarlane et al., 2005; Mahan et al., 2006b). Careful in situ work can produce precise constraints (with 2σ errors on the order of 10 Ma) on the age of particular fabrics or reactions, and thus allow the history of isobaric terranes to be interpreted and correlated.

Mahan et al. (2006b) used in situ monazite analysis to constrain the age of the major thrust zone that forms the eastern boundary of the Athabasca granulite terrane, and that played a key role in the ultimate exposure of the region. Dumond et al. (2005a, 2005b, 2007b) used similar techniques to show that early shallow fabrics in the terrane are Neoproterozoic and correspond with high-temperature peak metamorphism in the region (Fig. 9A). Multiple generations of steep, cross-cutting fabrics are generally Proterozoic in age and are associated with rheologically stronger conditions. The earliest S_2 fabrics were synchronous with ca. 1.9 Ga granulite-grade metamorphism and were subsequently cross-cut by younger retrograde steep fabrics (Dumond et al., 2006) (Fig. 9B). In contrast, shallow and steep fabrics overlap in age in the Upper Granite Gorge (D_1/S_1 at 1730–1698 Ma and D_2/S_2 at 1713–1685 Ma; Hawkins et al., 1996; Karlstrom et al., 2003), with the steep fabrics corresponding to peak metamorphism. In central Arizona (Big Bug block), peak metamorphism was also synkinematic with D_2 steep fabrics and both fabric intensity and metamorphic temperatures increase with proximity to 1.70–1.68 Ga granitoids (Karlstrom and Williams, 1995). These absolute constraints help to establish a fundamental difference in

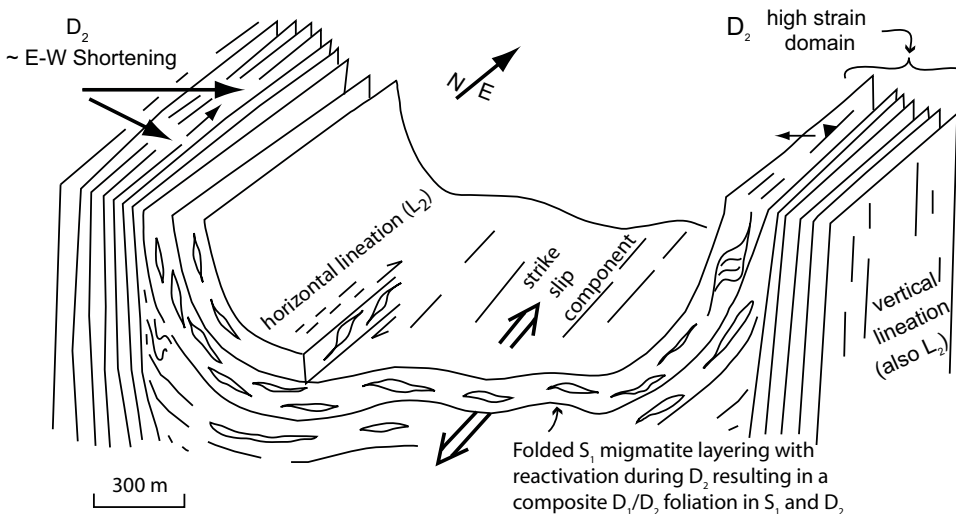


Figure 8. Schematic sketch showing reactivation of S_1 domains during D_2 deformation, Lower Granite Gorge, Grand Canyon. Modified from Karlstrom and Williams (2006).

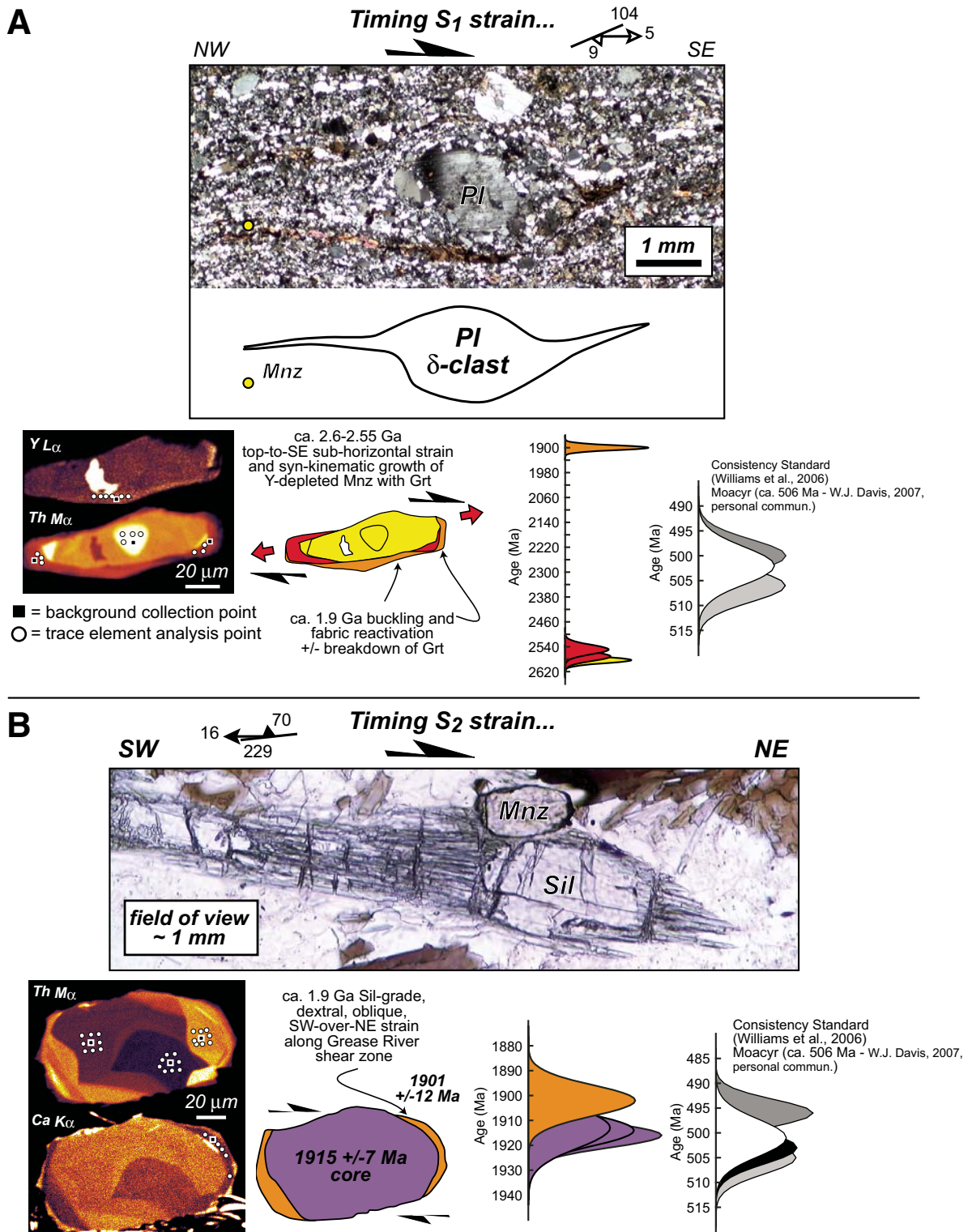


Figure 9. In situ monazite geochronologic constraints on timing of deformation and metamorphism in rocks from East Lake Athabasca. Monazite overgrowths tend to grow in extensional quadrants of strain and are linked chemically to syn-tectonic reactions (Dumond et al., 2006, 2007b). (A) Syn-tectonic monazite associated with Archean S_1 deformation. Small Paleoproterozoic overgrowths on top and bottom edges of grains reflect S_2 reactivation. (B) Syn-tectonic S_2 monazite associated with the upright Grease River shear zone.

the shallow-to-steep fabric transition between the deep and mid-crustal terranes.

Character and History of Plutonism

The nature of igneous rocks and especially their role in deformation/metamorphic processes is another characteristic that can be evaluated using isobaric terranes. Variation in size, geometry, distribution, age, and composition of the igneous bodies is common, and thus the lateral exposure of isobaric terranes allows a more robust assessment of these characteristics through time. Particularly valuable is the ability to evaluate the nature of deformation and metamorphic gradients between domains with a relatively more and relatively less abundant igneous component. These gradients have an important connection to the issues of steep and shallow fabric evolution and the regional block-type architecture.

Athabasca granulite terrane. The deep-crustal rocks of the eastern portion of the Athabasca granulite terrane are dominated by plutonic rocks (tonalite, granodiorite, charnockite, mafic dikes and sills). Although several workers have suggested that some migmatitic rocks were derived from sedimentary protoliths, it is likely that some or many of these rocks were also igneous in origin (i.e., derived from anatexis of orthogneisses: Baldwin et al., 2006). In nearly all areas, the emplacement of new igneous rocks was intimately involved with metamorphism, deformation, or recrystallization of preexisting rocks; that is, an important component of the thermal budget for generating these deep-seated rocks involves advective heating from plutonic rocks. For example, one of the most striking features of the southern domain is the interlayering of thick mafic granulite sheets with garnet-rich felsic granulite (Figs. 10A, 10B) (diatexite of Hanmer, 1994; “white gneiss” of Snoeyenbos et al., 1995; Baldwin et al., 2006). The mafic sheets are interpreted to have been emplaced as thick sills or “intraplates” of mafic magma (Baldwin et al., 2006). The felsic granulites are interpreted to be the restitic products of large amounts of melting of granodioritic or charnockitic rocks. The mafic sills are parallel to, and also contain, a strong S_1 fabric. Leucosomes are more abundant near mafic sills and are aligned and deformed along S_1 , all leading to the interpretation that the emplacement of mafic sills, intense migmatization, and D_1 deformation were broadly synchronous, and some of the heat necessary for the extreme melting came from the mafic underplating (Dumond et al., 2007b).

The dominant component of the Northwestern domain, the Mary granite/granodiorite, was also emplaced during the development of the S_1 , sub-horizontal fabric (Dumond et al., 2005a, 2005b). The pluton was emplaced as a large number of sheets with an assemblage of $\text{Opx-Pl-Kfs-Qtz} \pm \text{Hbl}$. The reaction



occurred during D_1 deformation and recrystallization may have been aided by the emplacement of later stages (sheets) of the same

pluton (Williams et al., 2000). In this case, heat associated with younger phases may have contributed to metamorphism of older phases during the progressive development of the S_1 gneissic fabric. Thus, intrusion, heating, and migmatization of deep-crustal rocks are associated with crustal flow (S_1) and a relatively weak stage in the history of these rocks. Dehydration from melt loss and cooling may lead to strengthening and the shift from shallow to upright deformation phases (Dumond et al., 2005b; e.g., Klepeis et al., 2003, 2004).

Igneous rocks are also associated with the younger S_2 fabrics. Granitoids and pegmatitic dikes were emplaced along zones of intense D_2 fabric and most also contain the D_2 fabric. The D_2 high-strain domains may have facilitated emplacement of these granitoid bodies, but the presence of magma may have equally played a role in weakening the crust and allowing localization of the D_2 strain (e.g., Hollister and Crawford, 1986). The Chipman dike swarm (Williams et al., 1995; Flowers et al., 2006a) is one noteworthy example. Near vertical, northeast-striking mafic dikes, one to ten meters in thickness, were emplaced into the Mesoproterozoic Chipman tonalite. Earlier dikes were metamorphosed and locally melted by heating interpreted to result from later Chipman magmatism, involving dikes and underplating. D_2 deformation was localized in the region of the dike swarm (Figs. 10C, 10D).

Upper Granite Gorge. Mafic, intermediate, and felsic arc-related plutonic and volcanic rocks are volumetrically significant components of the lowermost middle continental crust represented by Upper Granite Gorge of the Grand Canyon. Unlike the Athabasca region, the metasedimentary and metavolcanic rocks of most blocks were at or near the surface prior to the onset of tectonism. Thus, the nearly contemporaneous arc-related plutons were intruded relatively shallowly into low-temperature metasedimentary rocks, and had minimal effect on the rheology or metamorphic grade. In contrast, magmatism associated with peak metamorphism and D_2 deformation was dominantly 1.7–1.68 Ga granite and pegmatite (Hawkins et al., 1996). These felsic rocks occur primarily as swarms of meter-scale dikes associated with three large complexes (Figs. 10E, 10F). The dike swarms are spatially associated with increased metamorphic temperatures (Ilg et al., 1996; Dumond et al., 2007a). Although there is evidence for some in situ melting, a significant proportion of the melt is interpreted to have been introduced from below (Fig. 10G). Karlstrom and Williams (2006) suggested that these dike complexes represent granite melts that were in transition to higher structural levels; they acted as conduits feeding shallow-level ca. 1.7–1.68 Ga granite plutons. In addition, some zones of intense S_2 fabric are strongly migmatitic with abundant cm-scale leucosomes, suggesting that they may have been conduits through which magma has passed in a more dispersed fashion.

We suggest that the Upper Granite Gorge isobaric section captures a zone of transport through which felsic melts were passing to higher levels of the crust. This through-put certainly contributed advective heat and dramatically modified the bulk composition of the crust at this level, by the addition

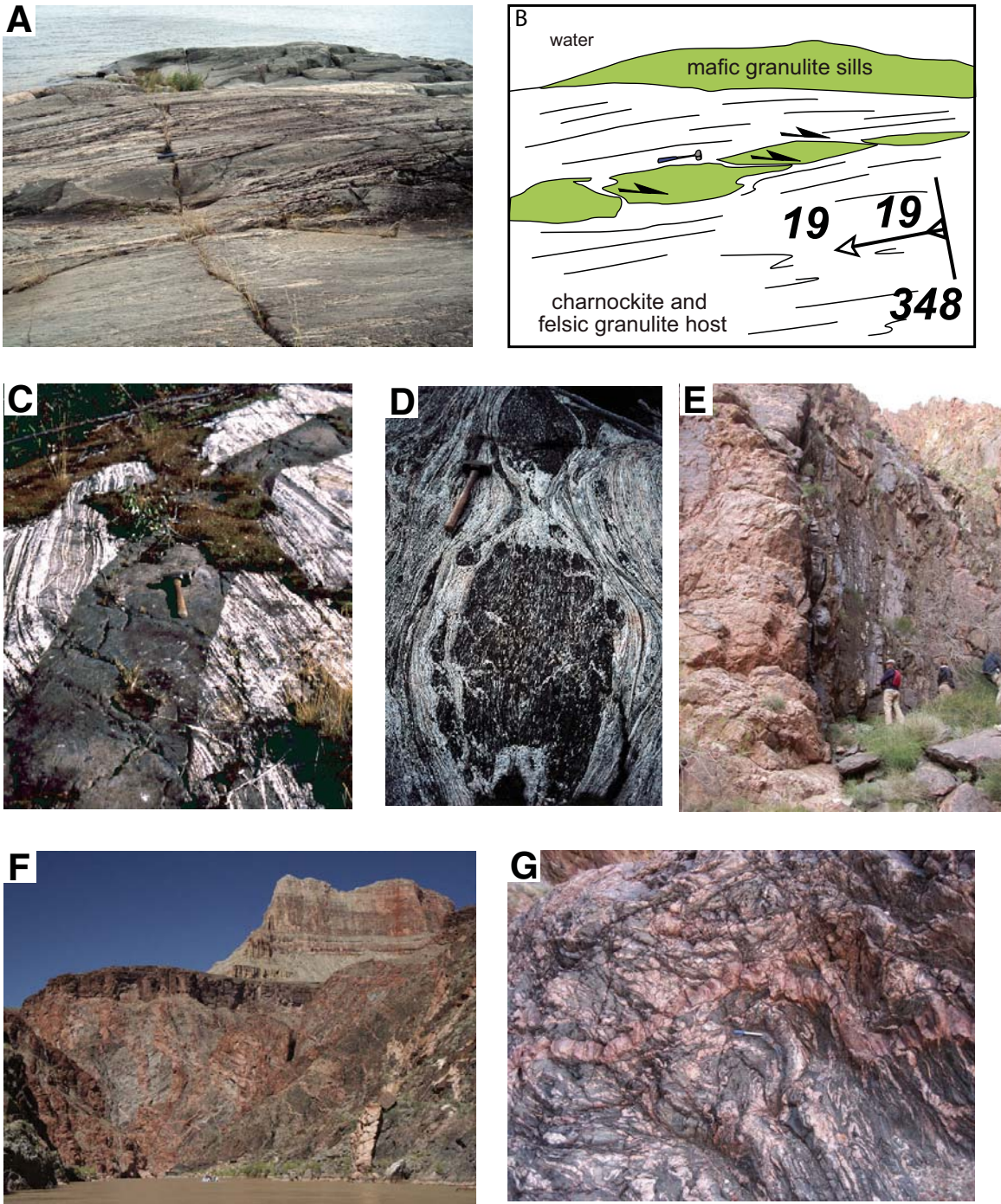


Figure 10. Photos showing relationships with igneous rocks. Photo (A) and line drawing (B) of sub-horizontal mafic granulite sills, derived from gabbroic protolith, emplaced in southern domain, East Athabasca. The sill-like bodies of mafic granulite (and locally eclogite) contain the penetrative S_1 fabric, and are intensely veined internally and at their contacts by felsic leucosomes. Relatively undeformed (C) and strongly deformed within S_2 fabric (D) sub-vertical mafic dikes, Chipman dike swarm, East Athabasca. (E) Large granitic-pegmatitic dike and strong S_2 fabric, Upper Gorge, Grand Canyon. (F) Pegmatite swarm near Phantom Ranch, Upper Gorge, Grand Canyon. (G) Close-up of migmatitic schist, Upper Gorge, Grand Canyon, interpreted to be injection migmatites in a zone of magma through-put.

of abundant granitoid materials. The Upper Granite Gorge isobaric terrane provides an excellent opportunity to compare the cooler less-modified rocks, away from the dike complexes, to those that have served as conduits for magma transfer. Unlike the Canadian deep crustal terrane, there is a notable lack of syn- S_2 mafic dikes in most of the exposed Upper Granite Gorge terrane. We speculate that such magmas may not have been able to pass through a zone of more abundant migmatite somewhat below the 20–25 km exposure level (Vernon et al., 1990). This level might correspond to the 16–21-km-deep “bright” seismic reflectors imaged by the INDEPTH profile beneath the Tibetan Plateau that are interpreted to mark the top of a mid-crustal partial melt zone (Nelson et al., 1996).

Central Arizona basement. At least 50% of the ~0.3–0.4 GPa basement rocks in central Arizona consists of granodiorite to granite. Similar to the Upper Granite Gorge, the granodiorite complexes tend to be older and more mafic, and are interpreted to be portions of arc batholiths. However, some of the largest plutons are ca 1.7–1.65 Ga syn-tectonic granite batholiths. For example, the Crazy Basin quartz monzonite (Fig. 5) is composed of a large number of sheets and dikes (Karlstrom and Williams, 1995), and screens of country rocks are present, but plutons can be readily distinguished. It is likely that some magma passed to even higher levels of the crust and perhaps erupted, but exposures at 0.3–0.4 GPa (10–15 km paleodepth) level are distinctly different from those of the Upper Granite Gorge. This crustal level is considered to be one of pluton-building rather than the site of through-put as inferred for the Upper Granite Gorge. This is compatible with the hypothesis that the 10–15-km-deep level represents a zone of neutral buoyancy for granitoid magmas (Vernon et al., 1990).

Calculated metamorphic pressures are relatively constant across much of the central Arizona basement terrane (0.3–0.4 GPa), but temperatures, and D_2 fabric intensity, increase toward the margins of syn-tectonic plutons. Regional (“background”) metamorphic temperatures may have been as low as 350–400 °C, but temperatures reached 600 °C or higher near plutons (Karlstrom and Williams, 1995). As in the Upper Granite Gorge, ca. 1.7–1.65 Ga felsic igneous rocks are an important component of the thermal budget, but the effects seem to be much more localized around the large plutons. Even though plutonic rocks are extremely abundant, migmatites are rare. They occur primarily near igneous bodies and in country rock screens where temperatures were highest. These migmatites are mainly injection migmatites and may have had the least affect on the overall rheology of this crustal level, although they may have helped accommodate pluton expansion during progressive syn-tectonic emplacement.

Summary of plutonic observations. All three isobaric terranes record different expressions of the transfer of heat and magma through the crust. At deep crustal levels, heat and mass are transferred from the upper mantle to the deepest levels of continental crust via basaltic magmas. In appropriate bulk compositions, the mafic rocks can lead to extensive melting with weakening, flow, and ultimately, upward transfer of tonalitic magma.

The 20–25 km level preserved in the Grand Canyon may be primarily a zone of granite magma transfer with local partial melting. The heat and fluids play an important role in partitioning S_2 fabric and localizing high-strain zones that serve to maintain and enhance the segmented block-type architecture. The relative lack of mafic igneous rocks in the Grand Canyon, in contrast to the abundant mafic dikes and sills in the Athabasca terrane, may suggest that mafic magmas were ‘filtered’ at some deeper level. The 10–15-km levels preserved across the southwestern United States host abundant granitic plutonic rocks with many plutons built by successive dike emplacement. This is clearly a level of accumulation of felsic igneous rock and the locus for a dramatic feedback between magmatism and deformation: the D_2/S_2 strain/fabric accommodated magma emplacement and in turn, the magma led to weakening and strain localization.

The combined picture is one of crustal differentiation and evolution driven by heat and magma and with important feedbacks with deformation and metamorphism at each level (Fig. 11) (see also Buddington, 1959; Pitcher, 1979; and Holm et al., 2005). Important questions in interpreting seismic sections include: (1) At what stage in this type of evolution is the particular seismic image? (2) Can we recognize the transient magma-related weakening within the overall image, as was postulated from the INDEPTH sections (Nelson et al., 1996) and from “bright spots” in rift zones (Brown et al., 1980); and (3) How is the history of the rock material presently captured in these images likely to influence its rheology and geophysical properties? Isobaric terranes can provide data on the distribution, abundance, and deformational character of igneous rocks through time that two-dimensional sections may miss or misrepresent.

IMPLICATIONS

Figure 11 is a composite section showing characteristics of the isobaric terranes highlighted here on a single depth axis. The sections that come from southwestern Laurentia involve rocks and tectonic events of similar age and thus might be reasonably stacked into a theoretical crust (e.g., central Arizona above the Upper Gorge section). However, our main purpose in stacking the sections is not to build a theoretical (model) crust, but to provide a comparison of tectonic style and process at specific depths as a general illustration for the following discussion.

Implications for Crustal Flow Models

Lateral flow in the crust at one crustal level or another has been increasingly invoked in models for the evolution of orogenic belts (Beaumont et al., 2001; Hodges et al., 2001; Grujic et al., 2002; Williams and Jiang, 2005; cf. Law et al., 2006). From fluid mechanics, two broad types of flow have been distinguished: Couette flow, in which vergence remains constant across the zone of flow and Poyseuille flow, in which vergence reverses within the zone of flow (e.g., Turcotte and Schubert, 2002; cf. Ch. 6). Couette flows are essentially shear zones and might be considered

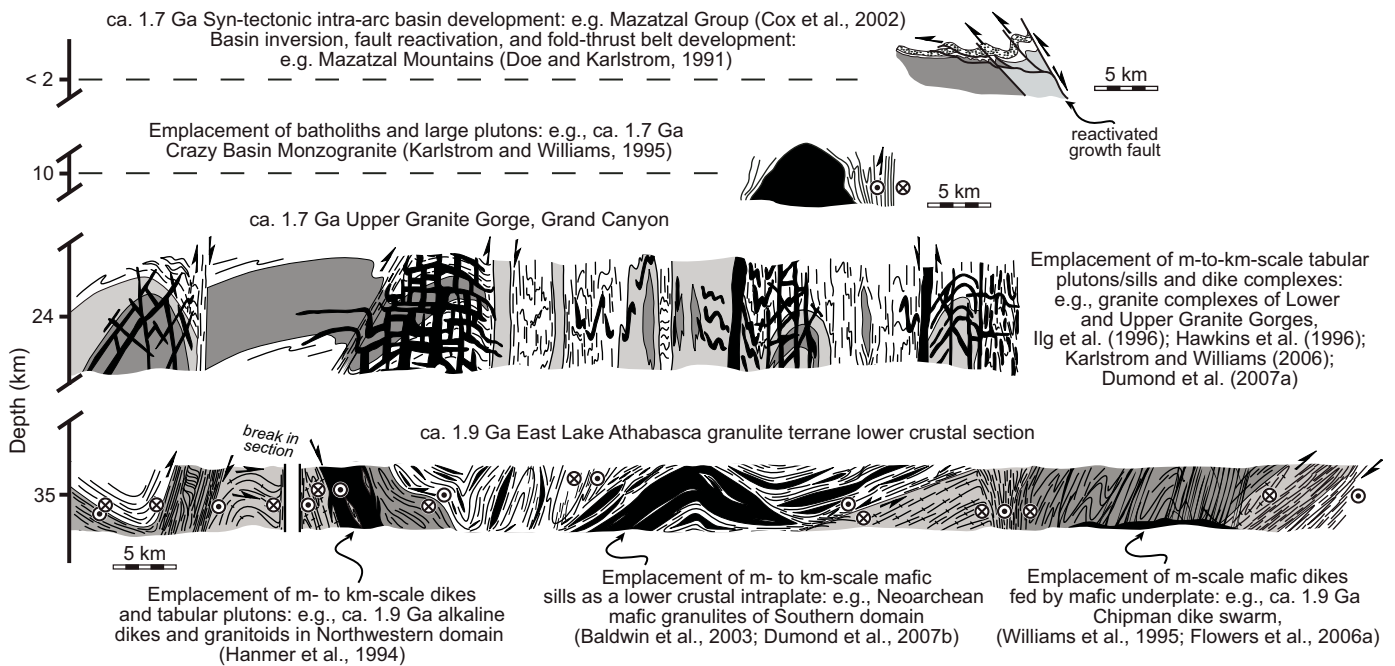


Figure 11. Schematic diagram showing isobaric sections from East Lake Athabasca and Proterozoic terranes from southwestern North America. This is not meant to depict a model crust but instead to provide a means of comparing tectonic styles and processes at different crustal levels. See text for discussion.

as detachment or partial detachment zones (Tikoff et al., 2002; Williams and Jiang, 2005). Pousseuille (pipe) flows are generally called channel flows and involve the ductile extrusion of crustal material between two rheologically stronger crustal layers. Both types of flow, but particularly channel flow, have been used to reconcile surface topography and surface processes with crustal and/or mantle dynamics (e.g., Clark and Royden, 2000). Many interpretations have been based on numerical or analog models or on interpretations of surface topography and structure (Royden et al., 1997; Beaumont et al., 2001, 2004), and most models are fundamentally two-dimensional. Isobaric terranes offer an opportunity to evaluate the third dimension, the aerial extent, of lateral flow process and the conditions that promote or inhibit crustal flow. This is particularly important for interpretations based on seismic images that might preferentially image gently-dipping fabrics (TRANSALP Working Group, 2002; Meissner et al., 2006).

Sub-horizontal transposition fabrics are extremely common, both in the examples described here and in many other metamorphic terrains (e.g., Williams and Jiang, 2005). One obvious first-order question involves evaluating the nature of the strain or flow that is implied by these fabrics. Distinguishing channel flow from a shear zone or detachment involves the recognition of a reversal in vergence within the zone. At first, this seems less feasible in an isobaric (i.e., horizontal) crustal exposure rather than in a crustal cross section. However, many isobaric terranes are at least somewhat oblique allowing some depth perspective, or as in all of the isobaric terranes described here, internal faults and shear zones within the terrane can allow evaluation of slightly

different depths. The isobaric terranes thus allow a broader survey of kinematics, deformational style, and strain partitioning at each level.

A comprehensive evaluation is not yet complete in any of these terranes. However, the sense of shear on the early (S_1) fabric in the Athabasca granulite terrane is remarkably consistent (i.e., top to the southeast), suggesting that this may be more a zone of partial detachment (Couette-type flow). If the fabrics do represent a channel flow, consistent with crustal extrusion, then only part of the channel is exposed. In the southwestern U.S. terranes, vergence on S_1 is more difficult to determine because of the intensity of syn- D_2 peak metamorphism. The orientation of the early mineral lineation is regionally consistent and the northwesterly orientation is also compatible with paleogeography and regional tectonic constraints (Jessup et al., 2005; Whitmeyer and Karlstrom, 2007). These may favor a detachment style of flow that is more typical of processes in accretionary orogens (e.g., Platt, 1986) rather than a channel flow.

Tikoff et al. (2002) identified three general levels of partial detachment or “clutch zones” that might be expected within continental lithosphere: one in the mid-crust, one in the deep crust above the Moho, and one near the lithosphere-asthenosphere boundary. The isobaric terranes described here provide exposures of the upper two of these levels. The following comments are meant to illustrate that isobaric terranes provide an important perspective and data source for understanding crustal flow, especially the conditions under which flow may occur or be inhibited, particularly in a typical heterogeneous crust.

The basic structural geometry of the three crustal levels described here is extremely similar, i.e., early penetrative S_1 fabric overprinted by upright S_2 fabric domains and shear zones. The details of the P - T history and the timing of fabric development relative to metamorphism, however, are different, and in turn, the interpretation of the S_1 fabric in terms of crustal flow is different. In the Athabasca granulite terrane, the early shallow fabric was developed regionally near peak metamorphic temperatures, with extensive migmatite development. This event represents the principal dehydration of biotite- and amphibole-bearing rocks. The rocks were apparently at their weakest during the development of the sub-horizontal S_1 fabric (Dumond et al., 2005b). If the S_1 fabric was the product of channel flow it might be interpreted to be analogous to the hypothesized flow of the deepest crust eastward away from the Tibetan Plateau today (Royden, 1996; Royden et al., 1997; Clark and Royden, 2000; Shapiro et al., 2004). However, indicators associated with S_1 are abundant and suggest a uniform vergence, as would be expected for a deep crustal partial detachment zone immediately above the Moho. Thus far, there is no evidence for a reversal of vergence or extrusion of material. Without such a reversal, the early fabric more likely represents a large scale shear zone or "clutch zone" (Tikoff et al., 2002). During S_2 time, even though metamorphic temperatures were locally as hot or hotter than during S_1 formation, the lower crust was rheologically stronger, mainly because it was drier and less fertile for melting. The lower crust was segmented by steep S_2 domains and shear zones and there was little tendency for lateral flow.

In both of the mid-crustal examples, the 20–25 km Grand Canyon and the 10–15 km central Arizona terrane, S_1 apparently developed during prograde metamorphism. During S_1 strain, the rocks were generally cooler with little or no melt component. The gently dipping deformational fabric may represent the deeper parts of thrust faults or shear zones associated with thickening and prograde metamorphism in an accretionary system. The metamorphic peak, amphibolite or lower granulite facies, occurred during the formation of the upright (S_2) fabrics, with local reactivation of S_1 . The crust was highly partitioned into the S_1 and S_2 domains, despite the abundance of water (hydrous phases like muscovite and biotite) and locally significant melting. There is little evidence for crustal flow at this time, even though the rheology of the hot domains was probably appropriate for flow. A regional channel flow would require a dramatic disruption of the segmented crustal architecture that seems to characterize this crustal level through a vast region and thus would probably require significant additional weakening and/or melting (see also Beaumont et al., 2004). The earlier S_1 fabric may represent a detachment or "clutch zone," and the prograde character of the P - T - t history indicates a connection with thrusting and crustal thickening.

An important characteristic of the S_1 fabric in each isobaric terrane is its lateral heterogeneity. The fabrics change from L-tectonite to L-S tectonite to S-tectonite, and some blocks within the overall flow regime were apparently characterized by a much stronger rheology such that the early flow fabric was partitioned against or around these blocks (Karlstrom and Bowring, 1988).

The fabric heterogeneity may be one strong control on the degree of coupling or detachment across the zone. Ultimately, it will be possible to build a map of strain and flow at specific crustal levels and specific times and even possibly stack appropriate maps to build a three-dimensional image of flow and coupling. These can be compared and combined with interpretations from tilted crustal sections (e.g., Klepeis et al., 2003, 2004, 2007).

Channel flows and/or detachment zones appear to require a special combination of conditions. Particular crustal levels may only exhibit a susceptibility to flow or detachment (i.e., weak behavior) during specific times in their P - T -deformation evolution, a behavior that is also heavily dependent upon bulk composition and fertility for melting. These interpretations can only come from accurately timing the P - T history and linking it to the tectonometamorphic history and thus are virtually impossible to infer from remote seismic images. More speculatively, regionally extensive isobaric domains may be a record of orogenic plateau development, such that flowing crust at some level precluded the maintenance of large topographic relief at the surface. Multi-disciplinary study of the distribution of isobaric terranes consequently provides important data for reconstructing aspects of the topography of ancient mountain belts, in addition to providing a window into orogenic plateaus at depth.

Implications for Interpretation of Seismic Data

The block-type architecture and common presence of steep and shallow fabric domains is important for the interpretation of seismic images of the middle and deep crust. Steep shear zones may not be directly recognized in many seismic reflection surveys and may show up as velocity transitions between disparate blocks, seismically slow and seismically fast domains, in teleseismic images (e.g., Levander et al., 1994). The presence of steep deformation zones may be inferred based on differences in the character of juxtaposed domains, but the presence of a relatively intense S_1 in most domains may lead to similar reflectivity, especially because similar metamorphic grades are generally involved in each case. Consequently, the relative invisibility of the steep domains may lead to erroneous interpretations about the continuity of domains and the associated subhorizontal structures. One might get the impression that lateral transport of material may have occurred or at least that there is a relatively homogeneous structural character. In addition, the significance of fabric domains for the overall tectonic history is difficult to deduce remotely, and similar architectures may represent very different tectonic histories.

The metamorphic grade and P - T history of a region are also very important for interpreting seismic data. Each terrane shows evidence for dramatic changes in mineralogy, fluid content, and texture during orogenic events and also after, perhaps long after, tectonism. For example the progressive growth of garnet at the expense of orthopyroxene or hornblende in deep-crustal charnockites may contribute to densification of the deep crust long after tectonism (Williams et al., 2000). Isobaric terranes can be

used to recognize styles of syn-tectonic and post-tectonic metamorphic reactions at different crustal levels and ultimately allow these effects to be identified in remote, geophysically derived sections (e.g., Fischer, 2002). Another consideration is the fabric anisotropy that is characteristic of each of the examples presented. Even in seismic studies that are focused on the mantle, the effects of crustal anisotropy and the extreme compositional heterogeneity are significant and must be considered (Mahan, 2006).

After decades of work, it is surprising how difficult it has been to recognize original microplate boundaries and/or sutures in each of these isobaric terranes. Each terrane is likely to include boundaries and paleosutures, and several have been proposed in the literature (Ilg et al., 1996; Tyson et al., 2002; Magnani et al., 2004; Duebendorfer et al., 2006). The lack of ophiolites, blueschists, and accretionary prisms has long been used to argue against plate tectonics (Stern, 2005; Ernst, 2006), but the counter to that argument is the recognition that the preservation potential of these rocks is very low at all levels in orogens. The isobaric sections discussed here reinforce this observation, but also make the point that such rocks may not be easily recognized at deep crustal levels. For example, the Grand Canyon transect (Fig. 6) is interpreted as a deep mid-crustal duplex in part because of the interleaving, at the 20–25 km levels, of pillow lavas and turbidites from the surface with ultramafic rocks of possible deep-crustal arc cumulate origin. This necessitates that these rocks have been translated >10's of km relative to each other before becoming stabilized at 20–25 km depths prior to final exhumation. This is another issue that would not be clear from remote images or xenolith data alone.

Implications for Understanding Stabilization of Continental Lithosphere

Each of the three isobaric terranes preserves a view of the transition from a less stable or less mature crust to a more stable or more mature one, but the transition is dramatically different in each case. The deep-crustal level records the progressive dehydration, local melt loss, and subsequent isobaric cooling and extensive garnet growth that reflects a temporal transition from a relatively weak and melt-laden crust to a strong, anhydrous deep crust (see also Klepeis et al., 2003, 2004). The mid-crustal examples document the establishment of a dynamic block-type architecture that fundamentally controls the crustal rheology. The overall strength may be high despite local zones of high strain and magma flow (Karlstrom and Williams, 1998). Igneous rocks play a number of critical roles at each level, contributing to the progressive evolution of lithologic and rheologic properties through time. They introduce significant heat and serve to localize deformation in a feedback relationship at each crustal level.

In terms of crustal evolution and stabilization, the deep flux of basaltic magma from mantle depths to the base of the crust has the tectonic effects of destabilizing the lithosphere (e.g., Flowers et al., 2006a), enhancing deformation and crustal flow through melt-weakening at appropriate levels, and instigating upward

flux of heat and melt that variably affect all higher levels. The longer-term effect involves depleting (and de-densifying) the upper mantle in terms of its Fe-component and causing thickening (and stabilization) of the lower crust (cf. Dufek and Bergantz, 2005). During isobaric cooling of deep-crustal rocks, there is a general tendency for rocks to grow garnet at the expense of pyroxene and plagioclase (Williams et al., 2000). This occurs because the rocks progressively cool into the field of high-pressure granulites (Fig. 1A). Although there may be kinetic barriers and small amounts of deformation and/or heating may be required, the general tendency is toward increasing density and probably strength (Williams et al., 2000). There is little evidence that surface-derived fluids reach this level to a significant degree. The lack of water may at least partly explain the general lack of coarsening and annealing of many rock types. The post-metamorphic evolution of the mid crust at both levels (0.7 GPa, Grand Canyon and 0.4 GPa, central Arizona) seems to involve local rehydration and annealing. Water may reach these levels from the surface but additional water may come from cooling plutonic rocks. This would be associated with a general decrease in density and strength and a general fertility for further deformation and or metamorphism in the future. It is interesting to note that both deep- and mid-crustal regions preserve evidence for major reactivation at a much later time, 1.9 Ga in Canada and 1.4 Ga in the southwestern United States. Both of these events are associated with new igneous activity. It seems likely that these igneous rocks provide not only heat but also new fertility for deformation and metamorphism especially at deeper levels, but the deformation was entirely different, as it was marked by development of steep cleavage rather than lateral flow. These observations emphasize that fundamental modifications may occur in a crustal terrane after the predominant tectonic event. This is an important consideration for interpretation of seismic images of ancient orogens.

SUMMARY

Isobaric terranes provide laboratories within which to evaluate the nature of continental crust and especially the nature and interplay of tectonic process through time at specific crustal levels. They provide a set of observable features against which geophysical models can be compared, and possible source rocks for igneous rocks and xenoliths. Clearly, each isobaric terrane is special and to some degree unique. We would not suggest that they can be simply stacked to make a model crust. Our hope is that these regions and interpretations can motivate studies of, and comparisons with, other isobaric terranes in order to better illuminate the common characteristics and processes that underlie the behavior of continental crust.

Numerous insights may emerge from integrating observations of isobaric terranes with crustal seismic cross sections and with data from other geophysical surveys, igneous petrology and xenolith studies. The most provocative commonalities of the 10, 20, and 35 km crustal levels discussed here are as follows.

(1) All crustal levels in continents can have quartz-rich lithologies (including metasedimentary rocks) such that rheological models for compositionally zoned mafic lower crust to felsic middle and upper crust are oversimplified, as are rheological models based on such zonation. (2) Foliation patterns of steep fabric domains segmenting earlier shallow fabric domains are common at all crustal levels; this heterogeneity of finite strain fabric may be as important as heterogeneity of composition in controlling crustal rheology, as shown in the Grand Canyon example where the rheology of hot domains would be consistent with crustal flow, but the intervening colder domains and shear zone architecture may have inhibited flow. (3) Advective heat transfer via melt flux is common to all crustal levels as are the resulting lateral temperature gradients due to melt partitioning, but the expression of melt-enhanced tectonism varies: basalt underplating and wholesale melting of the lower crust, melt flux through granitoid dikes in the Grand Canyon 20–25 km example, and construction of granitoid plutons at the 10 km level. (4) Isobaric terranes may represent frozen subhorizontal weak zones and hence these field laboratories offer potential for understanding both initiation and processes of crustal flow and the mechanisms of coupling across layers. The Canadian example is compatible with large distance crustal flow models in terms of temperature and melt flux, and the time-integrated overprinting of steep shortening fabrics on subhorizontal flow fabrics may represent the cessation of flow. The Grand Canyon example may be the most typical: high temperature domains are weak enough to flow, and flow is limited in scale because of strength factors introduced from crustal heterogeneity. Crustal flow at shallow crustal levels would seem to require large melt components. (5) The time-integrated behavior of continental crust is an essential element for understanding crustal rheology, a conclusion that strongly encourages the integration of observations from isobaric terranes with seismic and xenolith studies to constrain the dynamic behavior of continental lithosphere.

ACKNOWLEDGMENTS

The authors thank Scott Johnson, David Schneider, and Bob Miller (Guest Editor) for their careful and very helpful reviews of an earlier draft of this manuscript. This paper has benefited from discussions with a large number of people including: S.A. Bowring, M. Jercinovic, R. Flowers, J. Baldwin, C. Hetherington, N. Price, C. Kopf, D. Gibson, P. Goncalves, and many others. Work in the Athabasca granulite terrane has been supported by National Science Foundation (NSF) Grant EAR-0609935. Southwestern U.S. research has been supported by NSF EAR-9206045, 9508096, and 9305459. Electron Microprobe monazite geochronology technique development has been supported under EAR-0549639.

REFERENCES CITED

- Ague, J., and Brimhall, G.H., 1988, Magmatic arc asymmetry and distribution of anomalous plutonic belts in the batholiths of California: Effects of assimilation, crustal thickness, and depth of crystallization: *Geological Society of America Bulletin*, v. 100, p. 912–927, doi: 10.1130/0016-7606(1988)100<0912:MAADO>2.3.CO;2.
- Baldwin, J.A., Bowring, S.A., and Williams, M.L., 2003, Petrologic and geochronologic constraints on high-pressure, high-temperature metamorphism in the Snowbird tectonic zone, Canada: *Journal of Metamorphic Geology*, v. 21, p. 81–98, doi: 10.1046/j.1525-1314.2003.00413.x.
- Baldwin, J.A., Bowring, S.A., Williams, M.L., and Williams, I.S., 2004, Eclogites of the Snowbird tectonic zone: Petrological and U-Pb geochronological evidence for Paleoproterozoic high-pressure metamorphism in the western Canadian Shield: *Contributions to Mineralogy and Petrology*, v. 147, p. 528–548, doi: 10.1007/s00410-004-0572-4.
- Baldwin, J.A., Bowring, S.A., Williams, M.L., and Mahan, K.H., 2006, Geochronological constraints on the crustal evolution of felsic high-pressure granulites, Snowbird tectonic zone, Canada: *Lithos*, v. 88, p. 173–200, doi: 10.1016/j.lithos.2005.08.009.
- Baldwin, J.A., Powell, R., Williams, M.L., and Goncalves, P.G., 2007, Formation of eclogite, and reaction during exhumation to mid-crustal levels, Snowbird tectonic zone, western Canadian Shield: *Journal of Metamorphic Geology*, v. 25, p. 953–974, doi: 10.1111/j.1525-1314.2007.00737.x.
- Beaumont, C., Jamieson, R.A., Nguyen, M.H., and Lee, B., 2001, Himalayan tectonics explained by extrusion of a low-viscosity crustal channel coupled to focused surface denudation: *Nature*, v. 414, p. 738–742, doi: 10.1038/414738a.
- Beaumont, C., Jamieson, R.A., Nguyen, M.H., and Medvedev, S., 2004, Crustal channel flows: 1. Numerical models with applications to the tectonics of the Himalayan-Tibetan orogen: *Journal of Geophysical Research, Solid Earth*, v. 109, B06406, doi: 10.1029/2003JB002809.
- Bergh, S.G., and Karlstrom, K.E., 1992, The Proterozoic Chaparral fault zone of central Arizona; deformation partitioning and escape block tectonics during arc accretion: *Geological Society of America Bulletin*, v. 104, p. 329–345, doi: 10.1130/0016-7606(1992)104<0329:TCSZDP>2.3.CO;2.
- Berman, R.G., Davis, W.J., and Pehrsson, S., 2007, Collisional Snowbird tectonic zone resurrected: Growth of Laurentia during the 1.9 Ga accretionary phase of the Hudsonian orogeny: *Geology*, v. 35, p. 911–914, doi: 10.1130/G23771A.1.
- Bowring, S.A., and Karlstrom, K.E., 1990, Growth and stabilization of Proterozoic lithosphere in the southwestern United States: *Geology*, v. 18, p. 1203–1206, doi: 10.1130/0091-7613(1990)018<1203:GSAROP>2.3.CO;2.
- Brown, L.D., Chapin, C.E., Sanford, A.R., Kaufman, S., and Oliver, J., 1980, Deep structure of the Rio Grande rift from seismic reflection profiling: *Journal of Geophysical Research*, v. 85, p. 4773–4800, doi: 10.1029/JB085iB09p04773.
- Buddington, A.F., 1959, Granite emplacement with special reference to North America: *Geological Society of America Bulletin*, v. 70, p. 671–748, doi: 10.1130/0016-7606(1959)70[671:GEWSRT]2.0.CO;2.
- Burke, M.M., and Fountain, D.M., 1990, Seismic properties of rocks from an exposure of extended continental-crust—New laboratory measurements from the Ivrea Zone: *Tectonophysics*, v. 182, p. 119–146, doi: 10.1016/0040-1951(90)90346-A.
- Burr, J.L., 1991, Proterozoic stratigraphy and structural geology of the Hieroglyphic Mountains, central Arizona, in Karlstrom, K.E., ed., *Proterozoic geology and ore deposits of Arizona*: Tucson, Arizona Geological Society, Arizona Geological Society Digest 19, p. 117–133.
- Butler, R.W.H., Casey, M., Lloyd, G.E., Bond, C.E., McDade, P., Shipton, Z., and Jones, R., 2002, Vertical stretching and crustal thickening at Nanga Parbat, Pakistan Himalaya: A model for distributed continental deformation during mountain building: *Tectonics*, v. 21, doi: 10.1029/2001TC901022.
- Card, C.D., 2002, New investigations of basement to the western Athabasca basin: Summary of investigations 2002, Saskatchewan Geological Survey, v. 2, 17 p.
- Clark, M.K., and Royden, L.H., 2000, Topographic ooze; building the eastern margin of Tibet by lower crustal flow: *Geology*, v. 28, p. 703–706, doi: 10.1130/0091-7613(2000)28<703:TOBTEM>2.0.CO;2.
- Cox, R., Martin, M.W., Comstock, J.C., Dickerson, L.S., Ekstrom, I.L., and Sammons, J.H., 2002, Sedimentology, stratigraphy, and geochronology of the Proterozoic Mazatzal Group, central Arizona: *Geological Society of America Bulletin*, v. 114, p. 1535–1549, doi: 10.1130/0016-7606(2002)114<1535:SSAGOT>2.0.CO;2.
- Dann, J.C., and Bowring, S.A., 1997, The Early Proterozoic Payson ophiolite and the Yavapai-Mazatzal orogenic belt, central Arizona, in de Wit, M.J.,

- and Ashwall, L., eds., *Tectonic evolution of greenstone belts*: Oxford Monographs on Geology and Geophysics, v. 35, p. 781–790.
- Doe, M.F., and Karlstrom, K., 1991, Structural geology of an early Proterozoic foreland thrust belt, Mazatzal Mountains, Arizona, *in* Karlstrom, K.E., ed., *Arizona Geological Society Digest*: Tucson, Arizona Geological Society, p. 181–192.
- Duebendorfer, E.M., Chamberlain, K.R., and Fry, B., 2006, Mojave-Yavapai boundary zone, southwestern United States: A rifting model for the formation of an isotopically mixed crustal boundary zone: *Geology*, v. 34, p. 681–684, doi: 10.1130/G22581.1.
- Dufek, J., and Bergantz, G.W., 2005, Lower crustal magma genesis and preservation: A stochastic framework for the evaluation of basalt-crust interaction: *Journal of Petrology*, v. 46, p. 2167–2195, doi: 10.1093/petrology/egi049.
- Dumond, G., Goncalves, P., Williams, M.L., and Bowring, S.A., 2005a, Field-based constraints on lower crustal flow from the world's largest exposure of lower continental crust, northern Saskatchewan, Canada: *Eos (Transactions, American Geophysical Union)*, v. 86, Fall Meeting Supplement, abstract V21A 0592.
- Dumond, G., Goncalves, P., Williams, M.L., and McLean, N., 2005b, Shallow fabric, strain partitioning, and superposed deformation in deep continental crust: Implications for lower crustal flow and assembly of the western Churchill province, Snowbird Tectonic Zone, Canada [abs.]: *Geological Association of Canada–Mineralogical Association of Canada Annual Meeting*, Halifax, Nova Scotia, v. 30, p. 48.
- Dumond, G., Goncalves, P., Mahan, K., McClean, N., Williams, M., and Bowring, S.A., 2006, Minerals, mountains, and eleven orders of magnitude of intra-continental deformation: Monazite in the context of metamorphic and igneous tectonites: *Geological Society of America Abstracts with Programs*, v. 38, no. 7, p. 209.
- Dumond, G., Mahan, K.H., Williams, M.L., and Karlstrom, K.E., 2007a, Crustal segmentation, composite looping pressure-temperature paths, and magma-enhanced metamorphic field gradients: Upper Granite Gorge, Grand Canyon, USA: *Geological Society of America Bulletin*, v. 119, p. 202–220, doi: 10.1130/B25903.1.
- Dumond, G., Williams, M.L., Goncalves, P., and Jercinovic, M.J., 2007b, Flow of lower continental crust beneath Laurentia: Neoproterozoic sub-horizontal ductile flow in the Athabasca granulite terrane, Western Canadian Shield: *Geological Association of Canada–Mineralogical Association of Canada Joint Meeting*, Yellowknife, Northwest Territories, Abstracts, v. 32, p. 24.
- Dumond, G., McLean, N., Williams, M.L., Jercinovic, M.J., and Bowring, S.A., 2008, High-resolution dating of granite petrogenesis and deformation in a lower crustal shear zone: Athabasca granulite terrane, western Canadian Shield: *Chemical Geology*, v. 254, p. 175–196, doi: 10.1016/j.chemgeo.2008.04.014.
- Ellis, D.J., 1987, Origin and evolution of granulites in normal and thickened crusts: *Geology*, v. 15, p. 167–170, doi: 10.1130/0091-7613(1987)15<167:OAEOGI>2.0.CO;2.
- England, P.C., and Thompson, A.B., 1984, Pressure-temperature-time paths of regional metamorphism, Part I: Heat transfer during the evolution of regions of thickened continental crust: *Journal of Petrology*, v. 4, p. 1–30.
- Ernst, W.G., 2006, Preservation/exhumation of ultrahigh-pressure subduction complexes: *Lithos*, v. 92, p. 321–335, doi: 10.1016/j.lithos.2006.03.049.
- Fischer, K.M., 2002, Waning buoyancy in the crustal roots of old mountains: *Nature*, v. 417, p. 933–936, doi: 10.1038/nature00855.
- Flowers, R.M., Bowring, S.A., and Williams, M.L., 2006a, Timescales and significance of high-pressure, high-temperature metamorphism and mafic dike anatexis, Snowbird tectonic zone, Canada: *Contributions to Mineralogy and Petrology*, v. 151, p. 558–581, doi: 10.1007/s00410-006-0066-7.
- Flowers, R.M., Mahan, K.H., Bowring, S.A., Williams, M.L., Pringle, M.S., and Hodges, K.V., 2006b, Multistage exhumation and juxtaposition of lower continental crust in the western Canadian Shield: Linking high-resolution U-Pb and ⁴⁰Ar/³⁹Ar thermochronometry with pressure-temperature-deformation paths: *Tectonics*, v. 25, p. 1–20, TC4003, doi: 10.1029/2005TC001912.
- Flowers, R.M., Bowring, S.A., Mahan, K.H., Williams, M.L., and Williams, I.S., 2008, Stabilization and reactivation of cratonic lithosphere from the lower crustal record in the western Canadian shield: *Contributions to Mineralogy and Petrology*, v. 156, p. 529–549, doi: 10.1007/s00410-008-0301-5.
- Foster, G., Parrish, R.R., Horstwood, M.S.A., Chenery, S., Pyle, J., and Gibson, H.D., 2004, The generation of prograde P-T-t points and paths; a textural, compositional, and chronological study of metamorphic monazite: *Earth and Planetary Science Letters*, v. 228, p. 125–142, doi: 10.1016/j.epsl.2004.09.024.
- Gilboy, C.F., 1980, *Bedrock compilation geology: Stony Rapids Area (NTS 74P)*: Saskatchewan Geological Survey, Saskatchewan Energy and Mines, Preliminary Geologic Map, scale 1:250,000.
- Groome, W.G., Koons, P.O., and Johnson, S.E., 2008, Metamorphism, transient mid-crustal rheology, strain localization and the exhumation of high-grade metamorphic rocks: *Tectonics*, v. 27, TC1001, doi: 10.1029/2006TC001992.
- Grujic, D., Hollister, L.S., and Parrish, R.R., 2002, Himalayan metamorphic sequence as an orogenic channel: Insight from Bhutan: *Earth and Planetary Science Letters*, v. 198, p. 177–191, doi: 10.1016/S0012-821X(02)00482-X.
- Guidotti, C.V., and Cheney, J.T., 1989, Metamorphism in western Maine: An overview, *in* Chamberlain, C.P., and Robinson, P., eds., *Styles of metamorphism with depth in the Central Adirondack High, New England: A field trip honoring J.B. Thompson, Jr.*: Amherst, University of Massachusetts, p. 17–37.
- Guidotti, C.V., and Johnson, S.E., 2002, Pseudomorphs and associated microstructures of western Maine, USA: *Journal of Structural Geology*, v. 24, p. 1139–1156, doi: 10.1016/S0191-8141(01)00097-9.
- Handy, M.R., and Zingg, A., 1991, The tectonic and rheological evolution of an attenuated cross-section of the continental crust—Ivrea crustal section, southern Alps, northwestern Italy and southern Switzerland: *Geological Society of America Bulletin*, v. 103, p. 236–253, doi: 10.1130/0016-7606(1991)103<0236:TTAREO>2.3.CO;2.
- Hanmer, S., 1994, *Geology, East Athabasca mylonite triangle, Saskatchewan*: Geological Survey of Canada, Map 1859A, scale 1:100,000.
- Hanmer, S., 1997, *Geology of the Striding-Athabasca mylonite zone, northern Saskatchewan and southeastern District of Mackenzie, Northwest Territories*: Geological Survey of Canada Bulletin, v. 501, 92 p.
- Hanmer, S., Parrish, R., Williams, M., and Kopf, C., 1994, Striding-Athabasca mylonite zone: Complex Archean deep crustal deformation in the East Athabasca mylonite triangle, N. Saskatchewan: *Canadian Journal of Earth Sciences*, v. 31, p. 1287–1300.
- Hanmer, S., Kopf, C., and Williams, M., 1995, Modest movements, spectacular fabrics in an intracontinental deep-crustal strike-slip fault: Striding-Athabasca mylonite zone, NW Canadian Shield: *Journal of Structural Geology*, v. 17, p. 493–507, doi: 10.1016/0191-8141(94)00070-G.
- Harley, S.L., 1989, The origins of granulites: A metamorphic perspective: *Geological Magazine*, v. 126, p. 215–247.
- Harley, S.L., and Black, L.P., 1997, A revised Archean chronology for the Napier complex, Enderby Land, from SHRIMP ion-microprobe studies: *Antarctic Science*, v. 9, p. 74–91, doi: 10.1017/S0954102097000102.
- Hawkins, D.P., and Bowring, S.A., 1999, U-Pb monazite, xenotime and titanite geochronological constraints on the prograde to post-peak metamorphic thermal history of Paleoproterozoic migmatites from the Grand Canyon, Arizona: *Contributions to Mineralogy and Petrology*, v. 134, p. 150–169, doi: 10.1007/s004100050475.
- Hawkins, D.P., Bowring, S.A., Ilg, B.R., Karlstrom, K.E., and Williams, M.L., 1996, U-Pb geochronologic constraints on the Paleoproterozoic crustal evolution of the Upper Granite Gorge, Grand Canyon, Arizona: *Geological Society of America Bulletin*, v. 108, p. 1167–1181, doi: 10.1130/0016-7606(1996)108<1167:UPGCOT>2.3.CO;2.
- Hodges, K.V., and McKenna, L.W., 1987, Realistic propagation of uncertainties in geologic thermobarometry: *The American Mineralogist*, v. 72, p. 671–680.
- Hodges, K.V., Hurtado, J.M., and Whipple, K.X., 2001, Southward extrusion of Tibetan crust and its effect on Himalayan tectonics: *Tectonics*, v. 20, p. 799–809, doi: 10.1029/2001TC001281.
- Hollister, L.S., and Crawford, M.L., 1986, Melt-enhanced deformation: A major tectonic process: *Geology*, v. 14, p. 558–561, doi: 10.1130/0091-7613(1986)14<558:MDAMTP>2.0.CO;2.
- Holm, D.K., Van Schmus, W.R., MacNeill, L.C., Boerboom, T.J., Schweitzer, D., and Schneider, D., 2005, U-Pb zircon geochronology of Paleoproterozoic plutons from the northern midcontinent, USA: Evidence for subduction flip and continued convergence after geon 18 Penokean orogenesis: *Geological Society of America Bulletin*, v. 117, p. 259–275, doi: 10.1130/B25395.1.

- Ilg, B.R., and Karlstrom, K.E., 2000, Porphyroblast inclusion trail geometries in the Grand Canyon: Evidence for non-rotation and rotation: *Journal of Structural Geology*, v. 22, p. 231–243, doi: 10.1016/S0191-8141(99)00150-9.
- Ilg, B., Karlstrom, K.E., Hawkins, D.P., and Williams, M.L., 1996, Tectonic evolution of Paleoproterozoic rocks in the Grand Canyon: Insights into middle-crustal processes: *Geological Society of America Bulletin*, v. 108, p. 1149–1166, doi: 10.1130/0016-7606(1996)108<1149:TEOPRI>2.3.CO;2.
- Jamieson, R.A., Beaumont, C., Nguyen, M.H., and Culshaw, N.G., 2007, Syn-convergent ductile flow in variable-strength continental crust: Numerical models with application to the western Grenville orogen: *Tectonics*, v. 26, TC5005, doi: 10.1029/2006TC002036.
- Jessup, M.J., Karlstrom, K.E., Connelly, J., Williams, M.L., Livaccari, R., Tyson, A., and Rogers, S., 2005, Complex Proterozoic crustal assembly of southwestern North America in an arcuate subduction system: The Black Canyon of the Gunnison, southwestern Colorado, in Karlstrom, K.E., and Keller, R., eds., *The Rocky Mountain region: An evolving lithosphere-tectonics, geochemistry, and geophysics*: Washington, D.C., American Geophysical Union Geophysical Monograph, v. 154, p. 21–38.
- Karlstrom, K.E., and Bowring, S.A., 1988, Early Proterozoic assembly of tectonostratigraphic terranes in southwestern North America: *The Journal of Geology*, v. 96, p. 561–576.
- Karlstrom, K.E., and Williams, M.L., 1995, The case for simultaneous deformation, metamorphism and plutonism—An example from Proterozoic rocks in central Arizona: *Journal of Structural Geology*, v. 17, p. 59–81, doi: 10.1016/0191-8141(93)E0025-G.
- Karlstrom, K.E., and Williams, M.L., 1998, Heterogeneity of the middle crust: Implications for strength of continental lithosphere: *Geology*, v. 26, p. 815–818, doi: 10.1130/0091-7613(1998)026<0815:HOTMCI>2.3.CO;2.
- Karlstrom, K.E., and Williams, M.L., 2006, Nature of the middle crust: Heterogeneity of structure and process due to pluton-enhanced tectonism: An example from Proterozoic rocks of the North American Southwest, in Brown, M., and Rushmer, T., eds., *Evolution and differentiation of the continental crust*: Cambridge, UK, Cambridge University Press, p. 268–295.
- Karlstrom, K.E., Bowring, S.A., and Conway, C.M., 1987, Tectonic significance of an early Proterozoic two-province boundary in central Arizona: *Geological Society of America Bulletin*, v. 99, p. 529–538, doi: 10.1130/0016-7606(1987)99<529:TSAEP>2.0.CO;2.
- Karlstrom, K.E., Åhäll, K.I., Harlan, S.S., Williams, M.L., McLelland, J., and Geissman, J.W., 2001, Long-lived (1.8–0.8 Ga) Cordilleran-type orogen in southern Laurentia, its extensions to Australia and Baltica, and implications for refining Rodinia: *Precambrian Research*, v. 111, p. 5–30, doi: 10.1016/S0301-9268(01)00154-1.
- Karlstrom, K.E., Ilg, B.R., Williams, M.L., Hawkins, D.P., Bowring, S.A., and Seaman, S.J., 2003, Paleoproterozoic rocks of the Granite Gorges, Grand Canyon Geology, in Beus, S.S., and Morales, M., eds., *Grand Canyon geology*, 2nd edition: New York, Oxford University Press, p. 9–38.
- Karlstrom, K.E., Whitmeyer, S.J., Dueker, K., Williams, M.L., Bowring, S.A., Levander, A., Humphreys, E.D., Keller, G.R., and CD-ROM-Working-Group, 2005, Synthesis of results from the CD-ROM experiment: 4-D image of the lithosphere beneath the Rocky Mountains and implications for understanding the evolution of continental lithosphere, in Karlstrom, K.E., and Keller, R., eds., *The Rocky Mountain region: An evolving lithosphere-tectonics, geochemistry, and geophysics*: Washington, D.C., American Geophysical Union Geophysical Monograph, v. 154, p. 421–441.
- Klepeis, K.A., Clarke, G.L., and Rushmer, T., 2003, Magma transport and coupling between deformation and magmatism in the continental lithosphere: *GSA Today*, v. 13, no. 1, p. 4–11, doi: 10.1130/1052-5173(2003)013<0004:MTACBD>2.0.CO;2.
- Klepeis, K.A., Clarke, G.L., Gehrels, G.E., and Vervoot, J., 2004, Processes controlling vertical coupling and decoupling between the upper and lower crust of orogens: Results from Fiordland, New Zealand: *Journal of Structural Geology*, v. 26, p. 765–791, doi: 10.1016/j.jsg.2003.08.012.
- Klepeis, K.A., King, D., De Paoli, M., Clarke, G.L., and Gehrels, G., 2007, Interaction of strong lower and weak middle crust during lithospheric extension in western New Zealand: *Tectonics*, v. 26, doi: 10.1029/2006TC002003.
- Kopf, C.F., 1999, Deformation, metamorphism, and magmatism in the East Athabasca mylonite triangle, northern Saskatchewan: Implications for the Archean and Early Proterozoic crustal structure of the Canadian Shield [Ph.D. thesis]: Amherst, University of Massachusetts, 150 p.
- Krikorian, L., 2002, Geology of the Wholdaia Lake segment of the Snowbird tectonic zone, Northwest Territories (Nunavut): A view of the deep crust during assembly and stabilization of the Laurentian craton [M.S. thesis]: Amherst, University of Massachusetts, 90 p.
- Lafrance, B., and Sibbald, T.I.I., 1997, The Grease River shear zone: Proterozoic overprinting of the Archean Tantalito domain: Summary of investigations, 1997, Saskatchewan Geological Survey: Saskatchewan Energy and Mines, Miscellaneous Report 97-4, p. 132–135.
- Law, R.D., Searle, M.P., and Godin, L., 2006, Channel flow, ductile extrusion and exhumation in continental collision zones: *Geological Society of London Special Publication* 268, 620 p.
- Levander, A., Hobbs, R.W., Smith, S.K., England, R.W., Snyder, D.B., and Holliger, K., 1994, The crust as a heterogeneous 'optical' medium, or 'crocodiles in the mist': *Tectonophysics*, v. 232, p. 281–297, doi: 10.1016/0040-1951(94)90090-6.
- Magnani, M.B., Miller, K.C., Levander, A., and Karlstrom, K., 2004, The Yavapai-Mazatzal boundary: A long-lived tectonic element in the lithosphere of southwestern North America: *Geological Society of America Bulletin*, v. 116, p. 1137–1142, doi: 10.1130/B25414.1.
- Mahan, K.H., 2006, Retrograde mica in deep crustal granulites: Implications for crustal seismic anisotropy: *Geophysical Research Letters*, v. 33, doi: 10.1029/2006GL028130.
- Mahan, K.H., and Williams, M.L., 2005, Reconstruction of a large deep crustal exposure: Implications for the Snowbird tectonic zone and early growth of Laurentia: *Geology*, v. 33, p. 385–388, doi: 10.1130/G21273.1.
- Mahan, K.H., Williams, M.L., and Baldwin, J.A., 2003, Contractional uplift of deep crustal rocks along the Legs Lake shear zone, western Churchill Province, Canadian Shield: *Canadian Journal of Earth Sciences*, v. 40, p. 1085–1110, doi: 10.1139/e03-039.
- Mahan, K., Williams, M., Flowers, R., Jercinovic, M., Baldwin, J., and Bowring, S., 2006a, Geochronological constraints on the Legs Lake shear zone with implications for regional exhumation of lower continental crust, western Churchill Province, Canadian Shield: *Contributions to Mineralogy and Petrology*, v. 152, p. 223–242, doi: 10.1007/s00410-006-0106-3.
- Mahan, K.H., Goncalves, P., Williams, M.L., and Jercinovic, M.J., 2006b, Dating metamorphic reactions and fluid flow: Application to exhumation of high-P granulites in a crustal-scale shear zone, western Canadian Shield: *Journal of Metamorphic Geology*, v. 24, p. 193–217, doi: 10.1111/j.1525-1314.2006.00633.x.
- Martel, E., 2005, Geology of the Snowbird Lake area, western Churchill Province, NWT: Yellowknife, Northwest Territories, Northwest Territories Geoscience Office, Northwest Territories Open File Report, 2005-05, 26 p.
- Martel, E., Van-Breemen, O., Berman, R.G., and Pehrsson, S., 2008, Geochronology and tectonometamorphic history of the Snowbird Lake area, Northwest Territories, Canada: New insights into the architecture and significance of the Snowbird tectonic zone: *Precambrian Research*, v. 161, p. 201–230, doi: 10.1016/j.precamres.2007.07.007.
- McFarlane, C.R., M., Connelly, J.N., and Carlson, W.D., 2005, Monazite and xenotime petrogenesis in the contact aureole of the Makhavinekh Lake pluton, northern Labrador: *Contributions to Mineralogy and Petrology*, v. 148, p. 524–541.
- Meissner, R., Rabbal, W., and Kern, H., 2006, Seismic lamination and anisotropy of the lower continental crust: *Tectonophysics*, v. 416, p. 81–99, doi: 10.1016/j.tecto.2005.11.013.
- Metzger, K., 1992, Temporal evolution of regional granulite terrains: Implications for the formation of lowermost continental crust, in Fountain, D.M., Arculus, R., and Kay, R.W., eds., *Continental lower crust*, *Developments in Geotectonics*, 23: Amsterdam, Elsevier, p. 447–478.
- Mortimer, N., 2000, Metamorphic discontinuities in orogenic belts: Example of the garnet-biotite-albite zone in the Otago Schist, New Zealand: *International Journal of Earth Sciences*, v. 89, p. 295–306, doi: 10.1007/s005310000086.
- Nelson, K.D., Zhao, W., Brown, L.D., Kuo, J., Che, J., Liu, X., Klemperer, S., Makovsky, Y., Meissner, R., Mechie, J., Kind, R., Wenzel, F., Ni, J., Nabelek, J., Leshou, C., Tan, H., Wei, W., Jones, A.G., Booker, J., Unsworth, M., Kidd, W.S.F., Hauck, M., Alsdorf, D., Ross, A., Cogan, M., Wu, C., Sandvol, E., and Edwards, M., 1996, Partially molten middle crust beneath southern Tibet: Synthesis of project INDEPTH results: *Science*, v. 274, p. 1684–1688, doi: 10.1126/science.274.5293.1684.

- Percival, J.A., 1989, Granulite terranes and the lower crust of the Superior Province, *in* Mereu, R.F., Mueller, S., and Fountain, D.M., eds., Properties and processes of Earth's lower crust: Washington, D.C., American Geophysical Union, Geophysical Monograph, v.51, p. 301–310.
- Percival, J.A., and Card, K.D., 1983, Archean crust as revealed in the Kapuskasing uplift, Superior Province, Canada: *Geology*, v. 11, p. 323–326, doi: 10.1130/0091-7613(1983)11<323:ACARIT>2.0.CO;2.
- Percival, J.A., and West, G.F., 1994, The Kapuskasing uplift; a geological and geophysical synthesis: *Canadian Journal of Earth Sciences*, v. 31, p. 1256–1286.
- Percival, J.A., Fountain, D.M., and Salisbury, M.H., 1992, Exposed crustal cross sections as windows on the lower crust, *in* Fountain, D.M., Arculus, R., and Kay, R.W., eds., Continental lower crust, Developments in Geotectonics, 23: Amsterdam, Elsevier, p. 317–362.
- Pitcher, W.S., 1979, The nature, ascent, and emplacement of granite magmas: *Geological Society of London Journal*, v. 136, p. 627–662, doi: 10.1144/gsjgs.136.6.0627.
- Platt, J.P., 1986, Dynamics of orogenic wedges and the uplift of high-pressure metamorphic rocks: *Geological Society of America Bulletin*, v. 97, p. 1037–1053, doi: 10.1130/0016-7606(1986)97<1037:DOOWAT>2.0.CO;2.
- Pyle, J.M., and Spear, F.S., 2003, Four generations of accessory-phase growth in low-pressure migmatites from SW New Hampshire: *The American Mineralogist*, v. 88, p. 338–351.
- Royden, L.H., 1996, Coupling and decoupling of crust and mantle in convergent orogens: Implications for strain partitioning in the crust: *Journal of Geophysical Research*, v. 101, p. 17,679–17,705, doi: 10.1029/96JB00951.
- Royden, L.H., Burchfiel, B.C., King, R.W., Wang, E., Chen, Z.L., Shen, F., and Liu, Y.P., 1997, Surface deformation and lower crustal flow in eastern Tibet: *Science*, v. 276, p. 788–790, doi: 10.1126/science.276.5313.788.
- Rudnick, R.L., and Fountain, D.M., 1995, Nature and composition of the continental crust—A lower crustal perspective: *Reviews of Geophysics*, v. 33, p. 267–309, doi: 10.1029/95RG01302.
- Rutter, E.H., and Brodie, K.H., 1992, Rheology of the lower crust, *in* Fountain, D.M., Arculus, R., and Kay, R.W., eds., Continental lower crust, Developments in Geotectonics 23: Amsterdam, Elsevier, p. 201–267.
- Rutter, E.H., Khazanehdari, J., Brodie, K.H., Blundell, D.J., and Waltham, D.A., 1999, Synthetic seismic reflection profile through the Ivrea zone Serie dei Laghi continental crustal section, northwestern Italy: *Geology*, v. 27, p. 79–82, doi: 10.1130/0091-7613(1999)027<0079:SSRPTT>2.3.CO;2.
- Salisbury, M.H., and Fountain, D.M., eds., 1990, Exposed cross-sections of the continental crust; proceedings, NATO ASI Series—Series C: Boston, D. Reidel Publishing Company, 662 p.
- Shapiro, N.M., Ritzwoller, M.H., Molnar, P., and Levin, V., 2004, Thinning and flow of Tibetan crust constrained by seismic anisotropy: *Science*, v. 305, p. 233–236, doi: 10.1126/science.1098276.
- Shaw, C.A., Karlstrom, K.E., Williams, M.L., Jercinovic, M.J., and McCoy, A.M., 2001, Electron-microprobe monazite dating of ca. 1.71–1.63 Ga and ca. 1.45–1.38 Ga deformation in the Homestake shear zone, Colorado: Origin and early evolution of a persistent intracontinental tectonic zone: *Geology*, v. 29, p. 739–742, doi: 10.1130/0091-7613(2001)029<0739:EMMDOC>2.0.CO;2.
- Shaw, C., Karlstrom, K., and Heizler, M., 2005, Mid-crustal temperatures during ca. 1.4 Ga metamorphism in the southwestern United States: A regional synthesis of $^{40}\text{Ar}/^{39}\text{Ar}$ data, *in* Karlstrom, K.E., and Keller, R., eds., Lithospheric structure and evolution of the Rocky Mountains: Washington, D.C., American Geophysical Union, Geophysical Monograph, v. 154, p. 163–184.
- Sheraton, J.W., and Black, L.P., 1983, Geochemistry of Precambrian gneisses: Relevance for the evolution of the East Antarctic shield: *Lithos*, v. 16, p. 273–296, doi: 10.1016/0024-4937(83)90016-6.
- Slimmon, W.L., 1989, Bedrock compilation geology: Fond du Lac (NTS 74-O): Saskatchewan Geological Survey, Saskatchewan Energy and Mines, Map 247A, scale 1:250,000.
- Snoeyenbos, D.R., Williams, M.L., and Hanmer, S., 1995, An Archean eclogite facies terrane in the western Canadian Shield: *European Journal of Mineralogy*, v. 7, p. 1251–1272.
- Stern, R.J., 2005, Evidence from ophiolites, blueschists, and ultrahigh-pressure metamorphic terranes that the modern episode of subduction tectonics began in Neoproterozoic time: *Geology*, v. 33, p. 557–560, doi: 10.1130/G21365.1.
- Tikoff, B., Teyssier, C., and Waters, C., 2002, Clutch tectonics and the partial attachment of lithospheric layers: European Geophysical Union Stephan Mueller Special Publication Series, v. 1, p. 57–73.
- Tikoff, B., Russo, R., Teyssier, C., and Tommasi, A., 2004, Mantle-driven deformation of orogenic zones and clutch tectonics, *in* Grocott, J., McCaffrey, K.J.W., Taylor, G., and Tikoff, B., eds., Vertical coupling and decoupling in the lithosphere: Geological Society of London Special Publication 227, p. 41–64, doi: 10.1144/GSL.SP.2004.227.01.01.
- TRANSALP Working Group, 2002, First deep seismic reflection images of the Eastern Alps reveal giant crustal wedges and transcrustal ramps: *Geophysical Research Letters*, v. 29, doi: 10.1029/2002GL014911.
- Turcotte, D.L., and Schubert, G., 2002, *Geodynamics*: Cambridge, Cambridge University Press, 456 p.
- Tyson, A.R., Morozova, E.A., Karlstrom, K.E., Chamberlain, K.R., Smithson, S.B., Dueker, K.G., and Foster, C.T., 2002, Proterozoic Farwell Mountain–Lester Mountain suture zone, northern Colorado: Subduction flip and progressive assembly of arcs: *Geology*, v. 30, p. 943–946, doi: 10.1130/0091-7613(2002)030<0943:PFMLMS>2.0.CO;2.
- Vernon, R.H., Clarke, G.L., and Collins, W.J., 1990, Local, mid-crustal granulite facies metamorphism and melting: An example in the Mount Stafford area, central Australia, *in* Ashworth, J.R., and Brown, M., eds., High-temperature metamorphism and crustal anatexis: London, Unwin Hyman Mineralogical Society Series, p. 272–319.
- Whitmeyer, S.J., and Karlstrom, K.E., 2007, Tectonic model for the Proterozoic growth of North America: *Geosphere*, v. 3, p. 220–259, doi: 10.1130/GES00055.1.
- Williams, M.L., 1991, Overview of Proterozoic metamorphism in Arizona, *in* Karlstrom, K.E., ed., Proterozoic geology and ore deposits of Arizona: Tucson, Arizona Geological Society Digest 19, p.11–26.
- Williams, M.L., 1994, Sigmoidal inclusion trails, punctuated fabric development and interactions between metamorphism and deformation: *Journal of Metamorphic Geology*, v. 12, p. 1–21, doi: 10.1111/j.1525-1314.1994.tb00001.x.
- Williams, M.L., and Hanmer, S., 2006, Structural and metamorphic processes in the lower crust: Evidence from the East Athabasca mylonite triangle, Canada, a deep-crustal isobarically cooled terrane, *in* Brown, M., and Rushmer, T., eds., Evolution and differentiation of the continental crust: Cambridge, Cambridge University Press, p. 232–268.
- Williams, M.L., and Jercinovic, M.J., 2002, Microprobe monazite geochronology: Putting absolute time into microstructural analysis: *Journal of Structural Geology*, v. 24, p. 1013–1028, doi: 10.1016/S0191-8141(01)00088-8.
- Williams, M.L., and Karlstrom, K.E., 1996, Looping P-T paths and high-T, low-P middle crustal metamorphism: Proterozoic evolution of the southwestern United States: *Geology*, v. 24, p. 1119–1122, doi: 10.1130/0091-7613(1996)024<1119:LPTPAH>2.3.CO;2.
- Williams, M.L., Hanmer, S., Kopf, C., and Darrach, M., 1995, Syntectonic generation and segregation of tonalitic melts from amphibolite dikes in the lower crust, Striding-Athabasca mylonite zone, Northern Saskatchewan: *Journal of Geophysical Research*, v. 100, p. 15,717–15,734, doi: 10.1029/95JB00760.
- Williams, M.L., Melis, E.A., Kopf, C., and Hanmer, S., 2000, Microstructural tectonometamorphic processes and the development of gneissic layering: A mechanism for metamorphic segregation: *Journal of Metamorphic Geology*, v. 18, p. 41–57, doi: 10.1046/j.1525-1314.2000.00235.x.
- Williams, M.L., Jercinovic, M.J., Goncalves, P., and Mahan, K.H., 2006, Format and philosophy for collecting, compiling, and reporting microprobe monazite ages: *Chemical Geology*, v. 225, p. 1–15, doi: 10.1016/j.chemgeo.2005.07.024.
- Williams, P.F., and Jiang, D.Z., 2005, An investigation of lower crustal deformation: Evidence for channel flow and its implications for tectonics and structural studies: *Journal of Structural Geology*, v. 27, p. 1486–1504, doi: 10.1016/j.jsg.2005.04.002.
- Worley, B., and Powell, R., 2000, High-precision relative thermobarometry: Theory and a worked example: *Journal of Metamorphic Geology*, v. 18, p. 91–101, doi: 10.1046/j.1525-1314.2000.00239.x.

Evolution of the middle and lower crust during the transition from contraction to extension in Fiordland, New Zealand

Keith A. Klepeis*
Daniel S. King

Department of Geology, University of Vermont, Burlington, Vermont 05405-0122, USA

ABSTRACT

A deeply eroded orogen in southwest New Zealand preserves a record of changing flow patterns in the middle and lower crust during a transition from contraction and crustal thickening to extension and crustal thinning. The New Zealand exposures show that deformation patterns at mid-lower crustal depths were strongly influenced by local variations in crustal structure, temperature, composition, magmatic activity, and rheology. Kinematic parameters, including the orientation of shear zone boundaries, the degree of non-coaxiality and kinematic partitioning, strain symmetry, and whether shear zones were thickening or thinning in different planes of observation, were extremely variable spatially and changed repeatedly over an 8–10 Ma period. However, despite this variability, several aspects of superposed deformations remained constant and can be assigned to distinctive tectonic settings. All shear zones that formed during the 119–111 Ma period in Northern Fiordland record flow involving bulk horizontal (layer-parallel) shortening, vertical (layer-perpendicular) thickening, and >50% pure shear regardless of shear zone orientation, degree of non-coaxiality, strain symmetry, and temperature conditions. In contrast, all shear zones that formed during the 114–90 Ma period in Central Fiordland record flow involving vertical thinning, subhorizontal stretching, and 40%–50% pure shear. These patterns are correlative with regional contraction and regional extension, respectively. The data suggest that at length scales of ~100 km and time scales of ca. 10 Ma, the effects of changing plate boundary dynamics on deformation patterns in the middle and lower crust can be distinguished from the effects of changing local boundary conditions, including steep temperature gradients and variable rheology.

INTRODUCTION

One of the most important reasons for the failure of plate tectonics as a description of how continental lithosphere deforms is lower crustal flow. Unlike in oceanic regimes, many zones of

continental deformation are hundreds to thousands of kilometers wide and cannot be described by the rigid motion of plates that move laterally past and into one another along narrow boundaries (Buck, 1991; Clark and Royden, 2000; McKenzie et al., 2000; Jackson, J., 2002; Giorgis et al., 2004). Differences in the thickness, thermal profile, and strength of continental crust make lower crustal flow much more likely and important in continental

*Keith.Klepeis@uvm.edu

regions than it is in oceanic regions (Royden, 1996; Beaumont et al., 2001). However, despite recognition of its importance, the characteristics and consequences of lower crustal flow are among the least understood aspects of geodynamics. For example, what types of flow patterns evolve in the lower crust as tectonic settings and the driving forces of continental deformation change? How do flow patterns change as local rheologies and physical conditions in the deep crust change? What are the length and time scales of middle and lower crustal heterogeneity?

The study of deep-crustal exposures provides an important and useful approach to answering these questions. Geophysical images provide instantaneous views of lower-crustal structure but the age and kinematic significance of deep-crustal fabrics commonly is difficult to resolve (Nemes et al., 1997; McBride and Knapp, 2002; Jackson, H.R., 2002). Natural exposures of ancient middle and lower crust potentially allow us to determine directly how deformation in the deep crust relates to other observable features. However, studies of the middle and lower crust in different settings also have shown that the rheology and thermal structure of the lower crust are extremely heterogeneous and can change

rapidly during orogenic cycles (Miller and Paterson, 2001, Whitney et al., 2004; Rusmore et al., 2005; Karlstrom and Williams, 2006). This time-dependent, heterogeneous nature of deformation in most natural systems commonly obscures the nature of the forces that control lower-crustal deformation and complicates the application of numerical models to natural phenomena. Many numerical and analytical techniques employ algorithms that require steady-state conditions or limit the number of variables that operate simultaneously over geologic length and time scales (Royden, 1996; Lin et al., 1998, Jiang and Williams, 1998; Jiang et al., 2001; Beaumont et al., 2001). Our ability to predict the response of deforming continental lithosphere to changes in driving forces, including plate motions, relies on an adequate determination of lower-crustal behavior during orogenesis.

In this chapter, we report the results of a semiquantitative, field-based investigation of ductile flow in a deeply eroded section of exposed middle and lower crust in Fiordland, New Zealand (Fig. 1). The young age and well-constrained tectonic setting of these exposures allowed us to examine the physical response of the middle and lower crust to a major tectonic change from

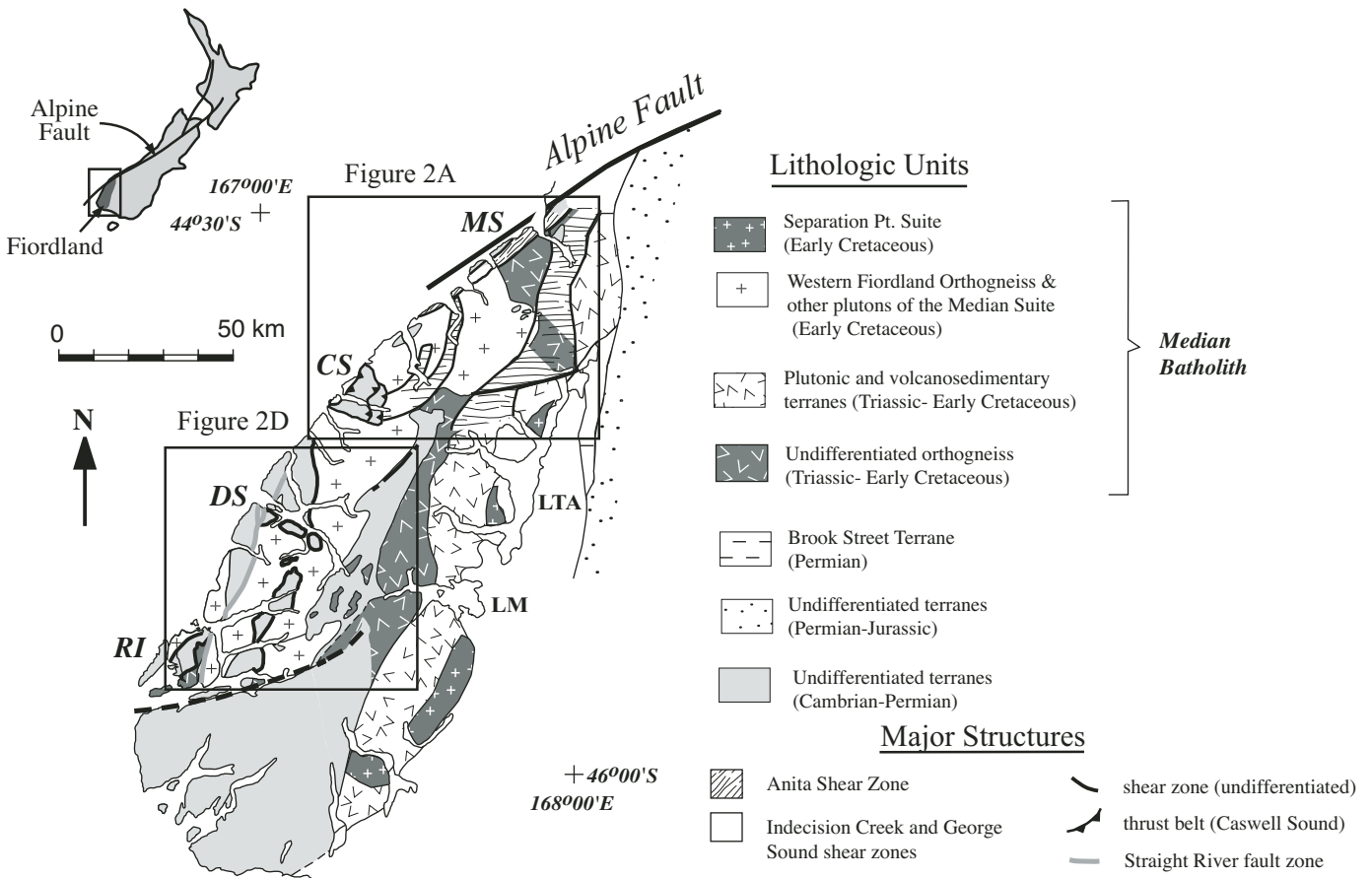


Figure 1. General geologic map of western New Zealand after Wood (1972), Oliver and Coggon (1979), J.Y. Bradshaw (1989a), Daczko et al. (2002a), Tulloch and Kimbrough (2003), and Klepeis et al. (2004). Area near Resolution Island from Turnbull et al. (2005). Abbreviations are as follows: CS—Caswell Sound; DS—Doubtful Sound; LM—Lake Manapouri; LTA—Lake Te Anau; MS—Milford Sound; RI—Resolution Island. Boxes show areas of study.

contraction to extension as plate boundary forces evolved from 114 to 111 Ma. During this interval, both the plate boundary kinematics and the regional style of deformation in western New Zealand changed (Tulloch and Kimbrough, 1989; Gibson and Ireland, 1995; Spell et al., 2000; Scott and Cooper, 2006; Klepeis et al., 2007). We obtained the first direct measure of changing lower-crustal flow fields over length scales of several hundred square kilometers during this transitional period. The exposures allowed us to relate the kinematic evolution of different fabrics in areas that record distinctive histories of magmatism and high-grade metamorphism. The data suggest a lower-crustal structure that is much more heterogeneous and transient than previously believed.

CONFLICTING OBSERVATIONS AND TESTABLE HYPOTHESES IN FIORDLAND

Most convergent margins record cycles of contraction and crustal thickening followed by extension and crustal thinning over periods of several tens of millions of years. In western New Zealand, Early Mesozoic contraction and arc magmatism thickened the ancient margin of Gondwana to a crustal thickness of at least 45 km by ca. 120 Ma (Oliver, 1980; Bradshaw, J.D., 1985; Bradshaw, J.Y., 1989a; Clarke et al., 2000; Tulloch and Kimbrough, 2003). This activity accompanied subduction and convergence along the ancient continental margin of Gondwana (Tulloch and Kimbrough, 2003) and produced a linear belt of Triassic–Early Cretaceous intrusive rocks known as the Median batholith (Fig. 1; Mortimer et al., 1999).

By ca. 110 Ma, structures that are typical of extending lithosphere had formed within the crustal column, including metamorphic core complexes and rift basins (Gibson et al., 1988; Tulloch and Kimbrough, 1989; Gibson and Ireland, 1995; Spell et al., 2000; Kula et al., 2005; Scott and Cooper, 2006; Klepeis et al., 2007). Geochemical and geochronologic data indicate that subduction-related magmatism lasted until ca. 105 Ma (Tulloch and Kimbrough, 2003) and appears to have overlapped with the transition to extension (Waight et al., 1998). This transition coincided with a reorganization of plate boundaries that ended subduction along the Gondwana margin (Bradshaw, J.D., 1989; Tulloch and Kimbrough, 2003). By ca. 84 Ma, the New Zealand continent had rifted away from Australia and Antarctica as the Tasman Sea opened (Gaina et al., 1998). This history and the unusual degree of exposure allow us to test two leading hypotheses that describe how local variations in lower-crustal strength (effective viscosity) and temperature affect lithospheric behavior during orogenic contraction and extension.

One leading hypothesis that explains conditions in the lower crust during the period 120–110 Ma, suggests that the development of extensional features following a period of crustal thickening reflects horizontal flow in lower crust that has been weakened by heat, magmatism and partial melting. Published models suggest that gravitational instabilities caused by a thick, weak lower crust and variations in crustal thickness may promote the flow of material away from thick zones resulting in extension within the crustal

column (McKenzie et al., 2000; Jackson, J., 2002). Relationships observed in Central Fiordland may support this hypothesis. Gibson and Ireland (1995) reported U–Pb isotopic data indicating that at or immediately before the initiation of extension in Central Fiordland, thick parts of the lower crust recorded elevated temperatures of > 750–800 °C. Zircon extracted from high-temperature granulite-facies fabrics at Doubtful Sound (DS, Fig. 1) yielded an age of 107.5 ± 2.8 Ma (Gibson and Ireland, 1995). The chemistry and age of the zircon suggested that it represented a new generation of zircon growth at high temperatures. These data, and the dependence of crustal viscosity on temperature (e.g., Royden, 1996; Ellis et al., 1998), suggest that the lower crust was weak and flowed easily at the time extension initiated. However, new high-precision data reported by Flowers et al. (2005) conflict with this interpretation. U–Pb ages on titanite, rutile, and apatite reported by these authors indicate isobaric lower crustal cooling through the range 650–550 °C by 113.5–111 Ma (Table 1).

A possible resolution to these conflicting observations was presented by Klepeis et al. (2007) who suggested that the initiation of extension coincided with areas of the lower crust that were weakened by heat and magma, but the transition occurred by ca. 114 Ma, significantly earlier than previously suggested. This interpretation is based on fabric studies at Doubtful Sound and ages from high-temperature granulites obtained by Hollis et al. (2004). Nevertheless, given the uncertainties in available ages (Table 1), the time of the shift from regional contraction to regional extension could have occurred at anytime during the interval 114–111 Ma. Evidence of magmatism during the interval 116–113 Ma (Table 1; Gibson and Ireland, 1998; Tulloch and Kimbrough, 2003; Hollis et al., 2004), granulite-facies metamorphism (Oliver, 1977; Oliver and Coggon, 1979; Oliver, 1980; Gibson and Ireland, 1995), and partial melting at Doubtful Sound (Hollis et al., 2004) support the interpretation of a weak lower crust at the time extension initiated.

An alternative hypothesis has been suggested on the basis of observations in Northern Fiordland. At Milford Sound (MS, Fig. 1), less than 100 km to the north of Doubtful Sound, metamorphic mineral assemblages and U–Pb isotopic data suggest that the lower crust there had cooled from temperatures of >800 °C to 650 °C prior to 111 Ma and probably as early as ca. 116 Ma (Daczko et al., 2002a; Hollis et al., 2003; Klepeis et al., 2004; Flowers et al., 2005). Even though partial melting appears to have occurred within the lower-crustal section at ca. 120 Ma, piston cylinder experiments on unmelted samples of dioritic gneiss from Pembroke Valley (Antignano, 2002) and petrological analyses (Daczko et al., 2001b) suggest that the total volume of melt probably remained low (Klepeis et al., 2003). The experiments showed that fluid-absent melting was controlled by the decomposition of hornblende \pm clinozoisite to produce garnet + melt and resulted in low (≤ 10 volume %) melt volumes at all temperatures up to 975 °C. Low melt volumes would have helped the lower crust remain strong even as it partially melted. Heat loss, the crystallization of magma, and the efficient removal of partial melt from the lower crust are interpreted to have resulted in isobaric cooling

TABLE 1. SELECTED MINERAL AGES FROM IGNEOUS AND METASEDIMENTARY ROCKS IN NORTHERN AND CENTRAL FIORDLAND

Location*	Rock type	Method	Mineral	Corrected age (Ma)	Source	Interpretation
Northern Fiordland						
Mt. Kepka	Syntectonic felsic dike	U-Pb, LA ICPMS	Zircon, r	119.0 ± 4.7	Marcotte et al. (2005)	ICSZ outlasted dike emplacement
Mt. Kepka	Syntectonic dike	U-Pb, LA ICPMS	Zircon, c	115 ± 3.6	Marcotte et al. (2005)	ICSZ outlasted dike emplacement
Mt. Kepka	Syntectonic dioritic dike	U-Pb, LA ICPMS	Zircon, r, c	117.4 ± 3.9	Marcotte et al. (2005)	ICSZ outlasted dike emplacement
Anchorage Cove	Syntectonic dioritic dike	U-Pb, LA ICPMS	Zircon, r	121.7 ± 4.2	Marcotte et al. (2005)	GSSZ outlasted dike emplacement
Mt. Daniel	WFO diorite	U-Pb, SHRIMP	Zircon, c	121.8 ± 1.7	Hollis et al. (2004)	WFO emplacement age
Selwyn Creek	Dioritic gneiss	U-Pb, SHRIMP	Zircon, r	125–115	Hollis et al. (2003)	Age of granulite-facies metamorphism
Caswell Sound	Monzodiorite	U-Pb, LA ICPMS	Zircon, c	116.8 ± 3.7	Klepeis et al. (2004)	Lower limit Caswell fold-thrust belt
Mt. Ada	Syntectonic dioritic dike	U-Pb, LA ICPMS	Zircon, r	115.7 ± 3.8	Klepeis et al. (2004)	ICSZ outlasted dike emplacement
Caswell Sound	Dioritic dike	U-Pb, LA ICPMS	Zircon, c	118.7 ± 3.8	Klepeis et al. (2004)	Lower limit Caswell fold-thrust belt
Arthur River Complex	Gabbroic gneiss	U-Pb, SHRIMP	Zircon, r	120–110	Hollis et al. (2003)	Ages of high-T metamorphism
Worsley	Monzodiorite	U-Pb, ID	Zircon	124 ± 1	Tulloch and Kimbrough (2003)	Granulite facies WFO
Central Fiordland						
0359, 0355	Orthogneiss, calcisilicate	U-Pb, ID	Titanite	113.4–111	Flowers et al. (2005)	Cooling through 550–650°C
Doubtful Sound	WFO	K-Ar	Hornblende	98–93	Gibson et al. (1988)	Cooling through ~500°C
0361	Granulite in WFO	U-Pb, ID	Rutile	~70	Flowers et al. (2005)	Cooling through 400–450°C
Supper Cove	Diorite	U-Pb, ID	Zircon	128 ± 1	Tulloch and Kimbrough (2003)	Youngest age of Median Suite
Wet Jacket	Diorite	U-Pb, ID	Zircon	116.6 ± 1.2	Tulloch and Kimbrough (2003)	Youngest known phase of the WFO
CA10	Granulite in WFO	U-Pb, SHRIMP	Zircon	114 ± 2.2	Hollis et al. (2004)	Age of granulite facies metamorphism
CA90	WFO diorite	U-Pb, SHRIMP	Zircon	115.6 ± 2.4	Hollis et al. (2004)	Crystallization age of WFO
CA39	Paragneiss	U-Pb, SHRIMP	Zircon, r	117.7 ± 2.8	Hollis et al. (2004)	Age of high-T metamorphism
Joseph Point	Syntectonic dioritic dike	U-Pb, LA ICPMS	Zircon, c	102 ± 1.8	Klepeis et al. (2007)	Age of DSSZ
0460	Post-extension felsic dike	U-Pb, LA ICPMS	Zircon, c	88.4 ± 1.2	King et al. (2008)	Upper limit of extension
Mt. Irene	Syntectonic dike	U-Pb, LA ICPMS	Zircon	107.3 ± 0.8	Scott and Cooper (2006)	Age of MISZ

* Sample locations are indicated in Figure 2. DSSZ—Doubtful Sound shear zone; ICSZ—Indecision Creek shear zone; ID—isotope dilution; GSSZ—George Sound shear zone; LA ICPMS—laser ablation inductively coupled mass spectrometry; MISZ—Mt. Irene shear zone; SHRIMP—sensitive high-resolution microprobe; WFO—Western Fiordland Orthogneiss. r indicates Zircon rim age; c indicates zircon core age.

($T = 650\text{ }^{\circ}\text{C}$) and a high viscosity lower crust before extension initiated in the mid-Cretaceous (Klepeis et al., 2003; Marcotte et al., 2005). A lower-crustal rheology controlled by the presence of feldspar rather than quartz also may have allowed crustal yield strengths to remain relatively high. This highly viscous lower crust may have led to a focusing of strain in a middle crust that was weak compared to the lower crust (Klepeis et al., 2007). A weak middle crust, rather than a weak lower crust, may have controlled the behavior of extending continental lithosphere.

These conflicting interpretations, which arise from observations in two different areas, raise questions about the physical conditions and behavior of the lower crust during the transition from regional contraction to regional extension. Within the resolution of available ages (Table 1) and thermobarometric calculations (Oliver, 1977; J.Y. Bradshaw, 1989a, 1989b; Gibson and Ireland, 1995; Clarke et al., 2000; Daczko et al., 2001a, 2001b, 2002a, 2002b; Hollis et al., 2004), Northern and Central Fiordland record divergent tectonic histories. Nevertheless, because they reflect observations made in different parts of Fiordland, it is possible that elements of both hypotheses are correct. This possibility is explored in detail in the "Discussion" of this article.

APPROACH TO THE ANALYSIS OF MID-LOWER CRUSTAL DEFORMATION

To resolve the conflicting interpretations described in the previous section, we measured kinematic patterns in shear zones and superposed ductile fabrics in both Northern and Central Fiordland that evolved through the transition from contraction to extension during the interval 126–90 Ma. Our goal was to determine which deformations in each locality, if any, displayed patterns that could be related to each tectonic regime and how the effects of extremely heterogeneous physical conditions also may have influenced the patterns. This approach relied on linking kinematic data with previously published age determinations and thermobarometry from key localities. Salient age determinations are summarized in Table 1. Key localities in Northern and Central Fiordland are shown in Figures 2A and 2D, respectively. We also present textural and microstructural data from lower-crustal fabrics that help us link the results of previously published thermobarometry to specific fabrics in lower-crustal shear zones.

Part of the problem with analyses of lower-crustal deformation is that both Northern and Central Fiordland display arrays of flat, moderately dipping, and steep fabrics (Fig. 2). In most localities, especially in zones of flat-lying shear zones, shear zone geometry and sense of shear are insufficient to distinguish contractional versus extensional tectonics because of the extreme heterogeneity and the possibility of at least some reorientation during exhumation. To overcome this problem, we evaluated a number of different kinematic and geometric parameters for superposed deformations, including the orientation of shear zone boundaries, bulk shear directions, orientation of the average vorticity vectors, average degrees of non-coaxiality, and whether zones of deformation were thickening or thinning in different

planes of observation (i.e., sectional kinematic vorticity numbers). Here we use the terms thinning and thickening in the sense that the boundaries of the deforming zone either moved toward or away from each other, respectively (Lin et al., 1998). Estimates of mean kinematic vorticity (W_m) provided us with a means of comparing the relative contributions of pure shear and simple shear for distinctive deformations. Absolute values of W_m vary from 0 to 1 and represent a nonlinear ratio between coaxial and non-coaxial components of deformation. Low numbers are highly coaxial and high numbers are mostly non-coaxial. This approach is a convenient way of determining whether a shear zone was thinning (positive W_m values) or thickening (negative W_m values) in different planes. These and other parameters, commonly used in studies of ductile deformation, are defined below in the context of our measurements. We also refer the reader to other publications for additional information (e.g., Lister and Williams, 1983; Passchier, 1987; Passchier and Urai, 1988; Simpson and DePaor, 1993; Tikoff and Fossen, 1995; Klepeis et al., 1999; Jiang et al., 2001; Daczko et al., 2001a; Bailey and Eyster, 2003; Law et al., 2004; Bailey et al., 2007).

To determine kinematic patterns for each deformation we identified local and regional strain gradients and determined how the geometry of structures varied across them. Three of the techniques we describe involved determining: angular changes in deformed vein and dike sets; rotation histories of asymmetric porphyroclasts; and progressive changes in the orientation of structural elements such as foliations, fold hinge lines and mineral stretching lineations. For some of the deformations, kinematic patterns have been reported in previous publications. In these cases, we provide a brief summary of salient results for comparison with other deformation events. Our study represents the first comprehensive comparison of all kinematic data from Fiordland. In all cases, our reference frame was the upper and lower contacts of the Western Fiordland Orthogneiss and the orientation of a regional compositional layering that parallels these contacts throughout the western side of the orogen. Thermobarometric data suggest that this layering originally formed in an approximately horizontal orientation and subsequently has been tilted (see also Klepeis et al., 2004, 2007). The P-T determinations also indicate that paleodepths increase from north to south across this layering and allow us to reconstruct paleohorizontal. In addition, most of the techniques we used, including analyses of kinematic vorticity, are insensitive to reorientation and tilting.

NORTHERN FIORDLAND

Geometry, Age, and Sequence of Structures

In Northern Fiordland (Fig. 2A), four sets of superposed shear zones record "snapshots" of evolving strain patterns during cooling from peak supra-solidus conditions ($P \approx 14\text{ kb}$, $T > 800\text{ }^{\circ}\text{C}$) to upper amphibolite facies conditions ($P \approx 14\text{ kb}$, $T \approx 650\text{ }^{\circ}\text{C}$). Structures in these shear zones allowed us to reconstruct changing kinematic patterns in the lower crust that accompanied

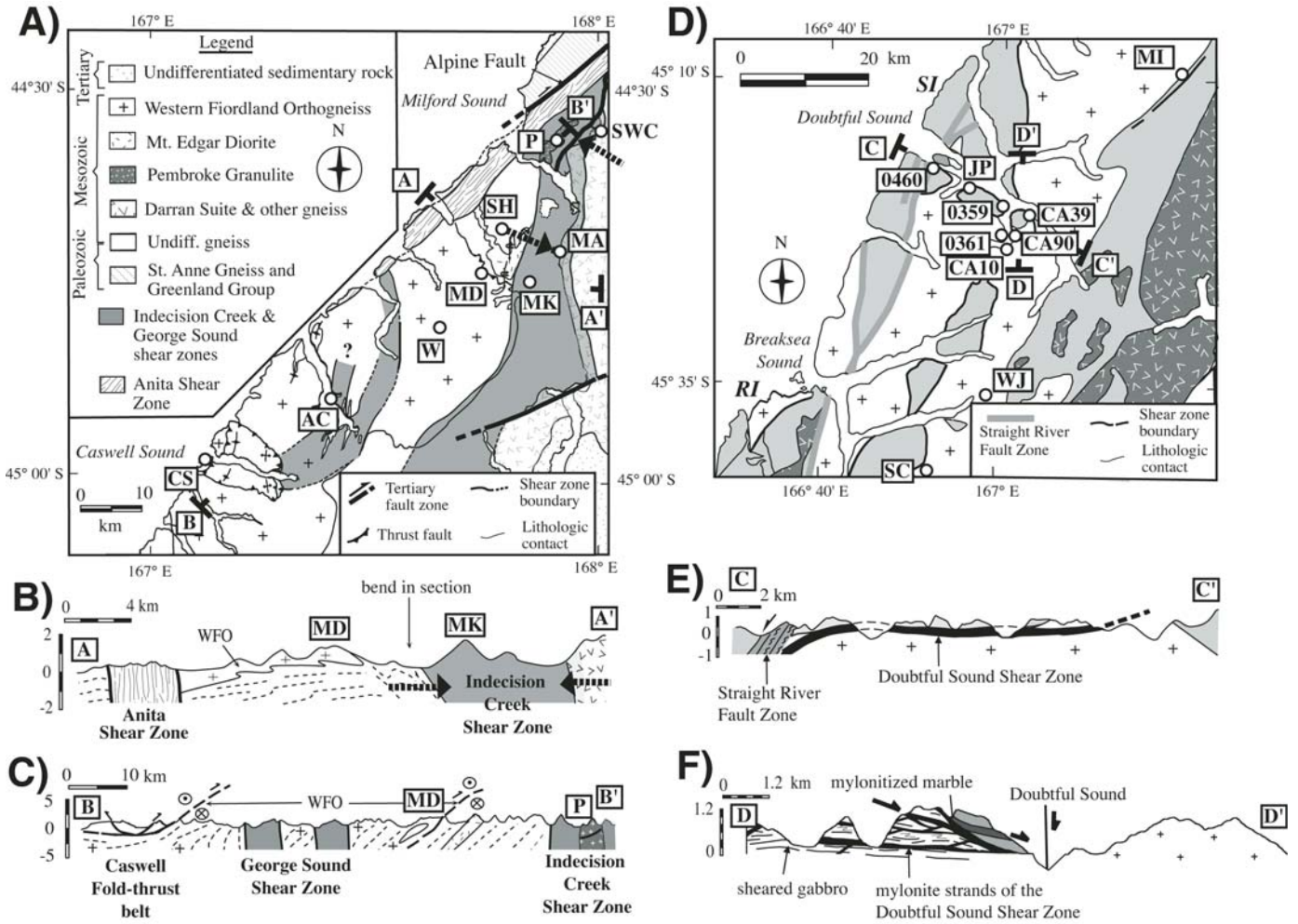


Figure 2. Simplified geologic maps of northern (A) and central (D) Fiordland. Two structural profiles are shown for each area: (B) and (C) for northern Fiordland and (E) and (F) for central Fiordland. Letters refer to key localities discussed in the text. Bold dashed arrows in (A) refer to regional-scale strain gradients along the margins of the Indecision Creek shear zone. Dashed lines in cross sections are the traces of foliation. Abbreviations are as follows: AC—Anchorage Cove; CS—Caswell Sound; JP—Joseph Point; MA—Mt. Ada; MD—Mt. Daniel; MI—Mt. Irene; MK—Mt. Kepka; P—Pembroke Valley; RI—Resolution Island; SC—Supper Cove; SI—Secretary Island; SH—Steep Hill; SWC—Selwyn Creek; W—Worsley; WFO—Western Fiordland Orthogneiss; WJ—Wet Jacket. Numbered abbreviations in B refer to samples listed in Table 1, patterns are same as in Figure 1.

cooling during the period 126–111 Ma. Klepeis et al. (2004) reconstructed the regional sequence of deformation, which we summarize here.

Between ca. 126 Ma and ca. 120 Ma, arc-related magmatism resulted in the emplacement of a >10-km-thick batholith, the Western Fiordland Orthogneiss. The oldest and hottest shear zones ($T > 800^\circ\text{C}$) in Northern Fiordland record supra-solidus deformation at the margins of intrusive sheets that make up this batholith. One of the best exposures of these shear zones occurs at Mount Daniel (Fig. 3) where a zone of penetrative magmatic foliations separates the Western Fiordland Orthogneiss above from the Milford Gneiss below. This shear zone is defined by successive sheets of intrusive rocks that were deformed at supra-solidus conditions during emplacement of the Western Fiordland

Orthogneiss. Textures that record flow in a semi-molten state are described in detail by Klepeis and Clarke (2004).

Another layer-parallel shear zone forms a ductile mid-crustal fold-thrust belt at the top of the Western Fiordland Orthogneiss at Caswell Sound (Figs. 2A and 2C). This belt was first identified by Daczko et al. (2002a). Both the Mt. Daniel and Caswell shear zones are generally less than 1 km thick and record sub-horizontal, layer-parallel shortening at high angles to the northeast-southwest trend of the Early Cretaceous magmatic arc. Deformation in the Caswell shear zone also accompanied emplacement of the Western Fiordland Orthogneiss and localized within its contact aureole, where strength contrasts between hot, magmatic material and cooler host rock occurred (Fig. 3C). Similar structures formed during arc magmatism on Stewart Island

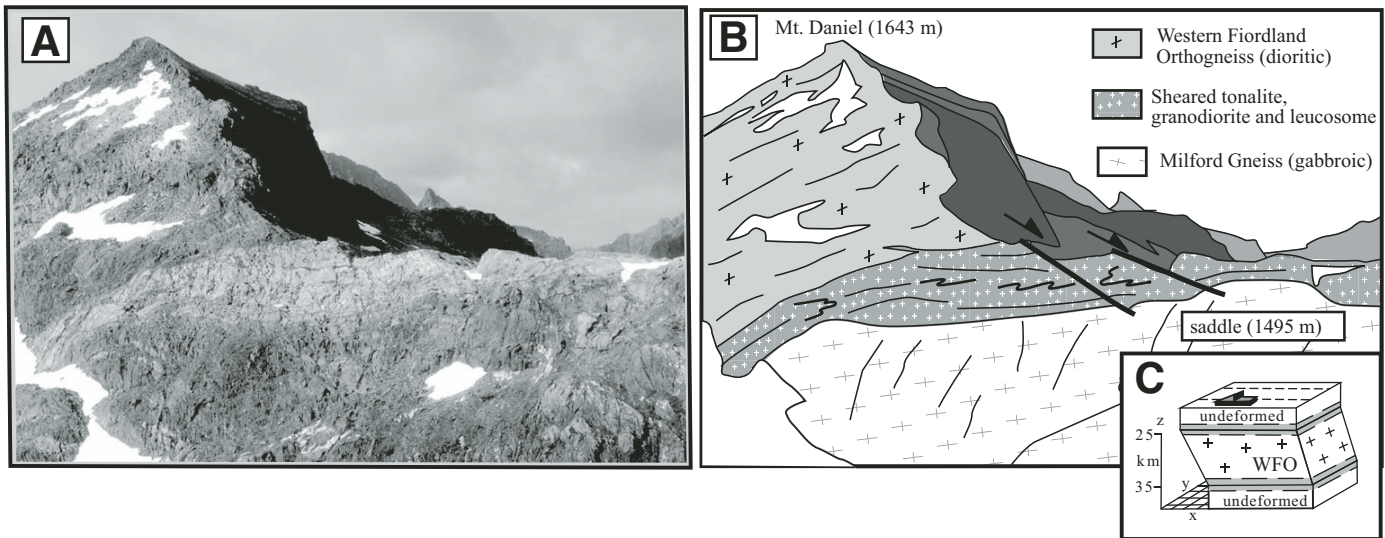


Figure 3. (A) Photograph and (B) interpretative sketch of igneous layering exposed on the northern face of Mount Daniel. View is to the south-east. Note presence of a melt-enhanced shear zone between Western Fiordland Orthogneiss (WFO) above and Milford Gneiss below. Normal faults shown in B are Tertiary brittle structures. Photo taken by Nathan Daczko. (C) Simple sketch showing the presence of layer-parallel ductile shear zones along the upper and lower contacts of the Western Fiordland Orthogneiss. See text for discussion.

south of Fiordland (Allibone and Tulloch, 1997; Tulloch and Kimbrough, 2003).

The input of heat accompanying emplacement of the Western Fiordland Orthogneiss resulted in the partial melting of the lower crust at temperatures of 750°–850° C (Clarke et al., 2000; Daczko et al., 2001b). The effects of this thermal pulse are reflected in the occurrence of migmatite and granulite-facies mineral assemblages within and up to 10 km below the batholith. Thin metamorphic rims around Paleozoic and Mesozoic zircon cores from below the batholith have yielded ages of ca. 120 Ma, suggesting that they reflect a period of partial melting and granulite-facies metamorphism that coincided with the emplacement of the batholith (Tulloch et al., 2000; Hollis et al., 2003). During this period of high-temperature metamorphism, a series of steep, thin (1–3 m) shear zones formed within and below the batholith (Figs. 4A and 4B). Analyses of the mineral assemblages that define foliations in the shear zones, including garnet, pyroxene, hornblende, plagioclase, rutile, and quartz, suggest that they record deformation at transitional granulite-facies conditions of ≈670 °C and ≈14 kb (Daczko et al., 2001a). These shear zones cut and recrystallize older foliations in migmatitic gneiss (Figs. 4A and 4B). Most contain mylonitic foliations defined by dynamically recrystallized plagioclase and stretched garnet, hornblende and clinozoisite aggregates. A sinistral set is dominant and strikes northeast. A second, subordinate set is dextral and strikes northwest. Both sets display gently plunging, hornblende mineral lineations and abundant asymmetric sense-of-shear indicators. They are preserved best in Pembroke Valley (P, Fig. 2A) north of Milford Sound (Daczko et al., 2001a).

Cross-cutting the steep shear zones in Pembroke Valley are a series of gently dipping, layer-parallel shear zones. Each

of these shear zones contains a central zone of 7–10-m-thick mylonite (Fig. 5A). Connecting each central zone of mylonite are thin (<1 m thick), curved shear bands that dip to the southeast and northwest (Fig. 5B). These shear bands envelop imbricated, asymmetric pods of mafic-intermediate orthogneiss. Relative displacement between groups of pods is indicated by the disparate orientations of foliation planes across mylonitic boundaries. Mineral lineations within the shear bands display similar trends but steeper plunges than the lineations that occur in the central mylonite zones. Boudinaged mafic layers and stretched garnet porphyroblasts show that these mineral lineations represent true stretching directions. The sense of shear displayed by these mylonitic zones and shear bands is dominantly top-to-the-northwest in a direction normal to the trend of the magmatic arc. Daczko et al. (2001a) interpreted these shear zones as forming part of a lower-crustal thrust duplex. This deformation also occurred at transitional granulite-facies conditions of ≈670 °C and ≈14 kb (Daczko et al., 2001a).

Following development of the gently dipping, duplex-style shear zones, two near vertical 10–15-km-wide zones of penetrative deformation, called the Indecision Creek and George Sound shear zones (Figs. 2A–2C), formed within the lower-crustal section. The structural elements that define the shear zones and the framework of the kinematic analysis described in this study are described by Marcotte et al. (2005). Both shear zones cut granulite-facies metamorphic mineral assemblages (ca. 120 Ma) in the Western Fiordland Orthogneiss and its granulite-facies host rock. Mineral assemblages, U-Pb determinations and cross-cutting relationships indicate that the shear zones developed before the shift to extension and before decompression and exhumation of the lower crust (Daczko et al., 2002c; Marcotte

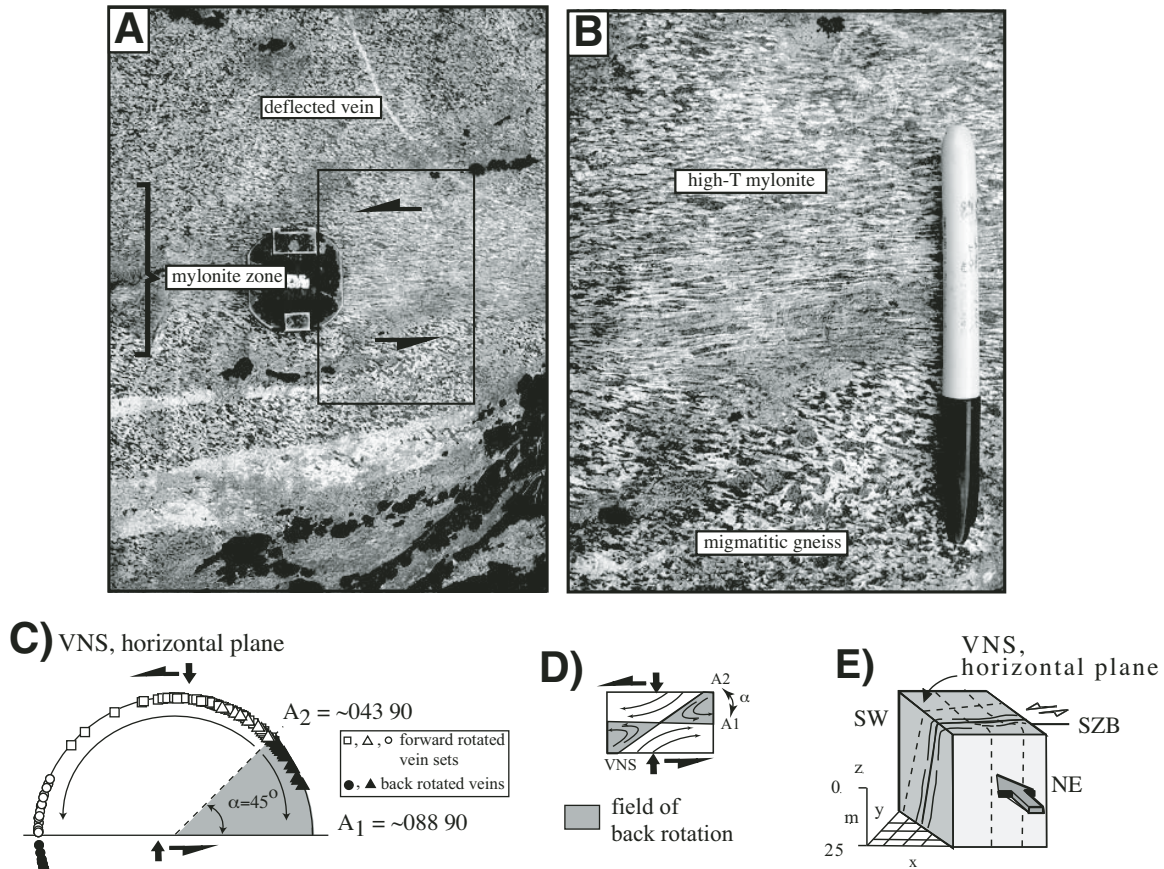


Figure 4. (A) Photograph of a vertical garnet-granulite-facies shear zone that cuts dioritic gneiss in Pembroke Valley. View is of a horizontal surface. For location see Figure 2A. Note deflected vein showing sinistral shear sense. (B) Close-up view of mylonite shown in A. Note stretched plagioclase ribbons. (C) Plot showing orientation (strike azimuth) of >250 rotated veins measured over a 0.75 km² area of Pembroke Valley. Plot represents a horizontal plane. Data and interpretation are from Daczko et al. (2001a). Symbols refer to different vein sets. The distribution of forward- and back-rotated veins relative to shear zone boundaries allows the width of the field of back rotation (D) to be defined in a horizontal plane. A_1 and A_2 refer to flow apophyses in a sinistral two-dimensional flow field. (E) Summary sketch showing geometry of parameters such as the vorticity normal section (VNS), the shear zone boundaries (SZB), and the rotated veins (dashed lines). Data show a pure-shear-dominated flow regime involving shortening in a horizontal plane.

et al., 2005). Their formation reflects a progressive widening and thickening of deformation zones that accompanied lower-crustal cooling, following emplacement of the Western Fiordland Orthogneiss batholith. The George Sound shear zone cuts up-section and merges with the mid-crustal Caswell fold-thrust belt. U-Pb data on zircon from the fold-thrust belt (Klepeis et al., 2004) and the Indecision Creek and George Sound shear zones (Marcotte et al., 2005) indicate that these structures all evolved during the same 119–111 Ma interval (Table 1).

The conditions of deformation that accompanied the formation of the steep shear zones during the interval 119–111 Ma were very heterogeneous, reflecting localized magmatic activity, some partial melting and rapidly changing lower-crustal temperatures. Kyanite- and paragonite-bearing assemblages indicate that the Indecision Creek shear zone records isobaric ($P = 14$ kb) cooling from >750 °C to ≈ 650 °C (Daczko et al., 2002c). The internal

structure of the shear zones is complex and includes multiple generations of foliations and folds (Fig. 6). Much of this complexity reflects a close relationship between deformation and the pre- and syn-tectonic emplacement of dikes displaying variable orientations (Marcotte et al., 2005). In some places, such as Selwyn Creek (SK, Fig. 2A) and Mt. Kepka (MK, Fig. 2A), garnet-bearing leucosome and numerous syntectonic dikes provide evidence of local partial melting, transient high temperatures and the transport of magma.

Microstructures in dioritic gneiss provide additional information on the conditions of deformation during this critical period immediately before the transition to extension in Northern Fiordland. In the high strain zones, large porphyroclasts of hornblende are surrounded by thin, commonly asymmetric mantles of small recrystallized grains (Fig. 7A). The mantles are stretched parallel to the foliation and grade into a fine-grained matrix consisting

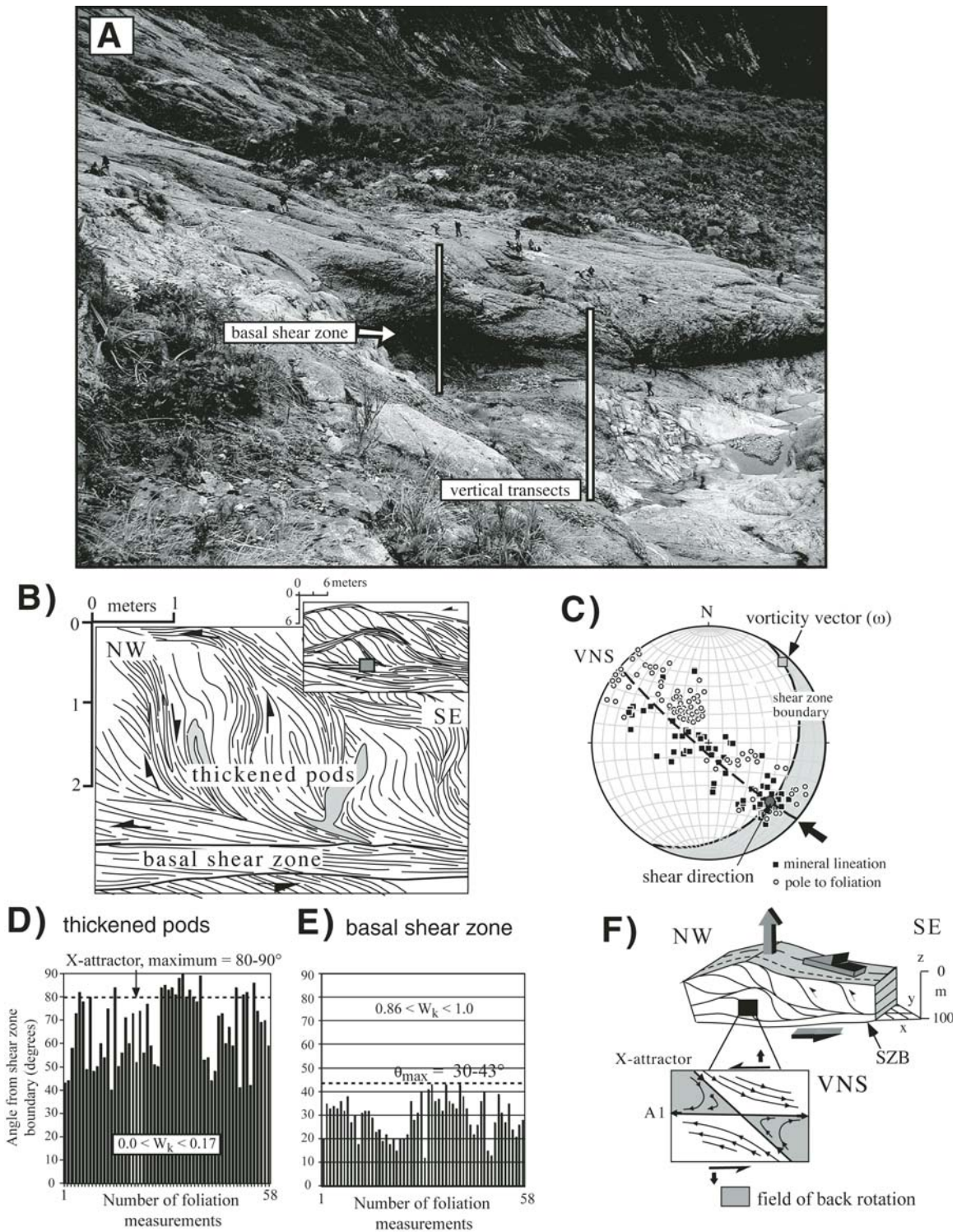


Figure 5. (A) Photograph of the Pembroke thrust fault. Photo by Stephen Marcotte. Note people in hanging wall for scale. Basal shear zone is one of several sub-parallel thrust zones that form a vertically stacked sequence. White lines are vertical transects along which structures were measured. (B) Vertical profiles showing the geometry of garnet-granulite-facies foliations within and above the basal shear zone. Shaded regions are pegmatite dikes. (C) Equal area lower hemisphere stereographic projections showing orientation of foliation (poles) planes and hornblende mineral lineations in the vertical transects. Structures allow the vorticity normal section (VNS), the vorticity vector and the shear zone boundaries (SZB) to be defined. (D and E) Histograms showing angle between foliation planes and the basal shear zone in the VNS plane. Data show a flow regime dominated by pure shear (~90%) and involving thickening in a vertical plane. (F) Sketch showing geometry of thrust zone, orientation of the VNS, and the shear zone boundaries. Sketch shows expected orientation of the X-attractor in a vertically lengthening shear zone.

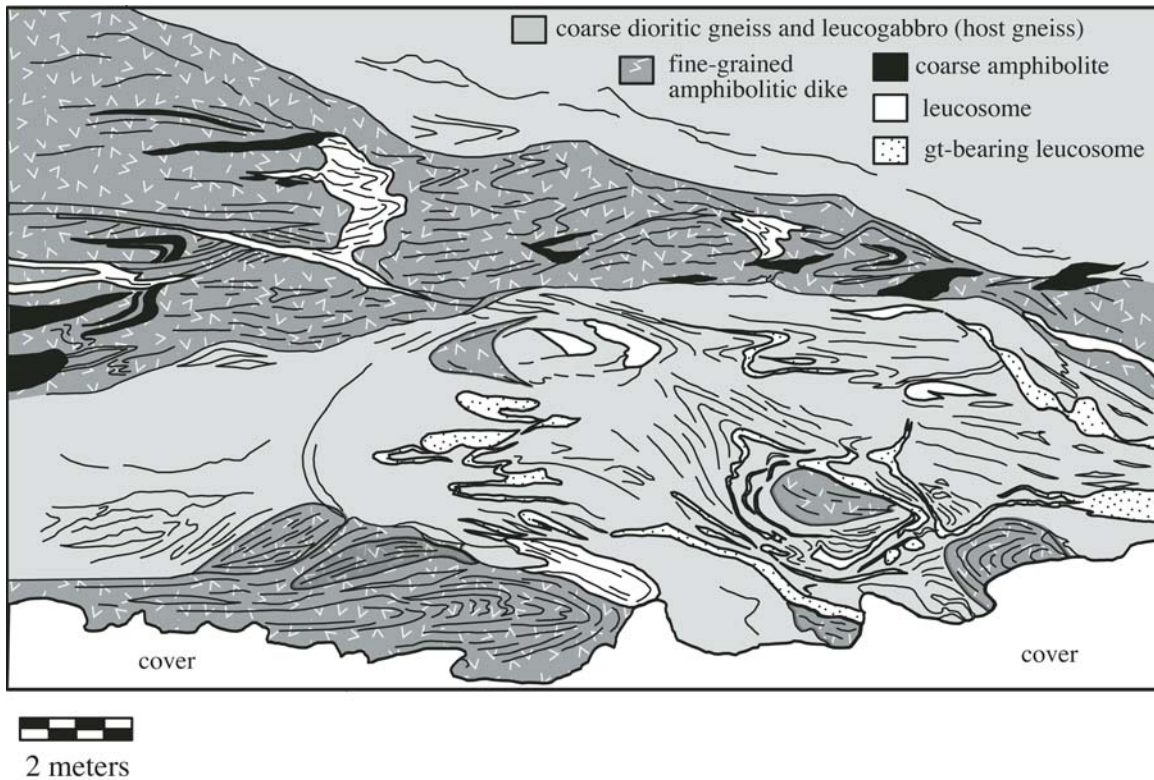


Figure 6. Sketch of a part of the Indecision Creek shear zone at Selwyn Creek. See Figure 2A for location. Note evidence of high strains and the heterogeneous structure composed of multiple igneous injections, folded foliations (thin dark lines), leucosome, and dikes. The geometry and grain size of the dikes controlled strain partitioning within the shear zone. View is toward 120° . Surface dips 29° NW.

mostly of recrystallized plagioclase (Fig. 7B). The cores of hornblende porphyroclasts display bent crystal lattices surrounded by bands of recrystallized grains, many of which display cuspatelobate grain boundaries (Fig. 7B, white arrows). These grain boundary shapes suggest that grain boundary migration was an important process that controlled the recrystallization of hornblende. In addition, the lack of neoblastic amphibole growth and the mixing of recrystallized hornblende and plagioclase grains in the mantle and tails of hornblende porphyroclasts (Fig. 7A) suggest that some diffusion-accommodated grain-boundary sliding also occurred (Gower and Simpson, 1992). In the matrix, deformation was accommodated mainly by dynamic recrystallization of plagioclase crystals. Plagioclase displays evidence of grain size reduction (Fig. 7C), cuspatelobate grain boundaries, and core-mantle structures (Fig. 7D), indicating high grain boundary mobility.

These textures suggest that deformation in the Indecision Creek shear zone occurred by recrystallization-accommodated dislocation creep in plagioclase (Tullis and Yund, 1985; Ji and Mainprice, 1990) and the recrystallization of hornblende, with some grain boundary sliding. Experimentally deformed aggregates of amphibole and plagioclase (Hacker and Christie, 1990) display amphibole microstructures at temperatures of $\geq 650^\circ\text{C}$ that

are similar to those we observed. Evidence of rotational recrystallization in plagioclase and recovery by dislocation climb suggest deformation at temperatures of $>550^\circ\text{C}$ (Olsen and Kohlstedt, 1985; Pryer, 1993), which are consistent with those obtained using thermobarometric techniques (Daczko et al., 2002c).

Estimates of Mean Kinematic Vorticity in a Horizontal Plane

Patterns of deformed and rotated veins adjacent to the steep shear zone pairs in Pembroke Valley reveal kinematic patterns in a horizontal (layer-parallel) plane over an area of 0.75 km^2 . Daczko et al. (2001a) used sets of near vertical veins as strain markers to infer that the shear zone pairs record a two-dimensional type of flow characterized by subhorizontal (layer-parallel) shortening and stretching with little displacement recorded in the vertical (layer-perpendicular) plane. The monoclinic rotation history of over 250 veins along the margins of shear zones allowed these authors to define fields of back rotation and forward rotation associated with the deformation (Fig. 4C). The dominant rotation sense was sinistral. Back rotation was indicated by the dextral rotation of a vein where it entered and was reoriented by a sinistral shear zone (see figure 6 in Daczko et al., 2001a). This history also allows the

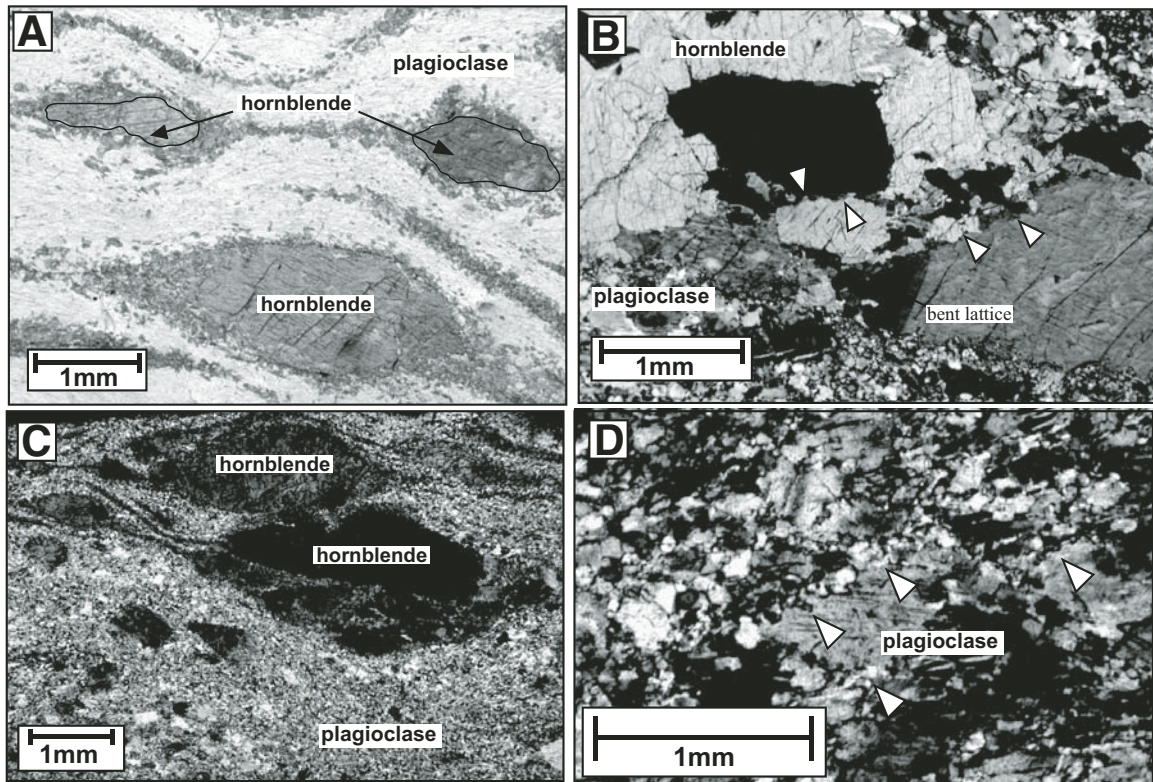


Figure 7. Photomicrographs from the Indecision Creek shear zone. All images are from thin sections of surfaces oriented perpendicular to foliation and parallel to lineation. Foliation planes in all images parallel the bottoms of the images unless otherwise indicated. (A) Hornblende subgrains in plane light form mantles and elongate tails of hornblende porphyroclasts. Intermixed mantles of plagioclase and hornblende suggest that mechanical mixing was important during deformation. The lack of subgrains in the matrix suggests that neoblastic growth was relatively minor. Two core grains are outlined. (B) Zone of recrystallized hornblende grains (arrows) that cut across a large core grain of hornblende (crossed polars). Openly bent lattice of core hornblende grain (arrows, bottom) grades into a band of subgrains that are strain free and share sharp grain boundaries with the host. (C) Asymmetric hornblende fish are surrounded by a fine-grained matrix of dynamically recrystallized plagioclase (crossed polars). Note evidence of grain size reduction in high-temperature mylonite. (D) Close-up view of dynamically recrystallized plagioclase shown in C. Arrows show core-mantle structures. Elongate grains define an oblique foliation from lower left to upper right.

determination of the orientation of the vorticity vector and vorticity normal section (VNS, Fig. 4E). The orientation and width of the fields of back rotation (Fig. 4D) provide an estimate of average sectional kinematic vorticity numbers (W_m) of $0.63 < W_m < 0.73$ for the horizontal plane (Daczko et al., 2001a). Daczko et al. (2001a) obtained similar results from measures of foliation traces and an estimate of the orientation of instantaneous strain axes at specific sites. This estimation involved measures of the orientation of >50 oblique grain-shape foliations preserved inside low strain pods within the margins of shear zones (see figure 8 of Daczko et al., 2001a). Wallis (1995) provides a full description of this technique. The similarity among the average and instantaneous measures of sectional kinematic vorticity suggests that the deformation was approximately steady at the scale of observation (0.75 km²). These patterns show that deformation in a horizontal plane involved subhorizontal arc-normal (northwest-southeast) shortening and arc-parallel (northeast-southwest) stretching (Fig. 4E) with ~43%–53% pure shear.

Estimates of Mean Kinematic Vorticity in a Vertical Plane

The geometry of structures that define the gently dipping, duplex-style shear zones in Pembroke Valley (Fig. 5A) allowed the estimation of the kinematics of deformation in a vertical (layer-perpendicular) plane. Above each basal shear zone, mineral lineations vary smoothly within a single plane that strikes to the northwest (131°) and dips steeply to the southwest (84°; Fig. 5B). This pattern defines the vorticity normal section (VNS) and allows estimation of the average orientation of the vorticity vector (ω) for the deformation (Fig. 5C). The vorticity vector is constrained to lie normal to the VNS for steady-state deformations. In addition, virtually all asymmetric microstructures such as recrystallized tails on porphyroclasts were observed in the VNS plane. The bulk shear direction for the shear zones is given by the intersection between the VNS and the shear zone boundaries. This direction parallels hornblende mineral lineations within the basal mylonite zones (Fig. 5C). The boundaries of the shear

zones parallel the thick zones of mylonite that underlie rotated foliation planes. These relationships establish that the deformation involved displacements in an interconnected network of flat and steep shear zones that displays monoclinic symmetry. Similar mid-crustal geometries have been described by Karlstrom and Williams (2006).

Structural relationships in areas where the vertical stacking of asymmetric pods are most abundant are distinct from those in areas that lack the antiformal stacks. Each pod contains a curved, oblique grain-shape foliation defined by coarse, elongate aggregates of garnet, clinopyroxene, plagioclase, hornblende, and clinozoisite. The angle between these internal foliations and the surrounding mylonitic foliations is at a maximum near the centers of each pod (Fig. 5B). The oblique foliations are either truncated by or smoothly merge into parallelism with the enveloping mylonites. The smooth deflections are accompanied by a reduction in the grain size of plagioclase and hornblende and an increase in the degree of grain elongation. This grain size reduction was accomplished by the dynamic recrystallization of plagioclase and the breaking apart of hornblende grains. The acute angles (θ) between the traces of the oblique foliations and the shear zone boundaries display angles as high as $\theta = 70\text{--}90^\circ$ in areas of antiformal stacking (Fig. 5D). In contrast, areas that lack stacked lenses display maximum angles of $\theta = 30\text{--}43^\circ$ and the spread of data is more homogeneous (Fig. 5E). The unusually steep angles of $\theta = 70\text{--}90^\circ$ only occur in areas of stacked pods and suggest that the deformation in these zones was dominated by pure shear and stretching at high angles to the shear zone boundaries. Mineral lineations in these stretching pods are steeply plunging within the VNS (Fig. 5C). The formation of fabrics oriented nearly 90° from the shear zone boundary is expected in zones of pure shear thickening (Teyssier and Tikoff, 1999).

If the areas outside the zones of thickened pods reflect the geometry of structures prior to the formation of the antiformal stacks then a comparison between these zones provide a means of estimating a mean kinematic vorticity number for the vertical plane. This assumption appears reasonable because the areas that lack antiformal stacks occur adjacent to areas that display the pile-ups. In addition, areas of stacked pods display ultramylonite textures indicating that these areas are highly strained. If correct, then the increase in angle (θ) from outside to inside the zones of thickened pods suggests that layer-parallel shortening and vertical thickening resulted in a progressive steepening of foliation planes. This interpretation agrees with the qualitative evidence of vertical thickening within a flow regime locally dominated by pure shear (i.e., less than 20% simple shear).

For a thickening shear zone undergoing steady flow, numerical models predict that the directions of maximum principal stretch (X) lie within or close to the trace of the VNS (Jiang and Williams, 1998; Lin et al., 1998; Jiang et al., 2001). This relationship holds true for triclinic as well as monoclinic shear zones. For steady-state deformations (Fig. 5F), the stable end orientation of the X-axis parallels an extensional flow apophysis

(or the X-tractor following the definition of Passchier, 1987). This apophysis is inclined relative to the shear zone boundary in a thickening shear zone (Jiang and Williams, 1998; Teyssier and Tikoff, 1999). With increasing strain the X-direction will rotate and converge on the extensional flow apophysis (A_1 , Fig. 5F). An estimate of the orientation of the extensional flow apophysis in these shear zones can be obtained if the trace of the rotating foliations approximately tracked the direction of maximum principal stretch (see descriptions by Wallis, 1995, and Daczko et al., 2001a). Even if the foliations did not track the finite strains perfectly they should approach the stable end direction if strains were high enough. Using this approach, the highest angles (θ) between traces of oblique mylonitic foliations and the shear zone boundaries in the VNS provide a minimum estimate of the sectional kinematic vorticity number (W_m). The range $\theta = 70\text{--}80^\circ$ suggests $-0.17 < W_m < -0.34$ on the scale of individual 20-m-thick antiformal stacks. The minus sign indicates thickening (after Simpson and DePaor, 1993).

Three-Dimensional Strain and Kinematic Vorticity Patterns at the Regional Scale

Kinematic data from Pembroke Valley suggest that deformation prior to ca. 111 Ma, at least locally, involved components of horizontal shortening and vertical thickening and >50% pure shear at the scale of several square kilometers. We tested this result at the scale of the entire lower-crustal section by measuring variations in the orientation of structural elements across two regional strain gradients. To use this approach, we assumed that the foliations and mineral lineations formed together and approximately tracked finite strain directions during deformation. We evaluate these assumptions later in this section.

One of the best exposed regional strain gradients occurs in a 5-km-wide zone adjacent to the western boundary of the Indecision Creek shear zone (SH to MA in Fig. 2A). From west to east across this zone (marginal domain in Fig. 8A), a positive strain gradient is defined by an increase in fold tightness (decrease in interlimb angle) and a decrease in the angles between deformed dikes and vein sets (strain data reported by Marcotte et al., 2005). Within the central parts of the shear zone, these folds and dikes are almost completely transposed parallel to foliation (Fig. 6). These geometric changes reflect an increase in the component of shortening from west to east across the section. Another, narrower (1–2-km-wide) strain gradient occurs from east to west across a second marginal domain adjacent to the eastern boundary (SC, Fig. 2A). Within these marginal domains, a steep foliation is developed parallel to the axial planes of the tightening folds. Hornblende mineral lineations appear together with this steep foliation. This fabric cross-cuts the 126–120 Ma Western Fiordland Orthogneiss and has been dated as having evolved during the interval of 119–111 Ma (Marcotte et al., 2005). These relationships justify our assumption that the foliations and mineral lineations we measured formed during the same approximate time interval.

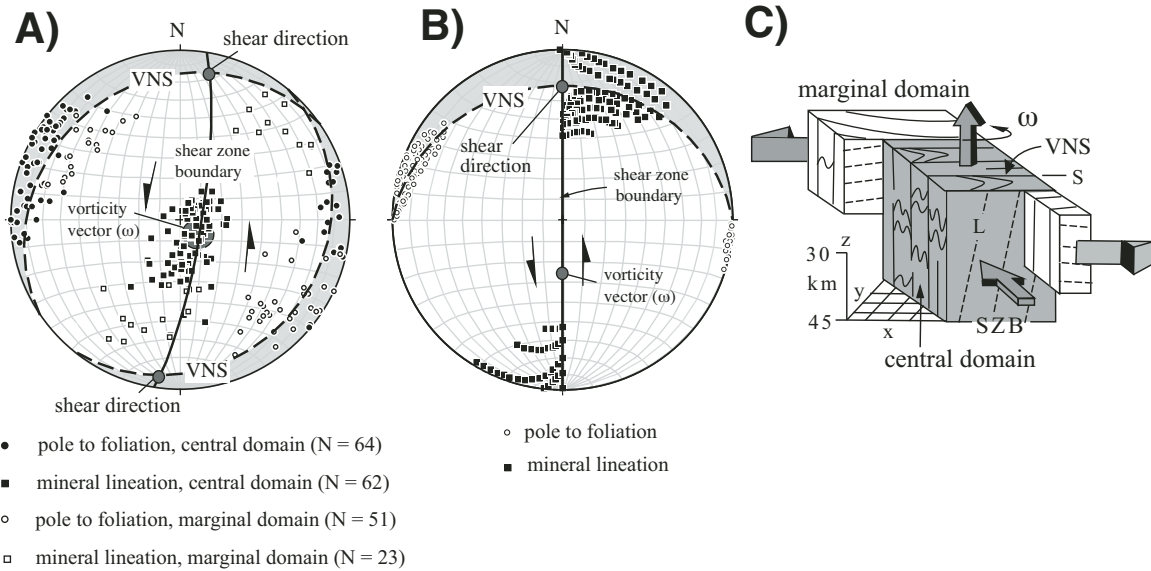


Figure 8. (A) Equal area, lower hemisphere, stereographic projections showing orientation of foliations and hornblende mineral lineations within the Indecision Creek shear zone. Central domain refers to high strain areas, such as Selwyn Creek (Fig. 6). Marginal domains refer to lower strain areas in the wall rock of the shear zone. Data were measured across two regional-scale strain gradients oriented perpendicular to the shear zone boundaries (for location see Fig. 2A). (B) Results of forward modeling of a vertical transpressional shear zone showing predicted changes in the orientation of extensional and contractional axes (poles to foliation and mineral stretching lineations, respectively) during progressive deformation in horizontally thinning and vertically thickening shear zones. Figure is modified from those presented in Jiang et al. (2001). See text for discussion. The angle of convergence is 20° from the normal to the shear zone boundary. Different lineation (squares) paths track the long axis of the finite strain ellipsoid with different values of simple shear and pure shear. Experiments were conducted with ratios of simple shear to pure shear of 1, 2, 4, 6, and 20. With an increasing component of pure shear, lineations plot progressively farther from the vorticity normal section and approach the vorticity vector. These patterns are similar to the changes in the orientations of lineations with increasing strain shown in part A, suggesting that the Indecision Creek shear zone was vertically thickening, horizontally thinning, and dominated by pure shear. (C) Sketch showing geometry of deformation in the Indecision Creek shear zone, including the orientation of the velocity normal section (VNS) and the shear zone boundaries (SZB).

A comparison of structures in the marginal and central domains allowed us to determine the kinematics of flow within the Indecision Creek shear zone. The boundaries of the shear zone are well defined and nearly vertical (Fig. 8A). These boundaries separate the domains and parallel the steep western margin of the Darran igneous suite (Fig. 2A). With increasing strain across the two marginal domains (black dashed arrows in Figs. 2A and 2B), foliation planes steepen and rotate counter-clockwise into parallelism with the vertical boundaries. For a steep shear zone accommodating a component of horizontal shortening perpendicular to its boundaries (i.e., a horizontally thinning shear zone), the spread of foliation poles defines the VNS and allows estimation of the vorticity vector (Lin et al., 1998; Jiang et al., 2001; Jones et al., 2004). This relationship is true for triclinic and monoclinic zones of steady-state deformation and is independent of any volume change. Each of the two marginal domains shows a spread of poles to foliation that define two gently-dipping planes on an equal-area stereoplot (Fig. 8A). These two dipping planes correspond to the western and eastern marginal domains, respectively. The intersection of the VNS and the shear zone boundary

gives nearly horizontal bulk shear directions (Jiang et al., 2001). The counter-clockwise sense of rotation indicates a component of sinistral strike-slip displacement parallel to the shear direction.

The hornblende mineral lineations change orientation from a few degrees from horizontal in the marginal domains to near vertical in the central domain (Fig. 8A). These lineations neither perfectly parallel the vorticity vector (ω) nor lie in the VNS. These patterns indicate that the deformation was dominated by pure shear because the farther the lineations plot away from the shear direction, the higher the percentage of pure shear relative to simple shear (Lin et al., 1998; Jiang et al., 2001). This pattern also implies that the marginal domains record a higher percentage of simple shear than the central domains because the lineations plot closer to the VNS in the latter. This result means that the margins of the shear zone were more efficient at maximizing offset relative to strain. It also indicates that the deformation deviated from plane strain and may have involved a significant component of sub-horizontal (layer-parallel) flattening, especially in the shear zone center. The migration of lineations toward the vertical dip-line of the shear zone with increasing strain (black arrows in

Fig. 5B) indicates that the zone was thickening in a down-dip or vertical direction. These patterns are diagnostic of triclinic transpression and are independent of any change in volume (Lin et al., 1998; Jiang et al., 2001; Czeck and Hudleston, 2003).

These results are in excellent agreement with the results from Pembroke Valley and also are compatible with interpretations of transpression. To test the interpretation and the assumption of steady-state flow, we compared our data to forward models of homogeneous triclinic deformation (original models presented by Lin et al., 1998, and Jiang et al., 2001). The models predict the progressive changes in the orientation of finite strain axes for various flow types. One model that approximates the patterns illustrated by the Indecision Creek shear zone involves components of horizontal shortening, vertical thickening and subhorizontal sinistral shear parallel to a steep shear zone boundary (Fig. 8B) (after figure 5b of Jiang et al., 2001). Nevertheless, the natural patterns display significant deviations from the model results. First, structural patterns within Fiordland indicate that the deformation was far from homogeneous. Structures are complex in part due to the heterogeneity of the strain and also due to compositional variations created by numerous superposed dikes and sills that form part of the shear zone fabric. Second, the spread of poles to foliations is greater than the predicted $\leq 45^\circ$ for transpression. The large spread we measured probably reflects folding and flattening within the marginal domain. Nevertheless, despite these complexities, the patterns we observed are compatible with deformation with components of vertical thickening, subhorizontal, arc-normal shortening, and sinistral arc-parallel translation (Fig. 8C). The result of this comparison suggests that, although the deformation probably was not truly steady state, the approximation is good enough to allow us to recognize the bulk kinematics of flow at the regional scale.

CENTRAL FIORDLAND

Geometry, Age, and Sequence of Structures

In Central Fiordland (Fig. 2D), the Doubtful Sound shear zone is composed of splays of upper-amphibolite-facies mylonite up to several hundred meters thick (Figs. 2E and 2F). The shear zone was originally interpreted as a ductile thrust fault by Oliver and Coggon (1979) and Oliver (1980) and later was reinterpreted as an extensional detachment fault by Gibson et al. (1988). Zones of high strain are mostly sub-horizontal with anastomosing branches that dip gently to the northeast and southwest (Fig. 9A). Curved zones of mylonite envelop asymmetric pods that preserve older gneissic fabrics and garnet-granulite mineral assemblages. These pods typically vary in size from <1 m to >30 m in horizontal length. One of the largest high strain zones separates two distinctive lithologies: an interlayered unit of coarse-grained pyroxene- and hornblende-bearing metagabbro and metadiorite of the Western Fiordland Orthogneiss and paragneiss, marble, amphibolite and granitoids that comprise an overlying Paleozoic cover sequence. North of Doubtful Sound the cover sequence

mostly dips gently to the north and northeast. Upper-amphibolite-facies mylonite zones up to 500 m thick also cut deeply inside the batholith (Fig. 2F). Foliations are defined by retrogressive biotite and hornblende that formed from the hydration of pyroxene. The branching nature of high strain zones in dioritic gneiss is similar to shear zones exposed in Pembroke Valley.

In the foot wall of the Doubtful Sound shear zone at Crooked Arm (CA10, Fig. 2D) strands of upper-amphibolite-facies mylonite (Figs. 9C and 9D) cut obliquely across an older granulite-facies fabric (Oliver, 1977; Oliver and Coggon, 1979; Klepeis et al., 2007). In these zones, garnet-granulite-facies foliations are transposed parallel to upper-amphibolite-facies foliation planes (Figs. 9C and 9D). Penetrative northeast-plunging mineral lineations defined by aggregates of plagioclase, pyroxene and amphibole are well developed on foliation planes in zones of both granulite-facies mylonite ($L_{GG}-S_{GG}$, Fig. 9D) and zones of upper-amphibolite-facies mylonite ($L_{SZ}-S_{SZ}$, Fig. 9E). The regional-scale geometry of these two fabrics, including sense-of-shear indicators, is similar (Klepeis et al., 2007).

Hollis et al. (2004) obtained U-Pb ages on zircon (Fig. 2D; Table 1) from Crooked Arm that suggest granulite-facies metamorphism occurred at 114 ± 2.2 Ma in this region. This age is in agreement with the ages of the youngest part of the Western Fiordland Orthogneiss (116–113 Ma; Table 1) obtained by Tulloch and Kimbrough (2003) and Hollis et al. (2004). Klepeis et al. (2007) obtained U-Pb ages on zircon from syntectonic dikes that indicate deformation in the shear zone occurred through 102 ± 1.8 Ma. This age determination is consistent with U-Pb thermochronology on titanite obtained by Flowers et al. (2005) from the same area (Table 1). These latter ages indicate cooling through 650–550 °C during the interval 113.4–111 Ma.

Microstructures and Changing Conditions of Deformation

Microstructures in the superposed fabrics from the hanging wall and foot wall of the Doubtful Sound shear zone provide a record of changing conditions within the lower crust, including its exhumation, during the period 114–90 Ma. Outside (above and below) the Doubtful Sound shear zone, grain sizes in undeformed diorite of the Western Fiordland Orthogneiss are relatively large, with most plagioclase grains falling within the range of 200 μm –1mm. A lattice preferred orientation (LPO) in plagioclase is visible. Plagioclase grains display deformation twins that taper toward grain boundaries and grain boundary bulging is commonly observed (Fig. 10A). Hornblende and biotite are clustered into aggregates that define a weak foliation (Fig. 10E) interpreted to reflect flow under partially molten conditions.

Within one kilometer of the Doubtful Sound shear zone, in its foot wall at Crooked Arm (CA10, Fig. 2D), garnet-granulite mineral assemblages record dehydration of host rock assemblages at temperatures of >700 °C and pressures of 12 kb (Oliver, 1977; Gibson and Ireland, 1995; Hollis et al., 2004). These exposures of sheared garnet granulite within Crooked Arm are composed of plagioclase, clinopyroxene, orthopyroxene, and garnet with

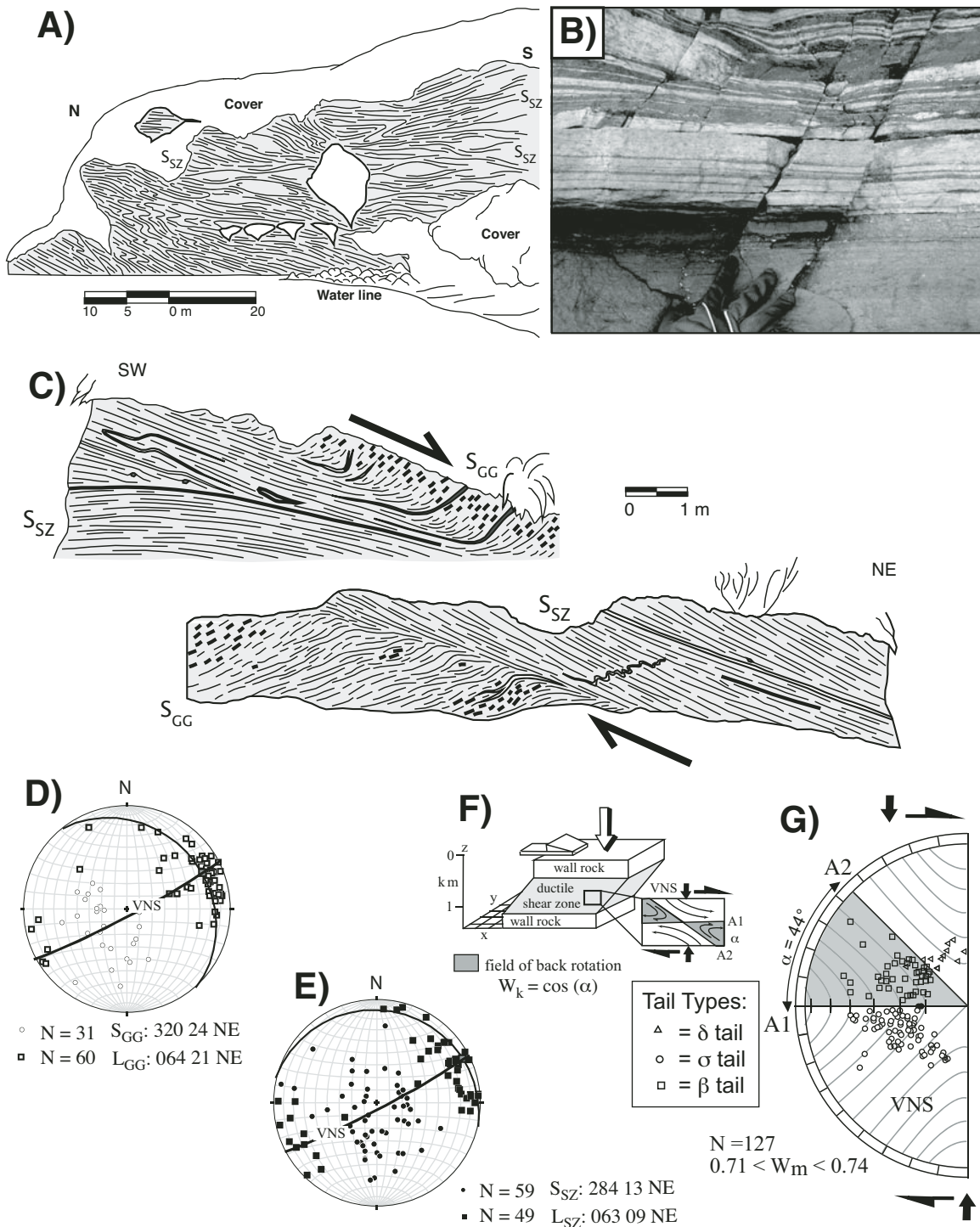


Figure 9. (A) Vertical profile of the Doubtful Sound shear zone exposed at Joseph Point. Note gently-dipping, oblate-shaped lozenges defined by foliation (S_{SZ}). (B) Photograph of a mylonitic part of the Doubtful Sound shear zone. Light colored layers contain elongate feldspar porphyroclasts in a fine-grained biotite- and hornblende-bearing matrix. These layers could represent deformed dikes in a highly sheared part of the Western Fiordland Orthogneiss. (C) Two vertical profiles of a high-strain branch of the Doubtful Sound shear zone at Crooked Arm. High strain zone is defined by a penetrative upper-amphibolite-facies foliation (S_{SZ}) that transposes a garnet-granulite-facies foliation (S_{GG}) in the foot wall and hanging wall (indicated by thick rectangles). (D) Equal area, lower hemisphere, stereographic projections showing orientation of garnet-granulite-facies foliations and plagioclase + hornblende mineral lineations at Crooked Arm. (E) Stereoplot showing orientation of upper-amphibolite-facies foliations and plagioclase + hornblende mineral lineations (L_{SZ}) within the Doubtful Sound shear zone. (F) Sketch showing predicted geometry of field of back rotation in a vertically thinning, horizontally stretching shear zone. (G) Hyperbolic plot showing distribution of forward rotated and backward rotated feldspar clasts in the Doubtful Sound shear zone. Data show a vertically thinning flow regime with approximately equal components of pure shear and simple shear. Plot combines data from five sites (from Klepeis et al., 2007).

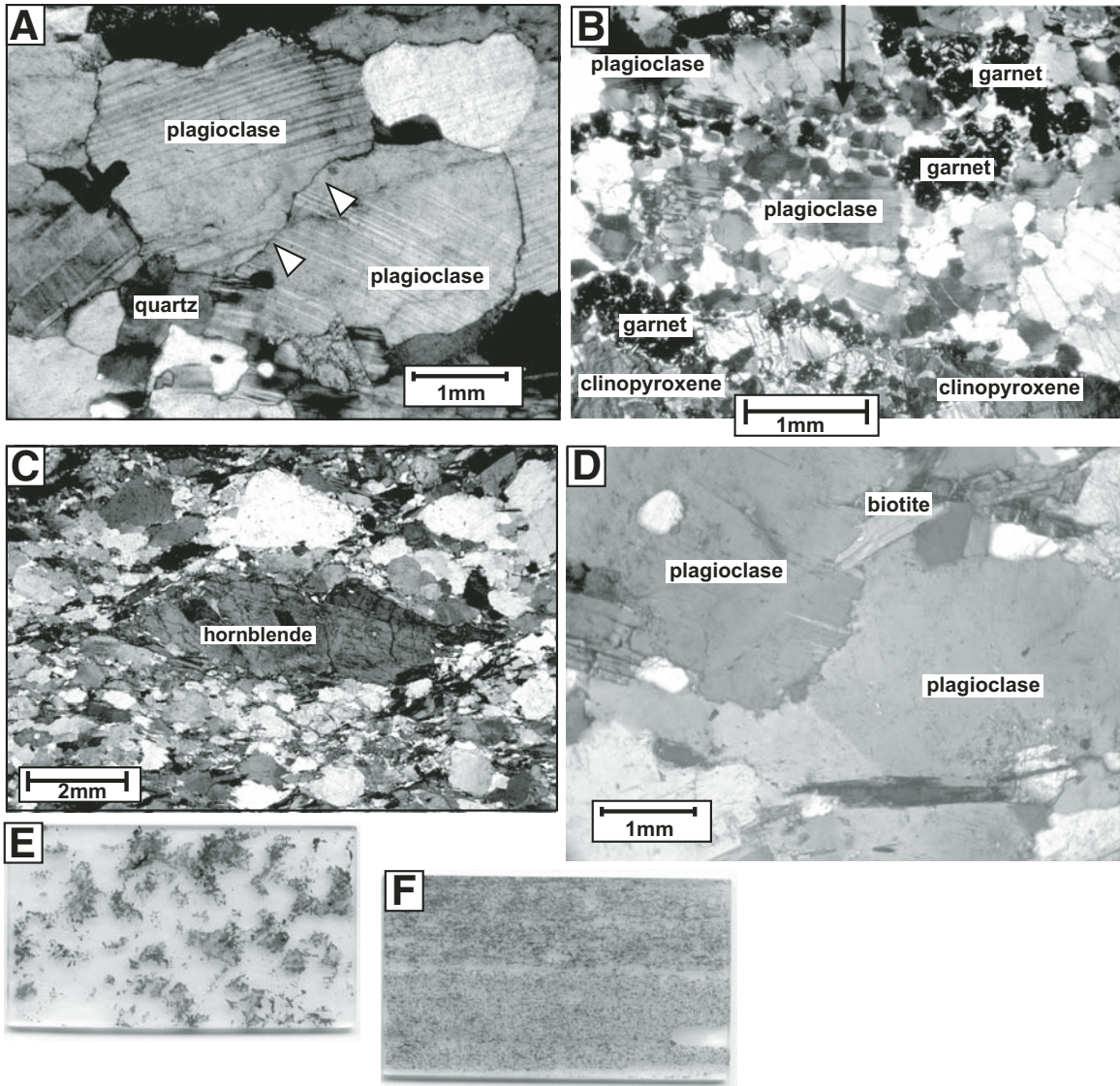


Figure 10. Photographs of microstructures from within the hanging wall and foot wall of the Doubtful Sound shear zone. All images are from thin sections of surfaces oriented perpendicular to foliation and parallel to lineation. Foliation planes in all images parallel the bottoms of the images unless otherwise indicated. (A) Photomicrographs of the dioritic part of the Western Fiordland Orthogneiss from the hanging wall of the Doubtful Sound shear zone at Bradshaw Sound. Image (crossed polars) shows plagioclase deformation twins as well as evidence for grain boundary bulging and grain boundary migration in plagioclase (arrows). (B) Photomicrograph of granulite-facies fabric in the foot wall of the Doubtful Sound shear zone in Crooked Arm. At the bottom of this image (crossed polars) is a deformed aggregate of clinopyroxene, orthopyroxene, garnet, and quartz. The plagioclase in the center of the image is almost completely recrystallized. (C) Photomicrograph (crossed polars) of upper-amphibolite-facies foliation within the Doubtful Sound shear zone at Joseph Point. Image shows an asymmetric hornblende fish (top-to-left, or -northeast, shear sense) surrounded by a matrix of dynamically recrystallized plagioclase. Grain boundary migration leading to recrystallization occurs along plagioclase grain boundaries. (D) Photomicrograph (crossed polars) showing subgrain formation within a plagioclase grain and recrystallization along a plagioclase grain boundary. Compare to Figure 10B. (E) Scanned image of a thin section (45 cm long) showing the macroscopic texture of dioritic orthogneiss (Western Fiordland Orthogneiss) below the Doubtful Sound shear zone. Note the relatively large grain size, weak foliation, and clustering of hornblende and biotite. (F) Scanned image of thin section at the same scale as in Figure 10E showing texture of dioritic orthogneiss (Western Fiordland Orthogneiss) within the shear zone. Note the extreme grain-size reduction and the anti-clustered distribution of hornblende and biotite.

small amounts of quartz and epidote. In most places within the samples, feldspar is completely recrystallized with sizes ranging from 100 to 500 μm in diameter (Fig. 10B). Recrystallization occurred through both grain boundary migration and subgrain rotation. A strong LPO is present. Many plagioclase grains intersect at 120° triple junctions. No growth twins were observed in plagioclase grains, but flame perthite and other deformation twin textures are common. A shape preferred orientation (SPO) in plagioclase defines a weak foliation oblique to the dominant foliation (S_{GG}). Orthopyroxene and clinopyroxene grains form asymmetric fish within a plagioclase matrix. These sense-of-shear indicators show both top-to-the-northeast (Fig. 10C) and –southwest senses of shear similar to shear indicators in the upper-amphibolite-facies strands of the Doubtful Sound shear zone.

Areas of the Western Fiordland Orthogneiss that are deformed by the Doubtful Sound shear zone display mineral assemblages that include plagioclase, hornblende, clinozoisite, K-feldspar and biotite with minor quartz and clinopyroxene. The composition is similar to that of samples outside the shear zone except there is a much greater percentage of hydrous phases. Plagioclase grain sizes are smaller within the shear zone than outside (Fig. 10F) with most grains only 50–100 μm and some up to 1 mm in diameter. Plagioclase shows exsolution lamellae and a well-developed SPO aligned with a penetrative foliation (S_{SZ}). The LPO appears visually weaker than outside the shear zone. Biotite and hornblende are aligned within the foliation. Plagioclase shows recrystallization through grain boundary migration (Fig. 10D). Klepeis et al. (2007) report deformation at upper-amphibolite-facies conditions of 550–650 $^\circ\text{C}$ and 7–9 kb.

On the basis of these microstructures, we interpret the relative importance of different deformation mechanisms as temperature and fluid conditions changed in the lower crust. Samples from outside the Doubtful Sound shear zone display features expected to result from dislocation creep in plagioclase. However, not all grains were recrystallized in these samples as evidenced by the presence of growth twins. This may suggest that high-grade metamorphic conditions did not last long enough to cause complete recrystallization everywhere within the Western Fiordland Orthogneiss. In addition, triple junctions of plagioclase grains are evidence for annealing. This process appears to have occurred after deformation through dynamic recrystallization ceased but while temperatures remained high. This pattern of a relatively short residence time at depth is consistent with evidence of rapid isobaric cooling during the interval 114–111 Ma (Flowers et al., 2005).

Sheared samples of garnet granulite from Crooked Arm display evidence for dislocation creep and recrystallization through grain boundary migration and subgrain rotation. The presence of a LPO suggests that diffusion creep was not an important process either during or after the time that dislocation creep was active. In contrast, samples from within the Doubtful Sound shear zone display textural evidence of diffusion creep assisted by the presence of hydrous phases. The LPO within these deformed samples is weaker than in samples outside the shear zone. Diffusion creep

does not produce a LPO and it can weaken a preexisting LPO. Biotite and hornblende grains form cusped intergrowths, with plagioclase parallel to the shear zone foliation. These patterns of the weak phases within a deformed sample are indicative of the activity of diffusion-creep-accommodated grain-boundary sliding (Gower and Simpson, 1992; Kruse and Stunitz, 1999). This evidence strongly suggests that fluids played an important role in controlling deformation mechanisms within the amphibolite-facies Doubtful Sound shear zone exposures. The activity of diffusion creep also may have been facilitated by the smaller grain size that resulted from recrystallization through dislocation creep. These features indicate that changes in temperature and fluid conditions occurred over a short (3–4 Ma) period of time after extension initiated. During the period 114–111 Ma, temperatures dropped from $>800^\circ\text{C}$ to 650–550 $^\circ\text{C}$ and the availability and importance of water in deformation became greater. The increased availability of water after ca. 111 Ma appears to have promoted a localization of strain into narrow ($<1\text{ km}$) zones during extension.

Strain Patterns and Estimates of Kinematic Vorticity

Klepeis et al. (2007) used measurements of shear zone boundaries, stretching lineations, different types of shear indicators, and the X-direction of finite strain ellipsoids to identify the VNS for both granulite-facies (L_{GG} - S_{GG}) and upper-amphibolite-facies (L_{SZ} - S_{SZ}) fabrics. Foliation and mineral stretching lineations in these superposed fabrics are nearly parallel and the VNS in both cases is approximately vertical (Figs. 9D and 9E). The bulk shear direction parallels the intersection between the shear zone boundary and the VNS. The parallelism among this bulk shear direction, mineral lineations and X-directions of 3-D finite strain calculations reported by Klepeis et al. (2007) indicate compatibility among the observations. In general, their data suggest that although both oblate and prolate strain ellipsoid shapes are represented, the bulk deformation involved mostly flattening strains.

Sense-of-shear indicators in the Doubtful Sound shear zone are best preserved in zones of upper-amphibolite-facies mylonite. In these areas, asymmetric tails of amphibole and quartz around plagioclase grains, hornblende and biotite fish (Fig. 10C), S-C fabric, and asymmetric tails around rotated garnet porphyroblasts yield top-down-to-the-northeast and –southwest senses of shear. Asymmetries associated with these kinematic indicators are best developed on surfaces oriented perpendicular to foliation and parallel to northeast-plunging stretching lineations. Rotated porphyroblast systems show σ -type, δ -type, and β -type tails that can be used to quantify the ductile flow field in the shear zone (Fig. 9F). Klepeis et al. (2007) obtained estimates of sectional kinematic vorticity (W_m) for the vertical plane by applying the porphyroblast hyperbolic distribution method of Simpson and DePaor (1993, 1997) in four sites within Crooked Arm. At each site over 30 clasts were measured at multiple length scales (thin section to a 10–20 m^2 outcrop) to obtain spatially averaged estimates of kinematic vorticity. For each shear zone the range of

clast sizes (vertical scale of semicircular plot in Fig. 9G) and orientations (perimeter of plot in Fig. 9G) were exceptional and allowed us to accurately determine the field of back rotation, which is defined by clasts that rotated in a direction opposite to the non-coaxial component of the bulk flow. One of the flow apophyses (A_1) in each case approximately paralleled the shear zone boundary, although this relationship is not required. Values of W_m were determined from the angular width (α) of the field of back rotation (shaded part of Fig. 9G). Two flow apophyses representing stable orientations of the clasts (A_1 , A_2) form the boundaries of this field of back rotation. The results ($0.71 < W_m < 0.74$) are similar among the sites and have been combined onto a single hyperbolic plot shown in Figure 9G. They indicate that the deformation involved approximately equal components of pure and simple shear and was characterized by vertical thinning and sub-horizontal stretching (Fig. 9F), irrespective of rock type and scale of observation. This result is consistent with the evidence of the flattening strains reported by Klepeis et al. (2007) at the scale of the middle and lower crust.

DISCUSSION

The Origin of Heterogeneity in the Middle and Lower Crust

Our analysis of superposed shear zones in Northern Fiordland indicates that most of the kinematic parameters used to describe ductile flow in the middle and lower crust changed repeatedly during a short 8–10 Ma time interval in the Cretaceous. Shear zone boundaries alternated between gently dipping (layer-parallel) and sub-vertical (layer-perpendicular) (Fig. 11A). The degree of non-coaxiality, kinematic partitioning and strain symmetry also were highly variable. Some of the spatial variability and transience of the deformations appears to reflect changes in the location and geometry of strength contrasts as the temperature, structure, and composition of the lower crust changed. For example, the cooling and crystallization of the Western Fiordland Orthogneiss batholith at ca. 120 Ma was accompanied by a change in the style of deformation in the lower crust. Deformation that was focused along the contacts of the batholith during intrusion affected a much broader part of the lower crust after the batholith and lower crust cooled. Microstructures from the Doubtful Sound region indicate that the presence of magma and/or partial melt, temperature and fluid availability strongly influenced patterns of strain partitioning and the mechanisms that accommodated ductile flow. During the period 114–111 Ma, as extensional deformation became dominant, temperatures dropped from >800 °C to 650–550 °C and the availability and importance of water in deformation became greater. The increased availability of water appears to have controlled the localization of strain into narrow (<1 km) zones during extension. These changes strongly suggest that flow in the lower crust was intrinsically unsteady and non-uniform and strongly influenced by local boundary conditions. The variability in kinematic

patterns also indicates that shear zone orientation and sense of shear alone are not diagnostic of tectonic regime.

Despite this high degree of variability, the data also show that some patterns remained constant through time. All of the lower-crustal deformations in Northern Fiordland record bulk horizontal (layer-parallel) shortening and vertical (layer-perpendicular) thickening (Fig. 11A). This result is independent of both the scale of observation and the orientation of the shear zone boundaries. In addition, all deformations involved between 50% and 90% pure shear (see Tikoff and Fossen, 1995, and Bailey et al., 2007 for discussion of general shear), in a manner consistent with a regime of lithospheric thickening and contraction. These results contrast with the deformations in Central Fiordland, which record flow involving vertical thinning, subhorizontal stretching and 40%–50% pure shear (Fig. 11B). The patterns suggest that transient, non-uniform flow histories can be assessed by comparing data from successive and sufficiently small time intervals and mesoscale observations following the approach we have outlined in this chapter.

The results of our analyses also demonstrate when and how patterns of lower-crustal flow changed during the transition from crustal thickening to crustal extension at about ca. 114 (and before ca. 111 Ma). During this transitional period, shear zones in northern Fiordland were characterized by diffuse, vertically thickening zones recording between 50% and 90% pure shear deformation. In contrast, lower-crustal shear zones that formed in Central Fiordland record focused, vertically thinning, horizontally stretching flows with approximately equal components of pure and simple shear. These patterns correspond to the stages of regional contraction and regional extension, respectively. Within the limits of precision in available ages, the timing of this transition appears diachronous. Our analysis of kinematic patterns in the lower crust combined with previously published geochronology indicate that the shift to extension in the Doubtful Sound region occurred by ca. 114 Ma, significantly earlier than implied by previous studies (ca. 108 Ma according to Gibson et al., 1988). In Northern Fiordland, the timing of the shift from regional contraction to regional extension is uncertain because no major extensional shear zones occur in this area. The limits of uncertainty on age determinations obtained from syn-tectonic dikes in the Indecision Creek shear zone indicate that contraction in the Milford region occurred during the interval 119–111 Ma (Marcotte et al., 2005).

Length and Time Scales of Changing Flow Patterns during the Transition from Contraction to Extension

A comparison of metamorphic and geochronologic data from the northern and central parts of Fiordland indicate that the lower crust of this orogen was characterized by extremely heterogeneous and transient thermal structures on length scales of less than 100 km. U-Pb geochronology indicates that the lower crustal section at Milford Sound cooled from >800 °C at ca. 120 Ma to ≈ 650 °C by ca. 116 Ma (Klepeis et al., 2004), while remaining at

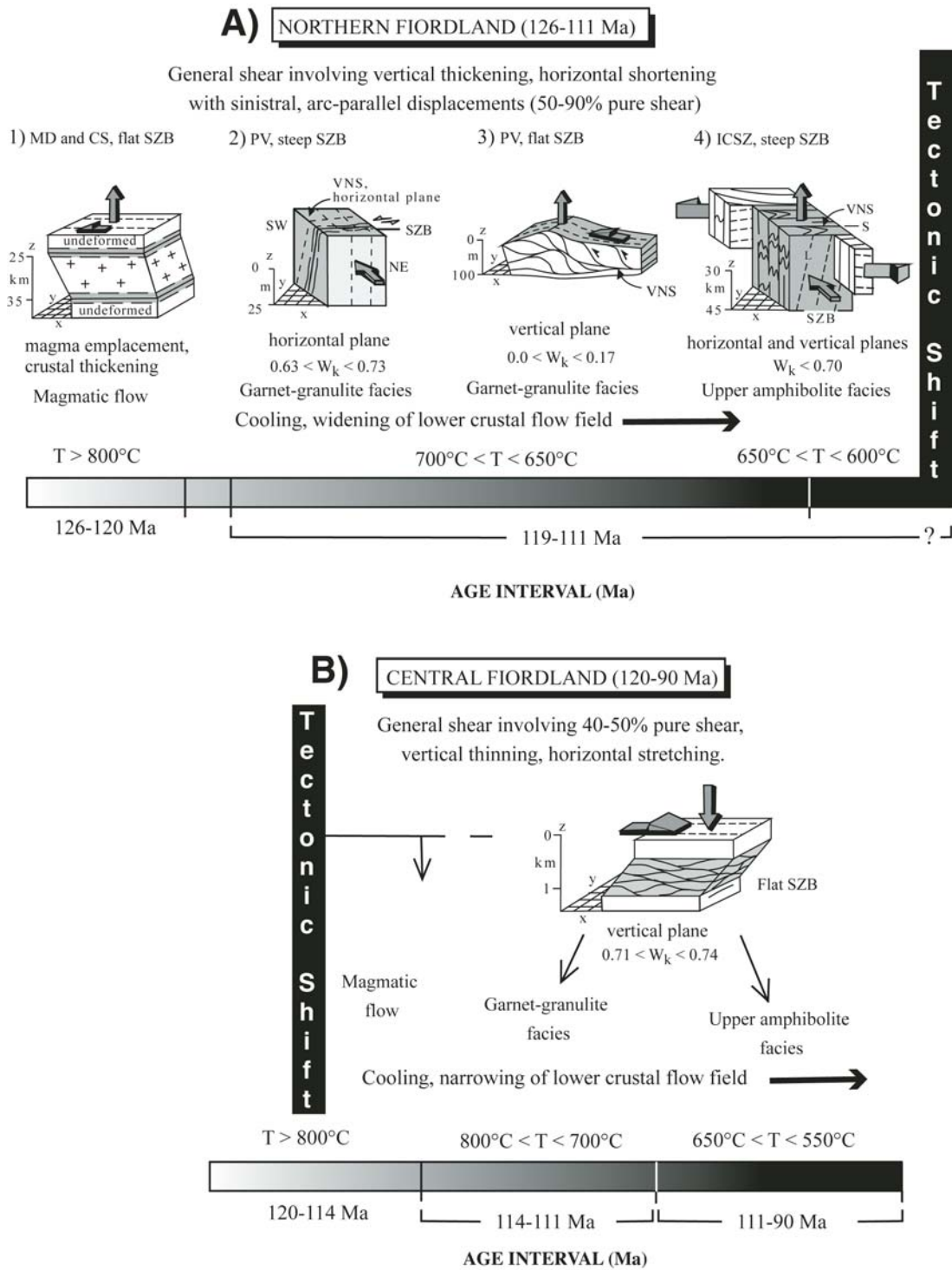


Figure 11. Diagram showing the diachronous evolution of lower-crustal structures in Northern (A) and Central (B) Fiordland. Upper diagram shows the evolution of contractional fabrics in Northern Fiordland from magmatic flow to high-temperature deformation at the garnet-granulite facies to cooler deformation at the upper-amphibolite facies. This section records contractional deformation and magmatism in the lower crust until at least ca. 111 Ma. (B) Evolution of extensional fabrics in Central Fiordland from magmatic flow to high-temperature deformation at the garnet-granulite facies to cooler deformation at the upper-amphibolite facies. This section records the initiation of extension at ca. 114 Ma. The block labeled 'Tectonic Shift' represents the time the tectonic regime changed from regional contraction to regional extension. This age is taken to be ca. 114 Ma but uncertainties in published ages indicate the shift could have occurred anytime during the interval 114–111 Ma. Abbreviations are as follows: CS—Caswell Sound; ICSZ—Indecision Creek shear zone; MD—Mount Daniel; PV—Pembroke Valley; SZB—shear zone boundary; VNS—vorticity normal section (for location see Fig. 2). See text for discussion.

high pressures (12–14 kb). Less than 100 km south of Milford Sound, however, U-Pb geochronology indicates that peak conditions involving temperatures of >800 °C persisted at Doubtful Sound until ca. 114 Ma (Table 1; Klepeis et al., 2007). The length and time scales of this variability imply that any single locality provides a part of the history of the lower crust that may not be representative of the whole section. It also suggests that elements of both of the hypotheses outlined earlier may explain how and why extension initiated following a period of crustal thickening.

In contrast to the first hypothesis, the geologic history of the Milford Sound region indicates that weakening of lower-crustal rocks by heating, magmatism and partial melting does not always promote horizontal flow that leads to crustal thinning and lithospheric extension. In this region, the peak of granulite-facies metamorphism in the lower crust at ca. 120 Ma was accompanied by magmatism and partial melting but did not develop thinning flows nor major extensional shear zones. Instead the data clearly show that, in this area, these events were accompanied by contractional deformation. However, the history of deformation in Central Fiordland partially supports the first hypothesis. This latter region record the development of major extensional shear zones that, at least initially, localized into areas of the lower crust that were weakened by magma and heat at ca. 114 Ma. These relationships indicate that a prerequisite for localizing extension in the lower crust is crustal weakening but that the overall style of the flow is controlled by the tectonic regime.

Elements of the second hypothesis, where a strong lower crust and a weak lower crust controlled extension, also appear to apply to Fiordland. Although extensional deformation in Central Fiordland was localized into areas that were weakened by magma and heat, this situation was transient. These hot, weak zones had declined and the lower crust had cooled through 650–550 °C by 113.5–111 Ma (Flowers et al., 2005). After ca. 111 Ma, extension was localized into the middle crust where quartz- and mica-dominated lithologies appear to have localized deformation (Klepeis et al., 2007). This result may explain why Northern Fiordland, which preserves the lower but not the middle crust, lacks evidence of extension; extension preferentially was partitioned into a weak middle crust after ca. 111 Ma. This process, whereby the transient nature of magma-induced hot spots in the deep crust controls strain partitioning, may help explain diachronous patterns of deformation and along-strike variability in arc structure, including the development of highly localized zones of extension and contraction.

CONCLUSIONS

Kinematic analyses conducted on superposed shear zones at multiple scales in Fiordland reveal extremely heterogeneous patterns of ductile flow and strain partitioning in the middle and lower crust. In Northern Fiordland, most of the parameters used to describe ductile deformation in shear zones were highly variable as both local conditions and plate motions changed. Over an ca. 8 Ma period (119–111 Ma), kinematic patterns were strongly

influenced by local variations in crustal structure, magmatic activity, composition, temperature, and rheology. In Central Fiordland, microstructures indicate that the grain-scale mechanisms that accommodated ductile flow also changed rapidly over a short 3–4 Ma interval as crustal compositions and fluid availability changed. The results imply that over periods of several million years flow in the lower crust of orogens is characterized by non-uniform, non-steady flow fields that reflect changing local boundary conditions.

The results also indicate that some kinematic parameters in lower-crustal shear zones were sensitive to changes in far-field plate boundary dynamics. All shear zones that formed during the 119–111 Ma period in Northern Fiordland record horizontal (layer-parallel) shortening and vertical (layer-perpendicular) thickening with 50%–90% pure shear. In contrast, all shear zones that formed during the 114–90 Ma period in Central Fiordland record vertical thinning and sub-horizontal stretching, with approximately equal amounts of pure shear and simple shear. These patterns are correlative with regional contraction and regional extension, respectively, and suggest that the transition to extension may have been diachronous over length scales of less than 100 km within the limits of precision in available ages. They also indicate that the orientations of shear zones and sense-of-shear indicators alone cannot be used to uniquely define different tectonic regimes in the middle and lower crust. A careful choice of length and time scales is important for interpreting the significance of deformation patterns in ancient orogenic belts where plate boundary conditions may be poorly defined. In New Zealand, these scales are ~100 km and ca. 10 Ma, respectively.

Areas of discord between published models of extension and observations in Fiordland center on the length and time scales of hot, weak zones in the lower crust and how such zones influenced the development of extensional structures. Metamorphic and geochronologic data collected from near Milford Sound suggest that part of the lower crust experienced rapid cooling from temperatures of between 850 °C and 750 °C to 700–650 °C by ca. 116 Ma following a period of mafic-intermediate magmatism and lower-crustal melting at ca. 120 Ma. This episode of lower-crustal cooling predated the tectonic shift from contraction to extension. However, less than 100 km to the south of Milford Sound, in Doubtful Sound, U-Pb zircon ages and metamorphic data suggest that magmatic activity there occurred later and that lower-crustal temperatures remained high (>800 °C) until ca. 114 Ma. At this latter locality, the lower crust was still hot when the shift to extension occurred. These observations indicate that the thermal structure and rheological transitions linked to magmatism and the partial melting of lower crust were spatially very heterogeneous and transient. Localized hot spots in the lower crust created by heterogeneous patterns of magmatic activity affected deformation patterns during cycles of extension and contraction within the arc. When the regional tectonic regime shifted at ca. 114 Ma, large (1-km-thick) extensional shear zones preferentially developed in hot, weak zones that thinned the lower crust. In contrast, areas of the lower crust that were relatively cool

at the time of the shift did not develop extensional structures and preserve older contractional shear zones. This example illustrates how the development of localized hot spots due to magmatism and metamorphism in the lower crust strongly influences deformation partitioning within arc crust.

ACKNOWLEDGMENTS

We thank the following people for valuable discussions and contributions in the field and laboratory: G. Clarke, G. Gehrels, N. Daczko, A. Tulloch, I. Turnbull, N. Mortimer, W.C. Simonson, S. Marcotte, A. Claypool, A. Goldstein, J. Fitzherbert, J. Hollis, and M. De Paoli. This work was supported by grants from the National Science Foundation (EAR-0087323 and EAR-0337111), the Geological Society of America (GSA Research grant to D.S. King), and the American Association of Petroleum Geologists (AAPG grant to D.S. King). We thank Richard Norris and Chuck Bailey for providing thorough reviews and many thoughtful comments on the original manuscript.

REFERENCES CITED

- Allibone, A.H., and Tulloch, A.J., 1997, Metasedimentary, granitoid and gabbroic rocks from central Stewart Island, New Zealand: *New Zealand Journal of Geology and Geophysics*, v. 40, p. 53–68.
- Antignano, A., IV, 2002, Experimental constraints on granitoid compositions in convergent regimes: A geochemical study [M.S. thesis]: Burlington, University of Vermont, 135 p.
- Bailey, C.M., and Eyster, E.L., 2003, General shear deformation in the Pinaleno Mountain metamorphic core complex, Arizona: *Journal of Structural Geology*, v. 25, p. 1883–1892, doi: 10.1016/S0191-8141(03)00044-0.
- Bailey, C.M., Polvi, L.E., and Forte, A.M., 2007, Pure shear dominated high-strain zones in basement terranes, in Hatcher, R.D., Jr., Carlson, M.P., McBride, J.H., and Martínez Catalán, J.R., eds., *The four-dimensional framework of continental crust*: Geological Society of America Memoir 200, p. 93–108.
- Beaumont, C., Jamieson, R.A., Nguyen, M.H., and Lee, B., 2001, Himalayan tectonics explained by extrusion of a low-viscosity crustal channel coupled to focused surface denudation: *Nature*, v. 414, p. 738–742, doi: 10.1038/414738a.
- Bradshaw, J.D., 1989, Cretaceous geotectonic patterns in the New Zealand region: *Tectonics*, v. 8, p. 803–820, doi: 10.1029/TC008i004p00803.
- Bradshaw, J.Y., 1985, Geology of the northern Franklin Mountains, northern Fiordland, New Zealand, with emphasis on the origin and evolution of Fiordland granulites [Ph.D. thesis]: Dunedin, University of Otago, 350 p.
- Bradshaw, J.Y., 1989a, Origin and metamorphic history of an Early Cretaceous polybaric granulite terrain, Fiordland, southwest New Zealand: *Contributions to Mineralogy and Petrology*, v. 103, p. 346–360, doi: 10.1007/BF00402921.
- Bradshaw, J.Y., 1989b, Early Cretaceous vein-related garnet granulite in Fiordland, Southwest New Zealand; A case for infiltration of mantle-derived CO₂-rich fluids: *The Journal of Geology*, v. 97, p. 697–717.
- Buck, W.R., 1991, Modes of continental lithospheric extension: *Journal of Geophysical Research*, v. 96, p. 20,161–20,178, doi: 10.1029/91JB01485.
- Clark, M.K., and Royden, L.H., 2000, Topographic ooze: building the eastern margin of Tibet by lower crustal flow: *Geology*, v. 28, p. 703–706, doi: 10.1130/0091-7613(2000)28<703:TOBTEM>2.0.CO;2.
- Clarke, G.L., Klepeis, K.A., and Daczko, N.R., 2000, Cretaceous high-P granulites at Milford Sound, New Zealand: Metamorphic history and emplacement in a convergent margin setting: *Journal of Metamorphic Geology*, v. 18, p. 359–374, doi: 10.1046/j.1525-1314.2000.00259.x.
- Czeck, D.M., and Hudleston, P.J., 2003, Testing models for obliquely plunging lineations in transpression: A natural example and theoretical discussion: *Journal of Structural Geology*, v. 25, p. 959–982, doi: 10.1016/S0191-8141(02)00079-2.
- Daczko, N.R., Klepeis, K.A., and Clarke, G.L., 2001a, Evidence of Early Cretaceous collisional-style orogenesis in northern Fiordland, New Zealand, and its effects on the evolution of the lower crust: *Journal of Structural Geology*, v. 23, p. 693–713, doi: 10.1016/S0191-8141(00)00130-9.
- Daczko, N.R., Clarke, G.L., and Klepeis, K.A., 2001b, Transformation of two-pyroxene hornblende granulite to garnet granulite involving simultaneous melting and fracturing of the lower crust, Fiordland, New Zealand: *Journal of Metamorphic Geology*, v. 19, p. 549–560, doi: 10.1046/j.0263-4929.2001.00328.x.
- Daczko, N.R., Klepeis, K.A., and Clarke, G.L., 2002a, Thermomechanical evolution of the crust during convergence and deep crustal pluton emplacement in the Western Province of Fiordland, New Zealand: *Tectonics*, v. 21, p. 1–18, 1022, doi: 10.1029/2001TC001282.
- Daczko, N.R., Stevenson, J.A., Clarke, G.L., and Klepeis, K.A., 2002b, Successive hydration and dehydration of high-P mafic granulites involving clinopyroxene-kyanite symplectites, Mt. Daniel, Fiordland, New Zealand: *Journal of Metamorphic Geology*, v. 20, p. 669–682, doi: 10.1046/j.1525-1314.2002.00397.x.
- Daczko, N.R., Clarke, G.L., and Klepeis, K.A., 2002c, Kyanite-paragonite-bearing assemblages, northern Fiordland, New Zealand: Rapid cooling of the lower crustal root to a Cretaceous magmatic arc: *Journal of Metamorphic Geology*, v. 20, p. 887–902, doi: 10.1046/j.1525-1314.2002.00421.x.
- Ellis, S., Beaumont, C., Jamieson, R.A., and Quinlan, G., 1998, Continental collision including a weak zone: The vise model and its application to the Newfoundland Appalachians: *Canadian Journal of Earth Sciences*, v. 35, p. 1323–1346, doi: 10.1139/cjes-35-11-1323.
- Flowers, R.M., Bowring, S.A., Tulloch, A.J., and Klepeis, K.A., 2005, Tempo of burial and exhumation within the deep roots of a magmatic arc, Fiordland, New Zealand: *Geology*, v. 33, p. 17–20, doi: 10.1130/G21010.1.
- Gaina, C., Muller, D.R., Royer, J.Y., Stock, J., Hardebeck, J., and Symonds, P., 1998, The tectonic history of the Tasman Sea: A puzzle with 13 pieces: *Journal of Geophysical Research*, v. 103, p. 12,413–12,433, doi: 10.1029/98JB00386.
- Gibson, G.M., and Ireland, T.R., 1995, Granulite formation during continental extension in Fiordland: *Nature*, v. 375, p. 479–482, doi: 10.1038/375479a0.
- Gibson, G.M., and Ireland, T.R., 1998, SHRIMP monazite and zircon geochronology of high-grade metamorphism in New Zealand: *Journal of Metamorphic Geology*, v. 16, p. 149–167.
- Gibson, G.M., McDougall, I., and Ireland, T.R., 1988, Age constraints on metamorphism and the development of a metamorphic core complex in Fiordland, southern New Zealand: *Geology*, v. 16, p. 405–408, doi: 10.1130/0091-7613(1988)016<0405:ACOMAT>2.3.CO;2.
- Giorgis, S., Markley, M., and Tikoff, B., 2004, Vertical-axis rotation of rigid crustal blocks driven by mantle flow, in Grocott, J., McCaffrey, K.J.W., Taylor, G., and Tikoff, B., eds., *Vertical coupling and decoupling in the lithosphere*: Geological Society of London Special Publication 227, p. 83–100.
- Gower, R.J.W., and Simpson, C., 1992, Phase boundary mobility in naturally deformed, high-grade quartzofeldspathic rocks: Evidence for diffusion creep: *Journal of Structural Geology*, v. 14, p. 301–313, doi: 10.1016/0191-8141(92)90088-E.
- Hacker, B.R., and Christie, J.M., 1990, Brittle/ductile and plastic/cataclastic transitions in experimentally deformed and metamorphosed amphibolite, in Dube, A.G., Durham, W.B., Handin, J.W., and Wang, H.F., eds., *The brittle-ductile transition in rocks*: Washington, D.C., American Geophysical Union, Geophysical Monograph Series, v. 56, p. 127–147.
- Hollis, J.A., Clarke, G.L., Klepeis, K.A., Daczko, N.R., and Ireland, T.R., 2003, Geochronology and geochemistry of high-pressure granulites of the Arthur River Complex, Fiordland, New Zealand: Cretaceous magmatism and metamorphism on the Palaeo-Pacific margin: *Journal of Metamorphic Geology*, v. 21, p. 299–313.
- Hollis, J.A., Clarke, G.L., Klepeis, K.A., Daczko, N.R., and Ireland, T.R., 2004, The regional significance of Cretaceous magmatism and metamorphism in Fiordland, New Zealand, from U–Pb zircon geochronology: *Journal of Metamorphic Geology*, v. 22, p. 607–627, doi: 10.1111/j.1525-1314.2004.00537.x.
- Jackson, H.R., 2002, Seismic refraction profiles in the Gulf of Saint Lawrence and implications for extent of continuous Grenville lower crust: *Canadian Journal of Earth Sciences*, v. 39, p. 1–17, doi: 10.1139/e01-054.

- Jackson, J., 2002, Strength of the continental lithosphere; time to abandon the jelly sandwich?: *GSA Today*, v. 12, no. 9, p. 4–10, doi: 10.1130/1052-5173(2002)012<0004:SOTCLT>2.0.CO;2.
- Ji, S., and Mainprice, D., 1990, Recrystallization and fabric development in plagioclase: *The Journal of Geology*, v. 98, p. 65–79.
- Jiang, D., and Williams, P.F., 1998, High-strain zones; a unified model: *Journal of Structural Geology*, v. 20, p. 1105–1120, doi: 10.1016/S0191-8141(98)00025-X.
- Jiang, D., Lin, S., and Williams, P.F., 2001, Deformation path in high-strain zones, with reference to slip partitioning in transpressional plate-boundary regions: *Journal of Structural Geology*, v. 23, p. 991–1005, doi: 10.1016/S0191-8141(00)00170-X.
- Jones, R.R., Holdsworth, R.E., Clegg, P., McCaffrey, K., and Tavarnelli, E., 2004, Inclined transpression: *Journal of Structural Geology*, v. 26, p. 1531–1548, doi: 10.1016/j.jsg.2004.01.004.
- Karlstrom, K.E., and Williams, M.L., 2006, Nature and evolution of the middle crust: Heterogeneity of structure and process due to pluton-enhanced tectonism, *in* Brown, M., and Rushmer, T., eds., *Evolution and differentiation of the continental crust*: Cambridge, UK, Cambridge University Press, p. 268–295.
- King, D.S., Klepeis, K.A., Goldstein, A., Gehrels, G., and Clarke, G.L., 2008, The initiation and evolution of the transpressional Straight River Shear Zone, central Fiordland, New Zealand: *Journal of Structural Geology*, v. 30, p. 410–430, doi: 10.1016/j.jsg.2007.12.004.
- Klepeis, K.A., and Clarke, G.L., 2004, Evolution of an exposed lower crustal attachment zone in Fiordland, New Zealand, *in* Grocott, J., McCaffrey, K.J.W., Taylor, G., and Tikoff, B., eds., *Vertical coupling and decoupling in the lithosphere*: Geological Society of London Special Publication 227, p. 197–229.
- Klepeis, K.A., Daczko, N.R., and Clarke, G.L., 1999, Kinematic vorticity and tectonic significance of superposed mylonites in a major lower crustal shear zone, northern Fiordland, New Zealand: *Journal of Structural Geology*, v. 21, p. 1385–1405, doi: 10.1016/S0191-8141(99)00091-7.
- Klepeis, K.A., Clarke, G.L., and Rushmer, T., 2003, Magma transport and coupling between deformation and magmatism in the continental lithosphere: *GSA Today*, v. 13, no. 1, p. 4–11, doi: 10.1130/1052-5173(2003)013<0004:MTACBD>2.0.CO;2.
- Klepeis, K.A., Clarke, G.L., Gehrels, G., and Vervoort, J., 2004, Processes controlling vertical coupling and decoupling between the upper and lower crust of orogens: Results from Fiordland, New Zealand: *Journal of Structural Geology*, v. 26, p. 765–791, doi: 10.1016/j.jsg.2003.08.012.
- Klepeis, K.A., King, D.S., De Paoli, M., Clarke, G.L., and Gehrels, G., 2007, Interaction of strong lower and weak middle crust during lithospheric extension in western New Zealand: *Tectonics*, v. 26, p. TC4017, doi: 10.1029/2006TC002003.
- Kruse, R., and Stunitz, H., 1999, Deformation mechanisms and phase distribution in mafic high-temperature mylonites from the Jotun Nappe, southern Norway: *Tectonophysics*, v. 303, p. 223–249, doi: 10.1016/S0040-1951(98)00255-8.
- Kula, J.L., Tulloch, A.J., Spell, T.L., and Wells, M.L., 2005, Timing of continental extension leading to separation of eastern New Zealand from West Antarctica; $^{40}\text{Ar}/^{39}\text{Ar}$ thermochronometry from Stewart Island, NZ: *Geological Society of America Abstracts with Programs*, v. 37, no. 7, p. 73.
- Law, R.D., Searle, M.P., and Simpson, R.L., 2004, Strain, deformation temperatures and vorticity of flow at the top of the Greater Himalayan Slab, Everest Massif, Tibet: *Journal of the Geological Society*, v. 161, p. 305–320, doi: 10.1144/0016-764903-047.
- Lin, S., Jiang, D., and William, P.F., 1998, Transpression (or transtension) zones of triclinic symmetry: Natural example and theoretical modelling, *in* Holdsworth, R.E., Strachan, R.A., and Dewey, J.F., eds., *Continental transpressional and transtensional tectonics*: Geological Society of London Special Publication 135, p. 41–57.
- Lister, G.S., and Williams, P.F., 1983, The partitioning of deformation in flowing rock masses: *Tectonophysics*, v. 49, p. 37–78.
- Marcotte, S.B., Klepeis, K.A., Clarke, G.L., Gehrels, G., and Hollis, J.A., 2005, Intra-arc transpression in the lower crust and its relationship to magmatism in a Mesozoic magmatic arc: *Tectonophysics*, v. 407, p. 135–163, doi: 10.1016/j.tecto.2005.07.007.
- McBride, J.H., and Knapp, J.H., 2002, Review of seismic reflector signatures of crustal deformation in the Appalachian-Caledonide orogen with reference to the Spanish Variscides and the Uralides, *in* Martínez Catalán, J.R., Hatcher, R.D., Jr., Arenas, R., and Díaz García, F., eds., *Variscan-Appalachian dynamics: The building of the Late Paleozoic basement*: Geological Society of America Special Paper 364, p. 281–300.
- McKenzie, D., Nimmo, F., and Jackson, J.A., 2000, Characteristics and consequences of flow in the lower crust: *Journal of Geophysical Research*, v. 105, p. 11,029–11,046, doi: 10.1029/1999JB900446.
- Miller, R.B., and Paterson, S.R., 2001, Influence of lithological heterogeneity, mechanical anisotropy, and magmatism on the rheology of an arc, North Cascades, Washington: *Tectonophysics*, v. 342, p. 351–370, doi: 10.1016/S0040-1951(01)00170-6.
- Mortimer, N., Tulloch, A.J., Spark, R., Walker, N., Ladley, E., Kimbrough, D.L., and Allibone, A.H., 1999, Overview of the Median batholith, New Zealand: A new interpretation of the geology of the Median Tectonic Zone and adjacent rocks: *Journal of African Earth Sciences*, v. 29, p. 257–268, doi: 10.1016/S0899-5362(99)00095-0.
- Nemes, R., Neubauer, F., Cloetingh, S., and Genser, J., 1997, The Klagenfurt Basin in the Eastern Alps: An intra-orogenic decoupled flexural basin?: *Tectonophysics*, v. 282, p. 189–203, doi: 10.1016/S0040-1951(97)00219-9.
- Oliver, G.J.H., 1977, Feldspathic hornblende and garnet granulites and associated anorthosite pegmatites from Doubtful Sound, Fiordland, New Zealand: *Contributions to Mineralogy and Petrology*, v. 65, p. 111–121, doi: 10.1007/BF00371051.
- Oliver, G.J.H., 1980, Geology of the granulite and amphibolite facies gneisses of Doubtful Sound, Fiordland, New Zealand: *New Zealand Journal of Geology and Geophysics*, v. 1, p. 27–41.
- Oliver, G.J.H., and Coggon, J.H., 1979, Crustal structure of Fiordland, New Zealand: *Tectonophysics*, v. 54, p. 253–292, doi: 10.1016/0040-1951(79)90371-8.
- Olsen, S.V., and Kohlstedt, D.L., 1985, Natural deformation and recrystallization of some intermediate plagioclase feldspars: *Tectonophysics*, v. 111, p. 107–131, doi: 10.1016/0040-1951(85)90067-8.
- Passchier, C.W., 1987, Stable positions of rigid objects in non-coaxial flow—A study in vorticity analysis: *Journal of Structural Geology*, v. 9, p. 679–690, doi: 10.1016/0191-8141(87)90152-0.
- Passchier, C.W., and Urai, J.L., 1988, Vorticity and strain analysis using Mohr diagrams: *Journal of Structural Geology*, v. 10, p. 755–763, doi: 10.1016/0191-8141(88)90082-X.
- Pryer, L.L., 1993, Microstructures in feldspars from a major crustal thrust zone: The Grenville Front, Ontario, Canada: *Journal of Structural Geology*, v. 15, p. 21–36, doi: 10.1016/0191-8141(93)90076-M.
- Royden, L., 1996, Coupling and decoupling of crust and mantle in convergent orogens: Implications for strain partitioning in the crust: *Journal of Geophysical Research*, v. 101, p. 17,679–17,705, doi: 10.1029/96JB00951.
- Rusmore, M.E., Woodsworth, G.J., and Gehrels, G.E., 2005, Two-stage exhumation of midcrustal arc rocks, Coast Mountains, British Columbia: *Tectonics*, v. 24, p. TC5013, doi: 10.1029/2004TC001750.
- Scott, J.M., and Cooper, A.F., 2006, Early Cretaceous extensional exhumation of the lower crust of a magmatic arc: Evidence from the Mount Irene shear zone, Fiordland, New Zealand: *Tectonics*, v. 25, p. TC3018, doi: 10.1029/2005TC001890.
- Simpson, C., and De Paor, D.G., 1993, Strain and kinematic analysis in general shear zones: *Journal of Structural Geology*, v. 15, p. 1–20, doi: 10.1016/0191-8141(93)90075-L.
- Simpson, C., and De Paor, D.G., 1997, Practical analysis of general shear zones using porphyroclast hyperbolic distribution method: An example from the Scandinavian Caledonides, *in* Sengupta, S., ed., *Evolution of geological structures in micro- to macro-scales*: London, Chapman and Hall, p. 169–184.
- Spell, T.L., McDougall, I., and Tulloch, A.J., 2000, Thermochronologic constraints on the breakup of the Pacific Gondwana margin; the Paparoa metamorphic core complex, South Island, New Zealand: *Tectonics*, v. 19, p. 433–451, doi: 10.1029/1999TC900046.
- Teyssier, C., and Tikoff, B., 1999, Fabric stability in oblique convergence and divergence: *Journal of Structural Geology*, v. 21, p. 969–974, doi: 10.1016/S0191-8141(99)00067-X.
- Tikoff, B., and Fossen, H., 1995, The limitations of three-dimensional kinematic vorticity analysis: *Journal of Structural Geology*, v. 17, p. 1771–1784, doi: 10.1016/0191-8141(95)00069-P.
- Tullis, J., and Yund, R.A., 1985, Dynamic recrystallization of feldspar: A mechanism for ductile shear zone formation: *Geology*, v. 13, p. 238–241, doi: 10.1130/0091-7613(1985)13<238:DROFAM>2.0.CO;2.

- Tulloch, A.J., and Kimbrough, D.L., 1989, The Paparoa metamorphic core complex, New Zealand; Cretaceous extension associated with fragmentation of the Pacific margin of Gondwana: *Tectonics*, v. 8, p. 1217–1235, doi: 10.1029/TC008i006p01217.
- Tulloch, A.J., and Kimbrough, D.L., 2003, Paired plutonic belts in convergent margins and the development of high Sr/Y magmatism: The Peninsular Ranges batholith of California and the Median batholith of New Zealand, *in* Johnson, S.E., Paterson, S.R., Fletcher, J.M., Girty, G.H., Kimbrough, D.L., and Martín-Barajas, A., eds., *Tectonic evolution of northwestern Mexico and the southwestern USA: Geological Society of America Special Paper 374*, p. 275–295.
- Tulloch, A.J., Ireland, T.R., Walker, N.W., and Kimbrough, D.L., 2000, U-Pb zircon ages from the Milford Orthogneiss, Milford Sound, northern Fiordland: Paleozoic igneous emplacement and Early Cretaceous metamorphism: Institute of Geological and Nuclear Sciences Report, 2000/6, 17 p.
- Turnbull, I., Allibone, A., Jongens, R., Fraser, H., and Tulloch, A., 2005, Progress on QMAP Fiordland: Geological Society of New Zealand 50th Annual Meeting, Kaikoura, New Zealand, 28 November–1 December.
- Waight, T.E., Weaver, S.D., and Muir, R.J., 1998, Mid-Cretaceous granitic magmatism during the transition from subduction to extension in southern New Zealand: A chemical and tectonic synthesis: *Lithos*, v. 45, p. 469–482, doi: 10.1016/S0024-4937(98)00045-0.
- Wallis, S.R., 1995, Vorticity analysis and recognition of ductile extension in the Sanbagawa belt, SW Japan: *Journal of Structural Geology*, v. 17, p. 1077–1093, doi: 10.1016/0191-8141(95)00005-X.
- Whitney, D.L., Teyssier, C., and Vanderhaeghe, O., 2004, Gneiss domes and crustal flow, *in* Whitney, D.L., Teyssier, C., and Siddoway, C.S., eds., *Gneiss domes in orogeny: Geological Society of America Special Paper 380*, p. 15–33.
- Wood, B.L., 1972, Metamorphosed ultramafites and associated formations near Milford Sound, New Zealand: *New Zealand Journal of Geology and Geophysics*, v. 15, p. 88–127.

MANUSCRIPT ACCEPTED BY THE SOCIETY 24 FEBRUARY 2009

A granulite-facies normal shear zone exposed in the Arunta inlier of central Australia: Implications for deep-crustal deformation during oblique divergence

Cheryl Waters-Tormey*

Department of Geosciences and Natural Resources, Western Carolina University, Cullowhee, North Carolina 28723, USA

Laurel B. Goodwin

Basil Tikoff

Kathy Staffier

Department of Geology and Geophysics, University of Wisconsin–Madison, Wisconsin 53706, USA

Paul Kelso

Department of Geology and Physics, Lake Superior State University, Sault Ste. Marie, Michigan 49783, USA

ABSTRACT

The Mount Hay block is a ~12-km-thick, deep continental crustal section exposed in the Arunta inlier in central Australia. The ~4-km-wide, granulite-facies (770–776 ± 38 °C) Capricorn ridge shear zone cross-cuts the dominant granulite-facies fabric of the Mount Hay block. In its present geometry, the Capricorn ridge shear zone contains a steeply south-southeast-dipping foliation, steeply east-southeast-plunging lineation, and south-side-up shear-sense indicators. When post-granulite-facies tilting is removed, the shear zone restores to a shallowly to moderately (30–50°) dipping, normal shear zone in which the lineation is oblique to the inferred Proterozoic plate boundary, suggesting oblique divergence. The field observations and reconstruction indicate that strain can be localized in the high-temperature, deep-crustal roots of extensional fault systems. This geometry of a discrete, moderately dipping, deep-crustal shear zone is consistent with simple-shear conceptual models of crustal extension.

INTRODUCTION

Although the upper-crustal geometry of extensional systems is relatively well understood, major questions remain concerning the geometry and kinematics of extensional deformation at greater depth. Several different conceptual models have been

proposed for crustal-scale deformation in this tectonic setting, which mainly differ in how the lower crust deforms (e.g., Lister et al., 1986). The pure-shear model (Fig. 1A) suggests that crustal thinning takes place in either a homogenous manner or within a complex of anastomosing shear zones. This geometry explains the lack of earthquakes on a single structure in the lower crust, which has been documented in some extending regions (e.g., Jackson and White, 1989). In contrast, Wernicke (1981, 1985) proposed

*cherylwt@wcu.edu

Waters-Tormey, C., Goodwin, L.B., Tikoff, B., Staffier, K., and Kelso, P., 2009, A granulite-facies normal shear zone exposed in the Arunta inlier of central Australia: Implications for deep-crustal deformation during oblique divergence, in Miller, R.B., and Snoke, A.W., eds., *Crustal Cross Sections from the Western North American Cordillera and Elsewhere: Implications for Tectonic and Petrologic Processes*: Geological Society of America Special Paper 456, p. 267–286, doi: 10.1130/2009.2456(10). For permission to copy, contact editing@geosociety.org. ©2009 The Geological Society of America. All rights reserved.

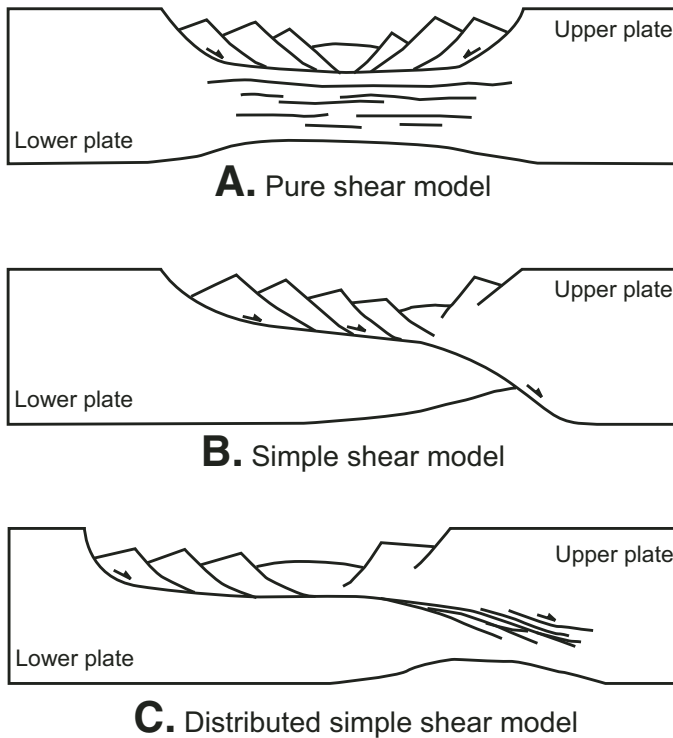


Figure 1. Conceptual models of crustal extension (after van der Pluijm and Marshak, 2004). (A) “Pure-shear” model, in which the ductile crust thins through either an array of anastomosing shear zones or by penetrative ductile deformation. (B) “Simple-shear” model where the basal detachment fault continues into the lower crust as a discrete shear zone. (C) Combination model where ductile shear is distributed over a significant portion of the deep crust.

that detachment faults extend into shear zones that steepen with depth and traverse the lithosphere. This geometry—described in the simple-shear model (Fig. 1B)—suggests a master fault/shear zone links crustal and mantle extensional zones. The last alternative, the distributed simple-shear model (Fig. 1C), is a composite of the two other models, and suggests that discrete surfaces in the upper crust extend into much more distributed features in the deeper crust. Thinning is distributed in the crust, and the shear system does not extend into the mantle. Reston (1990), interpreting seismic images of extended continental crust, suggests that the orientation of deep-crustal shear zones may not relate in a straightforward manner to the geometry of either upper-crustal or upper-mantle deformation. In other words, any of the above models may be appropriate for a given geometry of structures in the upper crust or upper mantle. The questions of geometry and degree of localization of deformation are especially important for depths below 25 km, where crustal strength is generally inferred to decrease substantially (e.g., Brace and Kohlstedt, 1980). This is particularly true where relatively high geothermal gradients, recorded by granulite-facies mineral assemblages, elevate the position of the brittle-ductile transition.

The main reason for the different models is the lack of direct evidence: extensional faults are rarely exhumed intact. Core

complexes can exhume the foot wall of a normal fault system, but place it in contact with brittlely deformed hanging-wall rocks (e.g., Coney, 1980; Wernicke, 1981; Davis, 1983). Although the original, mid-crustal orientation of the shear zone can commonly be determined (e.g., Livaccari et al., 1995; Axen, 2004), its geometric context is typically lost. Seismic data are useful, as sub-horizontal to gently dipping seismic reflections in extended regions have been interpreted as part of lower-crustal shear zones (e.g., Fountain et al., 1984; Carbonell and Smithson, 1991; Sachpazi et al., 1997), but seismic reflections do not provide information about kinematics of structures.

A direct approach to resolving these issues is to study exposures of extended lower crust, which provide constraints on the styles of deformation in the deep crust during extension. In this paper, we present results from a field study of a ~4-km-wide, granulite-facies, normal shear zone exposed in the lower continental crust of the Arunta inlier, central Australia. We describe fabrics formed in the Capricorn ridge shear zone during the Proterozoic Strangways tectonic event (ca. 1700 Ma), and its overprinting of adjacent granulite-facies structures in the Mount Hay block. By estimating the net rotation during later thrusting, and removing this rotation, the entire Mount Hay block is restored to its original orientation during shear zone movement. In this restored orientation, the Capricorn ridge shear zone dips 30 to 50°. We discuss the implications of this structure in the context of existing regional constraints in the North Australian craton.

GEOLOGIC SETTING

The Proterozoic Arunta inlier of central Australia has been divided into the east-trending northern, central, and southern provinces on the basis of distinct lithologic, metamorphic, and deformational histories (Shaw et al., 1984). Our work has focused on understanding the record of deep-crustal deformation preserved in the Mount Hay block, part of an ~160 × 50 km², ~east-west-trending belt of granulites and associated intrusive rocks exposed in the central Arunta province (e.g., Shaw et al., 1984; Zhao and Bennett, 1995; Fig. 2). Six tectonic events have been documented in the central Arunta province. Earlier events produced the granulite tectonites that are the focus of this research; younger events are responsible for their (largely pristine) exhumation. We include an abbreviated history below as context for our analysis of deep-crustal deformation and subsequent restoration of the Mount Hay block to its orientation prior to exhumation.

Granulites exposed in the central Arunta province originated as a variety of intrusive and supracrustal rocks; collectively, they record a long history of tectonism and associated magmatism along the active continental margin of the North Australian craton, including dominantly tholeiitic mafic magmatism at 1810–1800 Ma (Stafford event), 1790–1770 Ma (Yambah event), and 1740–1690 Ma (Strangways event) (e.g., Zhao and McCulloch, 1995; Collins et al., 1995; Clauoué-Long and Hoatson, 2005). The mafic intrusive protoliths to the majority of the granulites exposed in the Mount Hay block are interpreted to have formed

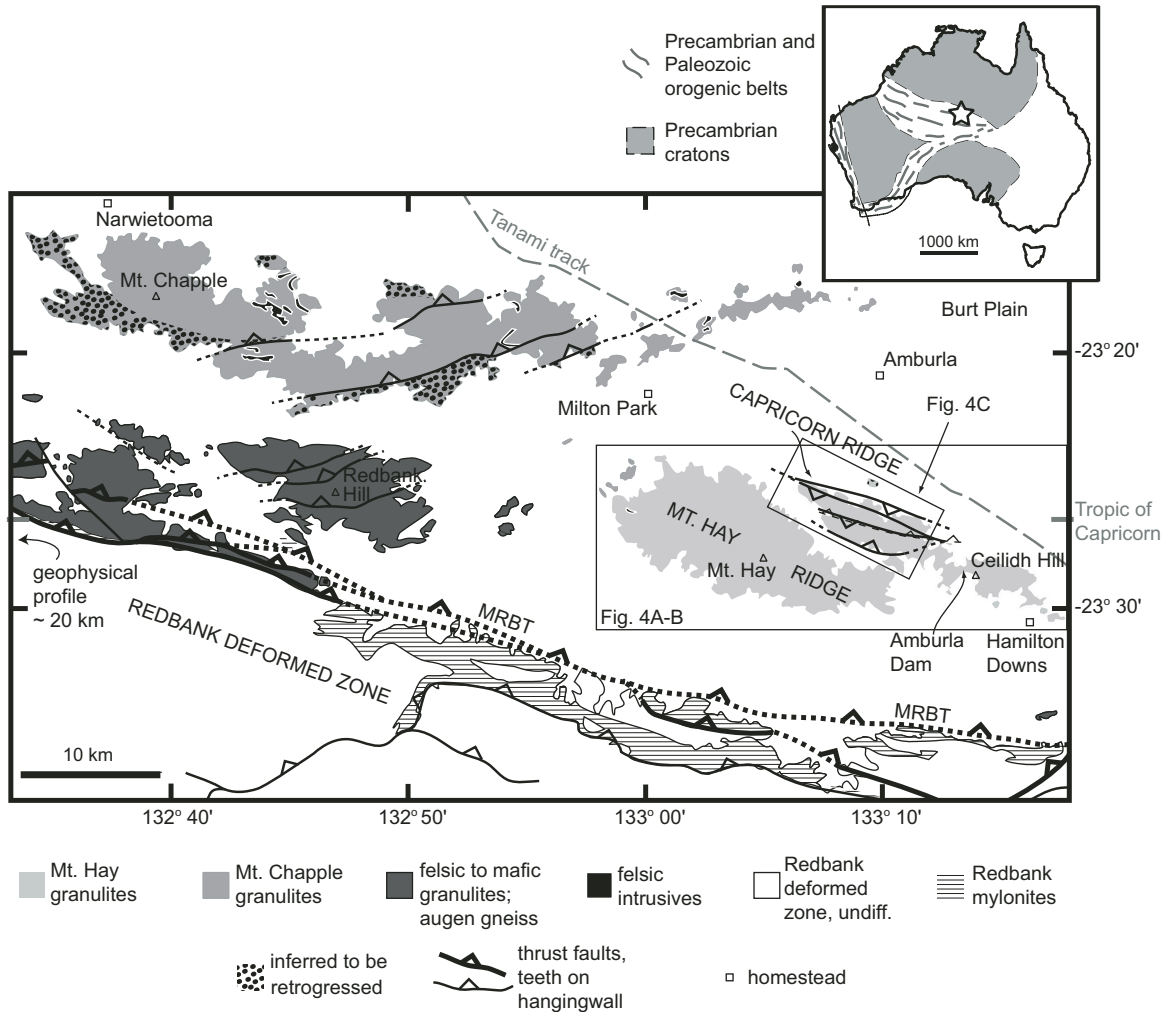


Figure 2. Inset shows location of study area within the Arunta inlier (star) at the southern margin of the North Australian craton (after Wellman, 1988; Myers et al., 1996; van der Hilst et al., 1998). Gray lines in inset indicate Precambrian orogenic belts, locally reactivated in the Paleozoic. Generalized geological map of the Mount Hay region shows the extent of granulite-facies complexes, and mylonites and inferred retrogression associated with the main Redbank thrust (MRBT). The Mount Hay block is structurally above this thrust and is located ~80 km northwest of Alice Springs in the Northern Territory. Map primarily after Warren and Shaw (1995), modified on the basis of Teyssier (1985a; Amburla Dam area and southeastern Mount Hay ridge), Teyssier et al. (1988: ~35 km southeast of Mount Hay), Shaw and Black (1991) and Black and Shaw (1992) (Redbank Hill area), Kelso (1993; Mount Hay and Mount Chapple blocks), Bonnay (2001: northwestern Mount Hay ridge), and our mapping. Boxes show locations of maps in Figure 4.

in a subduction or back-arc setting at 1803 ± 5 Ma on the basis of petrologic and U-Pb zircon analyses (Warren and Shaw, 1995; Zhao and Bennett, 1995; Hoatson et al., 2005; Claoué-Long and Hoatson, 2005). Metamorphic overgrowths on zircon from mafic granulites on Mount Hay ridge (Fig. 2) record high-temperature metamorphism at 1700 ± 17 Ma (Claoué-Long and Hoatson, 2005). Thus, at minimum, zircons in mafic granulites record emplacement during the Stafford event and metamorphism during the Strangways event. The timing of magmatism, peak metamorphism, and deformation varied spatially in the Arunta inlier, and previous workers have suggested regional deformation and

metamorphism occurred during both the Yambah and Strangways events (formerly the early and late Strangways events of Collins and Shaw, 1995; Goscombe, 1992a; Black and Shaw, 1992; Watt, 1992; Collins and Shaw, 1995; Zhao and Bennett, 1995; Biermeier et al., 2003; Claoué-Long and Hoatson, 2005). Claoué-Long and Hoatson (2005) note Yambah ages are recorded locally in domains in complex zircons from Mount Hay ridge, but attribute these to variable recrystallization of the older cores.

Three major post-Strangways tectonic events are recorded by deformation at amphibolite and greenschist facies in the central Arunta inlier: the Chewings event (ca. 1600 Ma), Anmatjira

event (ca. 1500–1400 Ma) and Alice Springs orogeny (ca. 400–300 Ma) (Collins and Teyssier, 1989; Shaw and Black, 1991; Collins and Shaw, 1995). The Chewings event is recorded by north-vergent, amphibolite-facies isoclinal folds and mylonite zones, which were then rotated from their subhorizontal orientation during subsequent events (Teyssier et al., 1988). The Anmatjira event is recorded by discrete, ~east-west-striking, south-vergent, amphibolite-facies mylonite zones (Shaw and Black, 1991; Biermeier et al., 2003). The Alice Springs orogeny was a major intracontinental, south-vergent contractional event (e.g., Teyssier, 1985b; Dunlap et al., 1997). Early Alice Springs deformation occurred at amphibolite facies, followed by later mylonitization at greenschist facies (e.g., Teyssier et al., 1988; Shaw and Black, 1991; Dunlap and Teyssier, 1995; Lafrance et al., 1995; Fliervoet et al., 1997; Scrimgeour et al., 2000). Some Alice Springs deformation reactivated older shear zones (Teyssier, 1985a; Teyssier et al., 1988; Shaw and Black, 1991; Dunlap and Teyssier, 1995).

Granulites of the central Arunta province are separated from amphibolites of the southern Arunta province by the north-dipping Redbank deformed zone, which includes thrusts, folds, and associated mylonites (Shaw et al., 1984; Zhao and McCulloch, 1995; Fig. 2). The Redbank deformed zone originated as a suture between tectonostratigraphic provinces within the Arunta inlier either prior to (Myers et al., 1996) or during (Shaw and Black, 1991) amalgamation with the other Australian cratonic elements. The zone has a long history, and was active most recently during the Alice Springs orogeny, when the rocks of the central Arunta province were exhumed along the main Redbank thrust and related structures (Collins and Teyssier, 1989; Shaw and Black, 1991). In the central Arunta inlier, the moderate (50–70°) north dip of mylonites in the Redbank deformed zone, foliation within Redbank thrust sheets, and foliation in the structurally overlying granulite blocks is attributed to rotation of the older metamorphic rocks into north-dipping thrust sheets during the Alice Springs orogeny (Teyssier et al., 1988; Collins and Teyssier, 1989). Biermeier et al. (2003) conducted extensive thermobarometric and thermochronologic work along a cross-strike traverse through the Mount Heughlin area, which occupies a structurally similar position to, but is roughly 70 km west of, the Mount Hay block. Granulites in Mount Heughlin record peak metamorphic conditions of ~850 °C and 1000 MPa, indicating total exhumation of ~35 km. Biermeier et al. (2003) proposed that ~15 km of exhumation occurred early in the rocks' history; they note evidence for decompression that they interpret as a record of exhumation at the termination of the Strangways event, although they do not specify a mechanism for this exhumation. Their data suggest that further exhumation from ~20 km to the surface occurred during the Alice Springs orogeny. Like previous workers, they contend that the Redbank deformed zone developed as a shear system during the Anmatjira event; however, they suggest that it was dominated by strike-slip motion at ca. 1450 Ma, and exhumation at that time was commensurately small.

Geophysical data constrain the geometry of the Redbank deformed zone and overlying structures at depth (Figs. 2 and 3).

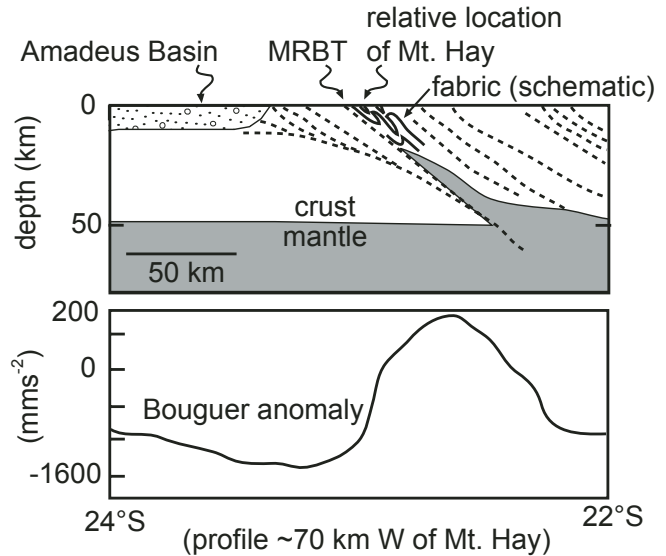


Figure 3. Geophysical cross sections across the Redbank deformed zone ~20 km west of map shown in Figure 2 (modified from Hand and Sandiford, 1999). The relative location of the Mount Hay block with respect to the main Redbank thrust (MRBT) is shown. The top diagram is the interpreted seismic line across the Redbank deformed zone (no vertical exaggeration). The bottom diagram is the Bouguer gravity model for the same profile.

A reflection seismic line located ~70 km west of Mount Hay, close to the traverse studied by Biermeier et al. (2003), indicates that major structures and lithologic contacts within and north of the Redbank deformed zone dip northward (e.g., Goleby et al., 1989). The main Redbank thrust and reflections in the granulites structurally above it are parallel in a region up to ~25 km north of the thrust and up to 40 km depth (Wright et al., 1990). A region of seismic transparency interpreted as mantle, and a strong positive gravity anomaly above the hanging wall, indicate that the crust-mantle transition has been offset ~25 km vertically across the main Redbank thrust, and also dips northward (Fig. 3) (Goleby et al., 1989). The crust-mantle transition is not a sharp contact; however, these data suggest that it is generally parallel to reflections in the overlying crust. It is reasonable to assume, therefore, that the overlying crust was tilted and displaced the same amount as the crust-mantle transition. This assumption is consistent with Biermeier et al.'s (2003) estimation of exhumation associated with movement on the Redbank thrust and associated structures.

THE MOUNT HAY BLOCK

Previous Work

The main granulite exposures in the Mount Hay block occur on two northwest-trending ridges, referred to here as the Mount Hay and Capricorn ridges, and a small hill called Ceilidh Hill (Figs. 2 and 4). Previous mapping by Glikson (1984) and Watt

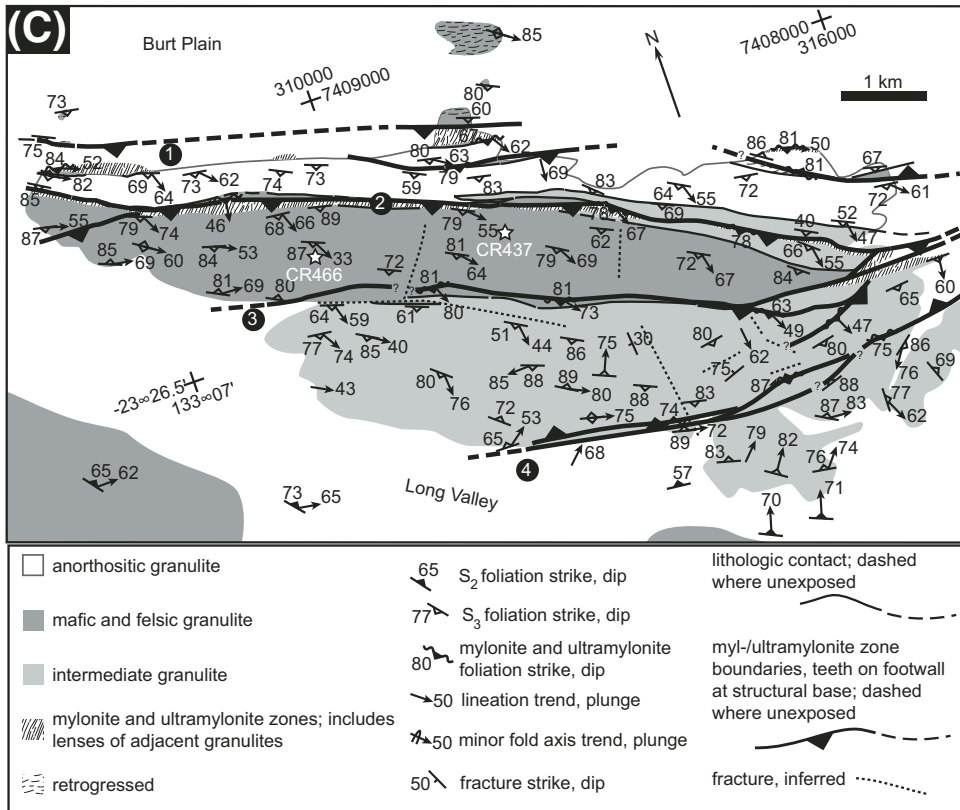
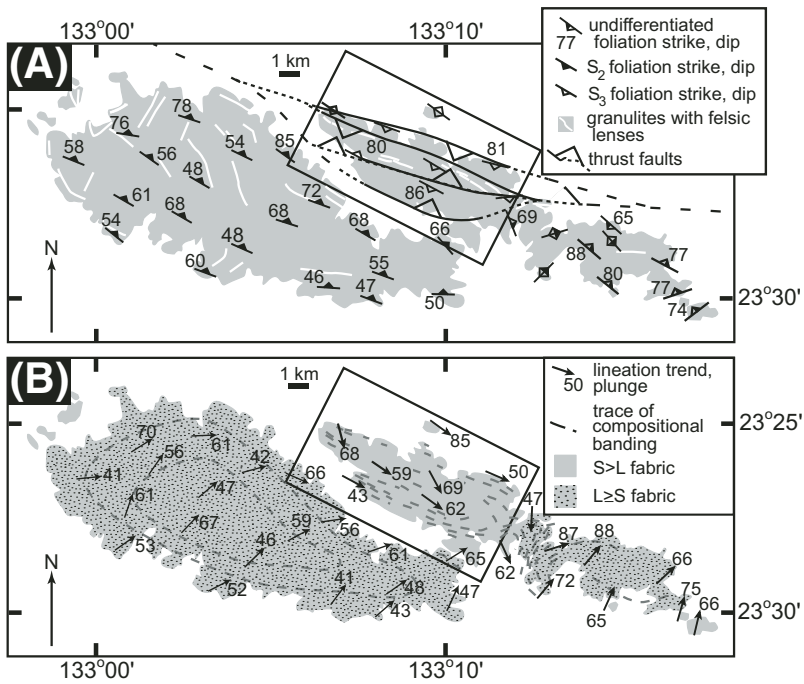


Figure 4. Simplified geological maps of the Mount Hay block showing extent of granulite exposures and spatial variations in structures. (A) Larger felsic lenses, minor thrust faults and dominant foliation orientations (see text for descriptions of foliations). Note that foliations are S₂ on Mount Hay ridge, S₃ on Capricorn ridge, and undifferentiated southeast of Capricorn ridge (Ceidilh Hill and the Amburla Dam area, Fig. 2). (B) Fabric types and lineation orientations. Dashed lines schematically illustrate variations in orientation of compositional banding; note fold closures in Mount Hay ridge and the Amburla Dam area (southeast of Capricorn ridge, refer to Fig. 2). (C) Relationships between lithologic units, foliations of different ages, and younger mylonite zones exposed on Capricorn ridge. Numbers in solid black circles refer to mylonite zones shown in Figure 9. White stars indicate locations of samples used for geothermometry. A–B include data from Teyssier (1985a) and Warren and Shaw (1995). Universal Transverse Mercator coordinates from grid 53K.

(1992) focused on geologic and petrologic descriptions, and is compiled into the 1:250,000 Hermannsburg geologic map and notes (Warren and Shaw, 1995). Prior to our work, detailed mapping of the study area was limited to a part of the northwestern edge of Mount Hay ridge (Bonnay, 2001), the Amburla Dam area, and the eastern end of Mount Hay ridge (Fig. 2) (Teyssier, 1985a).

Previous reconnaissance mapping relied heavily on aerial photography; as a result, structural relationships were largely inferred from color contrast, caused mainly by spatial variations in composition of exposed granulites. Compositional domains visible on air photos are typically felsic; they stand out with respect to adjacent, more mafic granulites. These felsic domains have a variety of origins. Bonnay et al. (2000) and Bonnay (2001) documented primary magmatic features, including evidence that irregular m- to 10-m-scale layering was derived from sill-like intrusion of tholeiitic basaltic magma into a silicic magma chamber. Evidence includes mafic granulite layers that exhibit sharp margins with underlying charnockite, along which load casts and flame structures record density contrast between protolith melts. Mafic granulite grades upward into granulite with hybrid compositions, including mafic granulite with K-feldspar megacrysts and tonalitic granulite, which is gradational into charnockite. These features were inferred to record shallow-crustal intrusion of a composite mafic and silicic intrusion (MASLI system; cf. Wiebe and Collins, 1998). Bonnay et al. (2000) provide U-Pb zircon ages (without supporting data) of 1819 ± 9 Ma as an intrusion age of charnockite. Mafic layers were subsequently dated at 1803 ± 5 Ma, as noted earlier (Clauoé-Long and Hoatson, 2005), consistent with the interpretation that the rocks were part of a single system. Additional dates on igneous zircon from granitoids inferred to be broadly syntectonic with respect to the metamorphism and deformation of the MASLI intrusion and metasedimentary country rocks, are reported as 1774 ± 7 Ma and 1783 ± 5 Ma (Bonnay et al., 2000). The MASLI intrusion makes up the majority of Mount Hay ridge, on which felsic domains occupy roughly 30% of the exposed granulites (Staffier, 2007). Less abundant anorthositic and intermediate granulites exposed mainly on Capricorn ridge are thought to have originated as intrusive rocks spatially and are geochemically related to the more voluminous mafic intrusions (Warren and Shaw, 1995).

Examples of discontinuous felsic domains are shown in Figure 4A, where it is evident that they have a regular orientation only on Capricorn ridge. Compositional layering, interpreted to be everywhere parallel to the main foliation in the rocks, is folded on a large scale on Mount Hay ridge and in the Amburla Dam area southeast of Capricorn ridge (Teyssier, 1985a; Watt, 1992). Compositional layering traces suggesting the formation of large fold closures are shown schematically in Figure 4B; they have been used to infer the presence of an antiformal sheath-like fold on Mount Hay ridge (Glikson, 1984; Shaw et al., 1984; Watt, 1992). Bonnay et al. (2000) provide evidence for four deformation episodes on the northwestern edge of Mount Hay ridge, including formation of the foliation defined by compositional

banding (their S_{1b}) and foliation parallel to the axial surface of the sheath-like fold in compositional banding (their S_{1d}). They assert that asymmetric K-feldspar porphyroclast systems on the northwestern edge of Mount Hay record north-side-up shear throughout this complex history. In contrast, compositional layering has a regular orientation on Capricorn ridge, and is everywhere parallel to a single foliation. Waters et al. (2002) and Waters-Tormey and Tikoff (2007) show that this consistent orientation reflects the transposition of older foliations in the Mount Hay block (described further below) into a south-side-up, >4-km-thick, high strain zone—the Capricorn ridge shear zone. Part of the transposition path is exposed across strain gradients straddling major compositional domain boundaries, where compositional domains become thinner, more planar, and more continuous at cm- to km-length scales. These strain gradients record strain localization along these compositional domain boundaries. Evidence such as sheath folds and transposition of compositional domains into the foliation provide evidence for high shear strain throughout the Mount Hay block (Hobbs et al., 1976; Cobbold and Quinquis, 1980).

Thermobarometric analyses of samples collected from the Mount Hay block range from 700 to 900 °C and 600–900 MPa (e.g., Warren, 1983; Glikson, 1984; Goscombe, 1992b; Collins and Shaw, 1995). Staffier's (2007) recent work shows temperatures and pressures within this same range, but provides a particularly useful comparison to data presented here because her samples spanned Mount Hay ridge. Temperatures calculated for four samples using Taylor's (1998) two-pyroxene geothermometer range from 795 ± 22 °C to 842 ± 18 °C, with a mean of 816 ± 27 °C, assuming a pressure of 800 MPa. One of these samples had a garnet-bearing mineral assemblage, allowing pressure to be calculated using a variety of geobarometers (Thermocalc; Holland and Powell, 1998), with results between 690 and 820 MPa for a temperature of 800 °C. It also allowed temperature to be estimated using garnet-orthopyroxene and garnet-clinopyroxene geothermometers (Ganguly et al., 1996). Temperatures calculated for this sample using the different thermometers are in reasonable agreement with one another: 801 ± 14 °C (two-pyroxene); 788 ± 51 °C (garnet-orthopyroxene), and 751 ± 35 °C (garnet-clinopyroxene). Variations in temperature recorded by samples across Mount Hay ridge show no systematic variations across the strike of the dominant foliation, parallel to strike, or with proximity to Capricorn ridge, implying that temperature was essentially invariant across the ridge, in spite of the variation in depth suggested by regional structural relationships (Fig. 3). Field relationships indicate that the last major stage of lower-crustal deformation occurred after the latest episode of magmatism (Teyssier, 1985a; Watt, 1992); thus, these thermobarometric data record regional deep-crustal metamorphism.

In the following sections, we add key structural observations on Mount Hay ridge and more detailed structural data from Capricorn ridge to this foundation of work. These data are subsequently integrated with previous work to provide a clearer picture of the tectonic history of the area.

Granulites

The main map unit in the Mount Hay block is lithologically heterogeneous. It is composed of mafic granulite interlayered with 10%–40% felsic granulite from the mm to m scales. Mafic granulites have a mineral assemblage of plagioclase + orthopyroxene + clinopyroxene + oxides \pm quartz \pm K-feldspar \pm biotite. They contain ~30%–50% pyroxenes, consistent with a gabbroic protolith. Mafic granulites are typically relatively fine-grained (up to 0.1 mm), but pyroxene grains are locally up to 3 mm in longest dimension on Capricorn ridge.

The felsic granulite contains plagioclase + quartz + orthoclase + oxide(s) \pm orthopyroxene \pm clinopyroxene, and on Capricorn ridge locally includes garnet and/or biotite. These most common mineral assemblages are consistent with tonalite and intermediate charnockite or granodiorite protoliths. Most felsic granulites are medium grained with grain sizes ranging from 0.1 to 0.2 mm in longest dimension. Coarser-grained, porphyroclastic felsic granulite is more common on Mount Hay ridge, with porphyroclasts as large as several centimeters in longest dimension preserved locally. Felsic granulites on Capricorn ridge are more uniformly fine grained than those on Mount Hay ridge and contain elongate, polycrystalline quartz ribbons with lengths up to 30 mm.

Other types of granulite are also present in the Mount Hay block. Metasedimentary granulites are locally exposed, but not mappable at the scale we have considered. Intermediate and anorthositic granulites are locally present, mainly on Capricorn ridge (Fig. 4). The mineral assemblage of the intermediate granulite is similar to that of the mafic granulite, but it has less than ~30% pyroxene, suggesting a broadly dioritic protolith. Pyroxene and plagioclase grains are ~0.2 mm in longest dimension. Anorthositic granulites are dominated by plagioclase, with trace amounts of quartz and K-feldspar and <10% pyroxenes \pm hornblende. Plagioclase grains are \geq 0.1 mm and mafic minerals are 0.1–3 mm in their longest dimensions. Centimeter to dm-scale variations in pyroxene abundance result in outcrop-scale heterogeneity in both intermediate and anorthositic granulites.

Despite the intrusive origin of virtually all of the rocks in the Mount Hay block, igneous microstructures such as internal compositional zoning are not observed in the samples we have studied and have not been noted by previous workers (Glikson, 1984; Teyssier, 1985a; Watt, 1992). All minerals in the granulite-facies assemblage, except garnet, locally exhibit evidence of intracrystalline strain, such as tapered deformation twins (plagioclase) and undulose extinction (quartz, rarely feldspar and pyroxene). Although the rocks locally exhibit a foam texture, grain and phase boundaries are typically interlobate to gently curved and minerals generally define a grain-shape preferred orientation. There is no evidence for reaction preserved in these rocks, and all the minerals are in stable contact with one another; thus, rocks throughout the block appear to exhibit equilibrium mineral assemblages. Porphyroclasts are relatively common in the felsic granulite, rare in the anorthositic granulite and generally absent

in the mafic and intermediate granulite. The combination of evidence for intracrystalline strain and dynamic recrystallization of granulite-facies mineral assemblages is consistent with ductile deformation at granulite-facies conditions.

Mount Hay Ridge

With the exception of local areas of metasedimentary granulite, intermediate granulite, and anorthositic granulite that are too small to map at the scale shown in Figure 4, Mount Hay ridge is composed entirely of interlayered mafic and felsic granulite. The amount of felsic granulite varies spatially, as noted earlier, from 10%–40%. Felsic domains are typically lens-shaped to tabular, and vary from ~1 mm to ~1 m thick over most of the ridge. Similarly shaped mafic domains vary from ~1 cm to several meters in thickness. These thicknesses contrast with domains reported to be tens of meters thick locally, where relict primary structures are preserved (Bonney et al., 2000).

Our observations are consistent with earlier interpretations (Glikson, 1984; Shaw et al., 1984; Watt, 1992) that the compositional banding described above defines a sheath-like fold on Mount Hay ridge. However, we clarify relationships where previously two foliations of different age were not distinguished over much of the ridge, as is still the case in the Amburla Dam area and on Ceilidh Hill (Fig. 4A). The older foliation is defined by a grain-shape preferred orientation everywhere parallel to compositional domain alignment; this S_1 foliation describes the large fold form (Fig. 4B), and is easiest to distinguish. We correlate this foliation with Bonney et al.'s (2000) S_{1b} foliation. The younger, NNE-dipping S_2 foliation (Fig. 5D) is defined by a grain-shape preferred orientation, and is present throughout the map area, not just in the eastern fold hinge and locally on the northwestern edge of Mount Hay ridge where it was previously described (S_{1d} of Bonney et al., 2000). It is parallel to S_1 on the northeastern and southwestern sides of Mount Hay ridge, and up to 90° from S_1 on the northwestern and southeastern ends of the ridge. In the tight eastern hinge of the fold, S_2 is demonstrably parallel to the axial surface of the fold, forming a divergent fan that is expressed at a large scale in a range of orientations that define a great circle girdle normal to the fold nose (Fig. 5D).

The lineation is a stretching lineation, defined by elongate porphyroclast systems, mineralogic domains, and a grain-shape preferred orientation. In the eastern fold hinge, it is demonstrably parallel to hinge lines of m-scale parasitic folds and the intersection between S_1 and S_2 . Thus, it is also parallel to the axis of the large folds, and is remarkably consistent in orientation, plunging steeply to the northeast (Fig. 5C).

The degree of development of foliation versus lineation, both defined by grain shape-preferred orientation and compositional domain alignment, varies on Mount Hay ridge. Overall, the lineation is stronger ($L > S$) than the dominant S_2 foliation (e.g., Fig. 6A). In detail, the tectonite fabric type varies with the relative orientation of S_1 and S_2 . S_1 is at an angle to S_2 mostly on the southeast and northwest ends of the ridge. Here, we observe

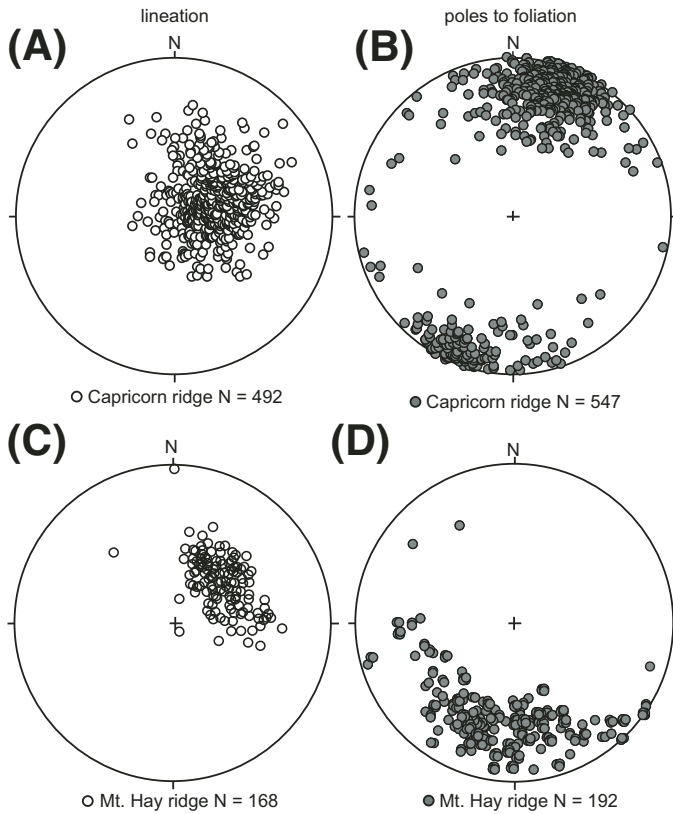


Figure 5. Equal area, lower hemisphere projections of lineation orientations on (A) Capricorn ridge and (C) Mount Hay ridge, and poles to dominant foliations on (B) Capricorn ridge (mainly S_3) and (D) Mount Hay ridge (mainly S_2).

$L > S$ to $L \gg S$ tectonites in which compositional domain boundaries are distinctly straighter on surfaces parallel to lineation than on faces perpendicular to lineation. On the northern and southern sides of the ridge, S_1 is subparallel to S_2 . Here, foliation tends to be better developed than elsewhere in the ridge, but tectonite fabric still ranges from $L > S$ to $L = S$. The most extensive $L = S$ domain is located on the northwest margin of Mount Hay ridge, opposite Capricorn ridge.

Northeastward across strike from the top of Mount Hay ridge to Capricorn ridge, the fabric type grades from $L > S$ to the $S > L$ fabric that characterizes Capricorn ridge. This change is accompanied, in a transition zone between the ridges, by progressive change in orientation of the S_2 foliation. On Mount Hay ridge proper, the foliation steepens toward the northeastern margin (Fig. 4A).

Plagioclase porphyroclast systems are found on Mount Hay ridge on faces that are perpendicular to foliation and sub-parallel to the lineation in locations in which grain-size reduction has not been complete (Fig. 6B). These porphyroclast systems are not strongly asymmetric, but consistently record north-side-up shear sense, consistent with those reported previously in a smaller area

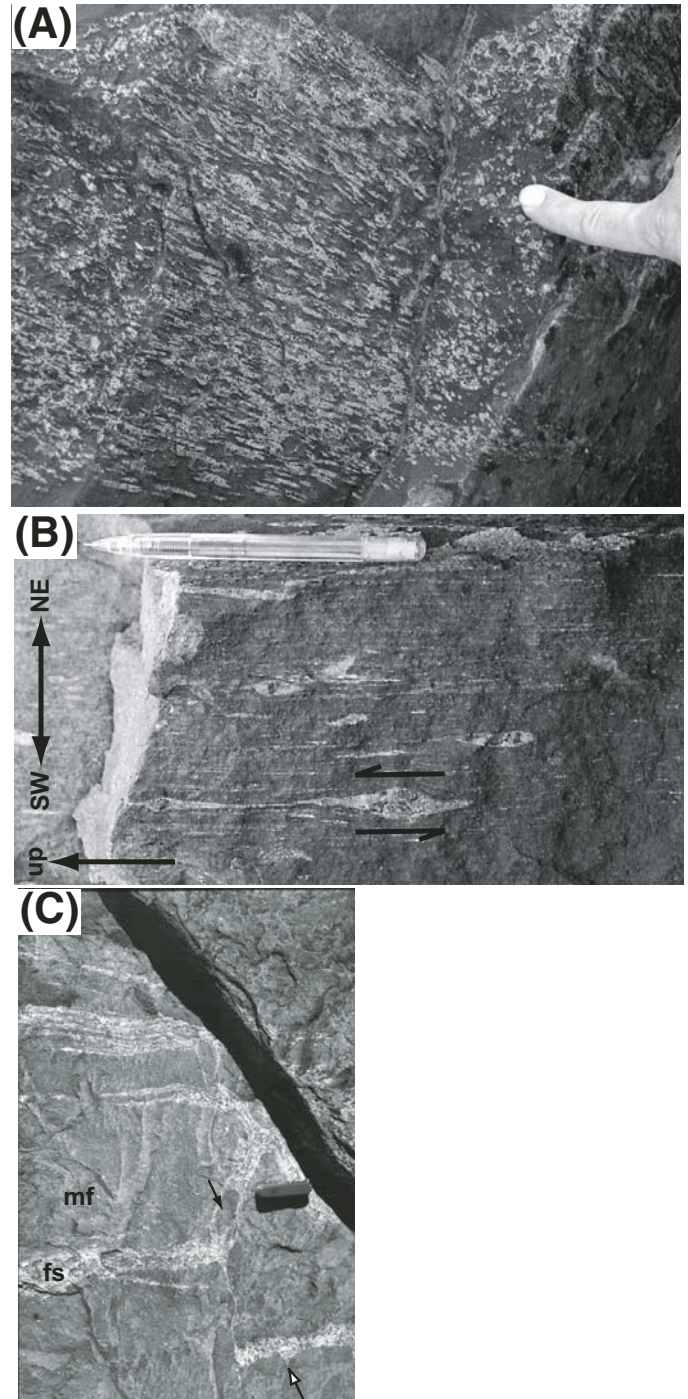


Figure 6. Outcrop photographs of mesoscale structures on Mount Hay ridge. (A) Three-dimensional view of $L \gg S$ fabric. Finger points to outcrop surface that is sub-perpendicular to lineation. (B) North-side-up shear sense indicated by asymmetry of plagioclase porphyroclast systems on surface parallel to lineation and at right angles to foliation. Pencil is 14 cm long. (C) Cusps (open arrow) and enclaves (closed arrow) in the mafic + felsic unit. These are interpreted as primary structures recording mixing of mafic and silicic magmas during formation of the protolith to the mafic + felsic granulite (Bonnay et al., 2000). Abbreviations: fs—felsic; mf—mafic. Penknife is 9 cm long.

(Bonnay et al., 2000). Viewed perpendicular to foliation and lineation, porphyroblast systems are symmetrical. Rare extensional shear bands record the same shear sense.

As mentioned above, some features evident in outcrop have been interpreted by previous workers to be primary magmatic structures created by magma mingling in a composite mafic and silicic intrusion (Bonnay et al., 2000; Bonnay, 2001). These features include lobate/cuspate contacts and enclaves (Fig. 6C). Our field observations indicate that these primary structures are only observed on surfaces (sub)perpendicular to lineation. We attribute preservation of these primary structures to the dominantly constrictional strain, an observation noted in other areas of L-tectonites (e.g., Pavlis et al., 2003).

Capricorn Ridge Shear Zone

The distribution of rock types on Capricorn ridge from northeast to southwest is anorthositic granulite, interlayered mafic and felsic granulite, and intermediate granulite (Fig. 4C). Map patterns indicate that the major lithologic units have tabular shapes that are parallel to the mesoscale foliation and compositional banding. Younger mylonite zones, described below, generally follow these boundaries, but granulite contacts are locally preserved. Felsic granulites occur as mm- to m-scale domains interlayered with mafic granulite and rarely in intermediate granulite on the southeast part of Capricorn ridge.

As on Mount Hay ridge, foliation in Capricorn ridge is defined by the shape-preferred orientation of grains, mineral aggregates, and compositional domains. These elements also define a lineation, which is parallel to mesoscopic fold axes locally. On Capricorn ridge proper, lineation and foliation show virtually no spatial variation in orientation (Figs. 5A and 5B). Foliation on average dips steeply south at $\sim 70^\circ$ and the lineation plunges steeply south-southeast. Mineral and stretching lineations are sub-parallel in adjacent compositional domains, and sub-parallel to fold hinge lines where present. The ~ 1 -km-wide transition from the south-dipping foliation on Capricorn ridge to the north-dipping S_2 foliation on Mount Hay ridge is poorly exposed in the intervening valley (Fig. 4C). However, foliation in the southwesternmost exposures on Capricorn ridge dip north, and the outcrops between the ridges show progressively more shallow northward dips with increasing proximity to Mount Hay ridge. Thus, southward across this transition between the ridges, foliation changes from south-southwest-dipping on Capricorn ridge to north-northeast-dipping on Mount Hay ridge and lineation changes from south-southeast-to-southeast-plunging on Capricorn ridge and the margin of Mount Hay ridge to northeast-plunging on Mount Hay ridge (Figs. 4 and 7). The transition in foliation orientation is illustrated by the poles to north-dipping foliations plotted on Figure 5B.

Although the penetrative $S > L$ (foliation dominated) fabric on Capricorn ridge does not show spatial variations in orientation, it does display across strike gradients in the degree of

development, or intensity, as described previously (Waters et al., 2002; Waters-Tormey, 2004; Waters-Tormey and Tikoff, 2007). With increasing foliation intensity, compositional bands become more tabular, parallel, and thinner (Figs. 8A and 8B). Sheath-like folds occur locally where the compositional layers are thinnest (Fig. 8D). Lineation intensity is essentially constant across this fabric gradient except in felsic granulite, where it increases with foliation intensity.

Mesoscale shear-sense indicators are mostly observed in the mafic + felsic granulite unit on faces parallel to lineation and perpendicular to foliation (Fig. 8C). These indicators include asymmetric plagioclase porphyroblast systems, orthopyroxene porphyroblasts with plagioclase wings, and garnet porphyroblasts with felsic wings. We have observed both σ - and δ -type geometries. The sense of shear recorded by these asymmetric objects varies, although most record south-side-up shear. Further, the most elongate clasts consistently exhibit asymmetry consistent with south-side-up shear. Asymmetric feldspar augen with the same shear sense also occur in rare quartzofeldspathic lenses and layers in the intermediate granulite. Most porphyroblast systems viewed on faces perpendicular to lineation are symmetric.

There are several mesoscale features observed on Capricorn ridge that are absent on Mount Hay ridge. Conjugate extensional shear bands and boudins occurring locally in the mafic + felsic unit, and oblate grain shapes in the anorthositic granulite, indicate that the increasing foliation intensity is partly the result of flattening. The conjugate shear bands and boudins are observed on faces perpendicular to foliation and lineation, and record a component of ESE-WNW extension sub-perpendicular to lineation in the foliation plane. Correlatively, the primary structures preserved locally on Mount Hay ridge, presumably due to the constrictional strain history, are absent from Capricorn ridge.

Relative Timing of Deformation on Mount Hay and Capricorn Ridges

The opposite senses of shear recorded on Capricorn and Mount Hay ridges require two different deformational episodes. The complete transposition of compositional banding into the foliation on Capricorn ridge is strong evidence that the Capricorn ridge shear zone is younger than the Mount Hay ridge sheath-like fold (Fig. 7). The change in orientation of foliation and lineation shown in Figures 4 and 7 also is interpreted as the result of deflection of foliation on Mount Hay ridge into parallelism with an S_3 foliation in the younger Capricorn ridge shear zone.

This interpretation that the Mount Hay ridge fold and axial-surface S_2 foliation were overprinted by the Capricorn ridge shear zone is supported by differences in strain inferred from differences in fabric type. The dominance of lineation and significant constrictional strain on Mount Hay ridge contrasts sharply with the stronger foliation and other mesoscopic structures on Capricorn ridge, which record a component of flattening and extension at right angles to the lineation.

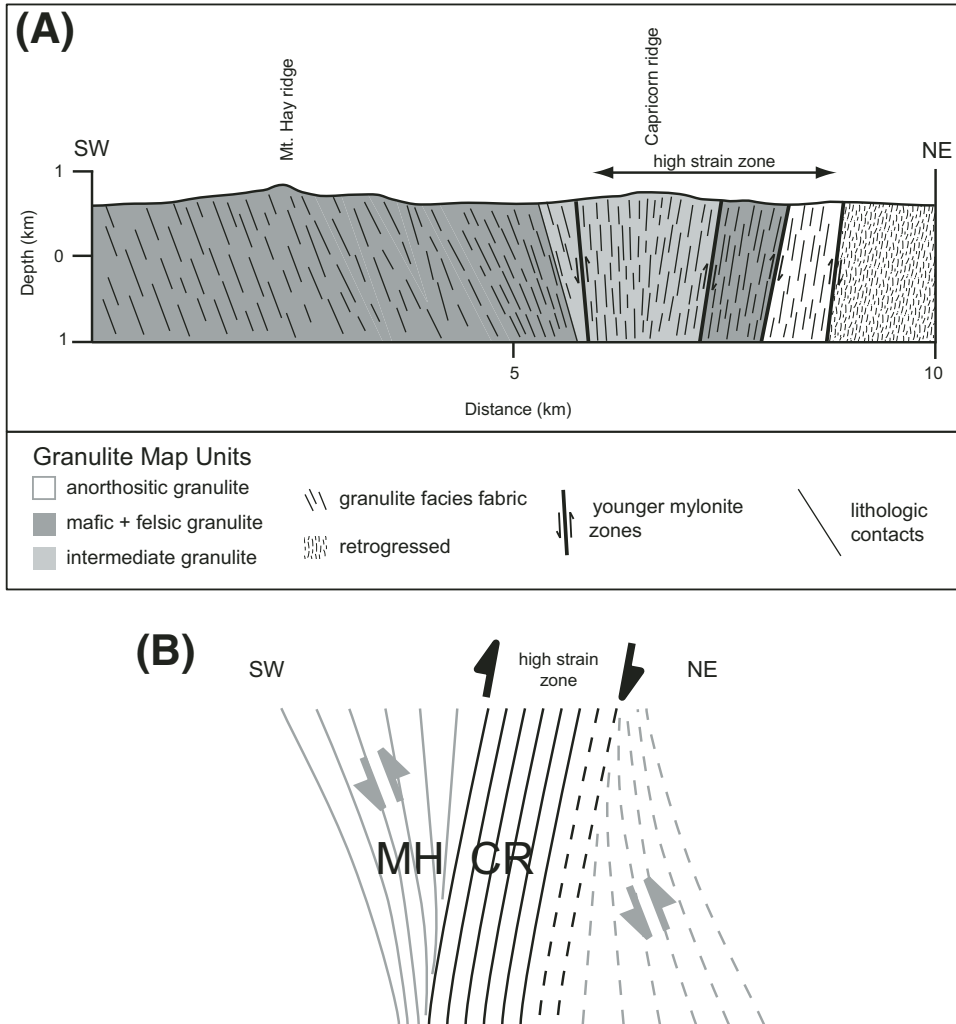


Figure 7. (A) Simplified northeast-southwest cross section through Mount Hay (north-side-up shear sense) and Capricorn (south-side-up shear sense) ridges in the Mount Hay block. The northeast end of the cross section is dominated by retrogressed granulite-facies rocks. Mylonite zones that post-date granulite-facies deformation conditions locally cross-cut the dominant fabric and are found preferentially on Capricorn ridge. (B) Interpretation of overprinting relationship between Mount Hay (MH) and Capricorn (CR) ridges shown as a schematic cross section looking northwest without younger mylonite zones. Dashed lines indicate other side of the Capricorn ridge shear zone (black), which is now truncated by younger mylonite zones, cross-cutting the older granulite fabric (gray).

We note that the Capricorn ridge shear zone has several distinctive characteristics: (1) It is wide relative to most shear zones reported from higher crustal levels. The width and high strain suggest the zone accommodated significant movement. (2) It does not have a sharp boundary with the wall rock; the boundary is a zone in which older foliation is deflected into the shear zone rather than truncated. (3) There is no evidence for significant grain-size reduction in the shear zone. Rather, the transposition of compositional domains into the foliation at all scales, and thinning of primary lithologic domains, are the main indicators of high strain.

Geothermometry in the Capricorn Ridge Shear Zone

The overprinting relationships we have documented skirt the question of whether, in spite of similar mineral assemblages, the Capricorn ridge shear zone formed at different pressure and temperature conditions than the older Mount Hay granulites it cross-cuts. We addressed this question through analysis of mineral

chemistry of appropriate samples. Unfortunately, the Capricorn ridge shear zone lacks the appropriate mineral assemblages to constrain metamorphic pressure, but we were able to use two samples of mafic granulite collected on Capricorn ridge to determine temperature using Taylor's (1998) two-pyroxene geothermometer, which facilitates a direct comparison with data Staffier (2007) reported from Mount Hay ridge. Sample locations are given in Figure 4C.

Geochemical data were collected on a Cameca SX50/51 (SN485 electron microprobe at the University of Wisconsin-Madison) using 15keV accelerating voltage and a 20nA probe current. Data were collected from four separate pyroxene pairs for each sample. At least five points were analyzed on the rim of each grain, and the average of the five points was used in the temperature calculations. Thus, the temperatures determined represent the conditions under which the final mineral assemblage equilibrated.

We used a Lotus 1-2-3 spreadsheet developed by Gordon Medaris (2005, personal commun.) to calculate temperature

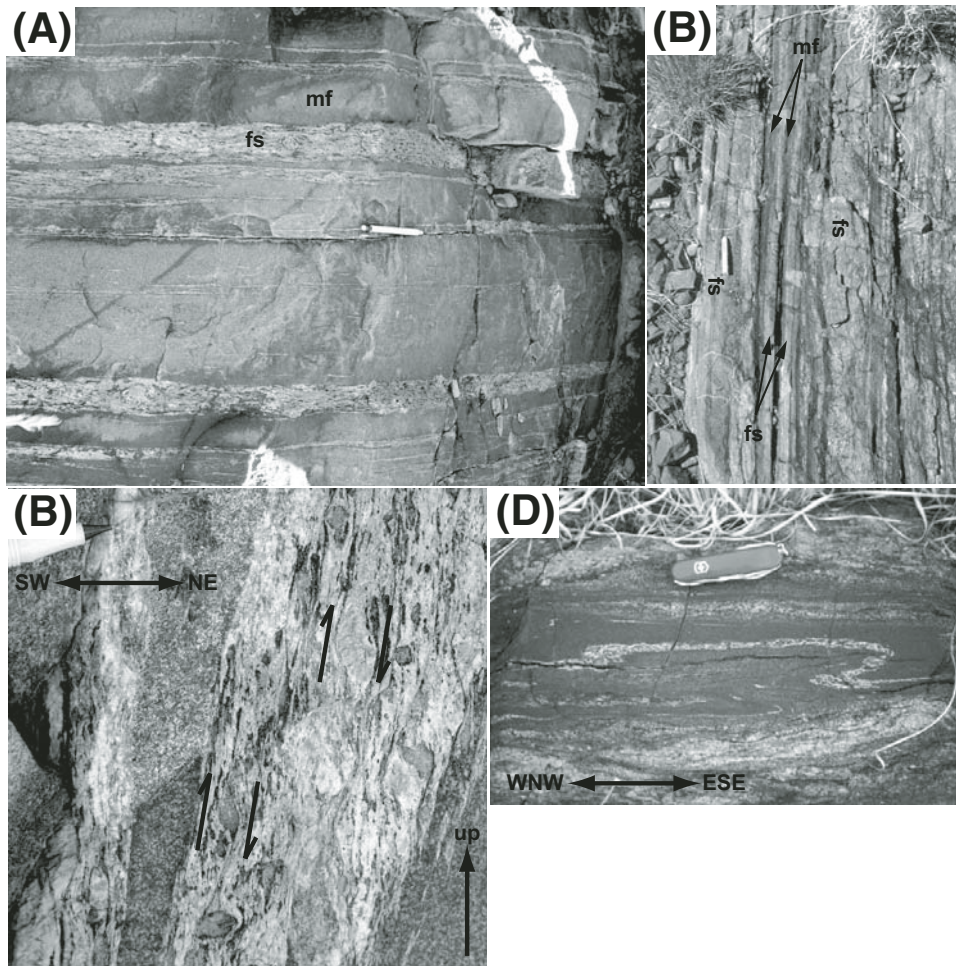


Figure 8. Outcrop photographs of meso-scale structures on Capricorn ridge. The outcrop surfaces are sub-perpendicular to lineation in (A), (B), and (D), and parallel to lineation and perpendicular to foliation in (C). (A) Three-dimensional view of S > L fabric in interlayered mafic + felsic granulite. Pencil is 14 cm long. (B) Thinner compositional layering in the same unit. Pencil is 12 cm long. Abbreviations: fs—felsic; mf—mafic. (C) South-side-up shear sense indicated by asymmetric feldspar porphyroclast systems and shear bands. End of pencil shown is 2 cm long. (D) Cross section of sheath-like fold. Penknife is 9 cm long.

based on Taylor's (1998) calibrations at pressures of 600, 700, and 800 MPa, which covers the range in pressures determined previously for other sites in the Mount Hay block. Temperatures were calculated for each grain pair for each sample. Geochemical data, temperatures for each grain pair, and the mean and standard deviation for each sample are given in Table 1. Several points are evident from these calculations. First, the temperatures are not strongly sensitive to pressure; there is only a 6 °C difference between temperatures calculated for 600 MPa and those calculated at 800 MPa. Second, the temperatures determined are essentially the same, within error. Third, the sample closest to Mount Hay ridge has a slightly higher mean temperature than that farther away (Fig. 4). However, both samples fall, within error, into the range reported by Staffier (2007) for samples from Mount Hay ridge. The mean of the two Capricorn ridge samples at 800 MPa is 776 ± 38 °C; the mean of the Mount Hay samples calculated for the same pressure is 816 ± 27 °C.

The lack of systematic variation in temperatures calculated from samples collected across the Mount Hay block suggests either that both deformation events occurred at essentially the same temperature, or that the mineral assemblage on Mount Hay

re-equilibrated when the Capricorn ridge shear zone was active. This similarity in temperature leads us to the conclusion that our best estimate of pressure is provided by the Mount Hay sample analyzed by Staffier (2007), which resulted in a range of pressures between 690 and 820 MPa. These pressures constrain depth at the time of deformation to 26–30 km, assuming a lithostatic gradient of 27 MPa/km. With these assumptions, the geothermal gradient would have been roughly 27–30 °C.

RECONSTRUCTION OF GEOMETRY OF THE ACTIVE CAPRICORN RIDGE SHEAR ZONE

The Mount Hay block has been rotated and exhumed subsequent to formation of the Capricorn ridge shear zone in the deep crust. To understand the tectonic significance of this major shear zone, we evaluate the effects of younger tectonic events in the Mount Hay block: (1) post-granulite shear zones that cut the Capricorn ridge shear zone (Fig. 4C) and (2) exhumation and tilting of the entire block.

Mylonitic and cataclastic shear zones that cut the north-east part of the Mount Hay block are described in detail in

TABLE 1. CHEMICAL ANALYSES OF PYROXENE PAIRS FOR EACH SAMPLE (SEE FIG. 4 FOR SAMPLE LOCATIONS) AND TEMPERATURES CALCULATED USING TAYLOR'S (1998) GEOTHERMOMETER AT PRESSURES OF 600, 700, AND 800 MPa

Sample	Grain	Na ₂ O	MgO	Al ₂ O ₃	SiO ₂	K ₂ O	CaO	TiO ₂	Cr ₂ O ₃	MnO	FeO	Sum	T (600 MPa)	T (700 MPa)	T (800 MPa)
CR437BY	opx1	0.004	16.57	1.3	50.342	0.003	0.454	0.039	0.023	0.624	29.198	98.557	759	762	765
CR437BY	cpx1	0.46	11.667	2.172	51.368	0.005	22.115	0.208	0.058	0.243	10.92	99.216			
CR437BY	opx2	0.004	16.633	1.184	50.301	0.004	0.399	0.041	0.033	0.674	28.961	98.234	755	758	761
CR437BY	cpx2	0.44	11.756	2.046	51.302	0.004	22.127	0.164	0.062	0.226	10.83	98.957			
CR437BY	opx3	0.002	16.666	1.324	50.289	0.007	0.493	0.05	0.022	0.59	28.841	98.284	759	762	765
CR437BY	cpx3	0.402	12.015	1.958	51.56	0.009	22.264	0.15	0.043	0.192	10.352	98.945			
CR437BY	opx4	0.005	16.693	1.312	50.402	0.006	0.473	0.048	0.014	0.658	29.096	98.707	707	710	713
CR437BY	cpx4	0.456	11.879	1.933	51.343	0.004	22.439	0.158	0.065	0.221	10.556	99.054	745±25	748±25	751±25
Mean values													745±25	748±25	751±25
CR466U	opx1	0.014	18.083	1.263	51.069	0.005	0.415	0.016	0.025	0.524	27.031	98.445	834	837	840
CR466U	cpx1	0.47	12.298	2.234	51.621	0.008	21.591	0.2	0.077	0.22	10.308	99.027			
CR466U	opx2	0.016	18.03	1.227	50.843	0.005	0.381	0.047	0.018	0.485	26.904	97.956	793	796	798
CR466U	cpx2	0.465	12.431	2.005	51.768	0.008	21.979	0.174	0.095	0.192	9.774	98.891			
CR466U	opx3	0.011	18.036	1.332	50.909	0.009	0.385	0.046	0.008	0.537	27.15	98.423	753	756	759
CR466U	cpx3	0.47	12.4	2.021	51.908	0.01	22.343	0.193	0.073	0.235	9.661	99.314			
CR466U	opx4	0.017	17.954	1.286	50.918	0.011	0.409	0.024	0.038	0.544	27.046	98.247	800	802	805
CR466U	cpx4	0.457	12.417	2.077	51.419	0.011	21.891	0.208	0.086	0.237	10.296	99.099	795±33	798±33	801±33
Mean values													795±33	798±33	801±33

Note: Sample means and standard deviations given for each pressure.

Waters-Tormey (2004). These zones are typically <10-m-wide, generally strike west-northwest or east-southeast, dip steeply, and exhibit down-dip lineations (Fig. 9). Shear zones with south-side-up sense-of-shear indicators have amphibolite-facies assemblages, whereas those with north-side-up sense-of-shear indicators have greenschist-facies assemblages, suggesting different periods of deformation. These zones locally cross-cut contacts and fabrics in the granulites, indicating that they formed after the cessation of granulite-facies deformation. Based on prior work in the region, we tentatively ascribe these shear zones to the ca. 1600 Ma Chewings event (south-side-up shear zones) and ca. 1500–1400 Ma Anmatjira or ca. 300–400 Ma Alice Springs orogeny (north-side-up shear zones). Granulite-facies fabrics are generally parallel across these shear zones (Fig. 4). Thus, these small-scale shear zones had negligible impact on the orientations of structures in the Capricorn ridge shear zone. Geophysical data and the pattern of these younger shear zones suggest that the Mount Hay block was rotated as a rigid block above the Redbank deformed zone (Collins and Teyssier, 1989; Goleby et al., 1989), forming a tilted and uplifted crustal cross section (Fig. 3) (Fountain and Salisbury, 1990). It is this latter rotation we seek to remove in our analysis.

Constraints on Rotation of the Redbank Deformed Zone

To rotate the Capricorn ridge shear zone back to its original orientation, we need to establish the most likely orientation of the rotation axis and constrain the magnitude and sense of rotation.

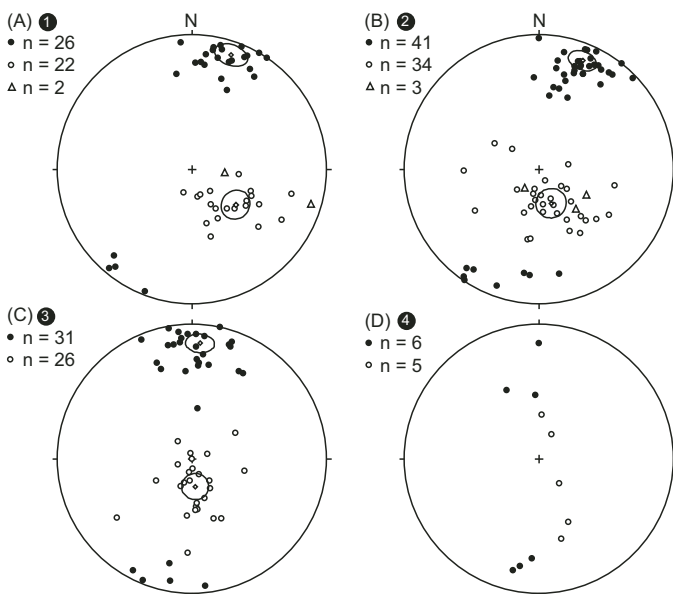


Figure 9. Equal area, lower hemisphere, projections of poles to foliation (black circles), lineation (unfilled circles), and fold hinge lines (triangles) in younger thrust shear zones exposed on Capricorn ridge: (A) mylonite zone 1, (B) mylonite zone 2, (C) mylonite zone 3, and (D) mylonite zone 4. Shear zone numbers are shown in Figure 4C. Small circles indicate orientation of maximum Bingham axial distribution (diamonds) and 95% confidence cones for poles and lineations.

As documented above in the “Previous Work” section of this paper, geologic constraints indicate that the Redbank deformed zone is responsible for the exhumation of the Mount Hay block (e.g., Collins and Teyssier, 1989; Biermeier et al., 2003). Thus, the orientations of major structures in the Redbank deformed zone offer the best constraints on the orientation of the rotation axis. In the Mount Hay region, faults of the Redbank deformed zone strike east-southeast. Associated mylonites strike east-southeast, dip 50–70° north, and generally have down-dip lineations (Fig. 2A) (Shaw and Black, 1991; Warren and Shaw, 1995). These observations indicate that the rotation axis most likely had an east-southeast trend and horizontal plunge, and that rotation was clockwise as viewed to the west.

The magnitude of rotation is less easily constrained. As discussed above, a seismic reflection profile shows that structures in the hanging wall of the main Redbank thrust are sub-parallel to both the thrust itself and the crust-mantle boundary it displaces (Fig. 3). The dip of the main Redbank thrust and other reflections to the north has been estimated at ~35–40° based on this profile (Goleby et al., 1990; Wright et al., 1990). Clearly, there is a discrepancy between this dip and the 50–70° dip of structures observed in the field. This discrepancy might be explained by the difficulty in imaging steeply-dipping structures using seismic reflection. Perhaps a second set of steep structures are present throughout the section imaged, but do not show on the profile. In this case, the shallowly dipping features would likely be younger structures. Because structures of this orientation have not been identified in the field, we reject this interpretation. A second possibility is that the structures we see in the field dip steeply only at the surface, and flatten out abruptly within the top 10 km of the crust. In this case, both field and seismic observations would be accurate. However, it would be highly fortuitous to have a change in dip occur everywhere at the same present-day depth, across a wide range of paleodepths.

We conclude that the structures documented in the field likely provide our best estimate of the orientation of the main Redbank thrust, and the discrepancy in orientation is an artifact of processing of the seismic data. The inclination of structures on the seismic profile may be low for several reasons. First, migration of the seismic data in the ~50-km-deep seismic section was accomplished with a constant velocity of 6.0 km/s (Goleby et al., 1990; Wright et al., 1990). Data from the survey indicate that P-wave velocities are 6.5 km/s at ~1 km depth and 7.2 km/s at ~31 km (Goleby et al., 1988), consistent with the range in velocities expected for a mixture of mafic and felsic granulite (Christensen and Mooney, 1995). Preliminary refraction data indicate that seismic velocities measured parallel to this seismic line are ~0.6 km/s slower than in the east-southeast-west-northwest direction (Wright et al., 1990). Further, gravity modeling along this profile requires mantle densities starting at ~25 km depth close to the main Redbank thrust (Goleby et al., 1989), which indicates seismic velocities of ~8 km/s in the lower half of the seismic section. Using a multi-layer velocity-depth function for migration would likely move deeper points on these reflections

to a deeper position, meaning that the dips of the main Redbank thrust and other reflections to the north would increase. Due to such factors as lateral variations in velocity across the Redbank deformed zone, however, it is impossible to predict exactly the effect of re-processing the data.

Assuming that the main Redbank thrust and parallel reflections in the overlying crust—and hence the crust-mantle transition—dip more steeply than 35–40°, it is necessary to estimate their inclination in the Mount Hay region. The main Redbank thrust can be traced along strike from the seismic line 70 km eastward to where the Mount Hay block lies structurally above it (Fig. 2) (e.g., Glikson, 1986; Shaw and Black, 1991). Immediately south of the Mount Hay block, mylonites within one km of the main Redbank thrust base dip 48°–80°N, with an average of 63°N (geometric average, weighted by distance from main Redbank thrust base) and strike 090–110 (data from Warren and Shaw, 1995). Gravity and magnetic lineaments associated with the Redbank deformed zone indicate that the uplifted wedge of lithospheric mantle material extends beneath Mount Hay (e.g., Wellman, 1988; Korsch et al., 1998). However, the gravity gradient associated with the Redbank deformed zone is steeper south of Mount Hay, relative to that in the location of the seismic study (Goleby et al., 1988), indicating that the orientation of the crust-mantle transition is steeper below the Mount Hay block. This information collectively suggests that a reasonable range in local dips for the main Redbank thrust and other parallel reflections is 50–70°, steeper than those calculated for the seismic data and consistent with the orientation of the outcrop foliation in the main Redbank thrust.

Rotations

Based on the regional constraints described above, we have rotated structures on Mount Hay and Capricorn ridges using three different potential magnitudes of rotation about three horizontal axes. The rotation axis azimuths (090, 100, 110) correspond to the range in local strike of thrusts in the Redbank deformed zone. Counterclockwise (looking west) rotations of 50°, 60°, and 70° were made about these axes, following the above discussion. The marker for this rotation is the crust-mantle transition, which we assume was sub-horizontal when the Capricorn ridge shear zone was active, prior to exhumation. Thus, we have conducted nine rotations, one for each combination of rotation axis azimuth and rotation magnitude.

Two sets of data were rotated: (1) lineations and foliations measured on central and western Capricorn ridge (to avoid the younger mylonite zones) and (2) lineations and the pole to the great circle girdle containing poles to foliation—i.e., the fold nose—from Mount Hay ridge. Comparison of the results of the nine rotations is facilitated by Bingham distribution axes and 95% confidence ellipses calculated using Stereonet© (Figs. 10C and 10D). Each rotation of lineations is represented by the restored orientation of the maximum eigenvalue of the lineation population with a 95% confidence ellipse. Similarly, each rotation of

poles to foliation on Capricorn ridge is represented by the orientation of the maximum eigenvalue of the population of foliations (Fig. 10C). The 95% confidence ellipse is smaller than each symbol for the Capricorn ridge data, reflecting the highly regular orientation of the structures. The average orientation of the maximum eigenvalue axes for poles to foliation on Capricorn ridge, and the corresponding confidence ellipse, is also indicated. Each rotation of the inferred fold nose on Mount Hay is shown with a 95% confidence ellipse. As indicated above, the mean lineation on Mount Hay ridge is essentially parallel to the axis of the map-scale fold, as is evident in Figure 10D.

A schematic cross section through the Mount Hay block allows its current and restored orientations to be compared (Figs. 10A and 10B). After rotation, foliation on Capricorn ridge dips 30–50° northeast and lineation plunges moderately north-northeast (Figs. 10B and 10C). The current south-side-up shear sense of the granulite-facies fabric on Capricorn ridge is re-oriented into a top-down-to-the-north-northeast normal shear sense (Fig. 10B). The lineation and fold axis on Mount Hay ridge become subhorizontal and trend NNE–SSW (Fig. 10D); the restored foliation is subhorizontal (Fig. 10B).

This restoration of the Mount Hay block is consistent with regional geological interpretations. For example, Teyssier et al. (1988) proposed a similar rotation in the Redbank deformed zone that restored the Proterozoic unconformity between the Chewings quartzite and underlying basement to subhorizontal or shallowly dipping. They postulated that a décollement separated the basement underlying the sediments from the lower crust (e.g., Mount Hay block) during the ca. 1600 Ma, top-to-the-north Chewings event, based on the absence of evidence for Chewings-age deformation in granulites north of the Redbank deformed zone. Our restoration of the Mount Hay block returns the south-side-up, amphibolite-facies mylonite zones on Capricorn ridge to a moderately north-dipping orientation with top-to-the-north shear sense, consistent with fabrics formed regionally during the Chewings event (cf. Teyssier et al., 1988). Our restoration therefore not only removes the necessity for a décollement, but also indicates that both the basement and cover sediments deformed during the Chewings event.

DISCUSSION

Summary

The Mount Hay block is a well-exposed cross section through ~12 km of deep, hot crust. This crustal cross section contains two, km-scale, penetratively deformed, granulite-facies structural domains: the Mount Hay ridge domain with north-side-up shear sense and $L \gg S$ to $L = S$ fabric and the Capricorn ridge shear zone with south-side-up shear sense and $S > L$ fabric. The field relations indicate that the Capricorn ridge shear zone overprinted the Mount Hay structures, including S_1 and S_2 , despite the similarly high metamorphic grade recorded by mineral assemblages in the two domains. Rotation of the Capricorn ridge shear zone,

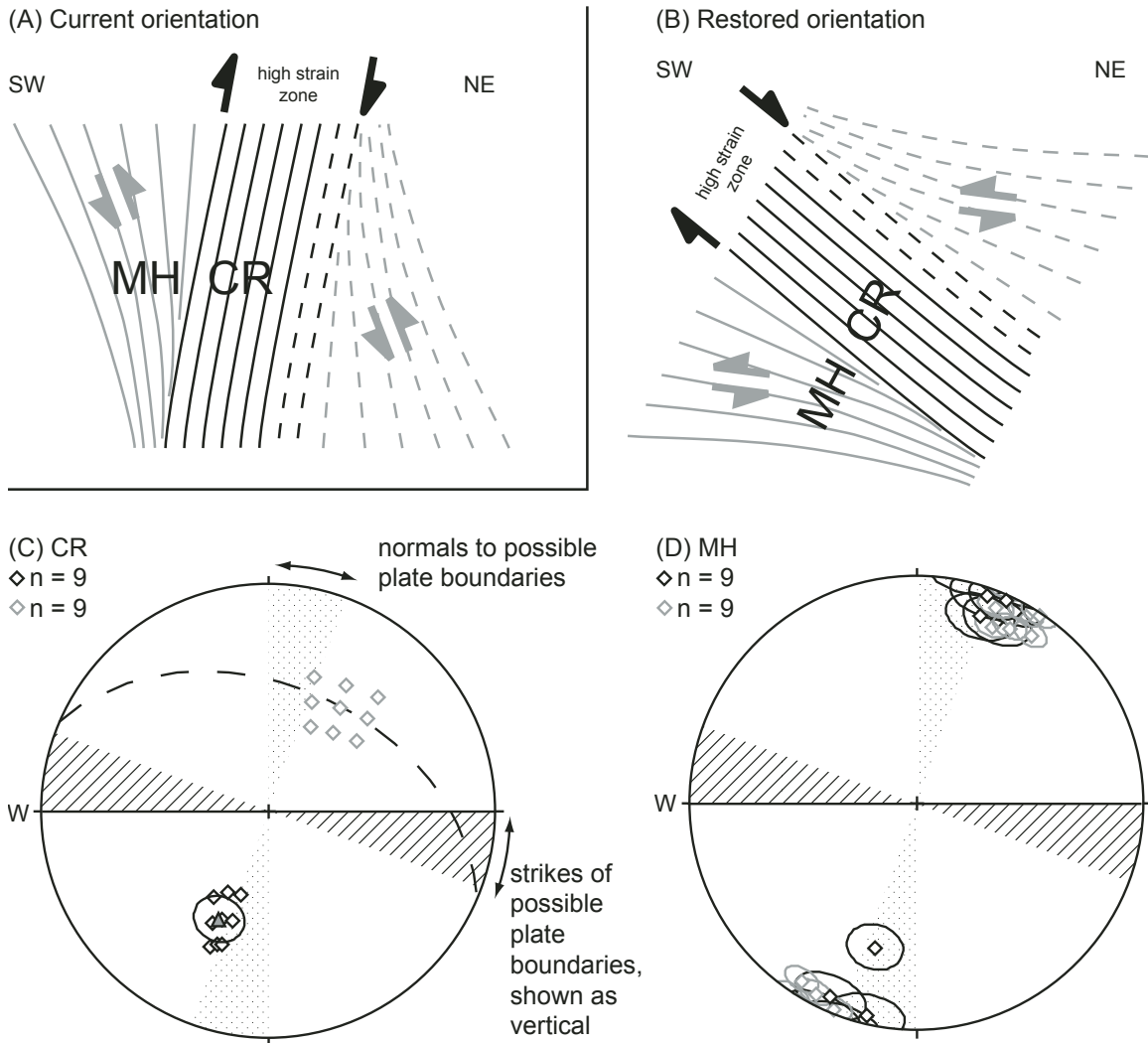


Figure 10. Results of removing net rotation of the Mount Hay block presented on lower hemisphere, equal area projections. Schematic cross section of the Mount Hay block in current (A) and restored (B) (with intermediate 60° rotation) orientations. Arrows show shear sense on Capricorn ridge (CR) (black) and Mount Hay (MH) ridge (gray). Lines indicate edges of foliation. (C) Rotation results for Capricorn ridge. Diagonally striped field indicates the orientation of the Paleoproterozoic plate boundary (shown as vertical) inferred from the Redbank deformed zone. Dotted field indicates the range of lines normal to the inferred plate boundary. Diamonds are Bingham distribution axes for rotated structures. 95% confidence cones (plotted as small circles) are smaller than the diamond symbols. Gray diamonds represent lineation rotation results. Black diamonds show positions of rotated poles to foliation. The dashed great circle corresponds to the average orientation of the Bingham distribution axes for the poles (gray triangle with 95% confidence cone). (D) Rotation results for the Mount Hay ridge sheath-like fold. Symbols as for (C) except: black diamonds represent the inferred fold nose, defined as the pole to the great circle girdle containing poles to S_1 and S_2 foliation. See text for further explanation. Small circles represent 95% confidence cones for rotated structures.

described in the previous section, restores its foliation (S_3) to a dip of $30\text{--}50^\circ$ to the NNE. In this orientation, the Capricorn ridge shear zone is a normal shear zone. The strike of the shear zone is restored to the local orientation of the Redbank deformed zone, which is interpreted as parallel to the local orientation of the Proterozoic plate margin (Shaw et al., 1984; Collins and Teysier, 1989).

Timing constraints can be inferred from prior work in the region. The protoliths to the tectonites exposed on Mount Hay ridge were penetratively recrystallized and deformed at granulite-facies conditions during an earlier event. As the only regional granulite-facies events identified to date are the 1790–1770 Ma Yambah and 1730–1690 Ma Strangways events, we tentatively relate the main fabric of Mount Hay ridge to the Yambah event

and the younger fabric exposed on Capricorn ridge to the Strangeways event. 1700 ± 17 Ma dates on zircon overgrowths support this conclusion, although we note that all these data are from Mount Hay ridge (Claoué-Long and Hoatson, 2005).

A Deep-Crustal Normal Shear Zone

Given the >4-km thickness of the Capricorn ridge shear zone, its formation was presumably related to regional-scale deformation during the Proterozoic. If we assume that the current exposure is close to the original thickness of the shear zone, deformation occurred within a zone ~6 km thick, including bounding transposition gradients ~1 km thick. Of the existing models for crustal extension, such strain localization is most consistent with the simple-shear model (Fig. 1B). The geometry of the shear zone is also consistent with the simple-shear model. If our reconstruction is correct, the Capricorn ridge shear zone was inclined $30\text{--}50^\circ$ at 26–30 km depth. Geological models for shear zones in crustal extension based on field studies call for deep, high-strain sections that are either sub-horizontal or moderately dipping based on kinematic or space constraints (e.g., Wernicke and Burchfiel, 1982; Lister *et al.*, 1986).

The current exposure may not represent the scale of the original shear zone, however, as deformation intensity does not demonstrably decrease toward the northeastern margin of Capricorn ridge (Waters-Tormey and Tikoff, 2007). The Capricorn ridge shear zone exposure therefore could be the edge of a broader zone of deformation or could be part of an anastomosing set of shear zones, such as that implied in the distributed simple-shear conceptual model (Fig. 1C). Exposures are not sufficiently continuous to allow us to determine if other granulite-facies extensional shear zones are present in the Mount Hay region. Aeromagnetic lineaments in the region surrounding the exposed Mount Hay block are interpreted to represent younger, lower-grade shear zones (e.g., Teyssier, 1985b; Collins, 2000). This inference is consistent with our observation of retrogressed, lower-grade rocks in isolated outcrops surrounding the main granulite-facies exposures. We know of no other extensional shear zones reported for the southern Arunta block active during the ca. 1800–1700 Ma time period.

In seismic sections, reflectors in extended lower continental crust typically have subhorizontal to gently dipping orientations (e.g., Klemperer, 1984; Carbonell and Smithson, 1991; Sachpazi *et al.*, 1997; Chadwick and Pharaoh, 1998; Singh *et al.*, 1998; Juhonjuntti *et al.*, 2001). Some of these reflectors have been interpreted as km-scale lower-crustal shear zones (e.g., Fountain *et al.*, 1984; Carbonell and Smithson, 1991; Sachpazi *et al.*, 1997). The Capricorn ridge shear zone appears to be too steep to be an analogy for these reflectors. However, given the anastomosing nature of shear zones observed elsewhere at deep-crustal levels (e.g., Martelat *et al.*, 2000; Arbaret and Burg, 2003) and the limited exposure in the Mount Hay region, the Capricorn ridge shear zone could represent a moderately inclined segment of a large-scale anastomosing array.

The first order observation from the Capricorn ridge shear zone, however, is that extensional deformation was not homogeneously distributed throughout the deep crust, even though it occurred at granulite-facies conditions. Rather, the deformation localized in the Capricorn ridge shear zone and overprinted, rather than simply reactivated, the existing foliation on Mount Hay ridge. This observation rules out the homogenous end-member of the pure-shear model for crustal extension, in which deformation is uniformly distributed throughout the deforming deep-crustal volume. Without knowing the complete crustal geometry of the shear zone, it is impossible to determine how much the earlier Mount Hay fabric was rotated by the younger Capricorn ridge shear zone. A reasonable assumption, however, is that foliation on Mount Hay ridge was sub-horizontal or shallowly inclined prior to uplift, similar to fabrics in other deep-crustal terranes (e.g., Moser, 1994), and was rotated only within the Capricorn ridge shear zone and in the adjacent ~1-km-thick strain gradient.

Orthogonal versus Oblique Divergent Tectonic Settings

The restored north-northeast-trending lineation of the Capricorn ridge shear zone is clockwise from the normal to the inferred regional-scale range of plate boundary orientations (Fig. 10C), which most strongly supports oblique divergence for the Strangeways event. However, the possible range in error for the geometric restoration of the Mount Hay block is sufficiently large that we cannot eliminate orthogonal divergence. Since most models of crustal-scale extension assume two-dimensional deformation for crustal- or lithospheric-scale extension (Fig. 1) (e.g., Davis, 1983; Lister *et al.*, 1986), it is worth briefly exploring the possibility that the Capricorn ridge shear zone records deep-crustal transtensional deformation during oblique divergence.

The argument that the lineation orientation suggests transtensional deformation is based on strain modeling. Within transtensional zones, the orientation of the overall stretching lineation is thought to reflect the orientation of the maximum finite stretch and not the orientation of the oblique plate motion (Fossen *et al.*, 1994; Fossen and Tikoff, 1998). At high strain, however, the long axis of the finite strain ellipsoid rotates into parallelism with the oblique plate motion vector. If the maximum finite stretch in the Capricorn ridge shear zone is represented by the prominent lineation, we can make a reasonable inference that the system is transtensional.

The upper-crustal response is well documented for both orthogonal divergence (e.g., Red Sea; Wolfenden and Ebinger, 2005) and oblique divergence (e.g., Gulf of California; Aragon-Areola and Morandi, 2005). In contrast, deep-crustal deformation during divergence is poorly documented (e.g., Dewey *et al.*, 1998). One reason for this is the difficulty in identifying extensional, high-grade terranes, both in terms of their pressure-temperature history, and because lower-crustal terranes are commonly rotated during the events that exhume them (Sandiford and Powell, 1986). The characterization of kinematics in deep-crustal

deformed zones is particularly difficult as the tectonic context for deformation is commonly obscured by younger events and the boundary conditions for deformation are unknown.

The presence of $L > S$ tectonites and folded foliations are two useful but not necessary criteria for inferring transtensional deformation; both of these features are expected to be better developed where the angle of divergence is low (Fossen et al., 1994; Venkat-Ramani and Tikoff, 2002; Dewey, 2003). The Capricorn ridge shear zone displays mainly $S > L$ fabrics and appears to be relatively tabular, suggesting the orientation of this structure was not modified by folding. These characteristics suggest a moderate to high angle of oblique divergence.

In high-angle oblique divergence, we expect upper crustal faults to have strikes oblique to the plate boundary. In contrast, the Capricorn ridge shear zone strike is parallel to the inferred Proterozoic plate boundary. This suggests that shallow and deep structures may be oblique to each other during oblique divergence (Fig. 11). This hypothetical geometry, necessarily pieced together from disparate field studies, requires further testing with additional studies of crustal cross sections and modeling to explore whether major structures change in strike with depth in divergent settings.

Tectonic Development of the Mount Hay Area

Our study of a crustal cross section and previous work allows us to propose a tectonic history for the Mount Hay area. In the Paleoproterozoic (ca. 1800 Ma), the Arunta inlier was part of a continental arc on the southern edge of the North Australian craton (e.g., Zhao and Bennett, 1995; Myers et al., 1996; Scott et al., 2000; Claoué-Long and Hoatson, 2005). Volcaniclastic sediments and intrusions related to this arc are the ca. 1800 Ma protoliths for the Mount Hay block granulites and other granulites with similar

crystallization ages in the central Arunta province (e.g., Warren, 1983; Warren and Shaw, 1995; Hoatson et al., 2005).

The 1790–1770 Ma Yambah event occurred while this continental arc was still magmatically active (Zhao and McCulloch, 1995; Claoué-Long and Hoatson, 2005; Hoatson et al., 2005). In the Mount Hay block, an earlier penetrative granulite-facies deformation resulted in the formation of a sheath-like fold through north-vergent shear after, or outlasting, minor felsic magmatism at ca. 1780–1770 Ma (Bonnay, 2001), presumably during the Yambah event.

Between ca. 1770 and 1730 Ma, a transition from a continental magmatic arc setting to a divergent, back-arc or intracontinental setting occurred in the central Arunta province. The evolution from distinct continental arc magmatism ending at ca. 1750 Ma (Zhao and McCulloch, 1995; Claoué-Long and Hoatson, 2005) to higher-silica magmatism at ca. 1730 Ma (Zhao and McCulloch, 1995) in granulites ~100 km east of the Mount Hay block may be related to the onset of divergence. Overlapping with this magmatic transition is the 1740–1690 Ma Strangways event, which resulted in a second stage of regional, penetrative, granulite-facies deformation (e.g., Goscombe, 1992a). At least locally, this involved oblique divergence, as indicated by the restoration of the Capricorn ridge shear zone. We correlate this deformation with the growth of zircon rims at 1700 ± 17 Ma (Claoué-Long and Hoatson, 2005). U-Pb zircon data also document intrusion of a diabase dike swarm in the Strangways Range northeast of the Mount Hay block at 1689 ± 8 Ma, which Claoué-Long and Hoatson (2005) have suggested records extension at the end of the Strangways event. Late Strangways extension might also account for the exhumation of that age proposed by Biermeier et al. (2003) on the basis of metamorphic decompression textures in the high-grade mineral assemblages of the Mount Heughlin area west of the Mount Hay block. Larger-scale regional studies also conclude that the southern margin of the North Australian craton underwent a tectonic transition between 1800 and 1700 Ma. Integrated petrological and sedimentary syntheses suggest that a reconfiguration of the West and South Australian cratons along the southern margin of the North Australian craton (e.g., Scott et al., 2000; Giles et al., 2002, 2004; Bagas, 2004) could have initiated a transition to (local) oblique divergence in the central Arunta block.

The majority of exhumation occurred after the Strangways tectonic event, although subsequent structural overprinting of the Redbank deformed zone obscures the exact timing (Black and Shaw, 1992; Zhao and Bennett, 1995; Biermeier et al., 2003). Granulites north of the Redbank deformed zone underwent up to 15 km of exhumation by ca. 1400 Ma (Biermeier et al., 2003). Regionally, the remaining exhumation occurred during the Paleozoic Alice Springs orogeny (Teyssier et al., 1988; Dunlap and Teyssier, 1995; Biermeier et al., 2003). Thrust faulting during the Alice Springs orogeny tilted the Paleoproterozoic Strangways lower crust and the Mesoproterozoic thrust sheets in the Redbank deformed zone into their present position (Teyssier et al., 1988).

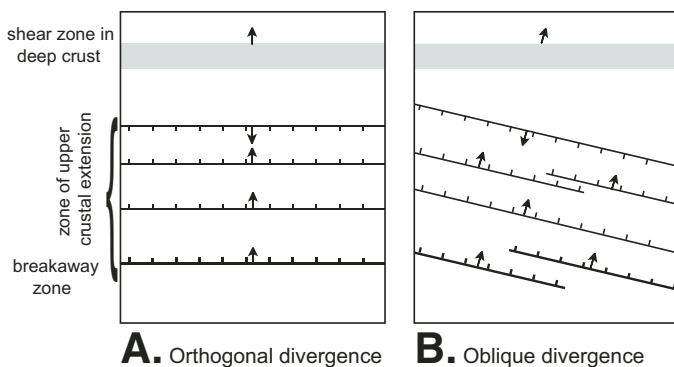


Figure 11. Rotation results (Fig. 10) indicate that the strike of the Capricorn ridge shear zone (east-west shaded region in this diagram) was subparallel to the inferred plate boundary. Map views show relationships between the Capricorn ridge deep-crustal shear zone and upper-crustal faults in cases of (A) extension resulting from orthogonal divergence and (B) transtension resulting from oblique divergence. Ornamented faults are normal faults in brittle crust.

CONCLUSIONS

The crustal cross section exposed in the Mount Hay block offers insight into deep, hot-crustal deformation during tectonic divergence. The ~4-km-thick, Capricorn ridge shear zone is inferred to have formed at 776 ± 38 °C during the 1730–1690 Ma Strangways event, and overprinted an older granulite-facies fabric exposed on the adjacent Mount Hay ridge. When post-Strangways tilting is removed, the Capricorn ridge shear zone restores to a moderately dipping (30–50°) normal shear zone, whose strike is sub-parallel to the inferred orientation of the plate boundary. This restored geometry and inferred localization within the ~4-km-thick zone are consistent with the simple-shear model of crustal extension. Lineations, however, restore to an orientation oblique to the Proterozoic plate boundary, suggesting that the Capricorn ridge shear zone formed during overall trans-tensional deformation in an obliquely divergent tectonic setting. These observations suggest that strain localization does occur at granulite-facies conditions, but in km-scale zones of penetrative deformation rather than the narrow discrete zones more commonly observed at lower metamorphic grades.

ACKNOWLEDGMENTS

This research was supported by a Packard Foundation grant to BT and NSF grant EAR-0440156 to LBG and BT. Vilas Travel (University of Wisconsin) and Sigma Xi grants provided additional support for CWT. The authors would like to thank the Danns and Evans families of Amburla and Hamilton Downs stations, respectively, for permission to carry out fieldwork and collect samples. The Alice Springs office of the Northern Territory Geological Survey is thanked for logistical support and invaluable discussions about regional geology. Laura Young and Bridget Diem are gratefully acknowledged for assisting in drafting figures. JoAnn Gage helpfully calculated temperatures for a wider range of pressures. Structural data were plotted using Stereonet v. 6.3.2 by R.W. Allmendinger. Helpful reviews by Bob Holdsworth, Bill Collins, and editors Bob Miller and Art Snoke significantly improved the manuscript.

REFERENCES CITED

- Aragon-Arreola, M., and Morandi, M., 2005, Structure of the rift basins in the central Gulf of California; kinematic implications for oblique rifting: *Tectonophysics*, v. 409, p. 19–38, doi: 10.1016/j.tecto.2005.08.002.
- Arbaret, L., and Burg, J.P., 2003, Complex flow in lowest crustal, anastomosing mylonites: Strain gradients in a Kohistan gabbro, northern Pakistan: *Journal of Geophysical Research*, v. 108, B10, p. 2467, doi: 10.1029/2002JB002295.
- Axen, G.J., 2004, Mechanics of low-angle normal faults, *in* Karner, G., Taylor, B., Driscoll, N., and Kohlstedt, D.L., eds., *Rheology and deformation in the lithosphere at continental margins*: New York, Columbia University Press, p. 46–91.
- Bagas, L., 2004, Proterozoic evolution and tectonic setting of the northwest Paterson Orogen, Western Australia: *Precambrian Research*, v. 128, p. 475–496, doi: 10.1016/j.precamres.2003.09.011.
- Biermeier, C., Stüwe, K., Foster, D.A., and Finger, F., 2003, Thermal evolution of the Redbank thrust system, central Australia: *Geochronological and phase-equilibrium constraints*: *Tectonics*, v. 22, p. 1–23, doi: 10.1029/2001TC901033.
- Black, L.P., and Shaw, R.D., 1992, U-Pb zircon chronology of prograde Proterozoic events in the central and southern provinces of the Arunta block, central Australia: *Australian Journal of Earth Sciences*, v. 39, p. 153–171, doi: 10.1080/08120099208728012.
- Bonnay, M., 2001, Felsic characterization and transfer of the magmas in the average crust to deep. Example: The Hay Mount in central Australia (translated title) [Ph.D. thesis]: Chicoutimi, Canada, University of Quebec–Chicoutimi, 537 p.
- Bonnay, M., Collins, W.J., Sawyer, E.W., and Wiebe, R.A., 2000, Introduction to the Arunta inlier, *in* Collins, W.J., ed., *Granite magma segregation and transfer during compressional deformation in the deep crust? Proterozoic Arunta inlier, central Australia*: Canberra, Geological Society of Australia, Field Trip Guide FA4, p. 8–46.
- Brace, W.F., and Kohlstedt, D.L., 1980, Limits on lithospheric stress imposed by laboratory experiments, *in* Hanks, T.C., and Raleigh, C.B., eds., *Magnitude of deviatoric stresses in the Earth's crust and uppermost mantle*: *Journal of Geophysical Research*, v. 85, p. 6248–6252.
- Carbonell, R., and Smithson, S.B., 1991, Large-scale anisotropy within the crust in the Basin and Range province: *Geology*, v. 19, p. 698–701, doi: 10.1130/0091-7613(1991)019<0698:LSAWTC>2.3.CO;2.
- Chadwick, R.A., and Pharaoh, T.C., 1998, The seismic reflection Moho beneath the United Kingdom and adjacent areas: *Tectonophysics*, v. 299, p. 255–279, doi: 10.1016/S0040-1951(98)00193-0.
- Christensen, N.I., and Mooney, W.D., 1995, Seismic velocity structure and composition of the continental crust; a global view: *Journal of Geophysical Research*, v. 100, p. 9761–9788, doi: 10.1029/95JB00259.
- Cloué-Long, J.C., and Hoatson, D.M., 2005, Proterozoic mafic-ultramafic intrusions in the Arunta region, central Australia Part 2: Event chronology and regional correlations: *Precambrian Research*, v. 142, p. 134–158, doi: 10.1016/j.precamres.2005.08.006.
- Cobbold, P.R., and Quinquis, H., 1980, Development of sheath folds in shear regimes: *Journal of Structural Geology*, v. 2, p. 119–126, doi: 10.1016/0191-8141(80)90041-3.
- Collins, W.J., 2000, ed., *Granite magma segregation and transfer during compressional deformation in the deep crust? Proterozoic Arunta inlier, central Australia*: Canberra, Geological Society of Australia, Field Trip Guide FA4, 104 p.
- Collins, W.J., and Shaw, R.D., 1995, Geochronological constraints on orogenic events in the Arunta inlier: A review: *Precambrian Research*, v. 71, p. 315–346, doi: 10.1016/0301-9268(94)00067-2.
- Collins, W.J., and Teyssier, C., 1989, Crustal scale ductile fault systems in the Arunta inlier, central Australia: *Tectonophysics*, v. 158, p. 49–66, doi: 10.1016/0040-1951(89)90314-4.
- Collins, W.J., Williams, I.S., Shaw, S.E., and McLaughlin, N.A., 1995, The age of the Ormiston Pound Granite; implications for Mesoproterozoic evolution of the Arunta inlier, central Australia: *Precambrian Research*, v. 71, p. 91–105, doi: 10.1016/0301-9268(94)00057-X.
- Coney, P.J., 1980, Cordilleran metamorphic core complexes; an overview, *in* Crittenden, M.D., Jr., Coney, P.J., and Davis, G.H., eds., *Cordilleran metamorphic core complexes*: *Geological Society of America Memoir*, v. 153, p. 7–31.
- Davis, G.H., 1983, Shear-zone model for the origin of metamorphic core complexes: *Geology*, v. 11, p. 342–347, doi: 10.1130/0091-7613(1983)11<342:SMFTOO>2.0.CO;2.
- Dewey, J.F., 2003, Transtension in arcs and orogens: *International Geology Review*, v. 7, p. 105–142.
- Dewey, J.F., Holdsworth, R.E., and Strachan, R.A., 1998, Transpression and transtension zones, *in* Holdsworth, R.E., Strachan, R.A., and Dewey, J.F., eds., *Continental transpressional and transtensional tectonics*: *Geological Society of London Special Publication* 135, p. 1–14.
- Dunlap, W.J., and Teyssier, C., 1995, Paleozoic deformation and isotopic disturbance in the southeastern Arunta block, central Australia: *Precambrian Research*, v. 71, p. 229–250, doi: 10.1016/0301-9268(94)00063-W.
- Dunlap, W.J., Hirth, G., and Teyssier, C., 1997, Thermomechanical evolution of a ductile duplex: *Tectonics*, v. 16, p. 983–1000, doi: 10.1029/97TC00614.
- Fliervoet, T.F., White, S.H., and Drury, M.R., 1997, Evidence for dominant grain-boundary sliding deformation in greenschist- and amphibolite-grade polyminerale ultramytonites from the Redbank deformed zone, central Australia: *Journal of Structural Geology*, v. 19, p. 1495–1520, doi: 10.1016/S0191-8141(97)00076-X.

- Fossen, H., and Tikoff, B., 1998, Extended models of transpression and tension, and application to tectonic setting, in Holdsworth, R.E., Strachan, R.A., and Dewey, J.F., eds., *Continental transpressional and transtensional tectonics*: Geological Society of London Special Publication 135, p. 15–33.
- Fossen, H., Tikoff, B., and Teyssier, C., 1994, Strain modeling of transpressional and transtensional deformation: *Norsk Geologisk Tidsskrift*, v. 74, p. 134–145.
- Fountain, D.M., and Salisbury, M.H., eds., 1990, *Exposed cross sections of the continental crust*: Boston, NATO ASI Series, Series C: Mathematical and Physical Sciences, v. 317, 662 p.
- Fountain, D.M., Hurich, C.A., and Smithson, S.B., 1984, Seismic reflectivity of mylonite zones in the crust: *Geology*, v. 12, p. 195–198, doi: 10.1130/0091-7613(1984)12<195:SROMZI>2.0.CO;2.
- Ganguly, J., Cheng, W., and Tirone, M., 1996, Thermodynamics of aluminosilicate garnet solid solution: New experimental data, an optimized model, and thermometric applications: *Contributions to Mineralogy and Petrology*, v. 126, p. 137–151, doi: 10.1007/s004100050240.
- Giles, D., Betts, P., and Lister, G., 2002, Far-field continental backarc setting for the 1.80–1.67 Ga basins of northeastern Australia: *Geology*, v. 30, p. 823–826, doi: 10.1130/0091-7613(2002)030<0823:FFCBSF>2.0.CO;2.
- Giles, D., Betts, P., and Lister, G., 2004, 1.8–1.5-Ga links between the North and South Australian cratons and the Early–Middle Proterozoic configuration of Australia: *Tectonophysics*, v. 380, p. 27–41, doi: 10.1016/j.tecto.2003.11.010.
- Glikson, A.Y., 1984, Granulite-gneiss terranes of the southwestern Arunta block, central Australia: Glen Helen, Narwietooma, and Anurla: Canberra, Bureau of Mineral Resources, Australia Record 1984-22, 1:100,000 sheet areas.
- Glikson, A.Y., 1986, Regional structure and evolution of the Redbank-Mount Zeil thrust zone; a major lineament in the Arunta inlier, central Australia: Bureau of Mineral Resources: *Journal of Australian Geology and Geophysics*, v. 10, p. 89–107.
- Goleby, B.R., Wright, C., Collins, C.D.N., and Kennett, B.L.N., 1988, Seismic reflection and refraction profiling across the Arunta block and the Ngalia and Amadeus basins: *Australian Journal of Earth Sciences*, v. 35, p. 275–294, doi: 10.1080/08120098808729447.
- Goleby, B.R., Shaw, R.D., Wright, C., Kennett, B.L.N., and Lambeck, K., 1989, Geophysical evidence for “thick-skinned” crustal deformation in central Australia: *Nature*, v. 337, p. 325–330, doi: 10.1038/337325a0.
- Goleby, B.R., Kennett, B.L.N., Wright, C., Shaw, R.D., and Lambeck, K., 1990, Seismic reflection profiling in the Proterozoic Arunta block, central Australia: Processing for testing models of tectonic evolution: *Tectonophysics*, v. 173, p. 257–268, doi: 10.1016/0040-1951(90)90222-T.
- Goscombe, B., 1992a, High-grade reworking of central Australian granulites. Part 1: Structural evolution: *Tectonophysics*, v. 204, p. 361–399, doi: 10.1016/0040-1951(92)90317-Y.
- Goscombe, B., 1992b, High-grade reworking of central Australian granulites: Metamorphic evolution of the Arunta complex: *Journal of Petrology*, v. 33, p. 917–962.
- Hand, M., and Sandiford, M., 1999, Intraplate deformation in central Australia, the link between subsidence and fault reactivation: *Tectonophysics*, v. 305, p. 121–140, doi: 10.1016/S0040-1951(99)00009-8.
- Hoatson, D.M., Claoué-Long, J.C., and Shensu, S., 2005, Proterozoic mafic-ultramafic intrusions in the Arunta region, central Australia, Part 1: Geological setting and mineral potential: *Precambrian Research*, v. 142, p. 93–133, doi: 10.1016/j.precamres.2005.09.004.
- Hobbs, B.E., Means, W.D., and Williams, P.F., 1976, *An outline of structural geology*: New York, Wiley, 571 p.
- Holland, T.J.B., and Powell, R., 1998, An internally consistent thermodynamic data set for phases of petrologic interest: *Journal of Metamorphic Geology*, v. 16, p. 309–343, doi: 10.1111/j.1525-1314.1998.00140.x.
- Jackson, J.A., and White, N.J., 1989, Normal faulting in the upper continental crust; observations from regions of active extension: *Journal of Structural Geology*, v. 11, p. 15–36, doi: 10.1016/0191-8141(89)90033-3.
- Juhonjuntti, N., Juhlin, C., and Dyrelius, D., 2001, Crustal reflectivity underneath the Central Scandinavian Caledonides: *Tectonophysics*, v. 334, p. 191–210, doi: 10.1016/S0040-1951(00)00292-4.
- Kelso, P., 1993, A magnetic study of deep crustal rocks from the Arunta block, Australia, and the implications for the interpretation of long-wavelength magnetic anomalies [Ph.D. thesis]: Minneapolis, University of Minnesota, 147 p.
- Klemperer, S., 1984, Seismic reflections of the continental crust: *Nature*, v. 311, p. 409, doi: 10.1038/311409a0.
- Korsch, R.J., Goleby, B.R., Leven, J.H., and Drummond, B.J., 1998, Crustal architecture of central Australia based on deep seismic reflection profiling: *Tectonophysics*, v. 288, p. 57–69, doi: 10.1016/S0040-1951(97)00283-7.
- Lafrance, B., Clarke, G.L., Collins, W.J., and Williams, I.S., 1995, The emplacement of the Wuluma granite: Melt generation and migration along steeply dipping extensional fractures at the close of the Late Strangways orogenic event, Arunta block, central Australia: *Precambrian Research*, v. 72, p. 43–67, doi: 10.1016/0301-9268(94)00046-T.
- Lister, G.S., Etheridge, M.A., and Symonds, P.A., 1986, Detachment faulting and the evolution of passive continental margins: *Geology*, v. 14, p. 246–250, doi: 10.1130/0091-7613(1986)14<246:DFATEO>2.0.CO;2.
- Livaccari, R.F., Geissman, J.W., and Reynolds, S.J., 1995, Large-magnitude extensional deformation in the South Mountains metamorphic core complex, Arizona; evaluation with paleomagnetism: *Geological Society of America Bulletin*, v. 107, p. 877–894, doi: 10.1130/0016-7606(1995)107<0877:LMEDIT>2.3.CO;2.
- Martelat, J.E., Lardeaux, J.M., Nicollet, C., and Rakotondrazafy, R., 2000, Strain pattern and late Precambrian deformation history in southern Madagascar: *Precambrian Research*, v. 102, p. 1–20, doi: 10.1016/S0301-9268(99)00083-2.
- Moser, D.E., 1994, The geology and structure of the mid-crustal Wawa gneiss domain: a key to understanding tectonic variation with depth and time in the late Archean Abitibi-Wawa orogen: *Canadian Journal of Earth Sciences*, v. 31, p. 1064–1080.
- Myers, J.S., Shaw, R.D., and Tyler, I.M., 1996, Tectonic evolution of Proterozoic Australia: *Tectonics*, v. 15, p. 1431–1446, doi: 10.1029/96TC02356.
- Pavlis, T.L., Marty, K., and Sisson, V.B., 2003, Constrictional flow within the Eocene forearc of Southern Alaska; an effect of dextral shear during ridge subduction, in Sisson, V.B., Roeske, S.M., and Pavlis, T.L., eds., *Geology of a transpressional orogen developed during ridge-trench interaction along the North Pacific margin*: Geological Society of America Special Paper 371, p. 171–190.
- Reston, T.J., 1990, The lower crust and the extension of the continental lithosphere; kinematic analysis of BIRPS deep seismic data: *Tectonics*, v. 9, p. 1235–1248, doi: 10.1029/TC009i005p01235.
- Sachpazi, M., Him, A., Nercessian, A., Avedik, F., Mc Bride, J., Loucoyanakis, M., Nicolich, R., and the STREAMERS-PROFILES group, 1997, A first coincident normal-incidence and wide-angle approach to studying the extending Aegean crust: *Tectonophysics*, v. 270, p. 301–312, doi: 10.1016/S0040-1951(96)00160-6.
- Sandiford, M., and Powell, R., 1986, Deep crustal metamorphism during continental extension: Modern and ancient examples: *Earth and Planetary Science Letters*, v. 79, p. 151–158, doi: 10.1016/0012-821X(86)90048-8.
- Scott, D.L., Rawlings, R.W., Page, C.Z., Tarlowski, M., Idnurm, M.J., Jackson, P.N., and Southgate, P.N., 2000, Basement framework and geodynamic evolution of the Palaeoproterozoic superbasins of north-central Australia: An integrated review of geochemical, geochronological and geophysical data: *Australian Journal of Earth Sciences*, v. 47, p. 341–380, doi: 10.1046/j.1440-0952.2000.00793.x.
- Scrimgeour, I., Smith, J.B., and Raith, J.G., 2000, Palaeoproterozoic high-T, low-P metamorphism and dehydration melting in metapelites from the Mopunga Range, Arunta inlier, central Australia: *Journal of Metamorphic Geology*, v. 19, p. 739–757.
- Shaw, R.D., and Black, L.P., 1991, The history and tectonic implications of the Redbank thrust zone, central Australia, based on structural, metamorphic and Rb-Sr isotopic evidence: *Australian Journal of Earth Sciences*, v. 38, p. 307–332, doi: 10.1080/08120099108727975.
- Shaw, R.D., Stewart, A.J., and Black, L.P., 1984, The Arunta inlier: A complex ensialic mobile belt in central Australia. Part 2: Tectonic history: *Australian Journal of Earth Sciences*, v. 31, p. 457–484, doi: 10.1080/08120098408729305.
- Singh, S.C., Hague, P.J., and McCaughey, M., 1998, Study of the crystalline crust from a two-ship normal-incidence and wide-angle experiment: *Tectonophysics*, v. 286, p. 79–91, doi: 10.1016/S0040-1951(97)00256-4.
- Staffier, K., 2007, Field and microstructural investigation of plagioclase deformation behavior in granulite facies rocks, Mount Hay, central Australia [M.S. thesis]: Madison, University of Wisconsin, 88 p.
- Taylor, W.R., 1998, An experimental test of some geothermometer and geobarometer formulations for upper mantle peridotites with application to the thermobarometry of fertile lherzolite and garnet websterite; Memorial

- volume for Matthias Rosenhauer: Neues Jahrbuch für Mineralogie-Abhandlungen, v. 172, p. 381–408.
- Teyssier, C., 1985a, High strain zones in the continental crust: The central Australian example [Ph.D. thesis]: Melbourne, Australia, Monash University, 350 p.
- Teyssier, C., 1985b, A crustal thrust system in an intracratonic environment: *Journal of Structural Geology*, v. 7, p. 689–700, doi: 10.1016/0191-8141(85)90144-0.
- Teyssier, C., Amri, C., and Hobbs, B.E., 1988, Southern Arunta block: The internal zones of a Proterozoic overthrust in central Australia: *Precambrian Research*, v. 40–41, p. 157–173, doi: 10.1016/0301-9268(88)90066-6.
- van der Hilst, R.D., Kennett, B.L.N., and Shibutani, T., 1998, Lithospheric and mantle structure beneath Australia, in Braun, J., ed., *Structure and evolution of the Australian continent: Geodynamics Series (American Geophysical Union)*, Washington D.C., v. 26, p. 39–57.
- van der Pluijm, B.A., and Marshak, S., 2004, *Earth structure*: New York, W.W. Norton and Company, 656 p.
- Venkat-Ramani, M., and Tikoff, B., 2002, Physical models of transtension folding: *Geology*, v. 30, p. 523–526, doi: 10.1130/0091-7613(2002)030<0523:PMOTF>2.0.CO;2.
- Warren, R.G., 1983, Metamorphic and tectonic evolution of granulites, Arunta block, central Australia: *Nature*, v. 305, p. 300–303, doi: 10.1038/305300a0.
- Warren, R.G., and Shaw, R.D., 1995, Hermannsburg, Northern Territory 1:250,000 Geological Series, Explanatory Notes and Map SF/53: Canberra, Bureau of Mineral Resources, Australia.
- Waters, C.L., Tikoff, B., Goodwin, L.B., and Little, T.A., 2002, Geological framework for deformation patterns and deformation-induced heterogeneity in the crust, in Goff, J.A., and Holliger, K., eds., *Small scale heterogeneity*: New York, Kluwer Press, p. 1–36.
- Waters-Tormey, C., 2004, Structural geology of a ten kilometer scale lower crustal shear zone: Mount Hay granulites, central Australia [Ph.D. thesis]: Madison, University of Wisconsin at Madison, 198 p.
- Waters-Tormey, C., and Tikoff, B., 2007, Characteristics of a kilometer-scale high strain zone in the lower continental crust: Mount Hay block, central Australia: *Journal of Structural Geology*, v. 29, p. 562–579, doi: 10.1016/j.jsg.2006.10.011.
- Watt, G., 1992, Geology of the Mount Hay–Mount Chapple massif (Arunta block, Hermannsburg 1:250,000 Sheet area, central Australia) Field Report: Canberra, Bureau of Mineral Resources: Record, v. 1992, no. 22.
- Wellman, P., 1988, Development of the Australian Proterozoic crust as inferred from gravity and magnetic anomalies: *Precambrian Research*, v. 40–41, p. 89–100, doi: 10.1016/0301-9268(88)90062-9.
- Wernicke, B.P., 1981, Low-angle normal faults in the Basin and Range Province: Nappe tectonics in an extending orogen: *Nature*, v. 291, p. 645–650, doi: 10.1038/291645a0.
- Wernicke, B., 1985, Uniform-sense normal simple shear of the continental lithosphere: *Canadian Journal of Earth Sciences*, v. 22, p. 108–125.
- Wernicke, B.P., and Burchfiel, B.C., 1982, Modes of extensional tectonics: *Journal of Structural Geology*, v. 4, p. 105–115, doi: 10.1016/0191-8141(82)90021-9.
- Wiebe, R.A., and Collins, W.J., 1998, Depositional features and stratigraphic sections in granitic plutons: Implications for the emplacement and crystallization of granitic magma: *Journal of Structural Geology*, v. 20, p. 1273–1289, doi: 10.1016/S0191-8141(98)00059-5.
- Wolfenden, E., and Ebinger, C.E., 2005, Evolution of a volcanic rifted margin; southern Red Sea, Ethiopia: *Geological Society of America Bulletin*, v. 117, p. 846–864, doi: 10.1130/B25516.1.
- Wright, C., Goleby, B.R., Collins, C.D.N., Korsch, R.J., Barton, T., Greenhalgh, S.A., and Sugiharto, S., 1990, Deep seismic profiling in central Australia: *Tectonophysics*, v. 173, p. 247–256, doi: 10.1016/0040-1951(90)90221-S.
- Zhao, J., and Bennett, V.C., 1995, SHRIMP U-Pb zircon geochronology of granites in the Arunta inlier, central Australia: Implications for Proterozoic crustal evolution: *Precambrian Research*, v. 71, p. 17–43, doi: 10.1016/0301-9268(94)00054-U.
- Zhao, J.X., and McCulloch, M.T., 1995, Geochemical and Nd isotopic systematics of granites from the Arunta inlier, central Australia: Implications for Proterozoic crustal evolution: *Precambrian Research*, v. 71, p. 265–299, doi: 10.1016/0301-9268(94)00065-Y.

Contents

CD-ROM Contents

Acknowledgments

- 1. The utility of crustal cross sections in the analysis of orogenic processes in contrasting tectonic settings**
R.B. Miller and A.W. Snoke
- 2. Petrology and geochronology of crustal xenoliths from the Bering Strait region: Linking deep and shallow processes in extending continental crust**
V.V. Akinin, E.L. Miller, and J.L. Wooden
- 3. Construction and evolution of the Kodiak Talkeetna arc crustal section, southern Alaska**
D.W. Farris
- 4. Mid-Cretaceous–Recent crustal evolution in the central Coast orogen, British Columbia and southeastern Alaska**
M.L. Crawford, K.A. Klepeis, G.E. Gehrels, and J. Lindline
- 5. Plutonism at different crustal levels: Insights from the ~5–40 km (paleodepth) North Cascades crustal section, Washington**
R.B. Miller, S.R. Paterson, and J.P. Matzel
- 6. Granulite- to amphibolite-facies metamorphism and penetrative deformation in a disrupted ophiolite, Klamath Mountains, California: A deep view into the basement of an accreted oceanic arc**
S.R. Garlick, L.G. Medaris Jr., A.W. Snoke, J.J. Schwartz, and S.M. Swapp
- 7. Mesozoic magmatism in an upper- to middle-crustal section through the Cordilleran continental margin arc, eastern Transverse Ranges, California**
S.K. Needy, J.L. Anderson, J.L. Wooden, R.J. Fleck, A.P. Barth, S.R. Paterson, V. Memeti, and G.S. Pignotta
- 8. Perspectives on the architecture of continental crust from integrated field studies of exposed isobaric sections**
M.L. Williams, K.E. Karlstrom, G. Dumond, and K.H. Mahan
- 9. Evolution of the middle and lower continental crust during the transition from contraction to extension in Fiordland, New Zealand**
K.A. Klepeis and D.S. King
- 10. A granulite-facies normal shear zone exposed in the Arunta inlier of central Australia: Implications for deep-crustal deformation during oblique divergence**
C. Waters-Tormey, L.B. Goodwin, B. Tikoff, K. Staffier, and P. Kelso

Index

